

The University of Nottingham
Faculty of Engineering
Department of Architecture and Built Environment



**NUMERICAL INVESTIGATION INTO A DOUBLE SKIN
FAÇADE SYSTEM INTEGRATED WITH SHADING
DEVICES, WITH REFERENCE TO THE CITY OF AMMAN,
JORDAN**

IKRIMA ABD EL-KARIM MOHAMMAD AMAIREH

BArch.Eng (Hons), MSc

Thesis submitted to the University of Nottingham for the degree of
Doctor of Philosophy

January 2017

ABSTRACT:

The aim of this research was to investigate the thermal performance of Double skin facades (DSFs) for office buildings in Amman. Special attention was given to the role of cavity-integrated shading slats. The study was conducted through a parametric study concerning configuration and design parameters of both DSF's cavity and shading slats, in addition to boundary conditions. For the purpose of this study, a CFD-Fluent model was developed and validated. Besides, a new method for more accurate representation of solar radiation (as boundary conditions) was developed. Both RNG $k-\epsilon$ and SST $k-\omega$ turbulence models were used. The Discrete ordinates (DO) radiation model with non-gray option was selected for modelling of radiation heat transfer.

Simulations confirmed that both the width of the cavity and the size and arrangement of openings would have a significant impact on overall performance of the system. The aspect ratio (H/W) of the cavity would further impact its operation, which could contribute to 77% and 26% increase in ventilation and temperature for inner glass surfaces, respectively, of a simple cavity. In addition, among other design parameters, the size and surface emissivity of integrated slats would have the largest influence on the natural ventilation rate in the cavity. The inner glass surface temperature is mainly influenced by the inclination angle and position of these slats in addition to the internal and external environmental conditions. The influence of these slats is also dependent on the aspect ratio of the cavity. Detailed design of these slats would play a further role,

together with the boundary conditions (incidence angle) and other design parameters of the cavity (H/W aspect ratio).

In Amman, DSFs were shown to have a good performance during heating seasons, as they would enable indoor thermal comfort and ventilation requirements to be met by passive means. During cooling seasons, DSFs with integrated slats would also be able to reduce total solar heat gains if sufficient ventilation could be provided for its cavity. However, artificial cooling is still required for such a hot climate. Controlling the cavity openings is highly recommended for both scenarios. It is recommended that the cavity width is at least 0.6m, the glass transmittance is about 0.8, the size for integrated slat is 20% of the cavity width, and the optimum surface emissivity of the slats is about 0.2. Slats should preferably be placed at mid of cavity or be adjustably according to the seasonal requirements. Optimum inclination angles for slats were found to be 45° degrees and 30° degrees for summer and winter, respectively. General recommendations and design guidelines were provided.

In the Name of Allah, the Entirely Merciful, the Especially Merciful.

ACKNOWLEDGMENT:

First of All, I would greatly thank Allah almighty for his countless mercy by accepting me among his servants, and for giving me the ability to reach this stage. All praises and thanks be to Allah, the lord of the worlds.

Secondly, I would like to express my deep gratitude to my main supervisor Dr Guohui Gan for his tremendous guidance, support, and patience throughout this research. As well, I would like to thank Dr Siddig Omer, second supervisor, for his contribution and advice. In addition, I would like to extend my thanks to IT staff at the University of Nottingham for their help and technical support.

Moreover, I would like to express my appreciations to the German-Jordanian University in Amman/Jordan for offering me a scholarship to pursue my PhD research. Besides, I would like to extend my deep thanks to my colleagues over there for their continuous support and help.

Last but not least, my sincere thanks go to my late Dad for his tremendous support over the course of my life, as he was more than a father. Deep gratitude from the bottom of my heart goes to my beloved Mum. Indeed, no words can express how much I do love and owe her. Special thanks go to my entire family: brothers, sister, brothers- & sisters-in-law, nephews and nieces.

TABLE OF CONTENTS:

ABSTRACT:	I
ACKNOWLEDGMENT:	III
TABLE OF CONTENTS:	IV
LIST OF TABLES:	X
LIST OF ILLUSTRATIONS:	XII
NOMENCLATURE	XXVI
GREEK SYMBOLS	XXVII
ABBREVIATIONS	XXVII
CHAPTER 1 INTRODUCTION	1
1.1 Overview:.....	1
1.2 Aim and Objectives:	5
1.2.1 Aim:	5
1.2.2 Objectives:.....	5
1.3 Framework of the Research:	6
CHAPTER 2 BACKGROUND OF CASE STUDY: CITY OF AMMAN IN JORDAN	12
2.1 Thermal Comfort:	12
2.2 Climate of Amman/Jordan: An overview of Amman City	15
2.3 Energy status, needs, and shortcomings in Jordan:	20
2.3.1 Energy Status:	20
2.3.2 Energy Consumption:	21
2.4 Architecture and Built Environment of Amman: Overview, Climate Issues, and Proposed Solutions	22
2.4.1 Trends of Architecture in Amman:	22
2.4.2 Energy-Efficient Building Codes and Energy Consumption in Amman:	24
2.4.3 Climatic Passive Design Solutions for Buildings in Amman:	27
2.4.3.1 Insulations and Thermal Mass Materials:	27

2.4.3.2	Passive Solar Shading:	28
2.4.3.3	Double Skin Facades “DSF”:	30
2.5	Conclusion:	35

CHAPTER 3 BACKGROUND OF DOUBLE SKIN FAÇADE (DSF)37

3.1	Introduction:.....	37
3.2	Definition of DSF:.....	39
3.3	History of DSF:	39
3.4	Advantages and Disadvantages of DSF:.....	40
3.5	The Architecture of DSF:.....	42
3.5.1	Structure of DSF:	42
3.5.2	Classification of DSF:	43
3.5.3	Components of DSF:.....	48
3.5.3.1	A pair of surfaces:	48
3.5.3.2	The cavity:	48
3.5.3.3	The openings:	54
3.5.3.4	Integrated Shading devices:	56
3.6	Cavity’s Airflow Modes and Ventilation Mechanisms:	57
3.7	The Operation of DSF:	60
3.7.1	System Function:	60
3.7.2	Work Mechanism:	60
3.8	Conclusion:	63

CHAPTER 4 LITERATURE REVIEW ON DOUBLE SKIN FAÇADES (DSF)65

4.1	Thermal Performance under Hot Conditions	65
4.1.1	Overview:	65
4.1.2	Insight into System’s Thermal Performance under Hot Conditions:.....	66
4.1.3	Design Considerations and Parameters:	68
4.1.4	Common Issues Associated with DSF Systems in Hot Conditions:	71
4.1.4.1	Excessive Direct Solar Gains:	71
4.1.4.2	Indoor Overheating:	72
4.1.5	Common solutions for Excessive Direct Solar Gains and Overheating by DSF Systems:	77
4.1.5.1	Window and Glass Characteristics:	78
4.1.5.2	Green Cavity “Plants in Cavity”:	81
4.1.5.3	Passive Shading & Ventilating the Cavity:	82
4.1.6	Conclusion:.....	82
4.2	Role of Cavity-Integrated Shading Devices in DSF	83
4.2.1	Overview:	83
4.2.2	Influence of cavity-integrated shading on thermal performance of DSF and Indoor:	85

4.2.3	Influence of cavity-integrated shading on airflow of ventilated DSF:	88
4.2.4	Design parameters of shading elements:	89
4.2.5	Geometrical Shape of Individual Cavity-integrated Shading Device:	93
4.2.6	Thermal and Airflow Modelling of DSF and Whole Building:	95
4.2.6.1	Modelling DSF system alone:	96
4.2.6.2	Modelling the whole building equipped with DSF (DSF-building):	100
4.2.7	Conclusion:	107
4.3	Natural Daylighting and Potentials with DSF	108
4.3.1	Overview:	108
4.3.2	Innovative daylighting systems:	109
4.3.3	Daylighting through DSF “Optical Performance”:	113
4.3.4	Glare caused by DSF:	115
4.3.5	Conclusion:	116

CHAPTER 5 THEORETICAL BACKGROUND AND METHOD VALIDATION.....118

5.1	Introduction:	118
5.2	The Mathematical Models:	119
5.3	Computational Fluid Dynamic (CFD) Modelling:	126
5.4	The Validation for Solution Method:	128
5.4.1	Case Description:	128
5.4.1.1	Measurements criteria:	129
5.4.1.2	Boundary and Operating Conditions:	130
5.4.1.3	Solution Method’s Set-up: Settings for Fluent Solver	131
5.4.2	Independence of Mesh Size:	135
5.4.3	External Extension for Computation Domain:	138
5.4.4	Turbulence Model:	140
5.4.5	Modelling Surface Emissivity:	144
5.4.6	Validation Cases and Results:	146
5.4.6.1	Non-shaded cavity: No shading slats inside the cavity	147
5.4.6.2	Shaded cavity: with integrated shading slats	150
5.4.7	Conclusion and Recommendations:	154
5.5	Further Validation Works	156
5.5.1	Model Validation against Simple Cavity with Horizontal Inlet and Outlet:	156
5.5.1.1	Investigating the importance of Height-to-Width ratio (h/w) on cavity’s air velocity profiles:	158
5.5.2	Fluent Model Validation against Established General Expressions	160

CHAPTER 6 MODEL SETUP AND DEVELOPMENT.....164

6.1	Introduction:	164
6.2	The Problem:	164
6.3	Boundary Conditions:	165

6.3.1	Solar Irradiance Magnitudes:	165
6.3.2	Air Temperature:.....	169
6.3.3	Indoor Boundary Conditions:	169
6.4	Solution Method's Set-up: Settings for Fluent Solver	169
6.4.1	Turbulence Model:.....	169
6.4.2	Radiation Model:.....	170
6.4.3	Material Modelling and Specifications:.....	170
6.4.4	Solution Methods, Control and Convergence Criteria:	172
6.5	Preliminary Studies:.....	173
6.5.1	Independence of Mesh Size:	173
6.5.2	Extension of the Computational Domain:.....	175
6.6	A New Method for Solar Radiation Representation:.....	176
6.6.1	Simple Cavity with Vertical Vents:	181
6.6.2	Simple Cavity with Horizontal Vents:.....	183
6.7	Amendments and Simplifications: Changes from Initial Configuration as Presented in Mesh Independence and Extension of Domain.....	188
6.8	Summary:	190

CHAPTER 7 GENERAL PARAMETRIC STUDY ON SIMPLE CAVITY WITH SIMPLE INTEGRATED SLATS191

7.1	Introduction:.....	191
7.2	Size of Integrated Slats:	192
7.3	Inclination Angles of Slats:.....	196
7.4	Position of Integrated Slats:	203
7.5	Surface Emissivity of Integrated Slats:.....	207
7.6	Surface Diffuse Fraction of Integrated Slats:	211
7.7	Surface Diffuse Fraction of Glass Panes:	215
7.8	Conclusion:	219

CHAPTER 8 PARAMETRIC STUDY ON SIMPLE CAVITY WITH HORIZONTAL VENTS AND VARIOUS INTEGRATED SLATS.....221

8.1	Introduction:.....	221
8.2	Performance of Different Integrated Slats with Surface Emissivity of 0.9 and Diffuse Fraction of 1; Under Summer Conditions:	227

8.3	Performance of Selected Integrated Slats with Surface Emissivity of 0.2 and Diffuse Fraction of 0; Under Summer Conditions:	236
8.4	Performance of Selected Integrated Slats with Surface Emissivity of 0.2 and Diffuse Fraction of 0; Under Winter Conditions:.....	243
8.5	Influence of Cavity Vents' Size on the Performance of Different Integrated Slats:.....	249
8.6	Influence of Integrated Slats' Position on Their Performance:	255
8.7	Influence of Size of Different Integrated Slats on Their Performance:.....	261
8.8	Influence of Aspect Ratio (Height-To-Width) of Cavity:	267
8.9	Combined Influence of Glass Transmittance and Height-to-Width Aspect Ratio:	284
8.10	Conclusion:	295

CHAPTER 9 DOUBLE SKIN FAÇADE (DSF) WITHOUT SHADING DEVICES.....298

9.1	Size of Cavity:.....	298
9.1.1	Summer Conditions	298
9.1.2	Winter Conditions:	300
9.2	Glass Transmittance:	303
9.2.1	Summer Conditions:.....	303
9.2.2	Winter Conditions:	307
9.3	Opening Control:	310
9.4	Uniting Cavity Size:	313
9.4.1	Summer Conditions:.....	313
9.4.2	Winter Conditions:	315

CHAPTER 10 DOUBLE SKIN FAÇADE (DSF) INTEGRATED WITH SLATS.....320

10.1	Size and Inclination Angle:.....	321
10.1.1	Summer Conditions	321
10.1.2	Winter Conditions	326
10.2	Slats' Surface Emissivity:.....	331
10.2.1	Summer Conditions	331
10.2.2	Winter Conditions	337
10.3	Slats' Position:	342
10.3.1	Summer Conditions	342
10.3.2	Winter Conditions	348

CHAPTER 11 EFFECT OF INTERNAL HEAT GAINS	355
11.1 Summer Conditions	355
11.2 Winter Conditions	359
CHAPTER 12 SUMMER ARTIFICIAL COOLING	366
12.1 Arrangement of Supply Vents:	366
12.2 The arrangement of Exhaust Vents:	372
12.3 Supply Air Temperature:	378
12.4 Ceiling Cooling Vents:	385
CHAPTER 13 OPTIMIZATION OF THE SYSTEM (SUMMARY AND APPLICATION)	392
13.1 Winter Scenario:	393
13.2 Summer Scenario:	396
CHAPTER 14 CONCLUSION, RECOMMENDATIONS AND FUTURE WORKS	401
14.1 Summary:	401
1.1 Conclusion, Key outcomes & Recommendations:	405
14.2 Contribution to the Body of Knowledge:	408
15.3 Research Limitations:	409
15.4 Future Works:	410
REFERENCES:	412
APPENDICES:	420
APPENDIX A: World Map of Koppen-Geiger Climate Classification.....	420
APPENDIX B: Jordan status in terms of applying Building Energy Code for residential and non-residential sectors. Worldwide Status of Building Energy Code/Standards.	421
APPENDIX C: Design and Specifications for Various Available Daylighting Products.	422
APPENDIX D: Design and Specifications for Common Shading Products.	445

LIST OF TABLES:

Table 1.1	Detailed description for the research framework, conducted tasks, and final chapters of the thesis.	10
Table 2.1	Percentage ratios of the sectoral distribution of final energy consumption during 2008-2012.	21
Table 2.2	Percentage rate of sectoral consumption of electricity during 2008-2012.	22
Table 2.3	U-values for Walls, Exposed Floors & Roofs and Window Types for Building in Amman according to Energy Efficient Building Code for Jordan.	25
Table 5.1	Boundary Conditions for the validation Case.	131
Table 5.2	Thermal and solar properties for different materials.	133
Table 5.3	set-up for solution methods in fluent.	134
Table 5.4	Characteristics for initial Mesh-1.	135
Table 5.5	codes for different levels of simplification.	147
Table 6.1	Parameters for Summer and Winter design days.	167
Table 6.2	Solar components and their values for the Actual Method; for south-vertical wall at 12pm on day# 187 (6th July); Amman/Jordan. Summer Design Day.	167
Table 6.3	Solar components and their values for the Equivalent Method; for south-vertical wall at 12pm on day# 187 (6th July); Amman/Jordan. Summer Design Day.	168
Table 6.4	Solar components and their values for the Actual Method; for south-vertical wall at 12pm on day# 23 (23rd Jan.); Amman/Jordan. Winter Design Day.	168
Table 6.5	Solar components and their values for the Equivalent Method; for south-vertical wall at 12pm on day# 23 (23rd Jan.); Amman/Jordan. Winter Design Day.	168
Table 6.6	Ambient air temperatures for both design days and at the specific hours.	169
Table 6.7	Energy band for Non-Gray radiation model with wavelength intervals.	170
Table 6.8	Characteristics for Angular Discretization.	170
Table 6.9	Thermal and solar properties for different materials.	171
Table 6.10	Absorption Coefficient (α) for two selected glass's thickness values δ (m) and various examined transmittance values (T).	171
Table 6.11	set-up for solution methods in fluent.	172
Table 6.12	Initial Under-Relaxation Factors used for different equations/parameters in the solution control.	173
Table 6.13	Characteristics for different examined meshes.	174
Table 7.1	Details for different examined positions of integrated slats.	203
Table 7.2	Maximum and minimum calculated values and associated variation for main reported outputs against various investigated parameters.	219
Table 7.3	level of influence of various investigated parameters on different reported outputs; 1st: highest influential whereas 6th lowest influential	220
Table 8.1	Revealed relationships between cavity's airflow rate and its characteristics (Height/Width=H/W), and for different integrated slats.	269
Table 8.2	Revealed relationships between cavity's airflow rate and its characteristics (Height/Width=H/W), and for different integrated slats; under winter conditions.	273

Table 8.3	Revealed relationships between surface temperature increase of cavity and its characteristics (Height/Width=H/W), and for desing#1 & desing#11 of integrated slats	276
Table 8.4	Revealed relationships between surface temperature increase of cavity and its characteristics (Height/Width=H/W), and for desing#1 & desing#11 of integrated slats	281
Table 8.5	Revealed relationships between cavity's airflow rate and its characteristics (Height/Width=H/W) for different glass transmittances and both integrated slats' designs: #1 & #11.	285
Table 8.6	Revealed relationships between surface temperature increase of cavity and its characteristics (Height/Width=H/W), for different glass transmittances and both integrated slats' designs: #1 & #11.	291
Table 12.1	Internal and solar heat gains used to calculate mass flow rate for initial setting of the artificial cooling loads.	367
Table 12.2	Adjusted sizes and corresponding velocity to achieve required flow rate (0.095m ³ /s-m	367
Table 12.3	Vent's sizes and arrangements for the three investigated proposals.	368

LIST OF ILLUSTRATIONS:

Figure 1.1	A Flowchart shows the framework of the research with generated chapters of the thesis.	9
Figure 2.1	Climate data for University of Jordan's weather station in Amman.	17
Figure 2.2	Psychometric Chart of Amman "University of Jordan's weather station".	18
Figure 2.3	Primary Energy Consumption of Jordan for 2008..	20
Figure 2.4	Composition of Jordan's Primary Energy Sources (2011-2020).	21
Figure 2.5	Panoramic View within Abdali mega project / Amman.	23
Figure 2.6	Abdali Boulevard Project / Amman.	24
Figure 2.7	large using of Concrete as a high thermal mass material at new building of QAIA / Amman.	28
Figure 2.8	Several passive techniques for Building Facades in Abdali Project / Amman, as sample of passive solution for modern buildings in the city.	28
Figure 2.9	Alabdali office building competition.	29
Figure 2.10	Arab insurance office building/Amman.	29
Figure 2.11	Full glazed facades with means of shading devices at new building of QAIA / Amman..	29
Figure 2.12	Figure 2.12: DSF as shown in office buildings of The Abdali Boulevard in Amman.	31
Figure 2.13	DSF as shown in office buildings of The Abdali Boulevard in Amman, Night-time View.	31
Figure 2.14	Shots of Rotana Amman Hotel in Amman. Full glazed facades with shading elements are shown.	32
Figure 2.15	LIVING WALL "a Mixed-use Complex Building" in AMMAN/JORDAN.	33
Figure 2.16	HIGH JUDICIARY HOUSE; AMMAN/JORDAN.	34
Figure 2.17	FDouble Skin Façade Concept suggested for HIGH JUDICIARY HOUSE; AMMAN/JORDAN.	34
Figure 3.1	American classifications of DSF.	45
Figure 3.2	Various concepts of Airflow paths for DSF systems.	59
Figure 3.3	Detailed sketch for thermal interactions (thermodynamic) and airflow (fluid dynamic) in DSF cavity with indoor space.	62
Figure 3.4	Schematic sketch for main thermal interactions (thermodynamic) and airflow (fluid dynamic) in DSF cavity.	63
Figure 4.1	DSF with dividing plates and grilles.	86
Figure 4.2	Geometrical Parameters of DSF cavity-integrated devices.	94
Figure 4.3	Concept for Simulation the entire building equipped with DSF system.	103
Figure 4.4	Light shelf can reflect the light to deep points inside.	109
Figure 4.5	Improving the indoor daylight distribution using the light shelf.	109
Figure 4.6	A) Shading slats act as lighting devices. B & C) Different designs of Light Shelf.	110
Figure 4.7	Several designs of Okasolar Glass systems.	110
Figure 4.8	Okasolar Glass system; Type Retro O & Retro U.	110
Figure 4.9	multi-slat combination blind of up-down-movement type.	111

Figure 4.10	Mini-optical light shelf daylighting system “Patent no.06714352”.	112
Figure 4.11	Mini-optical light shelf daylighting system “US-6480336-B2”.	112
Figure 4.12	Genius Slat.	112
Figure 4.13	Venetian blind system with perforated concave slats incorporated into DSF’s cavity.	113
Figure 5.1	Components of the experimental rig.	128
Figure 5.2	Constructed models for both non-shaded (A) and 45° shaded (B) cavities.	132
Figure 5.3	Generated mesh for validation structure. Mesh-2.	136
Figure 5.4	Zoom-in shows mesh for outer glass structure in both cases: Mesh-1 and Mesh-2.	136
Figure 5.5	Original generated mesh for cavity inlet (Mesh-2) and after-adaptation mesh (Mesh-3).	136
Figure 5.6	Air velocity and changes for cavity’s med-height (1.1m) and it’s outlet with the three mesh scenarios.	137
Figure 5.7	FSurface temperatures and changes for different structures with the three mesh scenarios.	137
Figure 5.8	Surface temperatures and changes for different glass surfaces under the effect of domain’s external extension.	139
Figure 5.9	Air velocity and changes for cavity’s med-height (1.1m) and it’s outlet under the effect of domain’s external extension.	139
Figure 5.10	Computational domain for validation case showing the extension for external domain with width of three times the cavity width.	139
Figure 5.11	Surface temperatures and changes for different glass surfaces under the effect of various turbulence models.	140
Figure 5.12	Air velocity averages and relative changes for cavity’s med-height (1.1m) under the effect of various turbulence models.	141
Figure 5.13	Air velocity profiles at mid-height (1.1m) of cavity for difference scenarios of structure simplification.	143
Figure 5.14	Surface temperatures and changes for different glass surfaces under the effect of various turbulence models.	145
Figure 5.15	Air velocity profiles at mid-height (1.1m) of cavity with different surface emissivities for inner surface of the double glass.	146
Figure 5.16	Surface temperatures and changes for different simplification levels for validated structure.	147
Figure 5.17	Air velocity averages and relative changes for cavity’s med-height (1.1m) under the effect of various turbulence models.	148
Figure 5.18	Air velocity profiles at mid-height (1.1m) of cavity for difference scenarios of structure simplification.	149
Figure 5.19	Experimental and calculated air velocity averages and relative changes for cavity’s med-height (1.1m) with integrated shading devices having different inclination angles.	151
Figure 5.20	Air velocity profiles at mid-height (1.1m) of the cavity with integrated slats with different inclination angles.	152
Figure 5.21	Schematic for the C-shape cavity investigated by La Pica et al. (1993) and simulated by the Author. Width = 0.07m, 0.125m or 0.170m.	157
Figure 5.22	Contours of Velocity Magnitude (m/s) for investigated cavity with width of 0.125m and total heat flux of 296W/m ² .	157
Figure 5.23	Comparison between measured air velocity (La Pica et al., 1993) and calculated air velocity using fluent model.	157

Figure 5.24	Air Y-Velocity profiles at mid-height levels along widths of both 0.125-wide cavity of La Pica et al. (1993) and 0.55-wide cavity of Mei et al. (2007).	159
Figure 5.25	(A) schematic for the simple simulated cavity. (B) velocity Contours for same cavity with total heat flux = 100W/m ² .	160
Figure 5.26	Comparison for “Re” Reynolds Numbers calculated using Gan-2011’s general expressions and predicted based on CFD results.	163
Figure 5.27	Comparison for “Nu” Nusselt Numbers calculated using Gan-2011’s general expressions and predicted based on CFD results.	163
Figure 6.1	Comparison of published and calculated Beam solar irradiance on south-wall in Nice city of France; on 21/7; at 12pm.	166
Figure 6.2	Comparison of published and calculated Diffuse solar irradiance on south-wall in Nice city of France; on 21/7; at 12pm.	166
Figure 6.3	Comparison of solar irradiance values calculated by SPECTRAL2 model and Excel sheet model for summer design day of Amman, 6th July.	166
Figure 6.4	Generated mesh for initial studied structure; Mesh4.	174
Figure 6.5	Surface temperatures and changes for different elements with the three mesh scenarios.	175
Figure 6.6	Air velocity and changes for cavity’s mid-height (1.1m) and its outlet with the three mesh scenarios.	175
Figure 6.7	Air velocity and changes for cavity’s med-height (1.1m) and it’s outlet under the effect of domain’s external extension.	176
Figure 6.8	Surface temperatures and changes for different glass surfaces under the effect of domain’s external extension.	176
Figure 6.9	Computational domains for initial studied case showing the domain’s extensions.	176
Figure 6.10	Extended computational domain with integrated slats (5cm; 45°) for either method.	178
Figure 6.11	Schematic diagrams showing both methods for representing solar irradiance in the computational model; Equivalent Method (left) and Actual Method (Right).	179
Figure 6.12	Schematic diagram showing the relation between original (a) and equivalent (b) solar beam components.	180
Figure 6.13	Investigated Designs for integrated slats: (A) Design-1 and (B) Design-6; with cavities having Horizontal vents.	180
Figure 6.14	Airflow through cavity for both investigated scenarios with percentage of changes; with both diffuse and specular characteristics for glass and slats surfaces.	181
Figure 6.15	Glass’s surface temperatures for both investigated scenarios with percentage of changes; with diffuse characteristics for glass and slats surfaces.	182
Figure 6.16	Glass’s surface temperatures for both investigated scenarios with percentage of changes; with specular characteristics for glass and slats surfaces.	182
Figure 6.17	Airflow through cavity for both investigated scenarios with percentage of changes; with specular characteristics for glass and slats surfaces.	183
Figure 6.18	Glass’s surface temperatures for both investigated scenarios with percentage of changes; with design-1 slats and specular characteristics.	184
Figure 6.19	Glass’s surface temperatures for both investigated scenarios with percentage of changes; with design-6 slats and specular characteristics.	184
Figure 6.20	Contours of Air velocity magnitude (m/s) for the examined structure and its extended domain with both investigated methods; integrated slats were Design-6.	186

Figure 6.21	Contours of Static Temperatures (k) for the examined structure and its extended domain with both investigated methods; integrated slats were Design-6.	186
Figure 6.22	Old and New (Final) configurations for initial case; showing the amendments for both cavity configuration and extended computational domain.	189
Figure 7.1	A schematic for simple tested structure with flat integrated slats.	191
Figure 7.2	Changes of airflow rates with integrated slats size.	192
Figure 7.3	Changes in cavity's permeability for flow and calculated airflow changes.	192
Figure 7.4	Contours of velocity magnitude (m/s) for simple cavity with integrated slats having different sizes.	193
Figure 7.5	Average surface temperature increase for inner surfaces of outer glass (left) and inner glass (right) panes, with cavity/openings size.	194
Figure 7.6	Comparison for changes of both surfaces' temperatures and openness ratios.	195
Figure 7.7	Average surface temperature increase with integrated slats size.	195
Figure 7.8	contours of air temperature (k) for simple cavity with integrated slats having different sizes.	195
Figure 7.9	A) Airflow rates changes with slats angle. B) Changes in cavity's permeability for flow and calculated airflow changes.	197
Figure 7.10	contours of velocity magnitude (m/s) for simple cavity with integrated slats having different inclination angles.	198
Figure 7.11	Average surface temperature increase for inner surfaces of outer glass (left) and inner glass (right) panes, with integrated slats angle.	199
Figure 7.12	Airflow rates and relative changes for sub-cavities with integrated slats angle.	200
Figure 7.13	Comparison for changes of both surfaces' temperatures and openness ratios	200
Figure 7.14	Average surface temperature increase for integrated slats, with changes in their angle.	200
Figure 7.15	contours of temperature (k) for simple cavity with integrated slats having different sizes.	202
Figure 7.16	airflow rates changes with integrated slats' position.	203
Figure 7.17	Relationship between relative width of front sub-cavity and relative changes in total airflow rate.	203
Figure 7.18	contours of velocity magnitude (m/s) for simple cavity with integrated slats having different positions.	204
Figure 7.19	Average surface temperature increase for inner surfaces of outer glass (left) and inner glass (right) panes, with integrated slats position.	205
Figure 7.20	Average surface temperature increase for integrated slats, with slats position.	205
Figure 7.21	comparison between ratio of inner sub-cavity width to outer sub-cavity width, and relative changes in surface's temperatures; with slats position.	205
Figure 7.22	contours of temperature (k) for simple cavity with integrated slats having different positions.	207
Figure 7.23	airflow rates changes with surface emissivity of slat.	208
Figure 7.24	contours (and vectors) of velocity magnitude (m/s) for simple cavity with integrated slats having different surface emissivity.	208
Figure 7.25	Average surface temperature increase for inner surfaces of outer glass (left) and inner glass (right) panes, with integrated slats' surface emissivity.	209
Figure 7.26	Averages surface temperature increase for integrated slats, with surface emissivity.	210

Figure 7.27	comparison between ratio of inner sub-cavity width to outer sub-cavity width, and relative changes in surface's temperatures; with changes surface emissivity.	210
Figure 7.28	contours of temperature (k) for simple cavity with integrated slats having different surface emissivity.	211
Figure 7.29	Airflow rates through cavity with integrated slats having surface emissivity of 0.1 and various diffuse fraction.	212
Figure 7.30	contours (and vectors) of velocity magnitude (m/s) for simple cavity with integrated slats having different surface diffusivity.	212
Figure 7.31	Averages surface temperature increase for inner surfaces of outer glass (left) and inner glass (right) panes, with integrated slats having surface emissivity of 0.1 and various diffuse fractions.	213
Figure 7.32	contours of temperature (k) for simple cavity with integrated slats having different surface diffusivity.	213
Figure 7.33	Averages surface temperature increase for integrated slats having surface emissivity of 0.1 and various diffuse fractions.	214
Figure 7.34	Relative changes for all elements of the structure; with integrated slats having surface emissivity of 0.1 and various diffuse fractions.	214
Figure 7.35	Airflow rates through cavity with integrated slats having surface emissivity of 0.9 and diffuse fraction of 1, with various diffuse fraction for glass panes.	215
Figure 7.36	contours of velocity magnitude (m/s) for simple cavity with integrated slats having surface emissivity of 0.9 and diffuse fraction of 1, with various diffuse fraction for glass panes.	216
Figure 7.37	Averages surface temperature increase for inner surfaces of outer glass (left) and inner glass (right) panes, with integrated slats having surface emissivity of 0.9 and diffuse fractions of 1, with various diffuse fractions for glass.	217
Figure 7.38	Averages surface temperature increase for integrated slats having surface emissivity of 0.9 and diffuse fraction of 1, with various diffuse fractions for glass.	217
Figure 7.39	relative changes for all elements of the structure; with integrated slats having surface emissivity of 0.9 and diffuse fraction of 1, with various diffuse fractions for glass.	217
Figure 7.40	contours of static temperature (k) for simple cavity with integrated slats having different surface diffusivity.	218
Figure 8.1	A schematic for structure with horizontal vents and simple integrated slats.	221
Figure 8.2	A schematic for more advanced integrated element that could serve for both solar shading and light directing, which coded hereafter by "11".	221
Figure 8.3	A summary of geometrical characteristics of different investigated designs.	222
Figure 8.4	Schematic drawings for different designs of integrated shading elements. (Continued).	224
Figure 8.5	Schematic drawings for different designs of integrated shading elements. (Continued).	225
Figure 8.6	Schematic drawings for different designs of integrated shading elements.	226
Figure 8.7	(A) Airflow rates changes for simple cavity with horizontal inlets and different integrated slats. (B) Changes in cavity's flow permeability and calculated airflow changes.	227
Figure 8.8	contours (and vectors) of velocity magnitude (m/s) for simple cavity with horizontal vents and various designs of integrated slats.	230
Figure 8.9	contours (and vectors) of velocity magnitude (m/s) for simple cavity with horizontal vents and various designs of integrated slats; (Continued).	231

Figure 8.10	Averages of surface temperature increase for cavity's elements in summer with different tested designs of integrated slats; slats surfaces had emissivity of 0.9 and diffuse fraction of 1.	232
Figure 8.11	Contours of static temperature (k) for simple cavity with horizontal vents and various designs of integrated slats.	234
Figure 8.12	Contours of static temperature (k) for simple cavity with horizontal vents and various designs of integrated slats; (continued).	235
Figure 8.13	(A) Airflow rates changes for simple cavity with horizontal vents and selected designs for integrated slats. (B) Changes in cavity's overall opacity and calculated airflow changes.	237
Figure 8.14	Contours (and vectors) of velocity magnitude (m/s) for simple cavity with horizontal vents and selected designs of integrated slats; for both scenarios: EMS0.9-DIFF1 (slats' surface emissivity of 0.9 and diffuse fraction of 1) and EMS0.2-DIFF0 (slats' surface emissivity of 0.2 and diffuse fraction of 0)	239
Figure 8.15	Averages of surface temperature increase for cavity's elements in summer with different tested designs of integrated slats; slats surfaces had emissivity of 0.2 and diffuse fraction of 0.	240
Figure 8.16	Contours of temperature (k) for simple cavity with horizontal vents and selected designs of integrated slats; for both scenarios: EMS0.9-DIFF1 (slats' surface emissivity of 0.9 and diffuse fraction of 1) and EMS0.2-DIFF0 (slats' surface emissivity of 0.2 and diffuse fraction of 0).	242
Figure 8.17	(A) Airflow rates changes for simple cavity with horizontal vents and different designs of integrated slats. (B) Changes in cavity's overall opacity and calculated airflow changes.	243
Figure 8.18	Contours (and vectors) of velocity magnitude (m/s) for simple cavity with horizontal vents and selected designs of integrated slats; slats had surface emissivity of 0.2 and diffuse fraction of 0 (EMS0.2-DIFF0); results are for both winter and summer scenarios.	245
Figure 8.19	Comparison between summer and winter average surface temperature increase of cavity with different integrated slats; slats surfaces had emissivity of 0.2 and diffuse fraction of 0.	246
Figure 8.20	Contours of static temperature (k) for simple cavity with horizontal vents and selected designs of integrated slats; slats had surface emissivity of 0.2 and diffuse fraction of 0 (EMS0.2-DIFF0); results are for both winter and summer scenarios.	248
Figure 8.21	(A) Airflow rates changes for simple cavity with horizontal vents had size of either 0.1m or 0.5m; with different designs for integrated slats had emissivity of 0.9 and diffusivity of 1. (B) Changes in cavity's overall opacity and calculated airflow changes.	250
Figure 8.22	contours of velocity magnitude (m/s) for simple cavity with horizontal vents and selected designs of integrated slats; slats had surface emissivity of 0.9 and diffuse fraction of 1 (EMS0.9-DIFF1); results are for and summer scenario. Cavity's vents had sizes of 0.1m and 0.5m.	251
Figure 8.23	Comparison for average surface temperature increase of cavity with both vents' sizes (0.1m & 0.5m), with different integrated slats; slats surfaces had emissivity of 0.9 and diffuse fraction of 1.	252
Figure 8.24	Contours of static temperature (k) for simple cavity with horizontal vents and selected designs of integrated slats; slats had surface emissivity of 0.9 and diffuse fraction of 1 (EMS0.9-DIFF1); results are for and summer scenario. Cavity's vents had sizes of 0.1m and 0.5m.	254
Figure 8.25	(A) Airflow rates changes for simple cavity with horizontal vents, and different integrated slats with different installation positions; slats surfaces had	255

	emissivity of 0.9 and diffuse fraction of 1. (B) Changes in cavity's overall opacity and calculated airflow changes.	
Figure 8.26	Contours of velocity magnitude (m/s) for simple cavity with horizontal vents and selected designs of integrated slats; slats had surface emissivity of 0.9 and diffuse fraction of 1 (EMS0.9-DIFF1). Cavity's vents had size of 0.5m. Results are for three different positions for integrated slats and for summer scenario.	257
Figure 8.27	Comparison for average surface temperature increase of cavity with different integrated slats and different positions; slats surfaces had emissivity of 0.9 and diffuse fraction of 1.	258
Figure 8.28	Contours of temperature (k) for simple cavity with horizontal vents and selected designs of integrated slats; slats had surface emissivity of 0.9 and diffuse fraction of 1 (EMS0.9-DIFF1). Cavity's vents had size of 0.5m. Results are for three different positions for integrated slats and for summer scenario.	260
Figure 8.29	(A) Airflow rates changes for simple cavity with horizontal vents, and different integrated slats; slats had two different sizes (0.2m & 0.4m), surface emissivity of 0.9 and diffuse fraction of 1. (B) Changes in cavity's overall opacity and calculated airflow changes.	261
Figure 8.30	Contours of velocity magnitude (m/s) for simple cavity with horizontal vents and selected designs of integrated slats; slats had surface emissivity of 0.9 and diffuse fraction of 1 (EMS0.9-DIFF1). Slats were placed at middle of cavity (P5) and had two sizes: 40% and 80% of cavity width (0.5m). Cavity's vents had size of 0.5m. Results are for summer scenario.	263
Figure 8.31	Comparison for average surface temperature increase of cavity with different integrated slats; slats had two different sizes (0.2m & 0.4m), surface emissivity of 0.9 and diffuse fraction of 1.	264
Figure 8.32	Contours of temperature (k) for simple cavity with horizontal vents and selected designs of integrated slats; slats had surface emissivity of 0.9 and diffuse fraction of 1 (EMS0.9-DIFF1). Slats were placed at middle of cavity (P5) and had two sizes: 40% and 80% of cavity width (0.5m). Cavity's vents had size of 0.5m. Results are for summer scenario.	266
Figure 8.33	Airflow rates changes for simple cavity with horizontal vents and different height-to-width ratios (H/W), under Summer conditions. Integrated slats had width of 40% of cavity width (e.g. 0.12m for cavity width of 0.3m), surface emissivity of 0.9 and diffuse fraction of 1.	268
Figure 8.34	Contours of velocity magnitude (m/s) for simple cavity with horizontal vents and selected designs of integrated slats; slats had surface emissivity of 0.9 and diffuse fraction of 1 (EMS0.9-DIFF1). Slats were placed at middle of cavity (P5) and had size of 40% of cavity width (0.5m). Cavity's vents had size of 0.5m. Results are for summer scenario. Cavity's height was 4.0m and width changed from 0.1m to 0.5m.	271
Figure 8.35	Airflow rates changes for simple cavity with horizontal vents and different height-to-width ratios (H/W), under winter conditions. Integrated slats had width of 40% of cavity width (e.g. 0.12m for cavity width of 0.3m), surface emissivity of 0.9 and diffuse fraction of 1.	272
Figure 8.36	Contours of velocity magnitude (m/s) for simple cavity with horizontal vents and selected designs of integrated slats; slats had surface emissivity of 0.2 and diffuse fraction of 0 (EMS0.9-DIFF1). Slats were placed at middle of cavity (P5) and had size of 40% of cavity width (0.5m). Cavity's vents had size of 0.5m. Results are for winter scenario. Cavity's height was 4.0m and width changed from 0.1m to 0.5m.	273
Figure 8.37	Comparison for average surface temperature increase of cavity with different integrated slats and different height-to-width ratios (H/W), during Summer	274

	Conditions. Slats' had size of 0.2m, surface emissivity of 0.9 and diffuse fraction of 1.	
Figure 8.38	Contours of temperature (k) for simple cavity with horizontal vents and selected designs of integrated slats; slats had surface emissivity of 0.9 and diffuse fraction of 1 (EMS0.9-DIFF1). Slats were placed at middle of cavity (P5) and had size of 40% of cavity width (0.5m). Cavity's vents had size of 0.5m. Results are for summer scenario. Cavity's height was 4.0m and width changed from 0.1m to 0.5m.	278
Figure 8.39	Comparison for average surface temperature increase of cavity with different integrated slats and different height-to-width ratios (H/W), during winter conditions. Slats' had size of 0.2m, surface emissivity of 0.9 and diffuse fraction of 1. (A) Front glass_inner surface. (B) Back glass_inner surface. (C) Integrated slats' surface. All results and relative changes are plotted against H/W ratios.	279
Figure 8.40	Contours of temperature (k) for simple cavity with horizontal vents and selected designs of integrated slats; slats had surface emissivity of 0.2 and diffuse fraction of 0 (EMS0.9-DIFF1). Slats were placed at middle of cavity (P5) and had size of 40% of cavity width (0.5m). Cavity's vents had size of 0.5m. Results are for winter scenario. Cavity's height was 4.0m and width changed from 0.1m to 0.5m.	281
Figure 8.41	Relationship between the influence of design#1 and design#6 for both cavity's airflow rates and averages of temperature increase of surfaces, in summer.	282
Figure 8.42	Relationship between the influence of design#1 and design#11 for both cavity's airflow rates and averages of temperature increase of surfaces, in winter.	283
Figure 8.43	Airflow rates changes for simple cavity (with horizontal vents) with different height-to-width ratios (H/W) and glass transmittances ($t=0.5, 0.7$ & 0.9), under summer conditions. Integrated slats had width of 40% of cavity width (e.g. 0.12m for cavity width of 0.3m), surface emissivity of 0.9 and diffuse fraction of 1.	286
Figure 8.44	contours of velocity magnitude (m/s) for simple cavity with horizontal vents and selected designs of integrated slats; slats had surface emissivity of 0.9 and diffuse fraction of 1 (EMS0.9-DIFF1). Slats were placed at middle of cavity (P5) and had size of 40% of cavity width (0.5m). Cavity's vents had size of 0.5m. Different glass transmittance values were used, presented results are for $t=0.5$ & $t=0.9$. Cavity was with two different H/W ratios (8 & 40), and integrated with slats of design#1 and #11. Results are for summer scenario.	287
Figure 8.45	Comparison for average surface temperature increase of cavity (with horizontal vents) with different height-to-width ratios (H/W) and glass transmittances ($t=0.5, 0.7$ & 0.9), under summer conditions. Integrated slats had width of 40% of cavity width (e.g. 0.12m for cavity width of 0.3m), surface emissivity of 0.9 and diffuse fraction of 1.	290
Figure 8.46	Contours of temperature (k) for simple cavity with horizontal vents and selected designs of integrated slats; slats had surface emissivity of 0.9 and diffuse fraction of 1 (EMS0.9-DIFF1). Slats were placed at middle of cavity (P5) and had size of 40% of cavity width (0.5m). Cavity's vents had size of 0.5m. Different glass transmittance values were used, presented results are for $t=0.5$ & $t=0.9$. Cavity was with two different H/W ratios (8 & 40), and integrated with slats of design#1 and #11. Results are for summer scenario.	292
Figure 8.47	Relationships between the influence of design#1 and design#6 integrated slats, all in summer.	294
Figure 9.1	airflow rates and changes for both office and entire structure, with changes in cavity/openings size.	299

Figure 9.2	Indoor temperature at height of 1.6m for different cavity/openings size.	299
Figure 9.3	surface temperature increase averages for inner surfaces of outer glass (left) and inner glass (right) panes, with changes in cavity/openings size.	299
Figure 9.4	airflow rates and changes for both cavity and office in winter, with changes in cavity/openings size. Values for 0.35 and 0.45 were calculated from revealed polynomial relationship.	301
Figure 9.5	Indoor temperature at height of 1.6m for different cavity/openings size in winter.	302
Figure 9.6	surface temperature increase averages for inner surfaces of outer glass (left) And inner glass (right) panes, with changes in cavity/openings size; in winter.	303
Figure 9.7	airflow rates and changes for both offices an entire structure, with various glass transmissivities.	304
Figure 9.8	Indoor temperature at height of 1.6m for various glass transmissivities.	304
Figure 9.9	Variation in surface temperature increase (surface temperature-outdoor temperature) averages for inner surfaces of outer glass (left) and inner glass (right) panes, in summer, due to changing their transmittance.	305
Figure 9.11	Airflow rates and changes for both cavity and offices with various glass transmissivities; in winter.	307
Figure 9.11	indoor temperature at height of 1.6m for various glass transmissivities.	307
Figure 9.12	Variation in surface temperature increase (surface temperature-outdoor temperature) averages for inner surfaces of outer glass (left) and inner glass (right) panes, in winter, due to changing their transmittance.	308
Figure 9.13	Airflow rates and changes for both cavity and office in winter, due to the effect of changing outer opening size at range: 0.05-0.20m.	310
Figure 9.14	Indoor temperature at height of 1.6m with different outer opening sizes, in winter.	310
Figure 9.15	Surface temperature increase averages for inner surfaces of outer glass (left) and inner glass (right), under the effect of adjusting external openings' size, in winter.	312
Figure 9.16	Airflow rates and changes for both office and entire structure, with varied cavity width and fixed opening size to 0.4m.	313
Figure 9.17	Indoor temperature at height of 1.6m, with varied cavity width and fixed opening size to 0.4m.	313
Figure 9.18	Variation in surface temperature increase (surface temperature-outdoor temperature) averages for inner surface of outer glass (left) and inner glass (right) panes, with changed cavity width and fixed opening size.	314
Figure 9.19	Airflow rates and changes for both office and entire structure, with varied cavity width and fixed opening size to 0.1m and 0.2m for outer and inner, respectively.	315
Figure 9.20	Contours of velocity magnitude (m/s) for structure with different cavity sizes (0.2-1.0), where openings sizes fixed to its optimum.	317
Figure 9.21	indoor temperature at height of 1.6m, with varied cavity width and fixed opening size to 0.4m.	318
Figure 9.22	variation in surface temperature increase (surface temperature-outdoor temperature) averages for inner surface of outer glass (left) and inner glass (right) panes, with changed cavity width and fixed opening size.	319
Figure 10.1	airflow rates and changes for both office and entire structure, with changes in size for 45 degrees slats.	322
Figure 10.2	airflow rates and changes for both office and entire structure, with changes in size for 60 degrees slats.	322

Figure 10.3	contours of velocity magnitude (m/s) at both inlets and outlets of each of 10% 30% and 50% cases; where size, offset and arrangements for 45 degrees integrated slats are shown.	323
Figure 10.4	Indoor temperature at height of 1.6m for integrated slats with different sizes and angle of 45 degrees.	324
Figure 10.5	increase in indoor average temperature wit relative changes at height of 1.6m for integrated slats with different sizes and angle of 45 degrees.	324
Figure 10.6	Indoor temperature at height of 1.6m for integrated slats with different sizes and angle of 60 degrees.	324
Figure 10.7	increase in indoor average temperature wit relative changes at height of 1.6m for integrated slats with different sizes and angle of 60 degrees.	324
Figure 10.8	surface temperature averages for inner surfaces of outer glass (left) and inner glass (right) panes, with changes in cavity/openings size. Inclination angle 45 degrees.	325
Figure 10.9	surface temperature averages for inner surfaces of outer glass (left) and inner glass (right) panes, with changes in cavity/openings size. Inclination angle 60 degrees.	325
Figure 10.10	airflow rates and changes for both office and entire structure, with changes in size for 60 degrees slats.	327
Figure 10.11	contours of velocity magnitude (m/s) showing variations in both flow rates and distribution inside cavity and attached office; under the effect of adjusting slats' inclination angles.	329
Figure 10.12	Indoor temperature at height of 1.6m with the effect of adjusting slats' inclination angles during winter.	330
Figure 10.13	increase in indoor average temperature with relative changes at height of 1.6m with the effect of with adjusting slats' inclination angles during winter.	330
Figure 10.14	surface temperature averages for inner surfaces of outer glass (left) and inner glass (right) panes, with the effect of adjusting slats' inclination angles during winter.	330
Figure 10.15	airflow rates and changes for both office and entire structure, with changes in integrated slats emissivity.	332
Figure 10.16	contours of velocity magnitude (m/s) for the cavity integrated with slats of different surface emissivities.	333
Figure 10.17	Indoor temperature at height of 1.6m for integrated slats with different surface emissivities for slats.	334
Figure 10.18	increase in indoor average temperature wit relative changes at height of 1.6m for integrated slats with different surface emissivities.	334
Figure 10.19	Fcontours of static temperature (k) for the cavity integrated with studied slats at different positions.	335
Figure 10.20	surface temperature averages for inner surfaces of outer glass (left) and inner glass (right) panes under the effect of varied slats surface emissivity; and relative changes in reference to no-slats case.	335
Figure 10.21	Temperature averages for outer glass's inner surface, inner glass's inner surface and slats' surface under the effect of varied slats surface emissivities. Relative changes are in reference to no-slats case for glass surfaces; and in reference to emissivity of 0.2 for slats surface; all for summer conditions.	336
Figure 10.22	airflow rates and changes for both office and entire structure, with changes in integrated slats emissivity.	338
Figure 10.23	contours of velocity magnitude (m/s) for the office, under the effect of surface emissivity for cavity integrated slats.	339
Figure 10.24	Indoor temperature at height of 1.6m for integrated slats with different surface emissivities during winter.	339

Figure 10.25	increase in indoor average temperature with relative changes at height of 1.6m for integrated slats with different surface emissivities during winter.	339
Figure 10.26	contours of static temperature (K) for the office, under the effect of surface emissivity for cavity integrated slats.	340
Figure 10.27	surface temperature averages for inner surfaces of outer glass (left) and inner glass (right) panes under the effect of varied slats surface emissivity; and relative changes in reference to no-slats case.	341
Figure 10.28	Temperature averages for outer glass's inner surface, inner glass's inner surface and slats' surface under the effect of varied slats surface emissivities. Relative changes are in reference to no-slats case for glass surfaces; and in reference to emissivity of 0.2 for slats surface; all for winter conditions.	341
Figure 10.29	airflow rates and changes for both office and entire structure, with changes in position of integrated slats. Left: All changes in reference to no-slats case. Right: Results' changes in reference to their minimum values.	343
Figure 10.30	contours of velocity magnitude (m/s) for the cavity integrated with studied slats at different positions.	344
Figure 10.31	Indoor temperature at height of 1.6m for integrated slats with different sizes and angle of 45 degrees.	345
Figure 10.32	increase in indoor average temperature with relative changes at height of 1.6m for integrated slats with different sizes and angle of 45 degrees.	345
Figure 10.33	contours of static temperature (K) for the cavity integrated with studied slats at different positions.	346
Figure 10.34	surface temperature averages for inner surfaces of outer glass (left) and inner glass (right) panes, with varied slats positions; and relative changes in reference to no-slats case.	347
Figure 10.35	Temperature averages for outer glass's inner surface, inner glass's inner surface and slats' surface under the effect of changing integrated slats position. Relative changes are in reference to no-slats case for glass surfaces; and in reference to emissivity of 0.2 for slats surface; all for summer conditions.	347
Figure 10.36	airflow rates and changes for both office and entire structure, with changes in position for integrated slats. Left: All changes in reference to no-slats case. Right: Results' changes in reference to their minimum values.	348
Figure 10.37	contours of velocity magnitude (m/s) for the cavity integrated with studied slats at different positions., during winter.	350
Figure 10.38	Indoor temperature at height of 1.6m with integrated slats having different positions.	351
Figure 10.39	Increase in indoor average temperature at height of 1.6m and relative changes, with integrated slats having different positions.	351
Figure 10.40	contours of static temperature (K) for the cavity integrated with studied slats at different positions in winter.	352
Figure 10.41	Surface temperature averages for inner surfaces of outer glass (left) and inner glass (right) panes, with varied slats positions; and relative changes in reference to no-slats case.	353
Figure 10.42	Temperature averages for outer glass's inner surface, inner glass's inner surface and slats' surface under the effect of changing integrated slats position. Relative changes are in reference to no-slats case for glass surfaces; and in reference to emissivity of 0.2 for slats surface; all for winter conditions.	353
Figure 11.1	Airflow rates and changes for office, cavity and entire structure for both scenarios: with and without internal heat gains.	356
Figure 11.2	Contours of velocity magnitude (m/s) for the office and attached cavity integrated with slats, for two scenarios: with and without internal heat gains.	356

Figure 11.3	Indoor temperature at height of 1.6m for studied scenarios: with and without internal heat gains.	357
Figure 11.4	Increase in indoor average temperature at height of 1.6m with relative changes for studied scenarios: with and without internal heat gains.	357
Figure 11.5	Contours of static temperature (k) for the office and attached cavity integrated with slats, for two scenarios: with and without internal heat gains.	357
Figure 11.6	Surface temperature averages for inner surfaces of outer glass (left) and inner glass (right) panes, with varied slats positions; and relative changes in reference to no-slats case.	358
Figure 11.7	Airflow rates and changes for office, cavity and entire structure for both scenarios: with and without internal heat gains. Left: All changes in reference to “no int. gain” case. Right: Results’ changes in reference to their minimum values.	360
Figure 11.8	Contours of velocity magnitude (m/s) for the office and attached cavity integrated with slats, for different scenarios.	361
Figure 11.9	Indoor temperature at height of 1.6m for studied scenarios: with and without internal heat gains.	362
Figure 11.10	Increase in indoor average temperature and relative changes at various levels and depths; for adjusted external vents.	363
Figure 11.11	Temperature averages for different inner surfaces of space with relative changes as a result of adjusting external vent size.	365
Figure 11.12	Averages for indoor surfaces temperature, air temperature and operating temperature with relative changes as a result of adjusting external vent size.	365
Figure 12.1	Schematics for the system showing proposals for artificial cooling vents.	368
Figure 12.2	airflow rates and changes for office, cavity and entire structure various proposals for artificial cooling vents.	369
Figure 12.3	contours of velocity magnitude (m/s) for the office and attached cavity integrated with slats, for investigated cases regarding office’s air supply vents.	369
Figure 12.4	Indoor temperature at height of 1.6m for different proposals for indoor air supply vents.	370
Figure 12.5	contours of static temperature (k) for the office and attached cavity integrated with slats for investigated cases regarding office’s air supply vents.	371
Figure 12.6	Indoor temperature averages and relative changes at various levels and depths; for investigated cases regarding office’s air supply vents.	371
Figure 12.7	Temperature averages for different inner surfaces of space with relative changes for investigated cases regarding office’s air supply vents.	372
Figure 12.8	Averages for indoor surfaces temperature, air temperature and operating temperature with relative changes for investigated cases regarding office’s air supply vents.	372
Figure 12.9	Tested proposals for the arrangements of exhaust vents at front facades’ layers.	373
Figure 12.10	airflow rates and changes for office and entire structure with tested proposals for the arrangements of exhaust vents at front facades’ layers.	374
Figure 12.11	contours of velocity magnitude (m/s) for the office and attached cavity; with tested proposals for the arrangements of exhaust vents at front facades’ layers.	375
Figure 12.12	Indoor temperature at height of 1.6m for tested proposals for the arrangements of exhaust vents at front facades’ layers.	375
Figure 12.13	contours of static temperature (k) for the office and attached cavity; with tested proposals for the arrangements of exhaust vents at front facades’ layers.	376

Figure 12.14	Indoor temperature averages and relative changes at various levels and depths; for tested proposals for the arrangements of exhaust vents at front facades' layers.	377
Figure 12.15	Temperature averages for different inner surfaces of space with relative changes for investigated cases regarding office's air supply vents.	377
Figure 12.16	Averages for indoor surfaces temperature, air temperature and operating temperature with relative changes for investigated cases regarding office's air supply vents.	377
Figure 12.17	contours of velocity magnitude (m/s) for the office and attached cavity; with different temperature for cooling air.	379
Figure 12.18	Indoor temperature at height of 1.6m for different temperatures of inlet air.	379
Figure 12.19	contours of static temperature (k) for the office and attached cavity; for different temperatures of inlet air. Scale range: 18-57°C.	381
Figure 12.20	contours of static temperature (k) for the office and attached cavity; for different temperatures of inlet air. Scale Range: 24-28.5°C.	381
Figure 12.21	Indoor temperature averages and relative changes at various levels and depths for different temperatures of inlet air.	382
Figure 12.22	Temperature averages for different inner surfaces of space with relative changes for investigated cases regarding office's air supply vents.	384
Figure 12.23	Averages for indoor surfaces temperature, air temperature and operating temperature with relative changes for investigated cases regarding office's air supply vents.	384
Figure 12.24	Tested proposal for placing cooling air vents at ceiling (B) instead of back-wall (A).	385
Figure 12.25	contours of velocity magnitude (m/s) for the office and attached cavity, where cooling air vents located at ceiling; with different temperature.	386
Figure 12.26	Indoor temperature at height of 1.6m for different temperatures of inlet air.	386
Figure 12.27	contours of static temperature (k) for the office and attached cavity; where cooling air vents located at ceiling; with different temperature. Scale Range: 18-57°C.	387
Figure 12.28	contours of static temperature (k) for the office and attached cavity; where cooling air vents located at ceiling; with different temperature. Scale range: 24-28.5°C.	387
Figure 12.29	Indoor temperature averages and relative changes at various levels and depths for different temperatures of inlet air.	388
Figure 12.30	Temperature averages for different inner surfaces of space with relative changes for investigated cases regarding office's air supply vents.	389
Figure 12.31	Averages for indoor surfaces temperature, air temperature and operating temperature with relative changes for investigated cases regarding office's air supply vents.	389
Figure 12.32	Comparison between Back-wall vent and Ceiling-vents designs. Structures' schematic (A), Contours of Velocity magnitude (B) and Static temperature (C).	390
Figure 13.1	contours of velocity magnitude (m/s) for the office and attached cavity integrated with slats.	394
Figure 13.2	Indoor Air temperature at height of 1.6m with external vent size of 0.1m and internal size of 0.2m.	394
Figure 13.3	Indoor average temperature and relative changes at various levels (Left) and depths (Right) with external vents size of 0.1m.	395
Figure 13.4	Temperature averages for different inner surfaces of space with relative changes during winter.	396
Figure 13.5	contours of velocity magnitude (m/s) for the office and attached cavity served with artificial cooling with 24°C during summer conditions.	397

Figure 13.6	Indoor temperature at height of 1.6m for different temperatures of inlet air.	398
Figure 13.7	Indoor average temperature and relative changes at various levels (Left) and depths (Right) with external vents size of 0.1m.	398
Figure 13.8	contours of static temperature (k) for the office and attached cavity integrated with slats. Temperature scale: A) 296°C - 311°C. B) 297.15°C - 301.65 “thermal comfort”.	399
Figure 13.9	Temperature averages for different inner surfaces of space with relative changes during summer.	400

NOMENCLATURE

$A_{I,S}$	Solar Absorption by Inner Surface
$A_{O,S}$	Solar Absorption by Outer Surface
C_d	Discharge Coefficient
$^{\circ}\text{C}$	Celsius Degree ($^{\circ}\text{C}$)
C_p	Specific Heat (J/kg.K)
D_F	Diffuse Fraction of Surface
g	The gravitational acceleration (m/s^2)
g_d	Thickness of Double Pane Glass (m)
g_s	Thickness of Single Pane Glass (m)
h_c	Convective Heat Transfer Coefficient ($\text{W/m}^2.\text{K}$)
H_i	Specific Enthalpy (J/kg)
I	Incident Radiation (W/m^2)
k	Thermal Conductivity (W/m.K)
k	Turbulent Kinetic Energy (M^2/S^2)
L_T	Light Transmittance
Nu	Nusselt Number (Dimensionless Number)
P	Pressure (Pascal Pa)
Q	Flow Rate (m^3/s)
q_{sun}	Incident Solar Heat Radiation (W/m^2)
q_{avg}	Average Heat Flux (W/m^2)
$q_{radiation}$	Radiative Heat Flux (W/m^2)
$q_{convection}$	Convective Heat Flux (W/m^2)
Ra	Rayleigh Number (Dimensionless Number)
Re	Reynolds Number (Dimensionless Number)
R_s	Reflected Solar Radiations (W/m^2)
R^2	R-Squared
T_s	Transmitted Solar Radiations (W/m^2)
t_{air}, T_{air}	Air Temperature ($^{\circ}\text{C}$, $^{\circ}\text{K}$)
ΔT_{Front}	Difference in Surface Temperature of Front Glass Pane ($^{\circ}\text{C}$, $^{\circ}\text{K}$)
ΔT_{Back}	Difference in Surface Temperature of Back Glass Pane ($^{\circ}\text{C}$, $^{\circ}\text{K}$)
ΔT_{Slats}	Difference in Surface Temperature of Slats ($^{\circ}\text{C}$, $^{\circ}\text{K}$)
T_{inlet}	Inlet Air Temperature ($^{\circ}\text{C}$, $^{\circ}\text{K}$)
V, U	Air Velocity (m/s)
$U - \text{value}$	Thermal Transmittance ($\text{W/m}^2.\text{K}$)
w_{inn}, w_{out}	Width of Inner and Outer Sub-Cavity, respectively, (m)
w	Width of Slats (m)

GREEK SYMBOLS

α	Absorption Coefficient (1/m)
β	Thermal Expansion Coefficient (1/K)
δ	Lateral Distance Between Slats And Glass (m)
ε	Turbulent Dissipation Rate (J/kg.s)
η_0	Constant
θ	Inclination Angle (degrees)
λ	Solar Wavelength (μm)
μ_e	Effective Viscosity
μ	Laminar Dynamic Viscosity (kg/m.s)
ν	Air kinematic viscosity (m^2/s)
ρ	Density (kg/m^3)

ABBREVIATIONS

1D, 2D, 3D	One-, Two-, Three-Dimensional
AC	Artificial Cooling
ANSYS	Computer-Aided Engineering Software Developer
BC	Boundary Condition
BDTRF	Bi-Directional Transmittance and Reflectance Function
BES	Building Energy Simulation Tool
BESTEST	Building Energy Simulation Test
CFD	Computational Fluid Dynamics
CFX	CFD Solver
CGI	CIE Glare Index
CIBSE	The Chartered Institution of Building Services Engineers
COMIS	Multizone Air Infiltration And Ventilation Simulation
CPU	Central Processing Unit
Design-Builder	Building energy simulation Software
DH	Dehumidification
DO	Discrete Ordinates (for Radiation Models)
DSF	Double Skin Facade
DGI	Daylight Glare Index
EC	Evaporative Cooling
EnergyPlus	Building Energy Simulation Software
EPSRC	UK's Engineering & Physics Sciences Research Council
etc.	et cetera
FLUENT	CFD Solver
FVM	Finite Volume method
GDP	Gross Domestic Product
GLAD	Physical Optics And Laser Analysis Software
G-value	Total Energy Transmittance for Window Unit

HPC	High Performance Computing
HELIOS	HELiOS Building Efficiency Software
HVAC	Heating, Ventilation and Air Conditioning
INV	High Inertia And Night Ventilation
N-S	Navier-stokes equations
PHONICES- FLAIR	CFD Solver
PCM	Phase change material
PV	Photovoltaics
QAIA	Queen Alia International Airport
RADIANCE	Simulation Tool for Daylighting Systems
RANS	Reynolds-Averaging Navier-Stokes
R&D	Research and Development
RNG	Re-Normalisation Group methods
RTE	Radiative Transfer Equation
SC	Solar Shading Coefficient
SHGC	Solar Heat Gains Coefficient (SHGC)
SPECTRAL2	Bird's Simple Solar Spectral Model - NREL
SST	shear stress transport formulation
TAS	Thermal Analysis Simulation Software
TRNSYS	TRaNsient System Simulation program
UAE	United Arab Of Emirates
VIE	Vertical Illuminance at the Eye
WINDOW 7.3	Optical Analysis Software
WWR	Window-to-Wall Ratio

CHAPTER 1 INTRODUCTION

1.1 Overview:

In addition to its attractive architectural appearance, a Double Skin Facade (DSF) system has many advantages such as improving thermal & optical comfort and natural ventilation. Hence, it is considered as a promising passive technology for building facades. Although it was basically introduced to buildings in cold climates, its applications are widely being transferred to hot climatic regions in recent years. Several studies have been conducted on the performance of DSF in hot conditions. To some extent, these works showed a promising and acceptable performance of the system if it is designed and operated properly (Hamza, 2004). At the same time, there is still a clear debate in particular regarding its thermal effectiveness during summer in hot regions whether it could work as a passive cooling strategy.

On the other hand, Jordan faces serious shortages in energy resources. At the same time, significant growth in constructional works is noticed in Amman over the past few years. This includes construction of new buildings with newly imported systems (e.g. DSF), which initially aim to work as passive techniques. The concept of DSF systems has been introduced to at least three buildings in Amman city, Jordan. Two of them have been built (Foster+Partners, 2007; NES, 2008) while the third was proposed through a competition (Architects, 2011). At the same time, there are no noticeable studies on DSF's performance in Jordan while the system has already been transferred to the state. Thus, it is highly important to investigate the

performance of such system there before it is widely being spread due to its advantages as a promising passive technology. Generally, the system is expected to perform well in winter but its performance is not guaranteed in hot summer of Amman. The city of Amman usually experiences a hot-dry summer with high solar radiation about 5kW.h/m^2 per day compared to cold winter (Bani-Domi, 2005; Al-Salaymeh et al., 2010).

Referring to the relevant literature of similar climates, both DSF's cavity and indoor space are highly likely to experience summer overheating due to large glazed areas exposed to excessive direct solar gains coincided with high ambient temperatures. In addition, visual glare in areas next to the façade is also common. However, enhancing DSF with cavity-integrated shading elements and proper ventilation mechanisms could be a good solution to protect occupants from summer's direct solar gains and extract cavity-trapped heat to outside while shading elements are being protected inside the cavity. In addition, it would enhance indoor daylighting and control glare.

At the same time, the presence of the shading devices in the cavity could influence both airflow and thermal operation of the system. This influence is usually determined by a combination of several factors that include design parameters of both DSF system and integrated shading devices (i.e. size, inclination angle, etc.). Whereas many previous works have already investigated the role of several design parameters of these devices on thermal performance of both DSF and occupied spaces, no significant works are noticed regarding the influence of the exact shape (i.e. cross-section profile) of these devices on such performance. In particular, its influence on solar

shading (thermal aspect), airflow (thermal & ventilation aspects), daylighting (optical aspect) and most importantly all of them together as expected role for a multifunctional cavity-integrated device for DSF. Furthermore, it is still required to optimize the configuration of DSF and integrated shading elements as either type of building or its location changes.

Hence, it is important to research the possibility of considering DSF system as a passive solution for Office buildings in Amman. This required an intensive investigation of the design parameters and configuration of such system under the climate of Amman. Next, integrated shading elements were also investigated as an auxiliary technique to improve the performance of DSF. Among other parameters, more attention was given to the role attributed to the shape of these elements. Consequently, the function of a potential combination of several parameters was further studied.

Generally speaking, these efforts are part of a long-term plan for the development of a new multifunctional device, which can effectively and comprehensively achieve different aspects of comfort required by occupants and meet standards of passive design. In other words, it aims to enhance the overall performance of facades' elements, which includes improving thermal & visual comfort for occupants, reducing energy consumption for air-conditioning & lighting and reducing the CO₂ impact on the environment. In addition, guidelines and recommendations for design and operation of such systems are expected. This research focuses on a detailed insight into the performance of DSF during both summer and winter times of Amman, and the role of cavity-integrated shading elements. Moreover, a good platform has

been established for continuing future research on DSF system (with cavity-integrated elements) with potential improvement of its overall performance.

A detailed computational model for fluid flow and associated heat transfer has been developed based on the Fluent code of ANSYS package. The model has been validated. To meet the objective of the study, a new method "ACTUAL METHOD" for solar source representation has been developed. The work was carried out through several stages where the outcome of each stage formed the foundation for next stage. Two main parametric studies were conducted on a simple cavity with different openings' configurations and set of design parameters regarding the integrated slats. Then, critical design and operation parameters were determined. Finally, a DSF system was investigated for integration into a one-storey office building located in Amman. Simulations were done for design days of summer and winter. Consequently, some recommendations were derived concerning the configuration of the system, its components, and solar characteristics. Moreover, the influence of integrated slats on airflow and thermal performance of the system and indoor was investigated and recommendations were set out. Generally, the study showed that DSF would be able to provide the thermal comfort of the office during winter. In summer, artificial cooling is still required even though DSF is expected to reduce the cooling demands.

Finally, general conclusions were drawn up, covering the contributions of the study to the body of knowledge, key outcomes and recommendations, research limitations and future work plans.

1.2 Aim and Objectives:

1.2.1 Aim:

This work aims to investigate and optimize both ventilation and thermal performance of Double Skin Façade (DSF) of Office buildings in hot-dry summer and cold winter regions. More specifically, investigate the role of integrated shading elements on the performance of DSF.

1.2.2 Objectives:

This work is planned to achieve the following objectives:

1. To develop a detailed computational model for fluid and associated heat transfer to simulate both airflow and thermal performance of DSF system.
2. To study the performance of non-shaded DSF applied to offices and determine vital parameters that influence its operation.
3. To study the influence of cavity's integrated shading devices on the system performance, and determine critical parameters/characteristics of these devices and how the interaction of different parameters/characteristics could influence the device's role.
4. To study the importance of geometrical shape (cross-sectional profile) of devices to its role in system's performance (i.e. thermal and flow).
5. To optimize the installation of integrated devices into DSF's cavity to ensure its better operation (enhance cavity's ventilation so minimize

its summer overheating, and maintain good solar shading to indoor thus help in reducing cooling demands).

6. To investigate and optimize the system's performance in heating seasons (winter) thus, reaching a dual mode of operation (cooling and heating).
7. To develop design guidelines and recommendations for applying DSF in Amman/Jordan as well as regions with similar climates. In addition, introducing DSF as an effective sustainable solution that can help to reduce energy bills of the buildings and protecting the environment by minimizing Carbon footprint (CO₂).

1.3 Framework of the Research:

The structure of the whole research was based on pre-designed frameworks, Figure 1.1. In addition, these frameworks were used to set out final chapters of the thesis as discussed and summarized in Table 1.1. Generally, thesis chapters present significant findings of the research along with relevant literature and adopted methods. The following summary draws what it entails:

A) Conceptual Framework "Rationality of work":

It clarifies the concept behind this research, its motivations and set out the aim & objectives. This is drawn in this thesis as:

- CHAPTER 1: INTRODUCTION.

B) Theoretical Framework "Background & Literature":

It identifies the case study (Amman, Jordan) and highlights its needs, problems and possible solutions. In addition, it investigates the background

of the research problem, suggested solution (DSF system) and current challenges (e.g. overheating) with this solution. Most importantly, it focuses on the relevant literature of the proposed system: DSF with multifunctional integrated shading devices. This is drawn in this thesis as:

- **CHAPTER 2: BACKGROUND OF CASE STUDY: CITY OF AMMAN IN JORDAN:** *It shows the local climate of Amman, energy status, growth of built environment and rationality of research there.*
- **CHAPTER 3: BACKGROUND OF DOUBLE SKIN FAÇADE (DSF):** *It reviews the general principles and basics of DSF system. Also, it shows the most relevant knowledge regarding DSF system as a proposed sustainable solution for energy-efficient facades.*
- **CHAPTER 4: LITERATURE REVIEW ON DOUBLE SKIN FACADES (DSFs):** *It presents up-to-date literature in the scope of researching and optimizing DSF within hot climates, and mainly using integrated shading devices. Literature deals with thermal & optical optimization, computer modelling, and state of the art regarding the available products of shading and daylighting elements.*

C) Operational Framework "Research Methodology & Validation":

This part concerns with the core work and shows a detailed plan for how the research was conducted through different stages. Within this thesis, this is presented as:

- **CHAPTER 5: THEORETICAL BACKGROUND AND METHOD VALIDATION:** *It shows the research problem and proposed solution method. Then, it provides necessary validation works for the proposed solution method.*
- **CHAPTER 6: MODEL SET-UP AND DEVELOPMENT:** *It summaries boundary conditions of the problem, and draws the solution method's structure and settings. Then, it shows preliminary studies within the*

research. After which, it demonstrates the new method for solar radiation representation for the purpose of accurate computational simulation. Finally, it summarizes both amendments and simplifications have been made to the initial configuration.

D) Analytical Framework "Results, Analysis & Conclusions":

It concerns with presenting research outcomes, interpreting outstanding results and drawing the net conclusions. Herein, this important part of work is shown through the following chapters:

- **CHAPTER 7: GENERAL PARAMETRIC STUDY ON SIMPLE CAVITY WITH SIMPLE INTEGRATED SLATS:** *It shows results of a series of parametric studies on simple cavity with vertical vents and integrated with simple flat shading slats. More parameters related to either cavity structure or characteristics of integrated slats were investigated.*
- **CHAPTER 8: PARAMETRIC STUDY ON SIMPLE CAVITY WITH HORIZONTAL VENTS AND VARIOUS INTEGRATED SLATS:** *It shows results of a series of parametric studies on simple cavity with horizontal vents and integrated with shading elements of various designs (including daylighting designs). It mainly aimed to differentiate the performance (thermal and airflow) of these designs. In addition, it aimed to investigate the influence of different design parameters on the role of the detailed design of these elements.*
- **CHAPTER 9: DOUBLE SKIN FAÇADE (DSF) WITHOUT SHADING DEVICES:** *It presents results of investigating the performance of a full model for office space with DSF system but without integrated shading elements.*
- **CHAPTER 10: DOUBLE SKIN FAÇADE (DSF) INTEGRATED WITH SLATS:** *Following the previous chapter, this chapter shows results of investigating the performance of the full model (of office space and DFS system) with integrated shading devices.*

- **CHAPTER 11: EFFECT OF INTERNAL HEAT GAINS:** This chapter shows the effect of including, in simulation, internal heat gains on the performance of the full model.
- **CHAPTER 12: SUMMER ARTIFICIAL COOLING:** This chapter presents the needs and requirements of providing summer artificial cooling to the designated office space (with DSF system).
- **CHAPTER 13: OPTIMIZATION OF THE SYSTEM (SUMMARY AND APPLICATION):** It shows the final optimization for the proposed DSF system in Amman, including integrated shading elements. Also, it summarizes its performance under both summer and winter conditions.
- **CHAPTER 14: MAIN CONCLUSIONS:** It draws the conclusions of the entire research including the rationality of research, modelling methods, significant outcomes, gained contributions and future research opportunities.

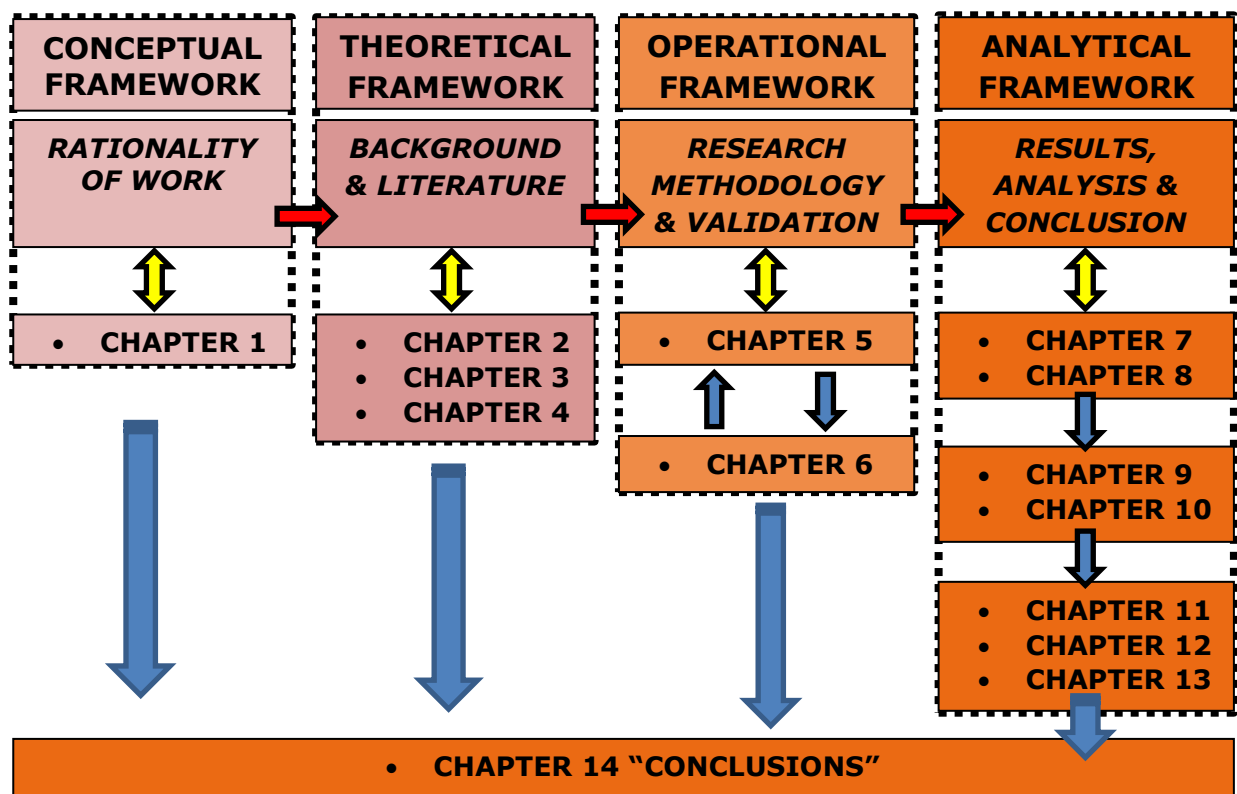


Figure 1.1: A Flowchart shows the framework of the research with generated chapters of the thesis.

Table 1.1: Detailed description for the research framework, conducted tasks, and final chapters of the thesis.

FRAME WORK	TASKS		CHAPTERS		
	MAIN TASKS	SUB-TASKS	#	KEY WORDS	TITLE
CONCEPTUAL FRAMEWORK	RESEARCH MOTIVATIONS		1	CLIMATE, ENERGY, BUILDINGS, PASSIVE DESIGN, RESEARCH, AMMAN.	INTRODUCTION
	AIM & OBJECTIVES				
	WORK RATIONALITY				
THEORETICAL FRAMEWORK	BACKG- ROUND	THE CITY OF AMMAN, JORDAN	2	OFFICES, OVERHEATING, ENERGY, AMMAN, PASSIVE DESIGN, DSF.	BACKGROUND OF CASE STUDY: CITY OF AMMAN IN JORDAN
		DSF: PRINCIPLES, APPLICATIONS & OBSTACLES.	3	DFS, SHADING ELEMENTS, OVERHEATING, CAVITY, VENTILATION.	BACKGROUND OF DOUBLE SKIN FACADE (DSF)
	LITERA- TURE	DSF PERFORMANCE	4	DFS, SHADING ELEMENTS, OVERHEATING.	LITERATURE REVIEW ON DOUBLE SKIN FACADES (DSF)
		DSF SHADING STRATEGIES			
		CAVITY-INTEGRATED ELEMENTS			
		EXAMINATION TECHNIQUES AND MODELLING METHODS			

Cont'd on next page

Cont'd

OPERATIONAL FRAMEWORK	RESEARCH METHODOLO -GY AND VALIDATION	PROPOSED METHOD AND VALIDATION	5	MODELLING, CFD, FLUENT, VALIDATION.	THEORETICAL BACKGROUND AND METHOD VALIDATION
		DEFINING BOUNDARY CONDITIONS, SETTING UP MODELS, PRELIMINARY STUDIES AND NEW METHOD FOR SOLAR RADIATION.	6	FLUENT, BC, MESH, DSF, SOLAR RADIATION	MODEL SET-UP AND DEVELOPMENT
ANALYTICAL FRAMEWORK	RESULTS, ANALYSIS AND DISCUSSION	INVESTIGATION THE PERFORMANCE OF SIMPLE CAVITY STRUCTURE WITH SIMPLE SHADING ELEMENTS THROUGH A PARAMETRIC STUDY OF VARIOUS DESIGN PARAMETERS AND CHARACTERISTICS.	7	PARAMETRIC STUDY, SIMPLE CAVITY, VERTICAL VENTS, SIMPLE SHADING SLATS	GENERAL PARAMETRIC STUDY ON SIMPLE CAVITY WITH SIMPLE INTEGRATED SLATS
		INVESTIGATION THE PERFORMANCE OF VARIOUS DESIGNS OF INTEGRATED SLATS UNDER VARIED DESIGN PARAMETERS, THROUGH A PARAMETRIC STUDY.	8	PARAMETRIC STUDY, SIMPLE CAVITY, HORIZONTAL VENTS, VARIOUS INTEGRATED SHADING & DAYLIGHTING ELEMENTS	PARAMETRIC STUDY ON SIMPLE CAVITY WITH HORIZONTAL VENTS AND VARIOUS INTEGRATED SLATS
		INVESTIGATION THE PERFORMANCE OF DSF SYSTEM FOR OFFICE BUILDINGS IN AMMAN.	9	DSF, OFFICE SPACE, AMMAN, PARAMETRIC STUDY	DOUBLE SKIN FAÇADE (DSF) WITHOUT SHADING DEVICES
		INVESTIGATION THE INFLUENCE OF CAVITY- INTEGRATED SHADING ELEMENTS ON THE PERFORMANCE OF DSF SYSTEM FOR OFFICE BUILDING IN AMMAN.	10	SHADING SLATS, DSF, OFFICE, AMMAN, PARAMETRIC STUDY	DOUBLE SKIN FAÇADE (DSF) WITH SHADING DEVICES
		INVESTIGATION THE EFFECT OF CONSIDERING THE INTERNAL HEAT GAINS.	11	SHADING SLATS, DSF, OFFICE, AMMAN, PARAMETRIC STUDY, INTERNAL HEAT GAINS	EFFECT OF INTERNAL HEAT GAINS
		OPTIMIZATION AND SIZING THE ARTIFICIAL COOLING SYSTEM.	12	SHADING SLATS, DSF, OFFICE, AMMAN, PARAMETRIC STUDY, INTERNAL HEAT GAINS, COOLING.	SUMMER ARTIFICIAL COOLING
		THE SYSTEM PERFORMANCE FOR BOTH WINTER AND SUMMER.	13	DSF, OFFICE, AMMAN BC, PARAMETRIC STUDY	OPTIMIZATION OF THE SYSTEM (SUMMARY AND APPLICATION)
	RESEARCH OUTCOMES, CONCLUSIONS AND RECOMMENDATIONS		14		MAIN CONCLUSIONS

CHAPTER 2 BACKGROUND OF CASE STUDY: CITY OF AMMAN IN JORDAN

This part of the work presents the concept of thermal comfort, the local climate of the Jordanian city of Amman, current needs of energy there, trends & developments in built environment of the city, the impact of this growth on energy needs and potentials for new passive solutions concerning new buildings.

2.1 Thermal Comfort:

The thermal comfort is defined as the state of mind that expresses satisfaction with the thermal environment (ASHRAE, 1992). In other words, it reflects the state of mind of occupants on how they do feel from a thermal perspective (e.g. hot, cold, etc.). Generally, the indoor thermal comfort is affected by different parameters, which include ambient climate, urban context, building design (configuration) and construction materials. Most importantly, People may respond differently to typical environmental conditions due to differences in their adaptation levels. Commonly, indoor thermal conditions are recommended to satisfy at least 80% of the occupants to be thermally considered as comfort. Meanwhile, the body's mean (core) temperature should be maintained around 37°C all the time (Gadi, 2010).

More precisely, indoor thermal comfort is usually determined by the combined influence of several factors: environmental and personal. Air temperature, thermal radiant (mean radiant temperature), air movement (velocity) and relative humidity are the environmental factors. The personal

factors cover metabolic rate and clothing thermal resistance. These factors are well-known as the six fundamental factors or the six basic parameters of indoor thermal comfort. Together, these factors influence the occupants' perception of their thermal environment. Consequently, their thermal response is based on the combination of these six factors. Some of these factors are dependent while others vary independently of each other (Fanger, 1970; Levin, 1995; Parsons, 2014). Moreover, a set of secondary parameters, which are related to the six main parameters, is also important for indoor thermal comfort of occupants. These parameters are: Sweat secretion rate, skin temperature, skin wittedness, clothing wittedness and permeation to moisture, clothing fit and air movement under and within clothing, and clothing surface temperature (Gadi, 2010).

However, whereas air temperature could be the most critical indicator of thermal comfort or thermal stress, other factors are still important and vital. For example, increasing air velocity (or enhancing air distribution) allows relatively higher air temperature values to be accepted within the thermal comfort range.

Generally, there are two main approaches regarding the investigation of indoor thermal comfort. The first approach is the heat balance model, which was based on extensive experimental works and developed by Fanger (1970). It mainly deals with Predicted Mean Vote (PMV) and Percentage People Dissatisfied (PPD) methods. Both PMV and PPD have been widely used in thermal assessment of indoor environments. The second approach is the adaptive thermal comfort model, which was based on series of field studies

(Humphreys, 1974; Humphreys, 1975) and was later introduced by Humphreys (1976) and supported through further works later on. The adaptive principle, on which the adaptive approach is based, says: "If a change occurs such as to produce discomfort, people react in ways which tend to restore their comfort" (Nicol and Humphreys, 2002).

With the Humphreys approach, the adaptive Predicted Mean Vote (aPMV) method would effectively extend the use of Predicted Mean Vote (PMV, based on Fanger approach) to cover different types of buildings with different microclimates, urban context, and cultures. Generally, aPMV method would more comprehensively define the indoor thermal comfort for free-running buildings, where occupants could continuously adapt themselves to changes in thermal environment of their spaces.

Thus, it is well established that the combined thermal effect of the six factors (e.g. air temperature, metabolic rate, etc.) is responsible for assuring occupants' thermal comfort. Therefore, measuring air temperature alone is not always a sufficient indicator of indoor thermal comfort. However, in this study, the air temperature and mean radiant temperature (together, form indoor operating temperature) were just used to partially evaluate indoor thermal comfort and highlight the possibility of severe overheating, where other factors were assumed to be within the normal ranges.

2.2 Climate of Amman/Jordan: An overview of Amman City

This section shows the characteristics and features of the local climate of Jordan and specifically the city of Amman. According to the climatic classification of Koeppen-Geiger-ASCII (Kottek et al., 2006), the climate of Jordan is mainly classified as hot dry, which is more evident in the east part of the state. However, it is still influenced by more than one category. This is due to the location of Jordan as it lies in the merging boundaries of the Arabian Desert regions and the Mediterranean Sea regions and between 29°3` N and 32°55` N (Bani-Domi, 2005). Referring to other sources, the climate of Jordan is considered as Mediterranean climate with long hot dry summer (Metz, 1989; Bani-Domi, 2005). More specifically, Jordan has a hot dry summer (November to April) with cool wet winter (May to October) especially the north, west or middle of the state.

Summer's temperatures have an average of 32°C and sometimes exceed 40°C while winter's average is about 13°C. A strong wind with hot dry air, known as *khamsin*, usually blows from the south and southeast sides of the state a month before and after the summer season. With much dust and drop in relative humidity up to 10%, it could cause a significant increase in air temperature between 10-15°C within a few hours.

Since 1992, the mean temperature of Jordan has increased by an average of 1.5-2°C. According to future expectations (2009-2018), mean minimum annual temperatures will decrease for different parts of the state while stay constant for the northern part. However, mean maximum annual temperatures will increase for the entire state. Clearly, this phenomenon

highlights a turning point in the country's climate, which makes it critical especially if it is being considered as a reference for environmental solutions. Jordan, as other similar states in the region, is expected to experience more hot summers that mean more energy demands for cooling due to unexpected increase in summer temperatures (Matouq et al., 2013).

Amman, the capital city of the state (latitude 32°, longitude 35°, altitude 980m), is being affected by such characteristics and significantly experiences hot dry summers and cool winters with most of the above features. Monthly temperature averages are 8°, 16° & 28°C for January, April, and July, respectively. However, it could reach 40°C in summer for many days. The annual average for daily solar irradiance in Amman is about 5 kWh/m² with significant diffuse radiation (Al-Salaymeh et al., 2010).

Figure 2.1 shows a summary of climate data from University of Jordan's weather station in Amman.

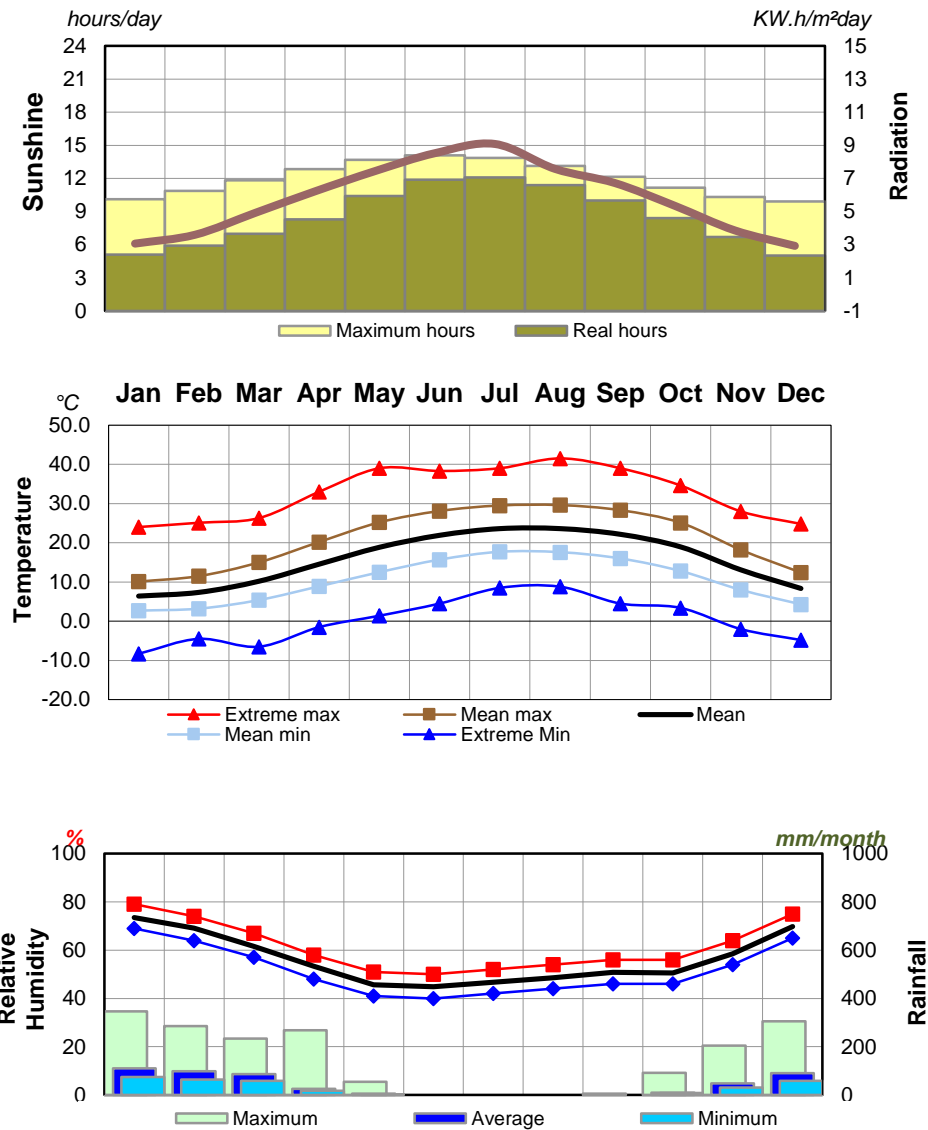


Figure 2.1: Climate data for University of Jordan's weather station in Amman.
Source: (Awadallah, 2013a).

In addition, Figure 2.2 shows a psychrometric chart for Amman city, which is based on previous data from University of Jordan's weather station in Amman. According to this chart, the annual thermal comfort zone is about 17.8°C-25°C. Although a considerable part of the year falls within the designated thermal comfort zone, there are still considerable needs for heating and cooling during the months out of designated comfort zone. While heating needs exceed the potentials of passive heating techniques to active one, most of cooling needs could be covered using passive cooling means.

Thus, good implementation of available passive cooling and heating strategies/techniques in buildings of Amman could be sufficient to achieve summer's thermal comfort and help to reduce requirements for winter's thermal comfort.

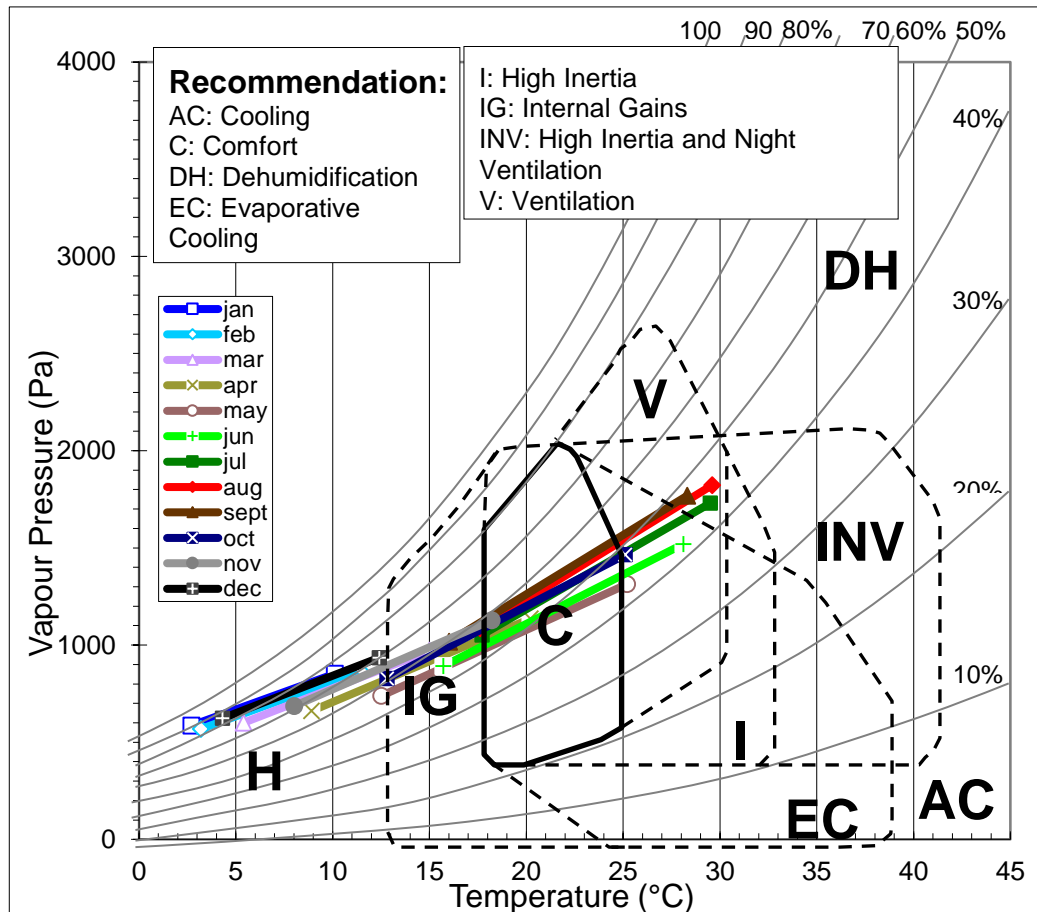


Figure 2.2: Psychrometric Chart of Amman "University of Jordan's weather station".
Source: (Awadallah, 2013b).

Taken into consideration expectations of a considerable increase in local temperatures of Amman, previous recommendation for passive techniques might be no longer valid. With possibilities of increasing indoor thermal discomfort, energy demands for air conditioning purposes would increase. Thus, more concerns have to be given to new passive strategies, especially with new modern techniques for constructions.

However, the thermal comfort zone of Amman for the purpose of this study was based on further climatic data from different weather stations including weather station of Amman's civil airport "Amman-AP" (Technologies, 2008). Thus, designated seasonal thermal comfort zone is 18.5°-24°C (winter) and 24°-28.5°C (summer).

2.3 Energy status, needs, and shortcomings in Jordan:

2.3.1 Energy Status:

Jordan, as a developing country located in the Middle East, faces an acute crisis in energy resources. Considering its very limited resources of traditional energy (oil, gas, etc.), it imported 97% of the national demands of energy in 2011, which formulated 16% of GDP (Gross Domestic Product) compared to 12.3% in 2009. Moreover, the annual growth for primary energy demands is 5.5%. In addition, the annual growth for electricity demands, in particular, is 7.1%. Both rates of growth are expected to keep increasing until 2020 (Elsagheer, 2013).

Although the state has abundant potentials of renewable energy resources including solar radiation (5-7 kW.h/m² per day) and the wind (7-11 m/s) (Hrayshat, 2007; Elsagheer, 2013), it mainly relies on traditional imported resources as shown in Figure 2.3.

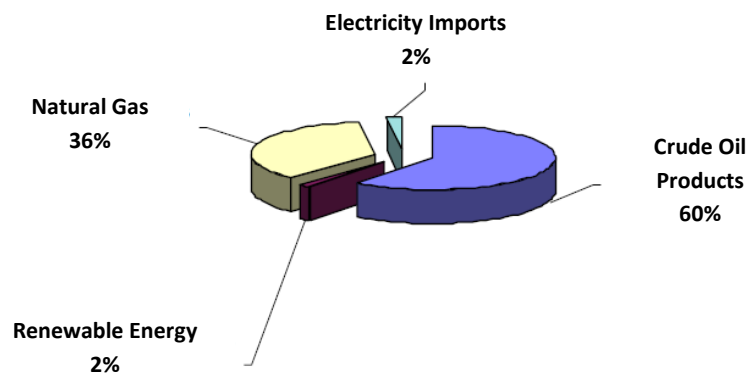


Figure 2.3: Primary Energy Consumption of Jordan for 2008. Source: (Secretariat, 2010).

Recently, the national government has issued new energy policies that work to turn this reliance toward local resources including renewable energy resources. By 2020, the National Energy Strategy "2007-2020" aims to provide up to 10% of the national demands from available renewable

resources including solar, wind and waste recycling (Commission, 2007; Secretariat, 2010). Figure 2.4 shows the expected share of different resources until 2020.

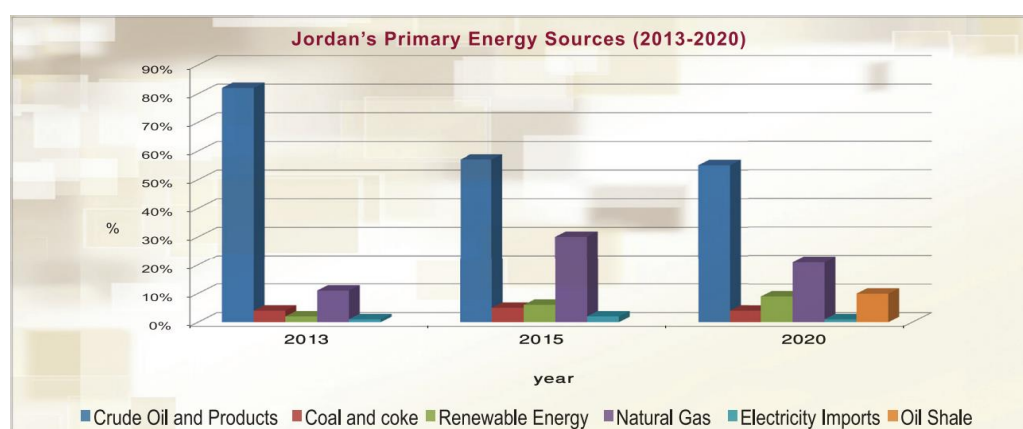


Figure 2.4: Composition of Jordan's Primary Energy Sources (2011-2020). Sources: (JORDAN, 2014).

2.3.2 Energy Consumption:

Table 2.1 shows the distribution of energy consumption in Jordan for the period 2008-2012. Commercial sector consumption is included within the others section. Moreover, Table 2.2 shows the distribution rates for the same period but regarding electricity consumption only, which is mainly produced from the traditional imported forms of energy. Electrical consumption in the commercial sector was almost constant at 17%. This consumption in commercial sector includes air conditioning (heating and cooling), lighting, etc.

Table 2.1: Percentage ratios of the sectoral distribution of final energy consumption during 2008-2012. Sources: (Jordan, 2012).

Year	Sector				Total %
	Transport %	Industry %	Household %	Others %*	
2008	38	23	21	18	100
2009	39	22	21	18	100
2010	41	21	21	17	100
2011	41	20	23	16	100
2012	49	14	23	14	100

* Including Commercial and Agricultural sectors along with streetlights.

Table 2.2: Percentage rate of sectoral consumption of electricity during 2008-2012.
Sources: (Jordan, 2012).

Sector type Year	Household %	Industry %	Commercial %	Water Pumping %	Street lights %	Total %
2008	39	27	17	15	2	100
2009	41	25	16	15	3	100
2010	41	25	17	15	2	100
2011	41	26	17	14	2	100
2012	43	24	17	14	2	100

2.4 Architecture and Built Environment of Amman: Overview, Climate Issues, and Proposed Solutions

2.4.1 Trends of Architecture in Amman:

Because of its distinguished location in the Middle East and because of the multi-political and economic developments in the region, Jordan becomes an active hub for trading, transportation and even living over the past few years. These changes increased the reputation of its capital “Amman” in the scope of estate investment and business. As a result, the city has experienced a noticeable growth in planning and construction works.

Since the early 1990s, Amman city has grown at an overwhelming rate. Relatively large-scale buildings have appeared in Amman. This includes office buildings (shops in ground level with offices in the upper floors), large retails buildings, large shopping malls and multi-use high-rise buildings (e.g. commercial, office and residential use). These large-scale buildings were scattered throughout the city. At the same time, these were no comprehensive long-term master plan for the urban development of the city (al-Asad, 2005; al-Asad, 2013).

Recently, a new center, known as Abdali district, was proposed. It compounds a business, social and residential facilities. For instance, office buildings (total area of 368,000 sqm) formed 36% of the project's phase-one. At the urban scale, green strategies have been adopted in this mega project including protecting the environs and saving energy (ABDALI, 2012b; ABDALI, 2012a).

Generally, in Amman, most of the new buildings are being constructed with modern and international styles. Recently, large openings and full glazed facades become common features there, Figure 2.5 and Figure 2.6. On the other hand, comfortable environments are still required under the hot summer of Amman with high internal heat gains, and for the cold winter over there, as well. As have been observed by the author, active auxiliary systems for air conditioning (i.e. artificial cooling and heating) are largely being adopted over there. This is due to the absence of sufficient passive design solutions.

To conclude, all these features of rapid urban growth, large-scale modern-design buildings and lack in comprehensive green strategies will affect the city infrastructures including energy resources, which are already scarce.

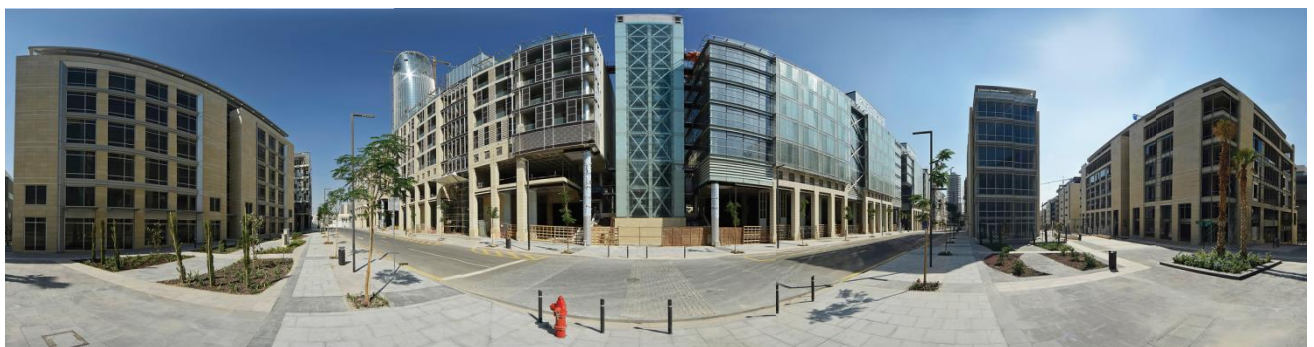


Figure 2.5: Panoramic View within Abdali mega project / Amman. Source: (Abdali, 2013b)



Figure 2.6: Abdali Boulevard Project / Amman. Source: (Abdali-Boulevard, 2013).

2.4.2 Energy-Efficient Building Codes and Energy Consumption in Amman:

A few years ago, an Energy-efficient code for buildings in Jordan known as “*Energy Efficient Building Code*” was set by Jordan National Building Council and Building Research Centre in Jordan (Awadallah et al., 2009). Jordan is among a few countries in the Middle East where building energy codes are, to a certain extent, mandatory by law for both residential and non-residential buildings; see Appendix B. While it mainly deals with mechanical & electrical devices in buildings, it also aims to enhance passively indoor thermal comfort and reduce air-conditioning demands, to face the overwhelming energy crisis there. This code deals with building design as well as a selection of construction materials, as follows:

- **Building envelope:** areas of openings should be determined according to spaces’ functions, location, and orientation.
- **Daylighting:** window-wall ratio is recommended to be more than 10% and 15% for services and residential functions respectively.
- **Shading devices:**
 - Using shading elements on both south and east facades is recommended.
 - The preference is for external shading.
 - Clear-space between external shading and openings is recommended.

- The shading coefficient is to be less than 0.2.
- The preference is for adjustable shading for east, southeast, west and southwest facades.
- **Ventilation:**
 - Night-ventilation, shaft, chimney and wind catcher means.
 - Humidity is to be 40-70%.
 - Shading the ventilation source.
 - Ensuring non-polluted ventilation source.
- **U-value:** Table 2.3 shows recommended U-values for walls, exposed floors & Roofs and Windows. It is obvious that the code deals with a window-to-wall ratio up to 40.7%. Thus, no obvious recommendations regarding larger or full glazed facades are available.

Table 2.3: U-values for Walls, Exposed Floors & Roofs and Window Types for Building in Amman according to Energy Efficient Building Code for Jordan. Source: (Awadallah et al., 2009)

Walls	U-value W/m ² .K	Exposed Floors and roofs		U-value W/m ² .K	Window Type	U-Value (window) W/m ² .K	Allowed ratio of window to wall
Opaque walls or any part of it	0.57	Exposed for outdoor air	Heat transfer towards the top	(1.2) 0.55	Aluminum/ steel frame, single glazing	5.7	20.1%
Total Wall including percentage of openings	1.6		Heat transfer towards the bottom	0.8	Aluminum/ steel frame, double glazing	3.4	32.9 %
Divider walls between 2 different energy source provider for 2 building spaces.	2.0	Floors/ Roofs dividing to floors with different energy source provider		1.2	Wooden/ plastic frame, single glazing	4.8	24.3 %
Divider walls between 2 parts of the building one of them is heated/ air conditioned and the other not.	2.0	Floors located above un heated/ air conditioned basements or spaces		1.2	Wooden/ plastic frame, double glazing	3.1	40.7 %

In a typical commercial building, air conditioning systems usually have the largest electricity consumption, which could reach more than 40% of the total consumption of the building (Chan et al., 2009). In hot conditions, cooling loads are an important part of this share, especially for office buildings where high standards of thermal comfort are usually required. In regions (e.g. Amman) where both hot summer and cold winter are significantly experienced, energy consumption could be even larger.

More specifically, facade's configuration in hot arid areas is predicted to be responsible for up to 40% of the building's cooling loads (Hamza, 2004). Therefore, under the hot dry summer of Amman, large or full glazed facades

would affect indoor thermal comfort and increase energy demands for air-cooling purposes. Added to winter heating demands, this would increase current shortages in energy resources over there. This indicates the importance of façades' design and their materials for energy saving in similar climates.

On the other side, constructions with sustainable and efficient energy techniques for facades could help to provide better thermal comfort and reduce air-conditioning loads (heating and cooling). At the same time, visual comfort might be enhanced and lighting energy consumption could be reduced.

Referring to Amman's psychometric chart, several means of passive strategies are available to cover each of heating and cooling demands, especially cooling ones. However, designers have to be careful in using any of these strategies in such climate of Amman (hot summer and cold winter) as it might give adverse results for the other season. Therefore, the proper combination with a good balance between different means could give better results. For instance, applying a sunspace to a living room would reduce heating loads in winter but could cause serious overheating in summer. This influence is affected by glass-to-wall ratio. However, having internal shading with sufficient night ventilation could efficiently reduce summer overheating. Thus, the proper combination of such passive techniques could lead to a reduction of about 42% of the annual heating and cooling loads in Amman (Bataineh and Fayez, 2010; Bataineh and Fayez, 2011).

2.4.3 Climatic Passive Design Solutions for Buildings in Amman:

This section shows some of the common and promising strategies for climate-based passive design solutions for buildings in Amman.

2.4.3.1 Insulations and Thermal Mass Materials:

Thermal insulation is widely used in residential buildings in Jordan. Heating and cooling energy requirements showed a reduction of more than 40% with proper thermal insulation for both ceiling and walls in a residential building (Shariah et al., 1997). Moreover, thermal insulation is widely being applied in office buildings in Jordan as well.

Moreover, and since the 1950s, concrete is widely being used as a principle construction material in Jordan, for structural skeleton (reinforced concrete) and walls (concrete masonry bricks). This includes residential and non-residential buildings. The concrete, with high thermal mass properties, could act as a passive design technique over there, where the local temperature would have a significant difference between day and night in summer.

Recently, the new building of Queen Alia International Airport (QAIA) in Amman was constructed and the concept of high thermal mass was largely implemented. The project was designed by Foster+Partners (E-Architect, 2013). Both building's roofs and structures were mainly constructed using concrete as shown in Figure 2.7.

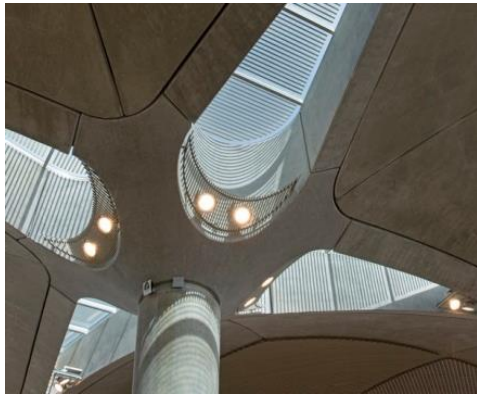
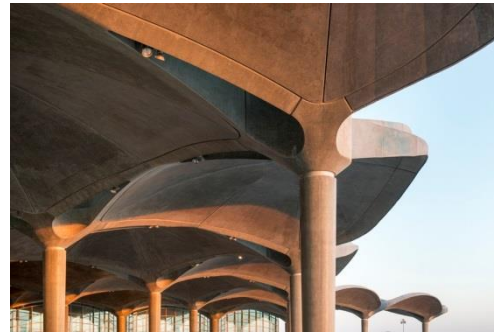


Figure 2.7: large using of Concrete as a high thermal mass material at new building of QAIA / Amman.

Source: (E-Architect, 2013).

2.4.3.2 Passive Solar Shading:

Various techniques of passive solar shading have widely been implemented into buildings in Amman, including the newly constructed ones. Openings' recess, louvers, and simple shading devices are seen over there, as shown in Figure 2.8, Figure 2.9 & Figure 2.10.



Figure 2.8: Several passive techniques for Building Facades in Abdali Project / Amman, as sample of passive solution for modern buildings in the city. Source: (Abdali, 2013a).



Figure 2.9: Alabdali office building competition. Source: (OMRAN, 2013a).



Figure 2.10: Arab insurance office building/Amman. Source: (OMRAN, 2013b).

In addition, the new building of QAIA (E-Architect, 2013) was constructed with almost full glazed facades however shading louvers techniques were intensively applied to these facades to reduce direct gains and control glare, as shown in Figure 2.11.

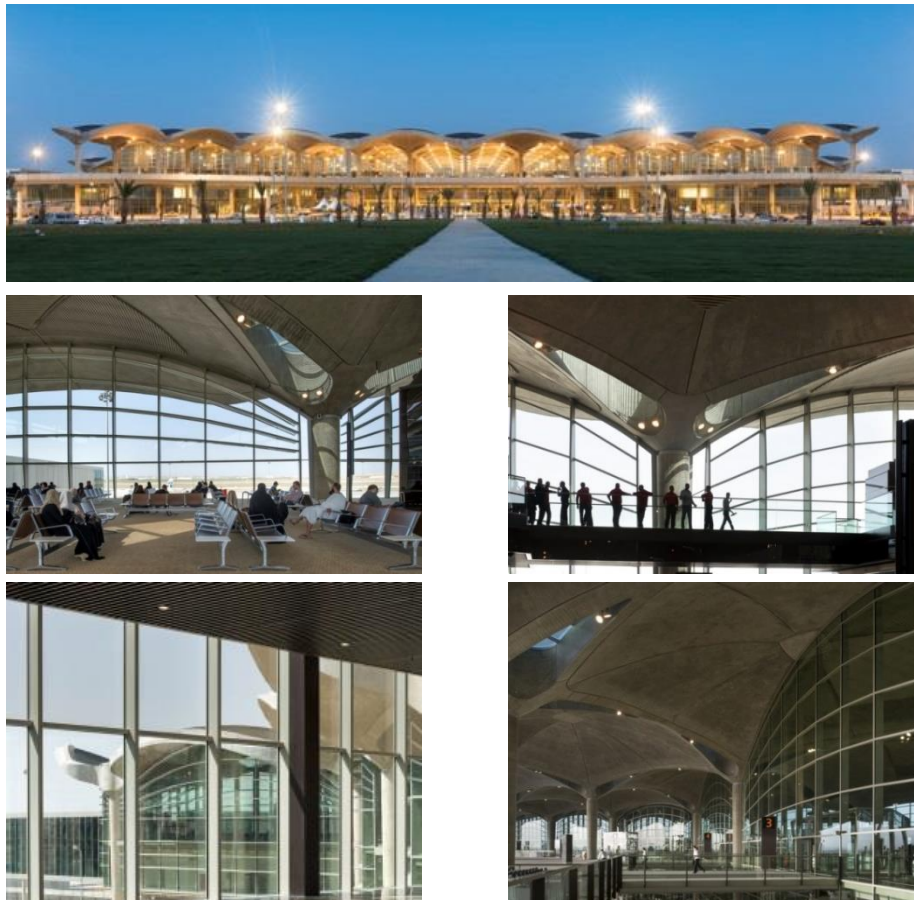


Figure 2.11: Full glazed facades with means of shading devices at new building of QAIA / Amman. Source: (E-Architect, 2013).

A research was carried out on the influence of different passive shading types on thermal performance of office buildings in Irbid city north of Amman. Generally, indoor temperature was reduced up to 13% throughout the day (Freewan, 2011). Another work by Alzoubi and Al-Zoubi (2010) investigated the effect of louvers on daylighting levels and associated energy for a typical office in Amman. Results showed the efficiency of such techniques in enhancing indoor light levels while reducing associated solar gains.

In his MSc research, Amaireh (2012) investigated the feasibility of using Photovoltaic integrated shading devices for glazed office buildings in Amman. Results showed a significant impact for such devices at different orientations. With Glass-to-Floor ratio about 50% at SW, annual reductions in solar gains might reach 59%. This could lead to a reduction of 56% in annual cooling loads and a net reduction of 52% in annual air conditioning loads (as heating would increase a bit). Accounting electricity generated from PV modules of the applied devices, the total contribution to energy saving might be up to 98% with proper installation and operation of these devices. This indicates the effectiveness of passive solar shading as cooling strategies for such buildings in Amman.

2.4.3.3 Double Skin Facades "DSF":

Following the significant growth in fields of construction in Amman, new constructional techniques have been imported to the city. Such techniques aim to produce building-images that are more attractive and sometimes bring in new sustainable solutions thus to reduce the building associated energy bills over there. Double Skin Façade "DSF" was one of these techniques. Until

the time this work was initiated, just four attempts for adopting DSF in Jordan were declared; all of them in Amman. Three of them are being brought to reality while the fourth was just proposed at conceptual levels. These are:

- **ABDALI BOULEVARD:**

The Abdali Boulevard consists of several parts. One is a block of office buildings. The block consists of four buildings and each has five storeys. Part of offices' facades was constructed with double skin curtain walls as shown in Figure 2.12 & Figure 2.13. This aims to enhance indoor daylight and control heat loss (McNamara, 2013).



Figure 2.12: DSF as shown in office buildings of The Abdali Boulevard in Amman. Source: (BRIEF, 2014).

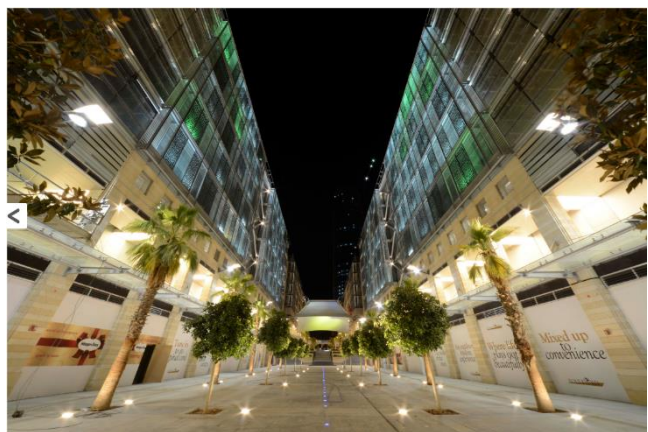


Figure 2.13: DSF as shown in office buildings of The Abdali Boulevard in Amman, Night-time View. Source: (MASAR, 2013).

Some of these DSFs consist of a glazed inner skin and an outer skin made of stone. The two skin are separated by a 0.75m-wide cavity. Integrated shading elements were used. These elements were either wooden or metal louvers (Musa, 2014).

- **ROTANA AMMAN HOTEL; AMMAN/JORDAN**

It is an 180m-high tower located within the Abdali district in Amman. It is a complex building designed by a French firm Architecture Studio. Third of its built-up area is designated as offices, Figure 2.14. Architecturally, the building consists of a tower emerges from a large platform. The tower is constructed using curtain walls with double glazed elements, which are protected by aluminum sun shading devices (i.e. vertical louvers). On the other hand, the platform zones (social spaces and restaurants) is designed with DSF protected by integrated retractable louvers (NES, 2008). As the project is still under-construction, detailed technical description and drawing are scarce and not available.



Figure 2.14: Shots of Rotana Amman Hotel in Amman. Full glazed facades with shading elements are shown. Source: (D'ingénierie, 2014).

- **LIVING WALL “Mixed-use Complex Building”;**

AMMAN/JORDAN:

Living Wall project, designed by Foster+Partners, consists of the a large podium with six inter-connected towers (Foster+Partners, 2007). The towers are designed with DSF protected with horizontal screens, which function to shade the inner spaces and enhance the air circulation next to facades, Figure 2.15. However, the work on the project was not completed. Again, at the time of this work, there was no technical description available concerning the DSF or its thermal and optical performance over there.



Figure 2.15: LIVING WALL “a Mixed-use Complex Building” in AMMAN/JORDAN. Source: (Foster+Partners, 2007).

- **HIGH JUDICIARY HOUSE in AMMAN/JORDAN: A Competition Proposed Project**

The proposed design was presented by a Jordanian Firm “Faris and Faris Architects” (Architects, 2011).The building’s envelope was suggested to be mostly made of glass (forming an inner skin) incorporated into another stone-box envelope (forming an outer skin) as shown in Figure 2.16.

Functionally, large glazed areas are suggested for better natural daylighting while the local well-known pattern “mashrabiyya” are cut into the

stone envelope to control levels of daylight and minimize solar heat gains then reduce the artificial cooling demands. The concept of DSF is suggested for natural cooling purposes, Figure 2.17.

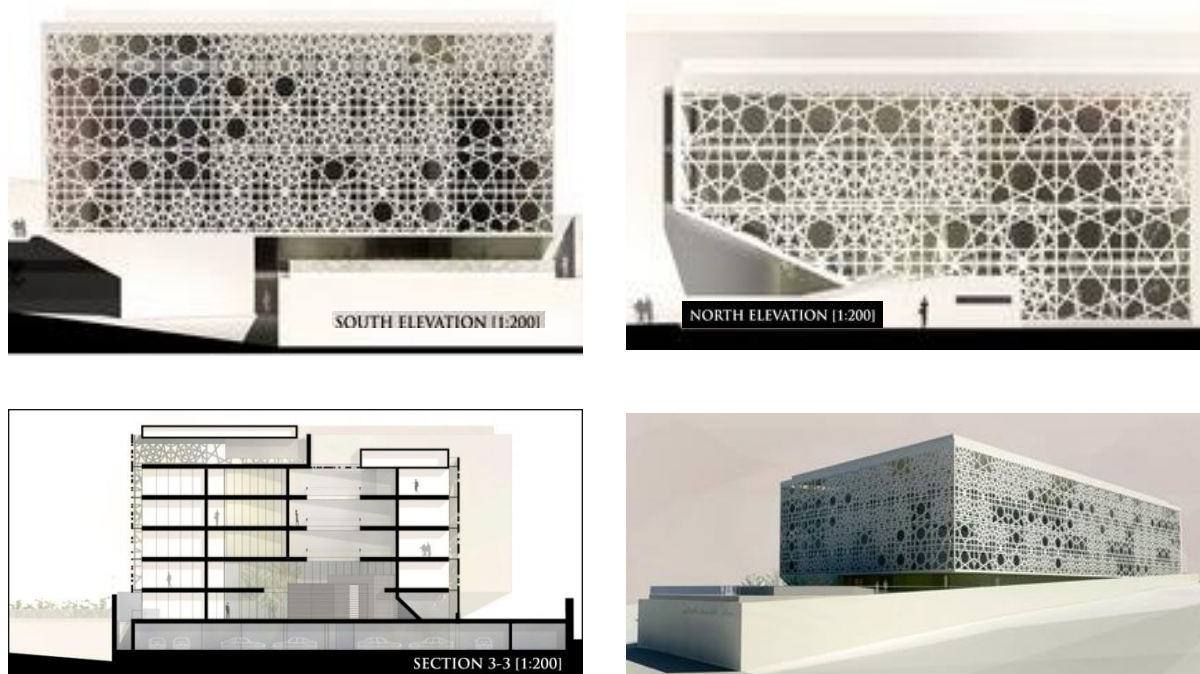


Figure 2.16: HIGH JUDICIARY HOUSE; AMMAN/JORDAN. Source: (Database, 2011).

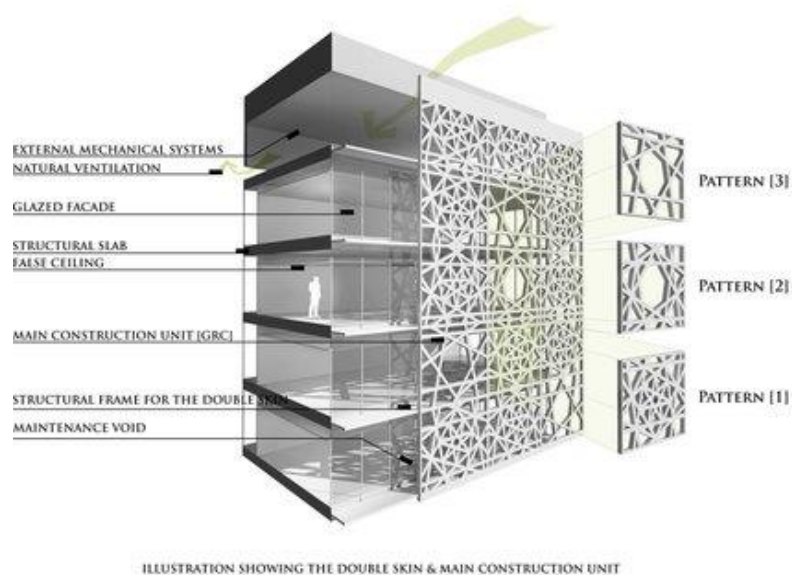


Figure 2.17: Double Skin Façade Concept suggested for HIGH JUDICIARY HOUSE; AMMAN/JORDAN. Source: (Database, 2011).

It is worth to mention that there are no published researches nor investigations concerning DSF performance and operation in Amman (or any Jordanian city) were conducted according to the available literature. Thus, it is not obvious yet whether this system would work properly over there especially for summer times.

2.5 Conclusion:

Amman city experiences hot dry summers with relatively cool winters. Such climatic characteristics highlight the necessity of considering the city as an individual case for the purpose of further studies regarding the thermal comfort and energy consumption for its buildings especially with the noticeable growth in construction works over there.

Obviously, Jordan is facing an acute crisis in its energy resources. For instance, commercial buildings are responsible for up to 17% of electrical energy consumption in the country. Even though there is no clear statistics regarding the air conditioning loads in office or commercial buildings in Amman, these loads are expected to have a considerable portion of total consumed energy by such buildings with hot summers and cool winters of the city.

Therefore, looking for proper passive energy solutions is highly recommended; where (1) hot dry summer with intensive solar radiation levels is usually experienced, (2) high standards of thermal comfort for office spaces are required, (3) significant growth in construction sectors with large glazed facades are widely being used and (4) critical shortages in traditional energy resources is part of reality.

For the last few years, more awareness is being noticed in Amman regarding sustainable solution and efficient energy codes for buildings. However, these codes still seem insufficient, or at least inappropriate aesthetically and technically, for such buildings with large glazed facades (e.g. fully glazed facades) especially in terms of cooling purposes.

Recently, DSF is imported to the city as a new construction technique. Although it is expected to perform well as a heating system with proper design in winter, there is no clear idea how it will perform in hot dry summer over there thus whether it will be considered as a passive cooling solution. Therefore, it is worthwhile to investigate its thermal performance over there before it is widely being used. And if possible, optimize its operation for both summer and winter times. In addition, equal attention has to be given to its optical performance in particular on sunny days of summer even though this is not part of this study.

CHAPTER 3 BACKGROUND OF DOUBLE SKIN

FAÇADE (DSF)

3.1 Introduction:

As one of the main functions of buildings is to protect the inside environment from the harsh and undesirable conditions of outside environment, the separation layer (shelter) between these two environments becomes highly important and sensitive. This shelter can take various shapes depending on many parameters including external intended architectural form, interior space, available materials, construction techniques, etc. While this shelter could be constructed with several diverse elements at the same time, the final product could be with regular or irregular forms. However, roofs and facades are still the most common elements that usually form the building shelter.

Each of these elements has an important effect on the relation between inside and outside environments; this is clearly seen through the climatic influence of ambient conditions on indoor space comfort. Thus, ambient conditions are among critical factors that can play a major role in determining the physical characteristics of these elements, in return. Therefore, optimizing these elements usually aims to achieve better controlling of indoor conditions in terms of thermal and optical comfort. In addition, it targets diverse purposes including energy-saving and aesthetic appearance. Hence, improving passively both thermal and optical indoor comfort and reducing

demands for active energy usually have the priority in sustainable design strategies.

Moreover, the importance of building's facades comes from the fact that facades usually shelter the largest area of the building exposed to ambient conditions, compared to other constructional elements, especially in mid- and high-rise buildings. Therefore, it is usually considered as a vital constructional element that plays a key role in defining the indoor environment and rate the building on energy efficiency scale.

As a result, façade's technologies are continuously being developed in terms of either construction techniques, materials, advanced sustainable technologies or all together. These enhancements usually aim to produce the façade as not only a constructional element but also a climatic moderator for the indoor space. As a result, this brought out new terminologies in façades' industry as curtain walls, climatic responsive facade/envelope, etc. These terminologies indicate many advanced systems and technologies that have been invented and developed during the last few decades.

One of these promising technologies is widely known as Double Skin Façades (DSFs). In the relevant literature, it is also mentioned as Double envelope façade, Multiple Skin Façade, Environmental second skin system, Double skin curtain wall, etc. (Poirazis, 2004). DSF has various pros including thermal, optical, ventilation aspects, etc. On the other hand, it can bring some cons if it is not designed and/or operated carefully.

3.2 Definition of DSF:

According to the relevant literature, many definitions for DSF were set; this indicates the diversity in system's purposes, characteristics, etc. For instance, Saelens (2002) defines DSF as simple as ***"an envelope construction, which consists of two transparent surfaces separated by a cavity, which is used as an air channel. This definition includes three main elements: (1) the envelope construction, (2) the transparency of the bounding surfaces and (3) the cavity airflow"***.

Also, DSF is widely considered as a system used for optimizing indoor daylight quality and enhancing the thermal performance of the space through adding a second glazed skin to the building façade (Wigginton and Harris, 2002). Moreover, the system's cavity is considered as a buffer zone that helps in protecting the inner glazed surface and provides a secure gap for installing proper shading elements (Oesterle et al., 2001).

3.3 History of DSF:

Roots of DSF go back to the nineteenth century and relate to the concept of greenhouse in Europe (Hamza, 2004). The initial concept of mechanical DSF was described by Jean-Baptiste Jobard in 1849 (Saelens, 2002). Also, by the late 20's, Le Corbusier has incorporated the concept of DSF in his proposed project "Murs Neutralisants" (Poirazis, 2004). However, according to Crespo (1999), the first constructed DSF was implemented in Steiff Factory in Giengen, Germany in 1903. The purpose was to enhance the indoor daylighting while providing a proper protector from the cold climate and strong

winds. Moreover, St. George School in Wallasey was probably the first solar double skin façade to be constructed in England in 1961 (Wigginton, 1996).

Consequently, developments in glass manufacturing and advanced mechanisms of glazing fixation and sealing have supported the trend of DSF in the last few decades (Hamza, 2004). By the end of 20th century, DSF was widely proposed as a climatic moderator in the European countries. Even though DSF have been used widely in cold and moderate climates for the last few decades, it is still a matter of controversy there in terms of best configuration, operation mechanism, optimal performance, etc. However, such controversy in DSF's feasibility in hot climates is highly raised and becomes more critical nowadays.

3.4 Advantages and Disadvantages of DSF:

DSF, as a sustainable solution, has advantages and disadvantages at the same time. Thus, for a successful implementation, it is highly important to ensure its suitability to the proposed building and specific location (i.e. climate).

- Advantages of DSF:

Well-designed DSF can offer many benefits (Pasquay, 2004; Poirazis, 2004; Ji et al., 2007; Zhou and Chen, 2010), including:

- *Providing a thermal buffer zone and pre-heating air in winter,*
- *Protecting the integrated shading elements,*
- *Reducing summer cooling loads,*
- *Reducing the external noise,*
- *Possibility of night-time cooling and natural ventilation,*

- *Filtering ventilation-air,*
- *Providing an aesthetic, modern and attractive architectural appearance; and*
- *Indicating the openness of users and inside functions through the high transparency.*

Equally important, proper use of DSF would greatly enhance the indoor daylighting (Hamza et al., 2007; Ji et al., 2007), which would save energy for artificial lighting. In addition, it is highly expected that occupant psychology, behaviour and productivity would be enhanced with the installation of such systems as it provides direct and comfort visual continuity to outdoor environments.

- Disadvantages of DSF:

On the other hand, several undesirable effects might result with DSF application, which are caused by either improper poor design or inefficient operation. These common cons are (Poirazis, 2004; Baldinelli, 2009; Zhou and Chen, 2010):

- *Possibility of summer overheating,*
- *Increasing undesirable inner-acoustics,*
- *Possibility of high moisture levels,*
- *Raising the risk of fire expansion; and*
- *Maintenance and cleaning difficulties.*

In addition, some other facts are still obstacles in front of wide expansion of this application, these include waste-areas of spaces (perimeters), needs for detailed technical design and high capital cost with additional running cost.

In spite of mentioned disadvantages and difficulties of implementing DSF, its application is still promising and recommended for several purposes as mentioned before. Whereas it is likely to face some of these cons, many improvements have already been taken to deal with them and enhance system's entire performance. Therefore, its use is still possible even in regions with extreme climates (e.g. hot-dry summer).

3.5 The Architecture of DSF:

3.5.1 Structure of DSF:

As an entire system, DSF might look complex because of its detailed structures and diverse designs. However, its structure could simply be divided into three sub-structures (Uuttu, 2001):

1. **Primary Structure:** indicates all main structures that are necessary to support the vertical and horizontal loads to construct the façade; include: bearing walls and structural columns.
2. **Secondary Structure:** includes sub-floor, vertical & horizontal partitionings, roof & façade elements, etc. As well, it includes three sub-structures: cantilever bracket structure, suspended structure, and frame structure.
3. **Tertiary Structure:** it is a part of the secondary structure but with less stability like, for instance, façade-integrated windows.

These details in the system's construction emphasize the importance of careful design. At the same time, such complexity indicates the needs for professional practice to construct the system and highlights the high cost of

such systems. However, professionalism and cost are highly affected by the intended details.

3.5.2 Classification of DSF:

In relevant literature, DSF has been classified upon different principles such as detailed construction, airflow pattern and system purposes (Poirazis, 2004). These principles lead to various categories of DSF with different characteristics. Two main classifications could be found in the literature, which are known as British and American (Boake et al., 2008).

The Environmental Engineering firm of Battle McCarthy in Great Britain classified DSF system into five categories, (Poirazis, 2004), which are:

- *Category A: **Sealed Inner Skin**: a mechanically ventilated cavity with controlled flue intake.*
- *Category B: **Openable Inner and Outer Skins**: subdivided into single storey cavity height versus full building cavity height.*
- *Category C: **Openable Inner Skin** with a mechanically ventilated cavity with controlled flue intake.*
- *Category D: **Sealed Cavity** either zoned floor by floor or with a full height cavity.*
- *Category E: **Acoustic Barrier** with either a massive exterior envelope or a lightweight exterior envelope.*

According to the above-mentioned British classification, three main principles were considered to vary these types, which are:

- 1. The configuration of cavity:** continuous or sub-divided.
- 2. Boundaries of cavity:** Openable inner and/or outer skins, light or massive construction.

3. Operation mode: Ventilation system and airflow pattern (i.e. mechanically or naturally, ventilated inside or not).

Under the American classification, just three main categories were originally set, Figure 3.1, based on their ventilation modes and energy efficiency (Lang and Herzog, 2000; Boake et al., 2008). Later on, in 2011, Hybrid System was added as a new category.

- **Buffer System:** using a pair of single-glass panes separated by 25-90cm air-cavity. These glazed surfaces are sealed so fresh air will not enter inside the building except by additional control means. However, inlets and outlets are provided at the bottom and top of the cavity to help circulate cavity's air. This design creates an insulated thermal zone between the inside and outside environments, which can accommodate shading elements if needed. Moreover, better sound insulation and daylight quality could be achieved as well.
- **Extract Air System:** in this case, another glass pane is fixed on the inner side of DSF external layer. System's cavity ranges from 15cm to 90cm and can accommodate shading means. Technically, heated air in system's cavity is extracted mechanically so lead to cool down the inner face of the glass. While fresh air is being supplied mechanically to indoor, this system is recommended where difficulties of having natural ventilation exist. As both supplying of fresh air and extracting of cavity exhausted air is driven mechanically, using this design would increase the energy consumption.
- **Twin Face System:** this design is based on curtain wall concept (could be with high thermal mass) that is placed behind the external single glass layer of the façade. Created space has to be *no less than 50cm* while shading systems can be integrated and protected by the external layer. The external single layer also works to protect the building from harsh winds and increase sound insulation. In addition, it can have vents to moderate the facades components. On the other

side, the added inner layer works to minimize heat losses by better thermal insulation. With this system, openings in space's facade can be operated for natural ventilation and fresh air.

- **Hybrid System:** some characteristics of this type are shared with previous categories however the final product is not following any of them. This includes the possibility of using non-transparent or even non-glazed materials for the system layers. In addition, it indicates the ventilation mode where natural, mechanical and mixed modes are available.

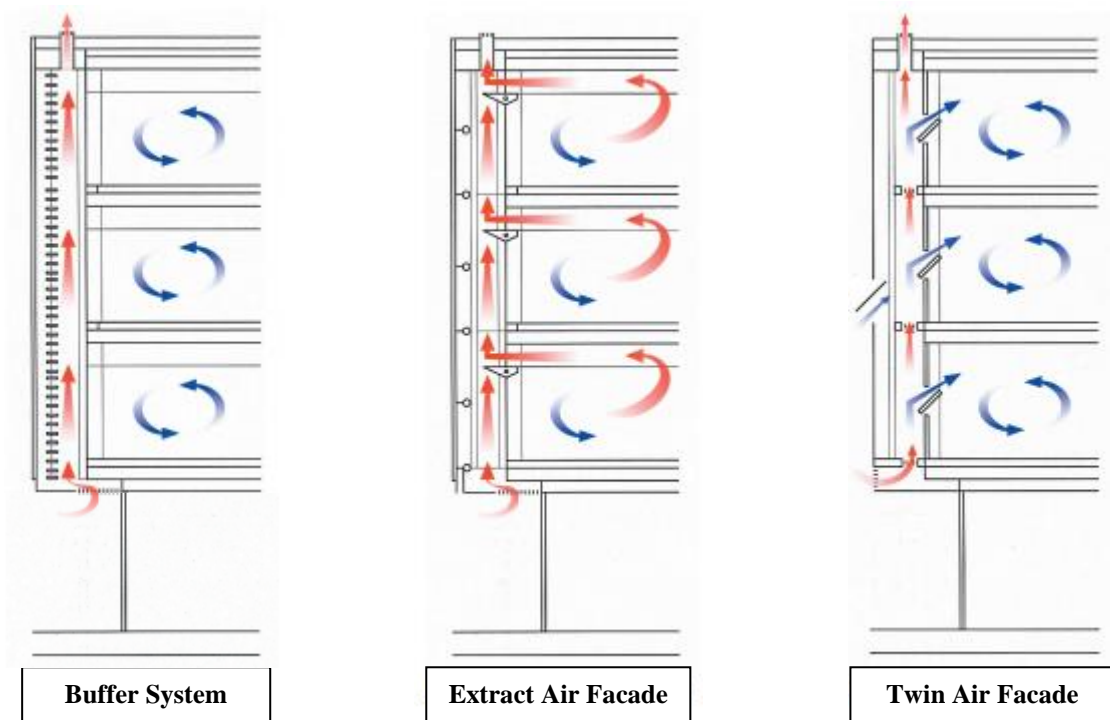


Figure 3.1: American classifications of DSF. Source: (Boake et al., 2008), edited by the Author.

For both British and American classifications, whereas system configuration seems to be the main classifying factor, all of the airflow patterns, modes of ventilation and thermal efficiency of the system are also used to vary different types within the same classification.

Moreover, another classification was set mainly based on ventilation modes (Kragh, 2000), as follows:

- **Naturally Ventilated Wall:** natural ventilation principles are the main drivers of airflow inside the system. To achieve sufficient stack effect and ensure better performance, it is recommended to install proper shading system inside the cavity to absorb more solar gains and heat up cavity air. However, this system is not recommended to be used in extreme hot climates.
- **Active Wall:** cavity's air is connected to space's ventilation system. While solar gains are absorbed by shading elements inside the cavity, these gains will be transferred to the circulating air and removed out in hot times or used for heating purposes in cold times. This type provides advantages of controlling indoor temperatures so ensures better thermal comfort for its occupants. This system is mainly recommended for cold climates.
- **Interactive Wall:** to overcome expected cavity's overheating in summer, this type was developed. It is similar to the natural ventilated wall type but with forced ventilation means to increase the air change rates. Thus, this type can be used in considerable hot climates. Mechanical means for forced ventilation should be selected with high energy-efficiency to reduce active consumed energy at the end.

Finally, another classification was set for DSF based on cavity configuration. This classification is well-known and used through most of the recent publications. Under this classification, four categories have been assigned, which are (Oesterle et al., 2001):

- **Box Window Type:** simply, several partitionings are placed vertically and horizontally along the façade to create separated boxes (Poirazis, 2004). This type seems to be the oldest among others (Hamza, 2004).
- **Shaft Box Type:** vertical partitionings are used to create vertical continuous sub-cavity within the entire cavity, which works as a solar chimney (Hamza, 2004). Many of Box-windows could be connected to this element to enhance the airflow through these constructions by

better stack effect (Poirazis, 2004). Instead of Box-windows, the storey-high cavity (corridor cavity) can be connected to the vertical shaft (central sub-cavity) with this type (Uuttu, 2001).

- **Corridor Façade:** the façade's cavity is divided by horizontal partitionings that are usually placed at each floor's level. This type provides better acoustical insulation and fire protection (Poirazis, 2004). Moreover, vents are provided on the bottom and top of the external layer to ease air circulation between inside and outside of cavity (Hamza, 2004). This system can be integrated with vertical central sub-cavity as shaft box type (Uuttu, 2001).
- **Multi Storey Double Skin Façade:** the entire façade's cavity is without any separations either vertical or horizontal, which helps in better airflow through the cavity. This cavity is designed with large openings at the lowest and highest levels for ventilation purposes while most of the façade could be solid without any openings. This system is highly recommended in the urban context with high levels of noise (Hamza, 2004).

As a promising solution, new concepts with more advancements are continuously added to these systems. For instance, another type is known as:

- **Louvers Façade:** movable louvers used to construct the outer layer of the façade so can be adjusted in winter and summer separately (BBRI, 2002). This concept has been developed and tested later on; and showed a good performance in warm climates (Baldinelli, 2009). This achievement gave a better reputation to DSF concept in general and opened further possibilities for its applications in hot climates.

As discussed earlier, variety in DSF classifications indicates its numerous features and highlights possibilities to produce DSF with various designs as a unique environmental solution relying on its specific purpose and microclimate (Poirazis, 2004). To sum up, previously presented classification given by

Oesterle et al. (2001) seems to be the most common classification according to the relevant literature. Probably, this is because of its simplicity in describing and distinguishing the several types of system. In some literature, it is noticed that combination between Oesterle's and Kragh's classifications could be used to indicate more specific types with shared characteristics.

3.5.3 Components of DSF:

According to relevant literature, DSF system usually and mainly consists of:

3.5.3.1 A pair of surfaces:

The external surface faces the ambient environment while the internal is connected to the indoor environment. These surfaces could be constructed using a variety of materials depends on intended features of the system. Usually, glass is the commonly used material, which offers wide ranges of thermal and optical benefits. These benefits are highly dependent on the type of glass like clear, low-E, absorptive, reflective, etc. (Poirazis, 2004). While the outer surface could be almost fully glazed, the inner could be constructed with varied glass-opaque ratios. Usually, the outer skin consists of a single glass pane while the inner could have double panes. For better fire protection, small modules for glass panes are recommended that increase the thermal resistance of the entire system (Chow WK and Hung WY, 2006).

3.5.3.2 The cavity:

It is the space created between the two boundary surfaces of the system, which is usually filled with normal air. It is considered as the most dynamic part of the system. This fact comes from its role as an intermediate zone between the two boundary surfaces while acting as transferring medium

for both solar gains and air. It is noteworthy mentioning that overall performance of the system is strongly affected by both air temperature and velocity inside its cavity. Usually, the cavity can be designed with varied geometries/configurations, which would affect the performance of the entire system differently. Several factors including the type of building, microclimate, and intended ventilation mode should be considered carefully to determine its configuration. These factors would help in characterizing cavity's height-to-width ratio, its airflow rate & patterns and even characteristics of its boundary surfaces (Hamza, 2004).

Cavity's Height, width (distance between boundary surfaces) and depth (distance between far sidewalls) are the main physical parameters that determine its configuration. According to literature, parameters of height and width are the most important.

- **Height of the Cavity:**

Hamza (2004) investigated the effect of changing cavity's height for west-oriented DSF at cooling loads of its attached zone (e.g. occupied office). Results indicated that average cooling loads were reduced by 12% as cavity's height was increased from 3.5m to 21m. This was a result of enhancing thermal buoyancy inside the cavity then increasing air velocity, which led to reduce cavity's overheating and minimize conductive gains through the internal glass. Accordingly, she continued her PhD study on DSF in hot arid climate while fixed cavity's height at 21m (7-storey) with 1m extra height to ensure better buoyancy.

While the height of cavity is mostly based on the number of storeys, it could be extended after the top storey as a solar chimney aiming to offer significant stack effect. Ding et al. (2005) investigated natural ventilation by DSF with solar chimney using CFD and reduced-scale model. They found that adding the chimney would ensure better natural ventilation even if there is no sufficient wind. Simply, increasing height of the chimney would create a larger difference in pressure between its bottom and top, which help in producing sufficient stack effect to enhance its ventilation. Finally, they suggested that height of the chimney is to be not less than the height of two storeys.

Also, an extra 1m parapet was added to the top of 17th-storey DSF to ensure better natural ventilation and airflow rates in investigated building in hot-humid climates (Wong et al., 2008). Mingotti et al. (2011) developed a model to investigate the influence of DSF's height on natural ventilation and its overall performance aiming to explore principles for optimal design and control. This was through two different modes of operations: summer and winter. Results showed how optimizing façade's height can considerably control natural buoyancy inside the cavity and then affect its ventilation, which will enhance the performance of the system in both winter (more preheating) and summer (more heat removal). The ratio of façade-to-space height was found to be a considerable factor for seasonal operation in summer and winter.

Alibaba & Ozdeniz (2011) conducted a parametric study on thermal comfort and airflow rate of DSF-building in a warm climate. The height of both building and chimney were among investigated parameters. TAS was mainly used to investigate these parameters after initial results were validated

against field measurements. Adding a 4.5m-high chimney to the last floor with a single-side opening led significantly to minimize reversed hot air to this floor. However, placing two opposite openings instead of single-side opening on that chimney helped in reducing its height to 1.5m for the same efficiency.

DSF with higher cavity would generally perform better in cooling seasons. As always, there are some restrictions regarding maximum height for single storey buildings, DSF is more recommended to multi storeys. As well, having a solar chimney at top of the system would enhance the airflow inside its cavity that helps to remove more trapped heat and overcome cavity overheating. Moreover, it could provide proper natural ventilation if needed. From an aesthetic and cost-wise perspective, adding 1-1.5m-high chimney is still acceptable and even recommended to enhance the performance of DSF-buildings.

- **Width of the Cavity:**

Cavity's width is a crucial design parameter for DSF, which could vary based on configuration and specific climate. Practically, cavity's width strongly affects air velocity and airflow patterns inside (Poirazis, 2004). According to Belgian Building Research Institute "BBRI" (2002), narrow-cavities could have widths in the range of 0.1-0.2m while wide-cavities could fall in the range of 0.5-1m.

Increasing cavity's width would generally enhance its airflow as a result of extra heated air inside (Afonso and Oliveira, 2000) and less flow resistance at vents. Moreover, another research indicated that cavities with small widths could lead to slight increase in its temperature during summer. However, this

increase would not be critical to inner space. Most importantly, as small cavities could help in allowing more direct solar gains to indoor in winter, the possibility of heat losses would increase at these times as well (Wang et al., 1999).

According to Balocco (2002), heat transfer through space's wall from inside to the ventilated cavity in summer was considerable with the 0.07m-wide cavity. However, as heat transfer rate increased for wider cavities, the rate of increase became more constant. As a result, with south-faced ventilated façade, summer's overheating was reduced by 7% with 0.07m-wide cavity compared to 27.5% with the 0.35m-wide cavity. According to that study, ventilated DSF with cavities wider than 0.07m might help in providing the acceptable solar cooling effect. In winter, closing the cavity is recommended as this would minimize heat losses from indoor space to the cavity and might cause positive reverse as the heat starts transferring from cavity to space. Moreover, as wider cavities have less frictional resistance at boundary walls to the air, this ensures better airflow thus natural ventilation. Therefore, increasing cavity width would enhance both natural ventilation and concept of passive solar cooling, which leads to more saving in cooling energy in summer.

According to Hamza (2004), most of literature indicates cavity's width at a range of 0.07-1.5m. However, she stated that wider cavities are more efficient in hot-arid regions as these ensure better thermal performance of the system due to better airflow. For her entire PhD research, she set cavity width at 1m. In addition to climate awareness, other considerations were taken in

her decision such as the type of investigated buildings. Later on, she used same width (1m) for similar DSF case but in another study (Hamza, 2008).

In extreme hot climate of United Arab of Emirates (UAE), a study on DSF by Radhi et al. (2013) showed that by decreasing cavity's width, heat transfer rates minimized. However, increasing heat transfer rates with cavity's width might be due to more heated-air trapped inside the cavity with insufficient ventilation. At the same time, DSF with narrow cavity would allow more direct solar gains that heat up indoor space. Therefore, this work recommended that good balance between heat transfer and direct solar gains could be achieved by optimizing the cavity width at a range of 0.7-1.2m.

With Singapore hot-humid climate, natural ventilated DSF was investigated using CFD while cavity's width was varied at a range of 0.3-1.2m. While air velocity was further enhanced within wider cavities, indoor operative temperatures were more comfort with 0.3m-wide cavity (Wong et al., 2008). According to Chan et al. (2009), width of DSF's cavity could be 0.2-2m; however, they fixed it to 1m for their work in Hong Kong. For warm climates, new design of DSF with cavity's widths of 0.3, 0.5 and 0.7m was tested, and width of 0.7m showed better airflow velocity (Baldinelli, 2009). Moreover, according to a parametric study on DSF in warm climates using TAS and field measurements (Alibaba and Ozdeniz, 2011), there was no significant effect for cavity's width on both predicted mean vote (PMV) and percentage of people dissatisfied (PPD).

However, it highly is recommended to investigate the optimal width for each DSF system individually to ensure good ventilation that will moderate its temperatures (Hashemi et al., 2010). Apart from the thermal performance, another benefit is associated with wider cavities, which is related to fire protection as the wide cavities are expected to be safer than small ones (Chow and Hung, 2006). To conclude, increasing width of DSF's cavity (with sufficient ventilation possibilities) would increase airflow rates inside and enhance its overall thermal performance including indoor space.

3.5.3.3 The openings:

Openings could be integrated into both outer and inner skins of DSF. The main purpose of inner openings is to provide natural ventilation and fresh air whereas the importance of outer openings is to cool down the cavity especially in hot conditions. Type, size, and location of openings influence air velocity, flow patterns and temperatures inside both cavity and behind spaces (Poirazis, 2004). Moreover, while outer skin is usually fully glazed, inner skin is generally constructed based on the window-wall ratio (WWR). For instance, field survey on office buildings in Cairo/Egypt indicated that WWR is between 20-60%. Using DSF as a refurbishing solution, WWR of 40% was used to construct the inner skin for the base model of office buildings in Cairo/Egypt (Hamza, 2004). However, the inner skin could be almost fully glazed in some cases, as well.

Opening's effective-area (based on the whole area and discharge coefficient C_d) has to be considered instead of its design-whole-area in design and calculation process to avoid flow turbulence near these openings and

inside the cavity (Oesterle et al., 2001). In case of separated inlet and outlet on the inner skin, these openings are preferred to be staggered from each other (not in a vertical axis) in order to avoid the returned exhausted-hot air from the cavity to inside (Safer et al., 2005b; Hamza et al., 2011).

Furthermore, cross ventilation could be considered throughout the space and between its opposite sides, which depends on the type of building and its surrounding. In such case, possibilities for ventilating DSF's cavity would be greater. However, the reasonable distribution should be considered for openings on different sides including the outer skin. Ding et al. (2005), in the city of Tokyo with hot humid summers and mild winters, recommended openings with an area of 2m² per floor between space and cavity, and similar openings at the opposite façade of space.

A new concept was invented for the outer skin of DSF in the *warm climates*. Baldinelli (2009) developed movable shading devices integrated into the outer skin, which could be opened in summer for better ventilation and shading at the same time while, in winter, it would be closed to provide a good thermal buffer zone and allow more direct solar gains to indoor. In regions with *hot-summer and cold winter*, external open-loop design for DSF (external respiration DSF) is recommended based on experimental investigations in China (Zhou and Chen, 2010). Wong et al. (2008) used CFD tool to investigate and determine optimum size for both cavity's width and its openings for the south- and east- faced DSF in hot and humid climates, where results showed that size of 0.3m would be best. In extreme hot arid climate of UAE, Radhi et al. (2013) investigated DSF with three openings for its outer skin (one per

floor) with a height of 0.6m. The study concluded that optimizing opening's configuration could noticeably help to overcome cavity's overheating. Hashemi et al. (2010) recommended finding out the optimal size of cavity's openings for each individual case of DSF in hot arid climates, to ensure sufficient ventilation that cools down the cavity in summer. At the same time, operable windows for inner layer is highly recommended for better control upon occupants' satisfaction. Generally, in case of adjustable and operable openings, small sizes are recommended for heating seasons to reduce ventilation heat losses while large sizes are needed for summer to minimize cavity's overheating (Mingotti et al., 2011). Generally, automatic operation is recommended for the external openings to ensure a better response to outside climate variations (Alibaba and Ozdeniz, 2011). However, while windows are recommended for naturally ventilated cavities with high concern to its configuration and size, simple slots can be used with mechanical ones (Zhou and Chen, 2010).

To conclude, determining position and size of external openings are highly important and recommended for individual cases of DSFs. This importance increases for hot regions, as external sufficient ventilation is highly needed to avoid cavity's overheating during summer. As well, controlling and operating modes for these openings could significantly affect thermal performance of both façade system and indoor space.

3.5.3.4 Integrated Shading devices:

Originally, DSF systems were introduced for cold climates however it was then transferred to different climatic conditions including Mediterranean

and hot climates. Furthermore, DSF is mainly a fixed construction system; therefore, it should be appropriate for all possible ambient conditions of its specific location.

In hot climates, DSF system would be exposed to high levels of solar irradiance that would increase direct solar gains to its cavity and indoor space, which may cause serious overheating. Thus, adding proper shading elements to the system could help blocking part of unwanted gains during hot times. However, these elements could still play a significant role in winter as it could help preheating cavity's air to be used for indoor heating (Zhou and Chen, 2010).

Technically, shading systems could be either internal, external or integrated into the cavity; and with different forms including roller blind (screen), Venetian blind and movable slats (Gratia and De Herde, 2007c). Most importantly, many parameters could significantly affect the influence of these elements on DSF's overall performance; such as position, size, material, colour, emissivity, tilt angle, etc. These parameters would be discussed in more details in following sections.

3.6 Cavity's Airflow Modes and Ventilation Mechanisms:

As mentioned before, the cavity can be either naturally, mechanically or hybrid ventilated (Safer et al., 2005b). Natural airflow inside the cavity is mainly driven by thermal buoyancy effect. Thus, it is strongly influenced by in-out temperatures difference that is in turn affected by both ambient temperature and incident solar radiation (Oesterle et al., 2001; Balocco,

2002). However, as natural airflow in the cavity is expected to fluctuate, it is then considered as the most dynamic component for system performance.

Obviously, increasing airflow rate would increase convective heat transfer in the cavity (Safer et al., 2005c; Xu and Yang, 2008) that helps in removing more trapped heat in summer. If airflow rates, due to natural buoyancy, are not sufficient to extract trapped heat from inside cavity, its temperatures will considerably rise. This causes an overheating inside cavity, which is one of the dominant problems accompanied with DSF in hot climates. As a result, inner surfaces' temperatures would dramatically increase, which simply leads to higher radiation exchange and convection to indoor space. In such cases, additional mechanical means for ventilation could be applied to enhance cavity's airflow and prevent unwanted overheating (Hamza, 2004).

On the other hand, placing shading elements in cavity helps to block excessive solar gains. These elements could be significant obstacles for cavity's airflow, which could affect dramatically air's velocity and patterns thus convective heat transfer (Zhou and Chen, 2010). Both shading position and inclination angles would affect cavity's airflow as it usually divides airflow field into two asymmetrical parts (Safer et al., 2005b; Xu and Yang, 2008). This is because of considerable variations in solar absorption of several elements of DSF (i.e. shading elements, inner glass, and outer glass) in addition to the direction of solar radiation and position of cavity's openings. In addition to flow turbulence due to the presence of shading elements, eddies are also predicated close to the inlet/outlet of the cavity.

Furthermore, DSF can be designed with various airflow modes, Figure 3.2. Moreover, it can be switched from one mode to another according to outside conditions and occupant's preferences.

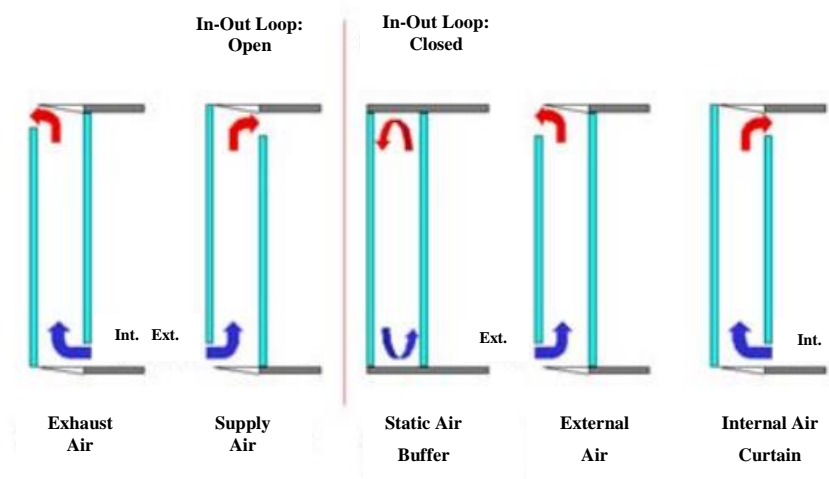


Figure 3.2: Various concepts of Airflow paths for DSF systems. Source: (Haase and Amato, 2006).

Practically, it is still not easy to precisely assess airflow inside DSF cavity because of the dynamic behaviour of airflow (Hensen et al., 2002). However, CFD applications are widely used to carry this job out. Fortunately, this application is being recommended as a reliable tool (Manz, 2003; Baldinelli, 2009). Successfully, it is capable to simulate both airflow and temperature fields inside both system cavity and indoor spaces.

To conclude, while natural ventilation is preferable as a passive solution, it is more complicated and difficult to be predicted based on expected fluctuations in ambient conditions. However, when natural ventilation is not sufficient to extract the trapped heat, mechanical ventilation means are highly recommended to prevent any possible overheating within the system cavity.

In addition, different modes are available for DSF to ensure better thermal performance, provide indoor natural ventilation and save energy.

3.7 The Operation of DSF:

3.7.1 System Function:

Thermally, the main purpose of DSF is to offer a thermal buffer zone and preheat trapped air for heating purposes (heat collector) in cold regions. However, this role is expected to be reversed in summer regions, as it should help reducing undesirable solar gains (heat removal). In moderate climates, the system is expected to operate with dual function, heating in winter and cooling in summer (Alibaba and Ozdeniz, 2011). Again, according to different thermal functions of DSF, high considerations should be taken to balance its operation and then ensure required benefits; as it is expected to perform differently in the different climates at different times.

In addition to the thermal aspect, DSF could also improve indoor air quality and reduce energy consumption (Zhou and Chen, 2010). Moreover, it could enhance indoor daylight (Hamza et al., 2007) but its components should properly be optimized to ensure comfort levels of daylight and avoid glare. Whereas DSF was widely tested and developed for several climate classifications (e.g. cold, moderate, hot), it is still worthy to optimize the system (i.e. configuration, components, and the operation mode) for specific microclimates and the given type of buildings.

3.7.2 Work Mechanism:

Heat gains and losses in buildings are mainly due to three components: internal heat, ventilation heat, and envelope heat. Obviously, transferred heat

through exposed glazed elements forms a significant portion of envelope's heat gains/losses. In sunny conditions, direct solar gains are the main contributor to these gains (through glass) while thermal conduction comes in second (Singh et al., 2008; Chan et al., 2009; Zhou and Chen, 2010).

Generally, total transmitted solar energy through glazed surfaces is highly important in determining energy balance indoors then required loads to maintain space's thermal comfort. In cooling times, large glazing elements of DSF are expected to increase direct solar gains then, unfortunately, increase cooling demands considerably. While direct solar gains fluctuate considerably over the year as sun altitude keeps changing, cooling demands are expected to be varied over the course of the year as well. Therefore, direct solar gains are considered as one of the main dynamic drivers for the system. Whereas glass properties can play a significant role in controlling these gains, installing proper shading elements can add more benefits not just for thermal performance but for optical as well. In heating times, large glazing elements of DSF would help to catch more solar gains for passive heating. However, it might cause significant losses of indoor heat.

In case of ventilated cavity, flowing air helps in increasing heat transfer rates inside the cavity. However, sufficient ventilation in summer will ensure extracting more trapped heat from the cavity to outside then avoid overheating and minimize heat transfer to spaces. In winter, trapped air in cavity would be heated by incident solar radiations thus work as thermal insulation (reduce heat losses to outdoor) while it could be used to heat spaces up through inner loop (or HVAC system).

As mentioned before, thermal performance of DSF is highly affected by both thermodynamic and fluid dynamic of its cavity, which depends on temperature and velocity of cavity's air. Indeed, complexity of the system's performance comes from the coupling of multiple physical phenomena: heat transfer mechanisms (conductive, convective, radiative) and cavity's unsteady airflow (Safer et al., 2005b) as shown in Figure 3.3 and Figure 3.4. To conclude, direct solar gains and outside temperatures (in addition to wind speed and direction) would significantly affect the performance of DSF system. However, this performance could be influenced by several parameters for design and operation. For instance, manipulating glass properties, having proper shading elements and providing sufficient ventilation would enhance system's performance in summer. In winter, cavity airflow has to be carefully controlled. At the end, all these modifications should be taken into consideration in advance before setting the design of the system.

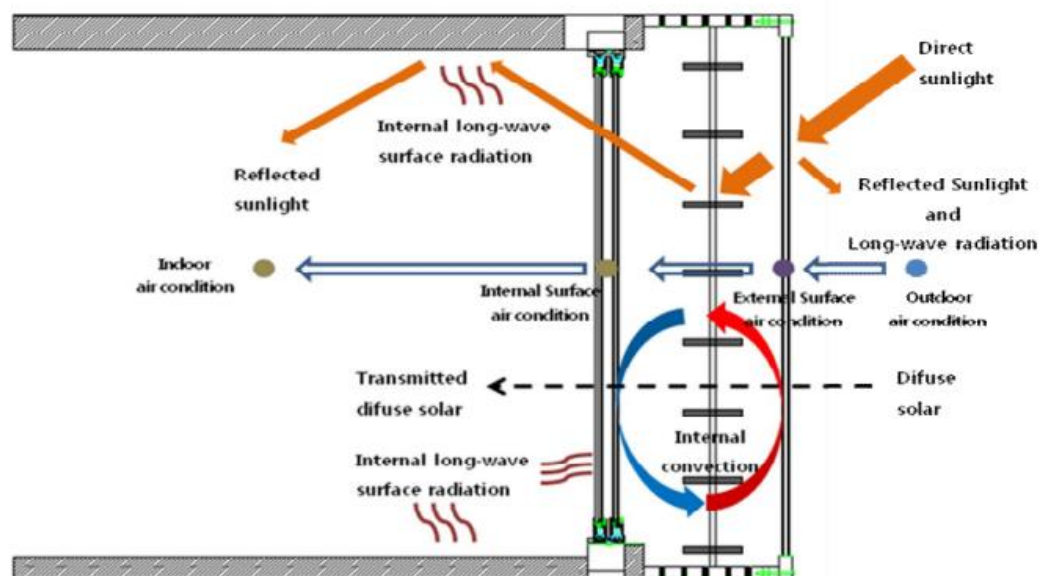


Figure 3.3: Detailed sketch for thermal interactions (thermodynamic) and airflow (fluid dynamic) in DSF cavity with indoor space. Source: (BOHRA et al., 2016).

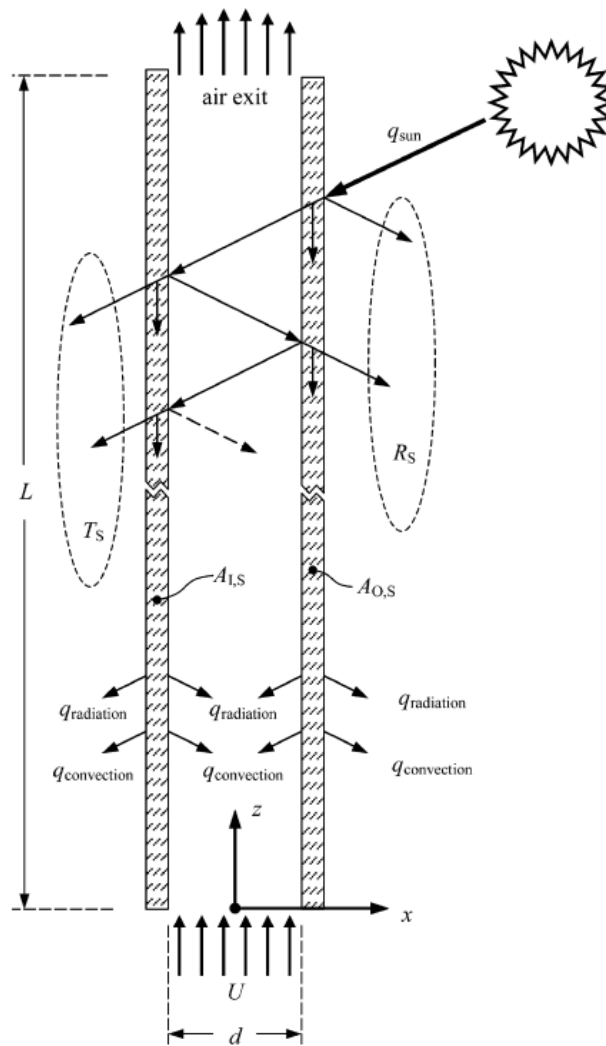


Figure 3.4: Schematic sketch for main thermal interactions (thermodynamic) and airflow (fluid dynamic) in DSF cavity. Source: (Pérez-Grande et al., 2005).

3.8 Conclusion:

- **A pair of surfaces:** it is highly important to ensure proper selecting for both thermal and optical properties of system's surfaces.
- **Cavity:** it is the most dynamic element of DSF's system as it controls both airflow and temperatures (air and surfaces).
- **Cavity's height:** DSF with higher cavities are expected to perform better in terms of natural ventilation due to better stack effect. It is recommended to add a solar chimney to the top of the cavity or at

least extend its height by 1-1.5m. However, both aspects of aesthetic appearance and cost have to be considered.

- **Cavity's width:** width has a significant impact on system thermal performance. The Wider cavity can enhance airflow to extract more trapped heat and then reduce possibilities of overheating. However, this might be inversed if there is no sufficient ventilation as a wider cavity in such case will trap a large amount of heated-air and cause serious overheating that increase heat transfer rates to indoor. Cavity's width at a range of 0.7-1.2m is recommended in hot conditions.
- **Opening:** it is necessary to determine configuration (i.e. position and size) of both inner and outer openings for each individual system. Adjusting openings' size according to ambient conditions is highly recommended for better seasonal operation. Regarding openings of the inner layer, these are recommended to be staggered to avoid returned exhausted air from the cavity.
- **Cavity ventilation & Airflow patterns:** successful design (including openings' size, position and operation modes) for naturally ventilated DSF would help to enhance passive cavity airflow thus reducing possibilities of cavity's overheating without needs of mechanical means. Whereas installing proper shading system in cavity works to block direct gains in summer and prevent indoor overheating, it might affect cavity airflow significantly. Thus, pre-investigation is highly

recommended to ensure its entire influence on both thermal and airflow of DSF.

- **System operation:** operation of DSF seems quite complex according to multi-coupling process occur at the same time. Careful design and proper selection of its components could efficiently lead to a better-controlled operation that ensures sufficient performance over the course of time.

CHAPTER 4 LITERATURE REVIEW ON DOUBLE SKIN FAÇADES (DSF)

4.1 Thermal Performance under Hot Conditions

4.1.1 Overview:

Generally, in hot regions, outdoor conditions are a challenge for indoor thermal comfort in buildings. In these regions, climate can be either constantly hot over the course of the year (humid, dry, arid) or partially hot (Moderate/Mediterranean). Where climate is more constant with hot features throughout the year, it seems easier to deal with the building's fabric in term of sustainable design. With partially hot climate, summer is expected to be hot while winter tends to be moderate, cool or cold. Thus, buildings might significantly experience fluctuated conditions during the year, which indicates the necessity for dynamic adaptation for its fabric.

Façade seems to be the most important dynamic element in building as it interacts directly with outdoor ambient conditions through large exposed

areas. In addition, it usually has various constructional elements including transparent components like glass. Thus, facades should be well-adapted to respond positively and passively to outdoor unsteady conditions.

For instance, in the Middle East where climates with hot features are widely common, roots of transferring façade's technology from European cities refer to the late of the 19th century (Mubārak, 1969). Moreover, interests in glazed facades have increased in many hot-arid cities in the Middle East since 1970's. However, adaptation techniques like shading systems and air conditioning became necessary for these types of buildings in such climates (Hamza et al., 2007). Double skin façade (DSF), as a promising technology for shading and climate moderating purposes, is widely used in several classifications of hot climates. Recently, DSF was transferred to many cities in the Middle East including Cairo and even Gulf's states like UAE. However, additional requirements are still required to ensure optimal performance of such system there.

4.1.2 Insight into System's Thermal Performance under Hot Conditions:

In hot conditions, the coupling of high irradiance levels with excessive ambient temperatures could seriously threaten thermal efficiency of DSF. Simply, a large amount of direct solar gains are expected to penetrate through the outer glazed skin and heat up cavity's components while some will directly pass to indoor space; all depends on irradiance levels, incident angles and properties of glass (Hamza, 2004; Zhou and Chen, 2010).

Many researches have been conducted on DSF performance under hot conditions; including: warm climate (Alibaba and Ozdeniz, 2011), hot arid (Hamza et al., 2007; Hamza, 2008; Hashemi et al., 2010) and hot humid (Wong et al., 2008; Haase et al., 2009). Moreover, DSF was investigated with hot summer & cold winter conditions (Baldinelli, 2009; Zhou and Chen, 2010), where more considerations should be given for system design and materials selection to ensure its optimum performance. Generally, DSF system shows an acceptable performance if it is designed properly even in extreme hot climates like UAE (Radhi et al., 2013).

Generally, installing proper shading systems and providing sufficient ventilation for cavity would help to block part of direct gains and then remove part of trapped heat from the cavity and cool down its components (e.g. glass and shading devices). This would reduce transferred heat to indoors thus maintain comfort levels or at least minimize cooling demands. Whereas using natural ventilation for the cavity is highly recommended, more attention has to be given for both air direction and velocity for the successful application (Zhou and Chen, 2010; Alibaba and Ozdeniz, 2011; Radhi et al., 2013). Furthermore, natural ventilation for cavity might be less efficient due to extreme temperature of ambient air in case of extreme hot conditions.

To conclude, excessive direct solar gains could lead to significant overheating of both system's cavity and indoor spaces, which still presents the most serious obstacle in front of DSF applications in hot conditions. As a result, indoor thermal conditions might exceed comfort levels if the system

was not designed nor operated properly, and consequently, more energy would be required for artificial cooling.

4.1.3 Design Considerations and Parameters:

Diversity in building envelopes, usage of space and urban context should be considered carefully in the design process of DSF. With regard to system's performance, three main parameters are considered to be vital: cavity geometry (e.g. height & width), airflow modes and solar & thermal properties for its components (Hamza, 2004). This includes properties for transparent elements (glass panes) and opaque elements (solid walls, partitions, frames and shading elements). Indeed, these parameters tend to be dependent and interchangeable. In her PhD's research on DSF in hot regions, N. Hamza (2004) defined the study's parameters for DSF's assessment as dependent and independent variables. She classified independent variables into climate profile, building morphology and operational profile of the building. Dependent variables include variations and alterations in geometrical and thermal characteristics of the façade. So far, many works have been conducted on DSF aiming to deliver clear recommendations and design guidelines for architects and building Engineers (Chan et al., 2009; Alibaba and Ozdeniz, 2011; Hamza et al., 2011; Mingotti et al., 2011; Zeng et al., 2012; Radhi et al., 2013).

Recently, the effect of outer skin's shape (i.e. inclination) on DSF's performance was investigated as three different shapes were tested using CFD application (Hamza et al., 2011). No significant variations were noticed for either cavity (airflow and thermal) or indoor spaces, which probably was because of slight differences in façade's design. Furthermore, a parametric

study was completed using field measurements and TAS simulation, to provide design guidelines for DSF in warm climates (Alibaba and Ozdeniz, 2011). Several parameters were included: cavity's width, openings' area, the arrangement of openings (opened and closed), building height and solar chimney height. Results showed that width of the cavity was found to be less important than openings' arrangements for system's performance. Based on a laboratory work and quantitative method, several parameters regarding DSF design and its operation were investigated (Mingotti et al., 2011). Results showed that system's performance (winter & summer) would be enhanced if openings' size (both room and cavity) and cavity's height are adjusted. In addition, EnergyPlus tool was used to assess the effect of varying glass characteristics (type, position, and #layers) on DSF performance (Chan et al., 2009). Results showed importance of the a proper combination of all these parameters as it could reduce cooling demands significantly (i.e. up to 26%).

Baldinelli (2009) developed a new type of DSF for warm climates while shading elements are integrated into the external skin, which works as fenestrated/breathing envelope. DSF with newly developed concept could lead to better performance in both winter and summer if the system is adapted accordingly to ambient conditions. In regions with hot summer and cold winter, DSF with shading blinds and natural ventilation is the most common type (Zeng et al., 2012). More concern should be given to shading elements and ventilation modes as dynamic parameters of DSF.

Most importantly, assessment of the dynamic performance of DSF is highly necessary to determine its overall efficiency over the course of time

(day, season and year). According to Zhou & Chen (2010), DSF's dynamic performance highly depends on following aspects:

- **Ventilation of cavity:** type and operation mode (Jiru and Haghighat, 2008).
- **Shading system:** location, characteristics and dynamic operation. Characteristics of shading include size, tilt angles, materials and colour (Gratia and De Herde, 2007c).
- **Materials,** mainly glass type and properties (Gratia and De Herde, 2007b; Chan et al., 2009). Properties of opaque elements are also important.
- **Cavity parameters,** including geometry and size (Zöllner et al., 2002; Gratia and De Herde, 2007b). Cavity's size is determined by height, width, and depth.
- **DSF's construction** (Gratia and De Herde, 2007a; Saelens et al., 2008).

The importance of dynamic performance increases in regions with considerable fluctuations in outdoor conditions. Nowadays, dynamic analysis is available through several computational applications.

To conclude, the plenty of researches on DSF indicates the complexity of its operation and difficulties of predicting its performance. However, many aspects would determine the performance of DSF's system: thermally and visually. These aspects include constructional (fixed) and operational (dynamic) parameters. Fixed parameters include cavity configuration, openings design, materials, etc. Dynamic parameters indicate the operation of shading, openings, and ventilation of cavity. Therefore, system performance would significantly rely on the successful combination of both fixed and dynamic parameters. Consequently, the successful integration of DSF system with its building depends on how the system would response to dynamic conditions including ambient and indoor conditions. The importance of dynamic response becomes greater when the system is expected to

experience considerable fluctuations in the ambient conditions like in regions with hot summer and cold winter.

4.1.4 Common Issues Associated with DSF Systems in Hot Conditions:

During the last few decades, increasing large glazed constructions in hot climates highlighted several relevant problems including uncomfortable thermal indoors and significant cooling demands (Simmler and Binder, 2008). Indeed, these two indications come out as results of two major relevant phenomena under hot conditions, which are excessive solar gains and indoor overheating. As DSF mainly consists of transparent glazed elements, it is highly predicted to face these two scenarios. Thus, its performance is always threatened in such conditions.

4.1.4.1 Excessive Direct Solar Gains:

Generally, using glass with large exposed areas for buildings in hot climates would increase total transmitted solar gains (g-value) by several means. Practically, transmitted rates depend strongly on several factors including properties of the glass (transmittance, reflectance & conductance) and ambient conditions (solar irradiance, incident angles). Optical properties of glass rely on the angle of incidence as solar transmissivity would decrease by increasing this angle (Baldinelli, 2009). On the other hand, solar irradiance relies considerably on the site's coordinates, season and daytime. Solar irradiance consists of the beam and diffuse components.

Direct beam solar gains are a shortwave irradiance and counted as the dominant contributor to total g-value in glazed buildings, which could

dramatically increase the indoor temperature in hot conditions (Simmler and Binder, 2008; Baldinelli, 2009). According to Zhou & Chen (2010), direct beam solar gains are considered as one of the main obstacles in applying DSF in hot-summer and cold-winter zone in China. Indeed, this fact is more common for extreme hot conditions. Direct beam solar gains to indoor space are expected to increase with decreasing cavity's width of DSF (Radhi et al., 2013). On the other hand, airflow rates in the cavity are highly affected by incident radiations (Balocco, 2002). Thus, with proper sun protector for indoor, high incident radiations could be helpful in removing more trapped heat from ventilated cavities.

4.1.4.2 Indoor Overheating:

In addition to excessive direct solar gains, high levels of internal heat gains (including human body metabolic radiations, electric lights, and equipment) will cause an overheating issue indoors. This section provides a general overview of the issue of overheating in buildings. Then, more details are presented regarding overheating in DSF's cavity itself and indoor spaces. Within this section, problem's causes and results are concluded while next section highlights common solutions and its feasibility for DSF system.

■ Overview of Overheating Phenomenon:

- What is Overheating?

Simply, overheating is a term that expresses undesirable/uncomfortable thermal conditions inside the space. Based on different sources, overheating could be defined as:

- *"the accumulation of warmth in a building to an extent where it causes discomfort to the occupants"* (Architects, 2012).
- Banfill (2012) highlighted indoor overheating based on the type of buildings. **In residential buildings:** *"High temperatures in a dwelling at night may cause discomfort"*. **In office buildings:** *"An office constantly exceeding an afternoon threshold may be deemed unfit for purpose"*.
- With more practical explanation: *"When the benchmark temperature is exceeded the building is said to have 'overheated' and if this occurs for more than the designated amount of time the building is said to suffer from 'overheating'"*(CIBSE, 2006).

Obviously, CIBSE definition provides more flexible scale where overheating of the building is assessed through measuring its temperature against specific temperature point that related to the precise thermal comfort of the building and its location. For instance, by this scale, temperature peak points were determined to be 26°C and 28°C for the bedroom and living spaces, respectively, in the residential building while the designated period was determined as 1% of the annual occupied time (CIBSE, 2006). However, these set points are highly likely to be different in office buildings according to the different occupancy's behaviour.

While thermal comfort is well-defined as "that condition of mind which expresses satisfaction with the thermal environment" (BSI, 2005), there is no specific comprehensive definition for the overheating phenomenon and most importantly its thermal thresholds (Architects, 2012). However, it could still be characterized in relation to the maximum acceptable temperature for the indoor thermal comfort of space (CIBSE, 2006; BSI, 2007). To conclude, overheating could be simply presented as a thermal phenomenon that occurs

inside the building because of an excessive increase in indoor temperature for relatively long period; consequently, it will cause uncomfortable thermal conditions and affect the satisfaction of occupants.

- **What causes Overheating?**

Mainly, high temperatures are the direct indication of overheating. Temperature is increased significantly because of high levels of heat gains that could be internal, external or both. In addition, insufficient ventilation and external high temperatures could contribute in increasing possibility of overheating (Architects, 2012; Dengel, 2012). All these factors are common in summer times in hot and Mediterranean climates, thus overheating is highly likely to occur in such conditions.

As solar gains pass through transparent structures of the fabric, it will partially be absorbed by indoor surfaces (i.e. floor & ceiling) and other elements (e.g. furniture); and then be reradiated as a heat to surrounding space. During summer time, if the fabric is well insulated, this heat will be trapped inside and cause overheating. On the other hand, internal heat is usually produced through different means including lighting equipment, domestic appliances, occupants' metabolic gains and building services systems. However, overheating will increase in case of limited air change of the space as proper ventilation will help in removing considerable part of these gains continuously (Architects, 2012; Dengel, 2012). To conclude, while outdoor conditions could maximize space's overheating through excessive solar gains, building's fabric design and equipments could considerably contribute to this issue as well.

- **How Overheating affects occupants' health?**

Similar to outdoor temperature, the indoor high temperature could cause health risks for people but at different levels. However, the effect of overheating on occupants can vary from thermal discomfort to less productivity and probably serious health issues if overheating was severe and for long times over the year (Dengel, 2012). These health issues may include illness from respiratory and cardiovascular diseases in addition to irritating to eyes, throat, and skin (Webster, 2014; HUB, 2015; Dengel et al., 2016). Hence, the impact of indoor overheating on human body should carefully be considered especially that occupants usually spend most of their time inside (Government, 2012). In office buildings, for example, this influence is highly critical as the majority of staff usually works during the daytime when outdoor temperatures are extremely high with high solar gains, in summer.

- **How to Reduce Overheating?**

Many strategies could contribute to overcome overheating issues in buildings, which include:

- **Occupant behaviour:** it is highly important to make the users aware about causes of overheating (Architects, 2012). Therefore, their awareness of the problem would help in minimizing its possibilities through either participation in space's design or operating & using of space's equipments.
- **Proper Ventilation:** high rates of air change would help in removing a large part of trapped hot-air from inside through what is called Purge Ventilation (Architects, 2012).
- **Thermal Mass:** materials with high thermal mass could temporary absorb more of indoor heat during the daytime. Simultaneously,

indoor air would be cooled down and opportunity of overheating is minimized. Stored heat could easily be removed to outside by proper night ventilation (Architects, 2012; Dengel, 2012).

- **Window Design:** should consider openings' area and materials that would determine the amount of solar gains. Also, it should consider the possibility of both daytime and night-time ventilation (Architects, 2012).
- **Shading systems:** shading could be provided for both openings and whole fabric. Different types of shading are available for glazed openings and building envelope (Architects, 2012). These elements can help in preventing a considerable portion of direct solar gains from passing to inside or heating up the envelope itself.

■ **Overheating with DSF systems:**

As discussed in above section, overheating is highly possible to occur in glazed buildings under hot conditions. Thus, it is highly expected in buildings with DSF in hot, warm and Mediterranean regions. Also, DSF's cavity is where overheating supposed to occur as its temperature might keep increasing significantly in hot conditions (Gratia and De Herde, 2004b). Obviously, possibilities of overheating increase when extreme outdoor temperature coincide with high levels of solar irradiance. As mentioned earlier, this thermal phenomenon is still considered as the main drawback in front of applying DSF in hot conditions (Hamza, 2004; Manz and Frank, 2005; Zhou and Chen, 2010).

With the overheated system, heated air would be trapped inside its cavity and, if not removed, its temperatures would be increased to dramatic levels. This would increase heat transfer rates to inside through the inner layer

as well as different infiltration and direct ventilation means. At the same time, large glazed layers would allow considerable solar gains to penetrate directly to indoors especially if the inner layer is fully glazed. As a result, indoor temperatures would rise and exceed the thermal comfort leading to a serious indoor overheating. Consequently, cooling demands would be increased significantly. In some cases, cooling loads might become much important than heating ones taking in consideration that DSF was initially introduced for heating purposes (Hamza, 2004; Gratia, 2006; Gratia and De Herde, 2007c). Technically, both poor design and improper operation are responsible for this scenario (Gratia and De Herde, 2007c; Zhou and Chen, 2010).

In regions with hot and cold times, microclimate conditions over the year should be considered carefully; and system components should be investigated well in early stages of design to avoid any overheating threats in future. Successfully, DSF could be adapted with several incorporated passive and active techniques to overcome this issue. Most importantly make good balance in intended savings of energy between heating and cooling times.

4.1.5 Common solutions for Excessive Direct Solar Gains and Overheating by DSF Systems:

Generally, several passive strategies can be used to overcome building overheating including passive cooling strategies. Indeed, these strategies are highly necessary for buildings with DSF in hot conditions to minimize the possible overheating thus reduce cooling loads. Passive cooling strategies include ventilating indoor spaces, ventilating system cavity, applying shading techniques (Gratia and De Herde, 2004b; Gratia and De Herde, 2007c; Zhou

and Chen, 2010) and manipulating glass characteristics (Wang et al., 1999; Hamza, 2004). Next, some techniques are summarized as follows:

4.1.5.1 Window and Glass Characteristics:

While DSF itself is considered as a mean of solar protecting “shading”, enhancing properties of its transparent elements would considerably improve its function. Therefore, glass properties are widely considered to adapt glazed facades in hot climates (Hamza, 2004). Thermal and optical properties of glass are vital factors in determining the efficiency of several means of solar heat transmission through these surfaces (Poirazis, 2004; Pérez-Grande et al., 2005).

In cold and moderate climates, the outer skin of cavity is used to be constructed with clear glass while inner skin has wide variations in terms of layer's number and thermal properties (Hamza, 2004). Obviously, using clear glass for outer skin would allow more solar gains into a cavity in cold conditions, which increases cavity temperatures and creates a better thermal buffer zone. At the same time, using double glass for inner skin would reduce heat losses from indoor to the cavity, leading to considerable reductions in heating demands. In warm conditions, the double glass for inner skin could reduce cooling loads slightly (Wang et al., 1999; Hamza et al., 2001). This is probably because of expected reduction in heat transfer (i.e. conduction) from the cavity to indoor through the double glass. However, such reduction and relevant savings in hot conditions should be investigated well to see its feasibility.

On the other hand, constructing DSF with double glass for outer skin is not guaranteed to perform greatly even in cold climates. For instance in the UK with such construction, while heating demands reduced slightly in winter, cooling demands increased by 30% in summer compared to single glass layer for outer skin (Wang et al., 1999). This is because of trapped heated-air inside the cavity in summer that would increase heat transfer to indoor. Consequently, results of DSF with double clear glass for outer layer are expected to be even worse in hot conditions. However, replacing clear glass of double glazed outer layer by proper selective glass could give better results (Chan et al., 2009).

In hot arid climate of Cairo, changing glass properties was the main shading technique that used to improve DSF performance (Hamza, 2004). System performance was investigated with three different types of glass for outer skin: clear, body-tinted and reflective. U-value was similar for all types while solar shading coefficient (SC) was set as 0.89, 0.59 and 0.27 for clear, body-tinted and reflective respectively. Compared to clear glass, DSF with body-tinted glass could largely reduce cooling demands for both seasonal and annual consumption rates. Moreover, a system with reflective glass indicated more reductions in cooling demands as it was reduced by 35% annually. This privilege for reflective glass with DSF was again confirmed (Hamza, 2008). In Hong Kong, DSF was investigated where outer and inner layers were constructed with double reflective glass and single clear glass respectively. This proper combination (type of glass, number of layers and out-in order) indicated 26% saving in annual cooling demands compared to single skin

façade with single absorptive glass (Chan et al., 2009). In UAE with extreme hot arid conditions, DSF was tested whereas three properties were investigated for glass: U-value, solar heat gains coefficient (SHGC) and emissivity (Radhi et al., 2013). SHGC had the largest impact on thermal performance and cooling loads reductions. In such conditions, it is recommended to decrease SHGC to reduce heat transfer rates. However, coupling low values of SHGC and U-value could increase overheating possibilities.

Window-wall ratio (WWR) of inner skin is thought to be vital for DSF performance (Gratia and De Herde, 2007a). Based on a field survey, this ratio was set to 40% in a study on DSF for office buildings in Cairo (Hamza, 2004). In Hong Kong, DSF was investigated with WWR was set to 60% (Chan et al., 2009). However, for some buildings, this ratio is required to be up to 100% forming a full glazed envelope. Surely, this could increase the possibility of overheating thus cooling demands.

Optically, considerable reductions in indoor daylighting are expected with some types of glass especially at back areas. At the same time, high levels of illuminance are still predicted in front areas (close to the façade), which require the use of optical adaptive means (Hamza et al., 2007). Thus, more balance between solar and optical influences should be done with changing glass characteristics (Radhi et al., 2013).

To conclude:

- While number of panes for outer skin seems to be not efficient in controlling summer overheating, enhancing its properties is much recommended to reduce total solar heat gains.
- While using double glass for inner skin would give some reductions in cooling demands under warm conditions, it is highly recommended to investigate the influence of double glass under hot conditions based on the individual case of study.
- Generally, improving thermal and optical properties of glass are highly recommended in hot regions. For instance, solar reflective glass is a good option to reduce total solar heat gains into both cavity and indoor, thus minimize the possibility of overheating then cooling demands.
- Optically, considering glass properties as the main cooling strategy would keep in-out visual continuity without interruption of using traditional shading elements. However, manipulating glass properties might affect negatively the quality of indoor daylighting with poor distribution and probably glare. Thus, indoor blinds might be needed!

4.1.5.2 Green Cavity “Plants in Cavity”:

In addition to the aesthetic and psychological effect of having plants in space, it can bring significant thermal benefits as well. In office buildings with DSF, plants can be placed inside the cavity to work as a climate moderator. In an attempt to investigate this influence, Stec et al. (2005) developed a model to perform the study. Compared to blinds, results showed that cavity integrated with plants can better contribute to indoor thermal comfort and energy saving. Significantly, temperature of the plant was two times lower than blinds, which led to considerable reduction in temperatures of both layers of the cavity. However, its influence on winter heating has to be further

investigated. In addition, methods of constructing these plants within the system have to be also investigated.

4.1.5.3 Passive Shading & Ventilating the Cavity:

As mentioned before, the cavity can be either naturally, mechanically ventilated or mixed-mode. Natural ventilation for the cavity is more recommended to avoid mechanical ventilation loads. With sufficient ventilation, cavity-trapped heat would be removed so overheating would be minimized. Furthermore, incorporating shading elements in cavity would also act as passive shading technique that would stop part of direct solar gains from passing to indoor. However, cavity's temperature might increase with these elements. But, with ventilated cavities, trapped heat would continuously be removed, which ensure lower heat transfer to indoor (Gratia and De Herde, 2007c; Zhou and Chen, 2010).

Thus, a successful combination of these two techniques would minimize possibilities of both indoor and system overheating. However, failure in applying or operating any of these two strategies (proper shading and sufficient ventilation) could result in reverse behaviour (Zhou and Chen, 2010). Therefore, precise planning for these techniques should be done carefully as early as possible through design stages. More details regarding the combination of shading and ventilation of the cavity are presented later in this chapter.

4.1.6 Conclusion:

The cavity is the core element of DSF, where overheating is supposed to occur in hot conditions, which is still the main drawback in front of wide

spreading of DSF in hot regions. Thus, more concern should be given to cavity design and most importantly its operation. Several cooling techniques are available to overcome cavity's overheating; including its ventilation, installing shading elements and manipulating glass characteristics. Applying both integrated-shading and cavity's ventilation can reduce predicted overheating during summer. However, these techniques should be addressed precisely in order to maximize its benefits and avoid unwanted effects.

4.2 Role of Cavity-Integrated Shading Devices in DSF

4.2.1 Overview:

As mentioned before, DSF is being recently used even in extreme hot arid climates such as UAE (Radhi et al., 2013). Referring to the construction of DSF, its outer skin could be almost fully glazed while being directly exposed to solar radiations over the year. In hot conditions, this increases total solar gains into both cavities and indoors, where the direct component is usually the main contributor to these gains.

To protect the system from excessive direct solar gains, proper shading elements are widely being used. These could be external, internal or integrated inside the cavity. Moreover, it could be screens, louvers, Venetian blinds etc. However, each of these techniques has its own pros and cons. At the same time, as one of DSF's functions is to protect shading elements itself from winds and other harsh ambient conditions, external shading option is usually excluded. In addition, the internal option could be a critical source for secondary heat gains (i.e. convection and re-radiation). Therefore, the cavity-integrated technique seems to be the most appropriate option.

To some extent, cavity-integrated shading is predicted to perform similarly to the internal shading in terms of heat reflection and absorption. Based on many design parameters, it will successfully block considerable portion of incident radiations inside the cavity and stop it from reaching indoor. Part of these reflections will stay inside the cavity and be absorbed by its components. Most importantly, this intermediate zone is not part of the occupied space.

As shading elements could act as heat collector (absorb part of incident solar and form a secondary energy source), it would heat up cavity's air and enhance its buoyant flow. Therefore, with sufficient natural ventilation, cavity-integrated elements could form a successful combination that enhances the performance of DSF systems in hot climates (Zhou and Chen, 2010; Zeng et al., 2012). However, the efficiency of such combination strongly relies on the design of shading elements (e.g. size, surfaces features), insulation level of the inner skin (Gratia and De Herde, 2004b) in addition to the quality of natural ventilation.

From an airflow perspective, a detailed analysis is usually required for suggested combination between cavity-integrated shading elements and its ventilation (Poirazis, 2004) as the presence of such elements could significantly influence both air velocity and airflow patterns inside the cavity, and then could influence heat transfer rates (Safer et al., 2005b). Following sections present characteristics of cavity-integrated shading system, and how could influence DSF operation. Finally, it highlights current problems and potential research gaps regarding this area.

4.2.2 Influence of cavity-integrated shading on thermal performance of DSF and Indoor:

DSF-integrated shading elements would divide its cavity into two asymmetrical thermo-flow fields, which is due to significant variations in solar energy absorption by different components of DSF; such as blind's surfaces, inner glass and outer glass (Xu and Yang, 2008). This would vary influence of these components on indoor thermal comfort through secondary heat transmissions.

Generally, convection heat transfer depends on the temperature difference between surface and air, the height of surface and velocity of air (in case of mechanical ventilations). As the presence of shading elements in cavity would influence its airflow rates, convection heat transfer associated with these elements would be affected. This covers convection by both elements themselves and glass layers (Safer et al., 2005b; Gratia and De Herde, 2007c). However, this influence depends on many parameters like the position of shading elements, their size and surface's characteristics. Radiation heat transfer mainly depends on the temperature difference between surfaces. In addition, size, shape and tilt angles of surfaces are also important for radiative heat exchange. This applies to integrated shading elements, where surface characteristics (i.e. emissivity) would have a significant role. Furthermore, solar radiation (incident levels and angles) would influence both convection and radiation caused by integrated slats.

In moderate summers, increasing secondary heat transmissions through DSF is expected to be low compared to reductions in direct solar

radiations. For instance, during summer in Germany, total energy transmittance to indoors was reduced effectively by using DSF with integrated shading (Eicker et al., 2008); and, cooling loads were consequently minimized. However, in extreme hot climates, as inner skin temperature could be significantly increased, secondary heat transmissions are highly critical to cooling loads even though integrated shading elements are still efficient to block direct solar gains.

With ventilated cavity in hot arid climate, it was revealed that shading's effect by simple dividing-plates, placed at floor-levels inside the cavity as shown in Figure 4.1, made cavity's temperature 7-12°C below ambient temperatures (Hashemi et al., 2010). Accordingly, the study claimed that shading the cavity properly could significantly reduce both cavity's temperatures and indoor cooling loads.

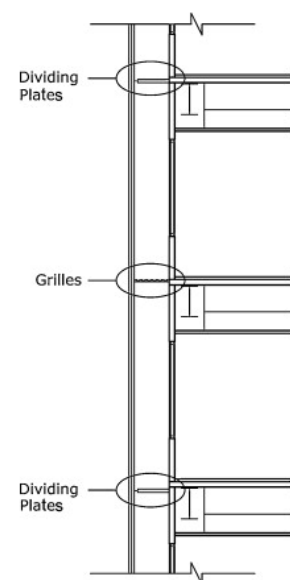


Figure 4.1: DSF with dividing plates and grilles. Source: (Hashemi et al., 2010).

Also, experimental and theoretical works were conducted on mechanical-ventilated DSF with Venetian blinds under hot summer conditions, where main variables were airflow rates and blinds' tilt angles (Gavan et al., 2007; Gavan et al., 2010). Results showed that temperatures for both cavity and indoor space were affected by blinds' tilt angle and cavity's airflow rates. Thus, successful control for blind inclination and airflow rates could prevent summer overheating and enhance indoor thermal comfort.

In regions with hot summer and cold winter, it is recommended to use DSF with integrated shading if shading is well-designed and -controlled with sufficient ventilation (Gavan et al., 2007; Zhou and Chen, 2010). This would minimize summer heat gains and winter heat losses, concerning indoor spaces; thus improve indoor thermal comfort and reduce energy consumption. For instance, a field study on DSF showed solar shading advantages to reduce energy consumption by 15% and 30% in summer and winter; respectively (Xu and Ojima, 2007).

Apart from DSF, a new multifunctional device was developed where solar collector was integrated into external shading devices (Abu-Zour et al., 2006). Absorbed heat by the surface of solar shading would be transferred to the integrated solar collector and more thermal energy would be captured. However, such idea highlights the concept of integrating proper solar collector system into cavity-integrated shading devices. By this combination, more thermal energy could be collected and extracted from the cavity. This would help to minimize possibilities of cavity overheating and thus reducing thermal loads of the façade. In addition, collected thermal energy could be stored and used for several purposes such as solar water heating.

To conclude, although using cavity-integrated shading elements would reduce direct solar gains, it could increase secondary heat transmissions to indoors due to possibilities of overheating of the cavity. However, ventilating the cavity sufficiently could help in overcoming this issue. Then, benefits from installing the shading element could be guaranteed without side-effects.

4.2.3 Influence of cavity-integrated shading on airflow of ventilated DSF:

Overheating inside the cavity is one of the dominant problems faced by DSF in hot climates. Its temperatures could considerably increase if airflow through the cavity is not sufficient to extract trapped heat. Mechanical ventilation could help overcoming this issue (Hamza, 2004) but it would increase total energy consumption. Therefore, natural ventilation is always preferred.

Airflow in naturally ventilated cavities is determined by either wind, buoyancy or both together. Buoyant airflow is driven by the difference in air density (due to temperature difference) between outside and inside of the cavity. For naturally ventilated cavities, complexity in airflow is usually experienced next to cavity's inlet, outlet and horizontal dividers (e.g. walkways) (Hamza et al., 2007). Furthermore, changes in flow fields are also expected in-between shading slats as well as between these slats and adjacent layers (e.g. outer skin). Level of changes usually depends on gap distance (Safer et al., 2005b; Zhou and Chen, 2010) and complexity of elements. However, good design/installation of shading elements (e.g. size, position, etc.) could successfully lead to significant enhancement in natural ventilation of the façade and avoid overheating (Ji et al., 2007).

In literature, airflow developments in DSF's cavity-integrated with Venetian blinds were studied (Safer et al., 2005b). 3D modelling with CFD was used while several design parameters were investigated including openings' position, slats' position, and its inclination angles. Results showed that shading

split cavity into two vertical sub-cavities. Lateral distance (by the position of shading) had a clear impact on air velocity. In addition, tilt angle for Venetian blinds influenced airflow field. This influence became more significant in case of a central position for blinds and became less important with large external lateral distance. Enlarging external lateral distance could enhance overall airflow and then extracting more trapped heat. However, in such case, blinds would be more close to the inner skin that could increase radiative heat exchange to indoors. Therefore, more attention has to be paid to ensure a balance between these two ways of heat transfer. In addition, Gratia and De Herde (2007c) confirmed the importance of the position of cavity-integrated slats on its airflow. Incorporating movable shading elements into the outer skin of cavity showed good results in terms of avoiding airflow complexity and overheating (Baldinelli, 2009).

Plenty of numerical computational models (e.g. CFD) are available to simulate developments in cavity's airflow and thermal fields (Zhou and Chen, 2010). However, the level of representation of cavity's components is a vital factor in simulation accuracy. **To conclude**, comprehensive modelling is highly necessary to understand the precise influence of cavity-integrated shading elements on its airflow and thermal performance.

4.2.4 Design parameters of shading elements:

These design parameters include the position of shading inside the cavity, size, inclination angle and shape. These usually determine shading impact on the cavity performance (Zhou and Chen, 2010); also surface's

characteristics (e.g. colour and emissivity) and material of shading could have a significant impact on the performance of DSF.

Several works on DSF have handled these parameters and under different ambient conditions (Safer et al., 2005c; Gavan et al., 2007; Gratia and De Herde, 2007c; Eicker et al., 2008; Gavan et al., 2010; Parra et al., 2015). Temperature and airflow in cavity were usually studied. In addition, indoor thermal performance was sometimes considered.

Effect of position and surface colour of cavity-integrated blinds on cooling loads of building was studied using TAS software. The effect was investigated for both closed and opened cavities. The building was assumed to be in Belgian (Gratia and De Herde, 2007c). Light-colour blinds showed better performance. Similarly, blinds with central position performed better. Most importantly, a proper combination between blinds' colour and position and good control for cavity openings could significantly enhance system performance as cooling loads were reduced by 24%. In addition, the research indicated that both colour and position of blinds could directly affect occupant thermal comfort through the undesirable radiative exchange in adjacent places to the façade.

The inclination angle of cavity-integrated Venetian blinds was investigated using 2D CFD model (Ji et al., 2007). Results showed that natural ventilation was improved by up to 35%. Consequently, solar heat loads of indoor was reduced by up to 75%.

Position and inclination angle of cavity-integrated shading slats were studied (Safer et al., 2004a; Safer et al., 2004b; Safer et al., 2005b). Results showed that impact of inclination angle on both temperature and flow fields inside the cavity would be influenced by the position of these slats as well as the level of direct solar radiations. Another work (Safer et al., 2005c) showed that convective heat transfer was significantly affected by airflow rates. However, these changes were not significant due to varying slats angles. Moreover, convection heat transfer was smaller than radiative heat transfer was. Nevertheless, the later was significantly influenced by slats angles. Based on CFD simulations, a nodal thermal energy model for DSF with Venetian blinds was developed to be implemented in BES tools (Building Energy Simulation). The new integration aimed to assess efficiently DSF's role in energy savings of buildings.

A mechanically-ventilated DSF with integrated Venetian blinds was studied by Gavan et al. (2007). The study was conducted using TRNSYS (transient system simulation tool) with DSF-nodal model from Safer et al. (2006). Moreover, climate data of Lyon (France) was considered. Both slat's angle and cavity's airflow rate were managed according to incident solar radiations and indoor temperatures. The system showed a good performance for both summer and winter. However, controlling the system was necessary to avoid summer overheating.

Full-scale model of mechanically-ventilated DSF with Venetian blinds was investigated under controlled environment (Gavan et al., 2010). System's behaviour was evaluated for different ventilation rates and inclination angles

of Venetian blinds. Both had a clear impact on the temperature of DSF and attached space. This was more obvious for inclination angles. With a maximum flow rate of the cavity, Venetian blinds with 35° angle led to best energy efficiency for DSF itself. However, the temperature of attached space reduced as inclination angle increased. Nevertheless, angles over 60° showed little further reductions. Therefore, large angles were not recommended, as they would dramatically reduce natural daylight with no significant thermal enhancement. Controlling both inclination angle of shading slats and external ventilation of cavity (by adjusting innovative outer-skin integrated louvers) enhanced the thermal performance of indoor space for both winter and summer (Baldinelli, 2009). The study recommended investigating further geometrical parameters (e.g. shape) of louvers and expected impact on daylight.

To conclude, using cavity-integrated shading slats would help in blocking part of direct solar gains to indoors. Therefore, adjusting slats' tilt angle could further reduce these gains, and save more energy by reducing cooling loads. However, tilt angle's adjustment could dramatically change cavity's airflow and then convection heat transfer. Moreover, it could increase radiation heat transfer to indoors. In addition to tilt angle, following design parameters of integrated slats could influence its role significantly and differently. These include size, position, materials and surface characteristics (e.g. colour, emissivity). Moreover, good control for these parameters (e.g. tilt angle) is highly efficient. Apart from thermal and airflow aspects, the

impact of these parameters on indoor daylighting should be taken into consideration.

4.2.5 Geometrical Shape of Individual Cavity-integrated Shading

Device:

As discussed earlier, with the presence of fenestrated shading elements, part of incident solar radiations will pass through the offset-distance between adjacent elements. However, the rest of radiation will be stopped by these elements then, be absorbed by its surfaces or reflected to outside, inside or next element. Scattering patterns for incident radiations are determined by the geometry of element, its surfaces' properties and direction of incident radiation. For different materials and shading designs, this character is known as bi-directional transmittance and reflectance function "BDTRF" (Lee et al., 2002).

So far, several studies have been conducted concerning different geometrical parameters (e.g. tilt, size, location) of integrated slats. Yet, exact shape (profile, layout, etc.) of more complex designs was not sufficiently investigated. In the literature of DSF, cavity-integrated shading devices were, not long ago, used to be introduced as horizontal slats while no extended description regarding the exact geometry of individual device-unit was clear (Poirazis, 2004).

However, some researches indicated the importance of geometry of slat-unit in addition to its surface's characteristics to system's performance (Manz and Frank, 2005). For instance, DSF with curvature Venetian blinds were modelled using CFD (Ji et al., 2007). Geometrical parameters including thickness (t_b), width (d), offset (P) and inclination angle were considered as shown in Figure 4.2. However, all parameters were constant except inclination angle varied throughout the study.

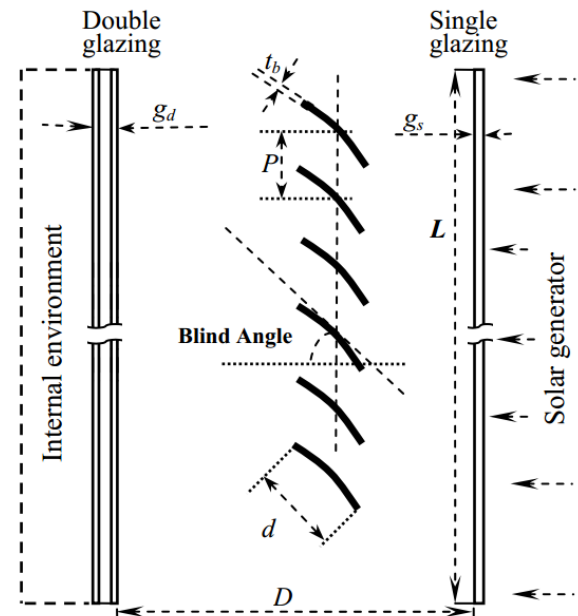


Figure 4.2: Geometrical Parameters of DSF cavity-integrated devices. Source: (Ji et al., 2007).

According to Arons (2000), absorbed heat by shading devices in ventilated cavity could be removed by convection process if sufficient air moved along surfaces of these devices. Therefore, the rate of conversion of stored heat into convection heat would depend on several factors including the geometry of devices (Mingotti et al., 2011). The shape could also affect both radiation heat transfer and natural daylight to indoor. Brownarch3230 (2011) proposed a multifunctional cavity-integrated louver with an elliptical shape. The concept was to enhance indoor daylighting and avoid cavity overheating. Design parameters included device's length, width, height, spacing, and angle. However, the design was not sufficiently investigated nor developed.

Therefore, it is among the author's objectives throughout this work, to investigate how manipulating different geometrical parameters of the device-unit would affect cavity's airflow and enhance its thermal performance. The work will include designs that are more complex than common ones (e.g. elliptical cross-section and simple curvature slat).

4.2.6 Thermal and Airflow Modelling of DSF and Whole Building:

It is still a time- and resource-consuming process to assess precisely the thermal performance of DSF-buildings. This is because of the interactive dynamic behaviour of DSF system in terms of airflow, thermal and optical aspects. This complexity becomes more significant as there is no efficient stand-alone simulation tool is capable to simulate accurately the comprehensive performance (with sufficient details and for transient period) of entire DSF-building (Hensen et al., 2002; Manz and Frank, 2005; Zhou and Chen, 2010). At the same time, comprehensive detailed modelling is highly necessary to understand the precise influence of cavity-integrated shading devices on the performance of DSF and its building as well.

Various mathematical models are used to simulate DSF and evaluate its performance. Other building energy simulation (BES) packages like TAS, TRNSYS, and EnergyPlus are also used to assess both DSF system and spaces serviced by the system. However, many contributions have been done to develop numerical models for DSF systems to be implemented into available BES tools.

Referring to relevant literature, there are two main trends concerning the modelling of DSF:

4.2.6.1 Modelling DSF system alone:

In addition to experimental work (field measurements or laboratory-works), different methods are available for modelling DSF systems and their buildings. This section presents a brief for some of these models:

- **The Lumped Model:**

The lumped model uses a single node approach to represent each element of the system including glass layers and its cavity. It uses a prediction technique to estimate several unknown parameters including convective heat transfer coefficients. Predictions are widely based on previous experimental works (Park et al., 2004). An example of lumped models for CFD with Venetian blind can be found in (Xu and Yang, 2008).

- **Airflow Network Model:**

This model uses a network of nodes to represent building zones (e.g. rooms), system components (e.g. glass layers) and flow paths inside the buildings (Hensen et al., 2002). Although it is based on a network of several nodes, it is still limited to simulate significant distribution and variations in fields of temperature and airflow inside both DSF and spaces. However, it could be coupled with different BES tools. For instance, Thermal building simulations (TRNSYS) were successfully coupled with nodal airflow network simulations (COMIS) for simulating ventilated DSF system (Haase et al., 2009).

- **Control-Volume Model:**

It is among available models used to simulate DSF (Ahmed et al., 2016). It is based on dividing DSF structure into several control-volumes in the flow direction (e.g. 1m-high each). Then, each control-volume is represented by set of one-dimensional nodal models in the other direction (i.e. perpendicular to façade's layers).

- **Zonal Model Approach:**

This model divides DSF again into several control-volumes using cells similar to that used in CFD but larger. Temperature distribution can be assessed based on this approach with more accuracy than other models except for CFD that still has the higher accuracy but time-consuming. The zonal approach was used to investigate a mechanically ventilated DSF system with Venetian blinds (Jiru and Haghighat, 2008).

- **Computational Fluid Dynamics (CFD):**

CFD is a robust tool for modelling thermodynamics and fluid dynamics of DSF structures. CFD could simulate heat transfer mechanisms as a full conjugate problem through considering heat convection, conduction, radiation in addition to potential complex airflow outside and inside the cavity (Manz and Frank, 2005; Hamza et al., 2007). In addition, it is able to simulate thermal performance and airflow of the entire DSF-building with high accuracy.

Safer et al. (2005) used 3D CFD model for simulating airflow of within DSF with Venetian blinds. These blinds were represented by a homogeneous porous media model to reduce the number of cells and save computing time. Porous media model aimed to represent the effect of Venetian blinds presence inside the cavity relying on relevant pressure losses. CFD showed a good capability to simulate DSF using either actual Venetian blinds or the porous model. Zeng et al. (2012) again used the porous model with CFD for modelling naturally ventilated DSF with Venetian blinds. Good agreement was achieved.

Ji et al. (2007) used 2D CFD to model airflow in DSF considering the effect of radiation, conduction, and natural convection. Generally, the results showed the ability of CFD to do the task with or without integrated Venetian blinds. However, 3D modelling was suggested for better accuracy in further works. Furthermore, Hamza et al. (2011) used CFD model (CFX code) to conduct a comparative analysis on natural ventilation by non-uniform DSF.

Pasut and De Carli (2012) proposed a comprehensive strategy for modelling DSF using CFD. Generated approach was based on a comparative and sensitive analysis. The aim was to set most the accurate but simplest model with lowest computing-resources. All set models were validated against experimental work. Results showed the importance of modelling outdoor environment. Less importance was found regarding the necessity of 3D modelling.

Brandl et al. (2014) studied, using a steady-state 3D CFD model, airflow and thermal performance of a multi-functional façade with three different

constructions. The variation was related to having either Photovoltaic module, solar thermal collector or transparent glass layers. Results showed that replacing the glazed outer skin by either PV modules or solar thermal collector would lead to higher air temperature inside the cavity. Thus, ventilating the cavity is highly recommended to avoid overheating in summer.

Parra et al. (2015) used CFD to model airflow and heat transfer for DSF system. The study aimed to assess the influence of optical properties of materials, construction (geometrical relationship of Venetian blinds) and operation (flow stream) parameters of the system on solar loads of building and energy saving. The system was investigated with and without Venetian blinds and for natural and forced ventilation mode. Results indicated that position of Venetian blinds (distance from outer skin), as well as surface characteristics of both inner and outer surfaces of Venetian blinds, could significantly affect DSF thermal performance and then total heat gains into the building.

In addition, different works to develop new nodal models for DSF were based on relevant CFD simulations (Safer et al., 2005a; Safer et al., 2005c). Furthermore, the reliability of CFD to simulate DSF was approved through several works (Manz, 2003; Manz et al., 2004; Manz, 2004).

Compared to CFD model, other models (e.g. nodal model) have clear limitations in its resolution and/or assumptions (e.g. convective heat transfer coefficients). In addition, CFD can efficiently consider precise details of DSF system including configuration, ventilation modes, and complex Venetian

blinds. Moreover, it can reliably model the complex airflow outside and inside the cavity.

Recently, Wang et al. (2016) used an improved zonal approach with a dynamic optical model of the Venetian blinds and airflow network model to model a mechanically ventilated DSF in hot summer and cold winter regions in China. The new approach showed a good agreement and more time-saving compared to conventional tools. Results showed that both inner glass temperature and total heat gains would decrease with increasing either cavity's flow rate or slats' angle. Slats had more significant impact. For example, heat gains dropped by 63% with slat angle of 60° compared to the angle of 0° .

4.2.6.2 Modelling the whole building equipped with DSF (DSF-building):

Nowadays, based on the nodal network method, many applications are able to model simultaneously both thermodynamics and fluid dynamics of buildings. This includes conduction, convection, radiation, ambient solar gains, internal gains, airflow and HVAC loads. The comprehensive integrated approach of these applications in addition to time-saving and possibility of transient simulation increase their reputation as good energy-design tools.

Based on this concept, many researches used individual Building Energy Simulations (BES) packages to simulate the whole DSF-building. TAS (Thermal Analysis Simulation Software) was used as a stand-alone tool for investigating the natural ventilation through DSF (Gratia and De Herde, 2004a; Gratia and De Herde, 2004c; Gratia and De Herde, 2004b). Later on,

same authors used TAS for investigating the operation modes of DSF (Gratia and De Herde, 2004d) and optimizing the shading devices within its cavity (Gratia and De Herde, 2007c). In addition, Alibaba & Ozdeniz (2011) used TAS to conduct a parametric study on DSF in a warm climate; generally, TAS results were in good agreement with results from real measurements. Hashemi et al. (2010) used EnergyPlus (version 2.1) tool to simulate the thermal performance of ventilated DSF in hot arid climate; however, there was significant disagreement between simulation results and field measurements due to the inability of EnergyPlus to simulate accurately the airflow in DSF cavity.

Obviously, relying only on BES (based on nodal network method) would lead to less accurate prediction of both indoor temperature and airflow distribution, which are necessary to assess indoor thermal comfort. For instance, DSF could experience significant variations in both temperature and air velocity along its height as well as width. Thus, it is not sufficient to represent the entire structure with just one zone.

For that reason, using results of detailed modelling of DSF for BES of the entire building is highly recommended. This could happen through coupling process.

Several works showed attempts to implement special developed nodal models of DSF into available BES applications. Gavan et al. (2007) implemented a nodal model of mechanically ventilated DSF with Venetian blinds into TRNSYS. Poirazis (2007) employed two different simulation tools

for investigating thermal and energy performance of DSF-office building with various constructions in Göteborg, Sweden. WIS3, a developed 2D simulation tool, was used for the parametric study and IDAICE3.0 (a BES) was used for energy analysis. Haase et al. (2009) linked a nodal airflow network model of ventilated DSF with roller blinds to TRNSYS, as well. In addition, more works on integrating nodal models of DSF into TRNSYS were done (Saelens et al., 2003; Saelens et al., 2005). Moreover, Chan et al. (2009) implemented an airflow network model of DSF into EnergyPlus tool to assess the energy performance of DSF with different configurations in Hong Kong.

All these attempts aimed to improve the accuracy of simulating DSF system as a part of the whole building. However, some shortcomings in these combined models are still cannot be ignored. This due to the concept of limited nodes in the developed integrated models.

Therefore, Manz & Frank (2005) set a method for simulating the whole DSF-building. This method is based on the concept of coupling of three different modelling levels, which are a *Spectral optical model*, *DSF simulation model* and *Building simulation model* as shown in Figure 4.3.

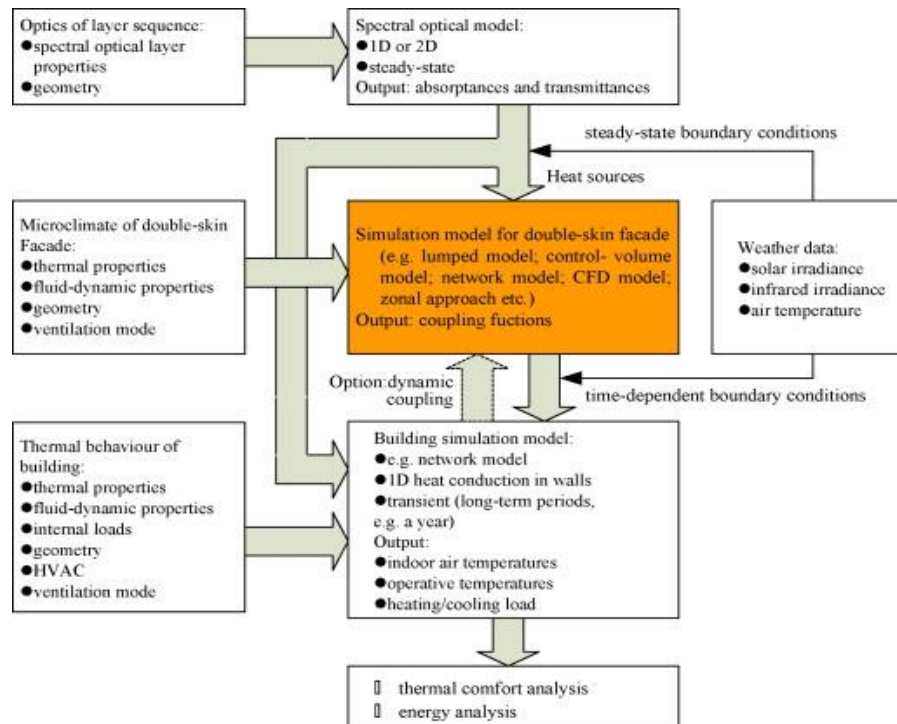


Figure 4.3: Concept for Simulation the entire building equipped with DSF system, provided by Manz & Frank (2005) and updated by Zhou & Chen (2010). Source: (Zhou and Chen, 2010).

Specifying the geometry's characteristics and materials' properties is highly important for each level. In addition, time-dependent weather data (e.g. 1h-time-step data) is required. Following a brief for each level of modelling:

- **Spectral optical model:**

Based on optics of different layers of multi-layer DSF, both absorptance and transmittance are calculated through special tools like GLAD (Research, 2015), WINDOW (Mitchell et al., 2013) or others. Using incident radiations, the calculated absorptance is used to find out heat sources in various components of DSF (glazed panes, integrated shading, opaque elements,

etc.). Consequently, given values of heat are implemented into DSF simulation model, like CFD. This implementation forms the first coupling stage (Manz and Frank, 2005).

- **DSF Simulation Model:**

This model aims to simulate accurately both airflow and associated heat transfer of DSF. Its main objective is to predict both temperature and velocity fields inside the cavity. CFD is a common and robust tool to do this task (Manz, 2003; Manz et al., 2004; Manz, 2004; Manz and Frank, 2005) but other models (e.g. lumped, airflow network models, etc.) could also be used instead of CFD (Zhou and Chen, 2010). However, CFD still has the best reputation among others in term of accuracy even though it is resource- and time-consuming. As mentioned earlier, the optical-model output is used to determine the boundary conditions (e.g. heat flux sources) for CFD model in addition to other boundary conditions (e.g. ambient air temperature, air velocity, etc.). However, simulations are usually performed as steady-state or for short transient periods (e.g. few hours).

- **Building Simulation Model:**

Results of modelling DSF are represented as functions to be implemented into Building energy simulation (BES) model. The later is used to simulate the whole building equipped with DSF. Another coupling is required to find out direct solar gains into the building. The calculated transmittance by the optical model is used to calculate these gains based on incident direct solar energy.

Manz & Frank (2005) gave an example of his proposed approach. Three models were employed. GLAD tool was used to calculate optical properties for the system then find out heat sources, which in turn were implemented into CFD model. CFD was used to calculate both cavity temperatures and indoor airflow as functions of ambient air temperature and solar radiation. Second coupling was between CFD and HELIOS program. Coupling was for the two functions: cavity temperature and indoor airflow induced by the cavity ventilation. By implementing these functions into HELIOS, both cavity temperatures and indoor airflow are being adjusted according to outdoor ambient conditions. This would ensure better accuracy for simulating cavity airflow and heat transfer with varied ambient conditions. Then, HELIOS is used to find out hourly operative room temperatures with more details. Later on, Baldinelli (2009) used the same approach to study his own innovative design of DSF for warm regions.

Hien et al. (2005) coupled CFD model with TAS tool to ensure precise simulating of airflow in the cavity. The work aimed to investigate the influence of DSF on energy loads, thermal comfort, and condensation issue for an office space in Singapore. Xu and Yang (2008) applied the three models approach (optical model, heat transfer model, and CFD model) to analyze natural ventilation through DFS with Venetian blinds. Radhi et al. (2013) conducted their work using a combination between Design-Builder (EnergyPlus engine-based) and CFD (PHONICES-FLAIR model). CFD was used to model both DSF's cavity and its outdoor surrounding. Coupling was done for temperature and

radiation between the two models. The work aimed to investigate possibilities of reducing cooling loads by implementing DSF for office buildings in UAE.

Loonen et al. (2014) worked to improve a simulation-based approach to support decision-making for research and development (R&D) of innovative building envelope technologies. To form a computational approach, BES was combined with analytical structured parametric studies to afford sufficient information regarding the performance of different technologies. This approach increases the reliability of analysis and decision-making based on whole-building performance information (with a variety of scenarios and boundary conditions) rather than depending on trial & error approaches (e.g. pilot studies). Recently, Angeli and Dama (2015) proposed a simplified model of heat transfer in DSF to be implemented with BES tools for dynamic simulation of natural ventilated DSF. The simplified model was validated against both CFD model and experimental data. The simplified model aimed to better simulated DSF performance at a reasonable time- and computing-resources.

Amarala et al. (2015) conducted a parametric study on the influence of the size of double glazed window, its orientation and shadowing on the energy performance of space in the Portuguese city of Coimbra. The parametric study was conducted based on two algorithms, and the operative temperature was determined using EnergyPlus(8.1.0). The dynamic study aimed to reduce the time of thermal discomfort and reduce both heating and cooling energy consumption. Results indicate that using windows' overhang could reduce cooling loads; and allow for larger glazed openings. However, considering

optimum window size is preferable over using overhangs with large openings for better thermal comfort.

4.2.7 Conclusion:

To conclude, the proper combination of both techniques (shading and airflow) is highly necessary for successful implementation of DSF in hot conditions. However, the additional concern should be given to the optical performance of the system. Moreover, careful design for DSF's cavity-integrated shading system is highly important as it could result in sufficient levels of indoor thermal comfort and energy saving in hot summer. In addition, controlling approaches for both shading system and ventilation are quite recommended. Good optimization of the system could result in dual benefits including cooling and heating year-round.

- **Influence of cavity-integrated shading:**

Several studies have already been conducted to investigate the influence of several geometrical parameters of cavity-integrated devices on both airflow and thermal performance of DSF System. These parameters include position, size, tilt angle, colour, etc. Generally, varying these parameters could lead to a significant influence on the performance of both system cavity and indoor spaces. However, this influence is also affected by both configuration of the system as well as microclimate boundary conditions.

At the same time, there is now sufficient knowledge regarding the influence of the exact shape of individual device-unit on such performance.

Therefore, it is among the author's objectives throughout this work, to investigate how manipulating different geometrical parameters of the device-unit would affect cavity's airflow and enhance its thermal performance. The work will include designs that are more complex than common ones (e.g. elliptical cross-section and simple curvature slat).

- **Modelling Tools:**

Regarding the modelling tools, various models were developed to simulate both thermal and airflow performance of DSF. Among all these models, CFD showed the best accuracy although it is still time-consuming and requires high computing facilities. CFD's accuracy comes from its ability to simulate comprehensively both airflow and associated heat transfer outside and inside the structure and with high resolution. For simulating the whole DSF-building, the tripartite coupling method (Manz and Frank, 2005) showed a good contribution for simulating both DSF structure and attached building; outside and inside environments.

4.3 Natural Daylighting and Potentials with DSF

4.3.1 Overview:

In highly luminous climates, artificial lighting of an office building can contribute in up to third of its net energy consumption on a summer day (Ochoa and Capeluto, 2006). However, while the minimum required indoor illuminance level for office work is 300Lux (CIBSE, 2006), utilizing natural daylight in such climates is highly recommended to reduce the associated consumed energy and get better visual comfort (Leslie, 2003; Ochoa and Capeluto, 2006). In addition, natural daylight could help controlling what is

called “circadian system” of occupants (Webb, 2006). Generally, daylight illuminance and then visual comfort depend on both weather conditions and sun altitude (Heim et al., 2011) in addition to the features of space.

Glass has a significant positive impact on human well-being through its high transparency to outside and ability to provide natural daylight. DSF as a glazed structure could increase natural daylight presence and enhance visual continuity to outdoor (Hendriksen et al., 2000; Hamza et al., 2007). Obviously, utilizing the natural daylight through DSF has a significant priority hand in hand with its thermal role. Therefore, proper investigating of DSF is highly recommended to control light levels and avoid both overheating and glare.

4.3.2 Innovative daylighting systems:

Innovative natural daylighting systems usually aim to improve indoor daylight quality (in particular for deep and back perimeters), enhance its uniformity, reduce glare issues, and also reduce direct solar heat gains (Littlefair et al., 1994). The light shelf is among various elements used for this purpose. Figure 4.4 and Figure 4.5 show how light-shelf works and could improve indoor daylight quality.

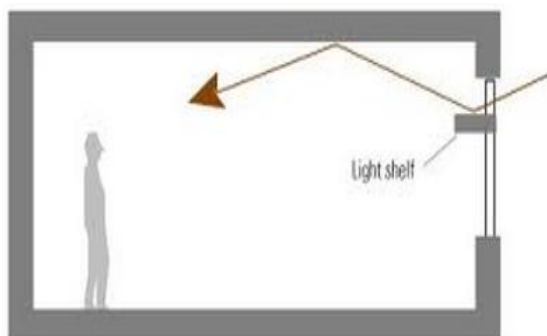


Figure 4.4: Light shelf can reflect the light to deep points inside. Source: (MGAE, 2017).

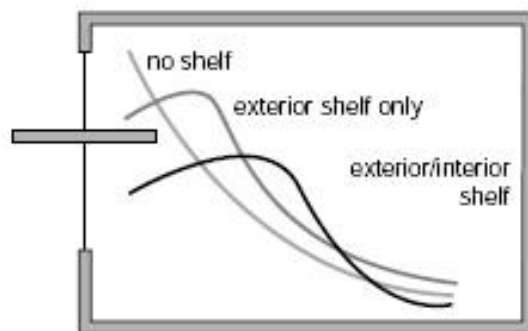


Figure 4.5: Improving the indoor daylight distribution using the light shelf. Source: (D.LiTE, 2017).

Plenty of daylighting systems were developed, which differ in terms of application and efficiency. Some are being used for direct sunlight while others for diffuse sunlight or skylight. While some are attached to either side of façade (interior or exterior), others can be incorporated between two pairs of glass. Simple Louvers, slats, and Venetian blinds can act as shading and lighting devices; Figure 4.6-A. Also, light shelves are available with several designs, Figure 4.6-B & C (Kischkoweit-Lopin, 2002).

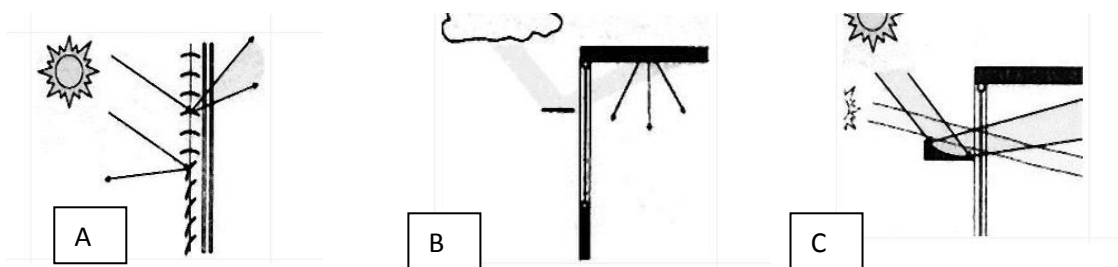


Figure 4.6: A) Shading slats act as lighting devices. B & C) Different designs of Light Shelf; source: (Kischkoweit-Lopin, 2002).

More advanced techniques for daylighting were developed under what is called “Okasolar System”, which is a pair of glasses enhanced with fixed microdevices in-between the two layers. These devices are designed with various shapes to ensure specific optical purposes; Figure 4.7 and Figure 4.8.

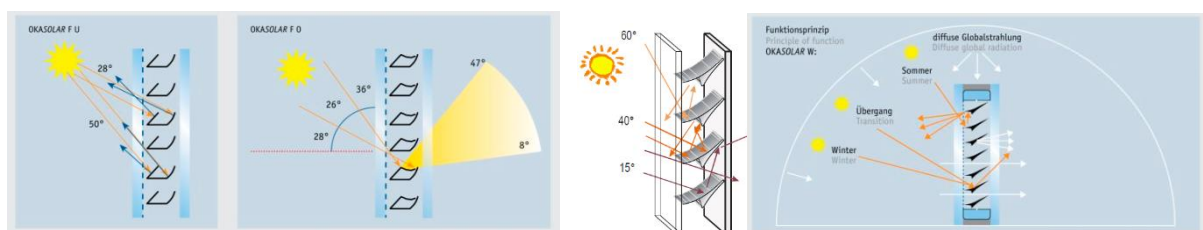


Figure 4.7: Several designs of Okasolar Glass systems. Source: (OKALUX, [n.d.]-a).

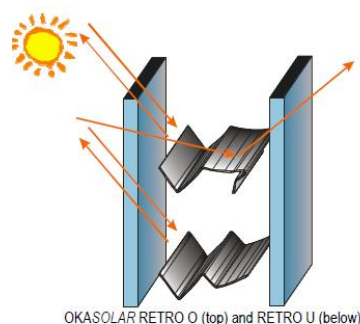


Figure 4.8: Okasolar Glass system; Type Retro O & Retro U. Source: (OKALUX, [n.d.]-b).

Furthermore, many researches have been done to develop new devices that can serve as shading and lighting devices. Recently, a multi-slat of up-down-movement type was invented (Zhang, 2013). With this flexible design, several shading-lighting combinations could be formed to achieve both

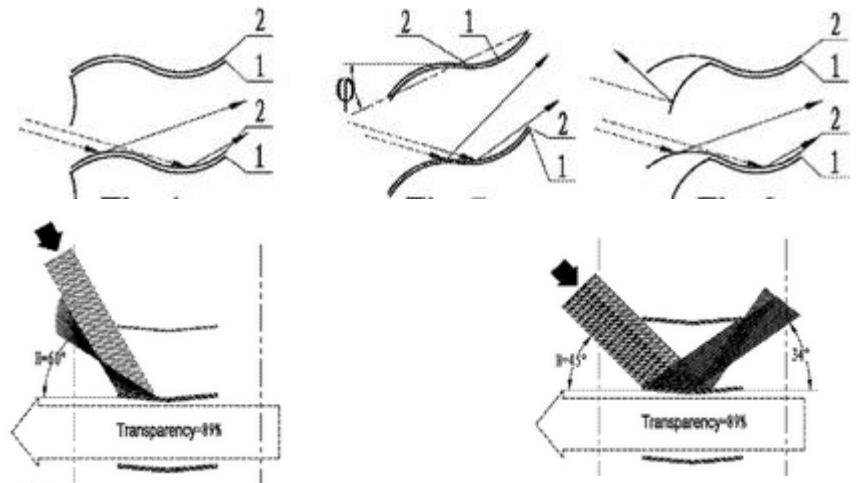


Figure 4.9: multi-slat combination blind of up-down-movement type; Source: (Zhang, 2013).

optimizations of solar shading and natural daylight; Figure 4.9.

Another system was developed under Patent no.06714352 and named as "*Mini-optical light shelf daylighting system*" (Rogers et al., 2003; Rogers et al., 2004). Figure 4.10 shows the new system. Light slat consists of three main segments. The upper surface is a light reflecting segment while the bottom surface comprises both light shading and light redirecting segments. It can reflect the light directly to the space ceiling by reflecting segment or through redirecting segment while shading segment can block unwanted low direct sun rays.

Another Mini-optical light shelf system was invented under the patent of US-6480336-B2 (Digert and Holtz, 2002). The system consists of a set of shelves with an identical optical-shaped top surface to collect incident light and redirect it to the space ceiling more efficiently; Figure 4.11.

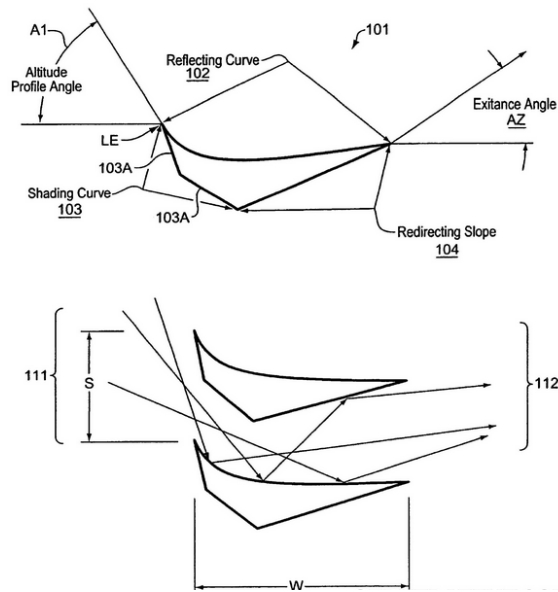


Figure 4.10: Mini-optical light shelf daylighting system "Patent no.06714352". Source: (Rogers et al., 2003).

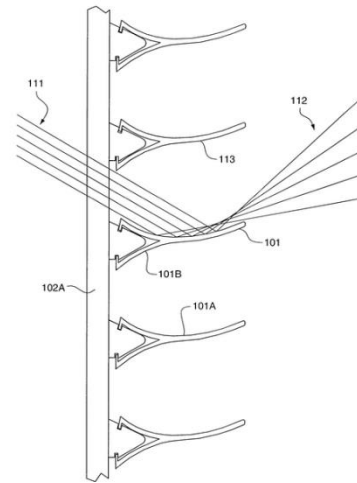


Figure 4.11: Mini-optical light shelf daylighting system "US-6480336-B2". Source: (Digert and Holtz, 2002).

Genius Slats, shown in Figure 4.12, was developed with significant design to ensure good performance under several conditions without the need for automated adjustment (Kuhn, 2006). It could enhance both direct solar gains control and daylight utilization with high reflective coating for its upper surface. At the same time, it controls the glare using a low-glare light coating for its bottom surface.



Figure 4.12: Genius Slat; source: (Kuhn, 2006).

Moreover, by this work more designs, products and patents concerning shading and daylighting aspects in buildings have been reviewed. A summary with a brief description is included in Appendix C and Appendix D. Based on the critical review of discussed and presented designs/products, base-cases and -samples for DSF-integrated shading elements were selected and regenerated as shown later in section 8.1.

4.3.3 Daylighting through DSF “Optical Performance”:

Fundamentally, the additional glazed layer (second skin) of DSF would reduce the light transmittance (LT) per façade-unit area to indoor. However, the relatively large glazed area of DSF would increase the light effective area of the façade. This increase in area would usually overcome the reductions in light transmittance (LT), which in turn enhance total natural daylight penetrations to indoor in comparison to common small windows (Hendriksen et al., 2000; Oesterle et al., 2001). Most importantly, expected multi-reflections through various façade’s elements (e.g. integrated shading/lighting devices) would increase the lit-depth of the space thus increase its effective usable depth. Indeed, the design of DSF itself would dramatically vary levels of natural daylight toward indoors. Generally, Façade’s configuration, its components, its materials, and shading system are among parameters that would determine the level of indoor daylight.

Apart from general attempts to enhance indoor natural daylight using discussed products, there were some efforts to enhance natural daylight through DSF in particular. For example, Venetian blind systems with perforated or half-perforated concave slats could be installed inside DSF’s cavity to

mainly utilize indoor daylighting; Figure 4.13. In addition, it could prevent indoor overheating (Warema, 2009). However, it is designed to be used either inside the

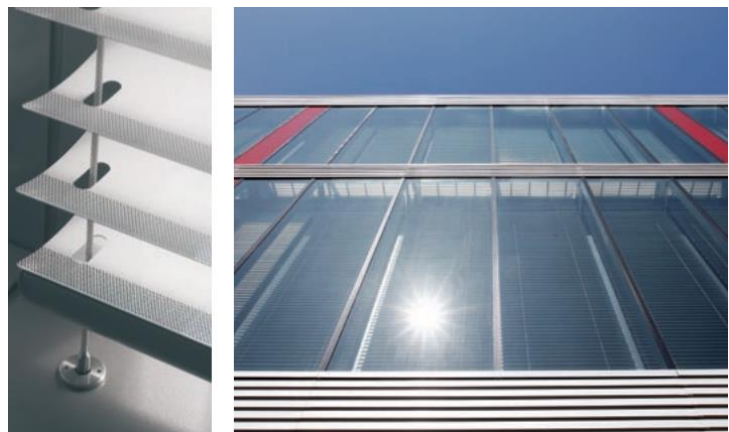


Figure 4.13: Venetian blind system with perforated concave slats incorporated into DSF’s cavity. Source: (WAREMA, 2009).

room or within closed DSF cavity. Therefore, in hot climates where the cavity is recommended to be naturally ventilated, the influence of such systems on the airflow inside the cavity and then heat transfer coefficients and thermal performance of entire DSF is not investigated nor guaranteed yet.

Hamza et al. (2007) analyzed the thermal and daylight performance of two configurations of DSF: continuous and corridor. Radiance software was used for analyzing the daylight performance. Results showed different indoor illuminance maps were produced by the different configurations. In the main work area (up to 6m depth from the façade), both configurations would provide sufficient daylight illuminance ($>300\text{Lux}$). During direct solar periods, the necessity for blinds was highlighted to avoid potential glare due to excessive illuminance levels in areas close to the façade. In addition, an area with a sharp contrast in daylight (stripes) was found next to the façade because of the reflections by the walkways elements. In the back of space, corridor-DSF would decrease the daylight further than continuous one. However, corridor-DSF reflected more light to the ceiling that may enhance the psychological aspect of occupants. The research recommended studying further the effect of walkways' position and materials on daylight distribution.

Heim et al. (2011) conducted a work to study both thermal and visual comfort of office buildings equipped with DSF. The office was constructed based on BESTEST model ($8\text{m} * 6\text{m} * 2.7\text{m}$) with facade depth of 1m. Desktop Radiance was used to define the daylighting model that was calculated based on Backward Ray Tracing Method (Larson et al., 1998). Visual comfort was assessed using indices of horizontal and vertical illuminance distribution. In

summer, where the sun is with high altitude, space is expected to be fully shaded by DSF's elements while just diffuse radiations would pass to indoor. Large variations in illuminance were noticed within the depth of 2m from the façade. However, authors suggested using Daylight Glare Index (DGI) and Vertical Illuminance at the Eye (VIE) for further works instead of illuminance distributions.

Other researchers have given further concerns about the daylight importance through DSF integrated with shading devices. For instance, Gavan et al. (2010) recommended using the smallest tilt angle for cavity-integrated Venetian blinds when it gives similar reductions in temperatures to higher angles; this is because the small angles would enhance indoor daylight. Even with new designs of DSF, improving natural daylight is still a critical issue so it is highly recommended to be addressed further (Gavan et al., 2007; Baldinelli, 2009; Radhi et al., 2013).

4.3.4 Glare caused by DSF:

Positively, DSF can provide much natural daylight under even overcast conditions. However, on sunny days, it will allow in dramatic light levels that could cause glare inside and affect the visual comfort for occupants (Straube and van Straaten, 2001; Gavan et al., 2007). Thus, glare is a common issue with DSF under clear sky conditions and expected to be significant with large open offices where depth is more than 6m (Hendriksen et al., 2000).

Glare Indices are used to assess the glare that occurs when indoor illuminance exceeds its comfort levels. Daylight Glare Index (DGI) and CIE Glare Index (CGI) are two common indices used for this purpose. DGI is

incorporated into DOE-2.1B (Wienold and Christoffersen, 2006) while CGI into RADIANCE (Ward, 1992).

4.3.5 Conclusion:

Installing DSF would generally increase indoor natural daylight with possibilities of having glare would also be increased. Any barrier in the cavity, including shading elements and even walkways, would affect indoor daylight levels and its quality. Therefore, further researches concerning daylight performance of DSF are highly recommended.

Several products of multi-functional devices are nowadays available, which could be used as external, internal or even within DSF cavity. Yet, there is no sufficient knowledge, in literature, on how such products would affect the airflow patterns inside the cavity and then the thermal performance of the entire system in hot conditions.

Generally, designing DSF with proper shading/lighting devices could enhance indoor natural daylighting, control potential glare and improve occupants' visual comfort. In addition, it would maximize daylight levels for deep areas. At the same time, these devices could act as solar shading and minimize unwanted solar gains while being secured inside the cavity. Therefore, the proper combination with sufficient compromising could result in a good multi-functional device, which could ensure both optical and passive solar shading aspects. This could be done through a good optimization of the features and characteristics of the device. This includes tilt, material, and geometry of the device.

Therefore, to ensure sufficient multi-functional performance of DSF, a detailed investigation should be conducted on all aspects of these elements. For example, the airflow pattern within the cavity should be considered carefully when designing or before applying such integrated devices. However, this work is only focussed on the thermal and airflow performance of these elements for a wide range of design parameters. However, due to the time limitation, daylighting investigation is recommended as future works.

CHAPTER 5 THEORETICAL BACKGROUND AND METHOD VALIDATION

5.1 Introduction:

In its simplest description, the Double Skin Façade (DSF) would generally work as a medium for airflow, heat transfer and daylighting penetration. This includes the air movement in/out of the cavity as well as through to indoor (e.g. space) or outdoor (e.g. ambient environment). In a bit more complex process, heat would transfer through the structure in its common forms: radiation, convection, and conduction; which in reality work together as a conjugate phenomenon. Furthermore, airflow and heat transfer are interactive in real life, which is more evident when talking about natural air movement (i.e. natural convection) through vertical heated structures; like solar cavities and DSF.

Most works so far on DSF focus on its performance: thermal and airflow; separately or as a combination. Usually, such works handle the performance at either investigation or optimization levels. For either purpose, a sensitive and accurate representation of the system's physics and the aforementioned phenomenon is highly required. Over the years, different methods have been developed to tackle these tasks. Generally, four different methods are available: experimental works (e.g. fields or small-scale), simple mathematical models (e.g. network model), building energy simulation BES (e.g. TAS) and computational fluid dynamics (CFD); (Ji et al., 2007; Zhou and Chen, 2010). However, CFD is still the most recommended technique due to

its advantages including high accuracy and detailed outputs (e.g. temperature, velocity and pressure fields) even though it could be highly resources- and time-consuming. In addition, it can efficiently deal with complex elements/structures.

In this chapter, the mathematical models for the given problem are presented followed by the concept of CFD as solving approach. Then, a validation work is shown for the selected solution technique, ANSYS Fluent solver.

5.2 The Mathematical Models:

Assuming normal air is a Newtonian fluid, Navier-Stokes equations are then applicable to analyze its behaviour under ordinary conditions. These equations are known as conservation equations, which govern both fluid flow and associated heat transfer. In addition to momentum equation, equations for continuity (mass) and energy transport are involved. For laminar flow, only equations of mass, momentum, and energy conservation are applied. The importance of energy conservation equation comes with the possibility of heat transfer through the fluid and structure, as conduction, convection, and radiation process supposed to occur. With turbulent flow, more transport equations (e.g. $k - \varepsilon$ turbulence equation) come along with other aforementioned equations.

Hereafter, a brief description is given for the aforementioned main conservation equations to be solved for analyzing the given problem (air flow associated with heat transfer through semi-transparent structures, i.e. DSF). Also, for such a given problem, both laminar and turbulent flows are expected

(Yakhot and Orszag, 1986; Gan, 2011b). For facilitating the solution (modelling) of turbulent flows, Reynolds-Averaging Navier-Stokes (RANS) method is usually used (RANS method is more applicable in term of required computational facilities, i.e. less CPU and computing-time, as it mainly governs the transported quantities based on time averaging). With RANS method, instantaneous variables (i.e. temperature, pressure, velocities) in instantaneous N-S equations are replaced by corresponding mean components. Therefore, a new set of terms is required to be solved, which ended by turbulent viscosity (Fluent, 2005; Hadlock, 2006). To solve these quantities for a specific turbulent flow, suitable turbulence model has to be first chosen to represent the occurred turbulence (Fluent, 2005; Hadlock, 2006). Among several available models, RNG $k - \varepsilon$ could be used for natural buoyant flow problems (Manz, 2004; Gan, 2011b).

General mathematical expressions, which work for both compressible and incompressible fluids, as well as steady and transient state, could be found in Fluent (2005). However, for an incompressible steady-state flow, in reference to tensor notation, the time-averaged governing equations for air flow and associated heat transfer could be mathematically expressed as following (Gan, 2011b):

- **Continuity (Mass) Conservation Equation:**

According to the law of conservation of mass, mass is neither created nor destroyed (Welty et al., 2009). Based on this fact, the rate of accumulated mass within controlled volume should equal to inflow's rate of mass subtracting outflow's rate of mass for that volume (Denton, 2009).

Equation (5.1) expresses the conservation of mass (Gan, 2011b):

$$\frac{\partial(\rho U_i)}{\partial x_i} = 0 \quad (5.1)$$

Where:

U_i : mean air velocity component (m/s) in i direction.

ρ : Air density (kg/m³)

- **Momentum Conservation Equation:**

Momentum transfer in a fluid involves the study of the motion of fluids and the forces that produce these motions. Equation of momentum conservation is based on Newton's second law of motion, which may be stated as follows "*The time rate of change of momentum of a system is equal to the net force acting on the system and takes place in the direction of the net force*" (Welty et al., 2009). Mainly, these forces include gravitational force, pressure force (pressure on volume boundary), shear stress and frictional force (Denton, 2009). Equation (5.2) presents the conservation of momentum and equations (5.3) to (5.8) presents the different terms for transport equations (Gan, 2011b):

$$\frac{\partial(\rho U_j U_i)}{\partial x_j} - \frac{\partial}{\partial x_j} \left[\mu_e \left(\frac{\partial U_i}{\partial x_j} + \frac{\partial U_j}{\partial x_i} \right) \right] = \rho g_i - \frac{\partial}{\partial x_j} \left[\left(P_s + \frac{2}{3} k \right) \delta_{ij} \right] \quad (5.2)$$

Where:

μ_e : The effective viscosity (kg/m-s).

g_i : The gravitational acceleration (m/s²) in i direction.

P_s : The static pressure (Pascal).

k : The turbulent kinetic energy (m²/s²).

δ_{ij} : The Kronecker delta; $\delta_{ij} = 1$ if $i = j$; $\delta_{ij} = 0$ if $i \neq j$.

To substitute the effective viscosity (μ_e), equation (5.3) is used in the RNG $k - \varepsilon$ turbulence model:

$$d\left(\frac{\rho^2 k}{\sqrt{\varepsilon \mu}}\right) = 1.72 \frac{(\mu_e/\mu)}{\sqrt{(\mu_e/\mu)^3 - 1 + C_v}} d(\mu_e/\mu) \quad (5.3)$$

Where:

ε : The turbulent dissipation rate (m²/s³).

μ : The laminar dynamic viscosity (kg/m-s).

C_v : Constant (≈ 100).

To substitute the turbulent kinetic energy (k), equation (5.4) is used:

$$\frac{\partial(\rho U_i k)}{\partial x_i} - \frac{\partial}{\partial x_i} \left(\frac{\mu_e}{\sigma_k} \frac{\partial k}{\partial x_i} \right) = \mu_t S^2 - \rho \varepsilon - \frac{g_i \mu_t}{\rho \sigma_t} \frac{\partial \rho}{\partial x_i} \quad (5.4)$$

Where:

σ_t : The turbulent Prandtl number.

σ_k : The Prandtl number for turbulent kinetic energy.

μ_t : The turbulent viscosity (kg/m-s).

S : The modulus of rate-of-strain tensor.

To compute turbulent dissipation rate (ε), equation (5.5) is used:

$$\frac{\partial(\rho U_i \varepsilon)}{\partial x_i} - \frac{\partial}{\partial x_i} \left(\frac{\mu_e}{\sigma_\varepsilon} \frac{\partial \varepsilon}{\partial x_i} \right) = C_1 \mu_t S^2 \frac{\varepsilon}{k} - C_2 \rho \frac{\varepsilon^2}{k} - C_3 \frac{g_i \mu_t}{\rho \sigma_t} \frac{\partial \rho}{\partial x_i} \frac{\varepsilon}{k} - S r \quad (5.5)$$

Where:

σ_ε : The Prandtl number for turbulent dissipation rate.

C_1 : Constant (1.42); C_2 : constant (1.68).

$C_3 = \tanh(V_v/V_h)$; V_v : vertical mean velocity component; V_h : horizontal mean velocity component.

Sr : The rate of strain.

To compute S and Sr terms, equations (5.6) and (5.7) respectively used:

$$S = \sqrt{\frac{1}{2} \left(\frac{\partial U_i}{\partial x_j} + \frac{\partial U_j}{\partial x_i} \right) \left(\frac{\partial U_i}{\partial x_j} + \frac{\partial U_j}{\partial x_i} \right)} \quad (5.6)$$

Where:

β : Constant (0.012).

η_0 : Constant (4.38).

$\eta = S k / \varepsilon$

$$S r = \frac{C_\mu \rho \eta^3 (1 - \eta/\eta_0)}{1 + \beta \eta^3} \frac{\varepsilon^2}{k} \quad (5.7)$$

To find out different terms of Prandtl numbers (σ_t , σ_k and σ_ε), inverse Prandtl number (α) could be calculated from (5.8):

$$\left| \frac{\alpha - 1.3929}{\alpha_0 - 1.3929} \right|^{0.6321} \left| \frac{\alpha + 2.3929}{\alpha_0 + 2.3929} \right|^{0.3679} = \frac{\mu}{\mu_e} \quad (5.8)$$

Then, $\sigma_t = 1/\alpha$ with α_0 is the laminar inverse Prandtl Number ($\alpha_0 = 1/\sigma$) and $\sigma_k = \sigma_\varepsilon = 1/\alpha$ with $\alpha_0 = 1$.

- **Energy Conservation Equation:**

The equation of energy conservation (5.9) is based *on the* first law of thermodynamics, which may be stated as follows: *If a system is carried through a cycle, the total heat added to the system from its surroundings is proportional to the work done by the system on its surroundings.* Evidently, it is possible to convert energy from one form to another whereas it cannot be either created or destroyed.

$$\frac{\partial(\rho U_j H_i)}{\partial x_j} - \frac{\partial}{\partial x_j} \left[\left(\frac{\mu}{\sigma} + \frac{\mu_t}{\sigma_t} \right) \left(\frac{\partial H_i}{\partial x_j} \right) \right] = q \quad (5.9)$$

Where:

H_i : The specific enthalpy (J/kg) in I direction; $H_i = C_p T$ for dry air with negligible pressure work and kinetic energy in incompressible flow.

C_p : The specific heat of air at a constant pressure (J/kg.K).

T : The absolute air temperature (K).

q : The volumetric heat production/dissipation rate (W/m³).

To compute the density of dry air (ρ) for the calculation of thermal buoyancy effect, ideal gas law could be used:

$$\rho = \frac{P}{RT} \quad (5.10)$$

Where:

P : The absolute pressure (pascal).

R : The gas constant (J/kgK)

- **Radiative Heat Transfer:**

Radiative components can be a main contributor to total heat transfer process, as it may be a direct way to heat up or cool down different involved elements, due to their temperature differences. And, the radiant heat flux is a good indicator for this contribution. Therefore, it is important to calculate radiative energy sources to be added to the energy balance of the system. To calculate radiative energy sources, radiation heat transfer should be modelled for different components of the system, using the radiative transfer equation (RTE) (Safer et al., 2005c). Among the different radiation models available with Fluent, the discrete ordinates (DO) radiation model was selected as it suits the given problem with low and high optical thickness. Furthermore, DO model proved its superiority in solving RTE with participating medium with spectral absorption coefficient, at semi-transparent walls, by using non-gray model and at a moderate computational cost (Fluent, 2005; Fluent, 2012a; Iyi et al., 2014; Hazem et al., 2015).

DO model solves the radiative transfer equation (RTE) for a finite number of discrete solid angles, each associated with a vector direction fixed in the global Cartesian system. With DO, RTE is transformed into a transport equation for radiation intensity in the spatial coordinates. For the given case assuming low optical thickness and negligible scattering coefficients for its medium (air), uncoupled option is used with DO model, where equations for the energy and radiation intensities are solved one by one (sequential not simultaneous approach) (Fluent, 2005; Fluent, 2012a). For DO model with

non-gray option, RTE for spectral intensity $I_\lambda(\vec{r}, \vec{s})$ could be written as following (5.11):

$$\nabla \cdot (I_\lambda(\vec{r}, \vec{s}) \vec{s}) + (a_\lambda + \sigma_s) I_\lambda(\vec{r}, \vec{s}) = a_\lambda n^2 I_{b\lambda} + \frac{\sigma_s}{4\pi} \int_0^{4\pi} I_\lambda(\vec{r}, \vec{s}') \phi(\vec{s}, \vec{s}') d\Omega' \quad (5.11)$$

Where:

λ : The wavelength. \vec{s} : assigned direction. \vec{r} : assigned position.

a_λ : The spectral absorption coefficient.

$I_{b\lambda}$: The black body intensity given by the Planck function. n : The refractive index.

Equation (5.11) can be applied to radiation heat transfer through a participating medium and between surfaces. For clean air which is transparent to radiation, the equation can be simplified for the calculation of radiation heat transfer between solid surfaces as a boundary condition in terms of radiation intensity or heat flux.

Incident radiation on opaque surfaces (e.g. integrated slats) could be reflected and absorbed differently, which depends on the absorptivity (assumed to be equal to emissivity) of that surface. Nature of reflection (specular or/and diffuse) also depends on the diffuse fraction of the surface. For an opaque wall with non-gray diffuse properties, following equations present different quantities of radiative heat transfer:

- Total incident radiative heat flux ($q_{in,\lambda}$) at the wall's surface, is expressed by Equation (5.12):

$$q_{in,\lambda} = \Delta\lambda \int_{\vec{s} \cdot \vec{n} > 0} I_{in,\lambda} \vec{s} \cdot \vec{n} d\Omega \quad (5.12)$$

Where: $I_{in,\lambda}$ is the spectral radiation intensity.

- Net radiative heat flux out ($q_{out,\lambda}$) of the wall's surface (reflected and emitted) is expressed by Equation (5.13):

$$q_{out,\lambda} = (1 - \varepsilon_{w\lambda})q_{in,\lambda} + \varepsilon_{w\lambda}\sigma T_w^4 n^2 [F(0 \rightarrow n\lambda_2 T_w) - F(0 \rightarrow n\lambda_1 T_w)] \quad (5.13)$$

Where:

n : The refractive index of the medium next to the wall.

$\varepsilon_{w\lambda}$: The wall emissivity in the band λ .

$F(n, \lambda, T)$: Provides the Planck distribution function.

T_w : The temperature of the wall.

σ : Stefan-Boltzmann Constant (5.669×10^{-8}).

- The net radiative heat flux at the wall's surface, could be calculated by Equation (5.14):

$$q_{net,\lambda} = q_{in,\lambda} - q_{out,\lambda} \quad (5.14)$$

- The boundary intensity $I_{0\lambda}$ for all outgoing directions \vec{s} in the band $\Delta\lambda$ at the wall's surface, could be calculated by Equation (5.15):

$$I_{0\lambda} = \frac{q_{out,\lambda}}{\pi \Delta\lambda} \quad (5.15)$$

Next, the computational fluid dynamics (CFD) approach is generally discussed; and, a brief introduction is given for ANSYS package and its well-known solver Fluent.

5.3 Computational Fluid Dynamic (CFD) Modelling:

For more practical applications, computing facilities are widely used to numerically solve the governing equations for a particular problem under given conditions. Computational fluid dynamics (CFD) indicates the employment of such facilities for the intended solution. With CFD, a full conjugate problem could be solved including the potential highly complex flow, and associated heat transfer mechanisms, outside and inside the cavity (Manz

and Frank, 2005; Hamza et al., 2007). Therefore, it is able to efficiently predict the thermal performance and ventilation phenomenon for DSF. Based on its concept of discretization, the computational domain is represented through a 2D or 3D meshing using a structured, unstructured or hybrid grid (cells). Then, for each cell, conservation equations (mass, momentum, and energy) are numerically solved to determine the values for dependent variables of temperature, velocity, and pressure at each cell (Fluent, 2005; Safer et al., 2005b; Asfour and Gadi, 2007). Thus, more cells will result in a higher accuracy, however, mean resources- and time-consuming.

Different commercial packages were developed for CFD including ANSYS, which provides several solvers such as Fluent, Polyflow, and CFX. Fluent, which is most commonly used, uses the finite volume method (FVM) to numerically solve the governing (conservation) equations. Fluent provides great possibilities to model different fluid flow phenomenon. Also, it allows for accurate modelling for turbulence within the flow through a set of robust turbulent models based on expected turbulence state (Fluent, 2005; Hadlock, 2006). Among several available models, RNG $k - \varepsilon$ could be used for natural buoyant flow problems (Manz, 2004; Gan, 2011b). For heat transfer phenomenon, several models are available to model natural, forced and mixed convection process. Radiative heat transfer process can be modelled via a wide range of models as well (Fluent, 2005; Fluent, 2012a; Fluent, 2012b).

Next, the proposed method for solution, ANSYS Fluent, was validated using proper data from the literature.

5.4 The Validation for Solution Method:

This section presents a detailed validation work for ANSYS Fluent solver, as a proposed solution method, using a published problem similar in principles to the intended work, herein.

5.4.1 Case Description:

An experiment work was conducted using a large-scale simulator at Loughborough University (Mei et al., 2007); which was funded by UK's Engineering & Physics Sciences Research Council (EPSRC). The rig consisted of a solar simulator (generator), DSF structure, and controlled internal environment (chamber); Figure 5.1.

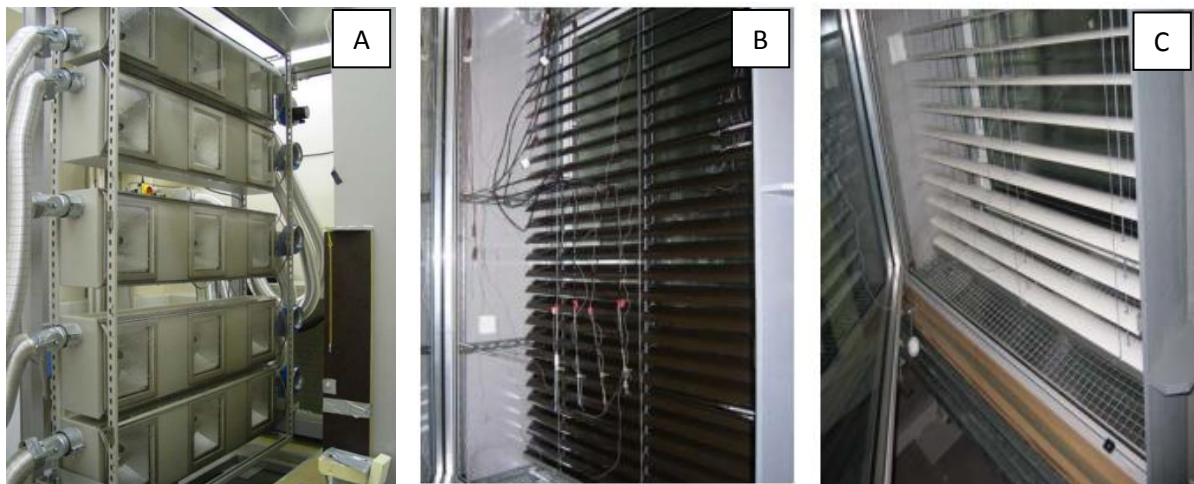


Figure 5.1: Components of the experimental rig; A) Solar Simulator. B) DSF with Dark venation blinds. C) DSF's below section shows bottom mesh grille and inlet grille; source: (Mei et al., 2007).

The solar simulator consisted of 15 Sol-1200 lamps and available irradiance range was $200\text{-}1000\text{W/m}^2$ with steps of 200W/m^2 using mesh attachments for levels control. Irradiance non-uniformity was of $\pm 10\%$. This simulator could test structures with maximum dimensions of 2.5m-length and 1.5-width. Simulated outdoor environment, in front of the tested structure, could be controlled in the temperature range of $12^\circ\text{-}30^\circ\text{C}$. The indoor environment was represented by the enclosure attached to the back of the

structure, where both temperature and airflow could be controlled. The rig could simulate naturally ventilated DSF that based on the buoyancy-driven phenomenon.

The Double Skin Façade (DSF) structure consisted of single storey “Box-window” with installed shading elements “sun-shading blinds”, which had two skins that were designed as openable doors to ease the work and adjustment. The outer skin was 1.44m (width) x 2.06m (height), which consisted of an aluminum frame and a single toughened clear glass pane with dimensions of 1.28m (width) x 1.91m (height) x 12mm (thickness). The inner skin was 1.38m (width) x 2.0m (height), which consisted of double glass panes separated by air gap (16mm). The glass was toughened clear with dimensions of 1.22m (width) x 1.85m (height) x 6mm (thickness); and there was a low-e coating on the inner face of the inner glass (Ji et al., 2007).

The cavity has single inlet and outlet; each had a grille that is 0.24m (height) x 1.45m (width), which consisted of three slots “spaces” of 4.5cm-high each. Also, there were two horizontal meshes installed in the cavity and shifted from bottom and top. The integrated shading elements were Venetian blinds type that made of aluminum (0.08m-wide), where the entire set for those blinds had the dimensions of 2.1m (height) and 1.45m (width). Validation was conducted for the work with blind’s colour of white having a reflectance of 0.762.

5.4.1.1 Measurements criteria:

- **Air velocity:** seven of TSI air velocity transducer (TSI Omni-directional Model 8475) with a range of 0.05-0.5m/s was used, which has an

accuracy of $\pm 3.0\%$ for a temperature range of 20°C - 26°C . Out of the given range, error of 0.5% per $^{\circ}\text{C}$ is added. One more thing that was not mentioned by the authors is that response time for the used transducer (model 8475) is 5.0s compared to 0.2s for other available transducer types by the same manufacturer (TSI UNDERSTANDING, 2012; INSTRUMENTS., 2015). Those transducers were placed along the cavity depth at middle height (1.1m from bottom).

- **Air temperature:** seven type-T thermocouples were attached to air velocity transducers.
- **Surface temperature:** twelve thermocouples were used and attached to the glass. Those thermocouples were covered with thermocouples pads to be shaded from direct solar radiation.
- **Solar radiations:** Kipp & Zonen CM3 pyranometer was used to measure actual incident solar radiations on outer skin façade, which was different from nominal value. For example, the measured value of $715\text{W}/\text{m}^2$ was recorded for the nominal value of $800\text{W}/\text{m}^2$ that was set by the solar simulator.

5.4.1.2 Boundary and Operating Conditions:

The experiment was run for several scenarios however, just two were, here, used for comparison: with & without integrated binds. Whereas cavity width was fixed to 0.55m , blinds were placed at the outer third of the width. Both indoor and outdoor temperatures were controlled to 20°C . Measured solar radiation was $715\text{W}/\text{m}^2$. The white blinds were tested for following inclination angles: 0° , 30° , 45° , 60° and 90° degrees. Table 5.1 summarizes the boundary conditions for conducted case.

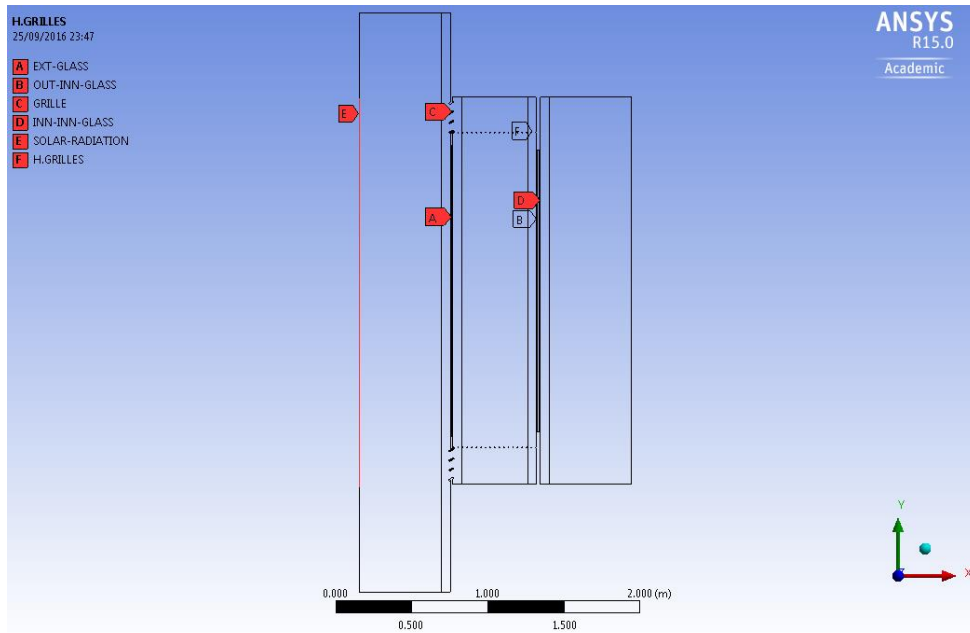
Table 5.1: Boundary Conditions for the validation Case.

Indoor Temp (°C)	Outdoor Temp (°C)	Nominal Solar Radiation (w/m ²)	Measured Incident Solar Radiation (w/m ²)
20	20	800	715

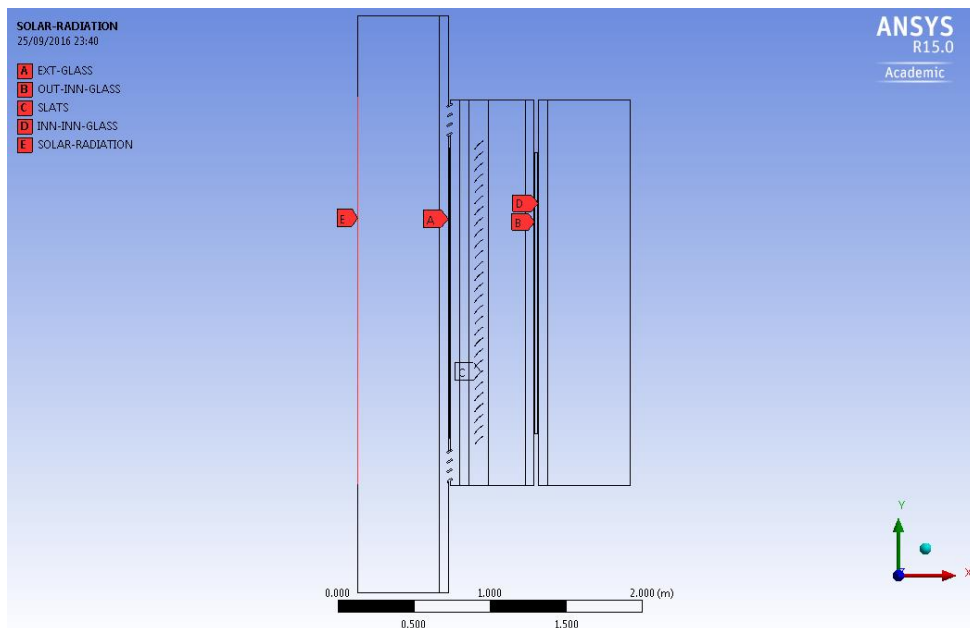
5.4.1.3 Solution Method's Set-up: Settings for Fluent Solver

■ General:

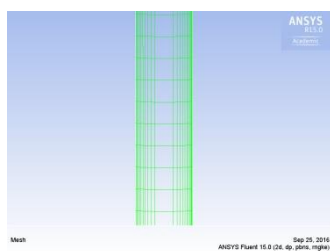
A two-dimensional (2D) model, Figure 5.2, was built with CFD Ansys and simulated using Fluent code to model the coupled convective, conductive and radiative heat transfer through DSF. Different commonly used turbulence models were examined as discussed later. Discrete Ordinate (DO) radiation model was selected; more details are presented later on. The solar heat source was represented by a vertical plane opposite to the front face of the structure, and the influence of offset distance on airflow distribution and its magnitude was further investigated as presented later. Just direct solar radiation was included.



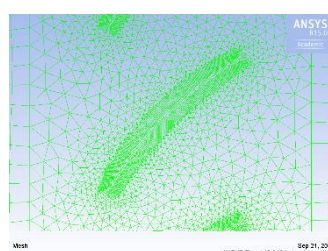
A) Constructed model for non-shaded cavity; Grilles for cavity's vents and mesh for cavity's bottom and top.



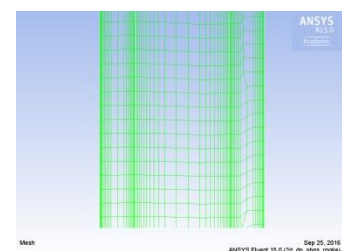
B) Constructed model with 45° degrees-integrated shading cavity; Grilles for cavity's vents.



C) Modelled medium for outer single glass pane.



D) Modelled medium for 45° integrated shading blinds.



E) Modelled medium for inner double glass panes.

Figure 5.2: Constructed models for both non-shaded (A) and 45° shaded (B) cavities.

■ Material Modelling and Specifications:

Air was modelled as a transparent medium; the glass was modelled as semi-transparent; aluminum Venetian blinds were modelled as opaque solid. Thermal and solar properties for different used materials are shown in Table 5.2.

Table 5.2: Thermal and solar properties for different materials.

SPECIFICATIONS		Air	Single-Glass (Draco; 2014)	Venetian-Blinds (Draco; 2014)
TEMP (°C)		20	-	-
THICKNESS (mm)		16	12	1
DENSITY (kg/m ³)		1.205	2500	2719
SPECIFIC HEAT C_p (J/kg-k)		1005	840	871
THERMAL CONDUCTIVITY (w/m-k)		0.0257	1.7	202.4
VISCOSITY (kg/m-s)		1.81e-05	-	-
ABSORPTION COEFFICIENT (1/m):				
1	SOLAR: 0-2.7	0	30	-
2	THERMAL: 2.7-1000	0	3000	-
SCATTERING COEFFICIENT (1/m)		0	0	0
SCATTERING PHASE FUNCTION		isotropic	isotropic	isotropic
EXPANSION COEFFICIENT (1/K)		0.00343	-	-
REFRACTIVE INDEX		1	1.5	1.44
EMISSION		-	0.84	0.7

■ Solution Methods, Control and Convergence Criteria:

- A) The case was solved using Fluent solver with double precision for better accuracy. The need for that was to minimize the numerical round-off errors, which could cause global imbalances of energy in the solid elements to fluctuate; such oscillations were due to a significant difference in the thermal conductivity between air and solid elements.
- B) Solution Methods: solution scheme was set as SIMPLE. And, spatial Discretization for different equations was as shown in Table 5.3:

Table 5.3: set-up for solution methods in fluent.

Spatial Discretization	
Gradient	Least Squares Cell Based
Pressure	PRESTO!
Momentum	Second Order Upwind
Turbulent kinetic Energy	Second Order Upwind
Turbulent Dissipation Rate	First Order Upwind
Energy	Second Order Upwind
Discrete Ordinates	Second Order Upwind

- C) All the solutions started with low values for under-relaxation factors to achieve good stability for the solution before being increased gradually toward default values for fast convergence. The target for all residuals was to drop for less than 1×10^{-3} for all solved equations except energy to 1×10^{-6} . Generally speaking, the target was achieved after a schematic control for the under-relaxation factors. However, higher residuals had to be accepted for some cases when such low values could not be achieved. For example, the residual for continuity equation was sometimes accepted around 1×10^{-2} .
- D) Relative change for all monitored values (of interest) was not to exceed 0.5%-1% at apart of 10,000 iterations. Generally, this was maintained for all cases and change was sometimes $< 0.1\%$. However, the solution was usually solved for not less than 20,000-30,000 iterations to achieve that target.

5.4.2 Independence of Mesh Size:

General recommendations for the mesh generation were adopted from previous relevant work (part of this research but not included in this thesis). However, mesh independence study was again conducted to assure independence of mesh size and quality for the given problem, where special attention was given to critical areas and boundaries. Mesh-1 was generated with characteristics given in Table 5.4. Mesh-2 was similar to Mesh-1 but with glass medium size of 5mm instead of 10mm. Moreover, additional region adaptation was done for different flow vents, Mesh-3. Furthermore, extra region adaptation was conducted later for regions where measurements were taken.

Table 5.4: Characteristics for initial Mesh-1.

CHARACTERISTICS FOR INITIAL MESH-1			
ITEM		SIZE(mm)	LAYERS(#)
GLASS	MEDIUM SIZE	10 (changed to 5mm for Mesh-2)	-
	INSIDE-INFLATION	-	22
	OUTSIDE-INFLATION	-	10
BOUNDARY SIZE		10	-
DOMAIN SIZE	INDOOR	10	-
	CAVITY	10	-
	OUTDOOR	10	-

Mesh-1 was with 261840 cells while Mesh-2 and Mesh-3 had 335044 and 465733 cells, respectively. Figure 5.3 presents generated mesh-2 with zoom-in at critical regions and boundaries. Figure 5.4 shows the difference between Mesh-1 and Mesh-2, which mainly relates to cells' size for glass medium that affects also mesh inflation quality at external faces (toward air domain) of glass structure. Lastly, Mesh-3 had an additional regional adaptation at both cavity's inlet and outlet as shown in Figure 5.5.

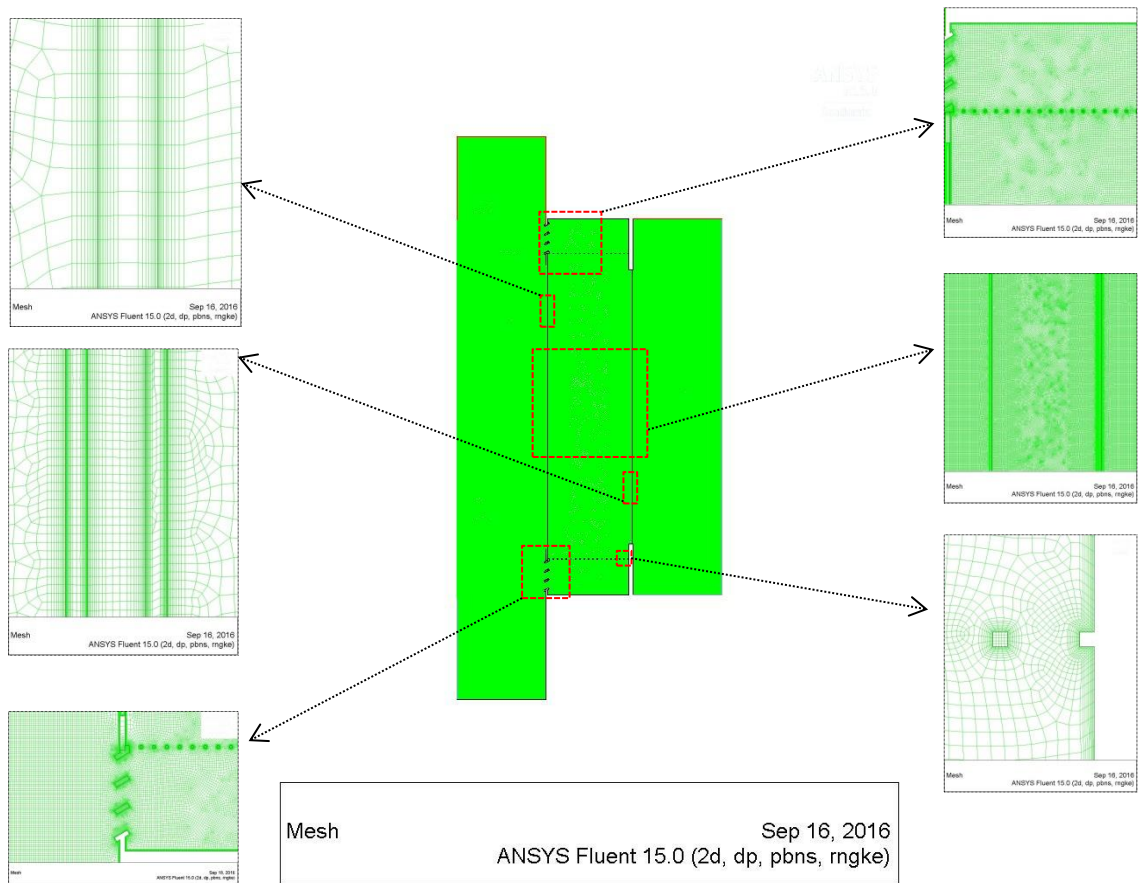


Figure 5.3: Generated mesh for validation structure. Mesh-2.

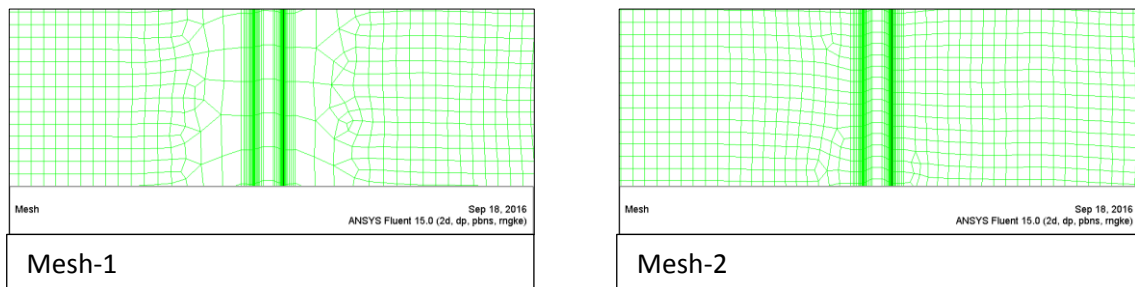


Figure 5.4: Zoom-in shows mesh for outer glass structure in both cases: Mesh-1 and Mesh-2.

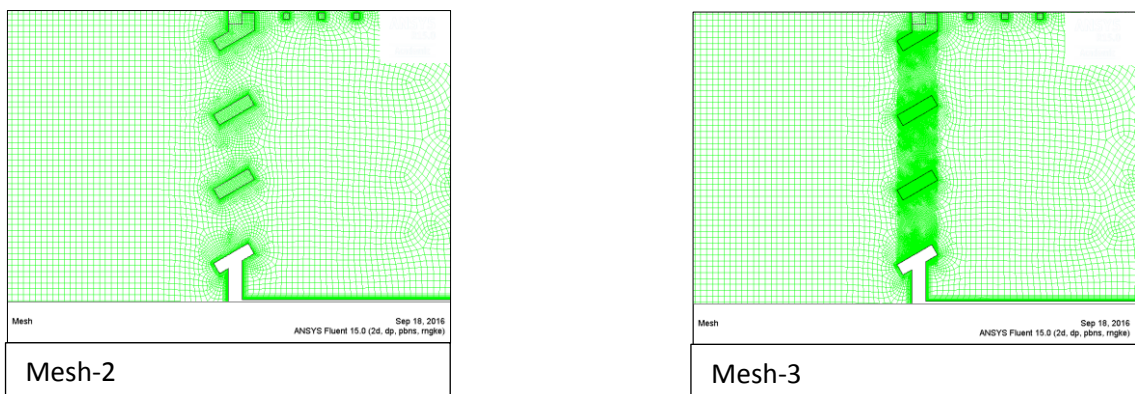


Figure 5.5: Original generated mesh for cavity inlet (Mesh-2) and after-adaptation mesh (Mesh-3).

As the differences for both surface temperatures, Figure 5.7, and air velocity, Figure 5.6, were small and nearly negligible (less than 1%) between the different mesh scenarios, Mesh-1 with the lowest number of cells was initially selected. However, further region adaptation was later done for areas of interest (e.g. mid of cavity $h=1.1\text{m}$ where data to be monitored).

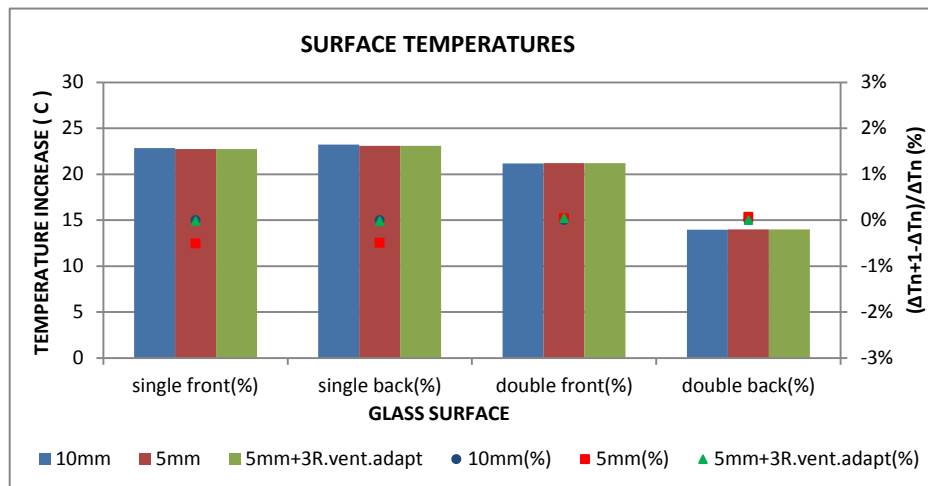


Figure 5.7: Surface temperatures and changes for different structures with the three mesh scenarios.

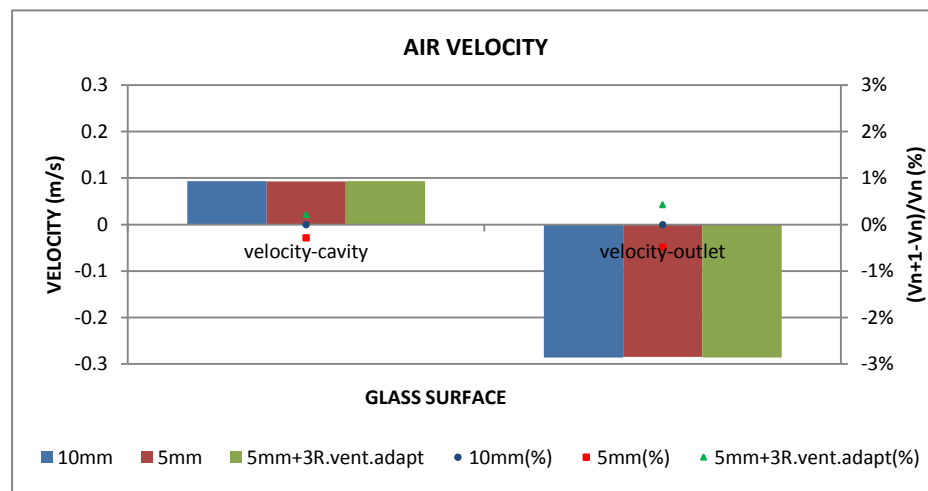


Figure 5.6: Air velocity and changes for cavity's med-height (1.1m) and it's outlet with the three mesh scenarios.

5.4.3 External Extension for Computation Domain:

Generally, including part of external boundary environment within the computation domain, is important as it eliminates any possible restrictions and critical simplifications on vital boundary conditions of the domain of interest; i.e. pressure vents and natural buoyant flow along external surfaces. Here, another preliminary study was conducted to determine to what level including this extension would affect the results and their independence.

It was found that each time distance for extension (offset from outer glass) increased, there was a change in both surfaces' temperatures, Figure 5.8, and air velocities, Figure 5.9, but these changes were negligible (i.e. <2% for temperature; 2.4% for air velocity). In general, such changes were not preferable however external extension equals to three times of cavity width (0.6m) was initially selected, which resulted in 1.8m; Figure 5.10. In spite of that, this decision was probably responsible for not matching experimental results, as the distance between the virtual source for heat (far boundary for the external domain) and the recipient (the external surface for outer glass pane) was three times the actual distance in the real rig (0.6m). Therefore, while the distance of 1.8m (3x) was considered for non-shaded cavity case, it was then set to original distance of 0.6m (1x) for cavities with integrated shading.

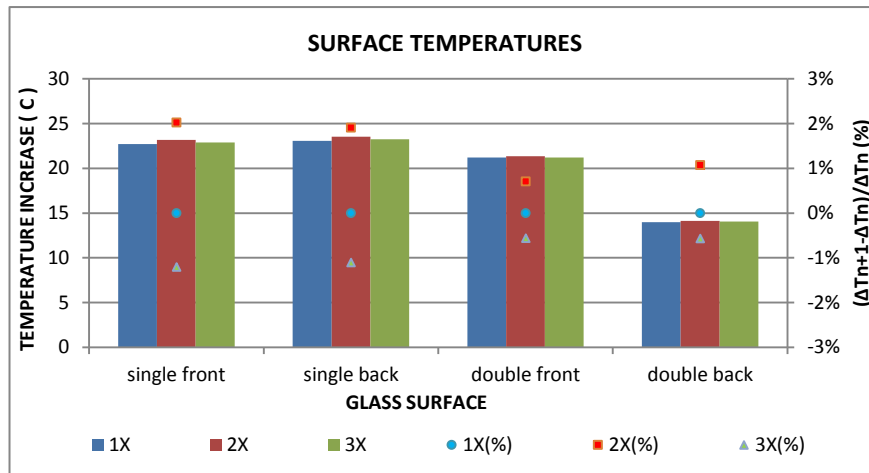


Figure 5.8: Surface temperatures and changes for different glass surfaces under the effect of domain's external extension.

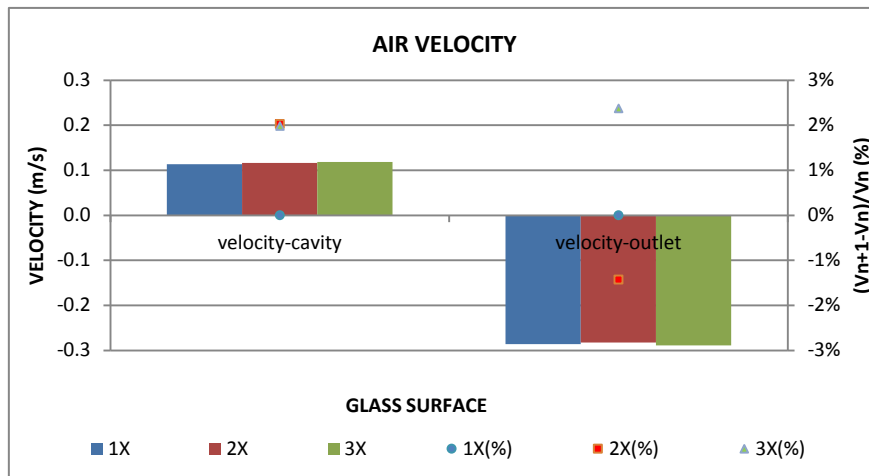


Figure 5.9: Air velocity and changes for cavity's med-height (1.1m) and it's outlet under the effect of domain's external extension.

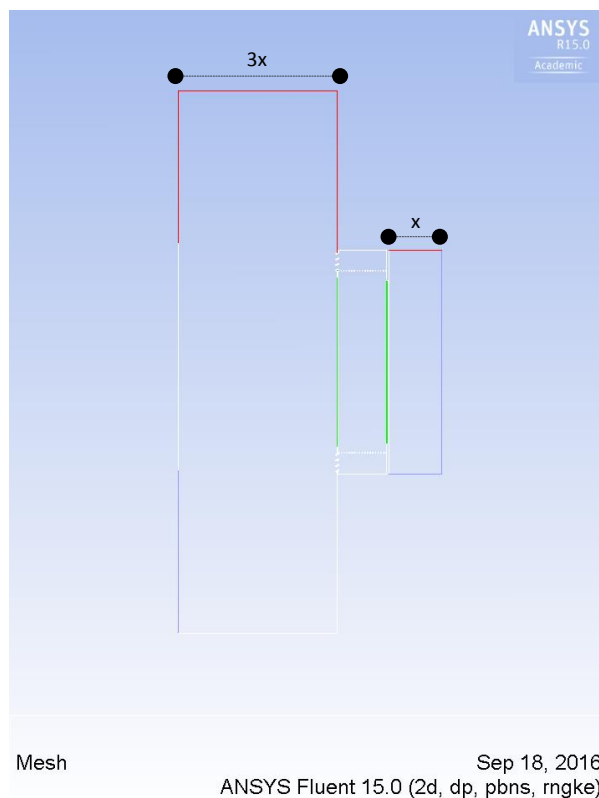


Figure 5.10: Computational domain for validation case showing the extension for external domain with width of three times the cavity width.

5.4.4 Turbulence Model:

Five different turbulence models were investigated under this validation work: **standard $k - \varepsilon$** , **RNG $k - \varepsilon$** , **realizable $k - \varepsilon$** , **standard $k - \omega$** and **SST $k - \omega$** . The purpose was to select the suitable model that represents properly the turbulence phenomenon inside the cavity thus would better predict both airflow and thermal performance of the system.

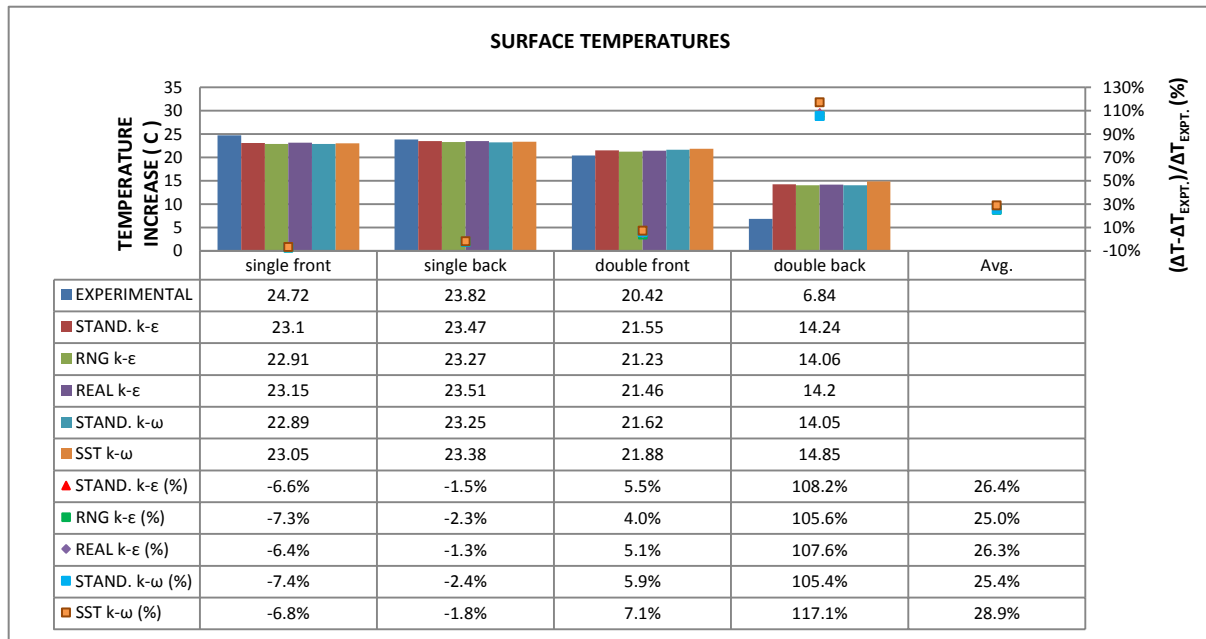


Figure 5.11: Surface temperatures and changes for different glass surfaces under the effect of various turbulence models.

As shown in Figure 5.11 all examined models produced surfaces' temperatures with good agreement with experimental ones with a maximum discrepancy of 7.4% for the front surface of the outer single glass, which was produced under the standard $k - \omega$ model. However, this applied to all surfaces except the back surface of the inner double glass, where differences between experiment results and simulation were significantly high and always over 100%. Possible reasons behind such disagreement include the fact that there was a layer of Low-e coating placed on that surface (the back-side of the inner double glass, toward indoor) that was not included in the simulation due to

inability to do so with the current method where glass surfaces had to be modelled as semi-transparent not opaque so excluding the option to determine their surfaces' emissivity. However, it is later thought that the low-e coating should be modelled as another semi-transparent medium attached to that surface, where solar and thermal characteristics should be provided but unfortunately were not given by the authors (discussed later). This simplification is highly likely the reason behind such over-predicting for that surface temperature (Ji et al., 2007). In addition, all experimental readings were point-based measurements that were limited to a few positions along the glass surfaces.

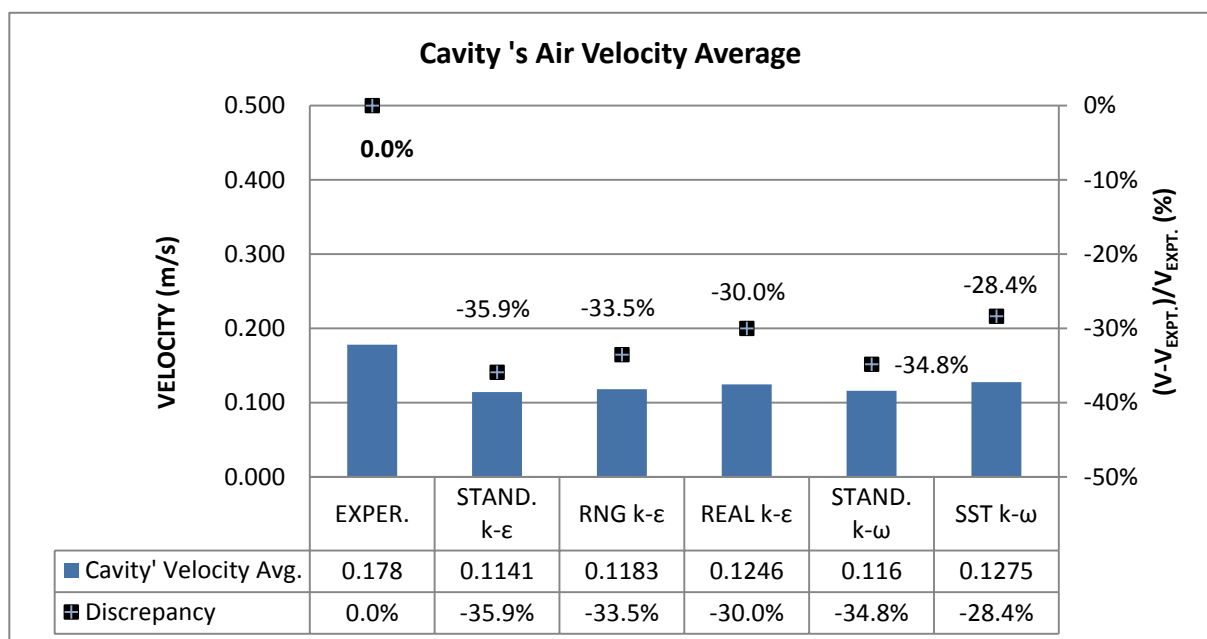


Figure 5.12: Air velocity averages and relative changes for cavity's med-height (1.1m) under the effect of various turbulence models.

On the other hand, cavity's average air velocity was under-predicted with noticeable disagreement with experimental ones as smallest discrepancy was 28.4% for SST k-ω model; Figure 5.12. It is worth mentioning that solar radiation value used in the simulation was 715W/m² as reported from the experimental work and also recommended through related validation work (Ji

et al., 2007). However, it was noticed later that this value refers to the measured value at the outer glass skin while its nominal value was 800W/m^2 , which produced by the solar simulator and was thus 12% higher.

In addition, it is worth mentioning that the calculated air velocity was available for 1000 points (measuring rake) along the cavity's width, 0.55m. However, experimental readings were limited to just 7 single points (air velocity transducers), which probably were not enough to represent the actual air flow: distribution and vector velocities along the cavity's width. In other words, while the experimental average was worked out from plotted graph of those 7-readings, the calculated average was produced from the 1000 points along the cavity's width. Figure 5.13 shows both experimental readings and calculated velocities under different examined turbulence models. It is clear that, in addition to the limited number of transducers, their distribution was not fair enough, as more attention should be given to boundary layers where changes in air velocity are usually more significant according to established theories and as revealed from the simulation. This limitation highlights another possible reason for such disagreement.

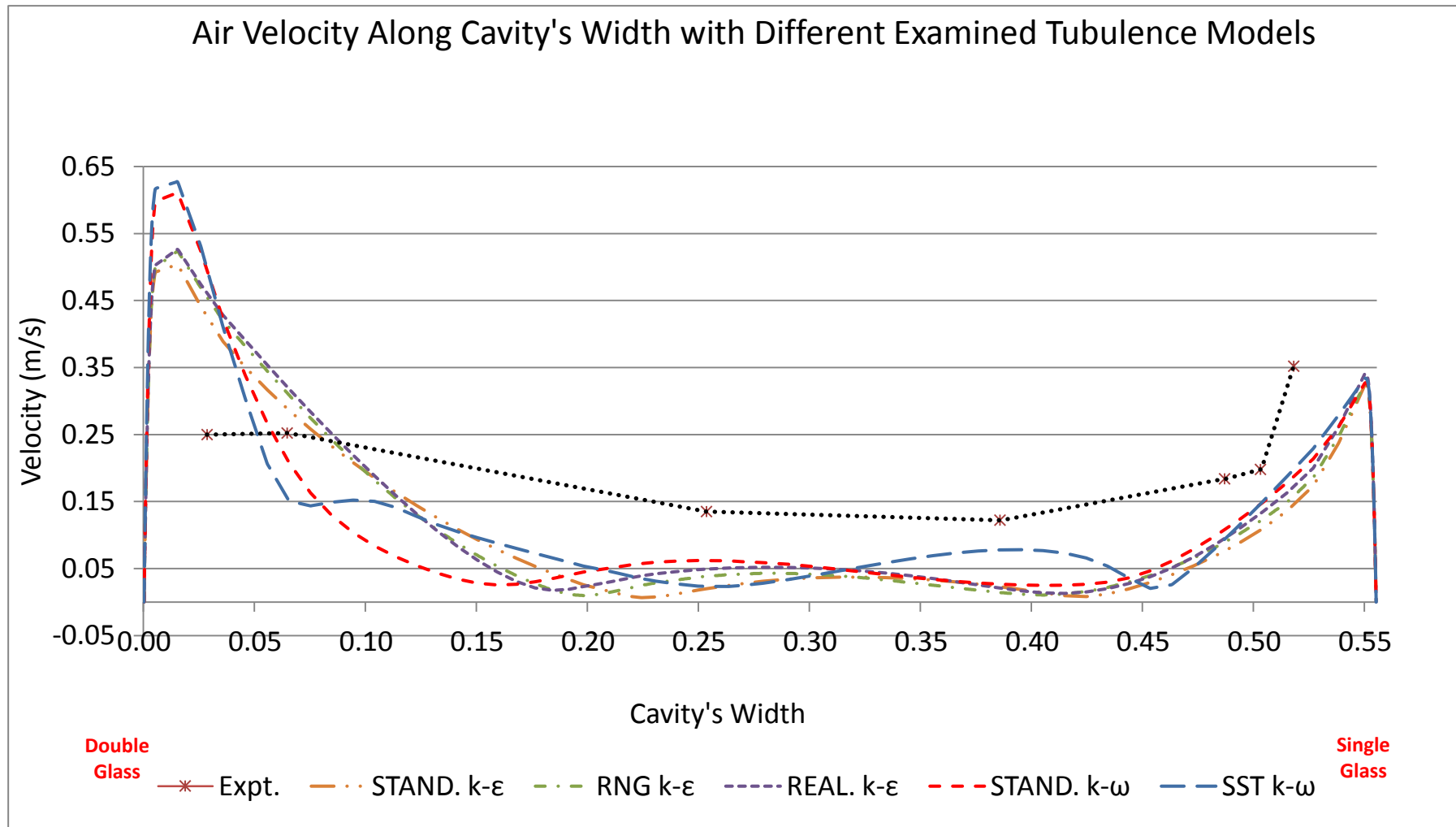


Figure 5.13: Air velocity profiles at mid-height (1.1m) of cavity for difference scenarios of structure simplification.

Moreover, as shown in Figure 5.13, a significant share of revealed discrepancy is attributed to the noticeable increase in air velocity for the boundary layer next to the double glass (inner glass), which in turn was due to over-predicting of its surfaces' temperatures due to not modelling the low-e coating.

Furthermore, even though relative coordinates for each transducer were provided and then considered for reporting corresponding values through simulations, it is generally not recommended to rely on single-point measurements for validation purposes, as it is practically quite difficult to ensure those coordinates from the experiment over the time.

Taking into consideration both the average for all temperatures' discrepancies and the average for air velocity discrepancy, RNG $k - \varepsilon$ model was initially selected; however, SST $k - \omega$ is still acceptable.

5.4.5 Modelling Surface Emissivity:

This section shows an attempt to model the effect of low-e coating film on the inner surface of the double glass by manipulating the emissivity for that surface. To do that, the boundary condition (BC) type for at least that surface had to be changed from semi-transparent to opaque so the option to determine the surface emissivity was activated. Indeed, this would not work with the concept of the adopted method (as no direct solar radiation would be transmitted to indoor with that opaque surface) however, it was tested especially that the indoor environment (rear chamber) was out of interest in the validation.

The simulation showed that with the new amendments to the boundary condition of the inner surface, the surface temperature would significantly further increase as disagreement became 331% and 309% for surface's emissivity of 0.84 and 0.2, respectively, compared to 106% when boundary condition was set as semi-transparent, Figure 5.14. In addition, the temperature for other surfaces would increase leading to increasing the disagreement with experimental readings.

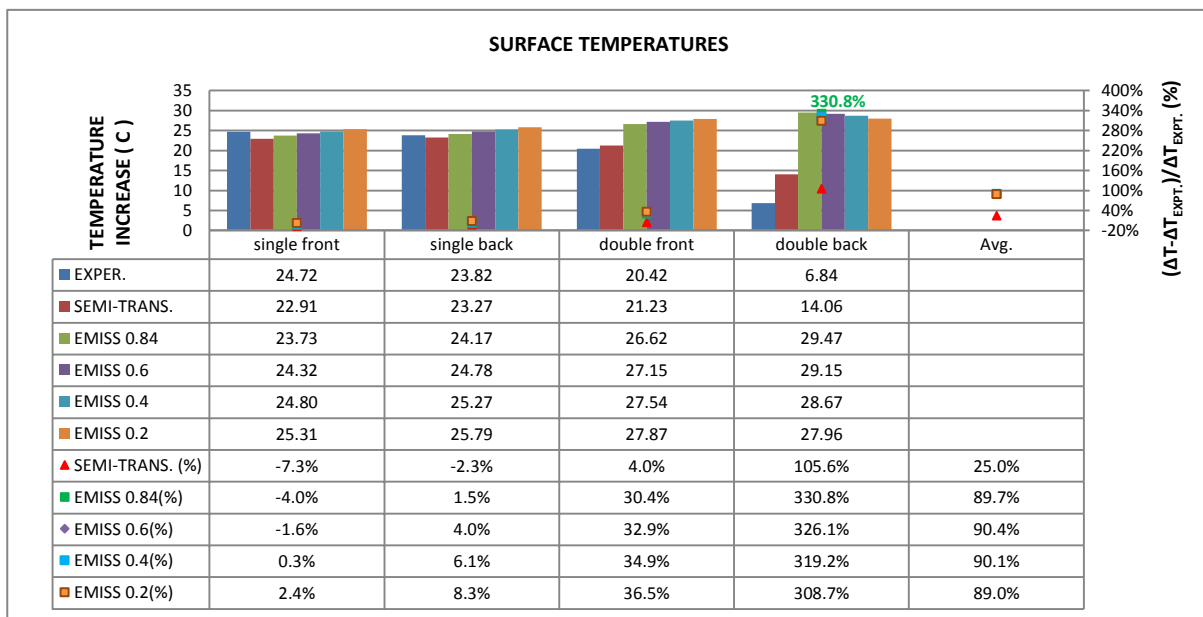


Figure 5.14: Surface temperatures and changes for different glass surfaces under the effect of various turbulence models.

Figure 5.15 shows velocity profiles at height of 1.1m inside the cavity with different examined surface's emissivities. Compared to results by semi-transparent BC, new profiles show nearly negligible improvements except for the boundary layer next to the inner double glass as velocity would increase due to the increase in surface temperature.

Therefore, it is concluded that to include the effect of the low-e coating film on the inner surface using the current method, it is necessary to model this film as a semi-transparent medium with exact solar and thermal

characteristics. However, this option was not available for this work, as the authors (of original published validation work) did not provide solar and thermal characteristics of that film.

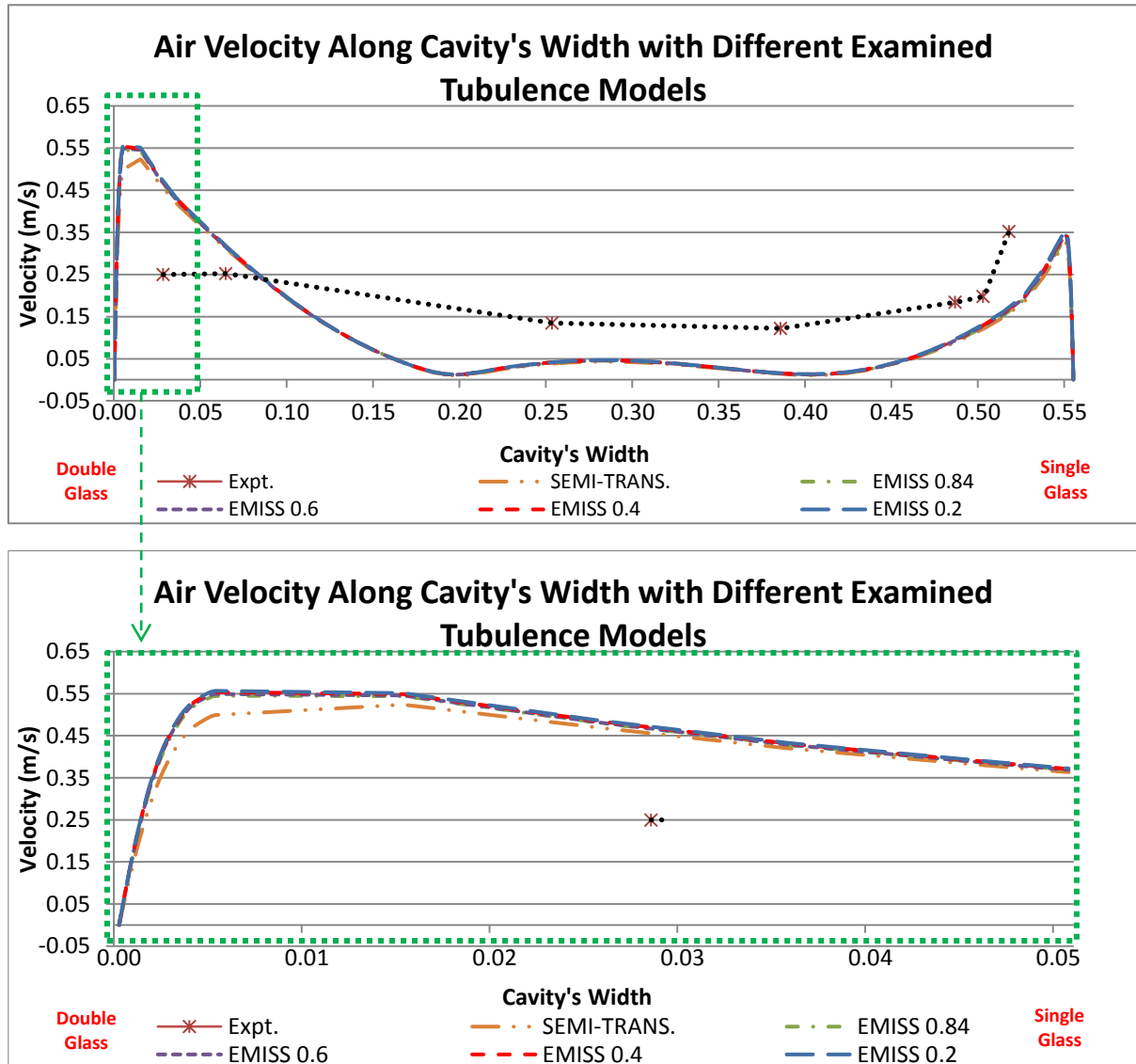


Figure 5.15: Air velocity profiles at mid-height (1.1m) of cavity with different surface emissivities for inner surface of the double glass.

5.4.6 Validation Cases and Results:

For the purpose of comprehensive validation, two cases were re-modelled: non-shaded cavity and shaded cavity with integrated slats. Both were with a measured solar irradiance of 715W/m². All previous conclusions were included in these simulations unless otherwise stated.

In addition, through this work, the level of simplification for the validated structure was further examined to determine to what extent this would influence predictions of both airflow and thermal behaviours of the system. Four different levels were examined as shown in Table 5.5:

Table 5.5: codes for different levels of simplification.

Code	Level of Simplification
A	Detailed representation for cavity vents (grilles).
B	Full detailed representation (vents grilles and cavity's bottom and top meshes).
C	No grilles at all.
D	Simple cavity structure (two vertical glazed walls with vertical inlet and outlet).

5.4.6.1 Non-shaded cavity: No shading slats inside the cavity

Figure 5.16 shows that all scenarios, except simple cavity, would be able to predict surface temperatures close to experimental ones for both faces of the single outer glass and front face of the double inner glass.

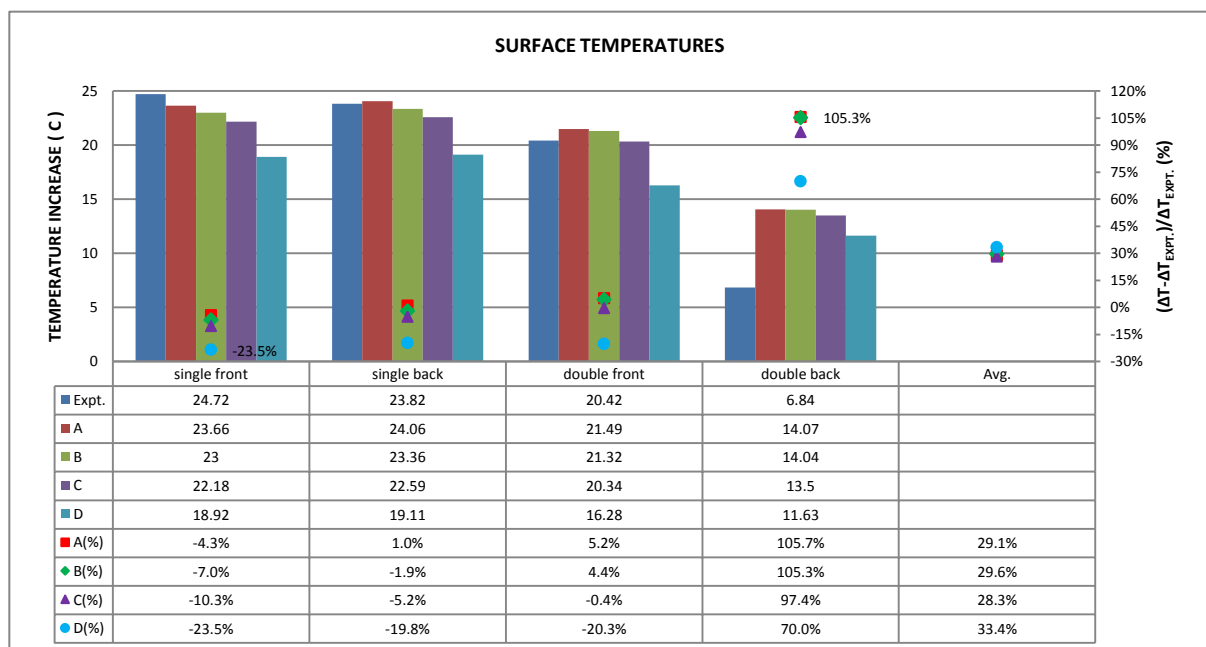


Figure 5.16: Surface temperatures and changes for different simplification levels for validated structure.

In general, better agreement was for A-scenario. For the back face of the inner glass, none of those scenarios was with good agreement even though D-scenario is still the closest with a discrepancy of 70%. This significant discrepancy is due to excluding the low-e film pointed out earlier.

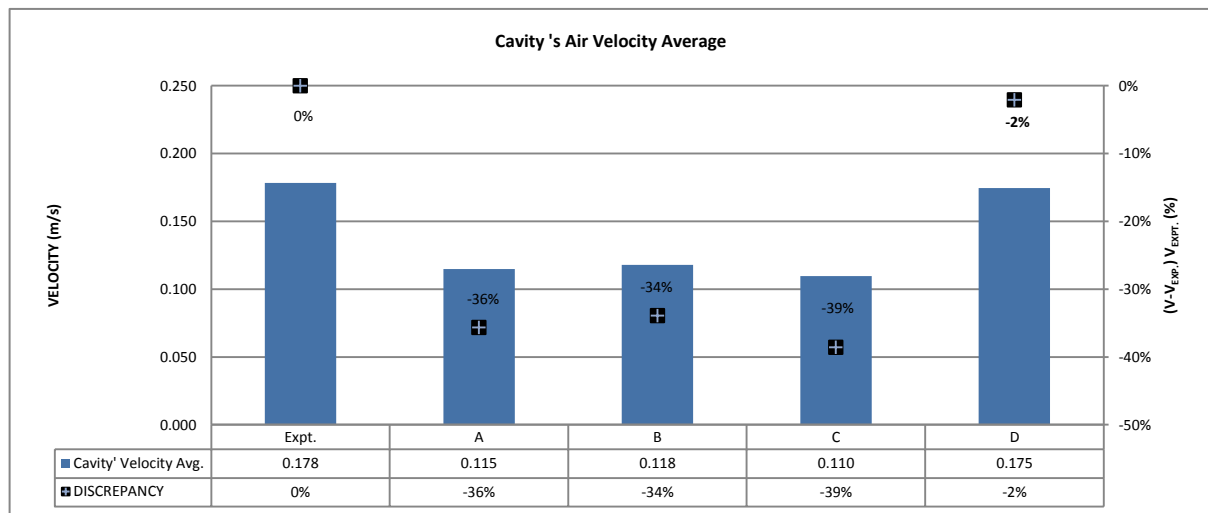


Figure 5.17: Air velocity averages and relative changes for cavity's med-height (1.1m) under the effect of various turbulence models.

On the other hand, Figure 5.17 shows velocity averages at mid-height (1.1m) of the cavity for all examined levels of simplifications. It was found that simple cavity (D-scenario) would produce an average close to experimental one (that was worked out from the plotted graph of 7 readings) with a change of just 2% (velocity profiles are shown in Figure 5.18). This is due to the fact that with a simple cavity that had vertical vents, air would be well-distributed with clear uniformity and higher magnitudes along the entire width due to less flow resistance at the wider vents. Also, noticeable enhancement in flow was noticed in the area next to single glass surface (outer layer) due to the change in flow direction with these vents. For other scenarios, air velocity would be relatively low in areas far from surfaces, as air would enter the cavity diagonally through the horizontal vents toward the double glass (inner layer). In fact, the wider vents for simple cavity (D-

scenario) that equals cavity width (0.55m) compared to typical vents' size (0.24m) for other scenarios was the reason behind the noticeable increase in air velocity magnitude for the aforementioned, because of lower flow resistance.

As also shown in Figure 5.18, velocity boundary layer next to inner double glass (with for all calculated scenarios) would be higher than experimental readings. This was due to the high-predicted temperatures for back surface of that glass due to the absence of low-e coating, which also affect the temperature for front surface of same glass and cause higher buoyancy effect. For example, when the calculated temperature (produced by D-scenario) of that surface was relatively close to experimental one, calculated air velocity profile was also relatively close to corresponding profile from the experiment.

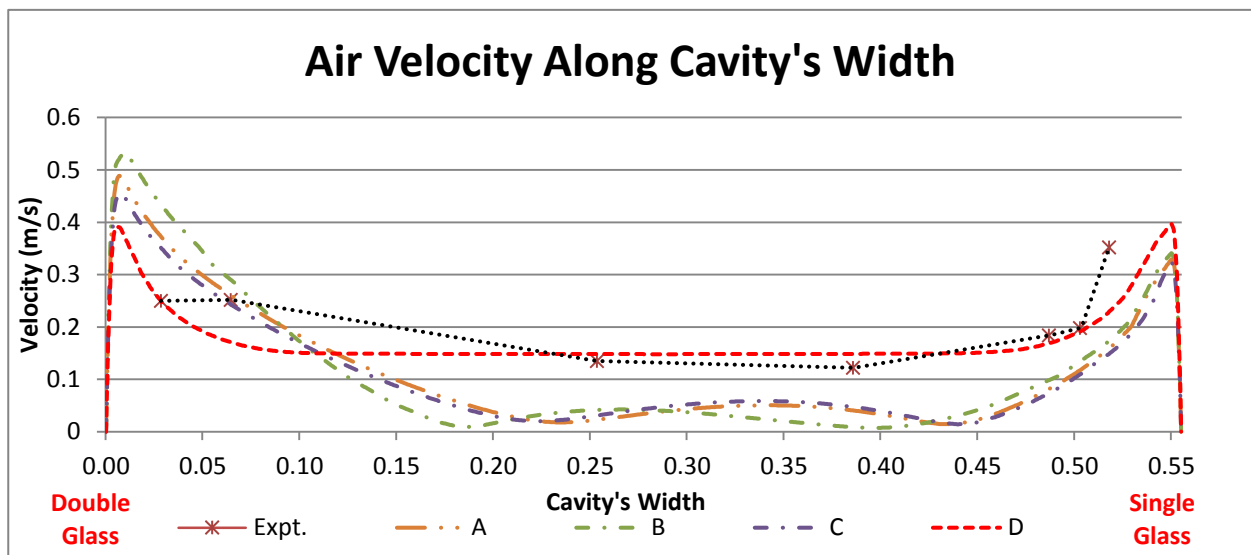


Figure 5.18: Air velocity profiles at mid-height (1.1m) of cavity for difference scenarios of structure simplification.

As discussed, simple cavity (D-scenario) would produce velocity results with best agreement with experiment but it would significantly under-predict surface temperatures (except inner face) due to the high airflow rate through its cavity. However, while simple cavity could theoretically better match experimental thermal and flow phenomenon, it still does not represent the real configuration of the structure; i.e. wide vertical vents instead of narrower horizontal vents. On the other hand, regarding the disagreement by more detailed representation (e.g. B-scenario), it was later noticed that two published works including one by same publishers of experimental results (Ji et al., 2007; Iyi et al., 2014), on the validation of this structure do not present any validation of air velocity, which may suggest a possible concern if reported velocity results would be suitable for validation. Hence, predicted results by modelling could still be valid.

Generally, it is concluded that detailed representation for the configuration of structure, characteristics of transparent & semi-transparent mediums and source of heat are really vital but resource- & time-consuming. Therefore, a good understanding of the case of interest is highly important for better balance between all these factors to ensure realistic representation, good results and save time & resources. Hereafter, either scenario A or B for simplification level could be used in this scope for exploring more details of the validated case.

5.4.6.2 Shaded cavity: with integrated shading slats

Again, the same structure was validated but with integrated slats. It is worth mentioning that external extension for computational domain, here,

was equal to the real distance in rig, 0.6m. Different turbulence models were again investigated and k-w SST model was found to be the best. Presented results are just for air velocity through the cavity, and for integrated slats with inclination angles of: 0°, 30°, 45° and 60° degrees. However, significant disagreements are still shown, Figure 5.19, between experimental results and calculated ones.

As shown in Figure 5.20, the computational model would again under-predict the air velocity for most of the target points, especially in the middle width of the cavity. However, this difference would be smaller with relatively larger inclination angles.

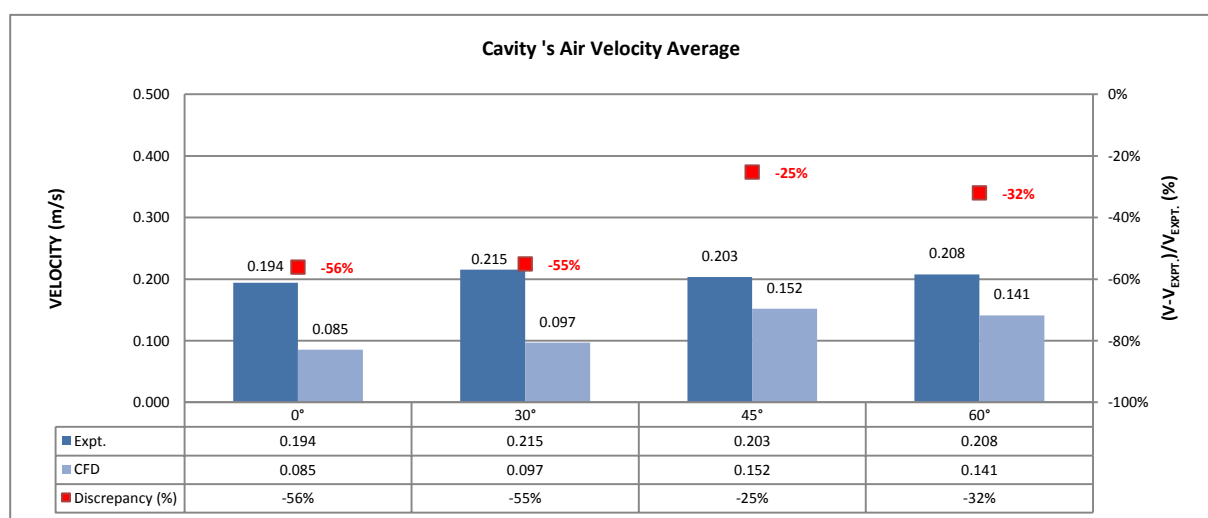
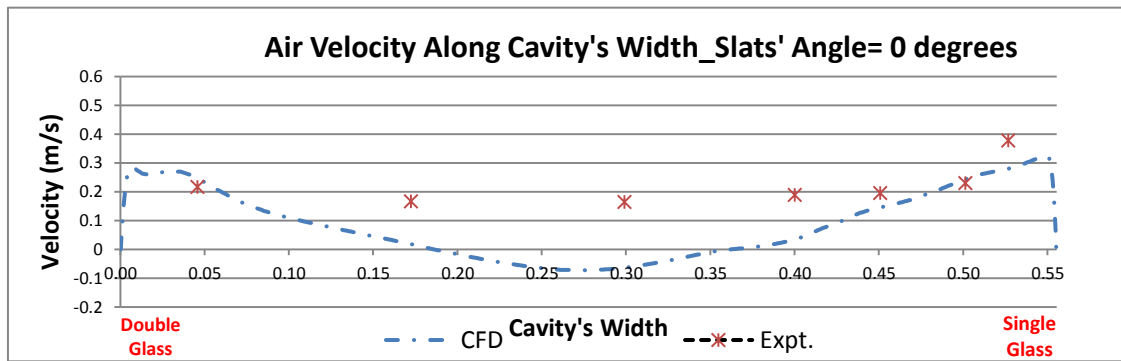
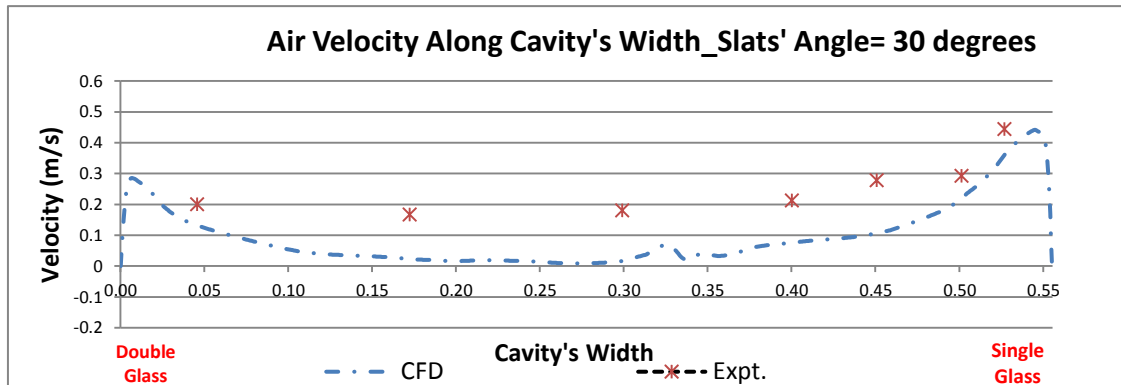


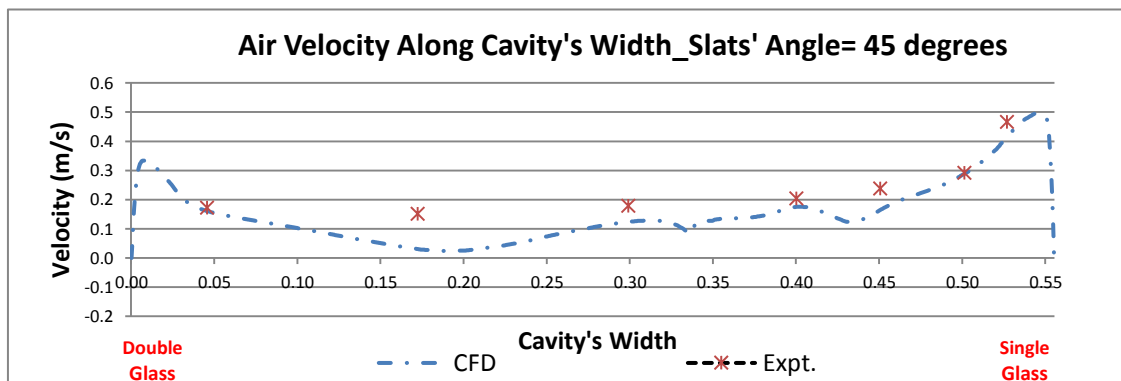
Figure 5.19: Experimental and calculated air velocity averages and relative changes for cavity's med-height (1.1m) with integrated shading devices having different inclination angles.



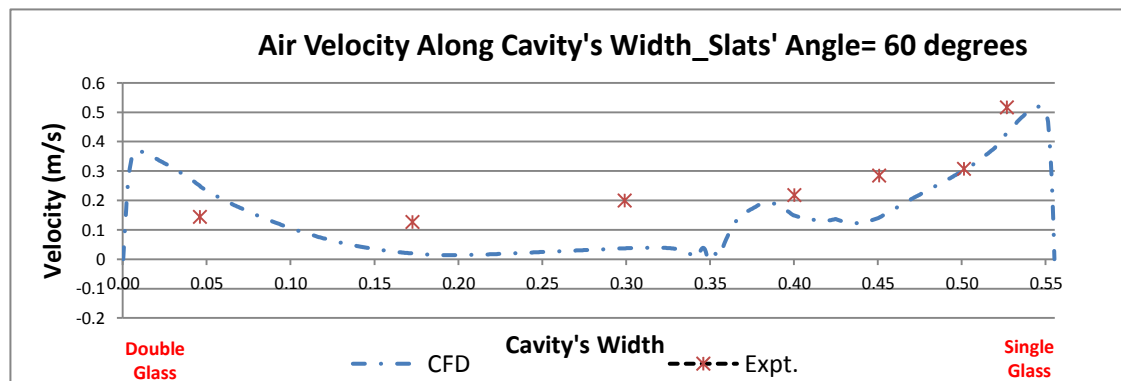
A) Inclination angle: 0 Degrees



B) Inclination angle: 30 Degrees



C) Inclination angle: 45 Degrees



D) Inclination angle: 60 Degrees

Figure 5.20: Air velocity profiles at mid-height (1.1m) of the cavity with integrated slats with different inclination angles.

In addition to previous potential reasons behind the noticeable discrepancy between measured and calculated results, especially for air velocity, the authors of the experimental work have stated some further possible reasons in their own validation work on same structure (Ji et al., 2007); these are:

- The little mixing occurs within the domain due to natural convection, as thermal boundary layers were still narrower compared to experiment.
- Glass properties: absorption coefficients at solar and thermal bands were determined based on measured transmittance and thickness using Beer's law. However, transmittance can vary depends on glass surface conditions.
- Uncontrollable air temperature in experiment; i.e. inlet air temperature and chamber's indoor air temperature.
- Exposing the thermocouples to direct solar radiation that caused higher surface temperatures for them and integrated slats in experiment compared to CFD, so producing higher buoyant air movement in experiment.
- Simplification of inner double glass where the low-e coating at the inner surface of the double glass was not included.

5.4.7 Conclusion and Recommendations:

Whereas the computation model has shown good capability for predicting surface temperatures with acceptable errors compared to experimental findings, corresponding results for cavity air velocities were still with significant disagreement. However, the following lessons and recommendations could be derived from this validation work:

→ General outcomes and Recommendations:

- A)** A better understanding of the physics of similar structures with more details.
- B)** Explore the vital factors that influence the performance of such structures.
- C)** Determine the level of simplification of structure for modelling purposes, which is still acceptable and maintain comprehensive representation for both thermal and flow phenomenon; and most importantly serves the objectives of the research's interest.
- D)** Investigate the importance of accurate representation for the solar source, and detailed modelling of semi-transparent mediums (i.e. glass) with correct solar and thermal characteristics, i.e. solar-band dependent values for transmittance and absorptance.

→ Specific outcomes and recommendations:

- A) Glass:** modelling its medium with correct thickness using independent mesh (e.g. inflation); more care should be given for boundary layers.
- B) Materials:** set the right characteristics and specifications for various materials; i.e. air, glass, aluminum, etc.

- C)** Source of heat: high importance of accurate representation of the solar source with both right magnitudes and beam directions.
- D)** Radiations: selection of proper radiation model, i.e. Discrete Ordinates (DO) with sufficient settings for Non-Gray Model: number of bands (2 bands) and its wavelength intervals: Solar (0-2.7 μm) and Thermal (2.7-1000 μm). Also, setting the sufficient parameters for Angular Discretization, i.e. Theta & Phi Divisions (both 6) and Theta & Phi Pixels (both 3).
- E)** Turbulence model: both RNG $k - \varepsilon$ and SST $k - \omega$ could possibly be used for such problems, which are generally recommended for natural convection in cavities.

Next section shows a further validation works for the same Fluent model, in particular, its ability to predict airflow rates (velocity) of structures having natural ventilation (buoyancy driven flow). The aim of these works was to further ensure the ability of the built Fluent model to effectively simulate the flow and associated heat transfer mechanisms through DSF systems investigated by this research.

5.5 Further Validation Works

5.5.1 Model Validation against Simple Cavity with Horizontal Inlet and Outlet:

This section presents a further validation work for CFD fluent model, in particular, its ability to predict airflow rates of structures having natural ventilation (buoyancy driven flow). A cavity with C-shape (Figure 5.21), and similar to that experimentally investigated by La Pica et al. (1993), was simulated using CFD fluent model with RNG $k-\varepsilon$ turbulence model with enhanced wall treatment. The cavity was with horizontal inlet and outlet; each had a height similar to cavity width. Boundary conditions and results for the experimental work were reproduced from Gan (2011b). And, cases were classified into three categories based on the width of cavity: 0.075m, 0.125m and 0.170m. For each width, there were five different cases; each had a different total heat flux. The heat source was limited to given heat flux assigned to the heated wall (inlet wall: the wall had both vents). Figure 5.22 presents contours of velocity magnitude for 0.125m-wide cavity with a total heat flux of 296W/m².

Figure 5.23 shows that predicted results by CFD model were with good agreement with experimental measurements. Maximum discrepancy was less than 10%; and average discrepancies were 5.4%, 4.9% and 1.3% for widths of 0.170m, 0.125m and 0.075m; respectively. Furthermore, overall average discrepancy for all widths was about 3.9%, which also agreed with corresponding findings by Gan (2011b) where the difference was less than 5%. Thus, it was concluded that CFD model would efficiently be able to predict

airflow rates in naturally ventilated cavities using tested model with RNG $k - \varepsilon$ turbulence model.

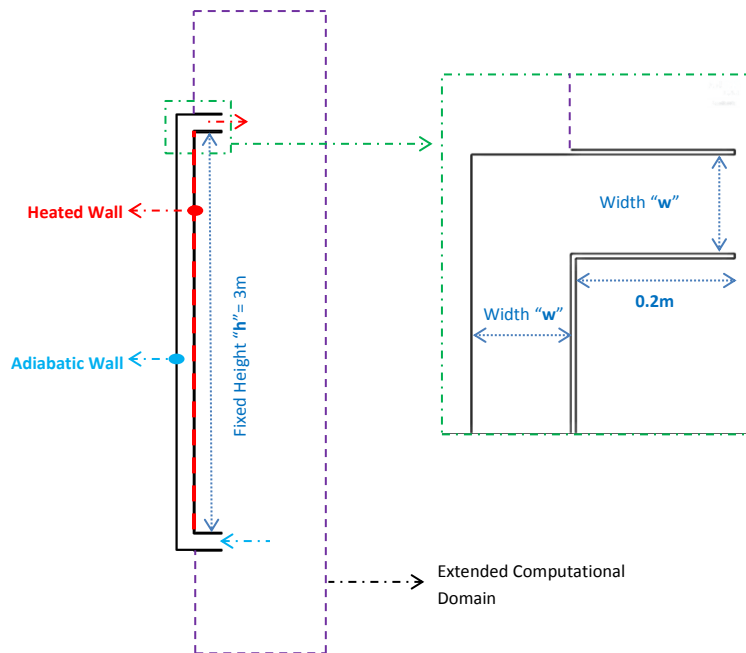


Figure 5.21: Schematic for the C-shape cavity investigated by La Pica et al. (1993) and simulated by the Author. Width = 0.07m, 0.125m or 0.170m.

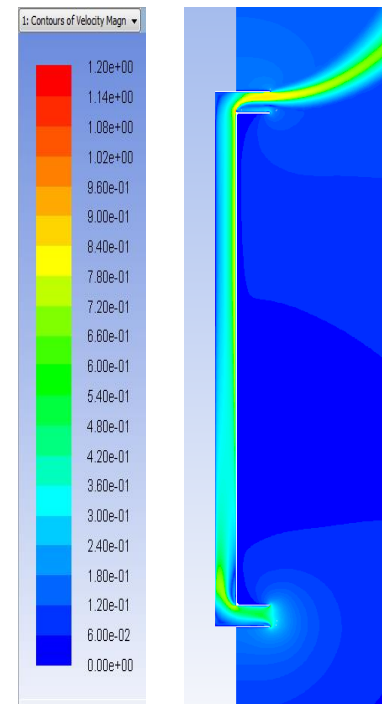


Figure 5.22: Contours of Velocity Magnitude (m/s) for investigated cavity with width of 0.125m and total heat flux of 296W/m².

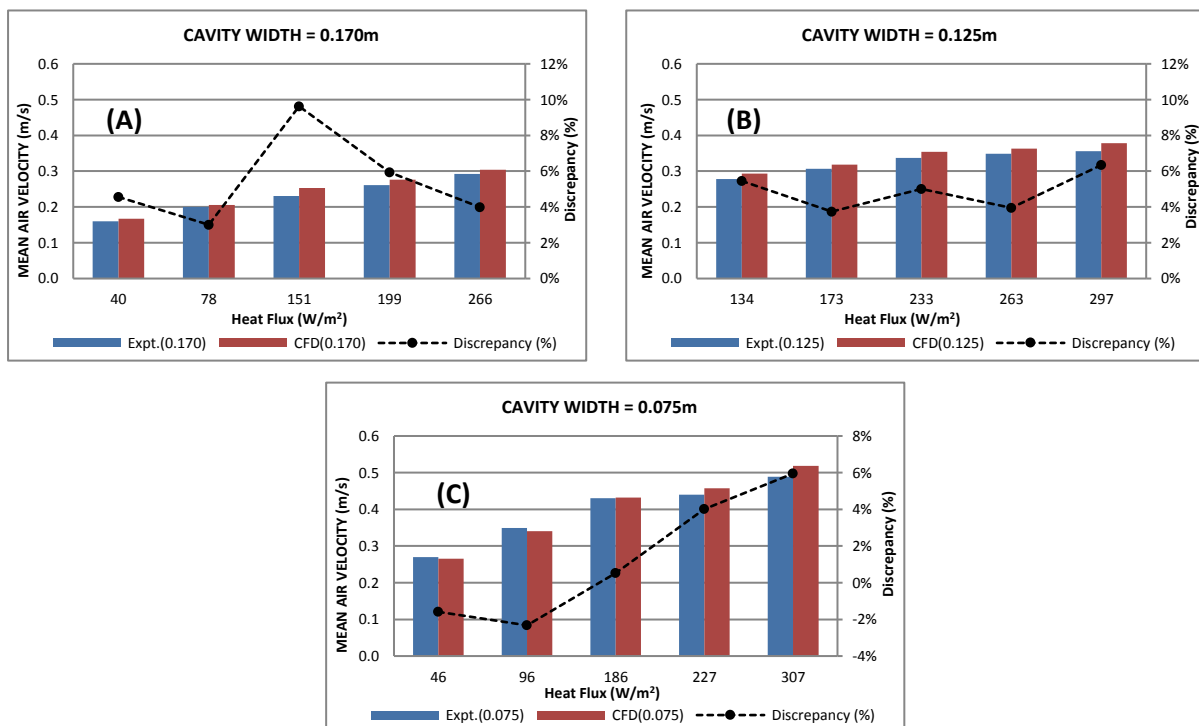


Figure 5.23: Comparison between measured air velocity (La Pica et al., 1993) and calculated air velocity using fluent model. (A) Cavity width=0.170m; (B) Cavity width=0.125m & (C) Cavity width=0.075m.

5.5.1.1 Investigating the importance of Height-to-Width ratio (h/w) on cavity's air velocity profiles:

Figure 5.24 shows that calculated air velocity profile at mid-height for the cavity of La Pica et al. (1993) was significantly different from calculated one for the cavity of Mei et al. (2007) (validated in previous section) even both had same total heat flux (200W) and distribution ratios (50% for each side-wall). For the aforementioned with cavity height of 3m, heat flux rate was 33.3W/m^2 whereas it was 50W/m^2 for the later with a height of 2m. Air velocity average was 0.286 m/s for the aforementioned and 0.118 m/s for the later as the aforementioned cavity (3m-high and 0.125m-wide) was relatively much taller with h/w ratio of 24 compared to just 3.7 for the later (2.05m-high and 0.55m-wide). It is also clear that the taller cavity had more uniform velocity profile with a maximum change of 18% (relative difference between two-peak-values average and total average) compared to a significant change of 259% for short cavity. For such tall cavities (e.g. h/w=24), velocity boundary layers are expected to merge at a certain level along the cavity height, and this why velocity profile seems to be more uniform afterward; according to the established theory. Again, this conclusion supports the concern about the reliability of experimental velocity results by Mei et al. (2007) as calculated velocity seems to be more reasonable as discussed in the previous section.

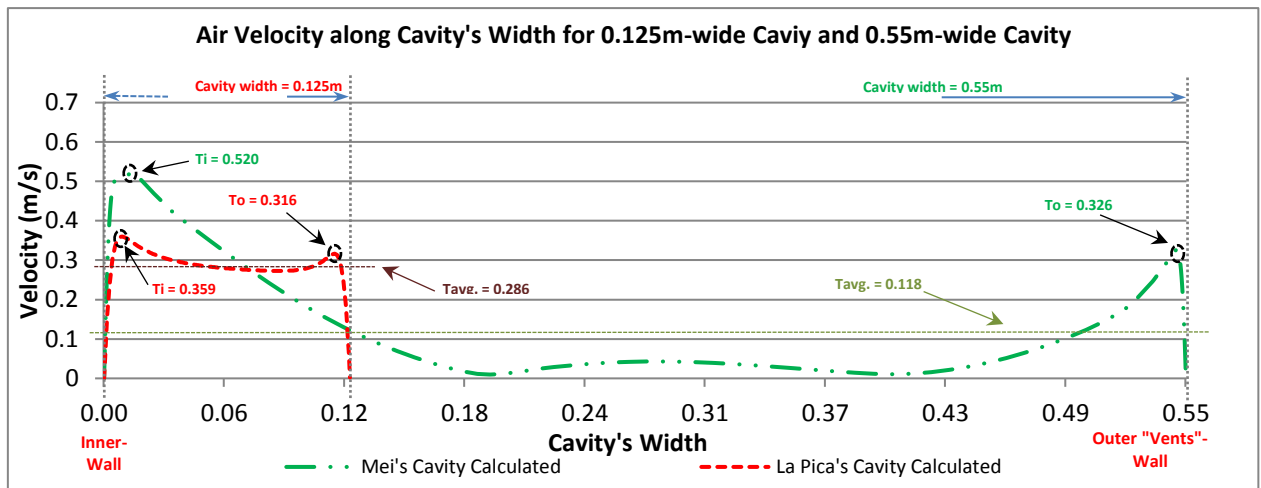


Figure 5.24: Air Y-Velocity profiles at mid-height levels along widths of both 0.125-wide cavity of La Pica et al. (1993) and 0.55-wide cavity of Mei et al. (2007).

5.5.2 Fluent Model Validation against Established General Expressions

This section presents an additional work aimed to further verify the validity of Fluent computation model to sufficiently predict both airflow and heat transfer rates. This validation was done for a simple cavity (3m-high and 0.3m-wide) with both inlet and outlet were vertical vents as shown in Figure 5.25. Also, total heat flux was equally distributed on both side-walls of the cavity (distribution ratio=50%).

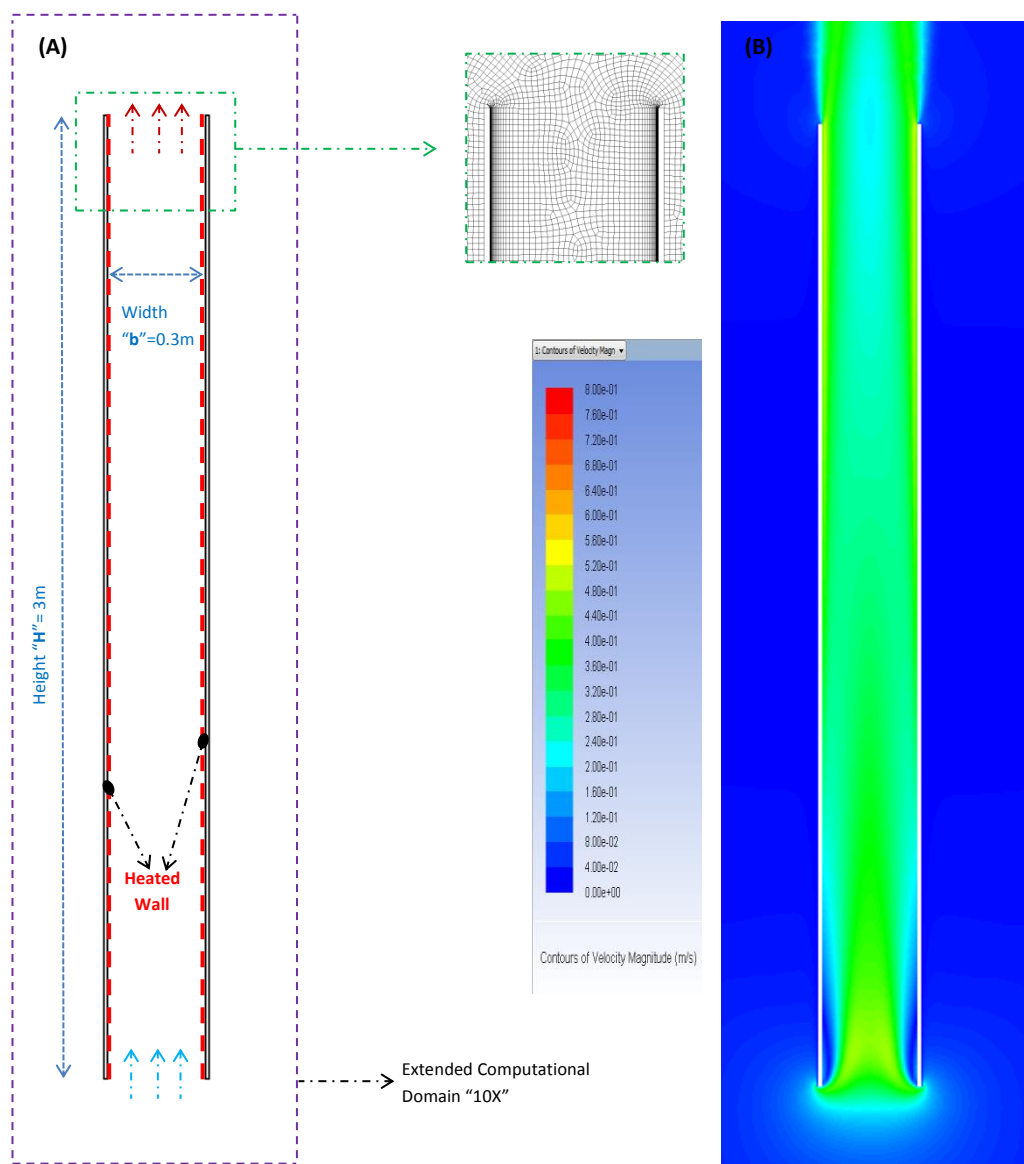


Figure 5.25: (A) schematic for the simple simulated cavity. (B) velocity Contours for same cavity with total heat flux = 100W/m^2 (B).

However, validation concept was based on non-dimensional numbers: Reynolds numbers "***Re***" (non-dimensional velocity) for airflow rates and Nusselt numbers "***Nu***" for heat transfer rates. These numbers were worked out through two different methods: the first is named as "*Predicted CFD*", which was based on Fluent simulation outputs and used equations (5.16) & (5.17) to calculate the ***Nu*** numbers and equation (5.18) to find out the ***Re*** numbers.

$$Nu = \frac{h_c b}{k} \quad (5.16)$$

Where:

Nu : Nusselt Number (non-dimensional);

h_c: Convective heat transfer coefficient (W/m²K);

b: Cavity's Width (m) "characteristic length";

k : Air Thermal Conductivity (W/mK), which is based on average temperatures of cavity wall surfaces and inlet air; i.e., [$\frac{1}{2}(t_1 + t_2) + t_{air}$]/2.

$$h_c = \frac{q_{avg}}{\Delta t} = \frac{\left(\frac{q_1 + q_2}{2}\right)}{\left(\frac{t_1 + t_2}{2}\right) - t_{air}} \quad (5.17)$$

Where:

q_{avg} : Average heat flux; ***q₁*** & ***q₂*** : heat flux on wall-1 & wall-2; respectively.

Δt : Temperature difference; ***t₁*** & ***t₂***: surface temperatures for wall-1 & wall-2; respectively; ***t_{air}***: Air temperature (K).

$$Re = \frac{Q}{v} = \frac{Vb}{v} \quad (5.18)$$

Where:

Re: Reynolds Number (non-dimensional).

Q: Airflow rate (m³/s); ***V***: Air velocity (m/s); ***v***: Air kinematic viscosity (m²/s).

$$Ra = \frac{g\beta \left(\frac{q_1 + q_2}{2}\right) b^4}{v\alpha k} \frac{b}{H} \quad (5.19)$$

Where:

Ra: Rayleigh Number (non-dimensional);

g: Gravitational acceleration (m/s²); **β** : thermal expansion coefficient (1/K);

α : Air diffusion coefficient (m²/s) as [$\alpha = k/(\rho C_p)$]; **ρ** : air density; ***C_p***: specific heat.

The second method is labelled as “Calculated Gan-2011” that used well-established general expressions with appropriate constants as provided by Gan (2011a) to calculate both Nu and Re using equations (5.20) and (5.21); respectively. However, to calculate Nu , Rayleigh number Ra was first calculated using equation (5.19) and based on cavity characteristics (both geometrical and thermal).

$$Nu = c_1 \left[Ra \left(\frac{H}{b} \right)^{3/2} \right]^m \quad (5.20)$$

Where:

c_1, m : Constants, which are for a cavity with vertical flow vents and heat distribution ratio between 20%-50% set as $c_1 = 0.137$ and $m = 0.265$.

$$Re = \frac{(Nu/c_2)^{1/n}}{Ra^a} \quad (5.21)$$

Where:

c_2, n, a : Constants, which are for a cavity with vertical flow vents and heat distribution ratio between 20%-50% set as $c_2 = 0.143$, $n = 1/m$ and $a = 0.391$.

Figure 5.26 shows a good agreement between calculated Re numbers using Gan-2011’s expressions and those based on CFD results as maximum deviation was 7% for small total heat flux “100W/m²”, whereas overall average disagreement was about 3%. This indicates suitability of CFD Fluent model to efficiently predict airflow rates throughout such heated vertical cavities. Similarly, Figure 5.27 presents calculated Nu numbers using general expressions and CFD results; however, results show that CFD Fluent model under-predicted heat transfer rates as predicted Nusselt numbers were lower than those mathematically obtained by Gan-2011’s expressions. Minimum difference was 7.9% for smallest heat flux (100W/m²) and maximum change

was about 17.6% for largest heat flux (1000W/m²). However, overall disagreement was about 14% that can still be acceptable. Furthermore, it was found that over-prediction for side-walls' surface temperatures (heated walls) and temperature gradient within their thermal boundary layer could be behind producing lower *Nu* values according to equations (5.16) and (5.17). Also, it was highlighted that the quality for generated mesh for thermal boundary layers could attribute to over-prediction of surface temperature, which was later given more attention throughout the rest of work.

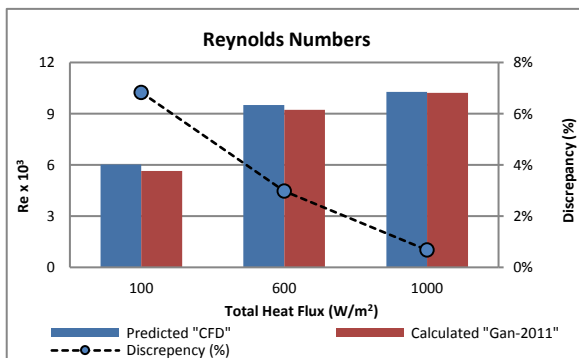


Figure 5.26: Comparison for "Re" Reynolds Numbers calculated using Gan-2011's general expressions and predicted based on CFD results.

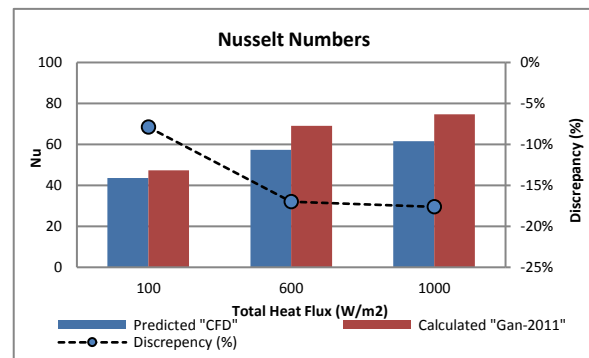


Figure 5.27: Comparison for "Nu" Nusselt Numbers calculated using Gan-2011's general expressions and predicted based on CFD results.

CHAPTER 6 MODEL SETUP AND DEVELOPMENT

6.1 Introduction:

This chapter presents the adopted methodology for simulating and analyzing the investigated DSF as a given problem; in particular, air flow and associated heat transfer. The general aim is to predict both airflow and thermal performance of the system. As concluded from the previous chapter, CFD approach would be used and ANSYS Fluent solver is considered.

A brief introduction is given for relevant boundary conditions and how to be represented. Then, general settings for Fluent solver are discussed (Turbulence, Radiation, Material and Solution method & control). Necessary preliminary studies for CFD work is conducted, which include mesh independence study and effect of computation domain's extension. Most importantly, a new solar radiation modelling technique was introduced and compared to common technique. Then, final updates to benchmark mode are presented.

6.2 The Problem:

Briefly, this work aimed to investigate and optimize the use of DSF in office buildings in Amman/Jordan. On another scale, special attention was given to the integrated shading devices, as additional works were carried out. Benchmarks for the DSF system and office was based on relevant studies and general regulations for office buildings in Amman. Whereas ventilation and thermal performance of the system are the main target, ANSYS Fluent was used to model airflow and associated heat transfer through.

6.3 Boundary Conditions:

The section mainly deals with the boundary conditions for the computational model. The common types of boundary condition are set, which include both solar irradiance and air temperature.

6.3.1 Solar Irradiance Magnitudes:

For better investigation of the influence of solar irradiance on both airflow and thermal performance of the structure, the interaction between the solar irradiance and various elements of the structure has to be carefully modelled, which requires a detail representation for different components of the solar irradiance. Thus, both diffuse and beam components were calculated; and defined into two wavelength bands as solar characteristics for different elements (glass and integrated slats) vary from one band to another. Both solar components for the two solar bands were computed using SPECTRAL2 model, which was developed and validated by Bird and Riordan (1984). However, an additional validation for SPECTRAL2 model was done by the author as part of this research, using a climatic data for the city of Nice (France) published by Safer et al. (2005c) for similar work.

Figure 6.1 shows both published and calculated values for beam solar irradiance for different solar bands on the south-oriented wall at 12 pm on 21st July in Nice city of France. Results have good agreement with a maximum discrepancy of 5% for the solar band of 0.78-2.7 μ m; and just 0.03% for the total band of interest (0.0-4.5 μ m). Similarly, Figure 6.2 shows corresponding results for the diffuse component; where the maximum discrepancy was about

6.4% for the solar band of 0.78-2.7 μ m, and just 0.14% for the total solar band.

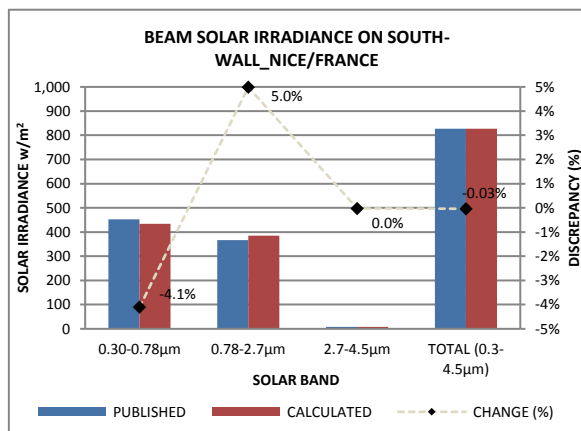


Figure 6.1: Comparison of published and calculated Beam solar irradiance on south-wall in Nice city of France; on 21/7; at 12pm.

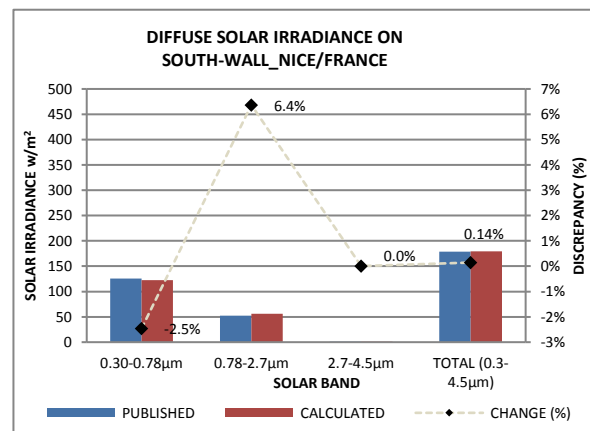


Figure 6.2: Comparison of published and calculated Diffuse solar irradiance on south-wall in Nice city of France; on 21/7; at 12pm.

Figure 6.3 shows a comparison of both beam and diffuse values for original solar irradiance on the south-oriented wall on the summer design day at 12 pm in Amman (Bird and Riordan, 1984; Amaireh, 2012; Amaireh, 2016). Results show a good agreement between the two calculation methods with a maximum discrepancy of 8% for beam component and 5% for total radiation. These data are the same used for modeling here, which again shows the validity of SPECTRAL2 model to calculate the solar irradiance components for this study.

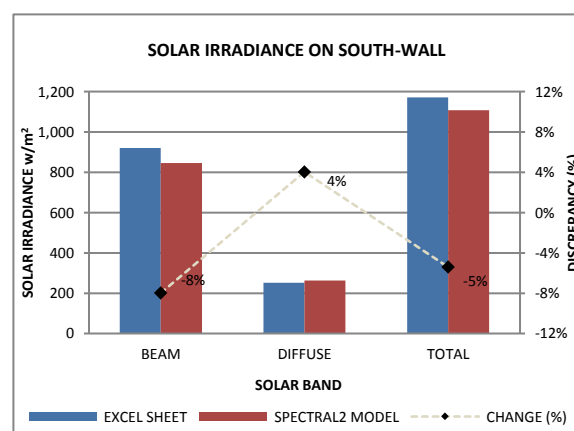


Figure 6.3: Comparison of solar irradiance values calculated by SPECTRAL2 model and Excel sheet model for summer design day of Amman, 6th July.

The required values were computed for both Summer and Winter design days; at 12 pm. Moreover, with the aforementioned model, generating the boundary conditions becomes more flexible to cover more scenarios. Detailed parameters for both design days are shown in Table 6.1.

Table 6.1: Parameters for Summer and Winter design days.

	PARAMETER	SUMMER	WINTER
SITE	Latitude °	31.98	31.98
	Longitude °	35.98	35.98
DAY	#(365)	187	23
TIME	Hour	12	12
	Angle °	81.0	38.9

Tabular data in Table 6.2 and Table 6.4 show breakdown details for Actual and Equivalent methods, respectively, regarding summer design day. Equivalent Method indicates the method that uses equivalent “worth” amount of solar irradiance with normal direction for incidence instead of the original amount with actual angle of incidence “Actual Method”.

Table 6.2: Solar components and their values for the Actual Method; for south-vertical wall at 12pm on day# 187 (6th July); Amman/Jordan. Summer Design Day.

THE ACTUAL METHOD _ SUMMER			
	SOLAR IRRADIANCE (w/m ²)		
WAVELENGTH BANDS	BEAM	DIFFUSE	TOTAL
0.00 - 0.78 µm	447.55	168.88	616.44
0.78 - 2.70 µm	390.48	91.54	482.02
> 2.7 µm	8.16	1.61	9.77
TOTAL	846.20	262.03	1108.22
DIRECTION	81° (ACTUAL)	NORMAL	
	BEAM	DIFFUSE	DIFFUSE (%)
Solar (<2.7 µm)	838.03	260.42	24%
Thermal (>2.7 µm)	8.16	1.61	16%

Table 6.3: Solar components and their values for the Equivalent Method; for south-vertical wall at 12pm on day# 187 (6th July); Amman/Jordan. Summer Design Day.

THE EQUIVALENT METHOD _ SUMMER			
	SOLAR IRRADIANCE (W/m ²)		
WAVELENGTH BANDS	BEAM (EQUIVALENT)	DIFFUSE	TOTAL
0.00 - 0.78 μm	69.85	168.88	238.74
0.78 - 2.70 μm	60.95	91.54	152.48
> 2.7 μm	1.27	1.61	2.88
TOTAL	132.07	262.03	394.10
DIRECTION	NORMAL	NORMAL	
	BEAM (EQUIVALENT)	DIFFUSE	DIFFUSE (%)
Solar (<2.7 μm)	130.80	260.42	67%
Thermal (>2.7 μm)	1.27	1.61	56%

Table 6.4 and Table 6.5 present corresponding details for same methods but for winter design day.

Table 6.4: Solar components and their values for the Actual Method; for south-vertical wall at 12pm on day# 23 (23rd Jan.); Amman/Jordan. Winter Design Day.

THE ACTUAL METHOD _ WINTER			
	SOLAR IRRADIANCE (W/m ²)		
WAVELENGTH BANDS	BEAM	DIFFUSE	TOTAL
0.00 - 0.78 μm	270.95	197.05	468.00
0.78 - 2.70 μm	319.87	102.27	422.14
> 2.7 μm	7.14	1.00	8.14
TOTAL	597.96	300.32	898.28
DIRECTION	38° (ACTUAL)	NORMAL	
	BEAM	DIFFUSE	DIFFUSE (%)
Solar (<2.7 μm)	590.82	299.32	34%
Thermal (>2.7 μm)	7.14	1.00	12%

Table 6.5: Solar components and their values for the Equivalent Method; for south-vertical wall at 12pm on day# 23 (23rd Jan.); Amman/Jordan. Winter Design Day.

THE EQUIVALENT METHOD _ WINTER			
	SOLAR IRRADIANCE (W/m ²)		
WAVELENGTH BANDS	BEAM	DIFFUSE	TOTAL
0.00 - 0.78 μm	210.82	197.05	407.86
0.78 - 2.70 μm	248.88	102.27	351.15
> 2.7 μm	5.55	1.00	6.56
TOTAL	465.25	300.32	765.57
DIRECTION	NORMAL	NORMAL	
	BEAM (EQUIVALENT)	DIFFUSE	DIFFUSE (%)
Solar (<2.7 μm)	459.70	299.32	39%
Thermal (>2.7 μm)	5.55	1.00	15%

6.3.2 Air Temperature:

Ambient air temperatures for different design days were derived from the weather data for Amman/Jordan, and specifically for the hours of interest. Table 6.6 shows the temperature values for both scenarios:

Table 6.6: Ambient air temperatures for both design days and at the specific hours.

Design Day	Date	Time	Ambient Temp. (°C)
Summer	6 th July	12pm	37°
Winter	23 rd Jan.	12pm	4°

6.3.3 Indoor Boundary Conditions:

Indoor boundary conditions refer to internal heat gains in addition to the requirements of artificial air conditioning, in case it was required. Both of these components are presented in relevant chapters hereafter.

6.4 Solution Method's Set-up: Settings for Fluent Solver

The study was conducted through two-dimensional (2D) modelling with Fluent code; work has been done via CFD Ansys package. The purpose was to simulate the airflow and associated heat transfer (coupled convective, conductive and radiative) through the structure (office and attached DSF) and surrounding environment (ambient air).

6.4.1 Turbulence Model:

For modeling expected turbulent airflow, the viscous model was set to *k-epsilon* ($k - \epsilon$) with sub-model as **RNG**, as this showed relatively best general performance with related validation cases. Furthermore, *Enhanced Wall Treatment* was chosen under the options for *Near-Wall Treatment*. However, at further stages of the work, turbulent model was switched to *k-*

$\Omega(k - \omega)$ with sub-model of **SST** as solution convergence criteria was difficult to be achieved with **RNG $k - \varepsilon$** . Still, that was accepted as both **RNG $k - \varepsilon$** and **SST $k - \omega$** are generally recommended for natural buoyant flow modelling in similar research problems through the wide literature; also, both are endorsed by the end of relevant validation work presented in this thesis. In addition, it is worth mentioning that just one was considered for the entire work on each of the parameters.

6.4.2 Radiation Model:

Radiation model was set to Discrete Ordinate (**DO**). The option of Non-gray model was activated with two bands named as solar and thermal; and distinguished with wavelength intervals as shown in Table 6.7. Also, Table 6.8 shows characteristics for the angular discretization for the radiation model; divisions were 6 and identical for both Theta and Phi angles whereas pixels were 3 and also identical for both angles (Iyi et al., 2014).

Table 6.7: Energy band for Non-Gray radiation model with wavelength intervals.

Name	Start (μm)	End (μm)
Solar	0	2.7
Thermal	2.7	1000

Table 6.8: Characteristics for Angular Discretization.

Angular Discretization	Divisions	Pixels
Theta	6	3
Phi	6	3

6.4.3 Material Modelling and Specifications:

Air was modelled as a transparent medium; the glass was modelled as semi-transparent; aluminum Venetian blinds were modelled as opaque solid. Based on general recommendations in addition to the conclusion of the validation on the specific problem, relevant specifications were defined for used materials in Table 6.9.

Table 6.9: Thermal and solar properties for different materials.

	Air "4°C"	Air "20°C"	Air "37°C"	Glass	Frames	Venetian -Blinds	Indoor Walls
TEMP (°C)	4°	20°	37°	-	-	-	-
THICKNESS (mm)	-	-	-	6	-	-	-
DENSITY (kg/m ³) "Boussinesq"	1.275	1.205	1.139	2500	2719	2719	2320
SPECIFIC HEAT "Cp" (J/kg-k)	1005	1005	1005	840	871	871	1138
THERMAL CONDUCTIVITY (w/m-k)	0.0245	0.0257	0.0269	1.7	202.4	202.4	0.5
VISCOSITY (kg/m-s)	1.74e-05	1.81e-05	1.89e-05	-	-	-	-
EXPANSION COEFFICIENT (1/K)	0.00361	0.00343	0.00323	-	-	-	-
REFRACTIVE INDEX	1	1	1	1.5	1.44	1.44	1

Moreover, additional solar and thermal characteristics for semi-transparent mediums were also determined. For instance, glass's absorption coefficient (α) was calculated based on its transmittance (T) and using Beer's law relationship, equation (6.1), (Ji et al., 2007). Table 6.10 presents calculated Absorption coefficients (α) for two different glass thickness (δ) values (6 & 12 mm) and with different nominal solar transmittance values.

$$\alpha = (-\ln T)/\delta \quad (6.1)$$

Where; δ is the thickness (m) of glass pane.

Table 6.10: Absorption Coefficient (α) for two selected glass's thickness values δ (m) and various examined transmittance values (T).

Transmittance (T)	α (1/m)	
	6mm Glass	12mm Glass
0.10	383.8	191.9
0.20	268.2	134.1
0.30	200.7	100.3
0.40	152.7	76.4
0.50	115.5	57.8
0.60	85.1	42.6
0.67	66.8	33.4
0.70	59.4	29.7
0.80	37.2	18.6
0.90	17.6	8.8

6.4.4 Solution Methods, Control and Convergence Criteria:

- A) As mentioned earlier, the cases were solved using Fluent code with double precision for better accuracy.
- B) Solution Methods: solution scheme was kept as default "SIMPLE" whereas Spatial Discretization for different equations was set as shown in Table 6.11:

Table 6.11: set-up for solution methods in fluent.

Spatial Discretization	
Gradient	Least Squares Cell Based
Pressure	PRESTO!
Momentum	Second Order Upwind
Turbulent kinetic Energy	Second Order Upwind
Turbulent Dissipation Rate	Second Order Upwind
Energy	Second Order Upwind
Discrete Ordinates	Second Order Upwind

- C) All the solutions started with initial low values for under-relaxation factors to achieve good stability for the solution before being increased gradually and schematically toward default values to speed up the convergence, Table 6.12. As discussed before, the target for all normalized residuals was to drop for less than 1×10^{-3} for all solved equations except energy to 1×10^{-6} . Generally speaking, the target was achieved after a schematic control for the under-relaxation factors. However, the residual for continuity equation was sometimes accepted between 1×10^{-2} and 1×10^{-3} .

Table 6.12: Initial Under-Relaxation Factors used for different equations/parameters in the solution control.

Equation / Parameters	Under-Relaxation Factors (URFs)	
	Initial URF	Default URF
Pressure	0.2	0.3
Density	1	1
Body Forces	1	1
Momentum	0.5	0.7
Turbulent Kinetic Energy	0.5	0.8
Specific Dissipation Rate	0.5	0.8
Turbulent Viscosity	1	1
Energy	0.9	1
Discrete Ordinates	1	1

D) Also, relative change for all monitored values (of interest) was not to exceed 0.5%-1% at apart of 10,000 iterations. Generally, this was maintained for all cases and change was sometimes <0.1%. However, the solution was usually solved for not less than 20,000-30,000 iteration to achieve that target. However, where there was a noticeable persistent oscillation, an average was taken for the monitored values with range not less than 10,000 iterations.

6.5 Preliminary Studies:

This section shows two preliminary studies prior to the main work, these are the independence of mesh and extension of computation domain.

6.5.1 Independence of Mesh Size:

In addition to the revealed recommendations from mesh independence study for relevant validation work as discussed earlier, another mesh independence study was done for the specific problem with initial configuration. Three meshing cases were investigated with different characteristics; Table 6.13. Generally, changes were either for domains sizes (glass medium and air) or surfaces' layer inflations. One more case was

investigated where region adaptation was conducted for all vents, which resulted in a mesh size of 287,253 cells. Figure 6.4 shows the final considered mesh, Mesh4.

Table 6.13: Characteristics for different examined meshes.

	Mesh1	Mesh2	Mesh3	Mesh4
#cells	145,121	188,943	201,517	287,253
SIZE				
GLASS SIZE (mm)	5	5	3	3
DOMAIN SIZE (mm)	100	100	50	50
INFLATION*	#layers			
GLASS (MEDIUM)	11	21	21	21
GLASS WALLS	10	20	20	20
DOMAIN WALLS	10	20	20	20
REGION ADAPTATION	-	-	-	Vents (2 times)
* is a technique “option” used in mesh generation to control both size and quality of mesh next to given boundary element.				

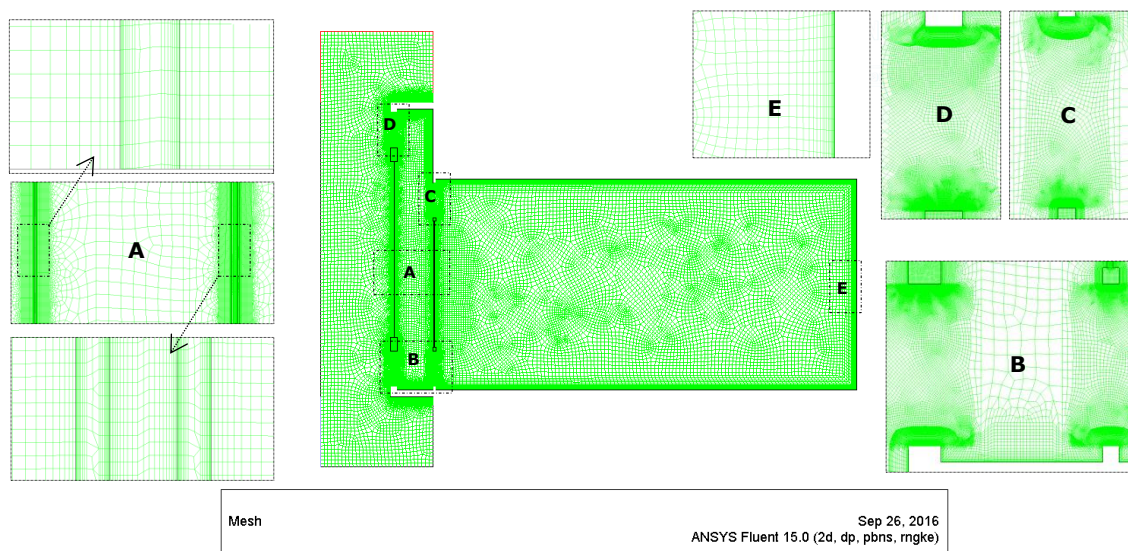


Figure 6.4: Generated mesh for initial studied structure; Mesh4.

Figure 6.5 shows the temperatures for glass surfaces with different meshing cases. Changes were always less than 2%. However, with Mesh4, change dropped to less than 1% except for Inner_Back (back surface for inner double glass) where it was 1.3%, which was also acceptable.

For airflow, averages for air velocities were calculated for both office and cavity outlets; Figure 6.6. Whereas Mesh3 had a change of 1.5% (DFS

outlet) and 1.2% (Office outlet) in reference with Mesh2, Mesh4 made no change to Office's outlet but 0.7% to DSF's outlet when compared to Mesh3. Therefore, either Mesh3 or Mesh4 could be used for the purpose of this study.

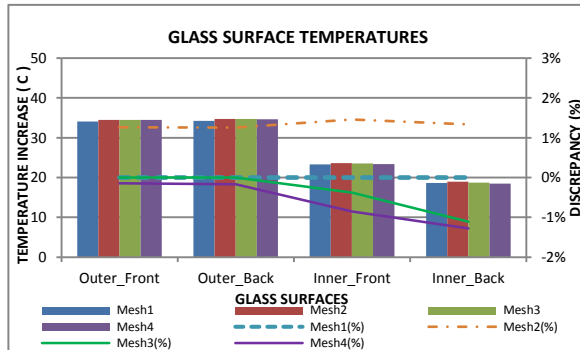


Figure 6.5: Surface temperatures and changes for different elements with the three mesh scenarios.

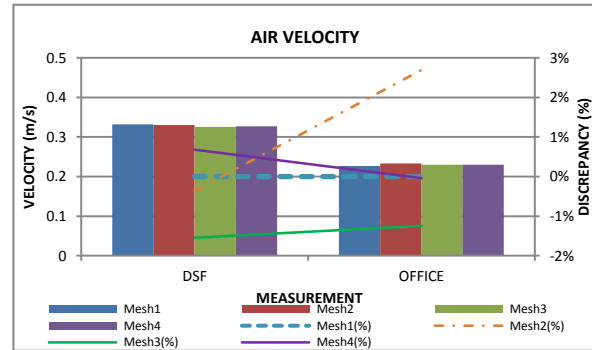
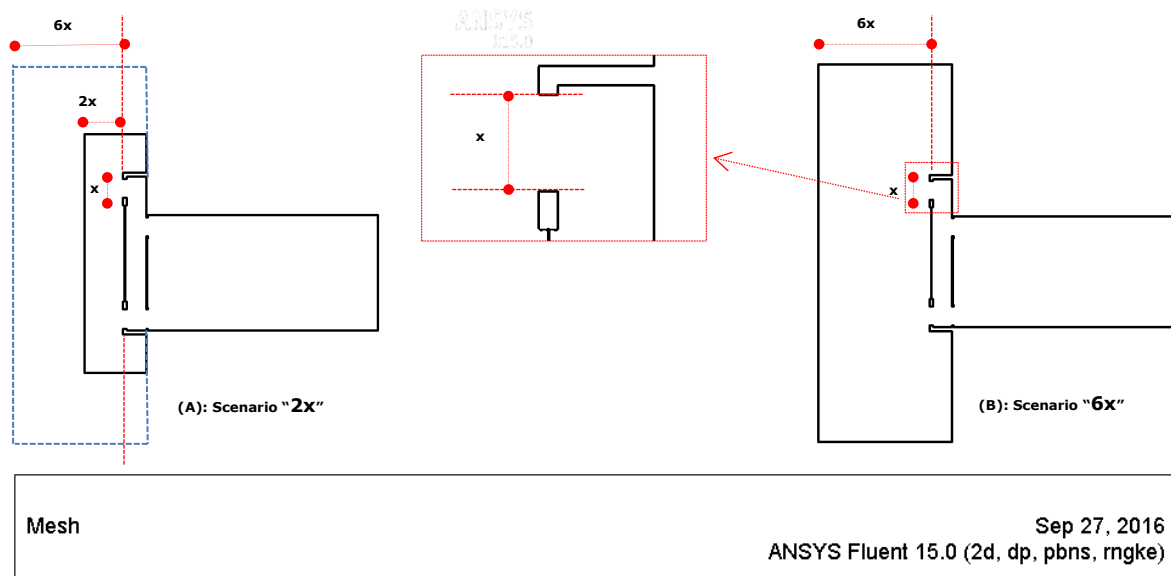
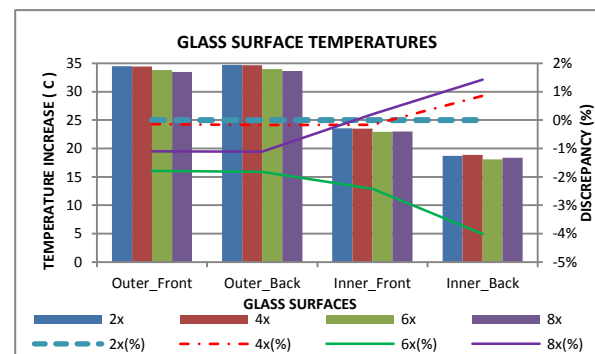
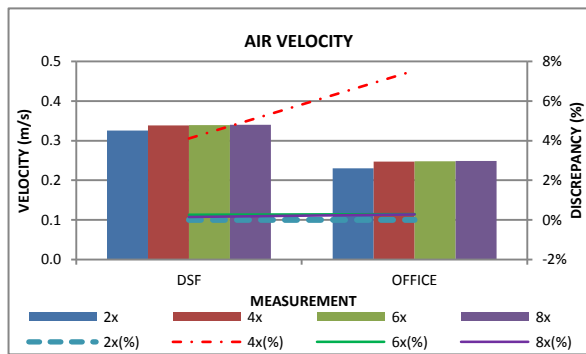


Figure 6.6: Air velocity and changes for cavity's mid-height (1.1m) and its outlet with the three mesh scenarios.

6.5.2 Extension of the Computational Domain:

Regarding the initial configuration of the cases, another study on the influence of extension of their computational domain was conducted. Four scenarios were set as: 2x, 4x, 6x and 8x; where x refers to the initial height for cavity's external vents (0.5m).

It was revealed that changes in air velocity for both the office and cavity were limited to 0.3% when the extension size was increased from 4x to 6x, Figure 6.7, which means feasibility of using 4x for smaller mesh size and less requirements for computing resources. On the other hand, corresponding changes for surface temperatures were still as high as 4% while it dropped to 1.4% between 6x and 8x; Figure 6.8. Therefore, it was decided that scenario 6x could be used for this study. This means that a distance (3.0m) between the outer glass pane and opposite boundary of the computational domain equals six times (6x) the cavity's width (0.5m) should be used. Figure 6.9 shows schematics for both scenarios: 2x and 6x; and highlight the main differences.



6.6 A New Method for Solar Radiation Representation:

Here, a brief description of both investigated methods: Equivalent and Actual is presented. The new method for representing solar irradiance in the model, named as "Actual Method" was introduced with a brief comparison to common "Equivalent Method". Next, a preliminary study on the differences between those two methods was conducted and results are presented with discussion on revealed pros and cons for each.

Generally, Equivalent refers to the component (worth amount) of solar irradiance that incidents on the outer face of the structure in the normal direction. This mainly deals with beam radiation component and includes different solar wavelength bands. Hence, the term "Equivalent" is hereafter used to distinguish the method where the equivalent amount of incident radiation is being calculated and then implemented into the computational model with normal incidence direction. Diffuse component is still assigned as diffuse with its actual magnitude. On the other hand, the term "Actual" refers to the method where the actual magnitude for both diffuse and beam radiation components are implemented in the computational model; combined with the hourly angle of incidence for beam component.

The purpose of this part of work is to explore the potential pros & cons for each method and then highlight main differences in order to select the proper method that serves the aim & objectives of this research.

Whereas the actual method needs a vertical extension to accommodate the correct position for beam solar transmitter with correct angle of incidence, this extension would vary depending on the hourly angle. However, for this study, the extension was determined based on the requirements for largest incident angle covered for this work, which was 81° degrees for Summer design day at 12 pm. Moreover, the new dimensions for the extended domain were also considered for the Equivalent method, even though there was no necessity, to eliminate any possible discrepancies due to changing the computational domain.

Figure 6.10 presents the final computational domain with a brief description of its different boundaries. The case shown was for Design-1 integrated slats (5cm with 45° degrees). The same computational domain was used for Design-6 integrated slats.

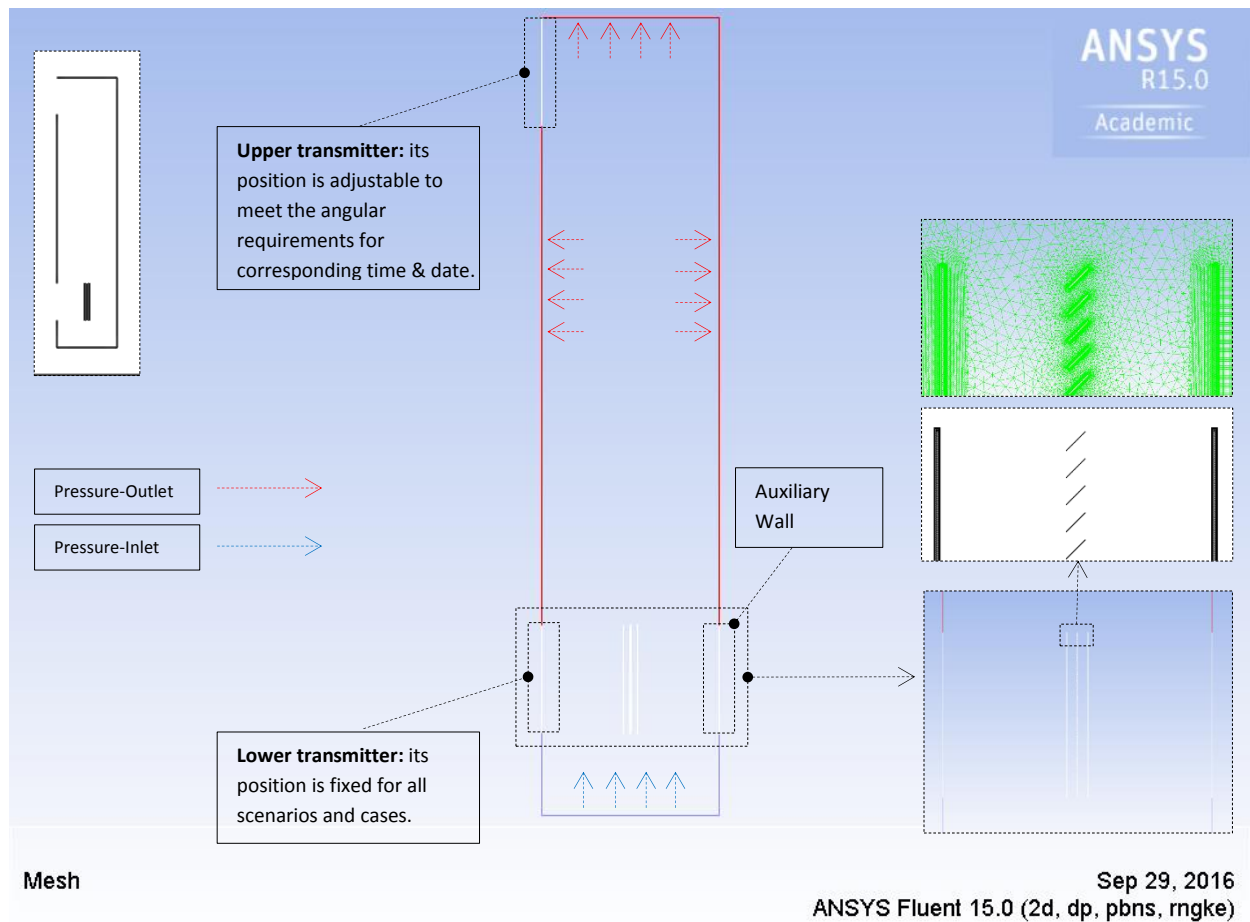


Figure 6.10: Extended computational domain with integrated slats (5cm; 45°) for either method.

Figure 6.11 shows both methods with more focus on solar transmitters' features. With the Equivalent method, just the lower transmitter is active as beam component was converted into the equivalent amount, Figure 6.12, which was assigned to that transmitter with normal incident direction, along with diffuse component. On the other hand, with the Actual method, both upper and lower transmitters are active. Whereas diffuse component was assigned to lower transmitter, beam component was assigned to the upper transmitter with real incident angle for better representation for direct beam

solar irradiance, thus better representation for the actual interaction between this component and various elements of the structure; i.e. glass panes, simple and arbitrary integrated elements.

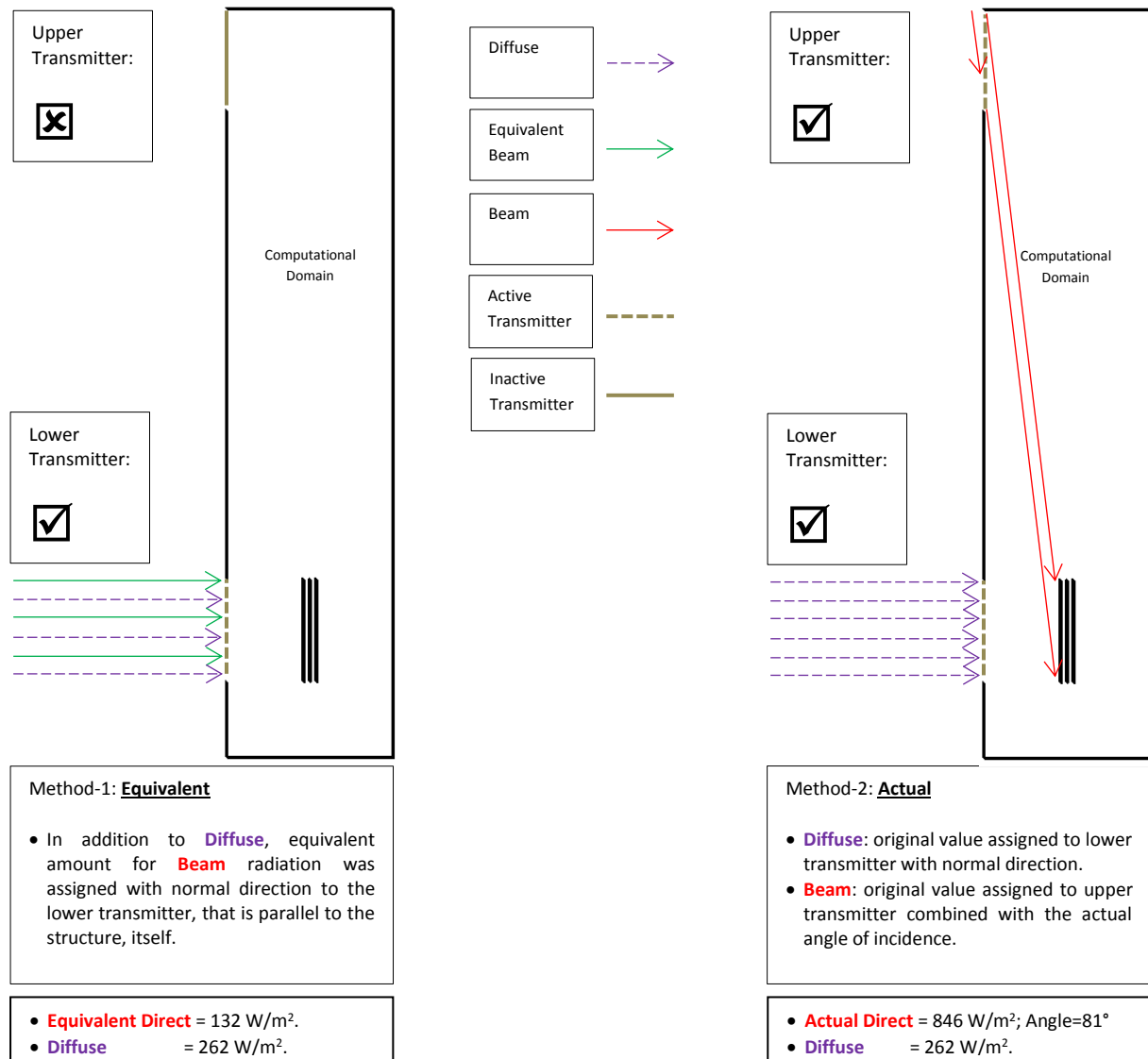


Figure 6.11: Schematic diagrams showing both methods for representing solar irradiance in the computational model; Equivalent Method (left) and Actual Method (Right).

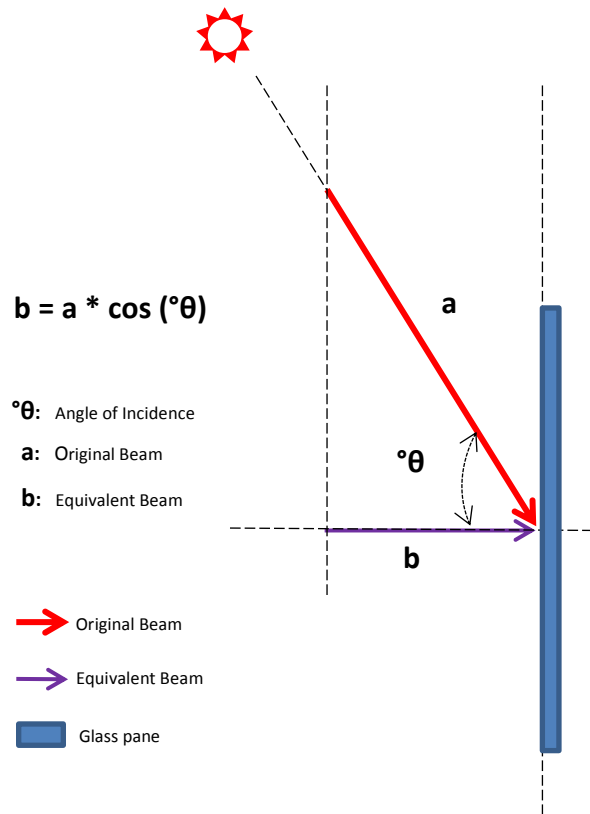


Figure 6.12: Schematic diagram showing the relation between original (a) and equivalent (b) solar beam components.

Figure 6.13 shows the investigated cavity with horizontal vents. In addition, schematic drawings are presented for two of the investigated designs of integrated slats.

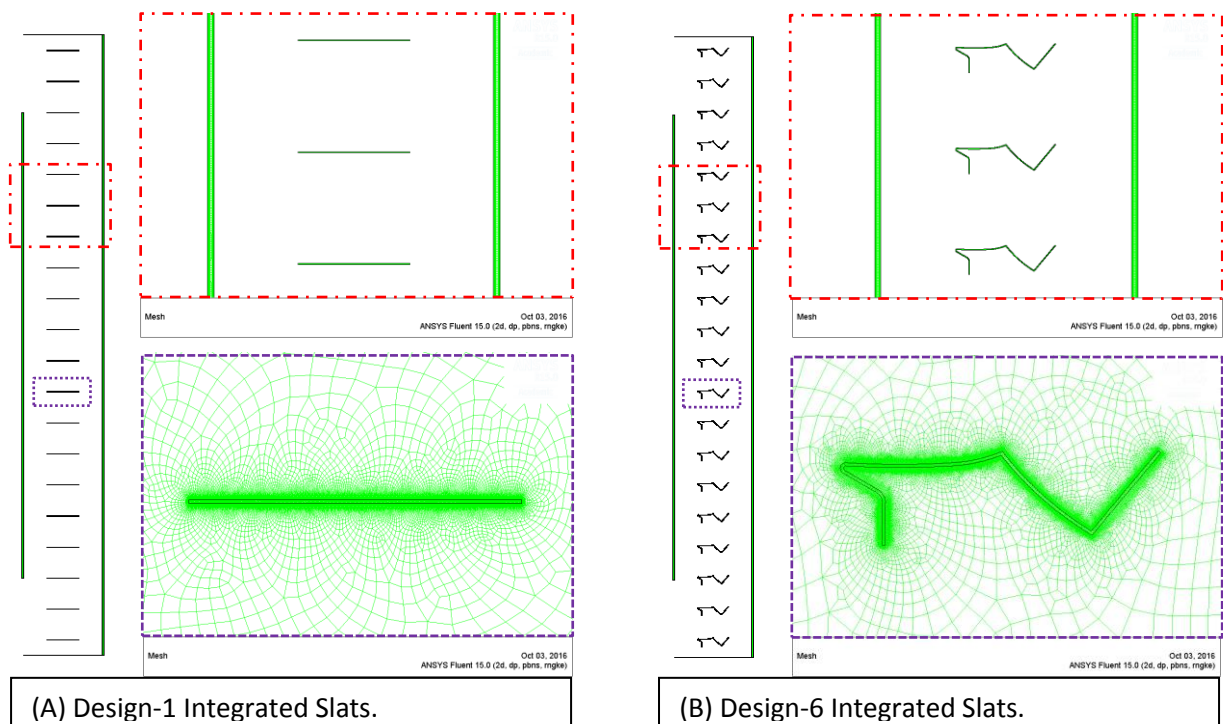


Figure 6.13: Investigated Designs for integrated slats: (A) Design-1 and (B) Design-6; with cavities having Horizontal vents.

6.6.1 Simple Cavity with Vertical Vents:

With diffuse characteristics for both glass and slats surfaces, results showed a difference in airflow rate of 4.2% between both suggested methods; with a higher magnitude for the Actual method; Figure 6.14. However, with specular characteristics, this difference increased to 11.8% but with a higher value for the Equivalent method.

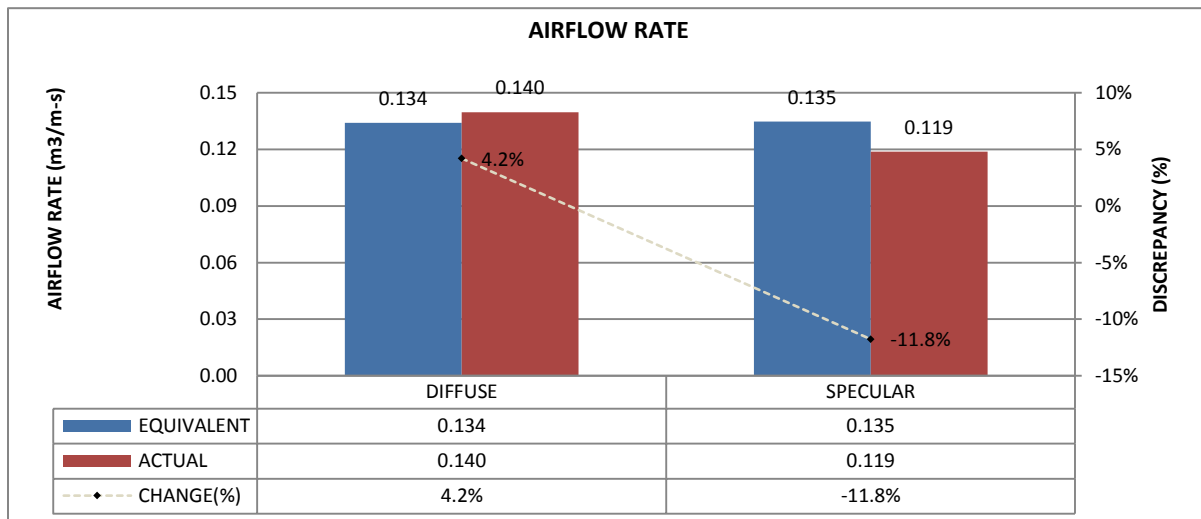


Figure 6.14: Airflow through cavity for both investigated scenarios with percentage of changes; with both diffuse and specular characteristics for glass and slats surfaces.

For surface temperatures, the actual method would produce temperatures higher than those for the equivalent method when those surfaces have diffuse characteristics; the difference was between 8-9%; Figure 6.15. On the other hand, corresponding differences increased to a 14% and 28% for outer and inner glass surfaces, respectively, as surface temperatures dropped significantly with the actual method; Figure 6.16. The reason behind this increase is due to the nature of glass surfaces with specular properties, as transmitted solar radiations would continuously be influenced by incident angle and, here, would hit the lower part of the inner glass pane. This also interprets why the change for inner glass temperature was double

that for outer glass (28%:14%). As a result, temperature average for inner glass surface would be lower than that for outer glass. The specular properties for integrated slats would also play a similar effect in the distribution of reflected radiation.

Hence, these findings highlight the necessity for accurate representation of incident solar radiation for better calculations of airflow and surface temperatures. This necessity becomes more important with materials having specular characteristics, which is more common in real constructions.

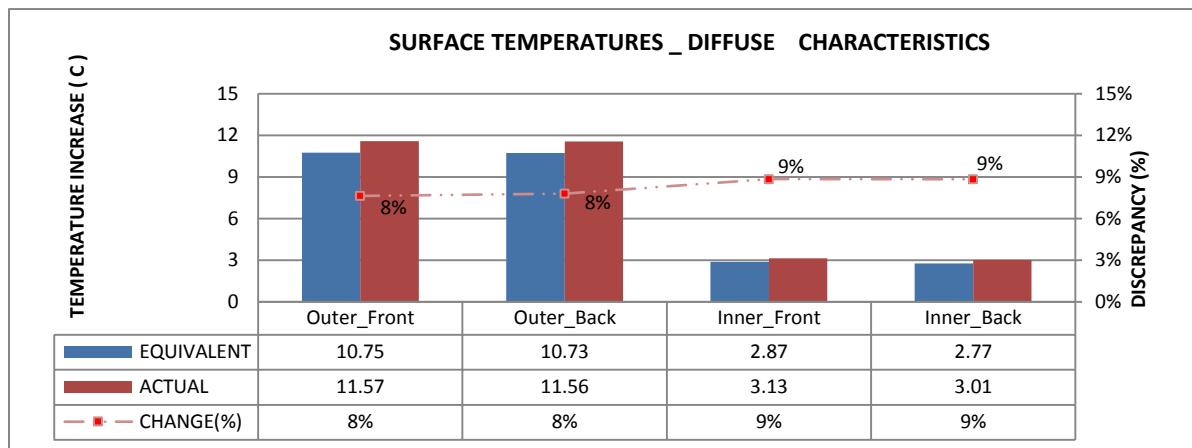


Figure 6.15: Glass's surface temperatures for both investigated scenarios with percentage of changes; with diffuse characteristics for glass and slats surfaces.

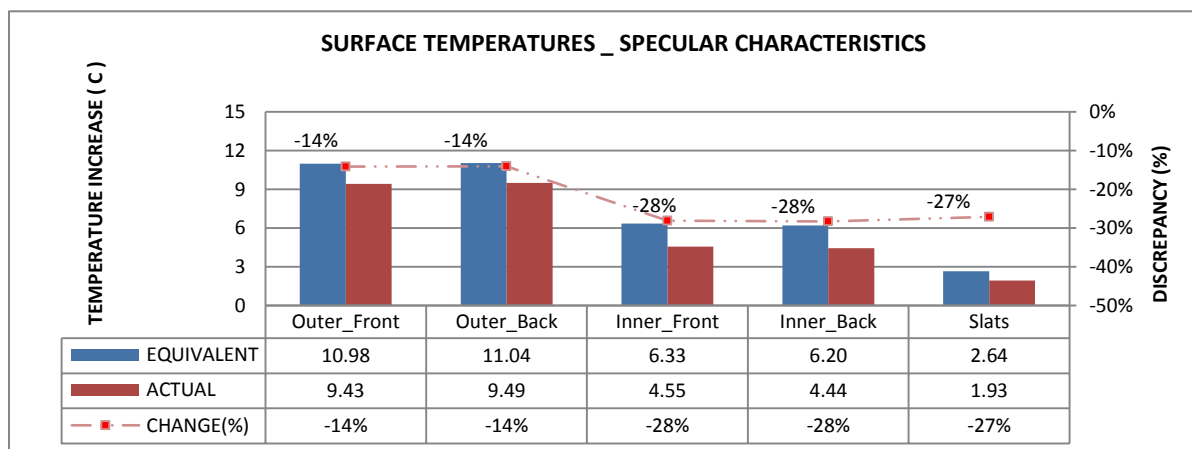


Figure 6.16: Glass's surface temperatures for both investigated scenarios with percentage of changes; with specular characteristics for glass and slats surfaces.

6.6.2 Simple Cavity with Horizontal Vents:

All the surfaces, here, were with specular characteristics. The aim of this part of work was to further investigate the difference in influence between both aforementioned methods: Equivalent and Actual. For better validation of the findings, the study was expanded to cover new configuration of the cavity and a different design for the integrated slats, which named, hereafter, as Design-6 whereas previous flat slats named as Design-1.

For design-1, airflow rate was 5.2% less with the actual method compared to equivalent one; similarly, this difference was 8.2% for design-6; Figure 6.17. This agrees with previous findings regarding the simple cavity (vertical vents) even though the difference due to changing solar representation method is also influenced by the cavity design itself.

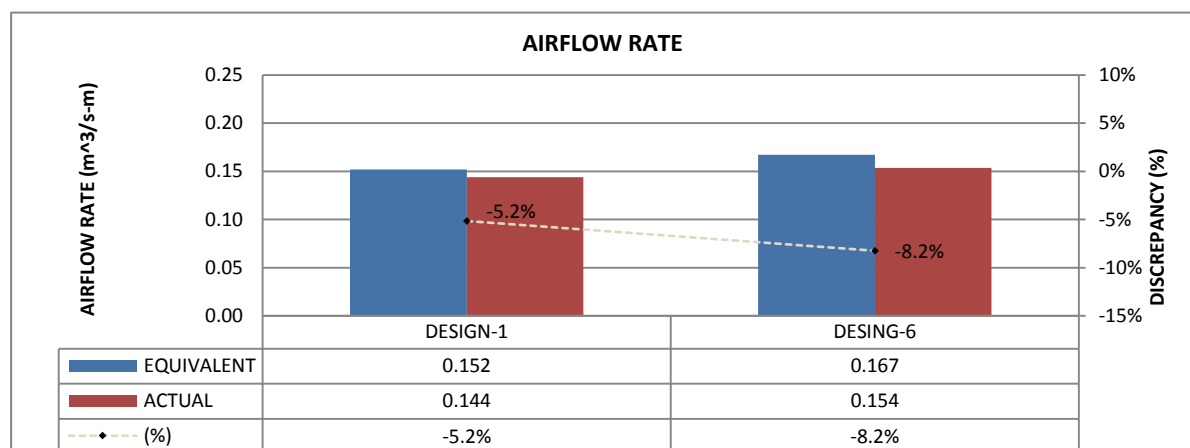


Figure 6.17: Airflow through cavity for both investigated scenarios with percentage of changes; with specular characteristics for glass and slats surfaces.

Similar to results of the simple cavity (vertical vents), simulations for new cavity (with horizontal vents) revealed that predicted surface temperatures for both glass and slats would be lower with the actual method compared to the equivalent method, Figure 6.19. This difference would vary depends on the position of glass as it was about 14% and 29% for outer and inner panes, respectively, which are still close to those of the previous cavity (with vertical vents) with specular properties. For Design-6 slats, the same findings were revealed but with slight changes in differences for glass and more dominant changes for slats, Figure 6.18.

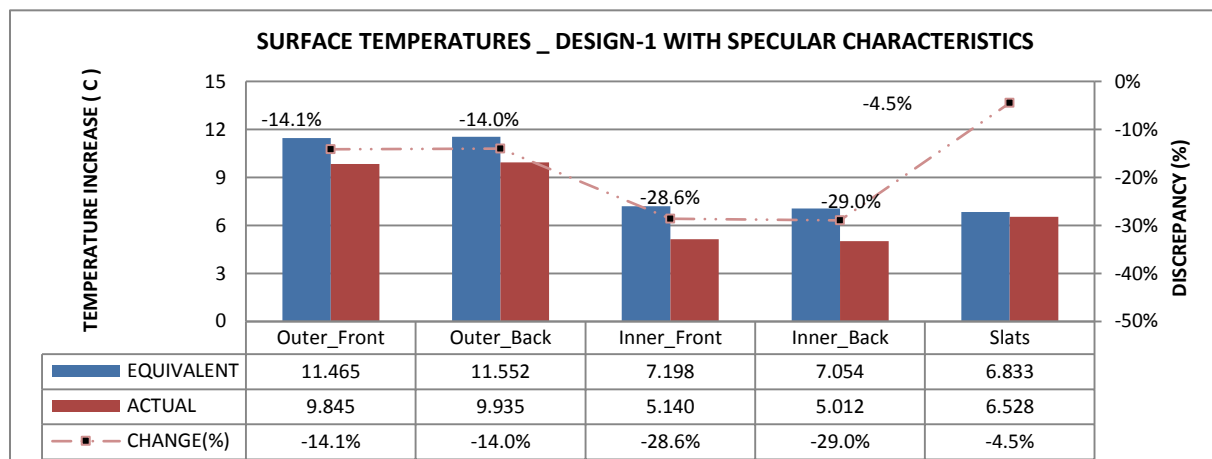


Figure 6.19: Glass's surface temperatures for both investigated scenarios with percentage of changes; with design-1 slats and specular characteristics.

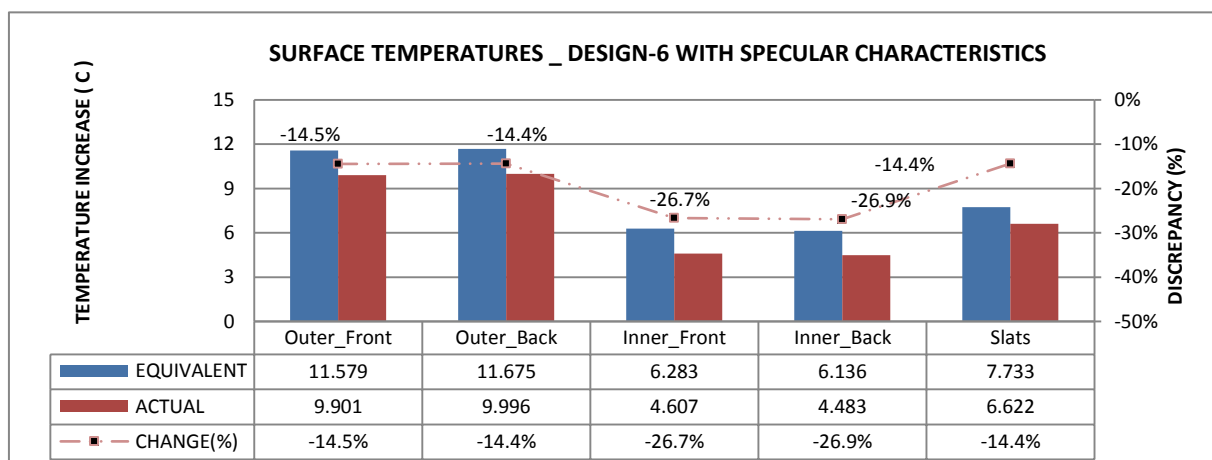


Figure 6.18: Glass's surface temperatures for both investigated scenarios with percentage of changes; with design-6 slats and specular characteristics.

To conclude, the influence of changing the solar irradiance representation method was clear and varied with other combined parameters including configuration of cavity and design of integrated slats. It was obvious that the common equivalent method (with equivalent magnitudes for incident solar radiation on front façade elements) would generally under-predict both airflow and surface temperatures with diffuse characteristics. However, it would significantly over-predict those values with specular characteristics, which applies for both simple and new configurations of cavity and also for both different designs of integrated slats.

Following figures present some graphical results for the investigated cases with horizontal vents and Design-6 integrated slats. Figure 6.20 presents the corresponding contours of air velocity, where magnitudes were higher for the Equivalent method, as a result. Figure 6.21 presents contours of temperature for those methods. Generally, air and surface temperatures would be higher with Equivalent method compared to Actual one, which was discussed before.

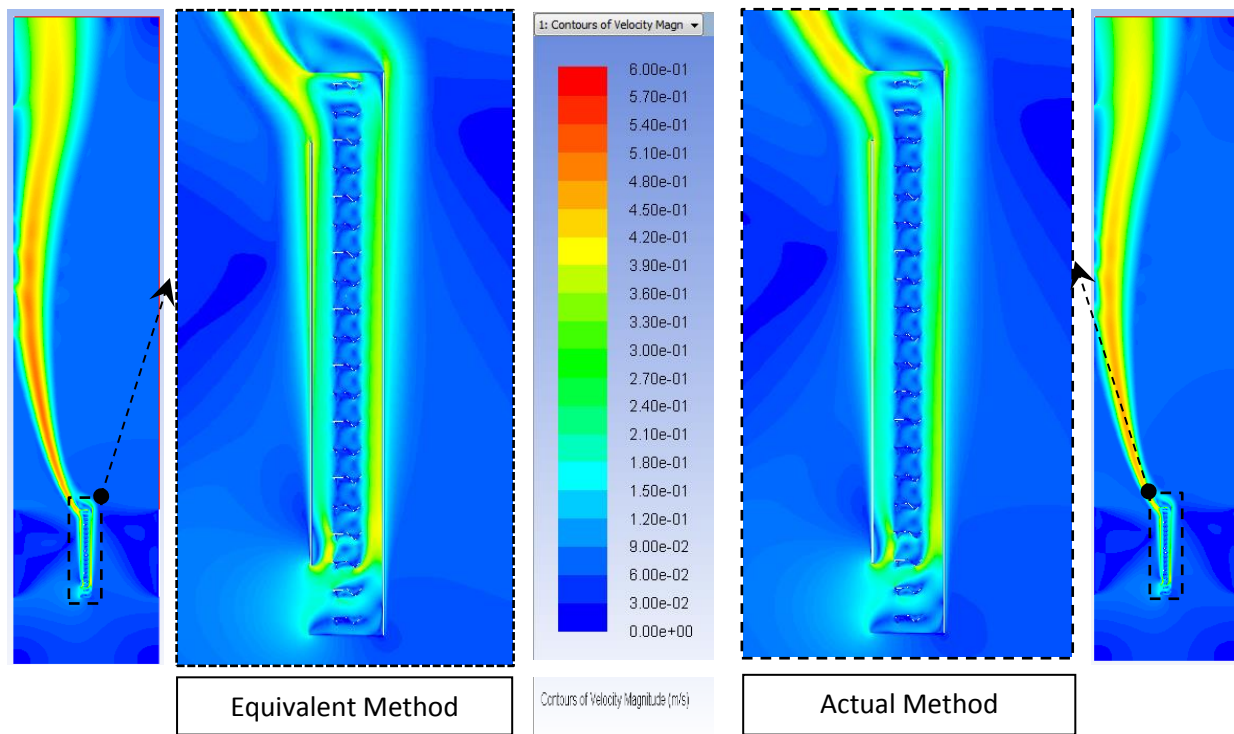


Figure 6.20: Contours of Air velocity magnitude (m/s) for the examined structure and its extended domain with both investigated methods; integrated slats were Design-6.

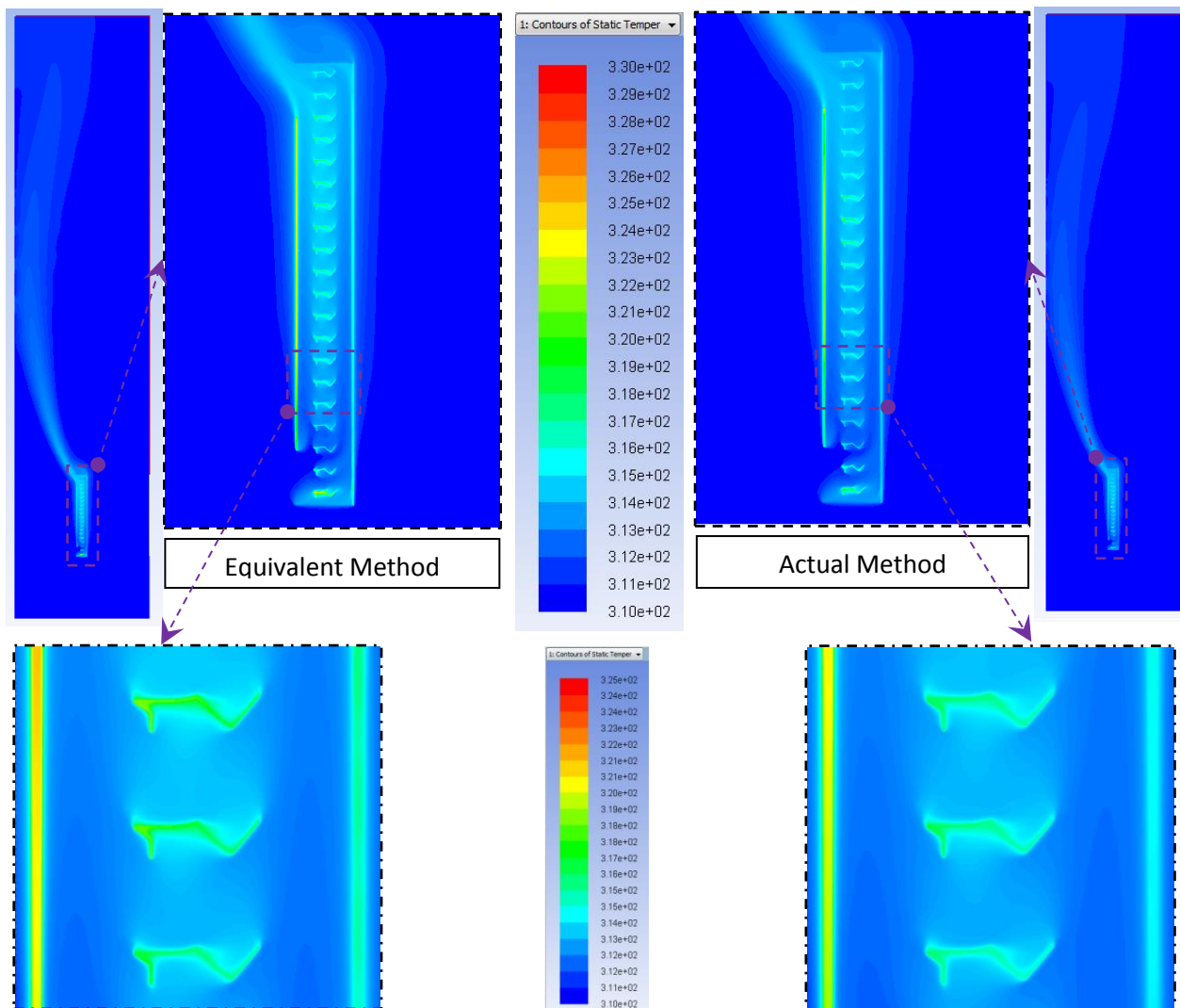


Figure 6.21: Contours of Static Temperatures (K) for the examined structure and its extended domain with both investigated methods; integrated slats were Design-6.

To conclude, it was revealed that the actual method is more suitable for the intended research with a wide range of parametric studies, which cover various design parameters for cavity's configuration, slats' design and ambient boundary conditions. The actual method simply refers to a more realistic representation technique for solar irradiance components, which include both diffuse and beam radiations with its wavelength bands, and the incident angle for beam component. One drawback for this new technique is its inflexibility for a wide range of ambient design boundary conditions, as both the extended domain and its meshing have to be adjusted continuously to match the corresponding changeable angle of incidence. However, for this study, this method was developed and adopted as the main aim of the study was to explore the different design parameters and related characteristics in more details that require a more accurate method. Indeed, it was also concluded that using 3D modelling would be more flexible for such studies, due to the possibility of applying the solar load model option. However, this option requires excessive time and computer memory requirements and therefore was not considered, here, due to a limitation in time and resources even though high performance computing (HPC) facility was used.

6.7 Amendments and Simplifications: Changes from Initial Configuration as Presented in Mesh Independence and Extension of Domain

Due to the extended time on which the work has been done, the benchmark case was continuously amended and level of simplification was modified until it was finally considered to be the best representation. Therefore, it is noticeable that the configuration used in mesh independence study, for example, would be different from that used for the final parametric study, and so on. Generally, previous conclusions on mesh independence and effect of domain extension would be considered for new configurations unless they are significantly different.

Figure 6.22 shows schematic drawings for both old and new configurations for the initial case of interest. It is clear that a few amendments were done, which is worth mentioning as following:

- The vertical extension for the extended domain to meet the requirements of the new method for solar representation as discussed before.
- Setting both the DSF's outer skin and the extensions of the front façade of the building (lower & upper of DSF) at the same vertical axis to meet common building configurations. Also, these extensions were modelled as solid wall indicating lower and upper storeys.
- Also, aluminum frames were removed and not modelled to reduce mesh size.
- Replacing the double-pane glass of inner skin by single-pane of the same characteristics. This simplification would help in reducing mesh size, and allow for better understanding of the performance of integrated slats.

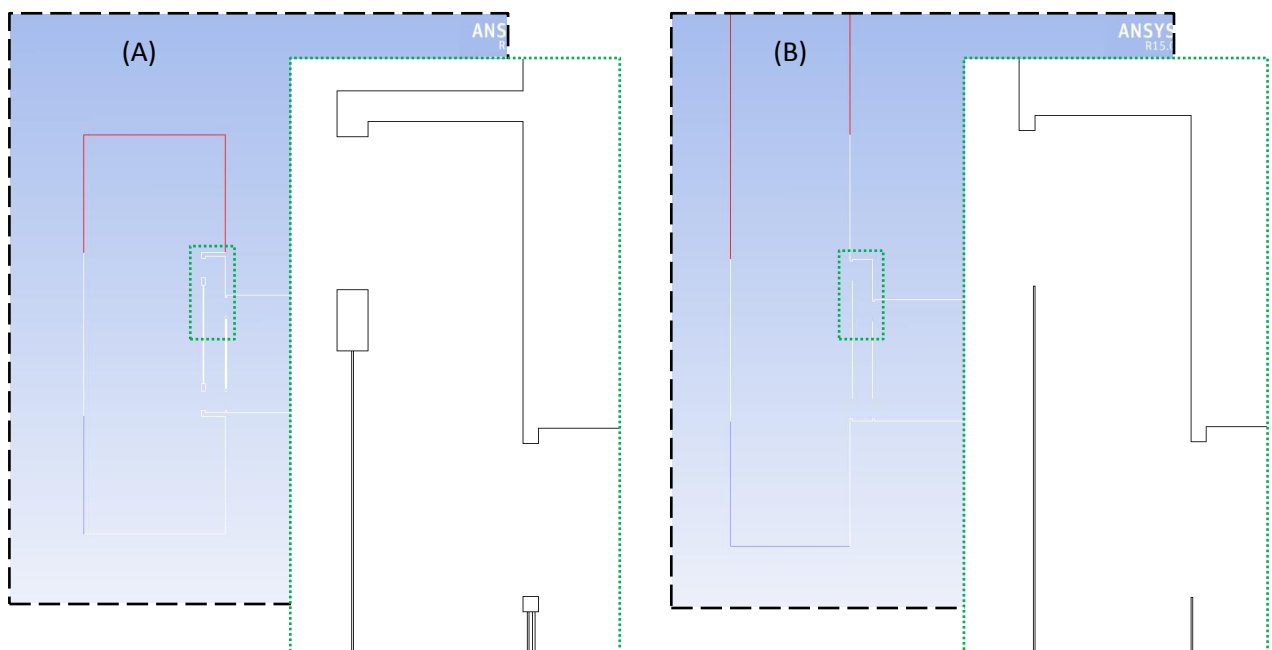
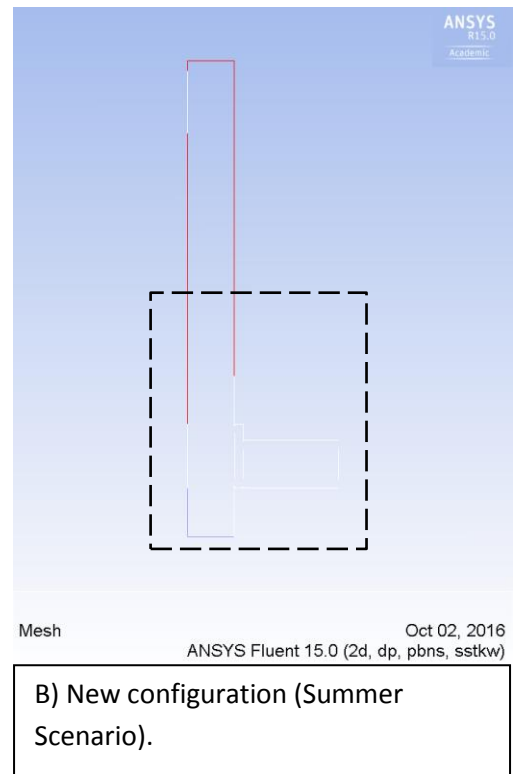
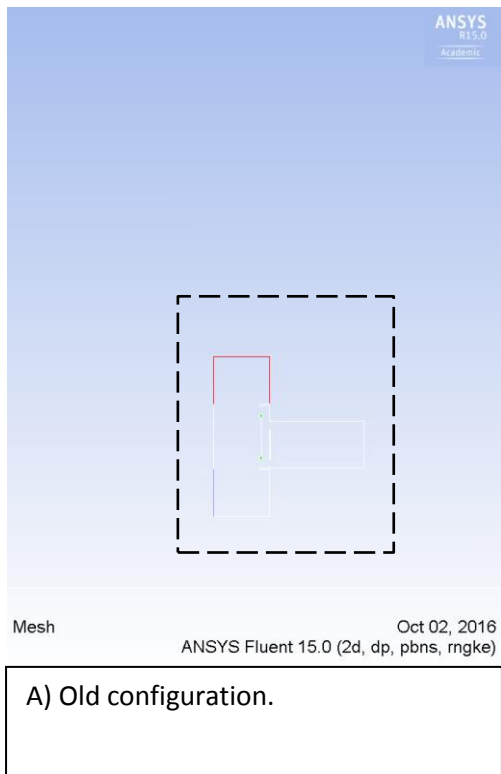


Figure 6.22: Old and New (Final) configurations for initial case; showing the amendments for both cavity configuration and extended computational domain.

6.8 Summary:

This chapter dealt with the work's general methodology at several aspects. After briefly reintroducing the problem, a detailed discussion is provided for the solution's boundary conditions: solar radiation and air temperature. Breakdown details are given for different solar radiation components with several wavelength bands.

Then, general settings for fluent setup are presented, where RNG $k - \varepsilon$ model is preferable for turbulence modeling. For radiation, Discrete Ordinate (DO) model with non-gray specification was selected. Related solar and thermal characteristics for used materials are also listed. Special attention was given to the solution's control and criteria of convergence, which based on a schematic approach to reach the good solution.

After that, a set of preliminary studies were carried out. First of all, a brief study was conducted for the mesh's independence after which final mesh specifications were agreed. Then, another study was carried out to determine the importance for the extension of the computational domain, where the extension of about six times of cavity's external openings is highly recommended. A new method for better representation for solar radiation was introduced, which showed a good enhancement compared to a common method.

Finally, a brief description of the latest amendments and changes on the initial case configuration is presented.

CHAPTER 7 GENERAL PARAMETRIC STUDY ON SIMPLE CAVITY WITH SIMPLE INTEGRATED SLATS

7.1 Introduction:

This chapter presents simulation results of a simple structure that could represent Double Skin Façade (DSF) system in its simplest configuration. The structure consists of two vertical panes of glass (6mm-thickness) with vertical vents having a size equal to cavity width (0.5m). Also, a set of simple shading slats was integrated inside the cavity. The aim behind this part of work was to facilitate investigation of the system performance with more parameters at the lowest cost (time and computing resources) before the next level of investigation with more realistic configurations as shown later.

Main characteristics of the tested structure were derived from previous benchmark model and conducted work on multi-storey building; i.e. the height of structure (4m), recommended cavity width (0.5m) and thickness of glass panes (6mm). Figure 7.1 shows a schematic of the tested structure with flat integrated slats.

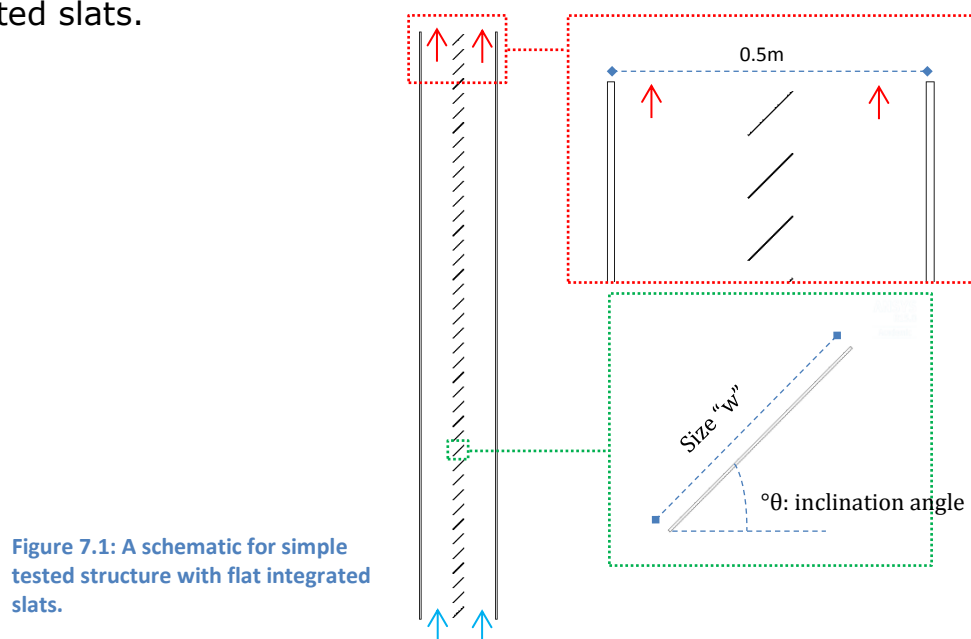


Figure 7.1: A schematic for simple tested structure with flat integrated slats.

The work was conducted through several sub-tasks each handled a specific parameter: slats' size, inclination angle, surface emissivity, position and surface diffuse fraction for both slats and glass. A brief introduction is given at the beginning of each section as follows:

7.2 Size of Integrated Slats:

The work, here, was carried out on the simple structure described earlier. For all cases, the integrated slats had the inclination angle of 45° and their set was placed at the central line of the cavity. This section shows the effect of changing the nominal size of the integrated simple slats on the airflow and thermal performance of the described cavity.

- **Airflow rate:**

Figure 7.2 shows the calculated airflow rates and relative changes due to changing the size for integrated slats. Figure 7.3 presents changes for both flow permeability of the cavity and its airflow.

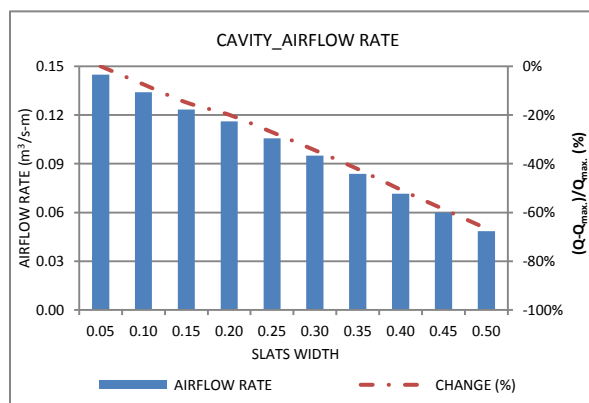


Figure 7.2: Changes of airflow rates with integrated slats size.

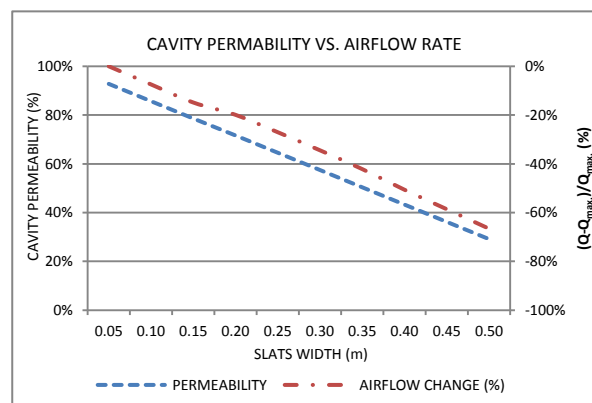


Figure 7.3: changes in cavity's permeability for flow and calculated airflow changes.

It is clear that airflow rate would be dropped significantly by increasing the size of integrated devices while other parameters were kept constant (i.e. opening's size). While airflow rate was $0.145\text{m}^3/\text{s-m}$ for slats size of 0.05m , it dropped to $0.048\text{m}^3/\text{s-m}$ for size of 0.5m . Hence, the maximum change

would be around 67%. Also, it's evident how airflow rate and cavity's flow permeability are correlated. Figure 7.4 shows contours of velocity magnitude (m/s) for the simple cavity with integrated slats having different sizes.

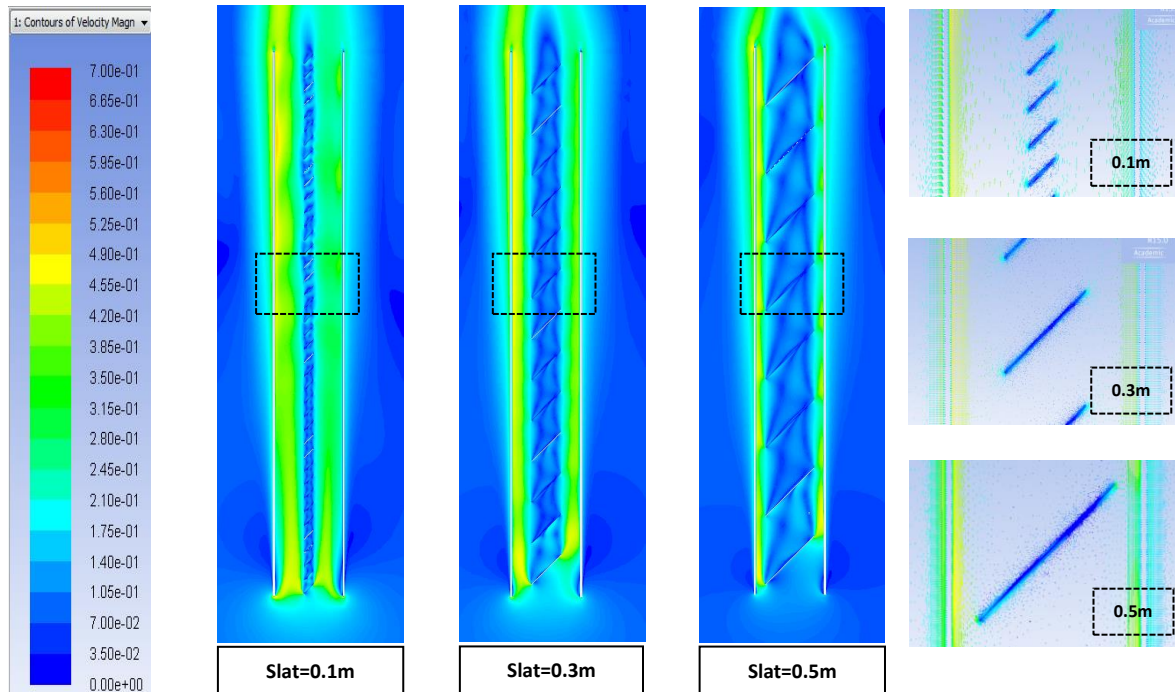


Figure 7.4: contours of velocity magnitude (m/s) for simple cavity with integrated slats having different sizes.

A second-order polynomial relationship between slats width (w) and predicted airflow rate (Q) was revealed from the simulation results as presented in equation (7.1). Also, cavity's Flow Permeability (FP) could be calculated from a revealed linear correlation (7.2).

$$Q = -0.0743 w^2 - 0.1717w + 0.1526 \quad (R^2 = 0.9993) \quad (7.1)$$

$$FP = -1.4142 w + 0.9986 \quad (R^2 = 1) \quad (7.2)$$

- **Temperatures:**

Figure 7.5 shows temperature differences (surface temperature – ambient air temperature “37°C”) for both surfaces of glass panes, which face the cavity inside. Generally, temperature difference would increase with slats' size. Whereas magnitude increase would be more significant for front glass,

up to 10.2°C compared to 4.5°C for back glass, corresponding changes with slat size would be less (i.e. max. 5% for the front glass compared to max. 17.2% for the back glass). Results showed that, for each pane, opposite faces' temperatures are almost identical in both magnitude and increasing rates, i.e. nearly uniform temperature across the glass thickness. This is due to the relatively high conductivity of the thin glass medium.

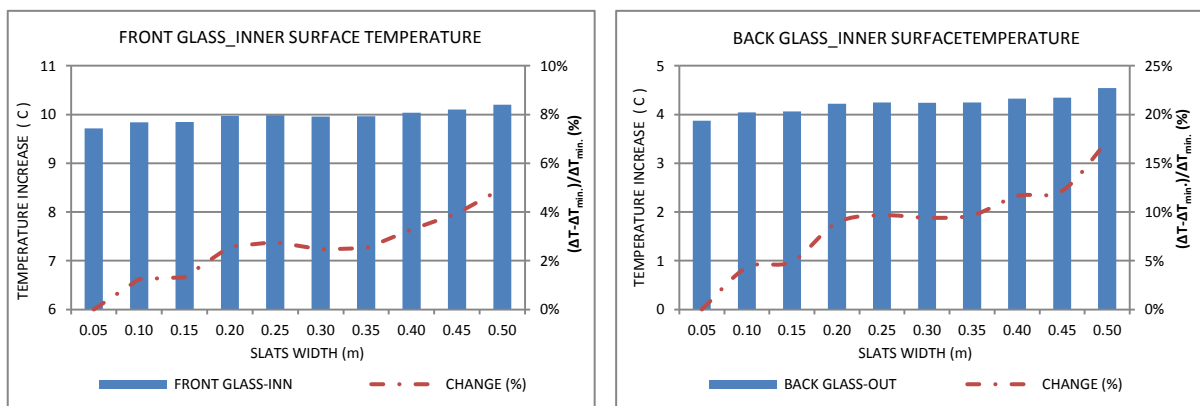


Figure 7.5: Average surface temperature increase for inner surfaces of outer glass (left) and inner glass (right) panes, with cavity/openings size.

The slight relative changes in front surface temperature were expected as solar radiation would hit the front glass pane before being interfered by the integrated slats, in contrast to the back glass pane. However, the non-smooth trends for relative changes were partially attributed to the slight fluctuations in the slats' openness ratio, Figure 7.6, which controls both solar reflection and transmission toward the front and back glasses, respectively. The uncontrolled changes in openness ratios were also due to the arrangement of changeable-width-slats (slat-slat offset) inside the fixed-tall-cavity.

Figure 7.7 presents average increase in slats' surface temperature; as the surface temperature would increase with increasing slat's size. the minimum increase was 5.1°C and the the maximum increase was 7.2°C with

a change of 42.7%. Figure 7.8 presents contours of temperature (k) inside the cavity.

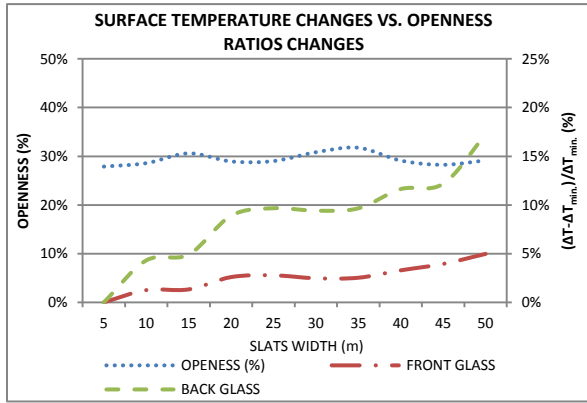


Figure 7.6: Comparison for changes of both surfaces' temperatures and openness ratios.

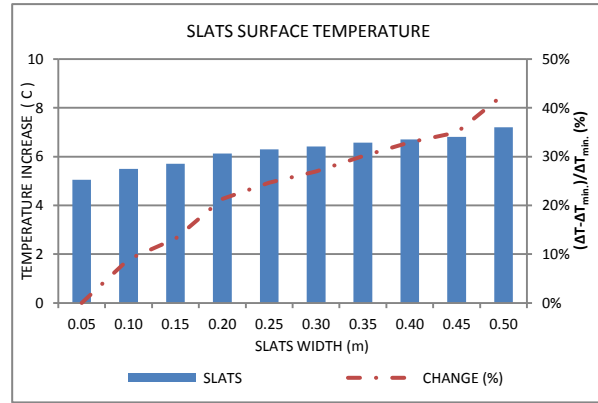


Figure 7.7: Average surface temperature increase with integrated slats size.

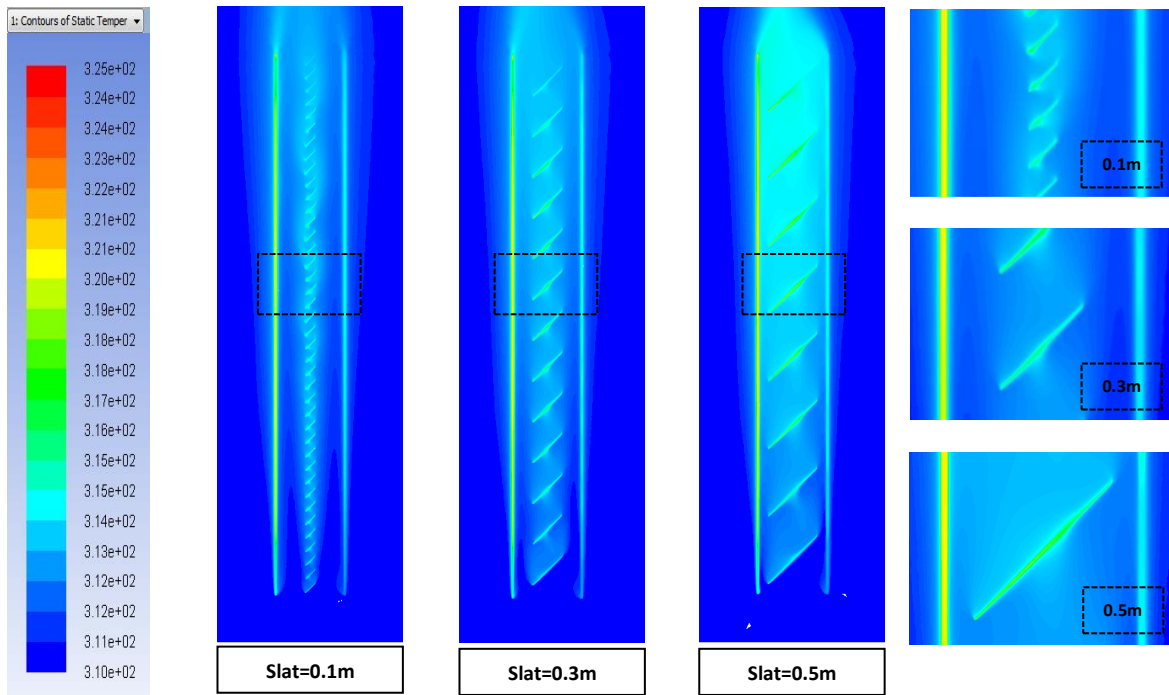


Figure 7.8: contours of air temperature (k) for simple cavity with integrated slats having different sizes.

Furthermore, simulation revealed polynomial relationships of third order between temperature increase (ΔT) and slat's width (w) as shown in equations (7.3) to (7.5).

$$\Delta T_{\text{Front}} = 16.32 w^3 - 13.56 w^2 + 4.0161 w + 9.5442 \quad (R^2 = 0.9662) \quad (7.3)$$

$$\Delta T_{\text{Back}} = 21.559 w^3 - 18.493 w^2 + 5.6452 w + 3.6273 \quad (R^2 = 0.9706) \quad (7.4)$$

$$\Delta T_{\text{Slats}} = 34.526 w^3 - 33.281 w^2 + 13.452 w + 4.4367 \quad (R^2 = 0.9933) \quad (7.5)$$

7.3 Inclination Angles of Slats:

This section shows the results of varying inclination angles of the integrated slats in the cavity. For all cases, slats had a constant size of 0.1m placed at the central line of the cavity. Examined inclination angles were: 0° (opened), 15°, 30°, 45°, 60°, 75° and 90° (totally closed). Both airflow and thermal performance were reported.

- **Airflow rate:**

Figure 7.9-A shows the calculated airflow rates for the cavity with different inclination angles of integrated slats. As inclination angle increased, cavity's flow rate increased. Compared to horizontal slats (0°), the flow rate would increase by about 35.4% with the angle of 75°. Moreover, having the slats on vertical position (openness =0) would enhance the flow only a bit more, 35.7%. Basically, higher flow permeability through the cavity due to higher angles would cause such an increase, Figure 7.9-B. Also, with higher angles, more solar would be reflected towards front glass than transmitted to back one, which (front glass) had a dominant effect on cavity buoyancy as shown in Figure 7.10.

Figure 7.10 shows contours of velocity magnitude (m/s) for the investigated cavity with integrated slats having different inclination angles. It is seen that with low angles (0°-45°), air would be turbulent for almost the upper two thirds of cavity and part of moving air would pass in-between slats and move from one sub-cavity to another.

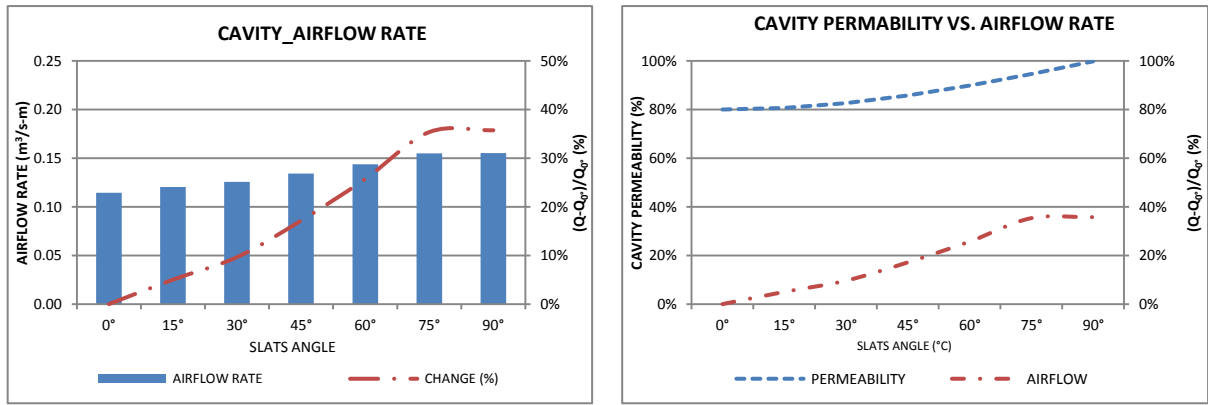


Figure 7.9: A) Airflow rates changes with slats angle. B) Changes in cavity's permeability for flow and calculated airflow changes.

The results indicate a second-order polynomial relationship, equation (7.6), between slats angle (θ) and calculated airflow rate (Q). Equation (7.7) could be used to calculate the flow permeability (FP) of the cavity using the inclination angle of slats.

$$Q = 4E-06\theta^2 + 0.0003\theta + 0.1147 \quad (R^2 = 0.9993) \quad (7.6)$$

$$FP = 2E-05\theta^2 + 0.0004\theta + 0.7977 \quad (R^2 = 0.999); \text{ where: } 0 \leq \theta \leq 90 \quad (7.7)$$

Where: $0 \leq \theta \leq 90$

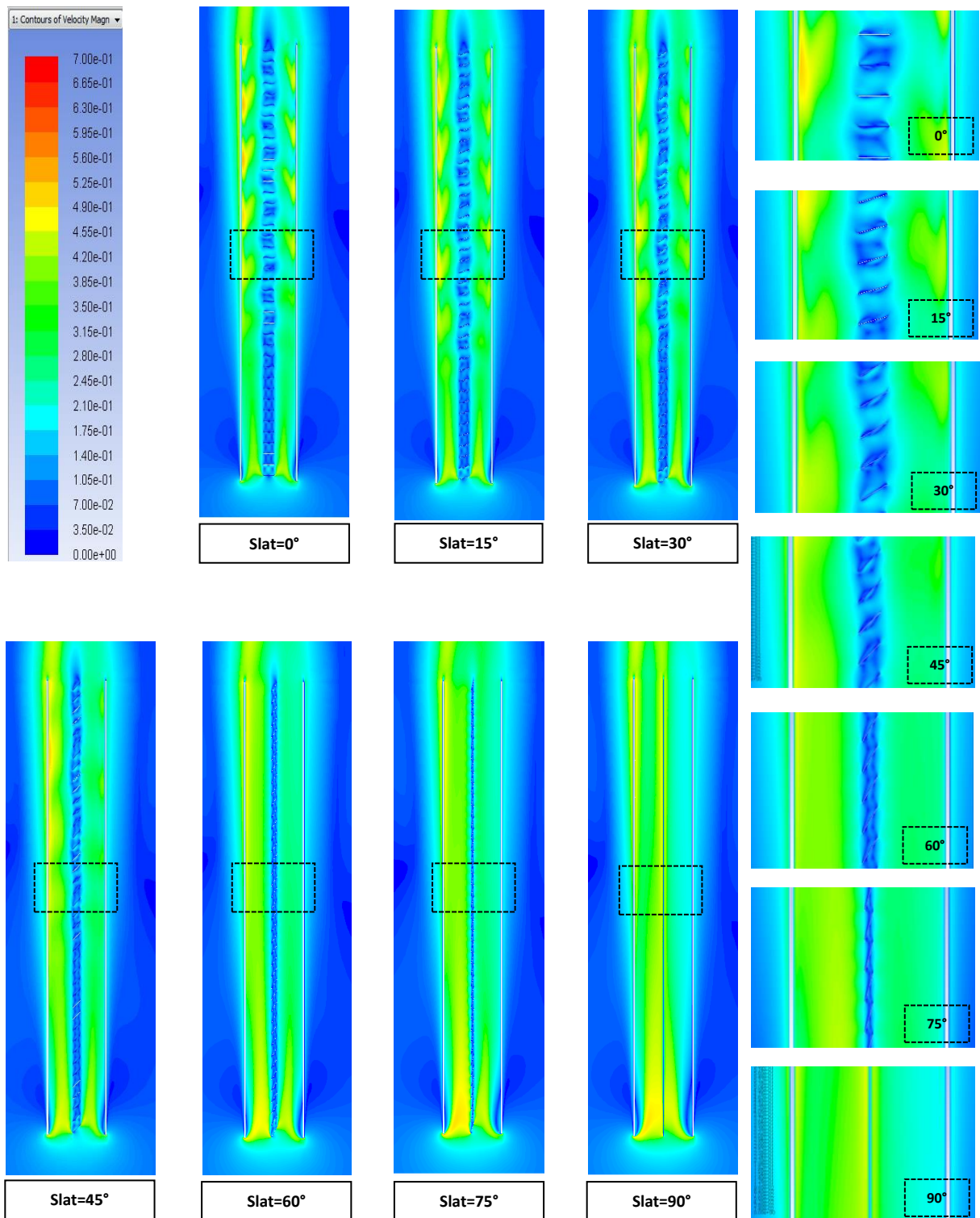


Figure 7.10: contours of velocity magnitude (m/s) for simple cavity with integrated slats having different inclination angles.

- **Temperatures:**

Figure 7.11 shows temperature increases (surface temperature – ambient air temperature “37°C”) for opposing surfaces of the cavity. For front glass, surface temperature would increase with inclination angle as more solar would be reflected towards it. Such increase would reach 5% and 12% with 75° and 90° (fully closed); respectively. With less solar penetration, surface temperature for back glass would reduce and maximum reduction was about 30% for inclination angle of 75°.

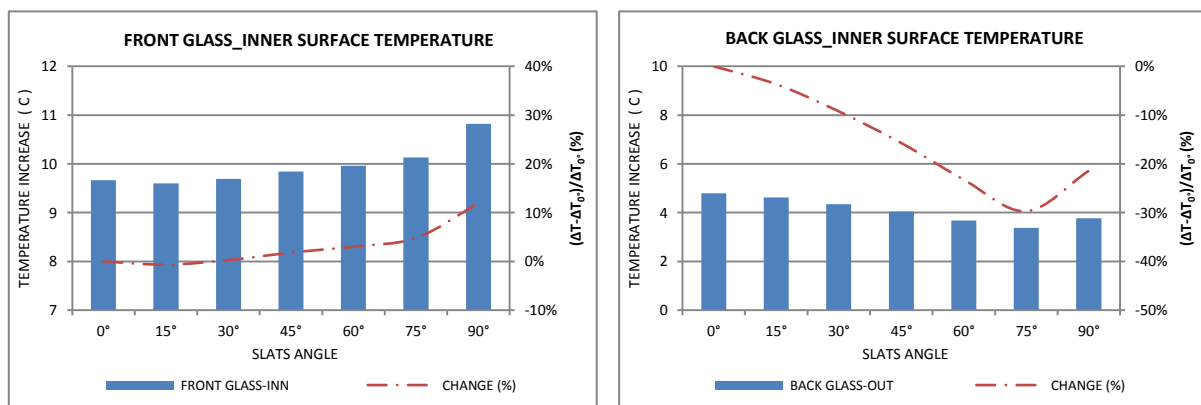


Figure 7.11: Average surface temperature increase for inner surfaces of outer glass (left) and inner glass (right) panes, with integrated slats angle.

However, compared to that for 75°, a slight increase in back glass surface temperature was recorded for 90°. That is mainly due to expected reduction in inner sub- cavity's ventilation, as air would tend to flow through front sub-cavity due to increasing surface temperature of the front glass with 90°-slats causing higher buoyancy effect there, Figure 7.12. Another reason is that, with 90°-slats, radiation exchange between closed slats (fully opaque aluminum sheet) and opposite back glass surface would increase due to relatively higher and lower surface temperatures for slats and back glass, respectively, as shown in Figure 7.13. Furthermore, increasing the angle

would lead to dramatically decrease the openness, minimize transmission towards back glass (decrease temperature) and increase reflectance towards front one (increase temperature).

Figure 7.14 presents averages increase in slats' surface temperature for different inclination angles. Obviously, surface temperature would increase as the angle increased except for 90°. Maximum increase was 6.3°C for 75°-angle with a change of 43% from that for 0°-angle.

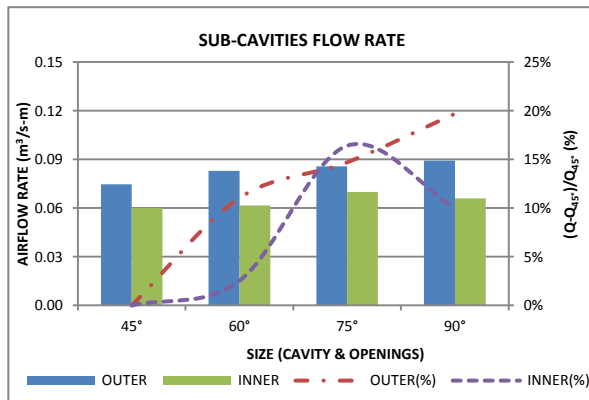


Figure 7.12: Airflow rates and relative changes for sub-cavities with integrated slats angle.

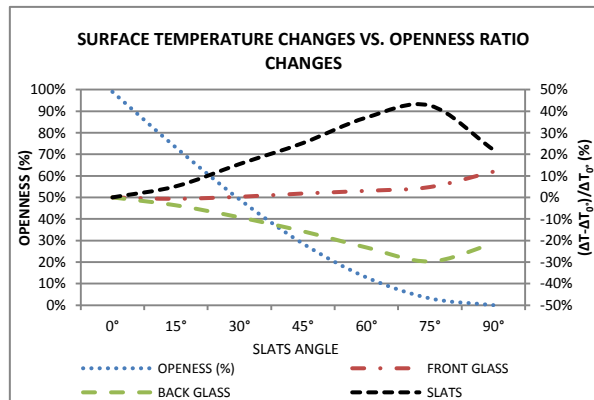


Figure 7.13: Comparison for changes of both surfaces' temperatures and openness ratios

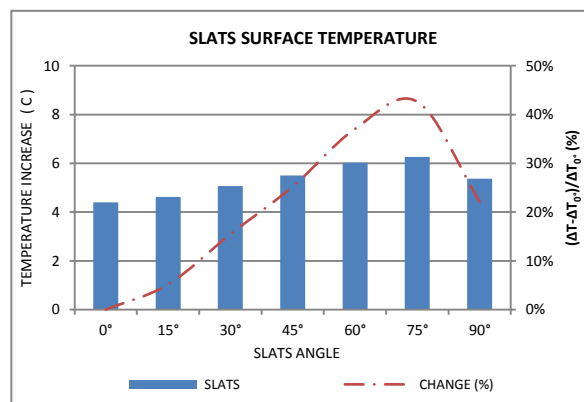


Figure 7.14: Average surface temperature increase for integrated slats, with changes in their angle.

The following polynomial relationships (7.8) to (7.10) between surface temperature increase (ΔT) and inclination angle (θ) for integrated slats could be used to further calculations.

$$\Delta T_{\text{Front}} = -2\text{E-}6\theta^3 + 0.0003\theta^2 - 0.0075\theta + 9.6593 \quad (R^2 = 0.9942) \quad (7.8)$$

$$\Delta T_{\text{Back}} = -8\text{E-}5\theta^2 - 0.0133\theta + 4.8115 \quad (R^2 = 0.9981) \quad (7.9)$$

$$\Delta T_{\text{Slats}} = -6\text{E-}6\theta^3 + 0.0007\theta^2 - 0.0062\theta + 4.3933 \quad (R^2 = 0.9988) \quad (7.10)$$

Where: $0^\circ \leq \theta < 90^\circ$

The influence of inclination angle of integrated slats on both air and glass temperatures of the simulated cavity are shown in Figure 7.15. As mentioned earlier, glass temperature with larger angle would increase for the front pane and decrease for the back pane. Also, with a smaller angle, air would mix at a lower level inside the cavity due to larger horizontal-width of integrated slats and associated thicker thermal boundary layer; also thicker boundary layer at back glass with more solar penetration.

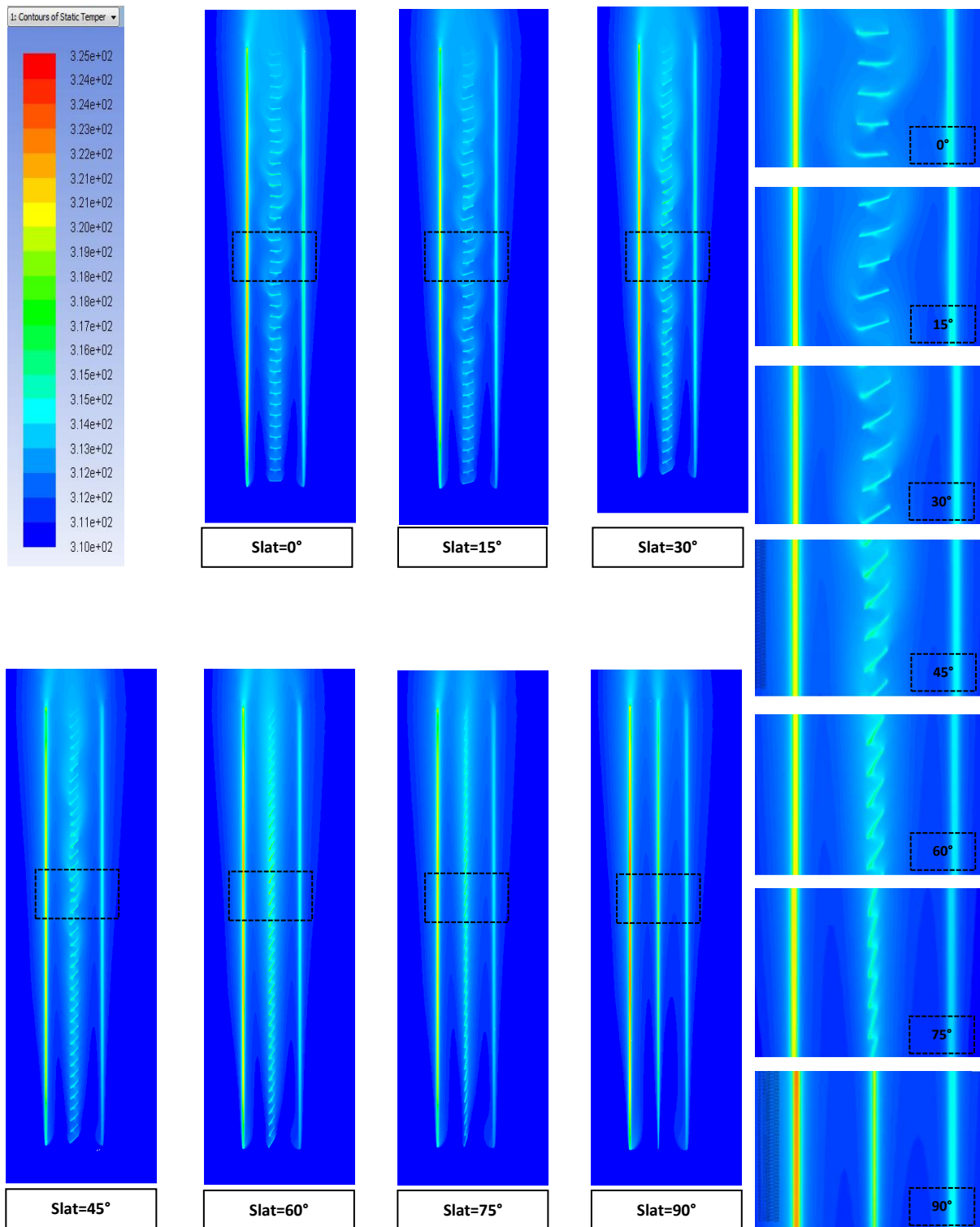


Figure 7.15: contours of temperature (k) for simple cavity with integrated slats having different sizes.

7.4 Position of Integrated Slats:

Under this section, results for the influence of the position of integrated slats are presented. Again, integrated slats were a simple flat and the cavity was 0.5m-wide. Slats had a size of 0.1m and angle of 45°. Table 7.1 shows the details for different positions of integrated slats.

Table 7.1: Details for different examined positions of integrated slats.

POSITION									
	P1	P2	P3	P4	P5	P6	P7	P8	P9
FRONT CAVITY (m)	0.414	0.364	0.314	0.264	0.214	0.164	0.114	0.064	0.014
BACK CAVITY (m)	0.014	0.064	0.114	0.164	0.214	0.264	0.314	0.364	0.414
SLATS-H-WIDTH (m)	0.071	0.071	0.071	0.071	0.071	0.071	0.071	0.071	0.071

• Airflow rate:

Results, Figure 7.16 show that total airflow rate would slightly increase (2.7%) as slats moved away from inner glass causing less flow resistance due to less interfering with adjacent velocity boundary layer. However, this effect became less important from P4 onwards as flow rate began decreasing with a maximum drop of 14.4% for P8. Figure 7.17 presents the relationship between relative changes in flow rate and relative width for front sub-cavity. Generally, the flow rate would decrease as front cavity getting narrower.

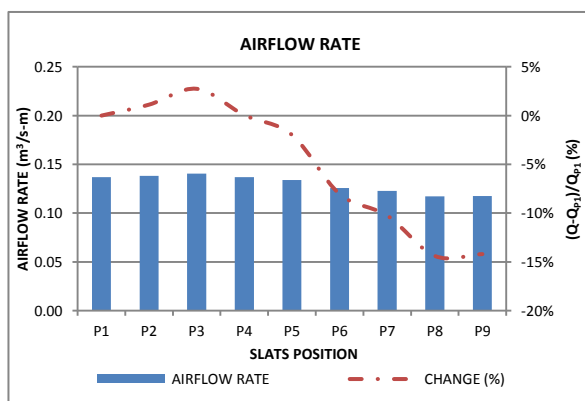


Figure 7.16: airflow rates changes with integrated slats' position.

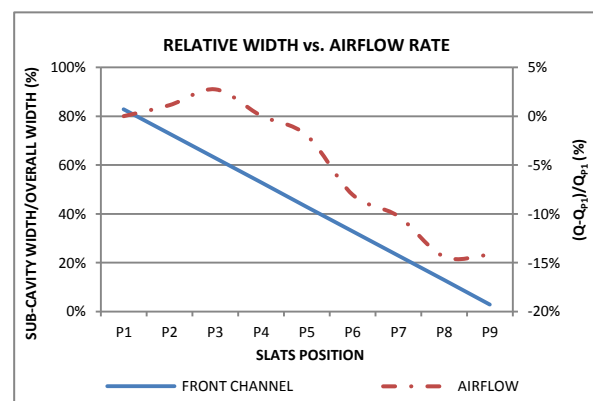


Figure 7.17: Relationship between relative width of front sub-cavity and relative changes in total airflow rate.

Equations (7.11) and (7.12) could be used to calculate relative widths for both inner and outer sub-cavities, respectively. Equation (7.12) gives the

relationship between total airflow rate Q_{total} and relative width for inner sub-cavity (w_{inn}).

$$w_{inn} = \frac{\text{inner subcavity width}}{0.5} \times 100\% \quad (7.11)$$

$$w_{out} = 0.8572 - w_{inn} \quad (7.12)$$

$$Q_{total} = 0.1745w_{inn}^3 - 0.2622w_{inn}^2 + 0.0766w_{inn} + 0.1341 \quad (7.13)$$

($R^2 = 0.9855$); where: $0.03 < w_{inn} < 0.83$

Figure 7.18 displays changes in velocity contours outside and inside simulated cavity under the influence of changing the position of integrated slats. It is clear how slats position would affect flow distribution at both inlet and outlet of the structure; as flow would be divided into almost two equal parts at the inlet with P5 while air would mainly flow through larger sub-cavity with either P1 or P9 positions. As slats placed close to either side, it would form with the far-opposite surface the main active boundaries where most of the flow passes through.

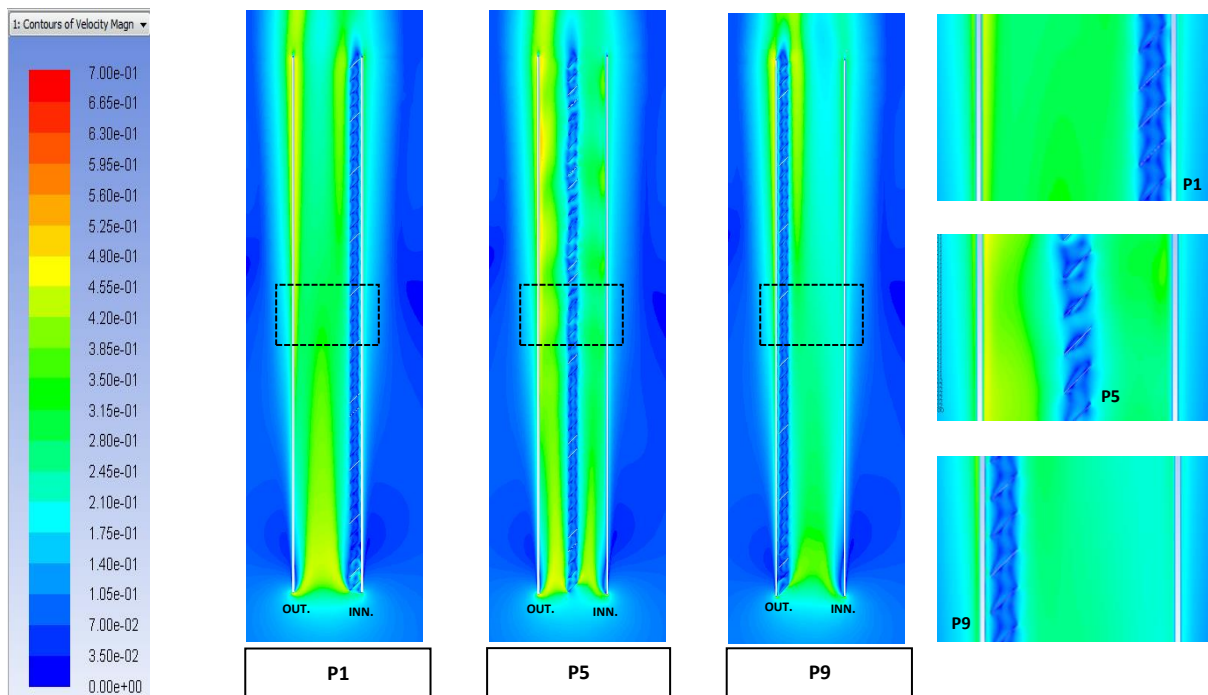


Figure 7.18: contours of velocity magnitude (m/s) for simple cavity with integrated slats having different positions.

- Temperatures:**

Generally, surface temperature increase for both outer and inner glass panes would be higher with slats placed close to those surfaces, Figure 7.19, due to less flow rate in between thus less efficient convection also higher radiation exchange as slats had an emissivity of 0.9. However, the temperature would start decreasing as the slats moved towards the middle of cavity allowing for better ventilation for surfaces. Noticeably, maximum change for front glass was about 5% compared to 26.4% for inner glass.

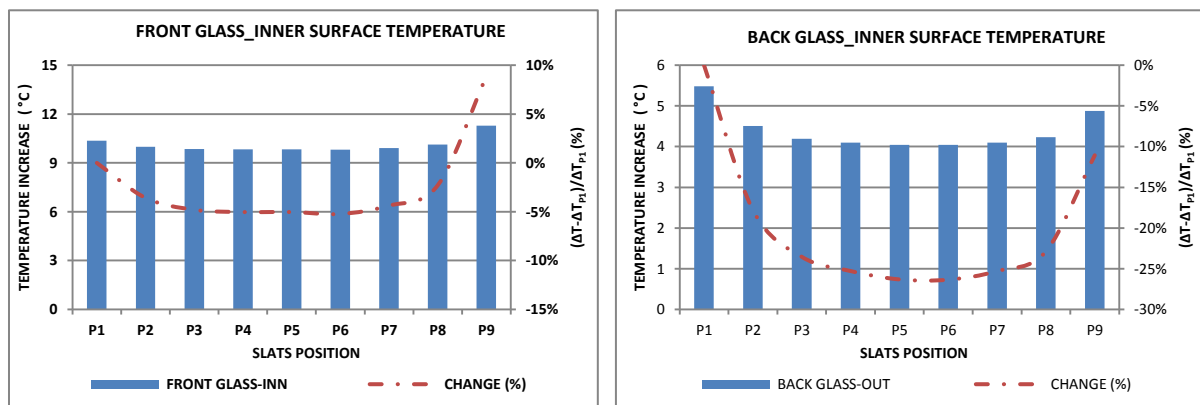


Figure 7.19: Average surface temperature increase for inner surfaces of outer glass (left) and inner glass (right) panes, with integrated slats position.

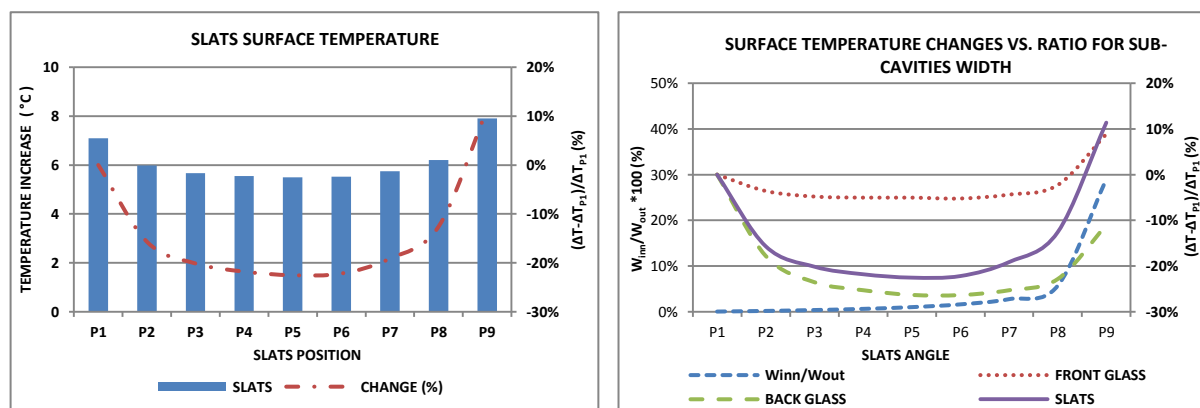


Figure 7.20: Average surface temperature increase for integrated slats, with slats position.

Figure 7.21: comparison between ratio of inner sub-cavity width to outer sub-cavity width, and relative changes in surface's temperatures; with slats position.

As shown in Figure 7.20, increases in slats' surface temperature would have a similar trend to those for glass panes as discussed earlier, where the temperature would increase in positions close to boundaries and started to

drop as moved towards the center. This is attributed to the increased ventilation for integrated slats as they placed away from boundaries, which lead to efficient convection. Also, results show that temperature would be around 10% higher for P9 compared to P1 as the aforementioned closed to outer glass thus more exposed to direct solar radiation.

Figure 7.21 gives an overview of different change rates for surfaces and also for the ratio of inner sub-cavity width to outer sub-cavity width. For positions within the outer half of cavity (P5-P9), all changes would increase as inner cavity's width increased; in contrast to positions of the inner half.

Equations (5.18) to (7.16) correlate relative width for inner cavity (w_{inn}) with surface temperature increase (ΔT) for different structures as denoted.

$$\Delta T_{Front} = 6.23w_{inn}^2 - 4.65w_{inn} + 10.55 \quad (R^2 = 0.8329) \quad (7.14)$$

$$\Delta T_{Back} = 7.13w_{inn}^2 - 6.70w_{inn} + 5.48 \quad (R^2 = 0.9172) \quad (7.15)$$

$$\Delta T_{Slats} = 12.55w_{inn}^2 - 10.09w_{inn} + 7.32 \quad (R^2 = 0.916) \quad (7.16)$$

Where: $0.03 < w_{inn} < 0.83$

Contours of temperature, Figure 7.22, reflect the flow patterns inside the cavity. Air temperature would be lower for areas where flow is more evident and vice versa. It is also obvious how glass thermal boundary layer would be seen clearly when slats were closely placed due to less flow in-between.

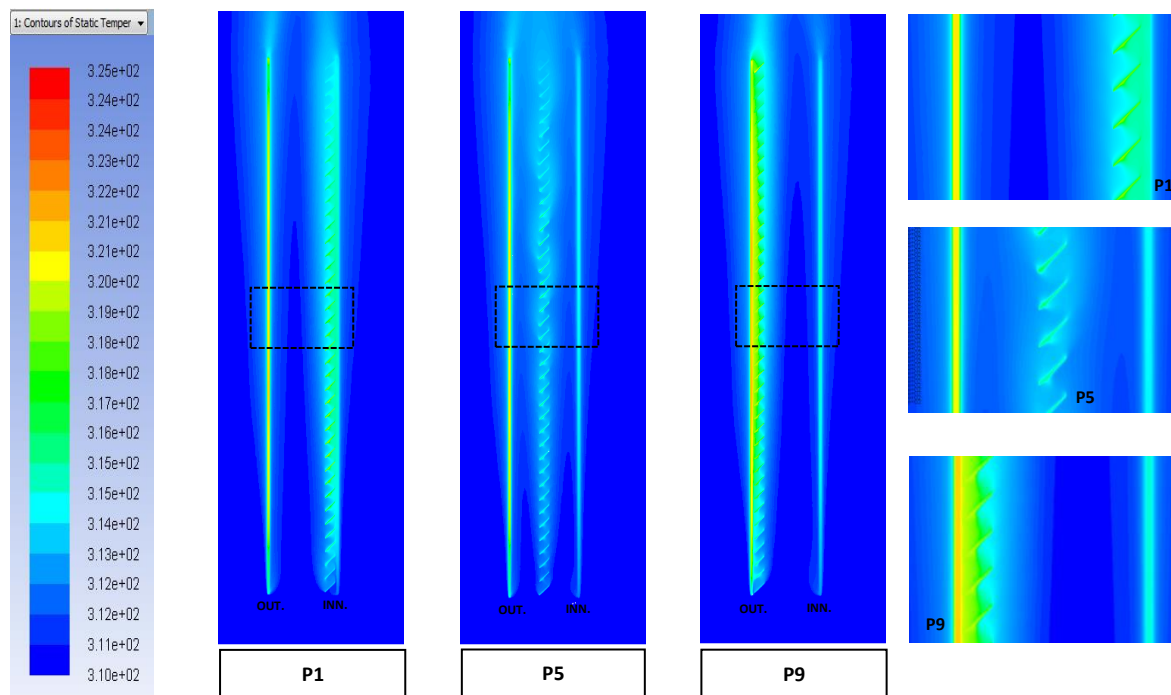


Figure 7.22: contours of temperature (k) for simple cavity with integrated slats having different positions.

7.5 Surface Emissivity of Integrated Slats:

Results presented here show the influence of changing the surface emissivity (ϵ) of integrated slats on both airflow and surface temperatures. The full range of emissivities was examined for slats size of 0.1m, inclination angle of 45° and placed in the middle (P5) of the 0.5-wide cavity.

- **Airflow rate:**

Cavity's flow would dramatically be enhanced by increasing slats' surface emissivity. In reference to mirror-like slats (emissivity =0), airflow could reach $0.14\text{m}^3/\text{s-m}$ with an increase of 42.5%, with ideal black-body slats (emissivity=1), Figure 7.23. Most importantly, increase rate was more evident for emissivities less than 0.5. Mainly, such increase is attributed to the fact that with higher emissivity more heat would be absorbed by the slats elements, which would, in turn, enhance the buoyancy inside the cavity so drag more air from the bottom of the cavity towards the top.

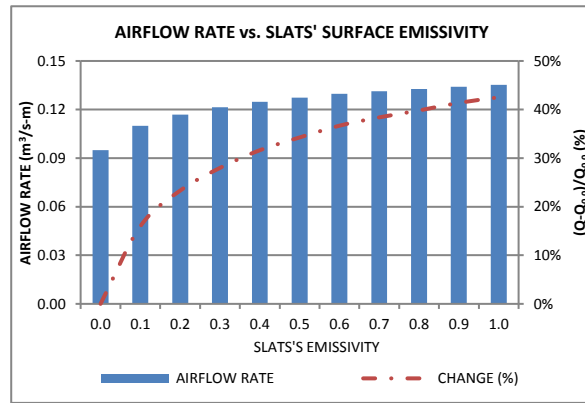


Figure 7.23: airflow rates changes with surface emissivity of slat.

Further calculations for airflow rate could be carried out using following polynomial equation (7.17):

$$Q = -0.0483 \varepsilon^2 + 0.0819 \varepsilon + 0.0994 \quad (R^2 = 0.9631) \quad (7.17)$$

Where: $0 \leq \varepsilon \leq 1$

Figure 7.24 shows changes in flow pattern as a result of changing surface emissivity of integrated slats. It is also shown how, with high emissivity (i.e. 0.9), the flow would be developed at relatively lower levels inside the cavity, which is more evident at upper part and outlet.

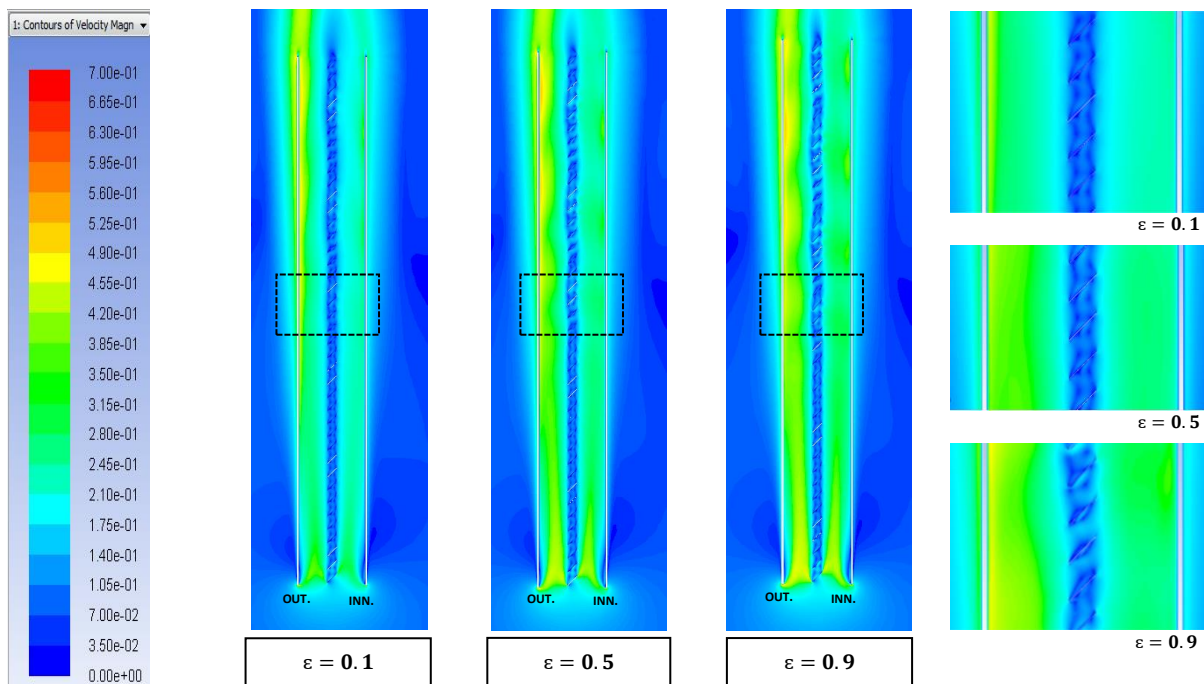


Figure 7.24: contours (and vectors) of velocity magnitude (m/s) for simple cavity with integrated slats having different surface emissivity.

- **Temperatures:**

As slats' surface emissivity increased, surface temperature for front glass would be decreased by up to 16%, Figure 7.25. Revealed surface temperature decrease was due to reducing reflection toward either side by high-emissivity-slats. Hence, surface temperature, for inner glass, would also be decreased by up to 19.3% as emissivity increased to 0.5; however, it then started increasing by up to 4% with higher emissivities. Marked increase for inner glass with emissivities higher than 0.5 was due to relatively high temperature slats that would increase radiation exchange between slats surfaces and glass surfaces at either side; however, with good ventilation through front sub-cavity, radiation influence would be decreased on final surface temperature for front glass (as it would keep decreasing but with lower changing rate as discussed) while the radiation influence would be more evident on back glass surfaces leading to a slight increase.

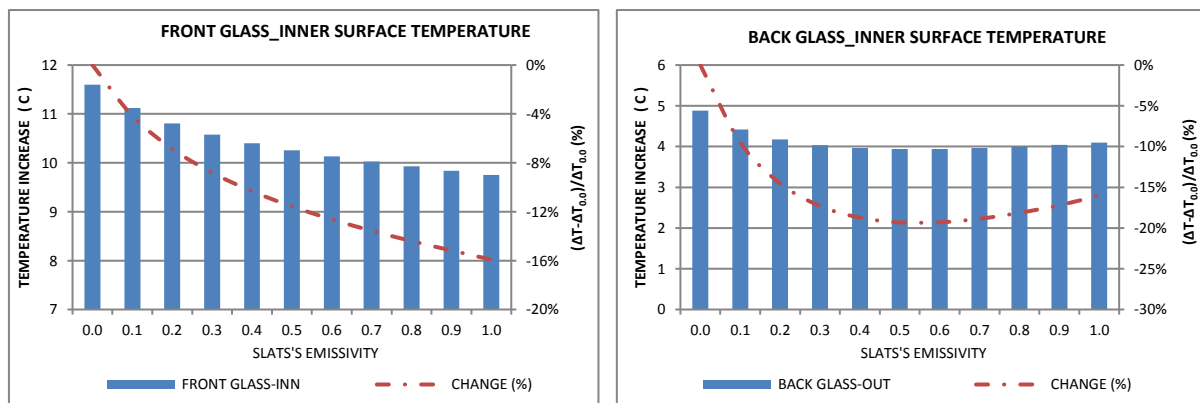


Figure 7.25: Average surface temperature increase for inner surfaces of outer glass (left) and inner glass (right) panes, with integrated slats' surface emissivity.

Figure 7.26 shows how changing surface emissivity for integrated slats would affect their surface temperature. With a negligible increase of 0.1°C (above incoming air temperature, 37°C) for mirror-like slats (emissivity=0.0), such increase would dramatically go up to 5.7°C for slats with a surface

emissivity of 1. Figure 7.27 presents the relative changes for all elements of the structure; it is clear that maximum change for both front and back glass panes would be almost equal, 16%.

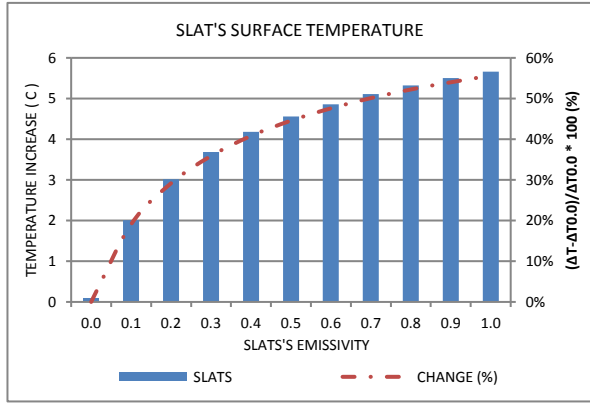


Figure 7.26: Averages surface temperature increase for integrated slats, with surface emissivity.

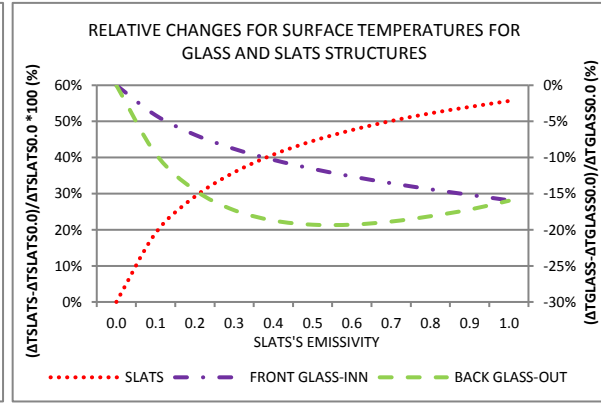


Figure 7.27: comparison between ratio of inner sub-cavity width to outer sub-cavity width, and relative changes in surface's temperatures; with changes surface emissivity.

Equations (7.18) and (7.19) show the empirical relationships between surface emissivity (ε) of integrated slats and expected increase in surface temperature (ΔT) for front and back glass panes; respectively. Similarly, (7.20) shows corresponding correlation between surface emissivity (ε) and temperature increase (ΔT) of those slats.

$$\Delta T_{\text{Front}} = 1.66\varepsilon^2 - 3.33\varepsilon + 11.49 \quad (R^2 = 0.9885) \quad (7.18)$$

$$\Delta T_{\text{Back}} = 2.19\varepsilon^2 - 2.75\varepsilon + 4.74 \quad (R^2 = 0.9252) \quad (7.19)$$

$$\Delta T_{\text{Slats}} = -6.58\varepsilon^2 + 11.33\varepsilon + 0.64 \quad (R^2 = 0.9729) \quad (7.20)$$

Where: $0 \leq \varepsilon \leq 1$

Contours of temperature, Figure 7.28, for air and both glass and aluminum slats mediums could provide an explanation to revealed variation. With lower surface emissivity (i.e. 0.1), glass temperature would be higher whereas slats temperature would be lower and vice versa; as discussed earlier.

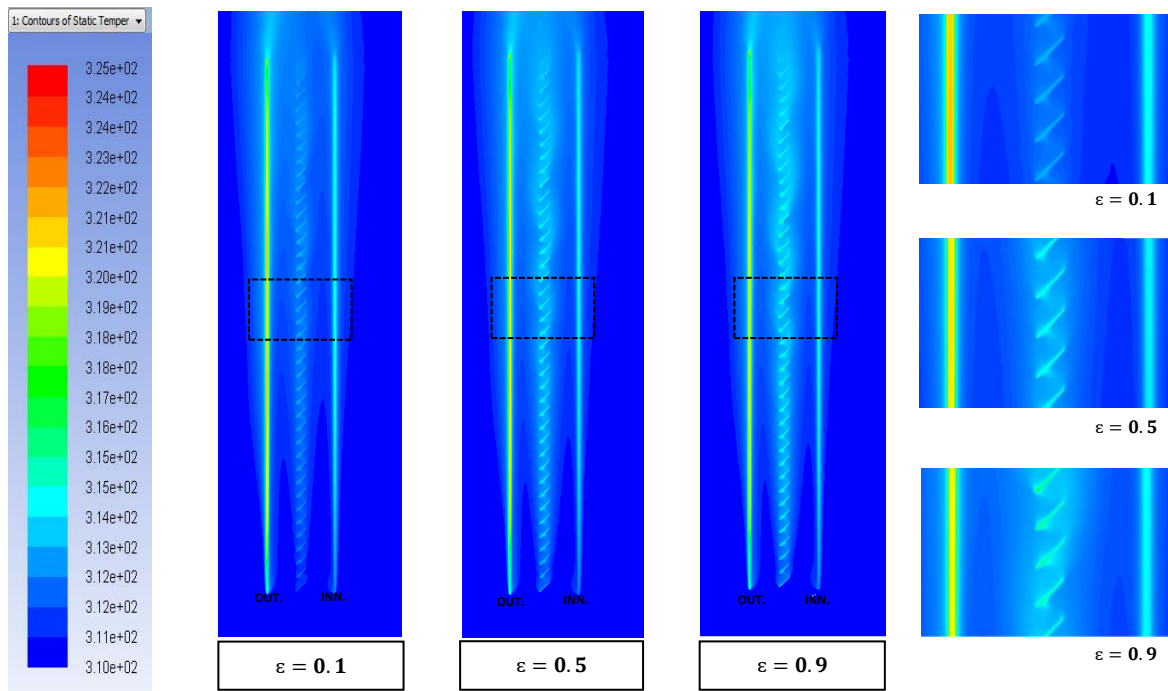


Figure 7.28: contours of temperature (k) for simple cavity with integrated slats having different surface emissivity.

7.6 Surface Diffuse Fraction of Integrated Slats:

All parameters were kept similar to the those in the previous section, however, slats' surface emissivity was set to 0.1 and diffuse fraction for surfaces of integrated slats was varied as a parameter of study. The low emissivity (0.1) was selected to easily explore the influence of surface diffuse fraction on both airflow and surface temperatures.

- **Airflow rate:**

Unlike surface emissivity where cavity flow was affected significantly (up to 42.5%), the diffuse fraction of same slats (combined with an emissivity of 0.1) had a negligible effect that was limited to 1.5%, Figure 7.29. The negligible influence is attributed to the simplicity of both integrated slats and the entire structure (cavity). Figure 7.30 shows that there was almost no

difference in flow patterns, which confirm the negligible variations in airflow rates.

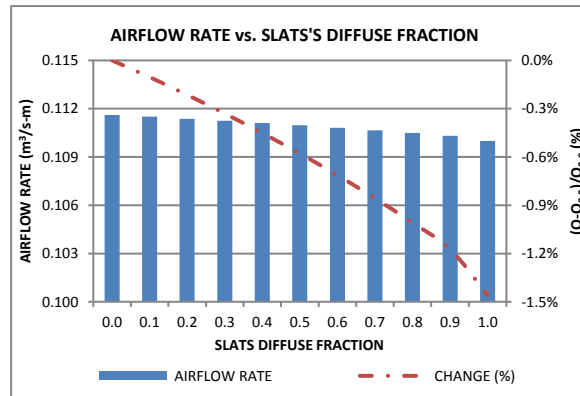


Figure 7.29: Airflow rates through cavity with integrated slats having surface emissivity of 0.1 and various diffuse fraction.

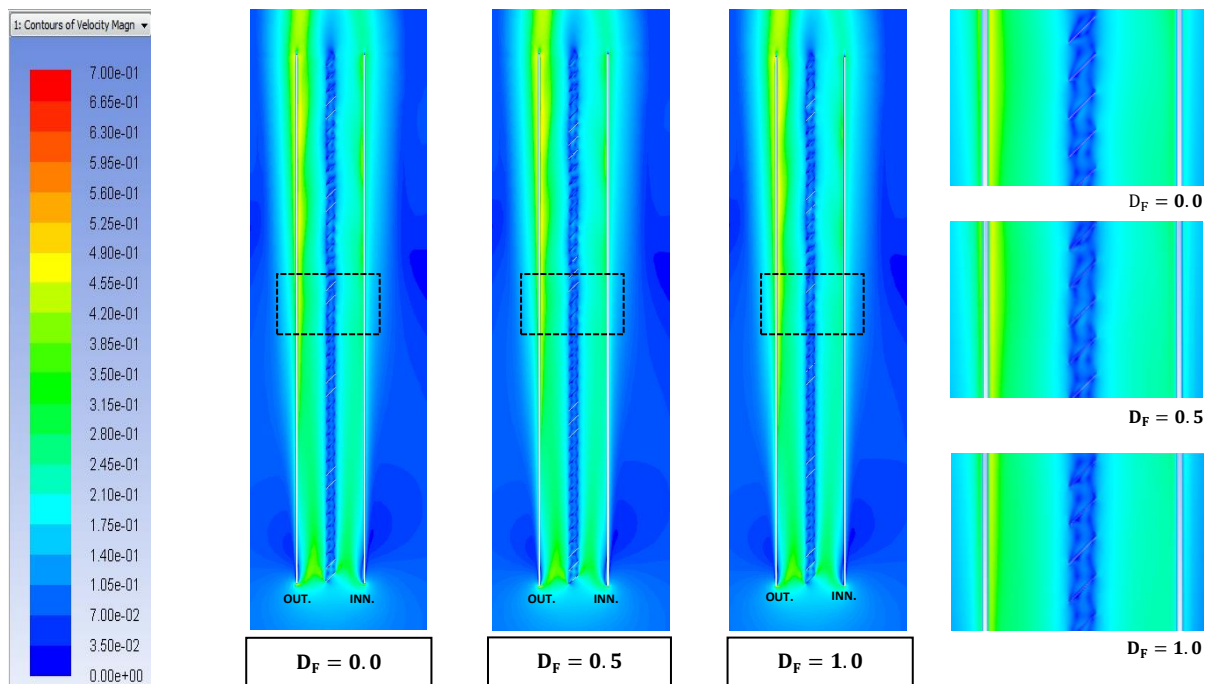


Figure 7.30: contours (and vectors) of velocity magnitude (m/s) for simple cavity with integrated slats having different surface diffusivity.

- ### Temperatures:

Changes for surface temperature increase for both front and back glass panes, Figure 7.31, were more evident than that for cavity flow rate as shown previously in Figure 7.29. This increase for front glass would be up to 6% as diffuse fraction increased toward 1.0 (diffuse surface). This was because, with simple flat integrated slats having an inclination angle of 45° (toward

outdoor), reflections would be better distributed over the front glass surface as diffuse fraction increased, rather than directed toward the upper part. On the other hand, the temperature for back glass would drop by a maximum of 12%, as value for diffuse fraction increased. This opposite trend for change was again attributed to less radiation reflected toward back glass with given slats having aforementioned stated characteristics. However, the absolute change between the maximum and minimum increases was same and about 0.61°C for either glass pane. Figure 7.32 shows contours of temperature for modelled structure with different diffuse fraction for integrated slats.

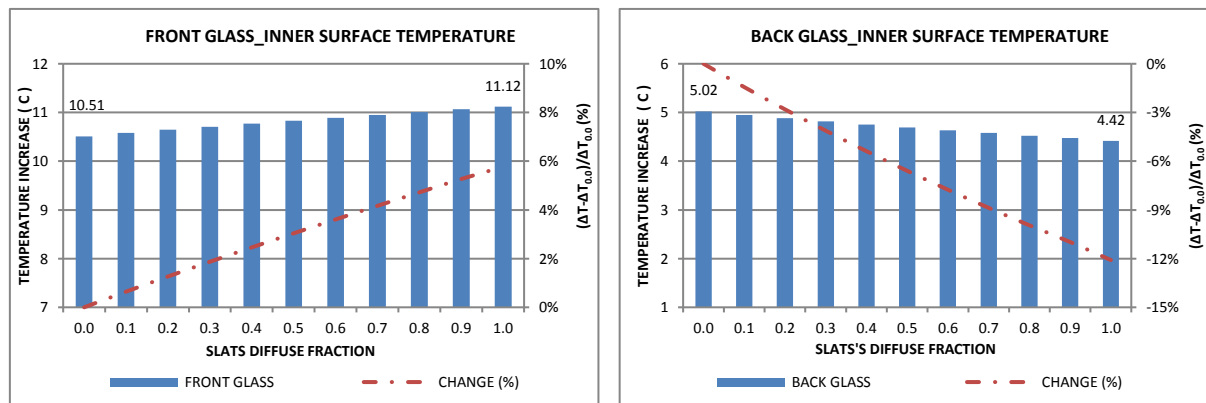


Figure 7.31: Averages surface temperature increase for inner surfaces of outer glass (left) and inner glass (right) panes, with integrated slats having surface emissivity of 0.1 and various diffuse fractions.

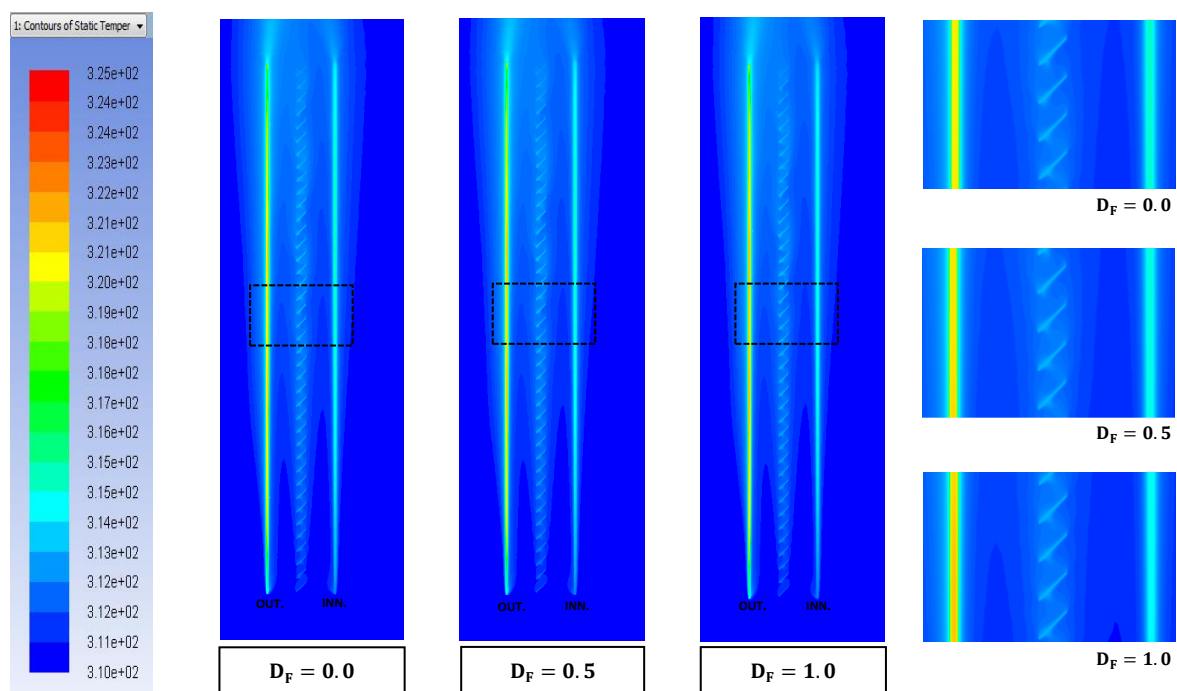


Figure 7.32: contours of temperature (k) for simple cavity with integrated slats having different surface diffusivity.

For integrated slats, its surface temperature would slightly be influenced by manipulating its diffuse fraction, Figure 7.33. As the later increased, increase in temperature would be slightly enhanced before it started to decrease. However, the maximum change was less than 3%. In turn, this decrease indicates a drop in surface temperature, which could be linked to both angle and direction of the installed slats. However, expanding this study for a wider range of inclination angles would help in understanding that. Finally, Figure 7.34 shows changes for all surfaces.

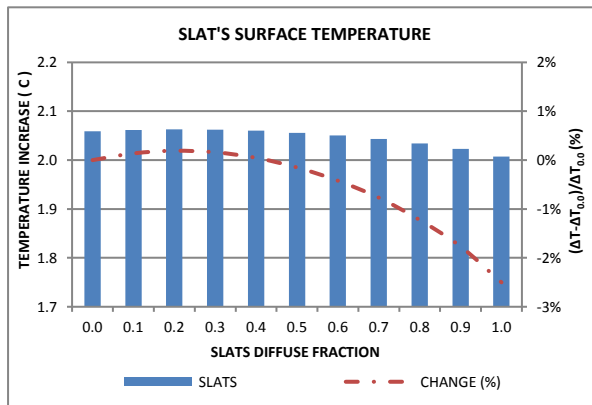


Figure 7.33: Averages surface temperature increase for integrated slats having surface emissivity of 0.1 and various diffuse fractions.

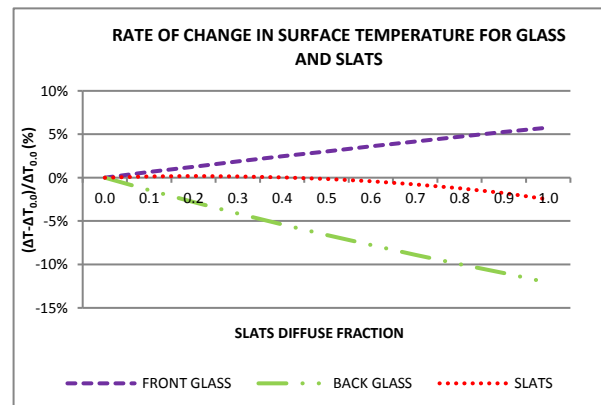


Figure 7.34: Relative changes for all elements of the structure; with integrated slats having surface emissivity of 0.1 and various diffuse fractions.

Equations (7.21) to (7.23) express the correlation between diffuse fraction D_F of integrated slats and calculated increase (ΔT) in the surface temperature of various elements of the structure as denoted.

$$\Delta T_{\text{Front}} = 0.6063 D_F + 10.522 \quad (R^2 = 0.9991) \quad (7.21)$$

$$\Delta T_{\text{Back}} = 0.1116 D_F^2 - 0.7143 D_F + 5.0229 \quad (R^2 = 0.9999) \quad (7.22)$$

$$\Delta T_{\text{Slats}} = -0.0906 D_F^2 + 0.0406 D_F + 2.0587 \quad (R^2 = 0.999) \quad (7.23)$$

Where: $0 \leq D_F \leq 1$

7.7 Surface Diffuse Fraction of Glass Panes:

Here, the influence of surface diffuse fraction of glass panes was investigated. All other parameters were kept similar to preceded work for slats. However, slats' surface emissivity and diffuse fraction were set to 0.9 and 1.0; respectively. Both cavity's airflow rate and surface temperatures are reported here.

- **Airflow rate:**

Similar to the influence by slats' diffuse fraction, that for glass had also a negligible effect on cavity's flow rate as the maximum change was 1.2%, Figure 7.35. With low values, incoming solar radiation with high incident angle would penetrate the front glass with specular direction and mainly hit the bottom of the cavity leading to slightly higher buoyant flow. Figure 7.36 proves negligible variations in airflow as shown in velocity contours for different diffuse fractions.

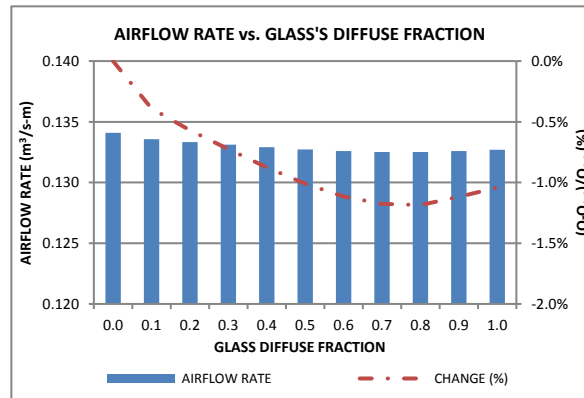


Figure 7.35: Airflow rates through cavity with integrated slats having surface emissivity of 0.9 and diffuse fraction of 1, with various diffuse fraction for glass panes.

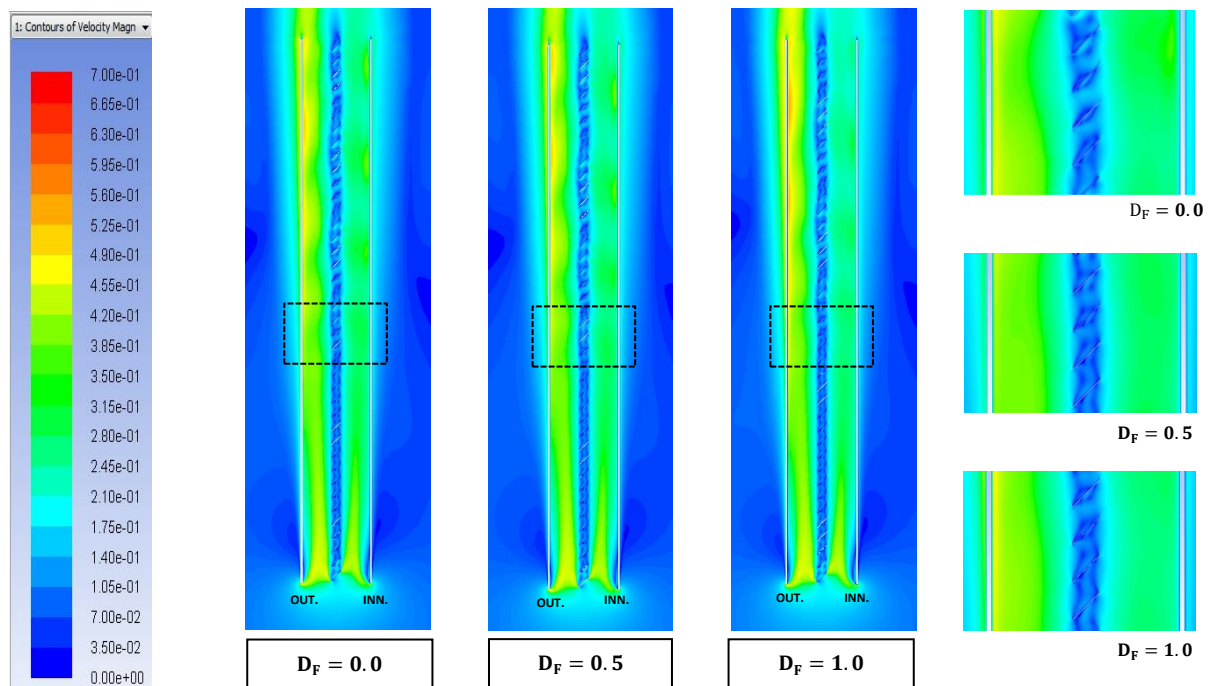


Figure 7.36: contours of velocity magnitude (m/s) for simple cavity with integrated slats having surface emissivity of 0.9 and diffuse fraction of 1, with various diffuse fraction for glass panes.

- ### Temperatures:

Similar to slats' diffuse fraction, increasing glass diffuse fraction would lead to increase surface temperature for front glass but reduce it for back glass, Figure 7.37. However, for back glass, maximum changes due to increasing diffuse fraction of slats and glass surfaces were close (12% and 10%, respectively) whereas corresponding changes for front glass were significantly different as the glass diffuse fraction would cause an increase up to 31.5% compared to just 6% by slats diffuse fraction. Simulations showed that with higher surface diffusivity (less specular characteristics), less incident radiation would be reflected to outdoor at the front glass and more being absorbed and transmitted. This increase in absorbed radiation would cause the significant increase in front glass surface temperature. However, the transmitted radiation (including the extra portion) would be distributed over wider angle thus would not increase the temperature of either integrated slats nor back glass as both would drop.

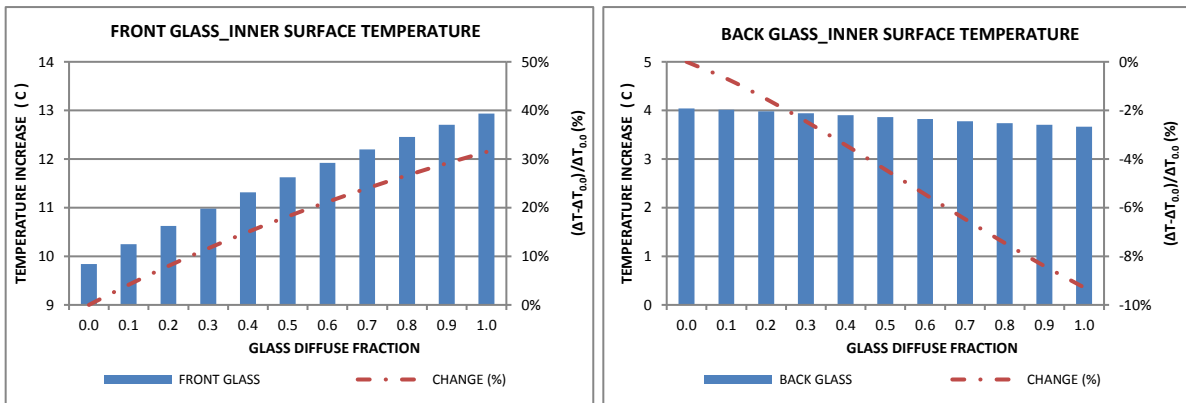


Figure 7.37: Averages surface temperature increase for inner surfaces of outer glass (left) and inner glass (right) panes, with integrated slats having surface emissivity of 0.9 and diffuse fractions of 1, with various diffuse fractions for glass.

With specular glass, incident beam radiation would penetrate the pane and mainly hit the bottom part of the structure (with relatively high incident angle, 81°) then increase the surface temperature of the lower set of integrated slats, which in turn cause the increase in total average temperature of slats with lower diffuse fractions, Figure 7.38. As diffuse fraction increased, this influence would be minimized. For the rest of the slats (middle and upper), there was no significant change in surface temperature between specular and diffuse glass panes. Figure 7.39 compares all changes in surface temperatures of both glass panes and integrated slats.

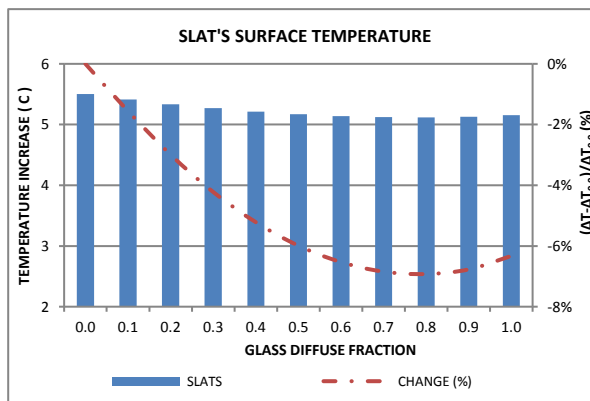


Figure 7.38: Averages surface temperature increase for integrated slats having surface emissivity of 0.9 and diffuse fraction of 1, with various diffuse fractions for glass.

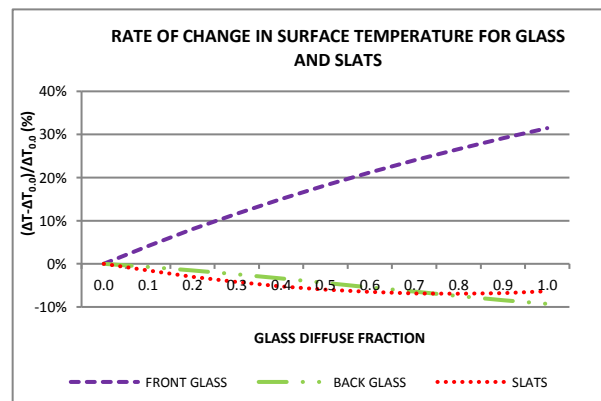


Figure 7.39: relative changes for all elements of the structure; with integrated slats having surface emissivity of 0.9 and diffuse fraction of 1, with various diffuse fractions for glass.

Magnitude changes in surface temperatures (ΔT : increase above inlet air temperature) for different elements could be calculated using the following correlations (7.24) to (7.26) and value of diffuse fraction D_F of glass surfaces.

$$\Delta T_{\text{Front}} = -0.97D_F^2 + 4.05D_F + 9.85 \quad (R^2 = 1) \quad (7.24)$$

$$\Delta T_{\text{Back}} = -0.03D_F^2 - 0.35D_F + 4.05 \quad (R^2 = 0.9992) \quad (7.25)$$

$$\Delta T_{\text{Slats}} = 0.62D_F^2 - 0.98D_F + 5.50 \quad (R^2 = 0.9998) \quad (7.26)$$

Where: $0 \leq D_F \leq 1$

Figure 7.40 displays contours of temperature for the simulated structure, where it is clear that external glass would have a higher temperature with higher diffuse fractions.

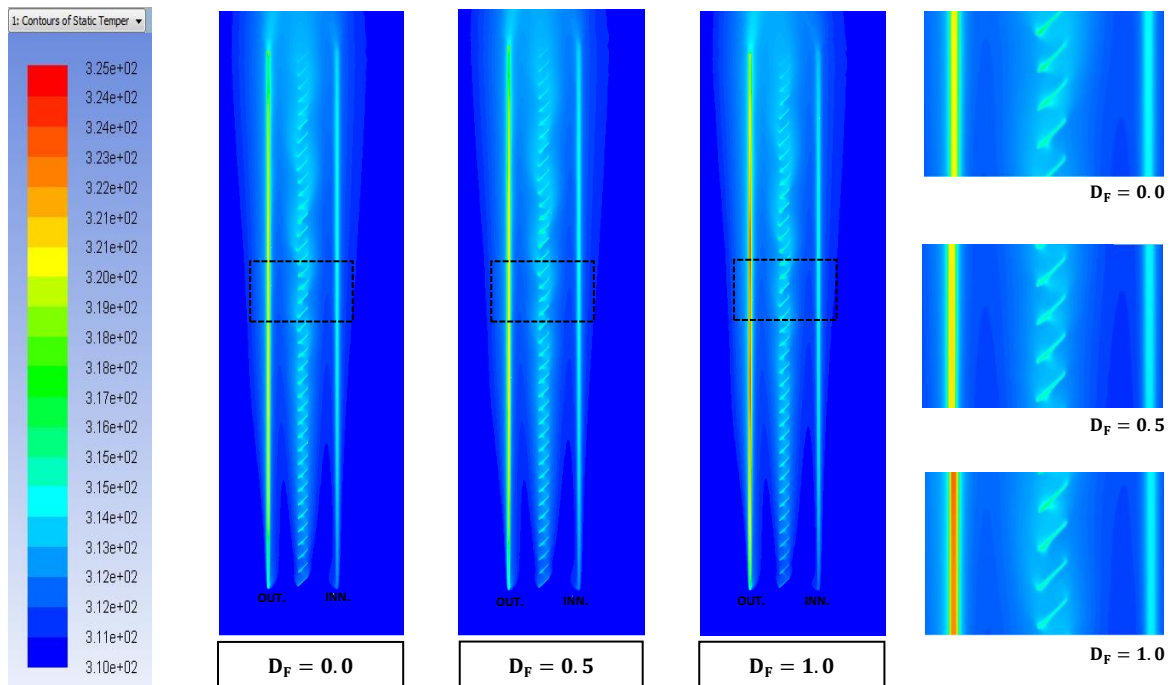


Figure 7.40: contours of static temperature (k) for simple cavity with integrated slats having different surface diffusivity.

7.8 Conclusion:


Previous sections show results and discussion for simulation outcomes for each investigated parameter. Key outcomes for each parameter are summarized in Table 7.2. It is clear how the impact of each parameter would vary from one perspective to another. For instance, the diffuse fraction (code: F) of glass would significantly affect surface temperatures, in particular, front glass pane, but it would have a negligible effect on flow rate of the cavity.

Table 7.2: Maximum and minimum calculated values and associated variation for main reported outputs against various investigated parameters. Code (A): influence of slat's size. Code (B): influence of slat's inclination angle. Code (C): influence of slat's position inside cavity. Code (D): influence of slat's surface emissivity. Code E: influence of slat's surface diffuse fraction. Code (F): influence of slat's glass diffuse fraction.

CODE	ELEMENT	PARAMETER	RANGE	AIRFLOW RATE (m ³ /s-m)			FRONT GLASS_ΔT			BACK GLASS_ΔT			INTEGRATED SLATS_ΔT		
				Min.	Max.	(%)	Min.	Max.	(%)	Min.	Max.	(%)	Min.	Max.	(%)
A	SLATS	Size	0.05 - 0.50 m	0.048	0.145	202	9.72	10.20	4.9	3.87	4.54	17.3	5.05	7.20	42.6
B	SLATS	Angle	0°- 90°	0.114	0.155	36	9.60	10.82	12.7	3.37	4.79	42.1	4.39	6.26	42.6
C	SLATS	Position	P1- P9	0.117	0.141	20.5	9.82	11.28	14.9	4.04	5.49	35.9	5.5	7.91	43.8
D	SLATS	Emissivity	0.0- 1.0	0.095	0.135	42.1	9.75	11.6	19	3.94	4.88	23.9	0.1	5.66	5560
E	SLATS	Diffuse Fraction	0.0- 1.0	0.1100	0.1116	1.5	10.51	11.12	5.8	4.42	5.02	13.6	2.01	2.06	2.5
F	GLASS	Diffuse Fraction	0.0- 1.0	0.1325	0.1341	1.2	9.84	12.93	31.4	3.66	4.04	10.4	5.12	5.50	7.4

Then, based on same data, tested parameters are classified according to their revealed influence on different reported outcomes, e.g. slats surface temperature, as shown in Table 7.3. This helps to understand how various outcomes are influenced by different parameters indicating right parameters to control specific aspect of the system.

Table 7.3: level of influence of various investigated parameters on different reported outputs; 1st: highest influential whereas 6th lowest influential

INFLUENCE		FLOW RATE	FRONT GLASS TEMPERATURE	BACK GLASS TEMPERATURE	SLATS TEMPERATURE
	1 st	A	F	B	D
	2 nd	D	D	C	C
	3 rd	B	C	D	B
	4 th	C	B	A	A
	5 th	E	E	E	F
	6 th	F	A	F	E

In general, diffuse fraction for either integrated slats or glass surfaces would have a very limited influence on airflow rate through the cavity but a varied effect on surface temperatures. Also, for better controlling of surface temperature of back (indoor) glass, more intention should be given to slat's inclination angle, position and surface emissivity.

CHAPTER 8 PARAMETRIC STUDY ON SIMPLE CAVITY WITH HORIZONTAL VENTS AND VARIOUS INTEGRATED SLATS

8.1 Introduction:

Whereas the previous chapter shows results of the simple cavity with vertical vents and simple integrated flat slats, this chapter presents results of another simple cavity but with horizontal vents, Figure 8.1, and various designs for integrated devices. Figure 8.2 shows a sample for an advanced integrated device that could serve for both solar shading and natural lighting, which is hereafter coded as 11. Other characteristics were kept typical to those for previously presented configuration including 4.0m-high and 0.5m-wide cavity, vents size equals to cavity width and 6mm-thickness glass. However, the major change was to have integrated devices with widely varied designs (configuration and profiles).

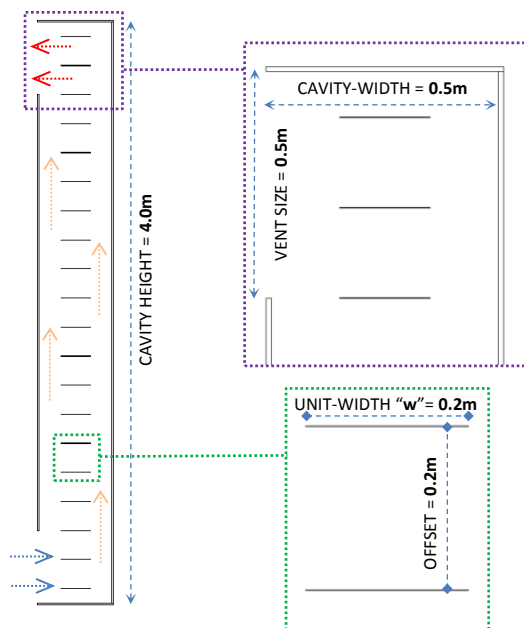


Figure 8.1: A schematic for structure with horizontal vents and simple integrated slats.

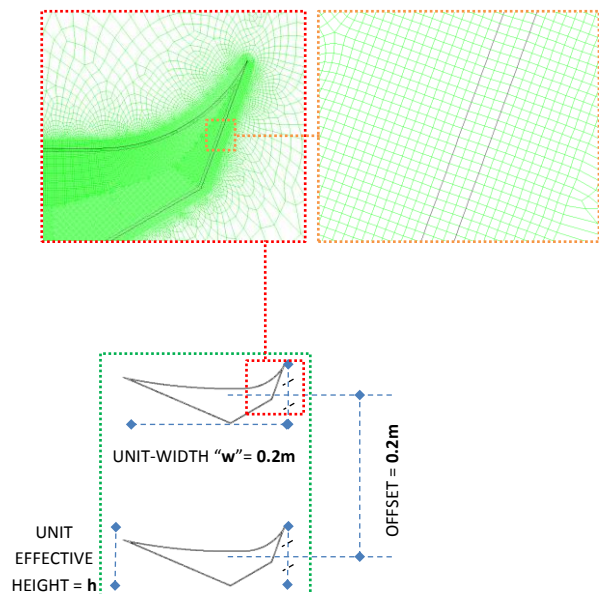


Figure 8.2: A schematic for more advanced integrated element that could serve for both solar shading and light directing, which coded hereafter by "11".

Based on general outcomes from previous work (simple cavity with simple slats), investigation here was narrowed down to fewer parameters and then fewer samples for integrated devices.

However, effective horizontal width for all slats was fixed to 0.2m (40% of cavity's width) and offset (distance from center-to-center of adjacent slats) was also 0.2m (equal to slat's width). The later, and due to varied effective heights for different designs (profiles), would results in varied openness ratios as shown in Figure 8.3-A.

It's worth mentioning that numbers-coding was originally assigned, by the author, to investigated devices based on their level of design's complexity, according to literature. However, they were re-arranged here based on their given effective heights;

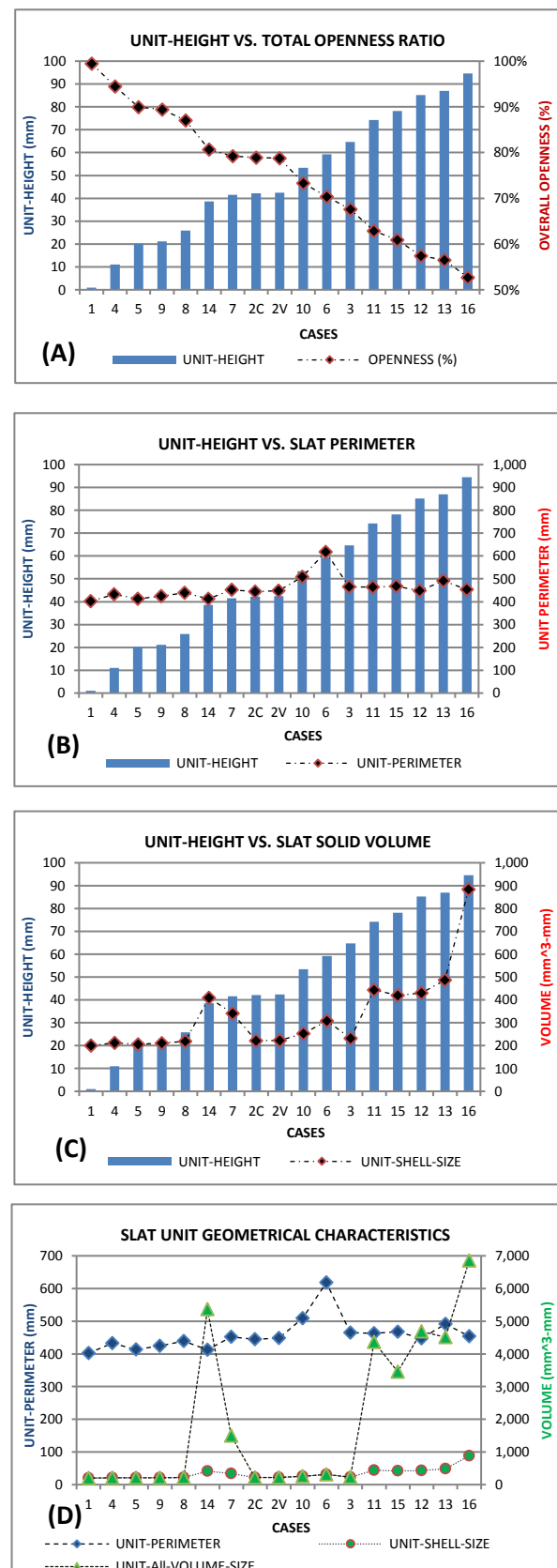


Figure 8.3: A summary of geometrical characteristics of different investigated designs. (A) Relation between effective unit-height and corresponding total openness ratio for the entire cavity. (B) Relation between effective unit-height and calculated perimeter for individual unit. (C) Relation between effective unit-height and calculated volume for individual unit. (D) Comparison between different geometrical characteristics for individual units.

i.e. 1's effective height is directly smaller than that for 4 and so on.

Figure 8.3-B compares between effective height and calculated perimeter for individual units. It shows that perimeters were between 400-500mm except for design-6 was 618mm due to its multi-folding layout. Figure 8.3-C presents calculated volumes of the outer shell of each unit, where shell thickness was fixed to 1mm for all designs. Finally, Figure 8.3-D summarizes different geometrical characteristics for all designs, including all-volume-size that counts both sizes of core and shell.

Figure 8.4 to Figure 8.6 shows schematic drawings for different designs of integrated shading elements that were examined under this work. As mentioned earlier, these designs were selected and regenerated from common shading & daylighting products and designs; Appendix C and Appendix D. Dimensions and coordinates could be derived from these drawings and based on provided grid. However, the thickness for shown designs was always 1mm. Design#15 is (also Design#17) not presented as it was eliminated from the study later on.

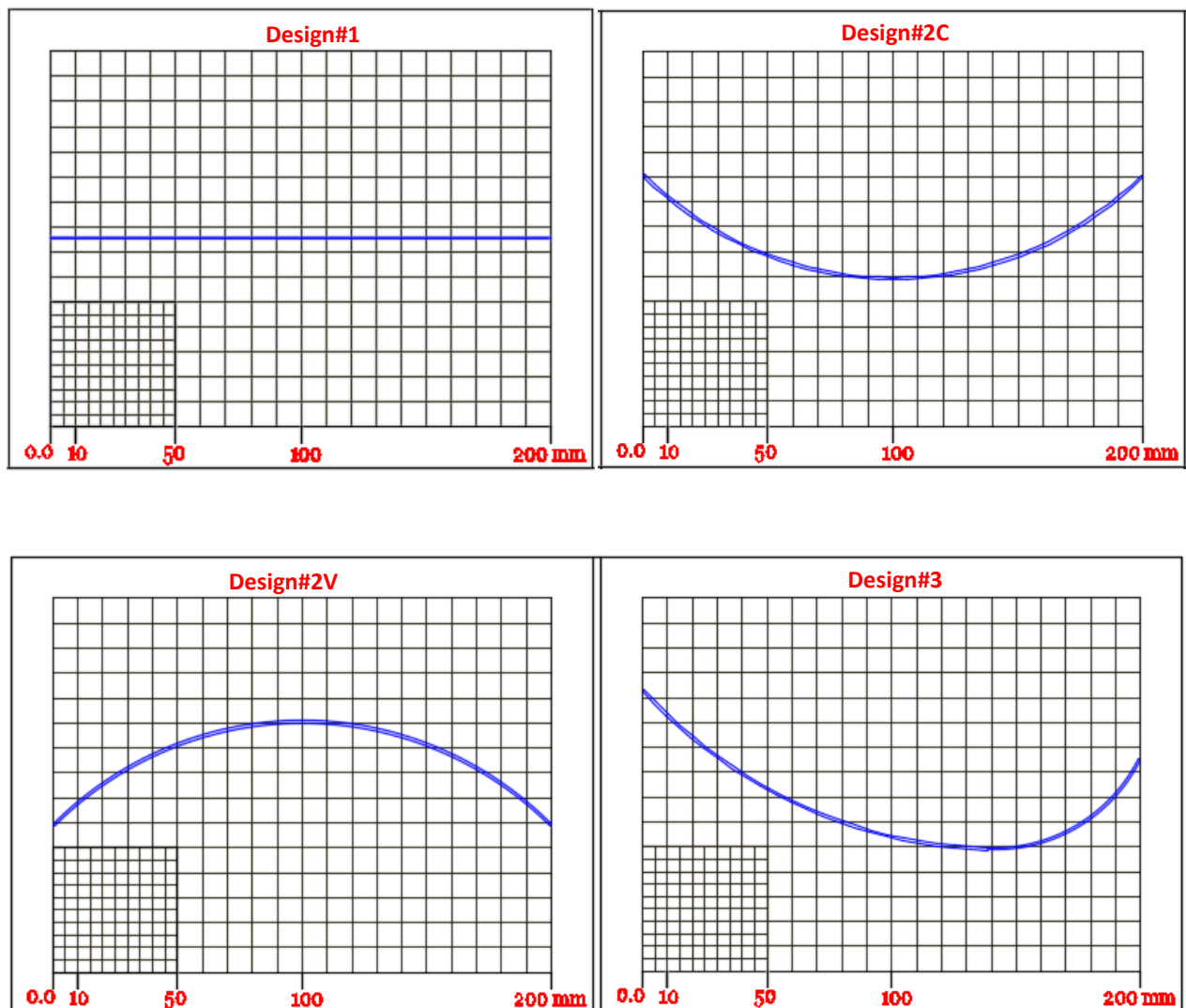


Figure 8.4: schematic drawings for different designs of integrated shading elements. (Continued).

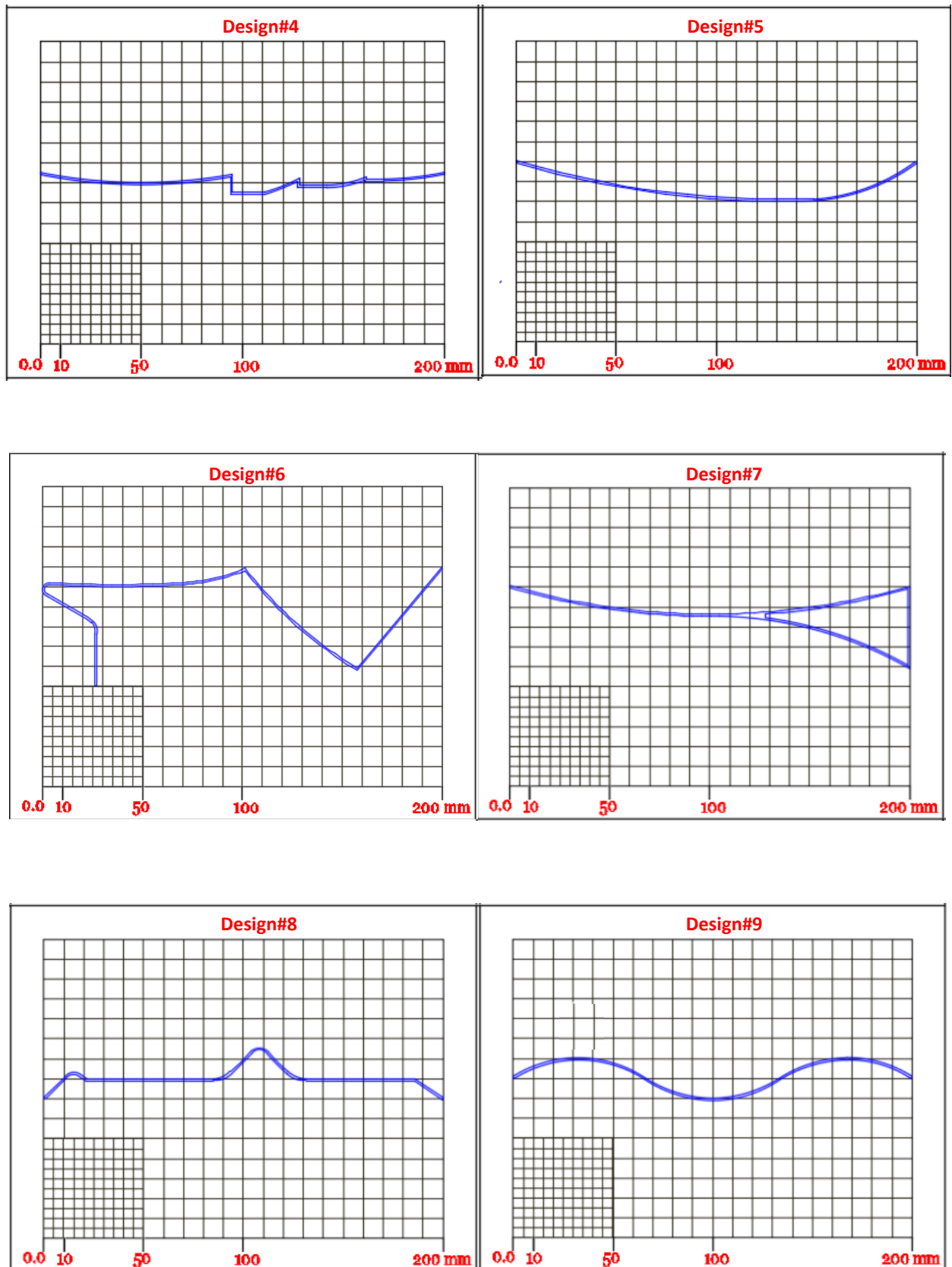


Figure 8.5: schematic drawings for different designs of integrated shading elements. (Continued).

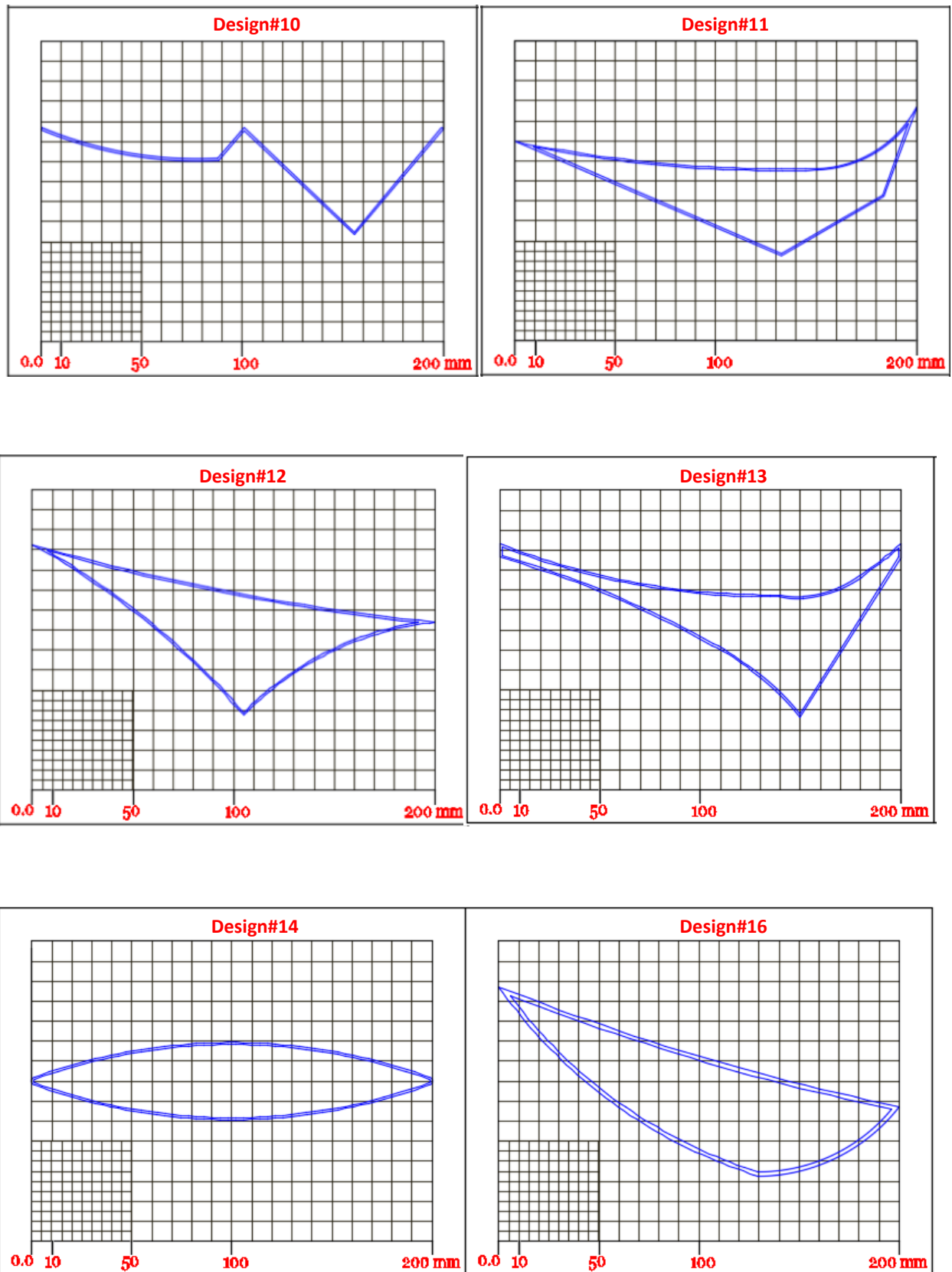


Figure 8.6: schematic drawings for different designs of integrated shading elements.

8.2 Performance of Different Integrated Slats with Surface Emissivity of 0.9 and Diffuse Fraction of 1; Under Summer Conditions:

This work was carried out for the simple structure as described earlier, and for all designs of integrated slats. Slats' set was always at the central axis of the cavity. The investigation was conducted under summer scenario with beam radiation having an incident angle of 81° . Slat's surface emissivity was 0.9 and the diffuse fraction was 1. Following results discuss the impact of changing the design for integrated slats on both airflow and thermal performance of the cavity.

- **Airflow rate:**

Figure 8.7-A shows calculated airflow rates for a cavity with integrated slats with different designs. Generally, airflow rate increased through the cavity with integrated slats compared to the non-shaded cavity. This increase was due to slat's ability to absorb more solar heat (in addition to absorption by glass panes) thus further enhancing buoyant airflow inside the cavity.

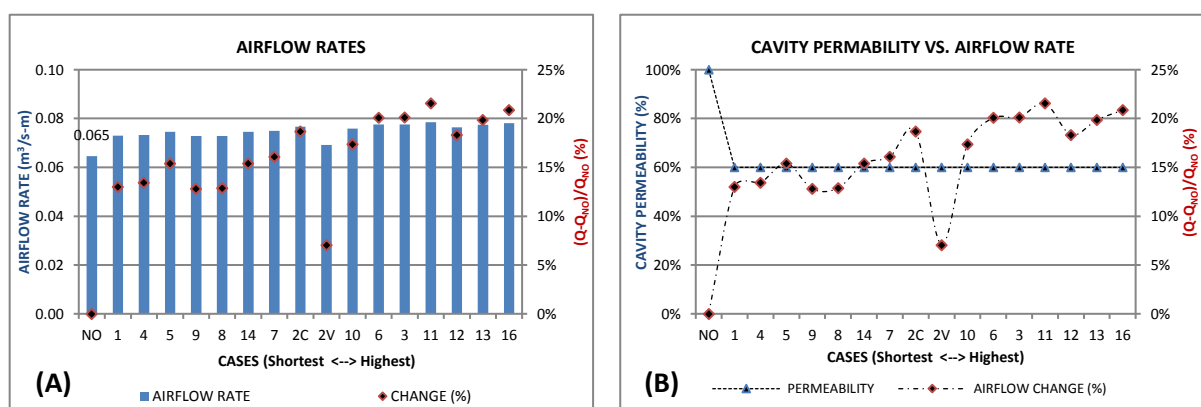


Figure 8.7: (A) Airflow rates changes for simple cavity with horizontal inlets and different integrated slats. (B) Changes in cavity's flow permeability and calculated airflow changes.

However, the rate of increase was found to be dependent on the slat's design (e.g. unit height and layout) but independent of its horizontal profile

that was fixed to 0.2m and resulted in constant cavity's flow permeability (60%) as shown in Figure 8.7-B.

In reference to the non-shaded cavity, maximum increase was 21.6% for design#11 and minimum was 7% for design#2V (convex slats); compared to 18.7% for design#2C (concave slats). However, average net increase for all investigated designs was about 16.4% ($0.011\text{m}^3/\text{s-m}$). Now setting the average net increase as a reference (this helps to assess the actual influence of design on cavity's airflow rates), design#11 (more influent design) could cause an increase of 131% compared to just 43% for design#2V (less influent design). Furthermore, design#1 (simple flat slat with 0° inclination angle) could lead to an increase of 79%.

Figure 8.8 and Figure 8.9 show contours of velocity magnitudes (m/s) for the investigated cavity (with horizontal vents) with and without integrated shading slats. Without shading slats (design#0), air would mainly flow toward the inner wall (inner glass) before it continues upward along the cavity height. It's clear that the distance needed for air stream to flow towards the outer glass of cavity was slightly more than the size of inlet (cavity' width). However, a vortex was created in this gap next to lower part of outer glass (the distance between the upper edge of the inlet and the point where air stream would flow towards outer glass). Also, vortex was created near the bottom of the cavity (inner corner).

Moreover, results are shown for different designs of integrated slats. It's clear that airflow patterns at the cavity's inlet (and, next area inside the

cavity) would vary based on the configuration of integrated devices. However, it is still common that air stream would initially tend to flow toward the inner wall (glass) before it turns up along the cavity. But, the presence of slats would divide the incoming flow into two unequal streams, and force the upper stream to go up directly along the front sub-cavity.

Furthermore, airflow mainly tended to move from back sub-cavity toward the front sub-cavity, which was due to higher surface temperature for front glass as well as front-face of integrated slats (that form the boundaries of front sub-cavity). However, the detailed design of integrated slats would significantly influence the flow between the two sub-cavities separated by these elements; for instance, air could have swirls and mainly return back to back sub-cavity with some designs (e.g. Figure 8.8-design#2C) whereas it could easily continue toward front sub-cavity with other designs (e.g. Figure 8.9-design#13). As a result, the flow (its density and velocity) in back sub-cavity would vary depends on the design of integrated slats (that would determine the effect height and then vertical free-offset between adjacent elements). This could be easily noticed when comparing the flow between design#11 and design#12 as shown in Figure 8.9.

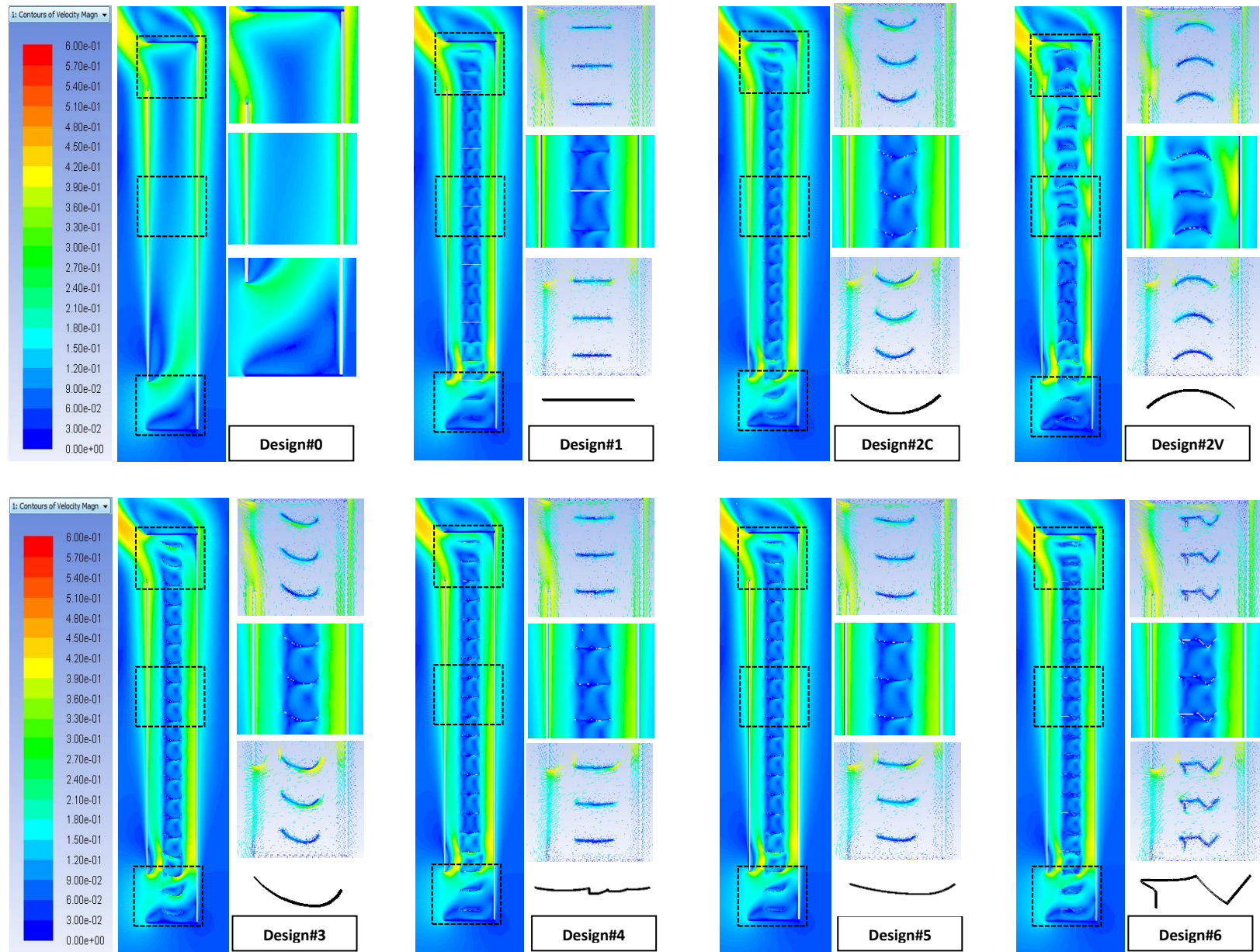


Figure 8.8: contours (and vectors) of velocity magnitude (m/s) for simple cavity with horizontal vents and various designs of integrated slats.

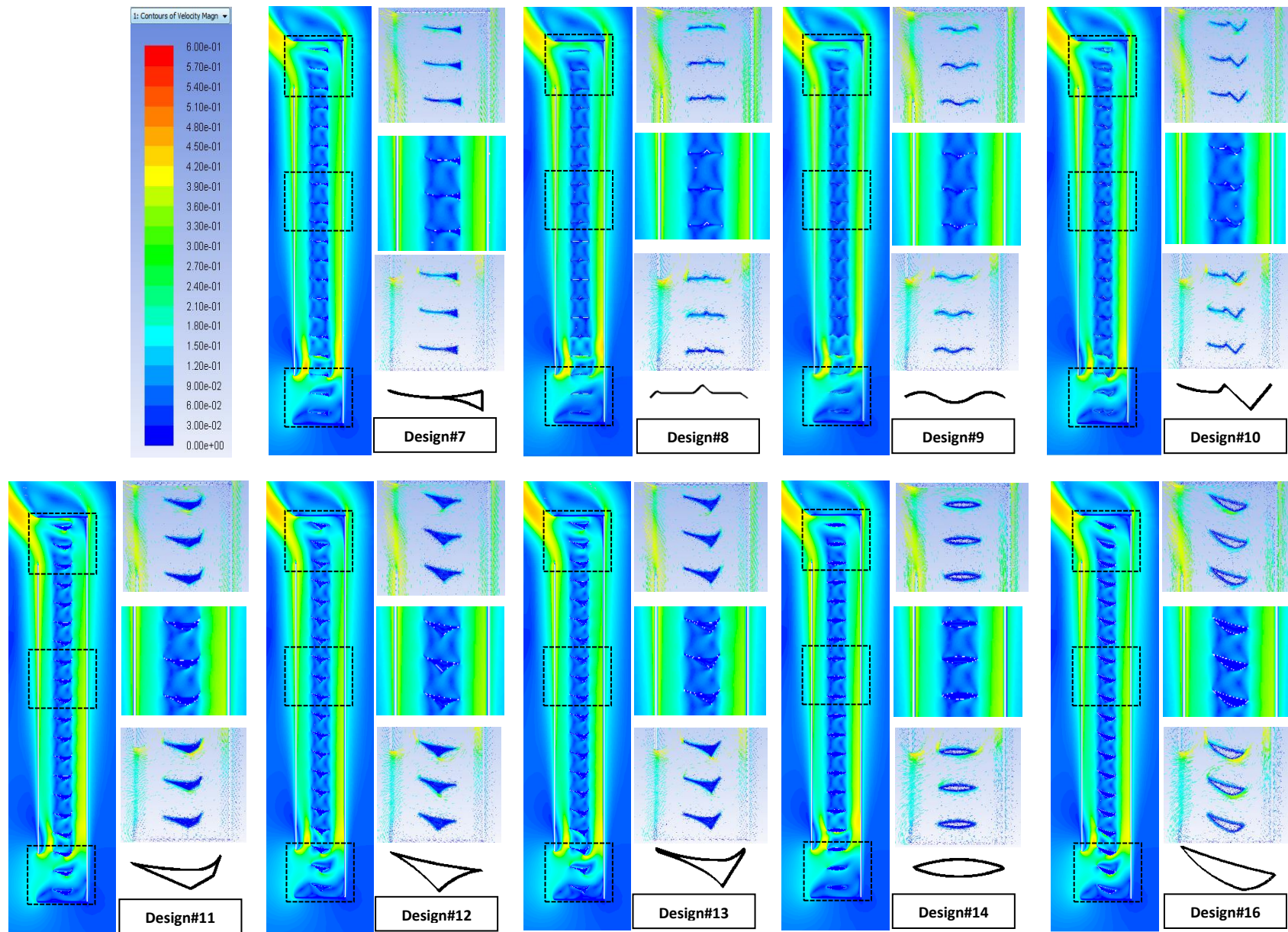


Figure 8.9: contours (and vectors) of velocity magnitude (m/s) for simple cavity with horizontal vents and various designs of integrated slats; (Continued).

- **Temperatures:**

Figure 8.10 shows surface temperature increase (surface temperature – ambient air temperature “37°C”) for both glass panes that face the cavity inside. Generally, temperature increase would drop with the presence of integrated slats. However, this drop for front glass was small as the maximum change was 4.3%, Figure 8.10-A. On the other hand, it was significant for back glass as maximum drop reached 45% with design#12 while average was 28% as shown in Figure 8.10-B. As mentioned earlier, drop in back glass temperature is attributed to less solar heat admitted toward it with the presence of integrated slats that had an emissivity of 0.9 and varied openness ratios. Obviously, changes in glass temperature were dependent on the design of those elements.

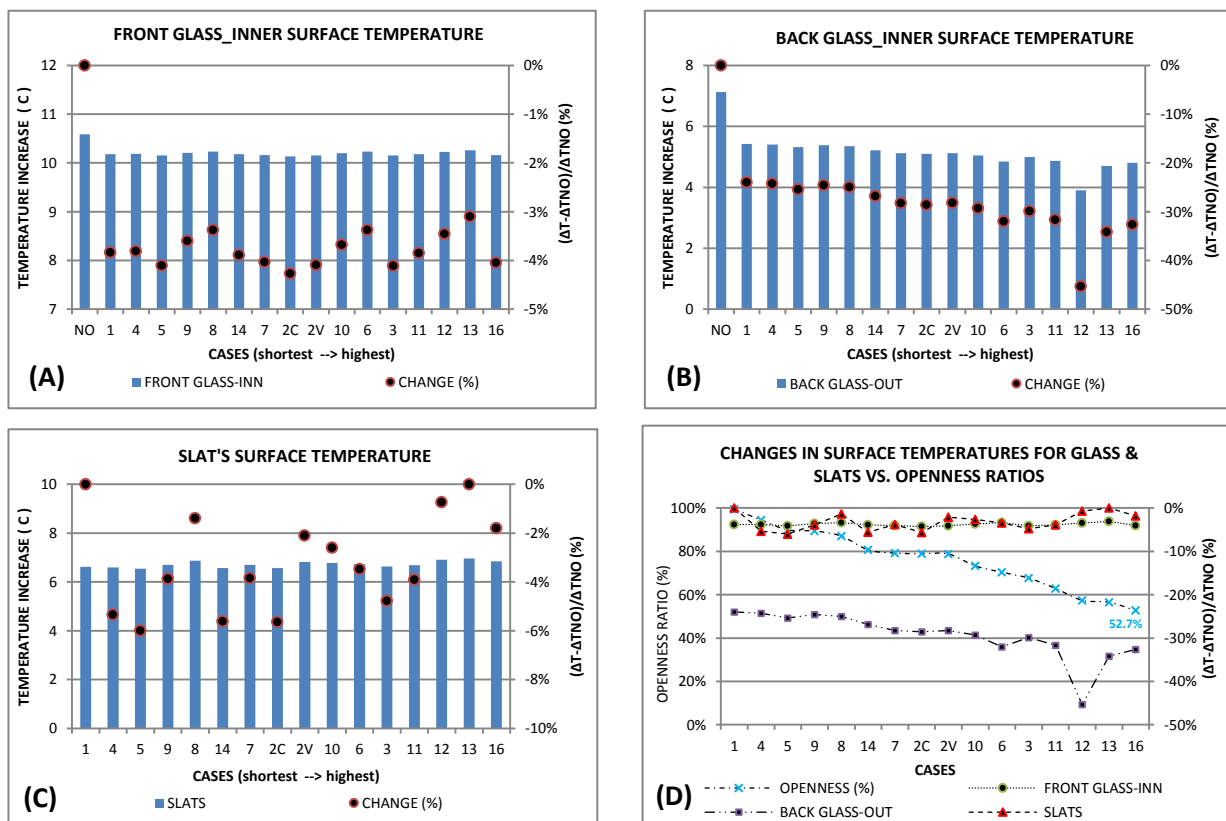


Figure 8.10: Averages of surface temperature increase for cavity's elements in summer with different tested designs of integrated slats; slats surfaces had emissivity of 0.9 and diffuse fraction of 1. (A) Front glass_inner surface. (B) Back glass_inner glass. (C) Integrated slats' surface. (D) Comparison for changes of all mentioned surfaces and openness ratios.

Also, Figure 8.10-C presents increase in average surface temperature of integrated slats; again the increase would vary with their designs. However, the maximum change was about 6% and these changes were related in somehow to those for outer glass. Finally, Figure 8.10-D shows a comparison between all revealed changes in surfaces' temperatures and changes in overall openness ratios; as shown, changes for back glass are highly related to those for openness ratios.

Both Figure 8.11 and Figure 8.12 present contours of temperature for the tested cavity. Contours show temperature gradient for both structure's elements (i.e. glass panes and integrated slats) and ventilation air. Thermal fields would be clearly developed along the height of cavity. Also, results show how the temperature of glass would vary between outer and inner panes; also, along with the height of each pane.

Moreover, with the presence of integrated slats, it's clear how it would help in developing the thermal fields at the middle height of cavity as it would be influenced not only by both heated walls but also the heated aluminum slats in the middle of the cavity. Also, the detailed design of these devices would influence the temperature contours inside the cavity and in particular in-between these devices as clearly seen when comparing design#1 and design#11.

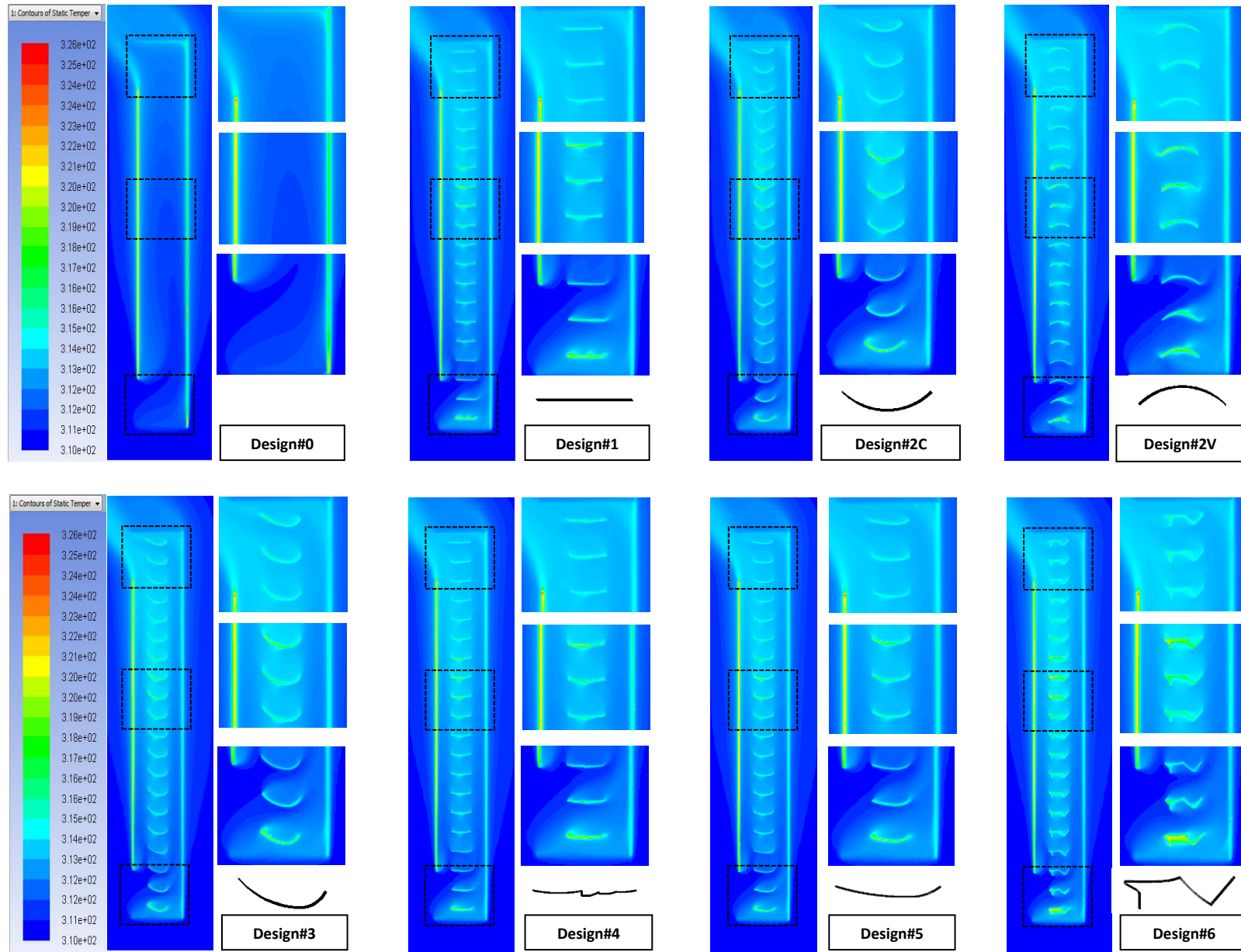


Figure 8.11: Contours of static temperature (k) for simple cavity with horizontal vents and various designs of integrated slats.

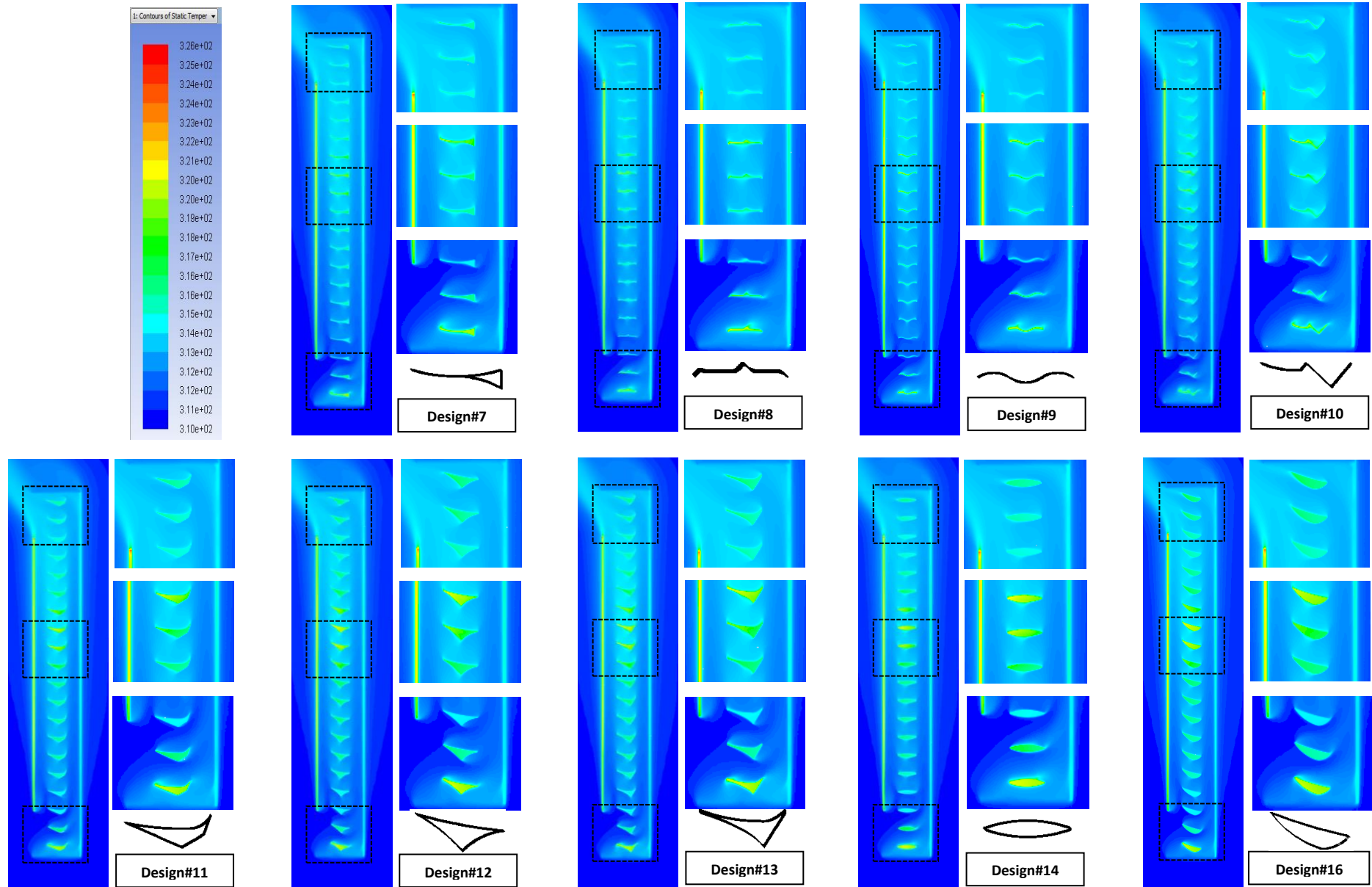


Figure 8.12: Contours of static temperature (k) for simple cavity with horizontal vents and various designs of integrated slats; (continued).

8.3 Performance of Selected Integrated Slats with Surface Emissivity of 0.2 and Diffuse Fraction of 0; Under Summer Conditions:

This section presents simulation results for similar structure used in the previous section but with some modifications to integrated slats; i.e. surface characteristics for these elements were changed and in particular, emissivity was set to 0.2 instead of 0.9, and diffuse fraction was set to 0 instead of 1. Furthermore, the study was narrowed down to just a few selected cases of integrated slats: design#1, design#14, design#6, design#3 and design#11. These cases were selected based on their variations in design complexity, multi-function and revealed performance as shown in the previous section; so they can still provide a good sample for tested cases to carry out the rest of study, which aims to explore the influence of unit-design and characteristics on both airflow and thermal performance of the system.

- **Airflow rate:**

Shown results here are for the five selected samples as mentioned earlier. However, for a better understanding of their performance, results are presented for both design assumptions regarding surface characteristics of individual unit-slat: (1) emissivity of 0.9 & a diffuse fraction of 1, and (2) emissivity of 0.2 & a diffuse fraction of 0; as shown in Figure 8.13. Yet, results for the emissivity of 0.9 & a diffuse fraction of 1 are hereafter indicated by "EMS0.9-DIFF1" whereas "EMS0.2-DIFF0" is used for the emissivity of 0.2 and a diffuse fraction of 0.

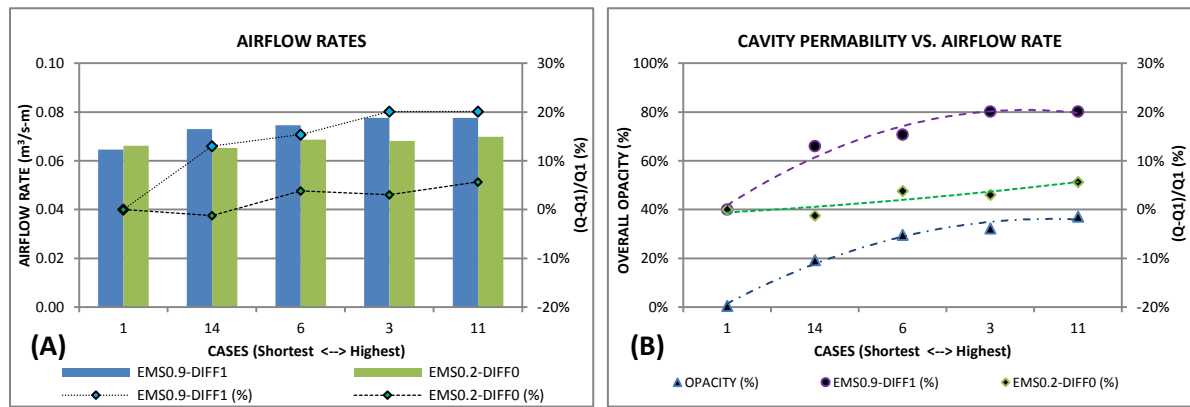


Figure 8.13: (A) Airflow rates changes for simple cavity with horizontal vents and selected designs for integrated slats. (B) Changes in cavity's overall opacity and calculated airflow changes.

As shown in Figure 8.13-A, airflow rate of the cavity with integrated slats of design#1 (simple flat) and surface characteristics of EMS0.2-DIFF0 was slightly higher (by 2%) than that for EMS0.9-DIFF1 with same slat design. In contrast, airflow rate for EMS0.2-DIFF0 was always lower than that for EMS0.9-DIFF1 with other designs (e.g. design#6). Such drop (with 10% average) could be interpreted as shading elements absorbing less solar heat with lower emissivity (0.2 instead of 0.9) thus providing smaller buoyancy effect. For design#1, such small increase was unexpected as it shows a contrast to the previous conclusion with respect to the effect of slat's emissivity on cavity airflow, where results showed that flow rate would decrease as slat's emissivity decrease and vice versa. However, changing slats' surface feature from fully diffuse (1) to purely specular (0) could have resulted in such small increase. However, such claim still needs to be further investigated.

Most importantly, variations in flow rates of the cavity with different designs were limited to a maximum of 5.7% for EMS0.2-DIFF0 compared to a maximum of 20.1% for EMS0.9-DIFF1. This highlights the value (as part of overall influence by given design) that surface's characteristics would have on

cavity airflow. In other words, surface characteristics (e.g. surface emissivity or diffusivity) of integrated devices could have more influence on cavity airflow than the degree of complexity (e.g. effective height) of these devices.

Additionally, Figure 8.13-B shows the relationship between the changes in cavity's airflow rates with different samples (and for both scenarios of surface characteristics of integrated slats) and the changes in overall opacity of this cavity with these samples. It is clear that as the overall opacity of cavity increased, its flow rate increased but with different rates depending on the scenario. Now, as opacity level ($h * \text{number of devices} / \text{height of cavity}$) depends on the effective height (h) of the individual integrated device, it was found that cavity's flow rate would increase as this height increases. This is mainly because of the capability of these devices have larger surfaces exposed to solar radiation to absorb more heat, and then enhance buoyant airflow. This also confirms why these devices with higher emissivity would cause more buoyant flow.

Figure 8.14 shows contours of velocity magnitudes (m/s) for the investigated structure with various integrated shading slats and for both scenarios of surface characteristics. It's shown how cavity flow rate would decrease as surface emissivity for slats decreased, which was evident through the changes in flow of inner sub-cavity.

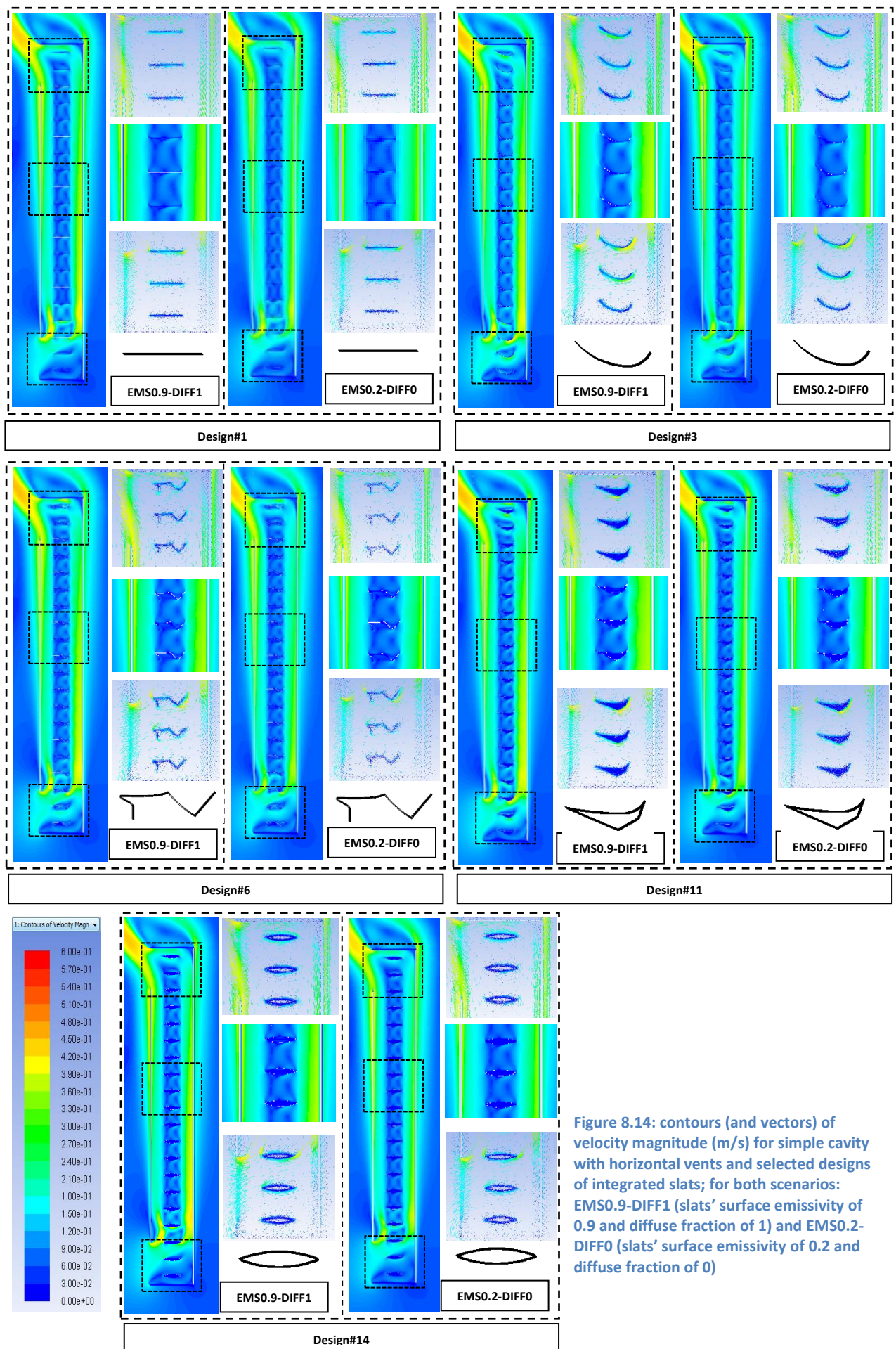


Figure 8.14: contours (and vectors) of velocity magnitude (m/s) for simple cavity with horizontal vents and selected designs of integrated slats; for both scenarios: EMS0.9-DIFF1 (slats' surface emissivity of 0.9 and diffuse fraction of 1) and EMS0.2-DIFF0 (slats' surface emissivity of 0.2 and diffuse fraction of 0)

- **Temperatures:**

Figure 8.15 shows average temperature increase for glass surfaces and different integrated slats along with relative changes. Unlike cavity's airflow, surface temperatures had more variations with lower surface emissivity and specular surfaces (EMS0.2-DIFF0) for integrated slats. For example, maximum change for front-glass's temperature-increase was about 6.8% with (EMS0.2-DIFF0) compared to a negligible change of 0.5% with (EMS0.9-DIFF1) as shown in Figure 8.15-A. This is mainly due to higher role of reflection by slats with lower surface emissivity as desing#6 shows. However, this role could be overtaken by the complexity of design as design#11 showed.

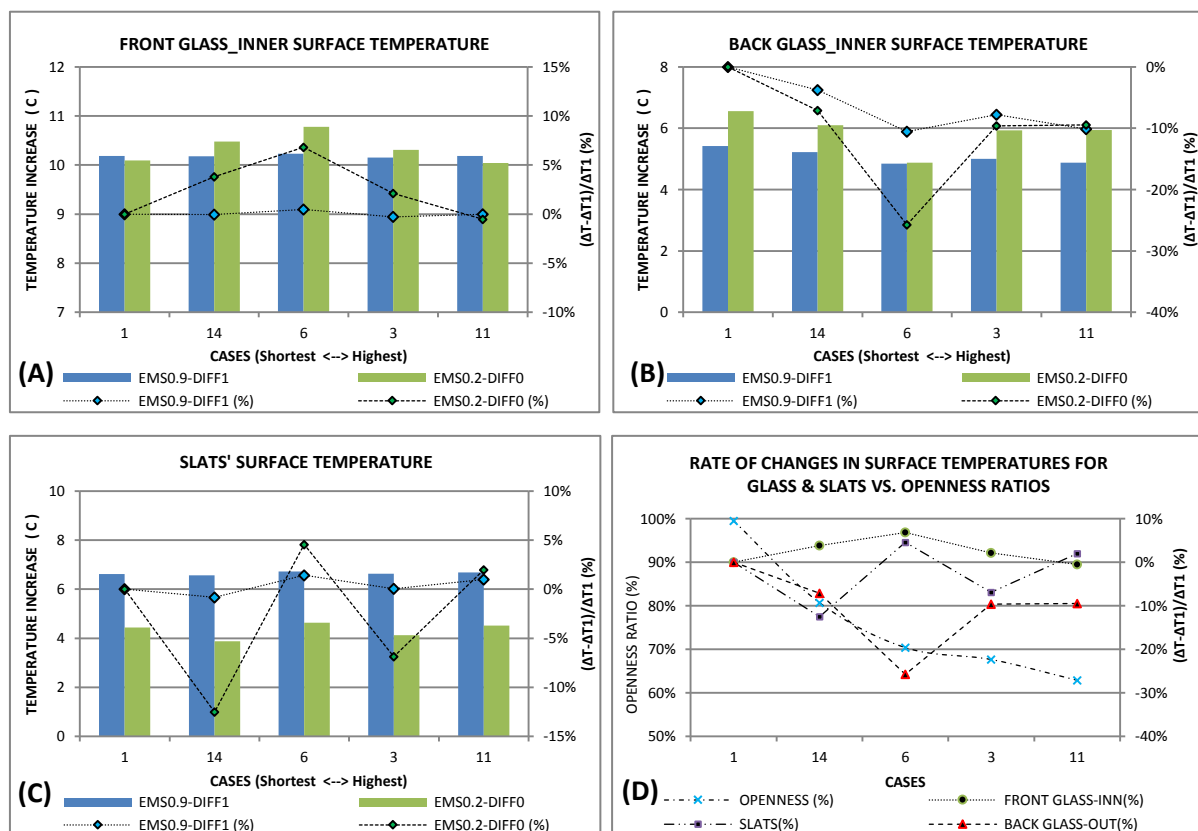


Figure 8.15: Averages of surface temperature increase for cavity's elements in summer with different tested designs of integrated slats; slats surfaces had emissivity of 0.2 and diffuse fraction of 0. (A) Front glass_inner surface. (B) Back glass_inner surface. (C) Integrated slats' surface. (D) Comparison for changes of all mentioned surfaces and openness ratios.

On the other side, Figure 8.15-B shows that design#6 also led to a maximum change of 25.7% for back-glass's temperature-increase with (EMS0.2-DIFF0) compared to just 10.5% with (EMS0.9-DIFF1). Again, this applies to integrated slats as their surfaces' temperature would vary significantly (max. 12.5%) with lower emissivity compared to higher emissivity (max. =4.6%) as shown on Figure 8.15-C. Nevertheless, there is no clear relationship between overall openness ratio of cavity and surface temperature changes for its elements as shown in Figure 8.15-D.

Figure 8.16 presents contours of temperature for the tested cavity with various designs of integrated slats and two scenarios of surfaces' characteristics. It is clear how changing thermal characteristics of the shading devices would affect the thermal field inside the cavity. For instance, increasing surface emissivity would lead to increase its temperature and surrounding air temperature with enhanced convection process. However, this change depended on the detailed design of integrated slats.

To conclude, whereas changes in surface temperatures for all elements (glass panes as well as integrated slats) were dependent on design of integrated slats with higher values for their surface characteristics (i.e. emissivity and diffusivity), this level of dependence could increase dramatically as those values decreases (i.e. lower emissivity and lower diffuse fraction).

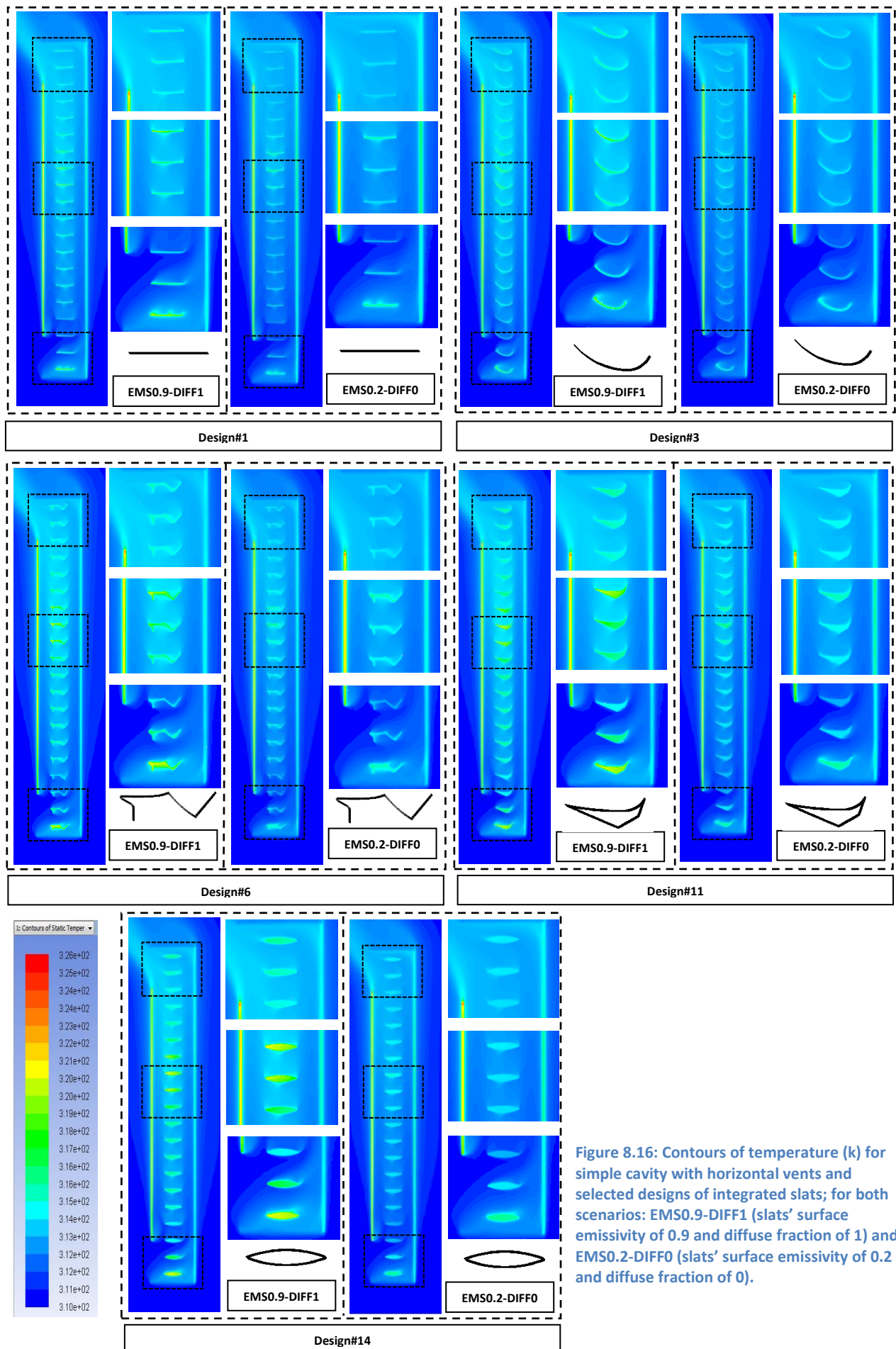


Figure 8.16: Contours of temperature (k) for simple cavity with horizontal vents and selected designs of integrated slats; for both scenarios: EMS0.9-DIFF1 (slats' surface emissivity of 0.9 and diffuse fraction of 1) and EMS0.2-DIFF0 (slats' surface emissivity of 0.2 and diffuse fraction of 0).

8.4 Performance of Selected Integrated Slats with Surface Emissivity of 0.2 and Diffuse Fraction of 0; Under Winter Conditions:

Simulations were repeated for same structure with same selected designs of integrated slats; however, boundary conditions were set for winter conditions instead of summer. Surface characteristics were kept as 0.2 for emissivity and 0 for diffuse fraction (specular).

- **Airflow rate:**

Figure 8.17-A provides a comparison for airflow rates of the cavity with different integrated slats, and both summer and winter conditions. Results show that cavity's airflow rates in winter were always higher than summer.

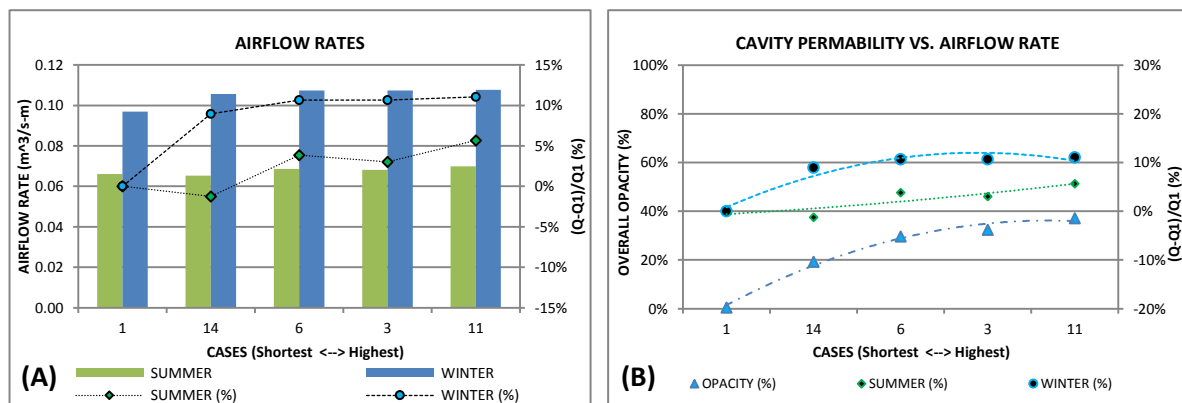


Figure 8.17: (A) Airflow rates changes for simple cavity with horizontal vents and different designs of integrated slats. (B) Changes in cavity's overall opacity and calculated airflow changes.

As discussed earlier in this work, this is because of the low angle of sun rays in winter compared to summer, thus more radiation would be absorbed leading to more buoyant force inside the cavity. However, except for design#1 (simple flat slat), less variations in cavity's flow rate were revealed with winter conditions, unlike summer. This indicates that detailed design of integrated elements would be with less important with low sun positions. However, this outcome may not fully be extended to effective height of slat-unit as

Figure 8.17-B shows that flow rate in both winter and summer would still increase with increasing total opacity of cavity (that depends on the effective height of slats).

Figure 8.18 shows contours of velocity magnitudes (m/s) for the investigated structure with various integrated shading slats and for both conditions: winter and summer. It is also shown how changing these conditions (radiation amount and incident angle) would affect flow patterns and its density inside the cavity.

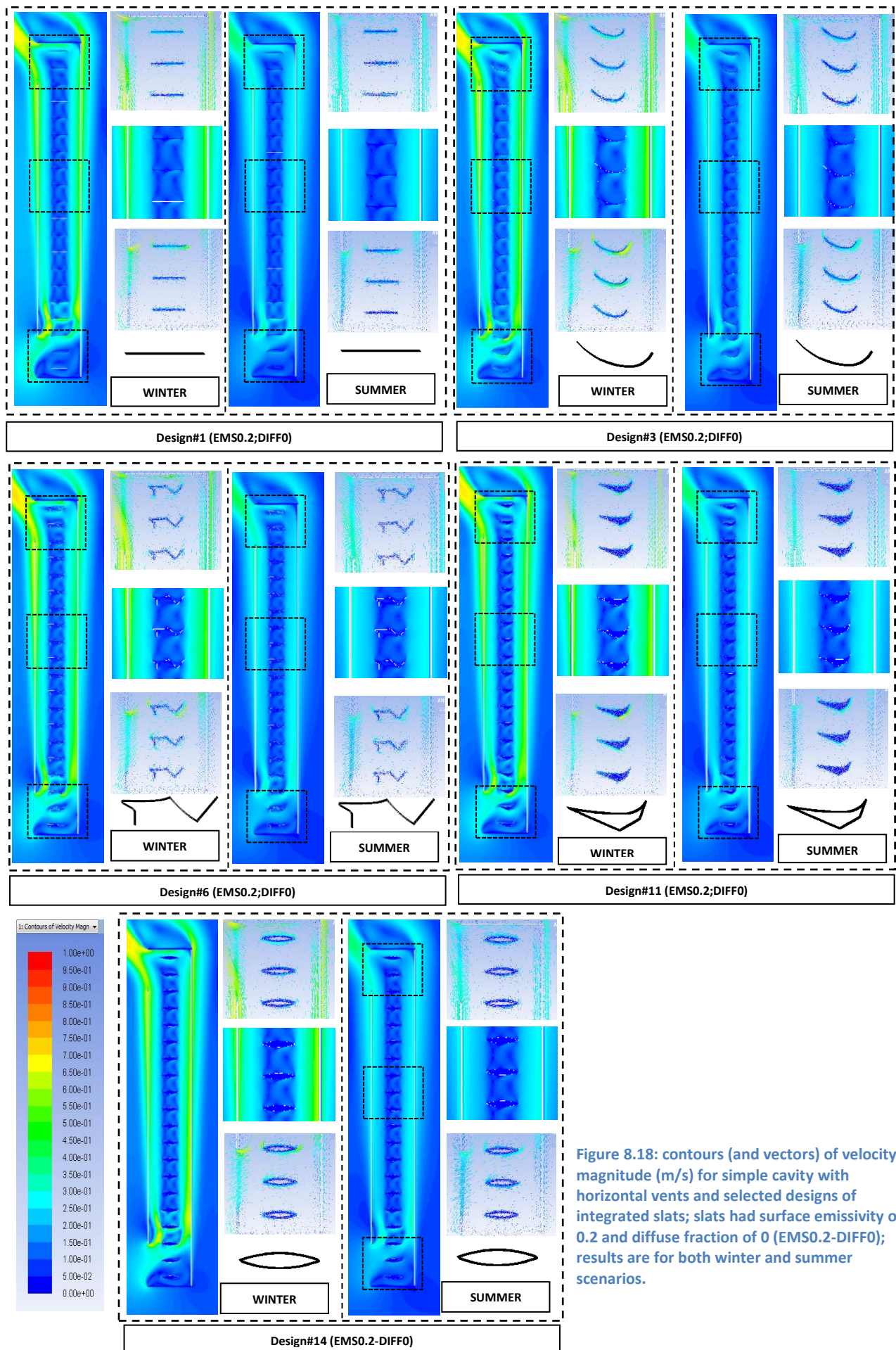


Figure 8.18: contours (and vectors) of velocity magnitude (m/s) for simple cavity with horizontal vents and selected designs of integrated slats; slats had surface emissivity of 0.2 and diffuse fraction of 0 (EMS0.2-DIFF0); results are for both winter and summer scenarios.

- **Temperatures:**

Figure 8.19 shows average surface's temperature increase in both summer and winter; generally, surface's temperature recorded a higher rate of increase in winter compared to summer. Moreover, relative changes in temperature due to various integrated slats were larger in winter for both front glass (Figure 8.19-A) and integrated slats (Figure 8.19-C). However, corresponding changes were close concerning back glass (Figure 8.19-B).

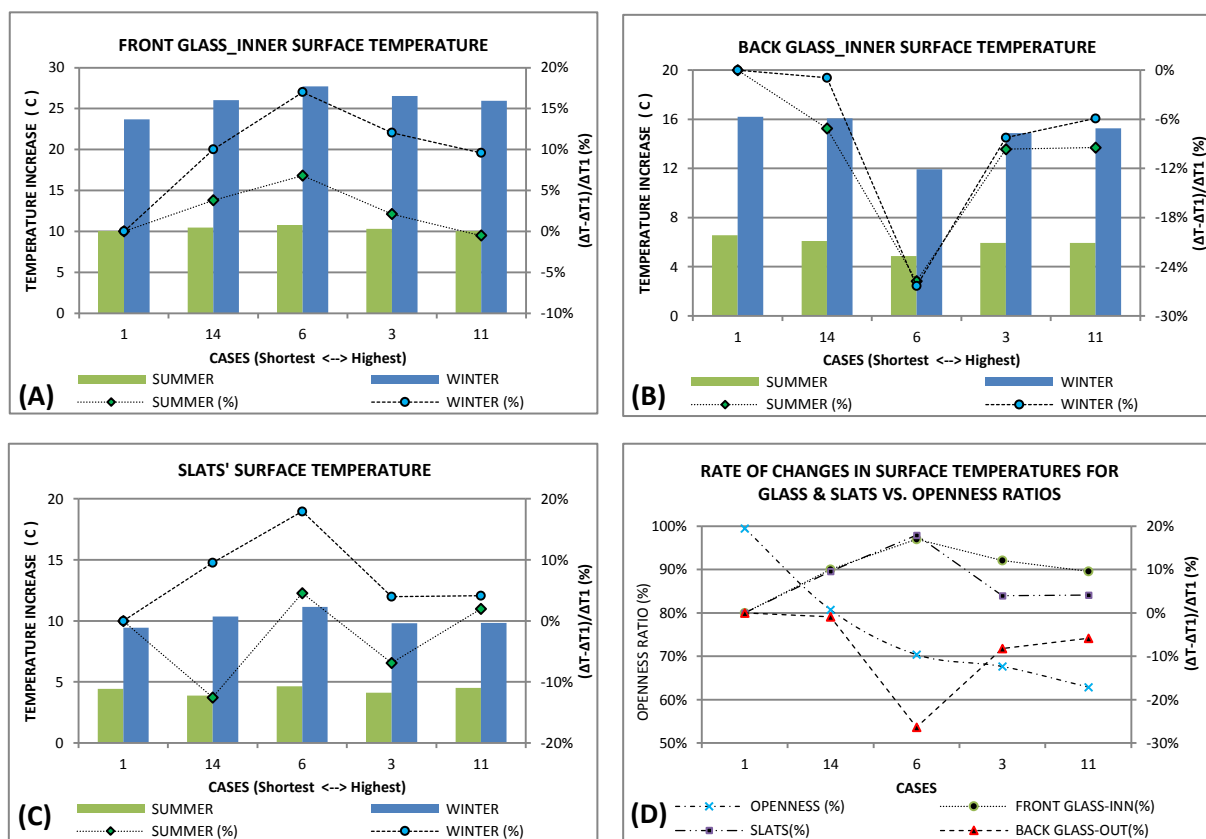


Figure 8.19: Comparison between summer and winter average surface temperature increase of cavity with different integrated slats; slats surfaces had emissivity of 0.2 and diffuse fraction of 0. (A) Front glass_inner surface. (B) Back glass_inner surface. (C) Integrated slats' surface. (D) Comparison for changes of all mentioned surfaces (winter) and openness ratios.

Figure 8.20 presents contours of temperature for the tested cavity. It is obvious that temperature for glass, slats and flowing air of cavity in summer would be higher than those in winter as incoming air in summer (37°C) is much higher than in winter (4°C).

To conclude, both cavity's airflow rate and its surfaces' temperatures would vary based on the detailed design of integrated devices and, also, given boundary conditions. These variations could be large and evident for surface temperature in both winter and summer but small in winter for cavity's ventilation with complicated devices.

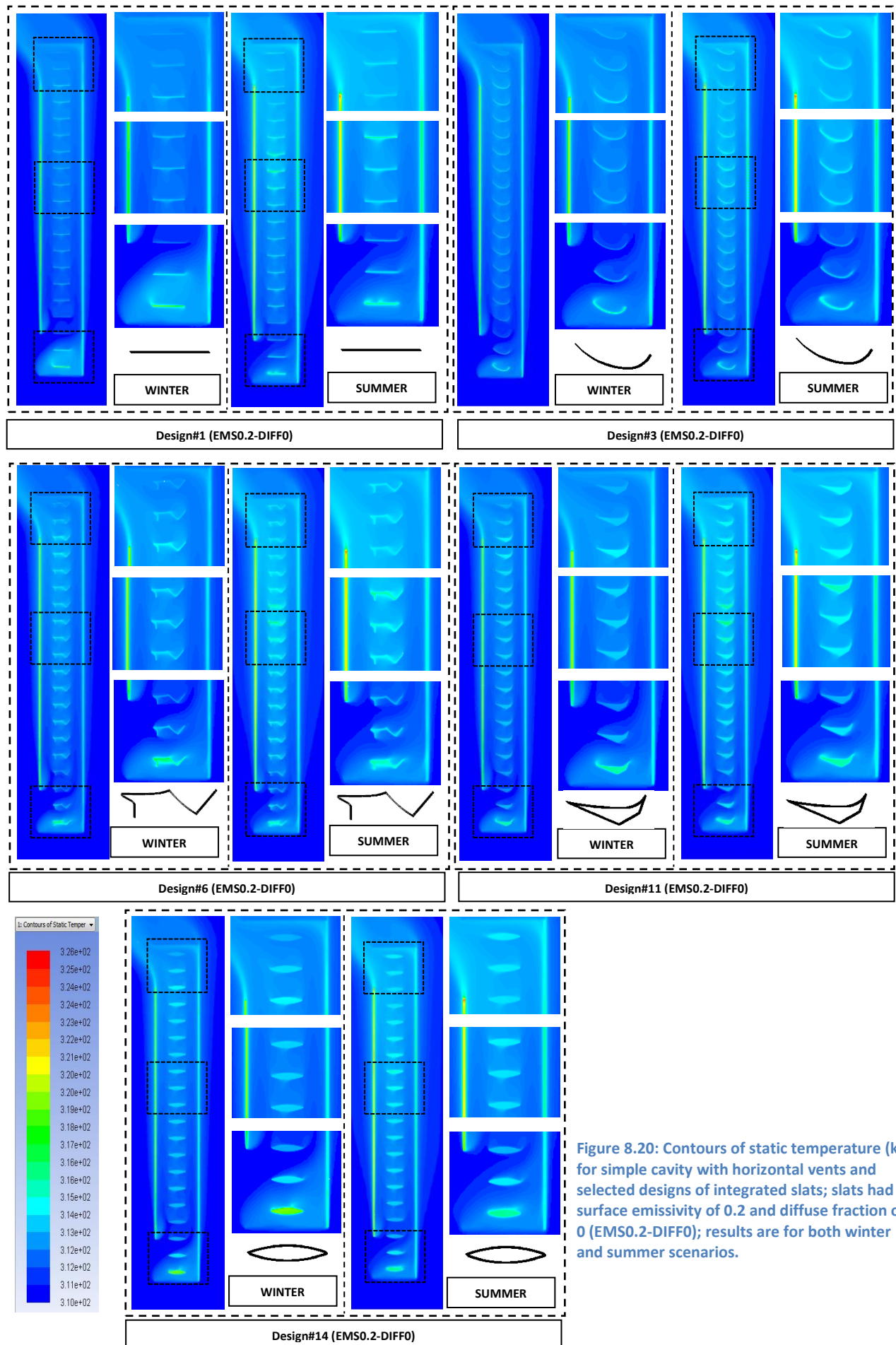


Figure 8.20: Contours of static temperature (k) for simple cavity with horizontal vents and selected designs of integrated slats; slats had surface emissivity of 0.2 and diffuse fraction of 0 (EMS0.2-DIFF0); results are for both winter and summer scenarios.

8.5 Influence of Cavity Vents' Size on the Performance of Different Integrated Slats:

This section shows simulation results for the same cavity structure but with two different sizes for its vents; i.e. 0.1m and 0.5m. Slats had a surface emissivity of 0.9 and a diffuse fraction of 1. In addition, simulations were conducted for summer conditions. The purpose behind this part of work was to assess the influence of flow resistance variations by cavity's vents on the role of different integrated slats (e.g. overall flow rate and surfaces' temperatures). In other words, to determine if variations in performance of given slat (e.g. simple slats) due to changing cavity vents' size could be generalized to other designs of integrated slats.

- **Airflow rate:**

As shown in Figure 8.21-A, cavity flow rate would be higher with larger vents' size due to lower flow resistance at these vents. For instance, cavity's flow rate with design#1 slats and 0.1m-size vents was 0.035m³/s-m compared to 0.073m³/s-m for same slats but 0.5m-size vents, which indicates an increase of 107% in flow rate. However, this rate of increase would vary based on the design of integrated slats as the corresponding increase was about 116% for design#11 slats.

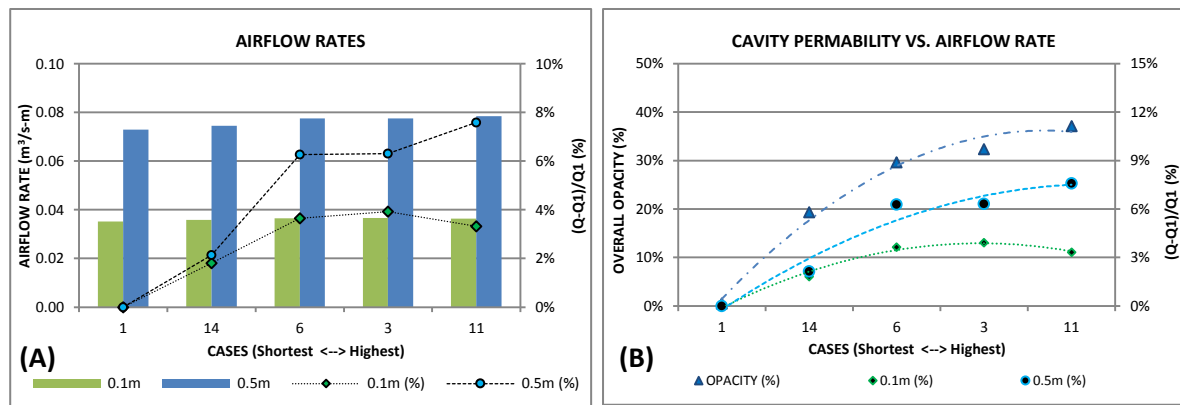


Figure 8.21: (A) Airflow rates changes for simple cavity with horizontal vents had size of either 0.1m or 0.5m; with different designs for integrated slats had emissivity of 0.9 and diffusivity of 1. (B) Changes in cavity's overall opacity and calculated airflow changes.

From another perspective, variations in cavity's flow rate, due to having different integrated slats, would be more evident when the initial flow rate is higher (that is determined by the level of flow resistance at both inlet and outlet; i.e. size of these openings), which is clear as shown in Figure 8.21-B.

Figure 8.22 shows contours of velocity magnitudes (m/s) for the investigated cavity with various integrated slats and for both sizes of cavity's vents. It is clear how reducing vents' size would affect the flow rate and its pattern inside the cavity. In general, incoming air through small vents of the cavity would tend to flow toward the inner skin and along the inner sub-cavity before it turns to outer sub-cavity, where this turn would be around half-height of the cavity. Also, it was found that detailed design of slats would affect airflow direction at the inlet. For example, with design#1, air would mainly flow toward the inner glass unlike the case of design#6 where the front side of lowest slat would redirect part of incoming flow upward through the front sub-cavity.

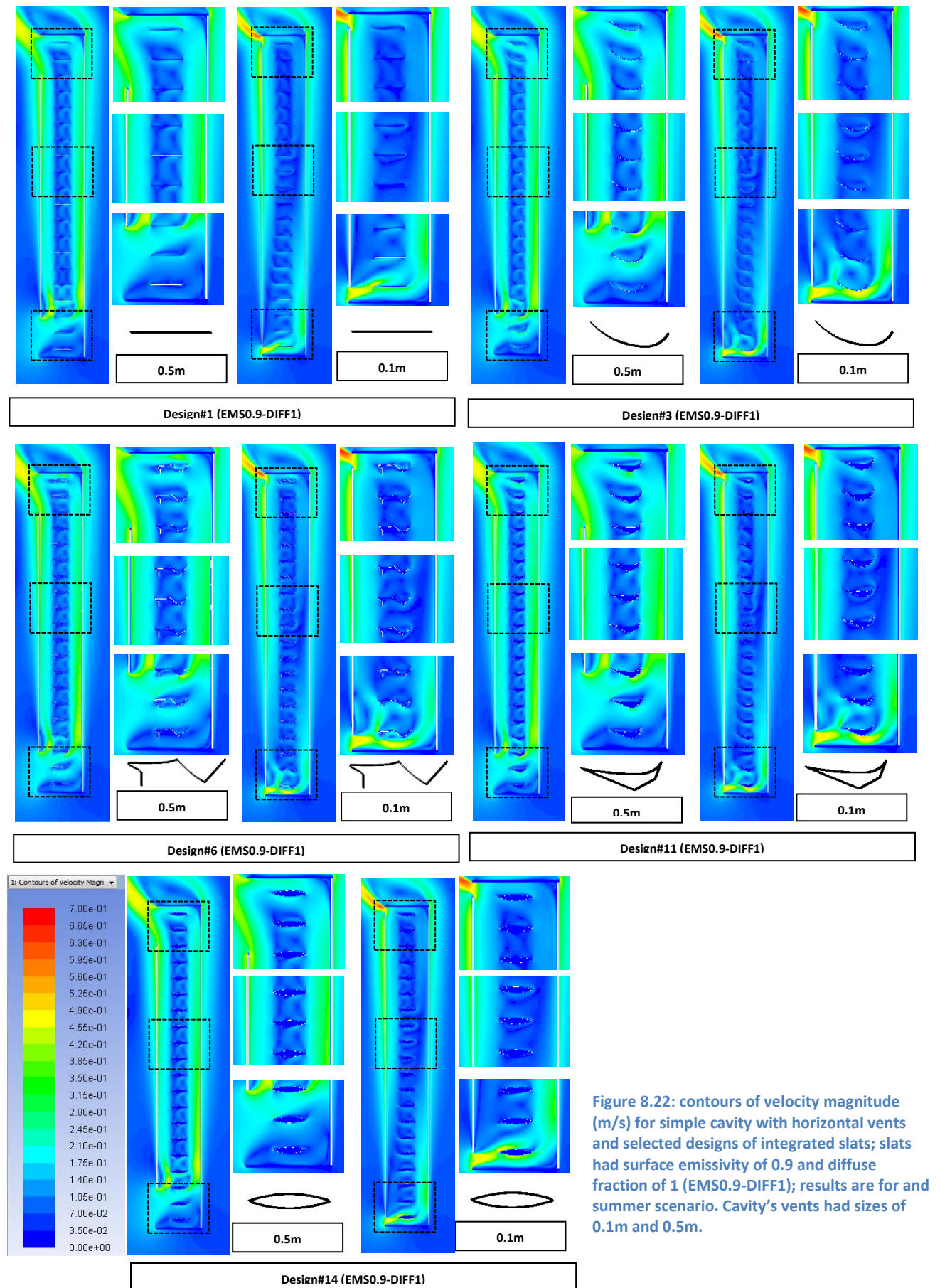


Figure 8.22: contours of velocity magnitude (m/s) for simple cavity with horizontal vents and selected designs of integrated slats; slats had surface emissivity of 0.9 and diffuse fraction of 1 (EMS0.9-DIFF1); results are for and summer scenario. Cavity's vents had sizes of 0.1m and 0.5m.

- **Temperatures:**

Figure 8.23-A shows variations in surface temperature averages for front glass, which were always less than 1% for both sizes of openings. Figure 8.23-B shows these variations could be more evident (up to 10.5%) for back glass, and most importantly, getting larger with larger vents' sizes. This also applies to temperature averages for integrated slats as variations between different designs would be based on the size of vents.

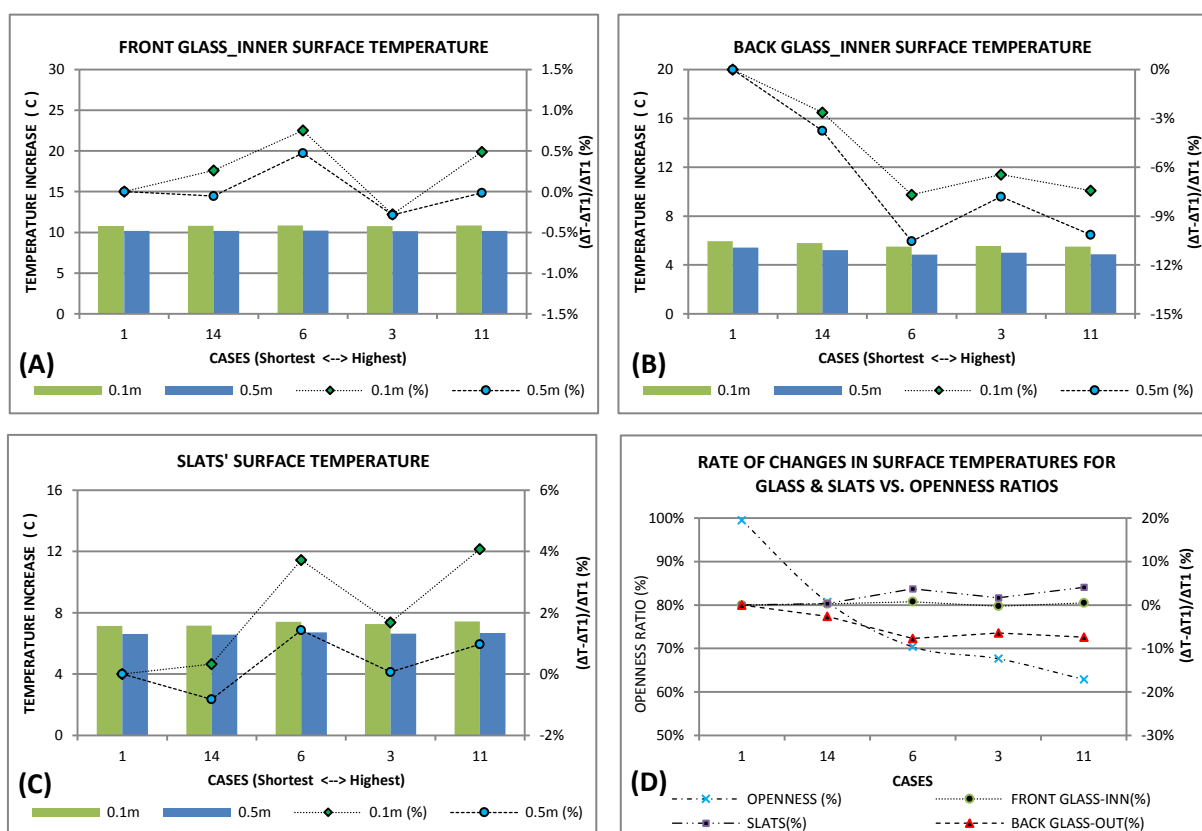


Figure 8.23: Comparison for average surface temperature increase of cavity with both vents' sizes (0.1m & 0.5m), with different integrated slats; slats surfaces had emissivity of 0.9 and diffuse fraction of 1. (A) Front glass_inner surface. (B) Back glass_inner surface. (C) Integrated slats' surface. (D) Comparison for changes of all mentioned surfaces (0.1m) and openness ratios.

As shown in Figure 8.24, air temperature inside the structure would increase with small vents as more heat would be trapped inside the cavity and especially near the top. This would also increase temperature of surfaces and in particular aluminum slats.

To sum up, the performance of integrated slats would depend on other parameters of cavity, e.g. size of openings. Generally, if design#A is performing better (for either flow rate or surface temperature) than design#B with a small opening for the cavity, the preference for design#A would still valid with large openings.

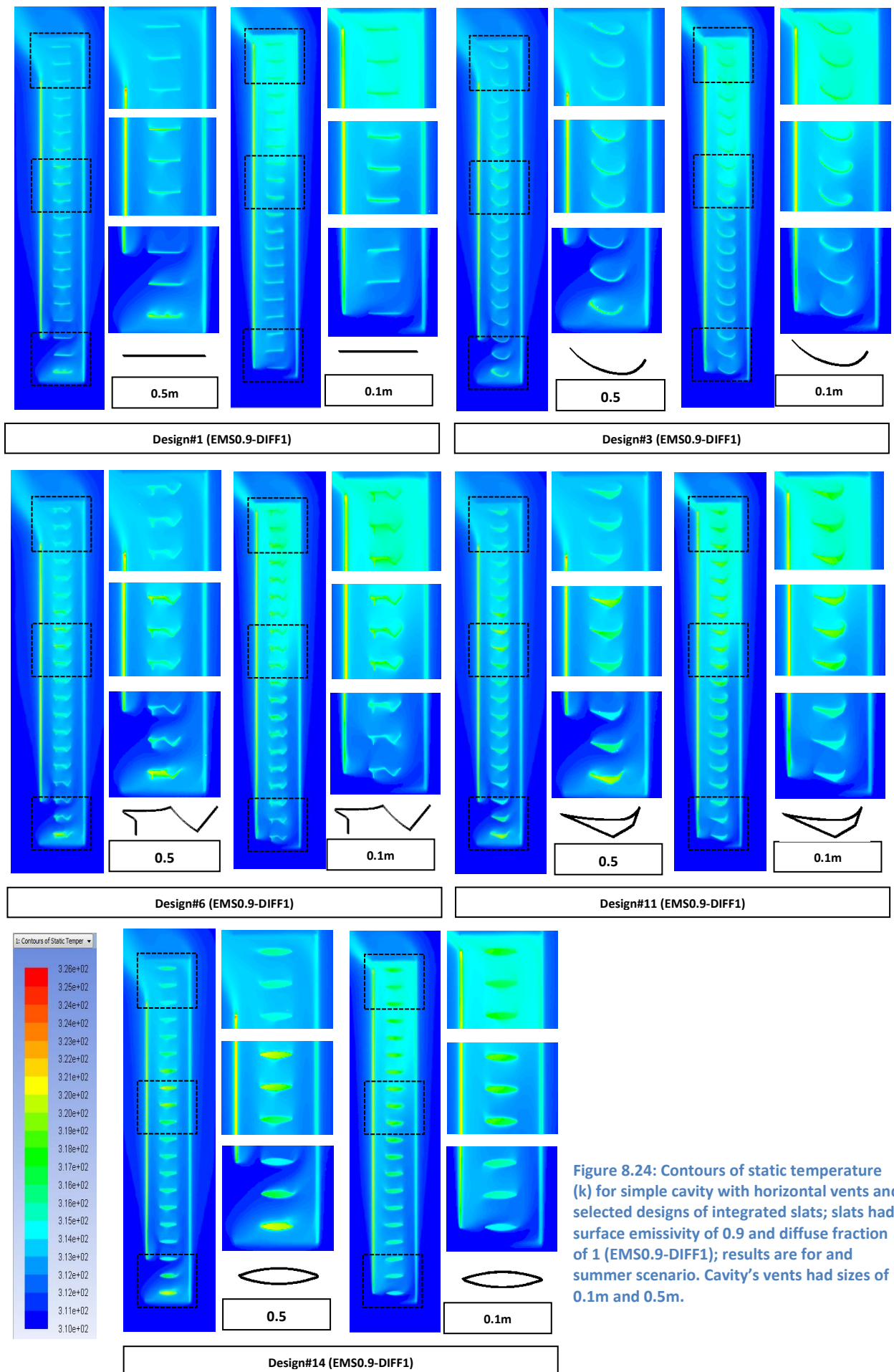


Figure 8.24: Contours of static temperature (k) for simple cavity with horizontal vents and selected designs of integrated slats; slats had surface emissivity of 0.9 and diffuse fraction of 1 (EMS0.9-DIFF1); results are for and summer scenario. Cavity's vents had sizes of 0.1m and 0.5m.

8.6 Influence of Integrated Slats' Position on Their Performance:

This section shows simulation results for the same cavity structure but with different positions for the integrated slats. Three positions were tested: P2 (next to inner skin), P5 (middle of the cavity) and P8 (next to outer skin). Slats had a surface emissivity of 0.9 and a diffuse fraction of 1. And, simulations were conducted for summer conditions. The purpose behind this part of work was to assess the influence of the position of integrated slats on their performance, and see if that influence could significantly be changed with different designs of integrated slats.

- **Airflow rate:**

As shown in Figure 8.25-A, cavity flow rate would vary with the combination of the design of integrated slats and its position inside the cavity; but, the maximum change was always less than 8%.

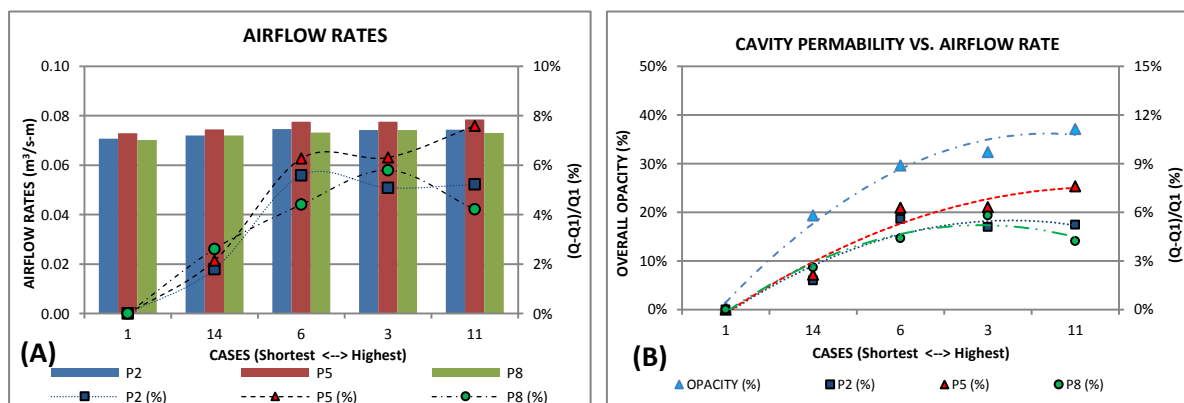
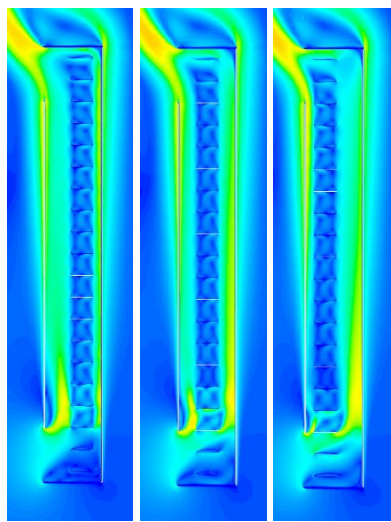


Figure 8.25: (A) Airflow rates changes for simple cavity with horizontal vents, and different integrated slats with different installation positions; slats surfaces had emissivity of 0.9 and diffuse fraction of 1. (B) Changes in cavity's overall opacity and calculated airflow changes.

However, the level of variation in flow rate with changing slats position was found to be related to the effective height of slat-unit; i.e. variations with relatively short slat-unit (e.g. design#14) were small for different positions while these variations became more evident with high slat-unit as shown in

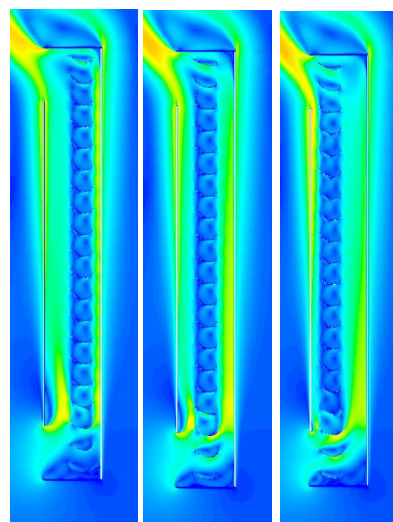
Figure 8.25-B. For example, flow rate with design#14 increased by 1.8% with position P2 and by 2.1% with position P5, however, with design#11 flow rate increased by 5.2% with position P2 and 7.6% with position P5.

Figure 8.26 shows contours of velocity magnitudes (m/s) for the investigated cavity with various integrated slats having different positions inside the cavity. It is clear how the position of these slats could change flow streams and patterns inside the cavity. For instance, with slats being set next to the outer skin (P8), most of the incoming air would flow through inner sub-cavity, especially for its lower half. Also, the position of integrated slats could affect the flow movement in-between adjacent unit, which is still dependent on its design.



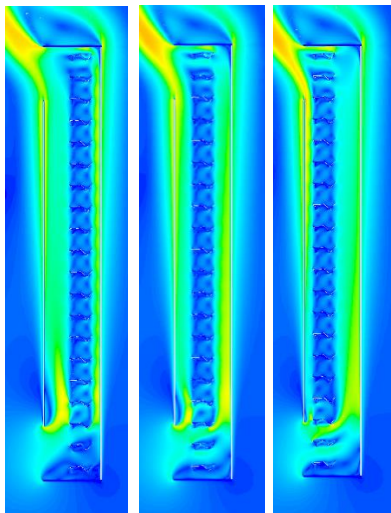
P2 P5 P8

Design#1 (EMS0.9-DIFF1)



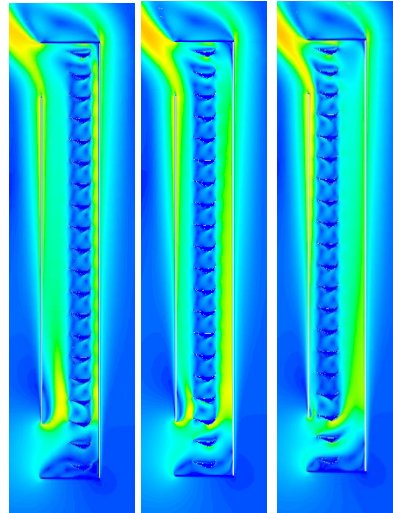
P2 P5 P8

Design#3 (EMS0.9-DIFF1)



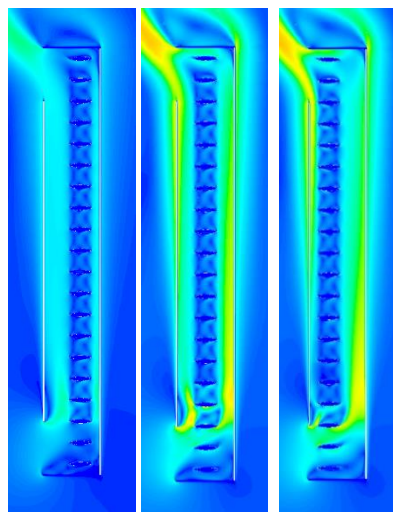
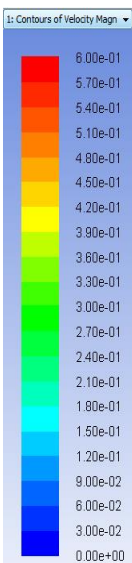
P2 P5 P8

Design#6 (EMS0.9-DIFF1)



P2 P5 P8

Design#11 (EMS0.9-DIFF1)



P2 P5 P8

Design#14 (EMS0.9-DIFF1)

Figure 8.26: contours of velocity magnitude (m/s) for simple cavity with horizontal vents and selected designs of integrated slats; slats had surface emissivity of 0.9 and diffuse fraction of 1 (EMS0.9-DIFF1). Cavity's vents had size of 0.5m. Results are for three different positions for integrated slats and for summer scenario.

- **Temperatures:**

Figure 8.27 shows that changes in surface temperature increase of cavity with different slats were also related to slats positions, and this relation was more evident for surfaces of front glass (Figure 8.27-A) and integrated slats (Figure 8.27-C) but less for back glass (Figure 8.27-B). However, these variations, in changing rates, due to changing position of slats were still small as maximum variation was about 2% for surfaces of integrated slats (design#6).

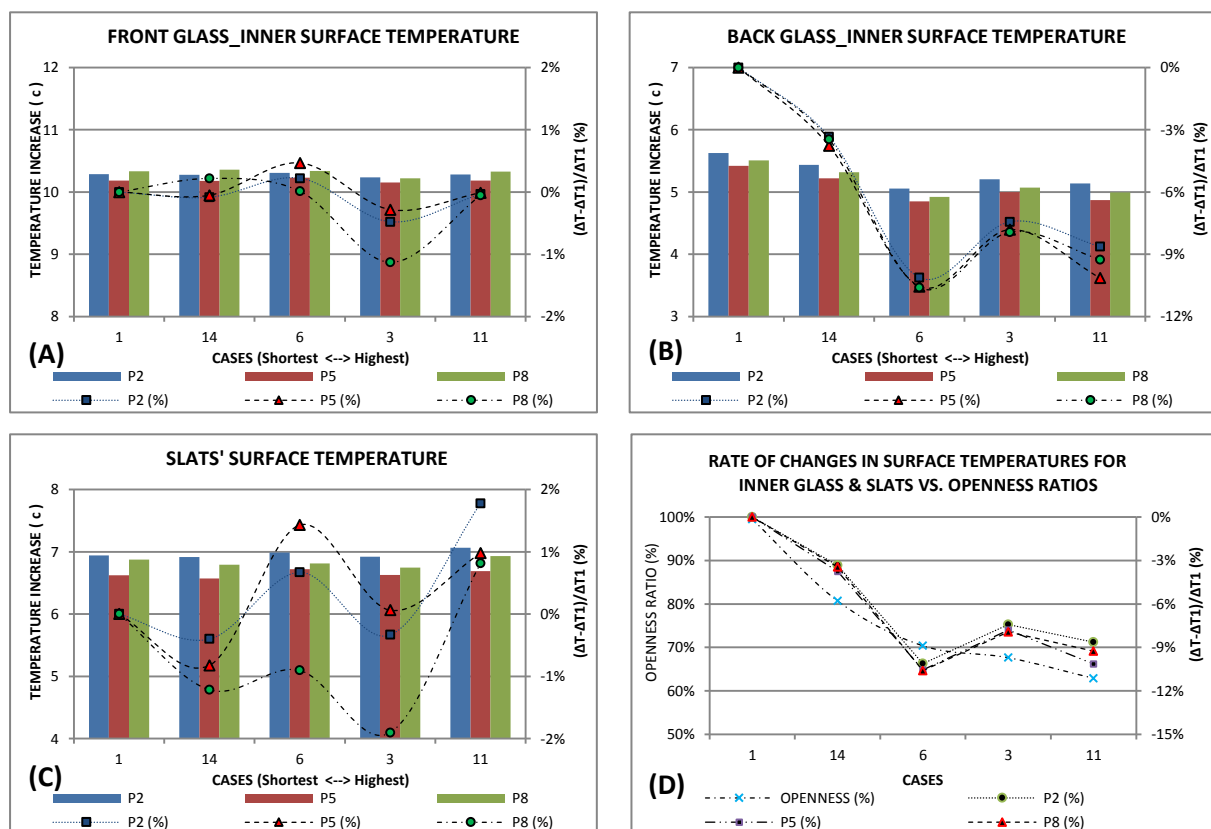


Figure 8.27: Comparison for average surface temperature increase of cavity with different integrated slats and different positions; slats surfaces had emissivity of 0.9 and diffuse fraction of 1. (A) Front glass_inner surface. (B) Back glass_inner surface. (C) Integrated slats' surface. (D) Comparison for changes of temperature of inner glass and openness ratios.

Figure 8.28 shows contours of temperature for the simulated structures. It's clear that temperature stratifications inside the cavity would dramatically be changed in particular for the upper half of cavity with changing the position of integrated slats. For example, the temperature would clearly be influenced

for inner sub-cavity as it would be increased with P2 (slats next to inner glass). This increase seemed to be related to the detailed design of these slats, as well.

To conclude, the position of integrated slats inside the cavity would generally have an impact on its performance. However, this impact would slightly be changed with changing the detailed design for these slats. This applies to both cavity airflow and its surfaces' temperatures.

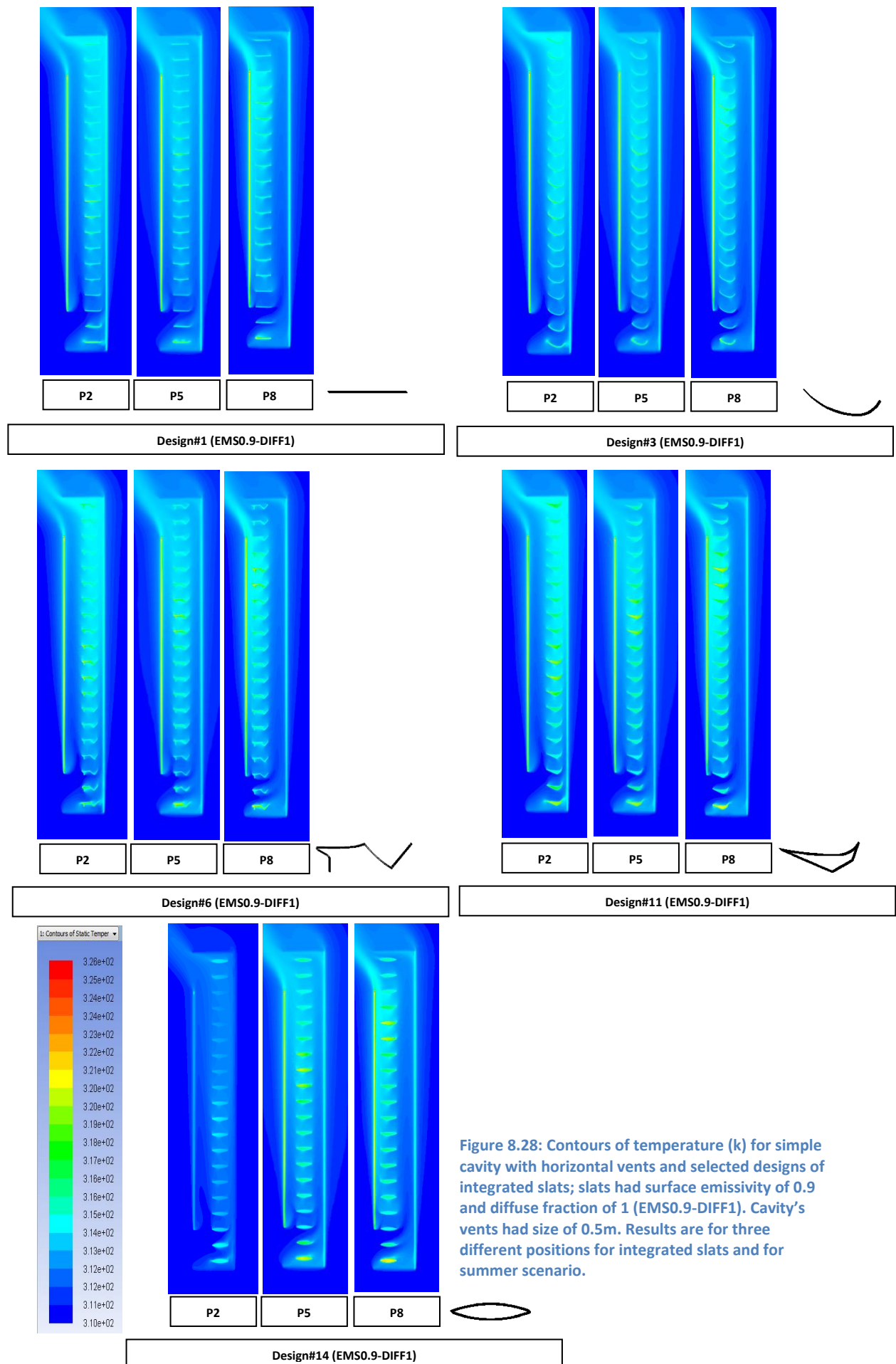


Figure 8.28: Contours of temperature (k) for simple cavity with horizontal vents and selected designs of integrated slats; slats had surface emissivity of 0.9 and diffuse fraction of 1 (EMS0.9-DIFF1). Cavity's vents had size of 0.5m. Results are for three different positions for integrated slats and for summer scenario.

8.7 Influence of Size of Different Integrated Slats on Their Performance:

This section shows simulation results for the same cavity structure with 0.5m width and 0.5m vents size but with different slat sizes. And, simulations were conducted for summer conditions. Integrated slats had a surface emissivity of 0.9 and a diffuse fraction of 1. However, slats had two different sizes: 0.2m (40% of cavity width) and 0.4m (80% of cavity width); and the purpose was to investigate the influence of slats' size on cavity performance with different designs for these slats.

- **Airflow rate:**

Figure 8.29-A presents airflow rates through two cavities integrated with slats that had two different sizes: 0.2m or 0.4m.

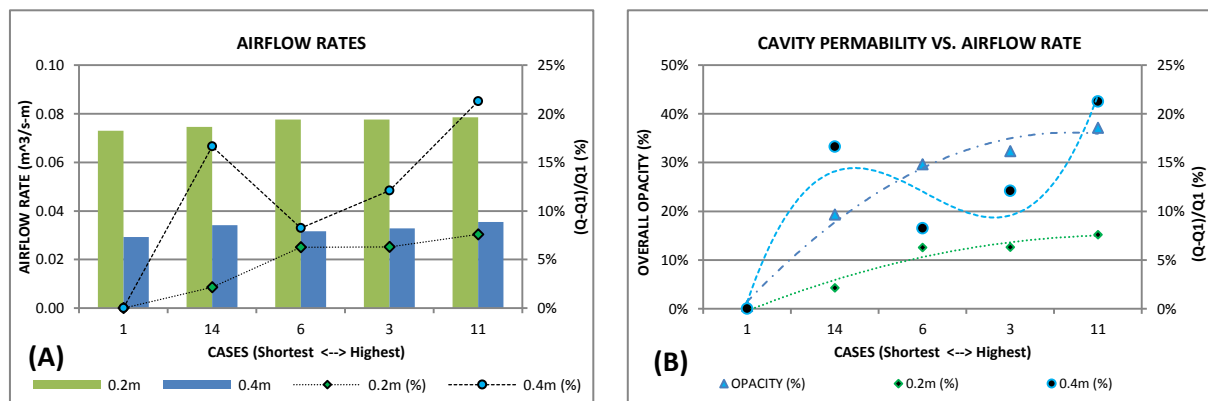


Figure 8.29: (A) Airflow rates changes for simple cavity with horizontal vents, and different integrated slats; slats had two different sizes (0.2m & 0.4m), surface emissivity of 0.9 and diffuse fraction of 1. (B) Changes in cavity's overall opacity and calculated airflow changes.

Generally, as slats size increased, cavity flow rate decreased due to additional flow resistance inside the cavity (less flow permeability with large slats). Also, it shows how the size of slats would affect their influence on flow rate of the cavity, as variations in the role of these slats would depend on their size; i.e., detailed design of a given slat would be more influential with large sizes. For example, the difference in airflow rate between design#1 and

design#14 cases was about 7.6% with slat's size of 0.2m whereas this difference increased to 21.3% with size of 0.4m.

Figure 8.29-B shows relative changes in flow rates for both sizes along with changes in cavity's overall opacity. It is worth mentioning that overall opacity of cavity was almost same with both sizes of slats. This is because of doubling the effective height of slat-unit for each design with increasing its size (effective width along cavity width) from 0.2m to 0.4m while the number of slats was reduced from 20 to 10.

In addition to revealed reduction in cavity's airflow rate with larger integrated slats, Figure 8.30 shows how enlarging these slats would affect the flow patterns inside the cavity, as well as at both inlet and outlet. Moreover, contours of velocity show changes in air movement between the two sub-cavities through the adjacent slats.

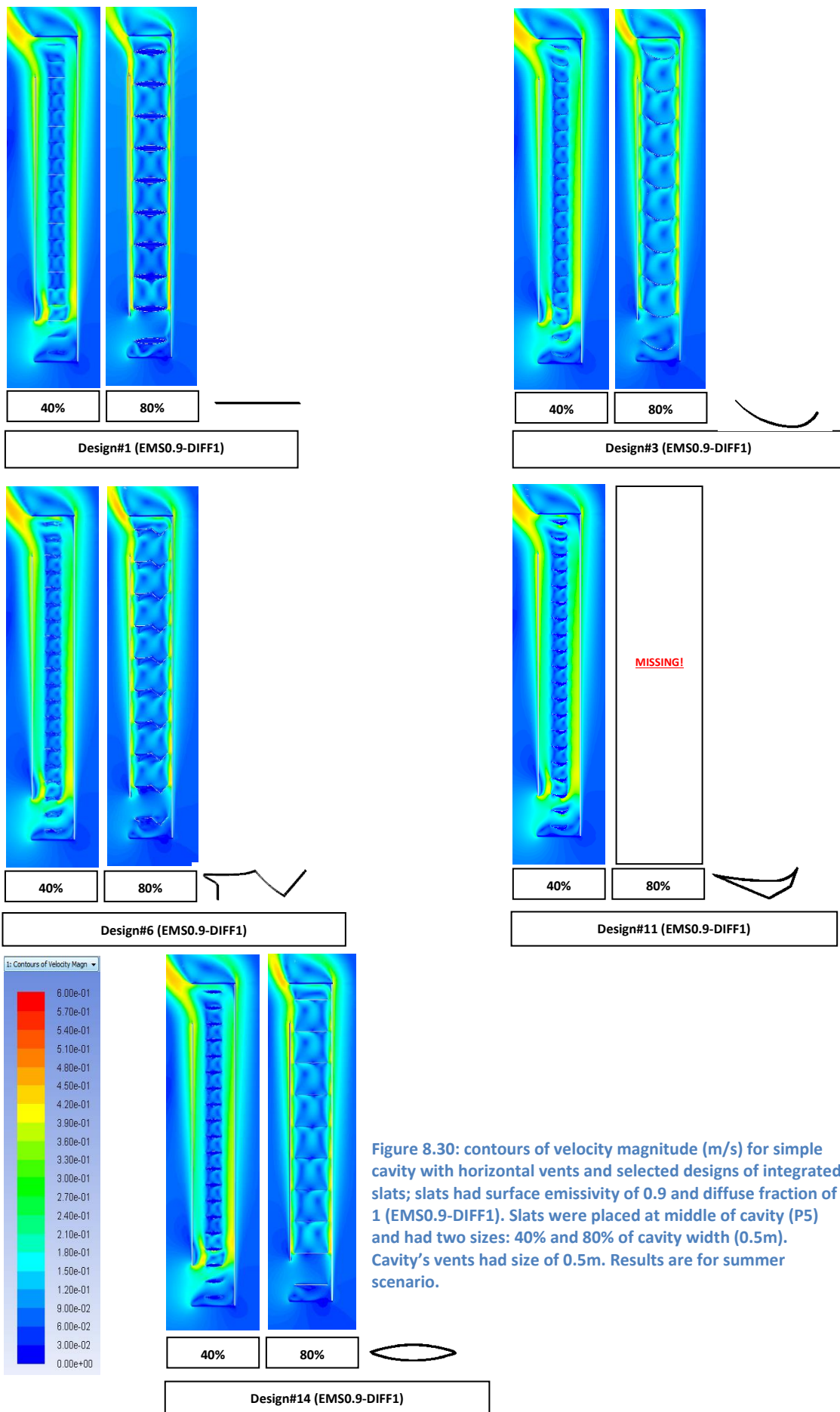


Figure 8.30: contours of velocity magnitude (m/s) for simple cavity with horizontal vents and selected designs of integrated slats; slats had surface emissivity of 0.9 and diffuse fraction of 1 (EMS0.9-DIFF1). Slats were placed at middle of cavity (P5) and had two sizes: 40% and 80% of cavity width (0.5m). Cavity's vents had size of 0.5m. Results are for summer scenario.

- **Temperatures:**

Figure 8.31 shows that temperatures for all surfaces increased with larger integrated slats as cavity's flow rate decreased so less heat was removed from these surfaces. However, size of integrated slat could affect its relative efficiency in terms of cooling down structure's surfaces as well as its surfaces. In other words, detailed design of the slat would determine to what extent varying its size could affect its efficiency in comparison to others. Furthermore, this change in efficiency for same design could vary with respect to the targeted surface. For instance and in reference to desing#1, desing#6 with either size led to a change of only about 0.5% for front-glass temperature (negligible change between the two different size) compared to an increase of 1.4% with 0.2m but drop of 3% with 0.4m for its surface temperature.

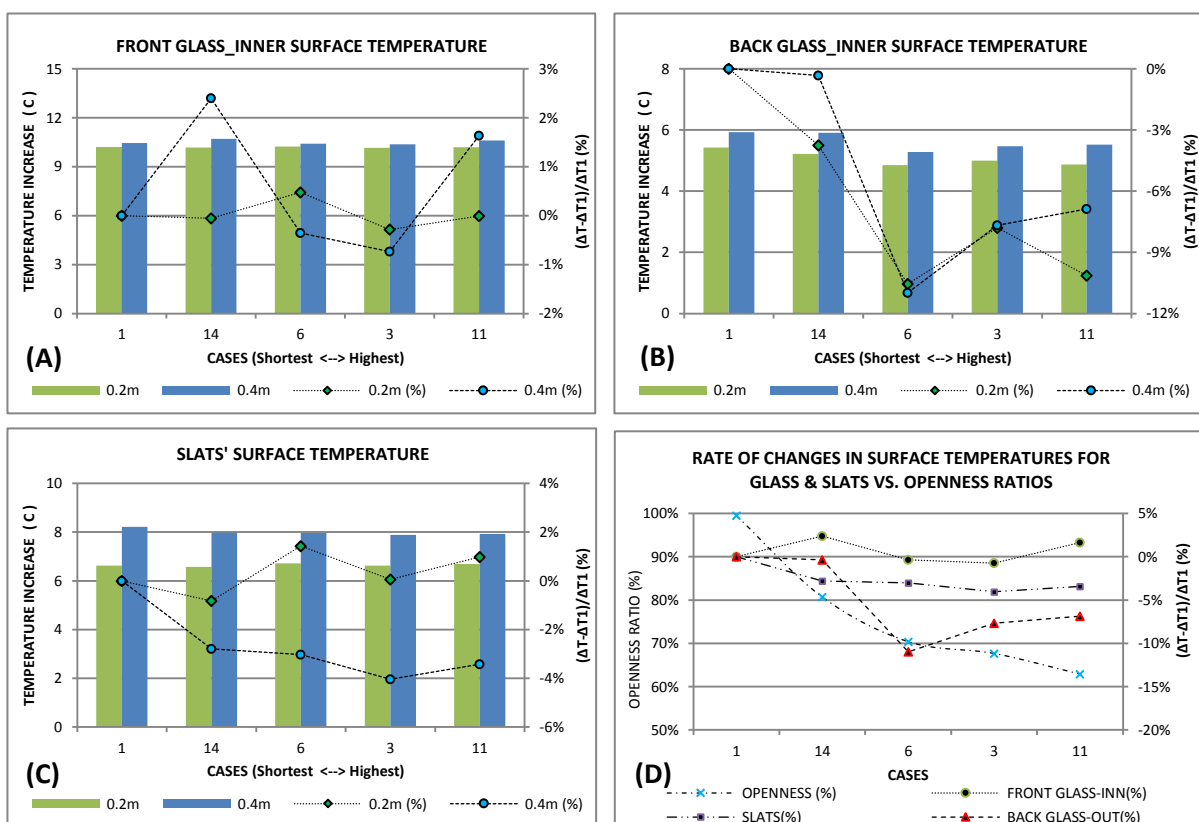


Figure 8.31: Comparison for average surface temperature increase of cavity with different integrated slats; slats had two different sizes (0.2m & 0.4m), surface emissivity of 0.9 and diffuse fraction of 1. (A) Front glass_inner surface. (B) Back glass_inner surface. (C) Integrated slats' surface. (D) Comparison for changes of surfaces' temperatures with 0.4m-integrated slats and changes of openness ratios.

Because of reducing air ventilation through the cavity, both air temperature and surfaces' temperatures would be increased noticeably as shown in Figure 8.32. This is clear at top of cavity and for both outer glass pane and front sides of integrated slats.

To conclude, the size of slat-unit is a vital parameter that would affect the level of influence that its detailed design would have on both airflow and thermal performance.

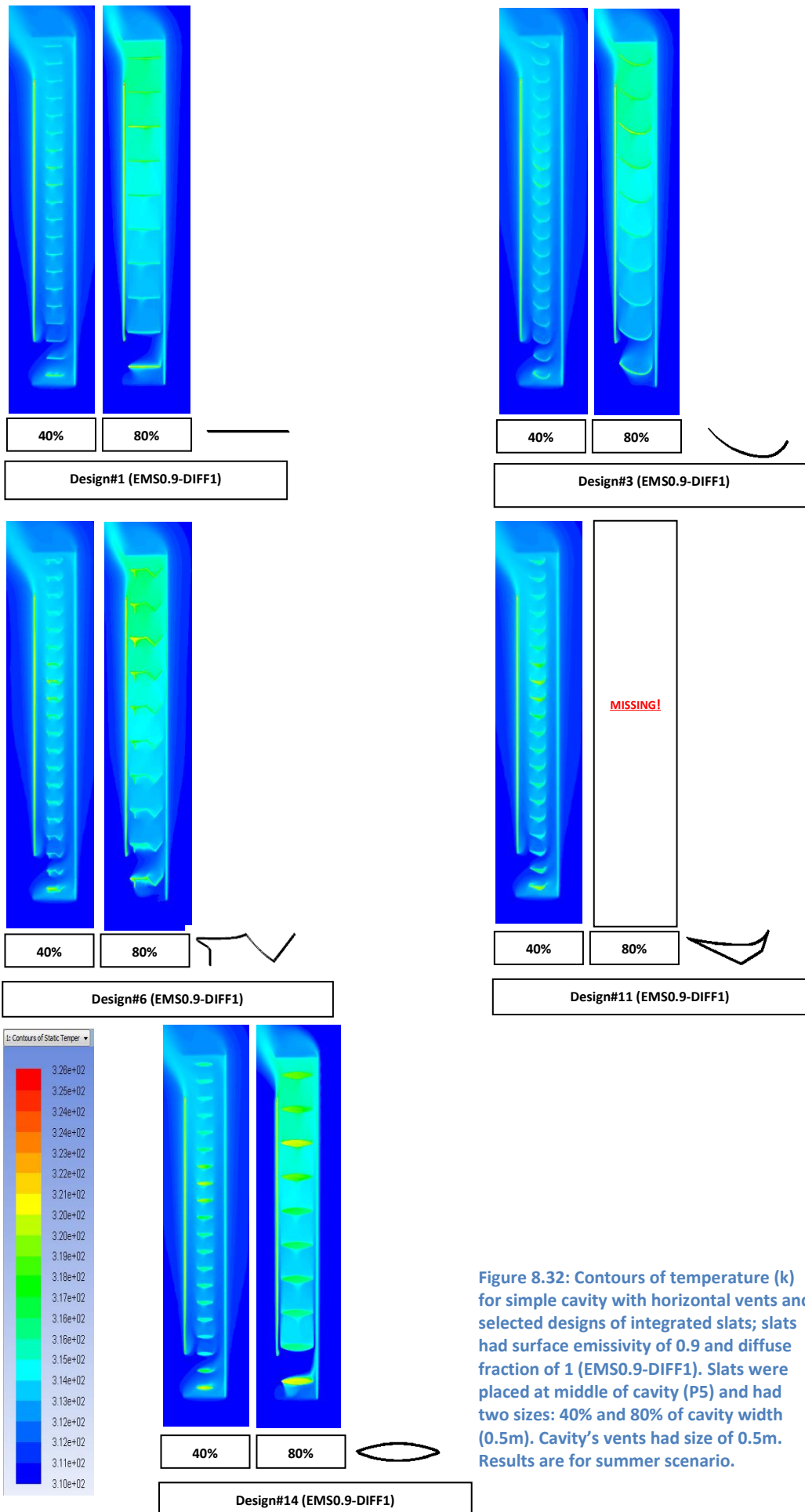


Figure 8.32: Contours of temperature (k) for simple cavity with horizontal vents and selected designs of integrated slats; slats had surface emissivity of 0.9 and diffuse fraction of 1 (EMS0.9-DIFF1). Slats were placed at middle of cavity (P5) and had two sizes: 40% and 80% of cavity width (0.5m). Cavity's vents had size of 0.5m. Results are for summer scenario.

8.8 Influence of Aspect Ratio (Height-To-Width) of Cavity:

The aim of this work was to investigate the importance of height-to-width (H/W) ratio of the cavity (with horizontal vents and different integrated slats) to its performance: airflow rate and surface temperatures. Furthermore, it also aimed to reveal how different designs of integrated slats would perform with different ratios of H/W. In other words, to see if difference in performance between design#A and design#B would vary as H/W of the cavity varies; especially that flow is expected to be mixed near the top of cavity with high H/W ratio; thus flow could pass in-between the two sub-cavities (separated by set of integrated slats) where detailed design of these slats could influence the flow patterns differently.

Cavity had a constant height of 4.0m while its width varied from 0.1m to 0.5m, which resulted in H/W ratios of 40 to 8, respectively. Cavity's vents size was always equal to cavity's width. Integrated slats were placed at mid cavity, and relative width of slat was fixed to 40% of cavity width (e.g. 0.2m-wide slat for 0.5m-wide cavity; and 0.04m-wide slat for 0.1m-wide cavity). The study was carried out for both summer and winter, to include both high (81°) and low (38°) angles of incident radiations. Three different designs of integrated slats were investigated for summer while just two designs for winter.

- **Airflow rate:**

Results under this section are for airflow rate for both summer and winter conditions:

- Summer Conditions:

Figure 8.33 shows airflow results for the examined cavity. As shown in Figure 8.33-A, cavity flow rate increased as cavity width increased due to the corresponding reduction in flow resistance. And, this applied to all designs of integrated slats.

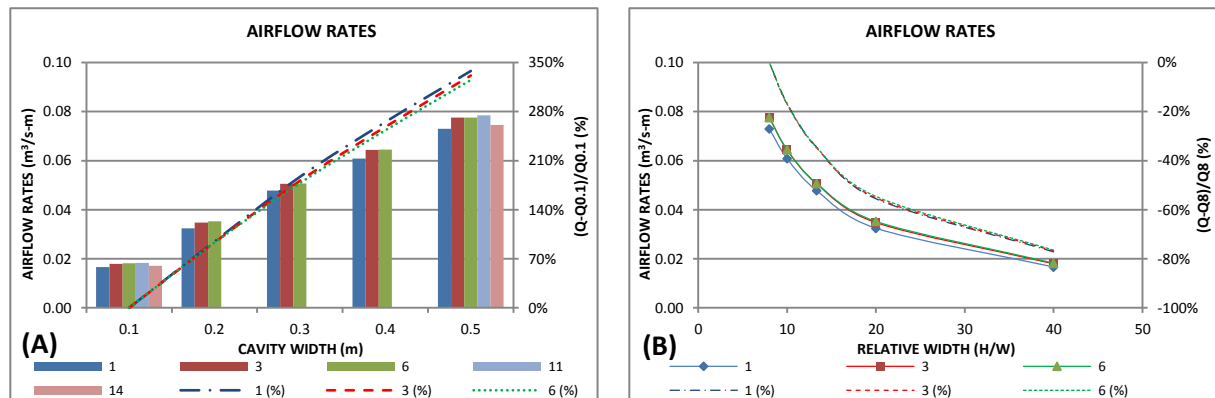


Figure 8.33: Airflow rates changes for simple cavity with horizontal vents and different height-to-width ratios (H/W), under Summer conditions. Integrated slats had width of 40% of cavity width (e.g. 0.12m for cavity width of 0.3m), surface emissivity of 0.9 and diffuse fraction of 1. (A) Results and relative changes plotted against cavity's width (0.1m-0.5m). (B) Results and relative changes plotted against H/W ratios (8-40).

Moreover, Figure 8.33-B shows same results are plotted against height-to-width (H/W) ratios of the cavity. Airflow rate would decrease as H/W increases (cavity's width decreases). However, the rate of decrease was more significant for small H/W ratios (i.e. 8-20); for instance, as H/W ratio increased from 8 to 20, flow rate decreased by about 55% while it just decreased by further 22% when H/W ratio increased from 20 to 40. This is expected as cavity width matters until it reaches a certain size after which it becomes less important to flow resistance by cavity's walls.

In addition, whereas airflow rate for the same width cavity (e.g. 0.1m) was influenced by the detailed design of integrated slats (e.g. flow rate was $0.0167\text{m}^3/\text{s-m}$ with design#1 compared to $0.0180\text{m}^3/\text{s-m}$ with design#3, all for 0.1m-wide cavity), the detailed design was found to have negligible

influence on relative changes in airflow rates with H/W ratios for either design. For example, airflow rate for cavity with design#1 decreased by about 77.2% when cavity's H/W ratio increased from 8 to 40 while it decreased by about 76.8% with design#3 and for the same change in cavity's H/W ratio (8 to 40).

Table 8.1 presents revealed polynomial equations that correlate cavity flow rate with its characteristics (i.e. H/W) and for different designs of integrated slats. For the three designs, it is shown that coefficients of corresponding variables, e.g. $(H/W)^2$, are almost equal. Also, constants are also close. Therefore, any of these correlations could be valid to represent the relationship whatever the design of integrated slats is.

Table 8.1: Revealed relationships between cavity's airflow rate and its characteristics (Height/Width=H/W), and for different integrated slats.

CAVITY'S AIRFLOW RATE (m ² /s-m)			
INTEGRATED SLAT'S DESIGN	(H/W) values	POLYNOMIAL RELATIONSHIP	R ²
#1	8 to 40	$Q = 8e-05 (H/W)^2 - 0.0056 (H/W) + 0.1106$	0.9923
#3	8 to 40	$Q = 9e-05 (H/W)^2 - 0.006 (H/W) + 0.1171$	0.9908
#6	8 to 40	$Q = 9e-05 (H/W)^2 - 0.0059 (H/W) + 0.1164$	0.9903

Figure 8.34 shows contours of velocity magnitudes for both 0.1m- and 0.5-m cavities and with different designs of integrated slats. It is shown how reducing the cavity width (increasing H/W ratio) could affect the flow patterns inside the cavity and, also, change the air distribution between the two sub-cavities. For example, airflow stream for 0.5m-wide cavity (with design#1 of integrated slats) was mainly passing through the back sub-cavity (e.g. at mid height) however this flow was almost divided equally between the two sub-cavities (and even tend to be more for front sub-cavity) when total width was

set to 0.1m instead of 0.5m. Also, this change was also clearer with design#11 integrated slats. This indicated the influence of detailed design of integrated slats on airflow distribution inside the cavity. And how this influence could significantly vary with narrow cavities (cavities with high H/W ratios).

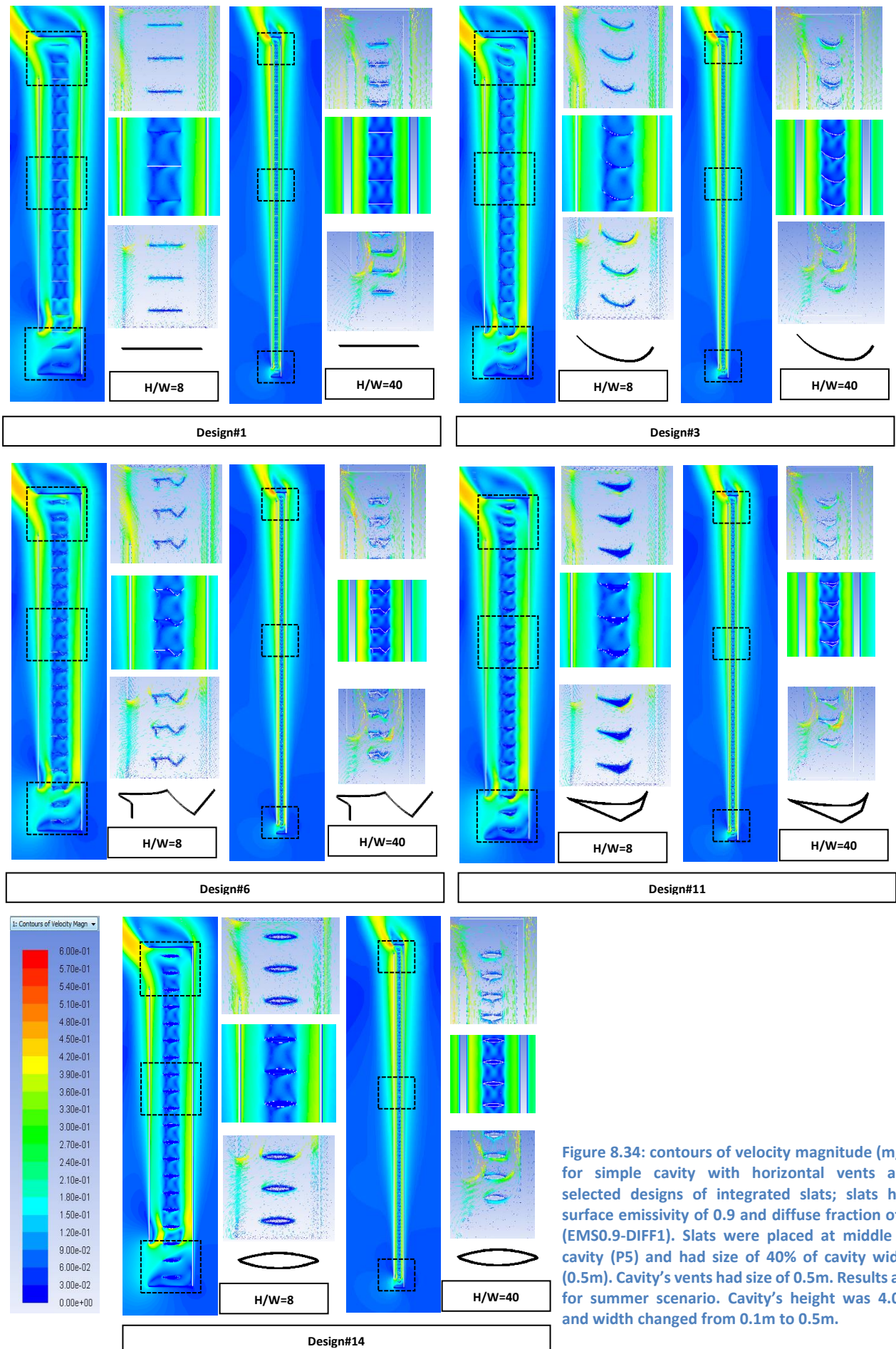


Figure 8.34: contours of velocity magnitude (m/s) for simple cavity with horizontal vents and selected designs of integrated slats; slats had surface emissivity of 0.9 and diffuse fraction of 1 (EMS0.9-DIFF1). Slats were placed at middle of cavity (P5) and had size of 40% of cavity width (0.5m). Cavity's vents had size of 0.5m. Results are for summer scenario. Cavity's height was 4.0m and width changed from 0.1m to 0.5m.

- Winter Conditions:

Similar to summer study, the following section presents findings for the same structure but under winter conditions. As shown in Figure 8.35, and similar to summer's findings, cavity's airflow rate would increase as its width increases (H/W decreases). Magnitudes of airflow rate were different and higher for winter compared to summer (i.e. with design#1 and H/W=8, airflow rate was $0.0245\text{m}^3/\text{s-m}$ in winter compared to $0.0167\text{m}^3/\text{s-m}$ in summer; an increase of 46.7%). But, relative changes in airflow rate (with increasing H/W ratio) were close for both summer and winter. For instance, as H/W increased from 8 to 40, changes in airflow rate with design#1 were 77.2% and 76% for summer and winter conditions, respectively.

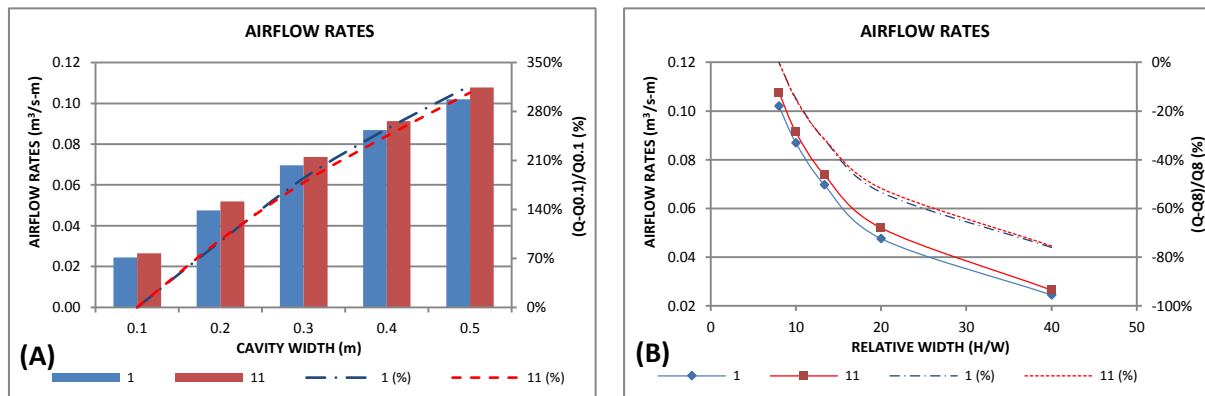


Figure 8.35: Airflow rates changes for simple cavity with horizontal vents and different height-to-width ratios (H/W), under winter conditions. Integrated slats had width of 40% of cavity width (e.g. 0.12m for cavity width of 0.3m), surface emissivity of 0.9 and diffuse fraction of 1. (A) Results and relative changes plotted against cavity's width (0.1m-0.5m). (B) Results and relative changes plotted against H/W ratios (8-40).

Finally, whereas flow rate with design#11 was always higher than that with design#1, relative changes in flow rate due to changing H/W ratios were close and similar to summer conclusion. Table 8.2 shows mathematical relationships that correlate cavity flow rate with its H/W aspect ratio for both design#1 and 11 under winter conditions. Similar to correlations of summer

airflow, coefficients for different corresponding variables of winter's correlations are also close.

Table 8.2: Revealed relationships between cavity's airflow rate and its characteristics (Height/Width=H/W), and for different integrated slats; under winter conditions.

CAVITY'S AIRFLOW RATE (m ² /s-m): WINTER CONDITIONS			
DESIGN#	(H/W) values	POLYNOMIAL RELATIONSHIP	R ²
1	8 to 40	$Q = 9E-05 (H/W)^2 - 0.0068 (H/W) + 0.145$	0.9991
11	8 to 40	$Q = 0.0001 (H/W)^2 - 0.0076 (H/W) + 0.1586$	0.9937

Figure 8.36 gives an insight into how changing H/W ratio of the cavity would affect its flow streams in winter. It's shown that with high H/W ratio (narrower cavity), airflow became more dense and was almost equal for both sub-cavities; that is similar to summer conclusion. However, there was a little difference between having either design of integrated slats unlike summer scenario.

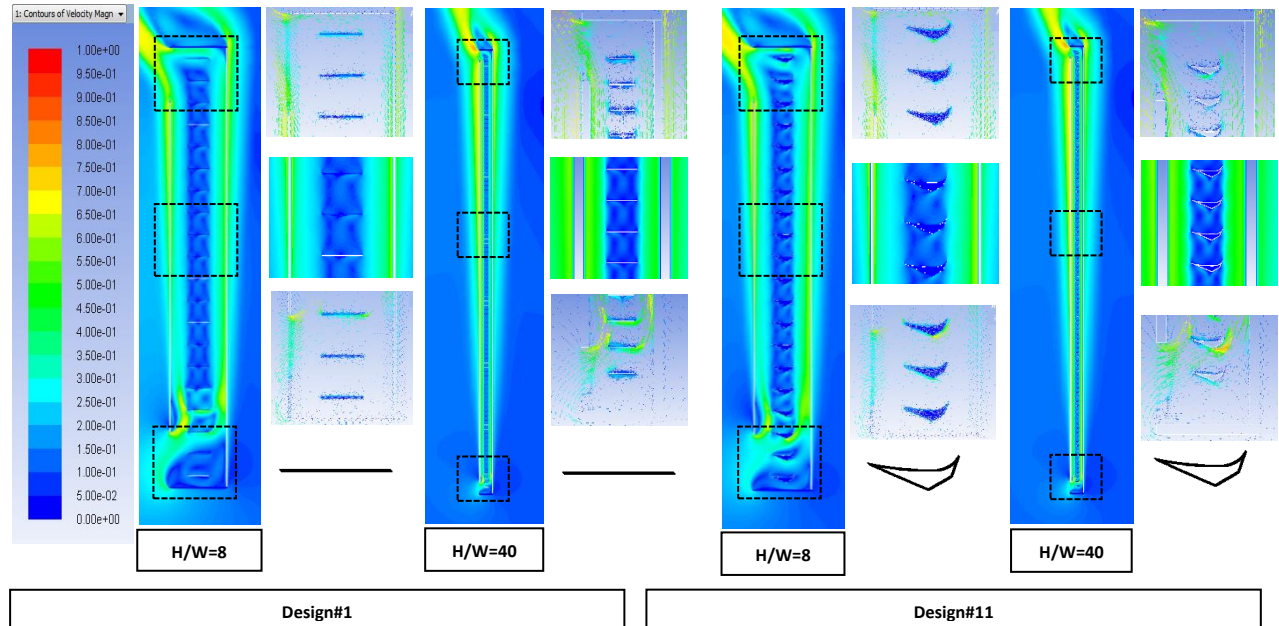


Figure 8.36: contours of velocity magnitude (m/s) for simple cavity with horizontal vents and selected designs of integrated slats; slats had surface emissivity of 0.2 and diffuse fraction of 0 (EMS0.9-DIFF1). Slats were placed at middle of cavity (P5) and had size of 40% of cavity width (0.5m). Cavity's vents had size of 0.5m. Results are for winter scenario. Cavity's height was 4.0m and width changed from 0.1m to 0.5m.

- **Temperatures:**

Results under this section are for surface temperatures of the cavity, for both summer and winter conditions:

- **Summer Conditions:**

Figure 8.37 shows average surface temperature increase of various elements. As shown in Figure 8.37-A, increase in surface temperature of front glass slightly dropped (less than 1%) as H/W ratio increased from 8 to 13; however, it rose again for higher ratios of H/W. The maximum change was about 9.5% with design#6 and H/W ratio of 40 (narrowest cavity, 0.1m). Furthermore, corresponding changes for design#1 & design#3 were close as 9.3% and 9.4%, respectively.

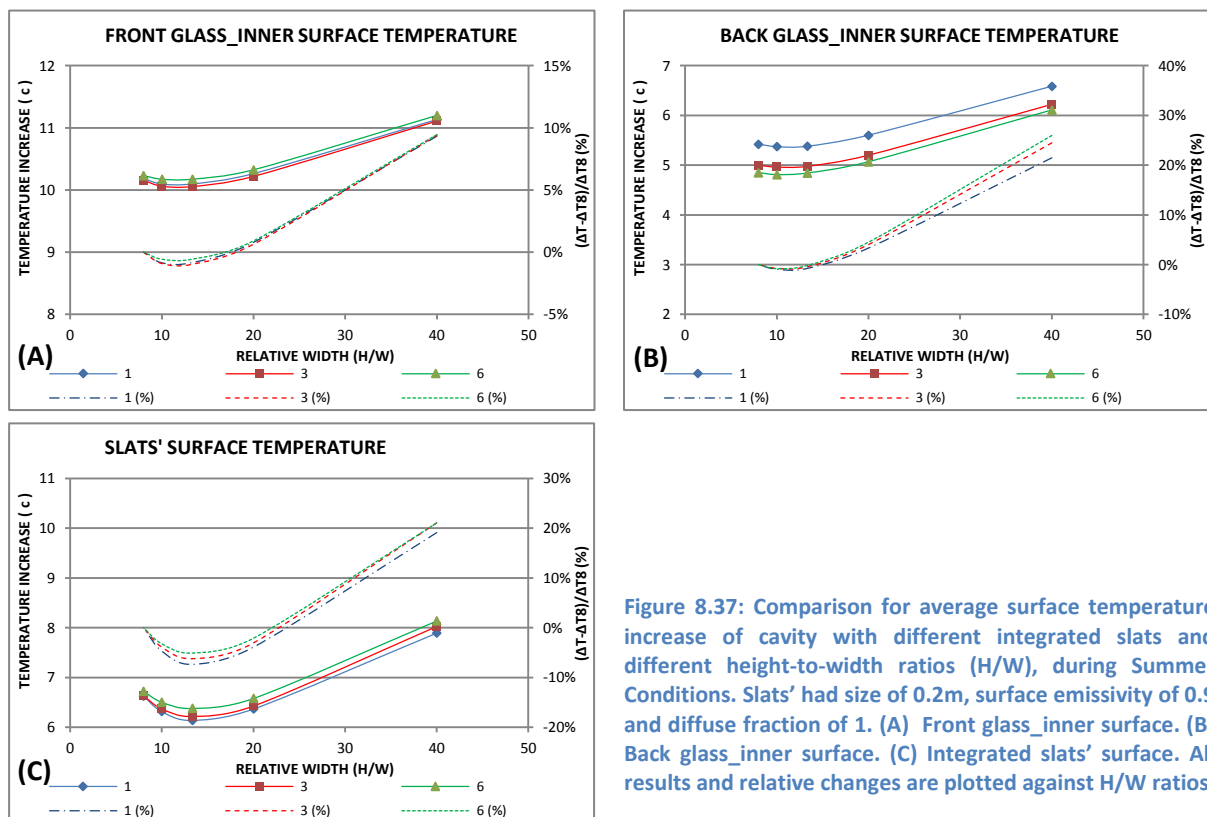


Figure 8.37: Comparison for average surface temperature increase of cavity with different integrated slats and different height-to-width ratios (H/W), during Summer Conditions. Slats' had size of 0.2m, surface emissivity of 0.9 and diffuse fraction of 1. (A) Front glass_inner surface. (B) Back glass_inner surface. (C) Integrated slats' surface. All results and relative changes are plotted against H/W ratios.

The shown increase in surface temperature was expected as cavity's flow rate was significantly reduced as presented before. But, regarding the

slight drop in temperature for small H/W up to 13, this drop could not be linked to changes in cavity's flow rate as results for flow rate showed a decrease as well. However, it is still possible because of changing flow patterns inside the cavity in a way that slightly helped to cooling down surfaces.

Now, Figure 8.37-B shows average surface temperature increase of back glass, along with relative changes. It is clear that temperature increase of back glass would perform similarly to that of the front glass. However, revealed changes in temperature increase of back glass for H/W ratios up to 13 were small and close to those of front glass (less than 1%, also). On the other hand, changes for larger H/W ratios ($13 < H/W < 40$) was found to be more evident than those of front glass; as maximum change for back glass was 26% (for H/W=40 and design#6) compared to just 9.5% for front glass (also, H/W=40 and design#6). Moreover, variations in maximum changes (for temperature increase) due to having different designs of integrated slats were more evident for back glass compared to front glass; e.g. maximum changes with design#1 & #6 were 21.5% and 26% (respectively) for back glass, compared to 9.3% and 9.5% (respectively) for front glass. This is expected as the distinguishment between different designs of integrated slats becomes more clear when it comes to heat controlled or transmitted to opposite side of the solar source (back glass).

Finally, Figure 8.37-C presents corresponding results but for surface temperature of integrated slat itself. Again, average surface temperature increase of integrated slats was found to have similar trends to those for glass panes, but with different magnitudes and changing rates. For instance, the

minimum average increase was found to be 6.14°C with design#1 and H//W=13, which was 7.4% lower than that of the same design but H/W=8. On the other hand, maximum increase was 8.13°C for design#6 and H/W=40 that was 21.1% higher than that of the same design and H/W=8.

Table 8.3 shows mathematical correlations between H/W ratio of cavity and temperature increase of its surfaces. All equations for glass surfaces were found to be with second degree and these for slats surfaces were with third degree. Moreover, equations seem to be typical except minor variations in constants, which reflect the variations in magnitudes as discussed before.

Table 8.3: Revealed relationships between surface temperature increase of cavity and its characteristics (Height/Width=H/W), and for desing#1 & desing#11 of integrated slats. (A) Front Glass (B) Back Glass & (C) Integrated Slats.

(A) FRONT GLASS: SURFACE TEMPERATURE INCREASE (°C)			
INTEGRATED SLAT'S DESIGN	(H/W) values	POLYNOMIAL RELATIONSHIP	R ²
#1	8 to 40	$\Delta T = 0.0012 (H/W)^2 - 0.0249 (H/W) + 10.263$	0.9925
#3	8 to 40	$\Delta T = 0.0012 (H/W)^2 - 0.0284 (H/W) + 10.255$	0.9922
#6	8 to 40	$\Delta T = 0.0011 (H/W)^2 - 0.0236 (H/W) + 10.317$	0.9963
(B) BACK GLASS: SURFACE TEMPERATURE INCREASE (°C)			
INTEGRATED SLAT'S DESIGN	(H/W) values	POLYNOMIAL RELATIONSHIP	R ²
#1	8 to 40	$\Delta T = 0.0011 (H/W)^2 - 0.0156 (H/W) + 5.438$	0.9953
#3	8 to 40	$\Delta T = 0.0011 (H/W)^2 - 0.0141 (H/W) + 5.0082$	0.9968
#6	8 to 40	$\Delta T = 0.0011 (H/W)^2 - 0.0116 (H/W) + 4.8404$	0.9971
(C) INTEGRATED SLATS: SURFACE TEMPERATURE INCREASE (°C)			
INTEGRATED SLAT'S DESIGN	(H/W) values	POLYNOMIAL RELATIONSHIP	R ²
#1	8 to 40	$\Delta T = 0.0032 (H/W)^2 - 0.1085 (H/W) + 7.1599$	0.9729
#3	8 to 40	$\Delta T = 0.0031 (H/W)^2 - 0.1029 (H/W) + 7.1476$	0.9837
#6	8 to 40	$\Delta T = 0.0029 (H/W)^2 - 0.0914 (H/W) + 7.1797$	0.9882

Figure 8.38 shows changes in both air and surfaces' temperatures for the investigated cavities with various designs of integrated slats, in summer. As discussed earlier, reducing H/W would lead to an increase in both

temperatures due to revealed reductions in cavity's ventilation. Also, it clearly shows the development in thermal stratification inside and along the height of the cavity, and with different designs of integrated slats.

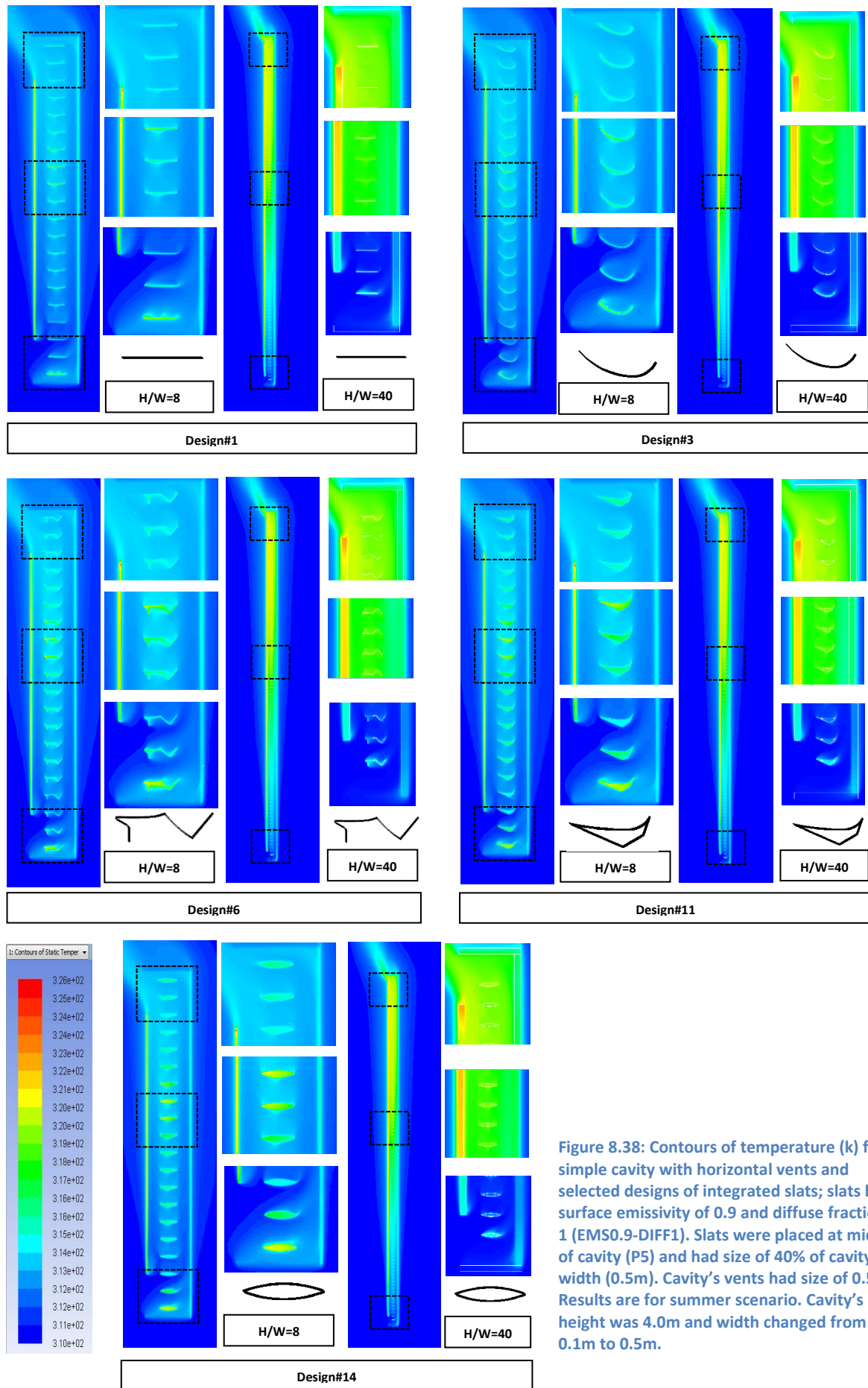


Figure 8.38: Contours of temperature (k) for simple cavity with horizontal vents and selected designs of integrated slats; slats had surface emissivity of 0.9 and diffuse fraction of 1 (EMS0.9-DIFF1). Slats were placed at middle of cavity (P5) and had size of 40% of cavity width (0.5m). Cavity's vents had size of 0.5m. Results are for summer scenario. Cavity's height was 4.0m and width changed from 0.1m to 0.5m.

- Winter Conditions:

Figure 8.39 shows results for surface temperature increase of the cavity under winter conditions.

As shown in Figure 8.39-A, increase in surface temperature of front glass of cavity with either design (#1 or #11) in winter had similar trend to those by other designs in summer (as shown before in Figure 8.37-A) but still with higher magnitude values and with slightly smooth transition at small H/W ratios. Furthermore, the relative change in surface temperature with H/W ratio seemed to be independent of the detailed design of integrated slats. In other words, maximum changes in surface temperature of front glass with both designs were close (5.6% with design#1 compared to 5.5% with design#11); which is similar to summer where maximum changes for the three examined designs were also close (9.3%-9.5%).

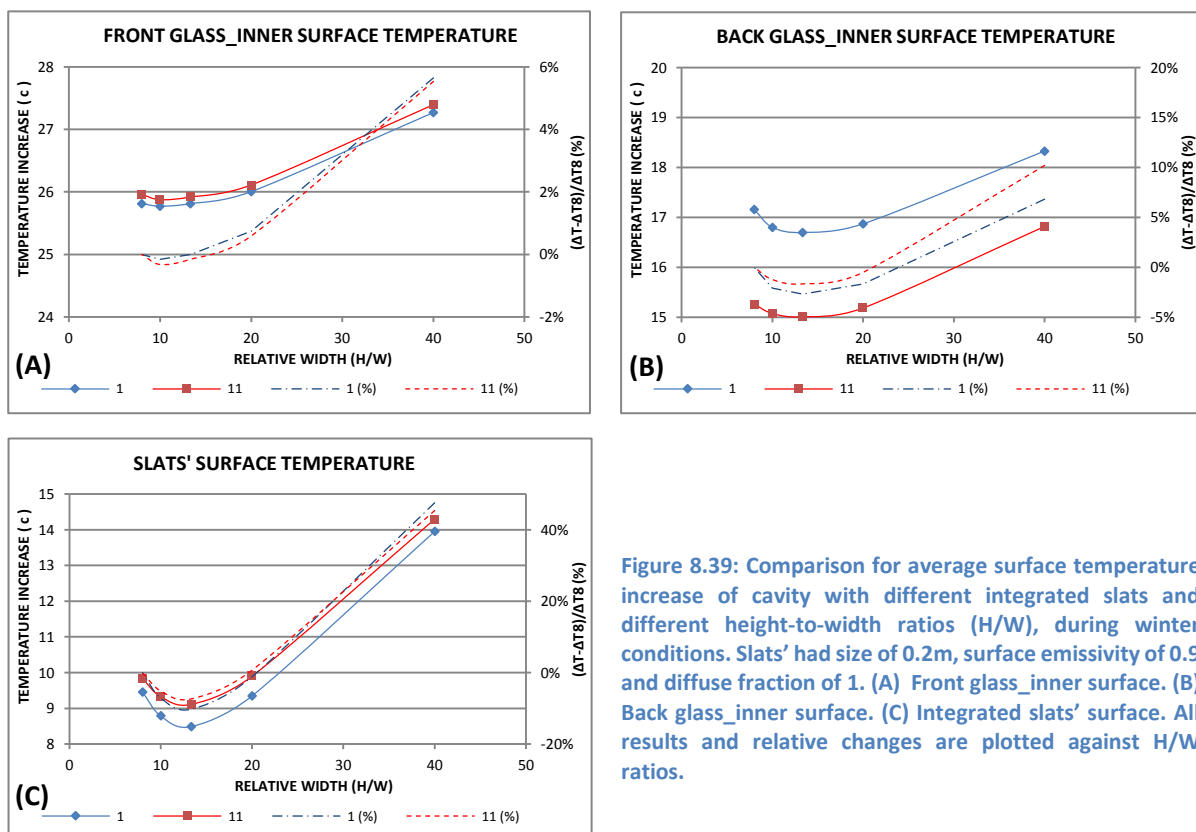


Figure 8.39: Comparison for average surface temperature increase of cavity with different integrated slats and different height-to-width ratios (H/W), during winter conditions. Slats' had size of 0.2m, surface emissivity of 0.9 and diffuse fraction of 1. (A) Front glass_inner surface. (B) Back glass_inner surface. (C) Integrated slats' surface. All results and relative changes are plotted against H/W ratios.

As presented in Figure 8.39-B, increase in surface temperature of back glass was always lower than that for front glass due to the shading effect associated with integrated slats. However, the difference in magnitudes of temperature increase for back glass (with different designs of integrated slats) was noticeably larger than that for the front glass. For example, the difference for back glass (between design#1 and design#11) was about 1.5°C-1.9°C but it was just 0.1°C-0.15°C for the front glass. This was mainly a result of the low incident angle of winter's sun, and the fact that openness ratio for design#1 was higher than that for design#11 (due to the difference in effective height of slat-units). It is worth mentioning that this difference for back glass would be lower in summer (0.5°C-1.3°C) as sun's angle would be much higher (81°) thus detailed design would be less important than winter.

Also, the influence of cavity's characteristics (i.e. H/W) on its thermal performance was more evident in summer than that in winter (e.g. with design#1, the maximum change in surface temperature of back glass was 21.5% in summer compared to 6.8% in winter).

Figure 8.39-C presents surface temperature of integrated slat itself. Generally, the influence of H/W ratio on the performance of these elements was more evident in winter compared to summer. For instance, as H/W increased from 8 to 40, surface temperature increased by 19.1% in summer (Figure 8.37-C) compared to 47.5% in winter (Figure 8.39-C).

Table 8.4 shows revealed equations that correlate H/W aspect ratio of the cavity with temperature increase of its surfaces.

Table 8.4: Revealed relationships between surface temperature increase of cavity and its characteristics (Height/Width=H/W), and for desing#1 & desing#11 of integrated slats. (A) Front Glass (B) Back Glass & (C) Integrated Slats.

(A) FRONT GLASS: SURFACE TEMPERATURE INCREASE (°C)			
INTEGRATED SLAT'S DESIGN	(H/W) values	POLYNOMIAL RELATIONSHIP	R ²
#1	8 to 40	$\Delta T = 0.0015 (H/W)^2 - 0.0246 (H/W) + 25.891$	0.9992
#11	8 to 40	$\Delta T = 0.0016 (H/W)^2 - 0.0304 (H/W) + 26.06$	0.9976

(B) BACK GLASS: SURFACE TEMPERATURE INCREASE (°C)			
INTEGRATED SLAT'S DESIGN	(H/W) values	POLYNOMIAL RELATIONSHIP	R ²
#1	8 to 40	$\Delta T = 0.0031 (H/W)^2 - 0.1057 (H/W) + 17.668$	0.9705
#11	8 to 40	$\Delta T = 0.0028 (H/W)^2 - 0.0828 (H/W) + 15.677$	0.9941

(C) INTEGRATED SLATS: SURFACE TEMPERATURE INCREASE (°C)			
INTEGRATED SLAT'S DESIGN	(H/W) values	POLYNOMIAL RELATIONSHIP	R ²
#1	8 to 40	$\Delta T = 0.0078 (H/W)^2 - 0.222 (H/W) + 10.423$	0.9837
#11	8 to 40	$\Delta T = 0.0069 (H/W)^2 - 0.1855 (H/W) + 10.632$	0.9892

Figure 8.40 presents changes in air and surfaces' temperature for the cavity, in winter, as its H/W ratio was increased. Again, temperature would be increased and with both designs of integrated slats (#1 & #11). This is obvious at the top of cavity.

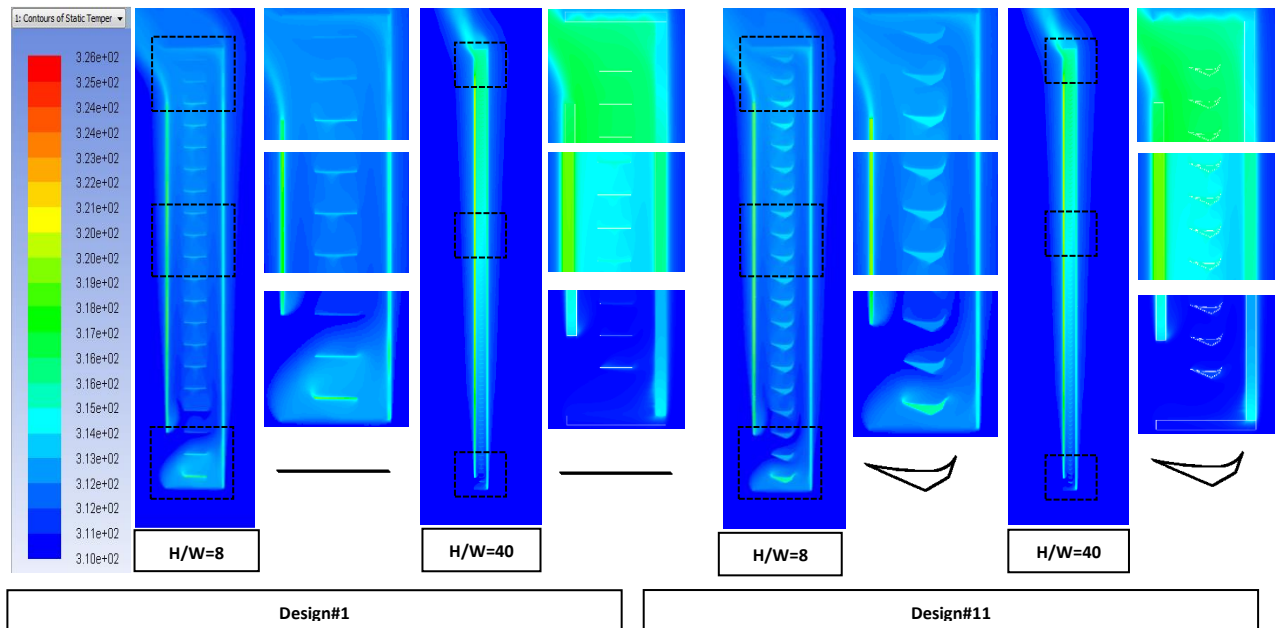


Figure 8.40: Contours of temperature (k) for simple cavity with horizontal vents and selected designs of integrated slats; slats had surface emissivity of 0.2 and diffuse fraction of 0 (EMS0.9-DIFF1). Slats were placed at middle of cavity (P5) and had size of 40% of cavity width (0.5m). Cavity's vents had size of 0.5m. Results are for winter scenario. Cavity's height was 4.0m and width changed from 0.1m to 0.5m.

- **Conclusion:**

To conclude, it was found that geometrical characteristics of the cavity (i.e. H/W) would dramatically affect both airflow and thermal performance of the system in summer. This influence could reach 77% for airflow and up to 26% for surface temperature depends on element's position, as it was more significant for back glass. Moreover, the study showed that detailed design of integrated slats could still influence both cavity's airflow and temperature of surfaces; which could reach 9.5% for airflow and 12% for surface temperature of back glass, Figure 8.41; all depends on the design of these slats. However, level of influence by the detailed design of slats are still controlled by the geometrical characteristics of the cavity (i.e. H/W). For instance, the difference in cavity flow rate between design#1 and design#6 was found to be 9.5% for $H/W=40$ compared to 6.3% for $H/W=8$.

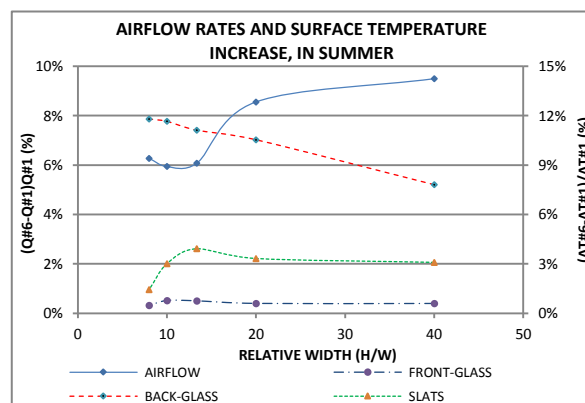


Figure 8.41: Relationship between the influence of design#1 and design#6 for both cavity's airflow rates and averages of temperature increase of surfaces, in summer.

In winter, the effect of H/W ratio on airflow rate would be similar and close to that in summer, as the maximum change could reach 76%. However, this effect would be different when it comes to surface temperature. As discussed earlier, H/W ratio would have a smaller effect on glass surface

temperature in winter compared to summer as maximum change for back glass was about 10% (with design#1) in winter compared to 21.5% (for same design#1) in summer. But, corresponding influence on surface temperature of integrated slats would be significantly higher in winter (i.e. 47.7% in winter and 21.1% in summer). For winter, detailed design of integrated slats would also influence both cavity's flow rate and surface temperature with almost close variations to those for summer. Also, the impact of H/W ratio on level of influence by this detailed design in winter was found to be close to those in summer; Figure 8.42 gives more details.

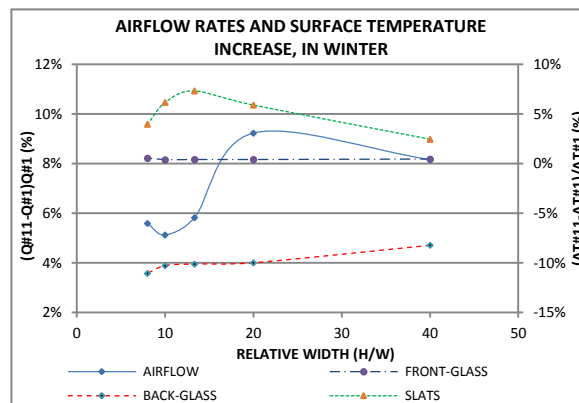


Figure 8.42: Relationship between the influence of design#1 and design#11 for both cavity's airflow rates and averages of temperature increase of surfaces, in winter.

8.9 Combined Influence of Glass Transmittance and Height-to-Width Aspect Ratio:

After investigating the influence of Height-to-Width (H/W) ratio on the performance of the cavity, this part of work further aimed to explore the influence of glass transmittance on that performance. In other words, to find out if varying glass transmittance would change the influence of H/W ratio on the cavity's performance. And, also, how this combination (different glass transmittances and H/W ratios) would affect the performance of integrated slats.

Cavity, with same characteristics to that used in the previous section, was considered here. Work was done for summer conditions. Two different slats were modelled: design#1 and design#11.

- **Airflow rate:**

Figure 8.43 shows airflow results for the examined cavity. Results are presented for both cases: design#1 and design#11. In Figure 8.43-A, results for different widths of the cavity are plotted against glass transmittance. It is clear that flow rate increased as cavity's width increased, which is also shown in Figure 8.43-B (results plotted against cavity width). Also, it was found that flow rate for the cavity with design#11 integrated slats was always higher than that with design#1 for same cavity width, due to a higher surface temperature of integrated slats as discussed earlier.

However, it was found that changes in cavity's airflow rate due to varying glass transmittance were negligible especially with design#1 (simple slats). For example, maximum change in flow rate with design#1 was 1.5%

(between $t=0.5$ & $t=0.9$; and for $w=0.5\text{m}$) while it was 3.4% (between $t=0.5$ & $t=0.9$; and for $w=0.4\text{m}$). That was because of the balanced changes in surface temperatures for both glass panes and integrated slats. For example, as glass transmittance increases, glass temperature would decrease (due to less absorption) but the temperature of integrated slats would increase (receive more heat), and vice versa; as discussed later. Finally, Figure 8.43-C shows same results plotted against H/W ratios. It is clear that changes in cavity's flow rate were more evident between small ratios (8-13) as discussed in the previous section. As said before, flow rates for a cavity with design#11 were always higher than those with design#1, however, relative changes in flow rates (with H/W ratios) were smaller with design#11 (max. 76.7%) compared to design#1 (max. 78.3%).

Table 8.5 presents revealed mathematical correlations between cavity's airflow rate and its H/W aspect ratio, and for different glass transmittances and both designs of integrated slats. Generally, relationships were best represented with power functions. It is also noticed that coefficient of the function (e.g. 5.229E-01) would slightly increase as transmittance increases, and for both designs. In addition, magnitude of the power constant (e.g. 9.329E-01) would increase with transmittance value.

Table 8.5: Revealed relationships between cavity's airflow rate and its characteristics (Height/Width=H/W) for different glass transmittances and both integrated slats' designs: #1 & #11.

CAVITY'S AIRFLOW RATE ($\text{m}^3/\text{s-m}$)					
GLASS TRANSMITTANCE (0-1)	(H/W) values	DESIGN#1	R ²	DESIGN#11	R ²
0.5	8 to 40	$Q = 5.229\text{E-}01(\text{H/W})^{-9.329\text{E-}01}$	0.9993	$Q = 5.273\text{E-}01(\text{H/W})^{-9.054\text{E-}01}$	0.9992
0.7	8 to 40	$Q = 5.387\text{E-}01(\text{H/W})^{-9.402\text{E-}01}$	0.9993	$Q = 5.358\text{E-}01(\text{H/W})^{-9.054\text{E-}01}$	0.9985
0.9	8 to 40	$Q = 5.512\text{E-}01(\text{H/W})^{-9.515\text{E-}01}$	0.9994	$Q = 5.522\text{E-}01(\text{H/W})^{-9.137\text{E-}01}$	0.9985

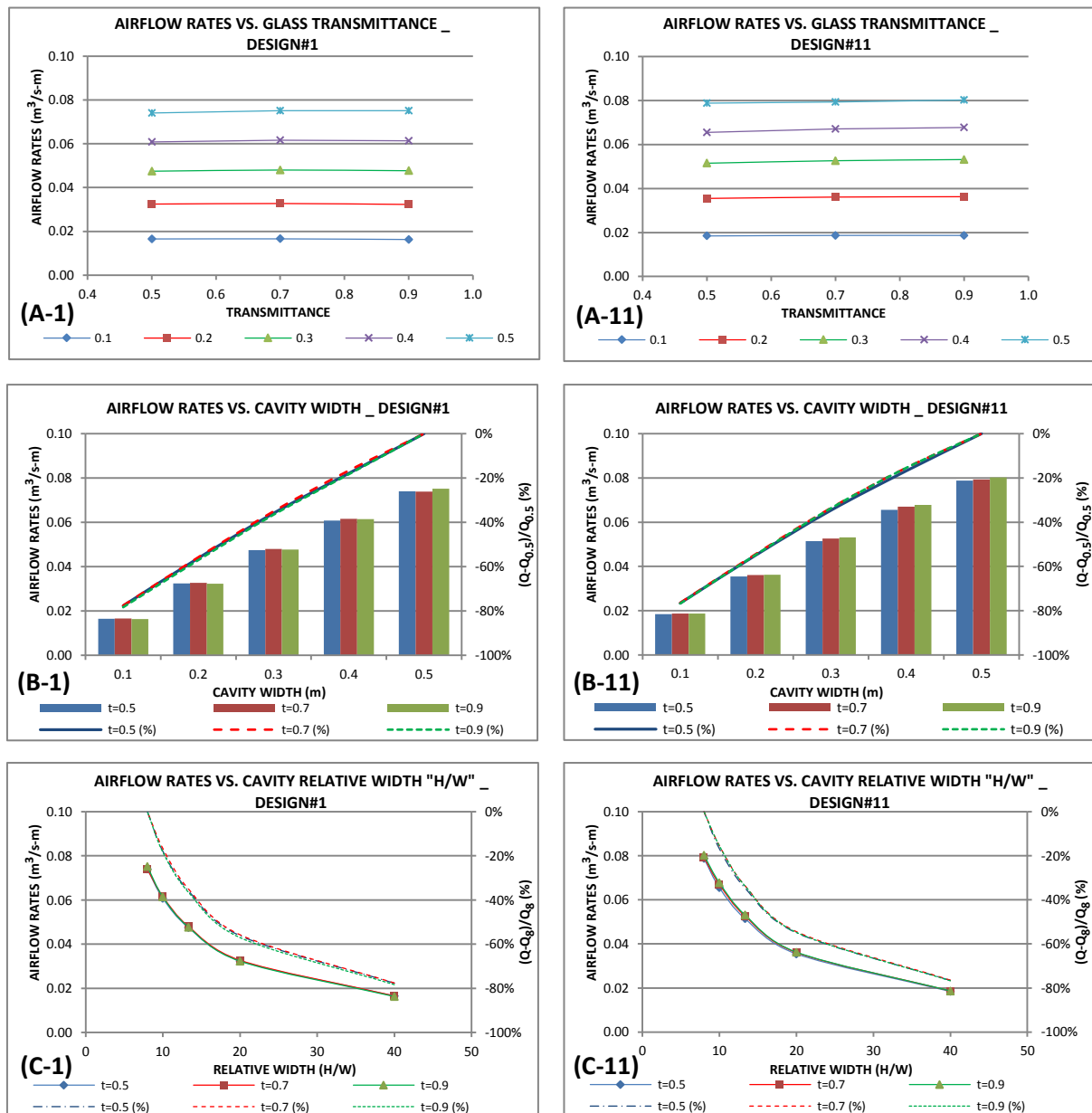


Figure 8.43: Airflow rates changes for simple cavity (with horizontal vents) with different height-to-width ratios (H/W) and glass transmittances ($t=0.5, 0.7$ & 0.9), under summer conditions. Integrated slats had width of 40% of cavity width (e.g. 0.12m for cavity width of 0.3m), surface emissivity of 0.9 and diffuse fraction of 1. (A) Airflow rates plotted against glass transmittances. (B) Airflow rates and relative changes plotted against cavity's width (0.1m-0.5m). (C) Airflow rates and relative changes plotted against H/W ratios (8-40). Left graphs denoted by 1 (e.g. A-1) for cases with design#1 integrated slats; and Right graphs for cases with design#11 (e.g. A-11).

Figure 8.44 shows contours of velocity magnitudes for the tested cavity; and for two ratios of H/W (8 & 40), two designs of integrated slats (#1 & #11) and two different values of glass transmittance (0.5 & 0.9). While total airflow through the cavity was slightly influenced by changing the glass transmittance (discussed earlier), the flow patterns were found to be different with different

values of transmittance. For example, air flow was better distributed (more uniformly) between the two sub-cavities with glass transmittance set to 0.5 compared to 0.9. This was more obvious for the upper half of cavity. Also, flow pattern (at top of cavity and just below its outlet) was found to be more varied with different designs of integrated slats as glass transmittance increased (i.e. $t=0.9$).

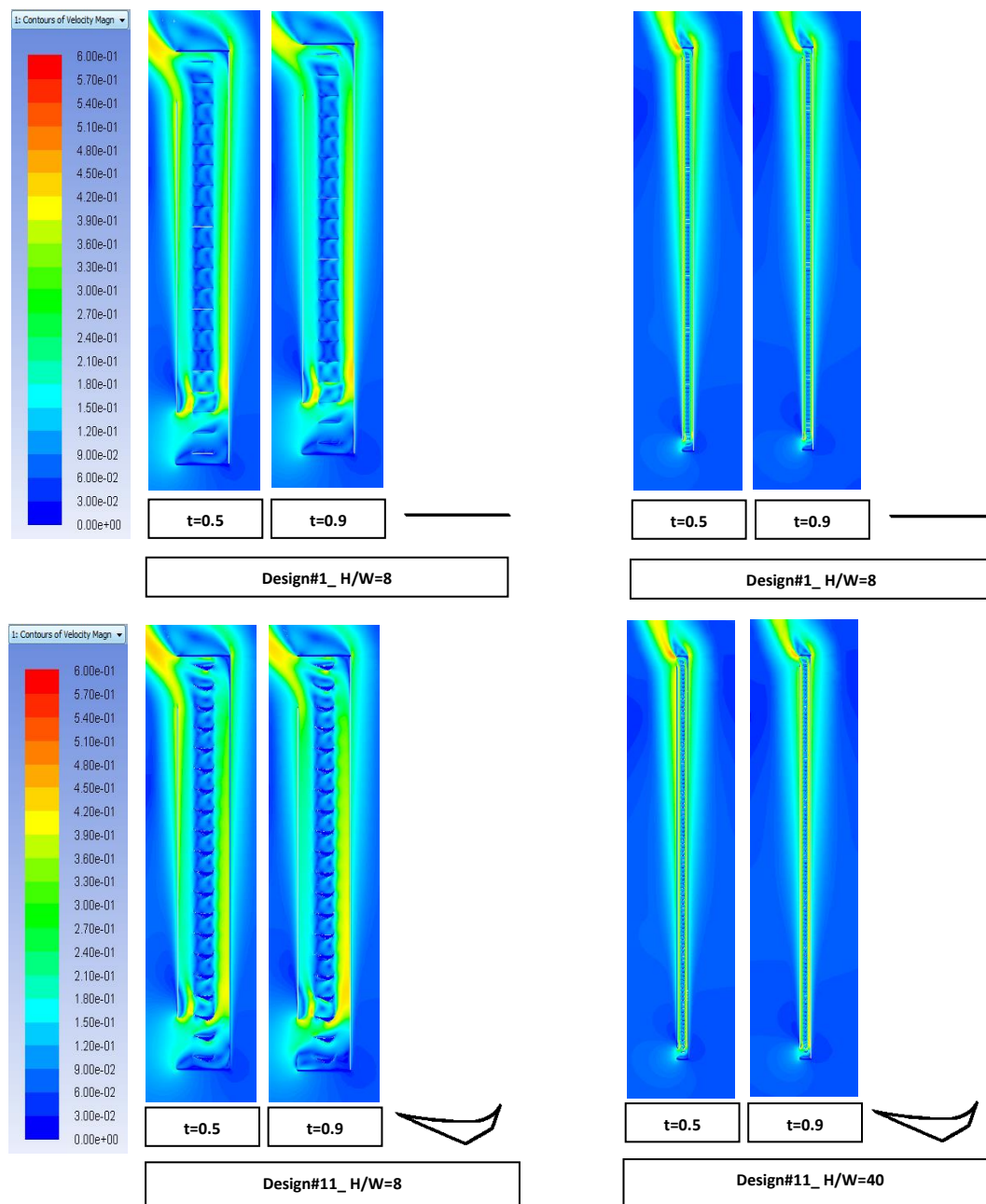


Figure 8.44: contours of velocity magnitude (m/s) for simple cavity with horizontal vents and selected designs of integrated slats; slats had surface emissivity of 0.9 and diffuse fraction of 1 (EMS0.9-DIFF1). Slats were placed at middle of cavity (P5) and had size of 40% of cavity width (0.5m). Cavity's vents had size of 0.5m. Different glass transmittance values were used, presented results are for $t=0.5$ & $t=0.9$. Cavity was with two different H/W ratios (8 & 40), and integrated with slats of design#1 and #11. Results are for summer scenario.

- **Temperatures:**

Figure 8.45 shows averages of surface temperature increase of the structure. As shown in Figure 8.45-A-1, the increase in surface temperature of front glass would decrease as its transmittance increases, this is due to its absorptance decreasing. Also, for any glass transmittance, increase magnitude slightly dropped as H/W ratio increased from 8 to 13. Also, this drop slightly enlarged as glass transmittance increased (e.g. with design#1, max. 1.4% for $t=0.5$ and max. 2.9% for $t=0.9$). After which, increase magnitude rose with H/W ratios. Again, change in increase magnitude was higher for higher glass transmittance. For instance, with design#1, maximum change was 9.1% for $t=0.5$ compared to 20.7% for $t=0.9$.

With design#11 integrated slats, surface temperature increase of front glass with different transmittances, as shown in Figure 8.45-A-11, had similar trends to those for design#1 but with different magnitudes and changing rates. Maximum changes in temperature increase were a bit higher with design#11 compared to design#1. For example, as H/W ratio increase from 8 to 40, increase in surface temperature of front glass (with $t=0.9$) rose by 20.7% with design#1 compared to 23.2% with design#11.

For both designs (#1), it was found that variations in glass temperature with H/W ratio would be higher for higher glass transmittances. For example, with design#11 integrated slats, the difference in surface temperature of front glass (between $H/W=8$ and $H/W=40$) was 1.0°C with $t=0.5$ compared to 1.2°C with $t=0.9$.

Now, for back glass, increase in surface temperature had also similar trends to those for front glass, and for both designs of integrated slats (#1), as shown in Figure 8.45-B-1 & B-11. However, magnitudes were different (always smaller) as well as relative changes. Similarly, as glass transmittance increased, increase in surface temperature dropped. Also, the difference between increase magnitudes for different transmittances was larger for higher transmittances, which means surface temperature would drop significantly as its transmittance is getting higher.

However, maximum change in temperature-increase for back glass (with $t=0.9$) was 26.7% (at $H/W=40$) for design#1 compared to 35.2% for design#11. This means that the performance of design#11 integrated slats (more detailed design as mentioned earlier) would be more influenced by characteristics of the cavity (i.e. H/W ratio). Moreover, and from a thermal perspective, the importance of the detailed design of integrated slats would be more vital with lower transmittances. For instance, with $H/W=8$, increase in temperature of back glass (with $t=0.5$) with design#11 integrated slats was 15% lower than corresponding increase with design#1. But, with $t=0.9$, the difference was just 5%.

Finally, as glass transmittance increases, increase in surface temperature of integrated slats would increase, unlike glass panes. This is expected with the high transparency of glass, as more heat would hit these devices causing higher heat absorption. Changes in increase of surface temperature for design#11 were close for the three investigated transmittance values, Figure 8.45-C-11, but a bit more varied for design#1

(simple flat), Figure 8.45-C-1. However, these changes were higher for design#11 (max. 20.3%) compared to design#1 (max. 15.1%)

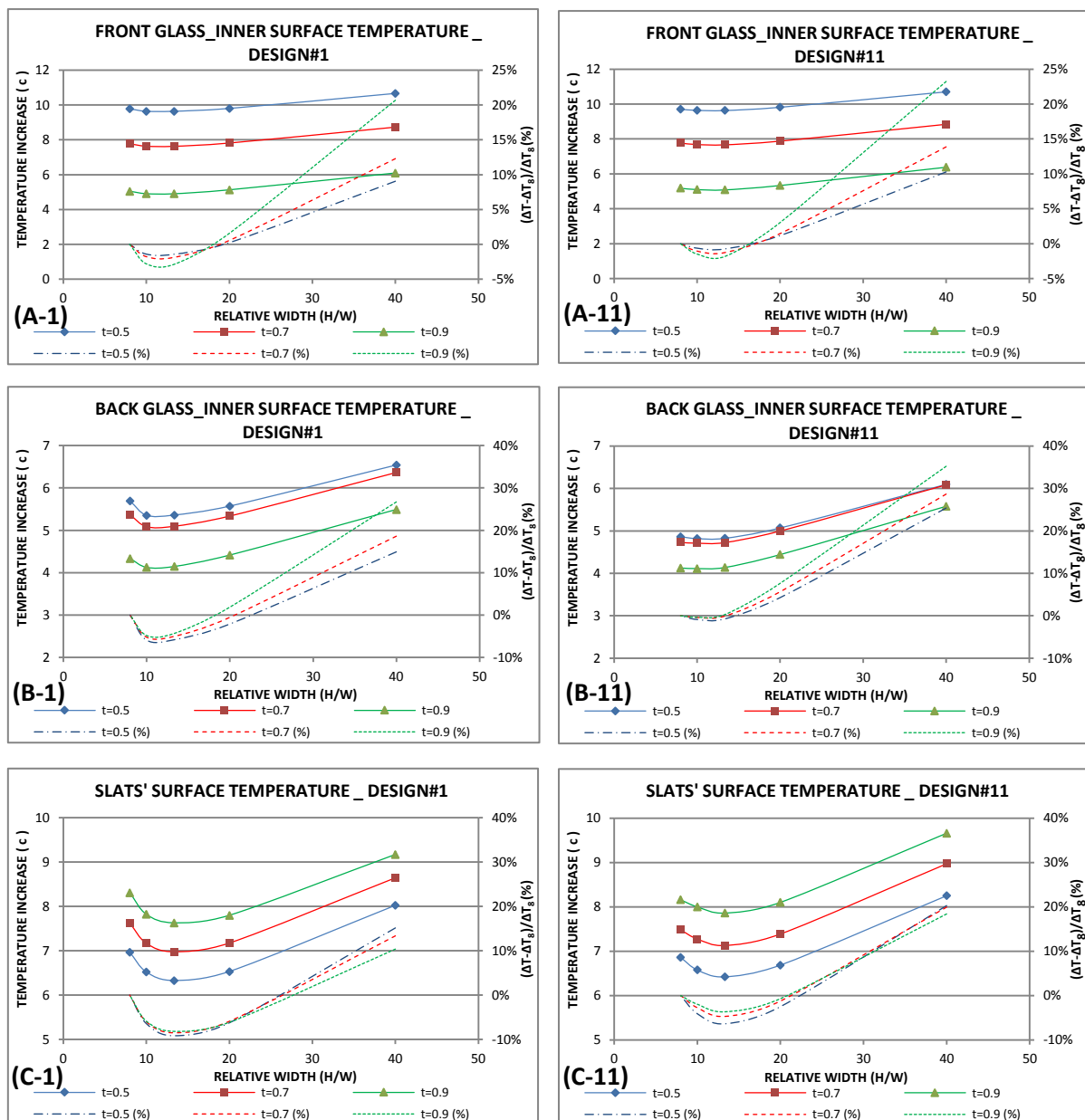


Figure 8.45: Comparison for average surface temperature increase of cavity (with horizontal vents) with different height-to-width ratios (H/W) and glass transmittances ($t=0.5, 0.7$ & 0.9), under summer conditions. Integrated slats had width of 40% of cavity width (e.g. 0.12m for cavity width of 0.3m), surface emissivity of 0.9 and diffuse fraction of 1. (A) Front glass_inner surface. (B) Back glass_inner surface. (C) Integrated slats' surface. All results plotted against H/W ratios (8-40). Left graphs denoted by 1 (e.g. A-1) for cases with design#1 integrated slats; and Right graphs for cases with design#11 (e.g. A-11).

Table 8.6 shows mathematical correlations between H/W aspect ratio of cavity and temperature increase of its surfaces. All correlations, concerning design#11, were best represented by polynomial functions with second order.

Regarding design#1, correlations were also represented by polynomial functions with second order; however, using higher orders (i.e. 3rd order) for these functions could still result in higher R-squared.

Table 8.6: Revealed relationships between surface temperature increase of cavity and its characteristics (Height/Width=H/W), for different glass transmittances and both integrated slats' designs: #1 & #11. (A) Front Glass (B) Back Glass & (C) Integrated Slats.

(A) FRONT GLASS: SURFACE TEMPERATURE INCREASE (°C)					
GLASS TRANSMITTANCE (0-1)	(H/W) values	DESIGN#1	R ²	DESIGN#11	R ²
0.5	8 to 40	$\Delta T = 1.300E-03(H/W)^2 - 3.253E-02(H/W) + 9.893$	0.9849	$\Delta T = 1.129E-03(H/W)^2 - 2.175E-02(H/W) + 9.764$	0.9937
0.7	8 to 40	$\Delta T = 1.339E-03(H/W)^2 - 3.211E-02(H/W) + 7.877$	0.9847	$\Delta T = 1.265E-03(H/W)^2 - 2.540E-02(H/W) + 7.836$	0.9916
0.9	8 to 40	$\Delta T = 1.337E-03(H/W)^2 - 2.899E-02(H/W) + 5.123$	0.9837	$\Delta T = 1.293E-03(H/W)^2 - 2.269E-02(H/W) + 5.224$	0.9914

(B) BACK GLASS: SURFACE TEMPERATURE INCREASE (°C)					
GLASS TRANSMITTANCE (0-1)	(H/W) values	DESIGN#1	R ²	DESIGN#11	R ²
0.5	8 to 40	$\Delta T = 1.814E-03(H/W)^2 - 5.554E-02(H/W) + 5.868$	0.9386	$\Delta T = 1.116E-03(H/W)^2 - 1.369E-02(H/W) + 4.861$	0.9952
0.7	8 to 40	$\Delta T = 1.687E-03(H/W)^2 - 4.536E-02(H/W) + 5.488$	0.9590	$\Delta T = 1.066E-03(H/W)^2 - 7.692E-03(H/W) + 4.690$	0.9964
0.9	8 to 40	$\Delta T = 1.490E-03(H/W)^2 - 3.176E-02(H/W) + 4.385$	0.9756	$\Delta T = 1.024E-03(H/W)^2 - 2.522E-03(H/W) + 4.045$	0.9963

(C) INTEGRATED SLATS: SURFACE TEMPERATURE INCREASE (°C)					
GLASS TRANSMITTANCE (0-1)	(H/W) values	DESIGN#1	R ²	DESIGN#11	R ²
0.5	8 to 40	$\Delta T = 3.557E-03(H/W)^2 - 1.317E-01(H/W) + 7.616$	0.9503	$\Delta T = 3.012E-03(H/W)^2 - 9.695E-02(H/W) + 7.319$	0.9769
0.7	8 to 40	$\Delta T = 3.560E-03(H/W)^2 - 1.329E-01(H/W) + 8.278$	0.9473	$\Delta T = 2.840E-03(H/W)^2 - 8.664E-02(H/W) + 7.901$	0.9858
0.9	8 to 40	$\Delta T = 3.547E-03(H/W)^2 - 1.369E-01(H/W) + 8.986$	0.9343	$\Delta T = 2.706E-03(H/W)^2 - 8.059E-02(H/W) + 8.560$	0.9899

Figure 8.46 shows changes in both air and surfaces' temperatures for the investigated cavities due to changing its glass transmittance. It was found that changing transmittance of glass of the cavity (with either integrated slats) would lead to change in temperatures of glass and slats mediums as well as passing air. However, this change was found to be much significant with narrower cavities (higher H/W ratios). For example, by increasing transmittance value to 0.9, temperature of external glass would drop while temperature of slats would increase, and, also temperature of air would rise

up. Moreover, air temperature stratification inside the cavity would tend to be symmetrical (around the slats set axis) unlike in the case of lower transmittance ($t=0.5$) where air temperature was much higher in front sub-cavity. Furthermore, detailed design of integrated slats would have a more evident influence on the air temperature development (e.g. top of the cavity) with narrower cavities compared to wider cavities.

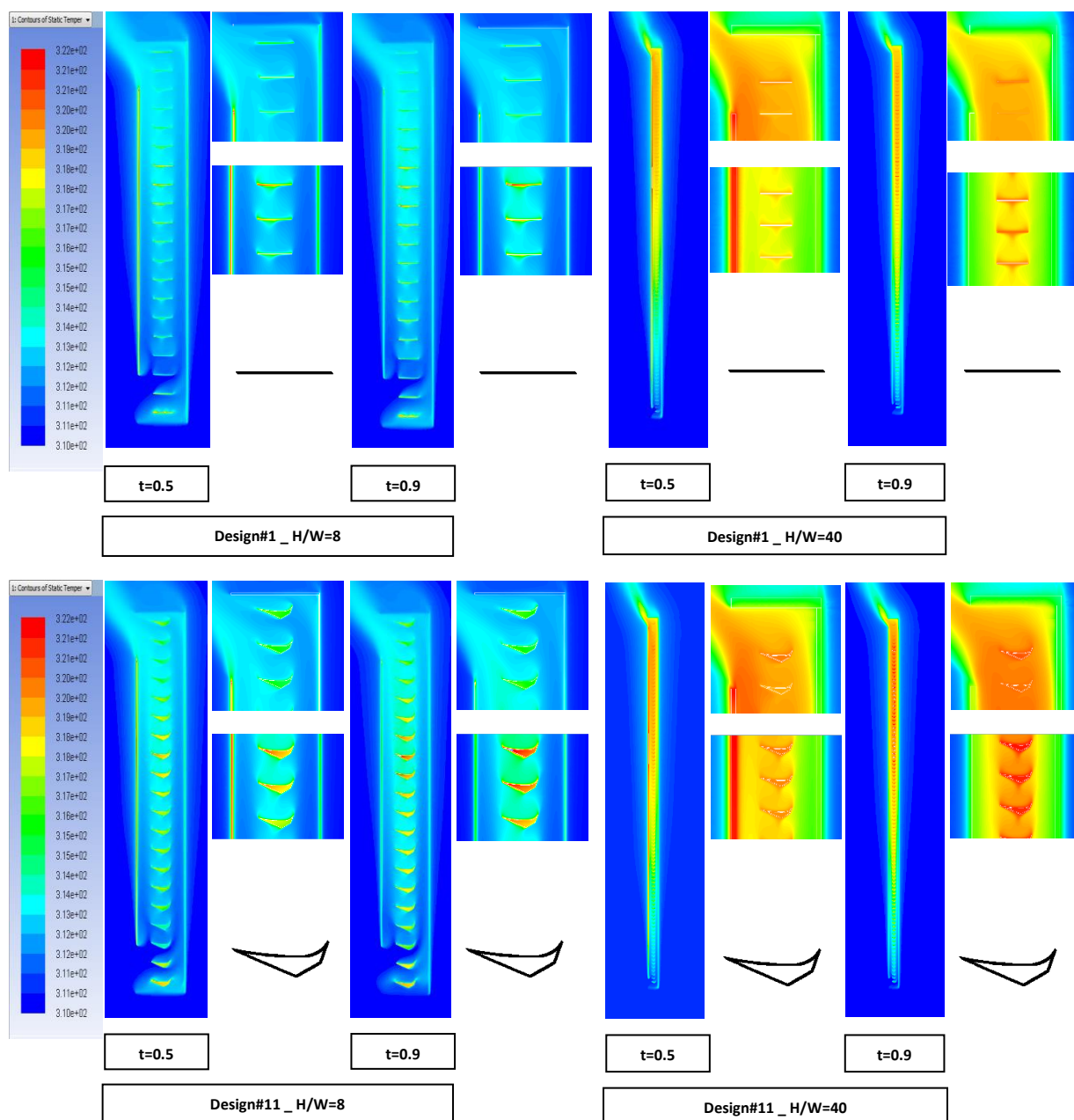


Figure 8.46: Contours of temperature (k) for simple cavity with horizontal vents and selected designs of integrated slats; slats had surface emissivity of 0.9 and diffuse fraction of 1 (EMS0.9-DIFF1). Slats were placed at middle of cavity (P5) and had size of 40% of cavity width (0.5m). Cavity's vents had size of 0.5m. Different glass transmittance values were used, presented results are for $t=0.5$ & $t=0.9$. Cavity was with two different H/W ratios (8 & 40), and integrated with slats of design#1 and #11. Results are for summer scenario.

- **Conclusion:**

To conclude, it was found that cavity's airflow would increase as its width increases (H/W ratio decreases). However, it was also found that changing glass transmittance would have negligible influence on cavity's airflow rates, as any decrease in glass' surface temperature would be balanced by a corresponding decrease in integrated slats' surface temperature. Also, detailed design of integrated slats would have an impact on cavity's airflow rate. However, this impact would vary based on both H/W ratio and transmittance of glass. Generally, as glass transmittance increases, the difference in airflow rate between different designs of integrated slats would increase as shown in Figure 8.47-A. Also, for the tested designs #1 & #11, such difference becomes more evident with higher H/W ratios (narrower cavities) where flow is expected to get merged near the top of narrower cavities more than wider cavities. This would help distinguishing the influence of detailed designs of integrated slats as flow would be forced to move between the two sub-cavities (separated by the set of slats). For instance, the difference in cavity's airflow rate for design#1 and design#11 increased from 6.7% to 14.6% as H/W ratio increased from 8 to 40, where transmittance was 0.9. Also, for $H/W=40$, such difference was increased from 11.6% to 14.6% as transmittance increased from 0.5 to 0.9. However, this conclusion depends on the configuration of cavity as well as detailed designs on integrated slats, as the conclusion for the simple cavity (with vertical vents instead of horizontal, here) with design#1 and design#6 integrated slats was slightly different as discussed in the previous chapter.

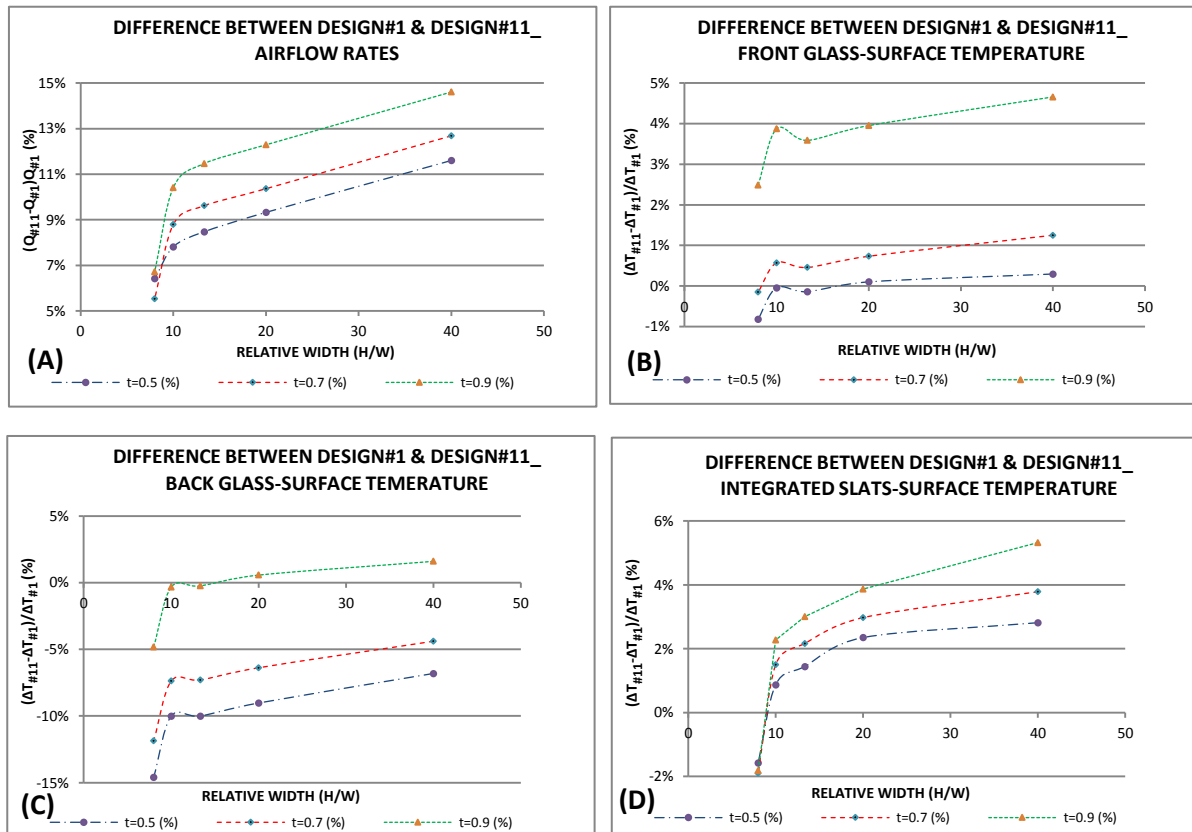


Figure 8.47: Relationships between the influence of design#1 and design#6 integrated slats, all in summer. (A) Cavity's airflow rates. (B) Front glass-Surface Temperature. (C) Back glass-Surface Temperature. (D) Integrated slats-Surface-Temperature.

On the other hand, it was found that surface temperature of both glass panes and integrated slats would be changed with varying the cavity's width (H/W ratio) and varying glass transmittance values.

The surface temperature of the glass panes would decrease as its transmittance increases. In contrast, the surface temperature of the integrated slats would increase. Furthermore, surface temperature for all elements would slightly drop for certain range of H/W ratios (8-13); then, it would increase for higher H/W ratios, which could be linked to changes in airflow rates for revealed increase.

Generally speaking, detailed design of integrated slats would have an evident impact on the surface temperature of different elements (i.e. glass

panes and integrated slats). For the given structure and tested designs of integrated slats, this influence would increase for front glass as transmittance value increases as shown in in Figure 8.47-B. For instance, the difference in surface temperature increase between design#1 and design#11 rose from 0.3% to 4.7% as transmittance increased from 0.5 to 0.9. For back glass, the difference in surface temperature increase also minimized as transmittance value increased as shown in Figure 8.47-C. For instance, for $H/W=8$, the difference was 14.6% with $t=0.5$ and 4.8% with $t=0.9$. Also, changes in this difference increased significantly with H/W ratio and in particular for small ratios.

Finally, the impact of the detailed design of integrated slats would also be evident for the surface temperature of these slats as shown in Figure 8.47-D. The role of design would get clearer as transmittance value increases, also as H/W ratio increases. The influence of H/W ratio would be clearer at small values (8-13). The influence of glass transmittance would be more evident at high H/W ratios.

8.10 Conclusion:

This chapter shows the performance for a simple cavity having horizontal vents and integrated with various designs of slats. A series of parametric studies were conducted on this cavity.

It was found that detailed design on integrated slats would influence both cavity's airflow (rate and patterns) and surfaces' temperatures. However, this influence is also affected by thermal characteristics (i.e. surface's emissivity and diffuse fraction) of these slats. Moreover, boundary conditions

(i.e. intensity of solar radiation, beam angle, and ambient air temperature) could play a significant role in distinguishing between the different designs of integrated slats (in terms of their performance). Also, flow resistance by cavity's vents would affect the difference in performance between these slats. Similarly, the size of slat would have a further role. However, it was concluded that such difference would slightly be changed as slats' position inside the cavity is changed.

Now, geometrical characteristics of the cavity (i.e. H/W ratio) would affect both its airflow and thermal performance. However, this influence could be altered by ambient boundary conditions (i.e. beam angle). Furthermore, whereas the detailed design of integrated slats would influence the performance of the cavity, it was revealed that this influence would further be controlled by the proportion of cavity (H/W ratio).

Moreover, it was revealed that glass transmittance could slightly affect ventilation rate of the given structure. However, while the detailed design of integrated slats could enhance cavity's ventilation, level of enhancement would still be influenced by glass transmittance. But, this is in turn still controlled by both complexity of slats' design and cavity's configuration. Furthermore, surface temperature of different elements could be affected by glass transmittance. Again, this influence is also enhanced by propositions of the cavity.

After the presented work for both simple cavities, following set of chapters show a continuation of this work but with a full model for the targeted

space (office space and cavity). However, similar investigation works were not repeated but relevant conclusions were used instead, with the need some time to further investigate some vital parameters to make sure their influence would not significantly be changed with major changes in structure's configurations.

CHAPTER 9 DOUBLE SKIN FAÇADE (DSF) WITHOUT SHADING DEVICES

9.1 Size of Cavity:

Results for changing the size of the cavity are presented in the following section. Opening height always equals to cavity width.

9.1.1 Summer Conditions

- **Airflow rate:**

As shown in Figure 9.1, all investigated sizes for cavity/openings would lead to airflow rates that exceed minimum ventilation rates for occupants ($10\text{L/s/person} = 0.01\text{m}^3/\text{s/person} = 0.005\text{m}^3/\text{s-m}$; given that office's area is $6\text{m} \times 8\text{m}$ "the third dimension" and accommodates 4 occupants). Minimum rate was $0.036\text{m}^3/\text{s-m}$ for narrower cavity (0.1m), which is 7 times more than minimum requirement. Both office (Q_{office}) and cavity (Q_{cavity}) ventilation would increase with cavity width (w) and opening height by a linear relationship (9.1) for the aforementioned and a polynomial relationship (9.2) for the later. For example, the office with 0.5m -cavity would have a ventilation rate around 160% higher than 0.1m -cavity.

$$Q_{\text{office}} = 0.1419 w + 0.0224 \quad (R^2 = 0.9995) \quad (9.1)$$

$$Q_{\text{cavity}} = 0.286 w^3 - 0.4031 w^2 + 0.2022 w - 0.0088 \quad (R^2 = 0.9997) \quad (9.2)$$

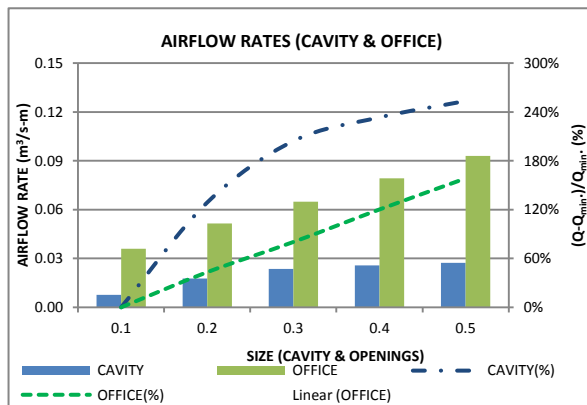


Figure 9.1: airflow rates and changes for both office and entire structure, with changes in cavity/openings size.

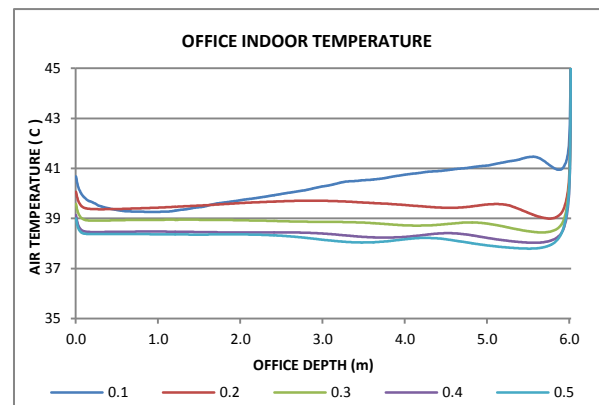


Figure 9.2: Indoor temperature at height of 1.6m for different cavity/openings size.

• Temperatures:

Figure 9.2 shows indoor temperature along the office depth at height of 1.6m. It's clear that increasing cavity width and opening size to 0.5m would help in reducing indoor temperature (38.2°C) by just about 5% compared to smallest size, 0.10m. This indicates that even narrowest cavity, 0.1m, would be able to provide good ventilation that partially removes solar gains and helps to maintain indoor temperature (40.3°C) close to outdoor temperature (37°C).

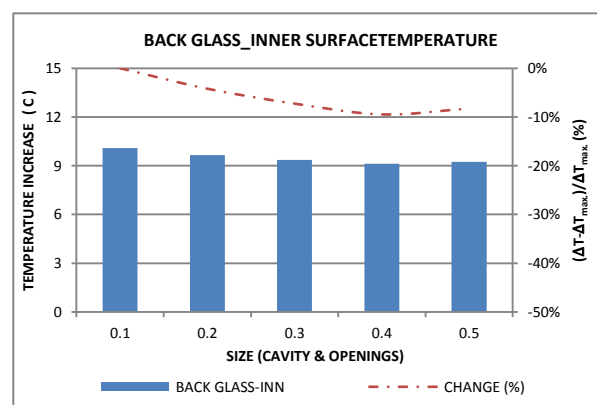
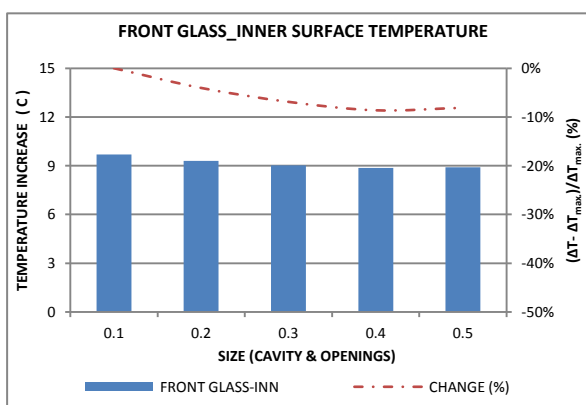


Figure 9.3: surface temperature increase averages for inner surfaces of outer glass (left) and inner glass (right) panes, with changes in cavity/openings size.

The aforementioned would also give more uniform distribution. However, all values are still much higher than comfort band (24-28.5°C) as lowest average was found to be 38.2°C for 0.5m-cavity, which is just 1.2°C

higher than the inlet temperature (summer peak: 37°C). Figure 9.3 presents the increase in average surface temperature for glass panes. Inner glass would have a bit higher temperature than the outer pane as the outer is better ventilated with lower temperature air. Both surfaces had similar trends for temperature changes that are just up to 10%. Moreover, results revealed polynomial relationships between the temperature increase (ΔT) average and cavity's width (w) as shown in equation (9.3) for front glass and equation (9.4) for back glass. However, relatively lower changes in each surface temperature were due to negligible changes in cavity ventilation itself particularly for wider cavities. Based on these findings, an initial optimum cavity size was considered to be 0.4m as it gives nearly same indoor temperature profile as the size of 0.5m while all provide sufficient ventilation.

$$\Delta T = 7.0855 w^2 - 6.2676 w + 10.257 \quad (R^2 = 0.9974) \quad (9.3)$$

$$\Delta T = 8.3926 w^2 - 7.2334 w + 10.738 \quad (R^2 = 0.9892) \quad (9.4)$$

9.1.2 Winter Conditions:

Results for changing the size of the cavity, in winter condition, are presented in this section.

- **Airflow rate:**

Similar to summer results, ventilation rates would increase for both office indoor and cavity; Figure 9.4. However, winter ventilation rate for the largest size (0.05m) increased by about 60% compared to that of summer conditions; which is due to more solar gains passing to indoor with low winter sun angle.

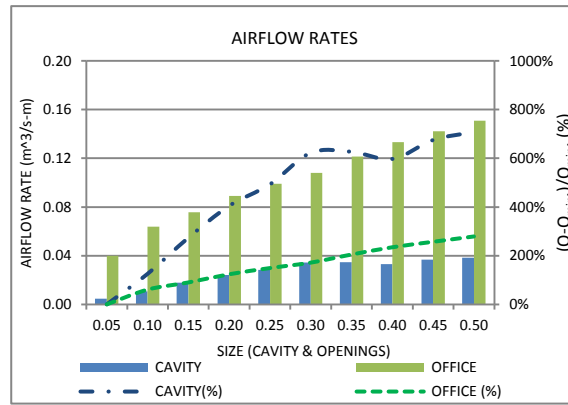


Figure 9.4: airflow rates and changes for both cavity and office in winter, with changes in cavity/openings size. Values for 0.35 and 0.45 were calculated from revealed polynomial relationship.

In reference to smallest size (0.05m), office's ventilation with largest cavity's size (0.5m) would be 279% more; and found to be well governed by a second-order polynomial equation (9.5). For cavity, increase rates were more dominant as maximum change from minimum value was about 708%; compared to 253% for summer conditions as discussed before. Also, cavity's airflow rate was governed by a polynomial equation of the fourth degree (9.6) for higher R-squared.

As shown, more cases have been investigated with 0.05m step-size; which was due to the sensitivity of winter operation and comfort to the size parameter.

$$Q_{\text{office}} = -0.1708 w^2 + 0.3292 w + 0.0282 \quad ; (R^2 = 0.995) \quad (9.5)$$

$$Q_{\text{cavity}} = 3.8823 w^4 - 4.1024 w^3 + 1.2382 w^2 - 0.0066x + 0.0026 \quad ; (R^2 = 0.993) \quad (9.6)$$

- Temperatures:**

Having winter's inlet temperature equals to 4°C, given structure with narrowest cavity (0.05m) would be able to keep indoor temperature up to

18.8°C (average) but with significant variation along its depth. However, larger cavity (0.1m) would help to maintain the average at 17.7°C with better uniformity; Figure 9.5. Also, average temperature for 0.2m-size would be close to 10.3°C with an increase of 6.3°C compared to 2.5°C in summer. Moreover, initial selected size for summer (0.4m) would cause an increase of 2.7°C in winter compared to just 1.4°C in summer.

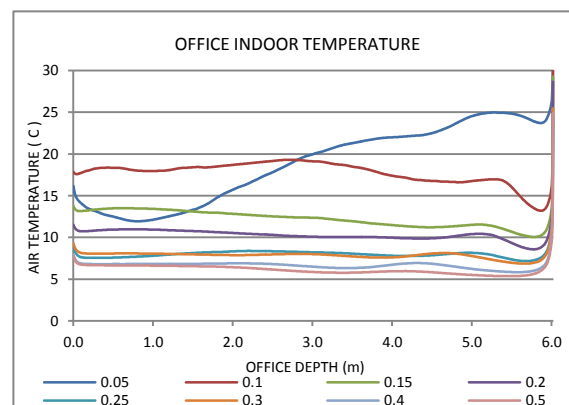


Figure 9.5: Indoor temperature at height of 1.6m for different cavity/openings size in winter.

Figure 9.6 presents averages for increase in surface temperatures for glass panes with investigated cavity sizes. This increase could reach 26.6°C and 29°C for outer and inner panes; respectively. However, changes in increase would be up to 19% and 33%; respectively, as wider cavities/openings would result in lower surface temperatures due to higher ventilation rates. Slight fluctuations were revealed from the change rates' trends, particularly for small sizes, which is possibly due to unsteady flow patterns inside both cavity and office structures with these sizes. Revealed mathematical relationships for calculated increase in surface temperature for outer and inner glass panes are given in equations (9.7) and (9.8), respectively.

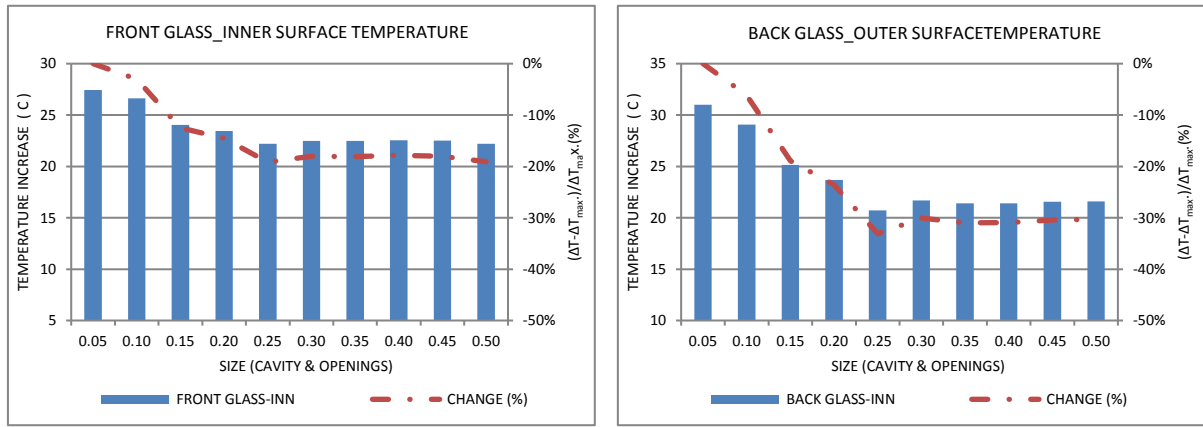


Figure 9.6: surface temperature increase averages for inner surfaces of outer glass (left) and inner glass (right) panes, with changes in cavity/openings size; in winter.

$$\Delta T = -852.41 w^4 + 806.92 w^3 - 185.15 w^2 - 15.964 w + 28.794 \quad ; (R^2 = 0.9736) \quad (9.7)$$

$$\Delta T = -1397.4 w^4 + 1385 w^3 - 337.72 w^2 - 26.25 w + 33.204 \quad ; (R^2 = 0.9736) \quad (9.8)$$

In conclusion, while all sizes would be able to provide minimum fresh air requirement, size of 0.2m was initially selected for winter as it would give good indoor temperature (10.3°C) even though sizes of 0.05m and 0.1m would give higher values but may exceed thermal comfort with expected internal heat gains (i.e. occupants, lighting, equipments). Also, wider cavities are preferred for maintenance/cleaning purposes. Further detailed study was conducted as discussed later.

9.2 Glass Transmittance:

9.2.1 Summer Conditions:

Effect of varying glass transmittance is presented in this section. Values were varied from nearly opaque glass ($t=0.1$) to highly transmitted one ($t=0.9$). Ventilation rates and surface & indoor temperatures were monitored. As stated in the Method chapter, corresponding absorption coefficient (1/m)

was calculated using Beer's law; e.g. for $t=0.9$, it is 17.56 (1/m). Cavity width and openings sizes were set to 0.4m.

- **Airflow rate:**

Glass transmittance could have a significant influence on ventilation rate for both cavity and office indoor, as shown in Figure 9.7. However, by increasing glass's transmittance, office's ventilation would be enhanced by up to 48.6% whereas cavity's flow would be reduced. For the later, its maximum flow rate would be with $t=0.1$ that was 61.1% higher than its minimum rate with $t=0.9$. The evident increase in office's ventilation was due to the fact that more solar gain being admitted to indoor thus enhance the buoyancy effect by heated structured, i.e. ceiling, floor.

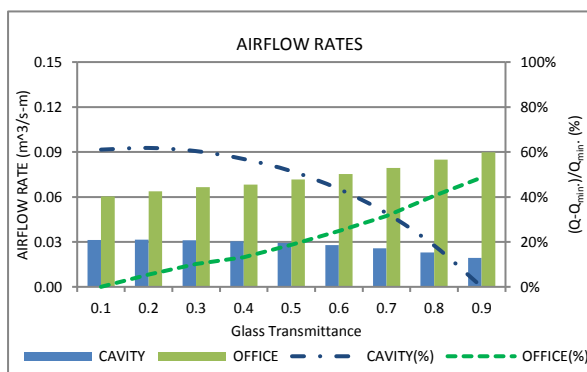


Figure 9.7: airflow rates and changes for both offices an entire structure, with various glass transmissivities.

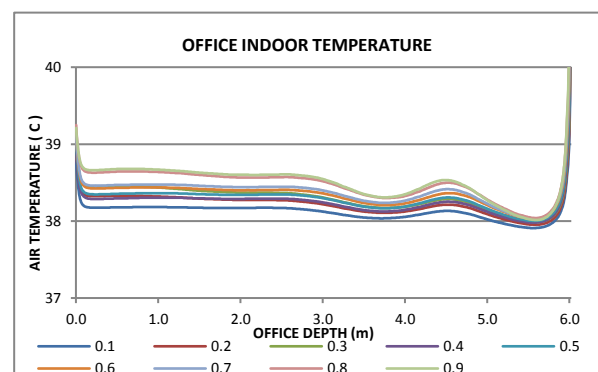


Figure 9.8: indoor temperature at height of 1.6m for various glass transmissivities.

For the cavity itself, increasing glass's transmittance would allow more solar gain to reach the second glass from the first glass; thus, heat would be better distributed on both sides of cavity rather than concentrated on just external side even though total absorbed heat could be less than in case of higher absorption coefficients (lower transmittance). So, due to decreasing total absorbed heat by cavity structures, expected thermal buoyancy inside the cavity would be weakened resulting in lower flow rates, which was more

evident for higher values of transmittance. Both office and cavity ventilation rates could be calculated using revealed equations (9.9) and (9.10), respectively.

$$Q_{\text{office}} = 0.0215 t^2 + 0.0141 t + 0.0594 \quad ; (R^2 = 0.9972) \quad (9.9)$$

$$Q_{\text{cavity}} = -0.0254 t^2 + 0.0111 t + 0.0303 \quad ; (R^2 = 0.9985) \quad (9.10)$$

• Temperatures:

As shown in Figure 9.8, the indoor temperature at height of 1.6m would be slightly increased with glass transparency. This is mainly due to sufficient airflow through the office that would be able to remove the additional solar gains and maintain space temperature close to outdoor incoming air temperature (37°C).

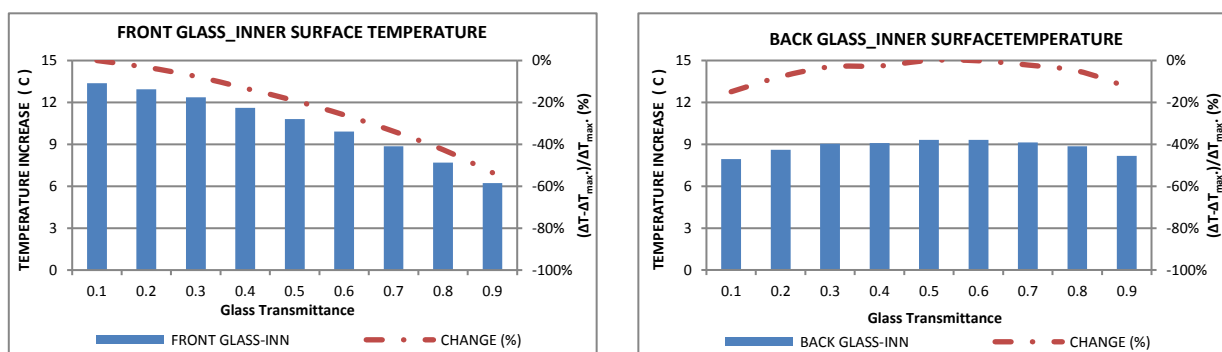


Figure 9.9: variation in surface temperature increase (surface temperature-outdoor temperature) averages for inner surfaces of outer glass (left) and inner glass (right) panes, in summer, due to changing their transmittance.

The temperature for the inner surface of external glass would dramatically drop due to less heat being absorbed by its medium with increasing its transmittance, Figure 9.9-left. This decrease could reach 54% with highly transmitted glass ($t=0.9$). For inner glass, the surface temperature would increase with glass transmittance until $t=0.5$ then it would start to fall in a symmetrical profile as shown in Figure 9.9-right. The maximum change would be 15% with $t=0.1$.

With low transmittance values, i.e. $t=0.1$, limited gains would reach second pane so small amount being absorbed, even with high absorptivity, then having a lower temperature. However, while transmittance value increases, more heat is being absorbed by the inner glass then surface temperature would increase to a certain point that found to be close to $t=0.5$, after which temperature starts decreasing. As the expected influence of increasing solar transmittance for the first glass (also, second glass) on increasing heat absorbed by the second glass would be dominant till $t=0.5$ before it is gradually being overcome by the corresponding decrease in the glass absorptivity due to the inverse relationship between both transmittance and absorptivity.

Following equations (9.11) and (9.12) present the revealed relationships between calculated temperature increase and glass transmittance for both outer and inner glass, respectively.

$$\Delta T = -6.3468 t^2 - 2.5089 t + 13.683 \quad ; (R^2 = 0.9997) \quad (9.11)$$

$$\Delta T = -22.939 t^4 + 44.422 t^3 - 36.198 t^2 + 14.869 t + 6.7716 \quad ; (R^2 = 0.9903) \quad (9.12)$$

Based on these findings, the highest transmittance ($t=0.9$) would provide better ventilation for the office's indoor and also overall structure even though have the lowest rate for cavity itself. Also, it would produce lowest surfaces' temperature while having same average air temperature as $t=0.8$. However, high transmittance is generally recommended for daylighting purposes.

9.2.2 Winter Conditions:

Effect of varying glass transmittance, under winter condition, is presented in this section. Similar to summer study, values were varied from nearly opaque glass ($t=0.1$) to highly transmitted one ($t=0.9$). Ventilation rates, surface & indoor temperatures were monitored. Cavity width and openings sizes were set to 0.2m.

- **Airflow rate:**

Like summer study outcomes, office's ventilation rates would go up with increasing glass transmittance as more heat admitted to indoor; Figure 9.10. Winter's highest change would be for $t=0.9$, and about 97.6% higher than the minimum rate that was for $t=0.1$, compared to 48.6% under summer conditions. Such increase in changes is mainly attributed to low angle of winter sun allowing more solar radiation toward indoor. This also explains the relatively higher increase in indoor temperature during winter (3° - 7°C), Figure 9.11, compared to summer (less than 2°C). The highest indoor average temperature was with $t=0.7$; this is clear in the first two meters as it had higher surface temperature than each of $t=0.8$ and 0.9 .

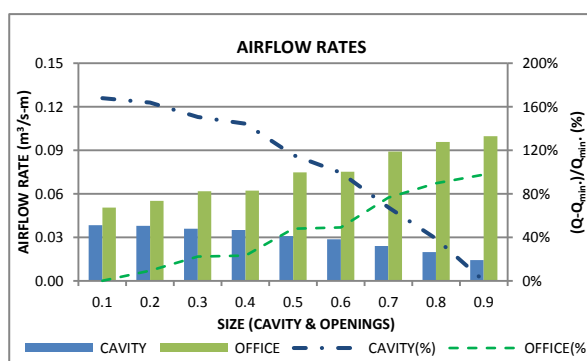


Figure 9.10: airflow rates and changes for both cavity and offices with various glass transmissivities; in winter.

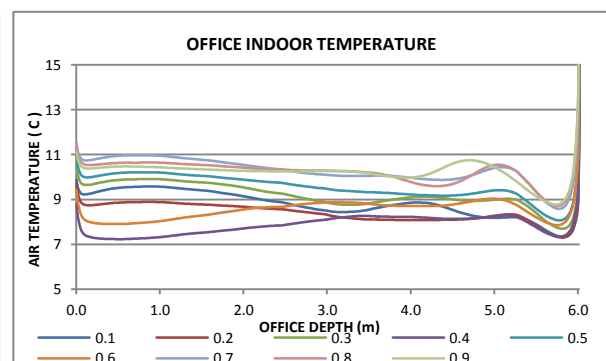


Figure 9.11: indoor temperature at height of 1.6m for various glass transmissivities.

For the cavity itself, airflow rates would again decrease as glass transmittance increases; which agrees with summer findings. However, in reference to the minimum, maximum rates' change in winter was much higher than that in summer, which was 167.8% and 61.8%, respectively. As discussed before, this is attributed to the influence of the relatively low angle of winter's sun. Results for both office's and cavity's flow rates could be extended using revealed functions with good R-squared as shown in (9.13) and (9.14), respectively.

$$Q_{\text{office}} = -0.0576 t^3 + 0.1108 t^2 + 0.0036 t + 0.0498 \quad ; (R^2 = 0.981) \quad (9.13)$$

$$Q_{\text{cavity}} = -0.0323 t^2 + 0.0023 t + 0.0385 \quad ; (R^2 = 0.9975) \quad (9.14)$$

- **Glass Temperatures:**

Under winter conditions, glass temperature changes would generally have a similar trend to that occurs in summer. Whereas temperature for outer glass would decrease with increasing its transmittance, the maximum temperature for inner glass would be for $t=0.5$ and minimum for both $t=0.1$ and 0.9 with a drop of about 20%; Figure 9.12.

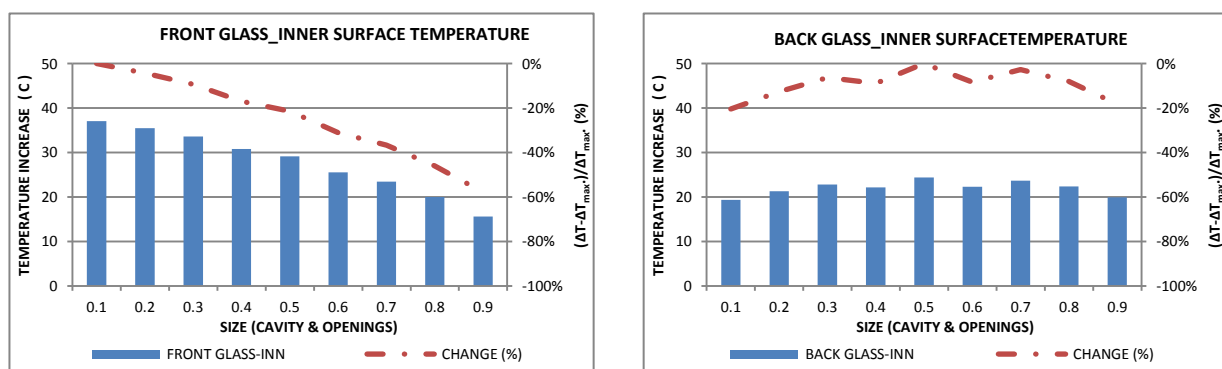


Figure 9.12: variation in surface temperature increase (surface temperature-outdoor temperature) averages for inner surfaces of outer glass (left) and inner glass (right) panes, in winter, due to changing their transmittance.

It is clear that while increasing transmittance would allow more solar to break through first glass then incident on the second one, this accounts for more solar being absorbed by the second compared to nearly negligible amount with lower transmittances (as with $t=0.1$, for instance, outer glass acts as opaque wall and very small amount would reach second glass). The structure would keep performing in this way until its transmittance reaches a point, where the effect of high transparency for the second pane would overcome the additional incident heat on it due to high transparency by the first glass. At this point, the temperature would drop and start to act similar to the that for first glass pane. Furthermore, given equations (9.15) and (9.16) could be used for further predictions of surfaces' temperatures of mentioned glass panes: front and back; respectively.

As mentioned earlier, $t=0.7$ would give highest indoor average temperature also produce nearly maximum surface temperature for inner glass. For indoor ventilation, it is 11% less than the highest rate ($t=0.9$). However, it's less efficient in daylighting than both $t=0.8$ and 0.9 . Referring to summer results, $t=0.9$ was found to be best in overall performance. Thus, $t=0.8$ was considered as an average for both optimum values, which can serve both summer and winter conditions.

$$\Delta T = -14.453 t^2 - 11.807 t + 38.324 \quad ; (R^2 = 0.9973) \quad (9.15)$$

$$\Delta T = -116.75 t^4 + 222.5 t^3 - 162.16 t^2 + 56.184 t + 15.111 \quad ; (R^2 = 0.8415) \quad (9.16)$$

9.3 Opening Control:

The following work aimed to investigate further the role of controlling both outer and inner openings, with fixed cavity size, on airflow and thermal performance. This study focused on winter conditions; and was conducted with two fixed cavity widths: 0.1 and 0.2m. However, shown results here are just for 0.2m as it gave more reasonable results and have a wider cavity. For 0.2m category, the internal inlet was fixed to 0.2m while changes happened to outer openings from 0.05-0.20m. Glass transmittance was set to 0.8.

- **Airflow rate:**

Compared to the case with same openings (0.20-0.20m), reducing the outer opening size to 0.05m would result in lowering airflow rate for office's indoor by up to 56%; Figure 9.13. This is expected due to the additional flow resistance occurred at the smallest external opening. Results showed that a polynomial equation (9.17) is governing the relationship between calculated flow rate and adjusted size (h) of the outer opening.

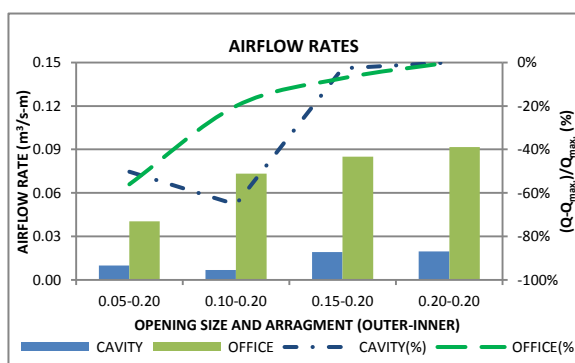


Figure 9.13: airflow rates and changes for both cavity and office in winter, due to the effect of changing outer opening size at range: 0.05-0.20m.

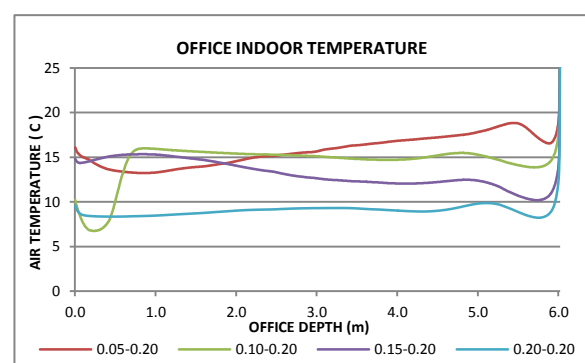


Figure 9.14: Indoor temperature at height of 1.6m with different outer opening sizes, in winter.

In addition, cavity's flow rate would be reduced because of decreasing outer opening's size. The reduction was relatively small just about 3% for

0.15m. However, this change increased significantly for smaller opening sizes as outdoor incoming air would be diverted more efficiently into the office through the inner skin opening; so just small part would rise up through the cavity. Still, results showed that cavity's flow rate would be higher for 0.05m than 0.10m, which is attributed to the diagonal direction (momentum) of incoming air through the outer opening. For example, for 0.05m opening size, outdoor air would enter with relatively higher angle into the cavity so part of the flow would be forced toward the top of the cavity leading to relatively higher flow through although the total flow was still much lower than that for 0.2m. Further investigations for more sizes within 0.05-0.15m range are needed to determine the exact turning point, but this is out of the current research scope. Furthermore, results indicate a polynomial equation of third degree (9.18) for cavity's airflow rate and size (h) of outer openings. However, more cases are needed to further expand the range of applications of this relationship.

$$Q_{\text{office}} = -2.6369 h^2 + 0.9912 h - 0.0018 \quad ; (R^2 = 0.9916) \quad (9.17)$$

$$Q_{\text{cavity}} = -36.241 h^3 + 13.941 h^2 - 1.5165 h + 0.0553 \quad ; (R^2 = 1) \quad (9.18)$$

Figure 9.14 presents average indoor temperature due to adjusting those openings. Clearly, average temperature would go up with small openings due to less heat being removed by cooler air coming from outdoor. Thus, highest average, 15.8c, was found under the effect of smallest size (0.05m) but with variation about 5.5c between front and back of space. Next highest was 14.5c with the size of 0.1m and showing better indoor uniformity except for the first

1m. On the other hand, while both 0.05m and 0.1m sizes would offer sufficient fresh air, the later showed better air distribution inside the office so the size of 0.1m was selected for outer openings with fixed inner openings at 0.2m. The difference in temperature between 0.05m and 0.1m is expected to be compensated by internal gains.

- **Glass Temperatures:**

Figure 9.15 presents changes in surface temperature averages due to adjusting outer openings' sizes. Generally, surface temperature would increase by reducing outer vents as overall airflow decreases thus less heat being transferred consequently. The drop could reach 17% and 23% for front and back glass, respectively.

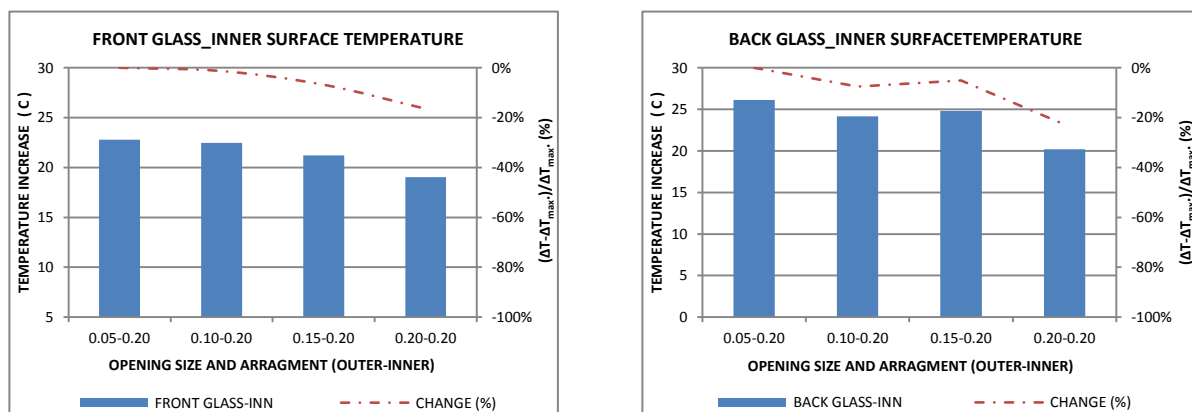


Figure 9.15: surface temperature increase averages for inner surfaces of outer glass (left) and inner glass (right), under the effect of adjusting external openings' size, in winter.

Following equations (9.19) and (9.20) were found to correlate both surface temperature increase and size of the outer opening for both front “outer” and back “inner” glass, respectively.

$$\Delta T_{\text{Front}} = -189.57 h^2 + 22.38 h + 22.134 \quad ; (R^2 = 1) \quad (9.19)$$

$$\Delta T_{\text{Back}} = -10474 h^3 + 3660.5 h^2 - 404.85 h + 38.516 \quad ; (R^2 = 1) \quad (9.20)$$

9.4 Uniting Cavity Size:

9.4.1 Summer Conditions:

The work under this section primarily aimed at uniting the cavity width for both summer and winter that has a different optimum width as discussed before. The opening size was fixed to 0.4m (its chosen value from the previous section). However, the cavity was further tested with three different widths: 0.6, 0.8 and 1.0m. New glass transmittance ($t=0.8$) was used.

- **Airflow rate:**

Increasing cavity width with fixed opening size would have a limited impact on indoor ventilation rate as the change was about 6% when width was increased from 0.4m to 1.0m; Figure 9.16. This change, however, would increase to 27% for cavity structure itself, which is preferable for heat removal thus preventing unwanted overheating during summer. The relatively significant increase in cavity's flow is interpreted because of reducing flow resistance inside the cavity with increasing its width. Therefore, wider cavities could be used with optimum openings size, as they would enhance the system performance while help in facilitating future services for cavity components, i.e. integrated slats maintenance and cleaning.

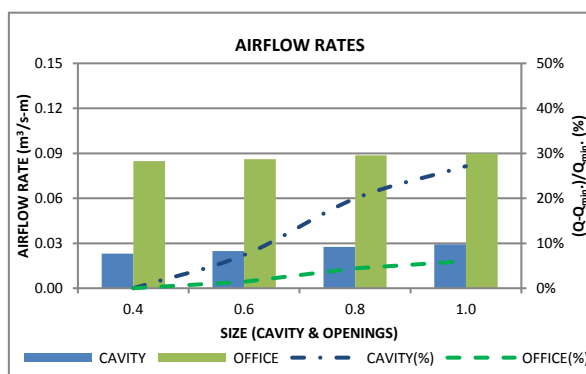


Figure 9.16: airflow rates and changes for both office and entire structure, with varied cavity width and fixed opening size to 0.4m.

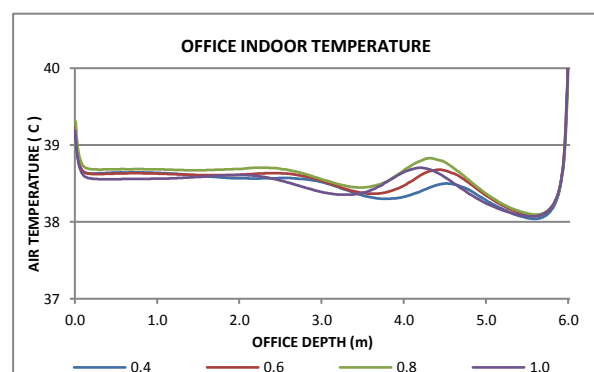


Figure 9.17: indoor temperature at height of 1.6m, with varied cavity width and fixed opening size to 0.4m.

New cavity width is set to 0.6m, which balances between revealed benefits for wider cavities from one side and good usage for perimeter areas in office buildings from another side.

Finally, it was found that correlations between calculated airflow rates and adjustable widths for cavity could be presented using following polynomial equations (9.21) and (9.22) for office and cavity structures, respectively.

$$Q_{\text{office}} = -0.0004 w^3 + 0.0032 w^2 - 0.0055 w + 0.0875 \quad ; (R^2 = 1) \quad (9.21)$$

$$Q_{\text{cavity}} = -0.0502 w^3 + 0.1051 w^2 - 0.0585 w - 0.0328 \quad ; (R^2 = 1) \quad (9.22)$$

- **Temperatures:**

Impact of increasing cavity is also found to be negligible on indoor temperature average, Figure 9.17, as nearly same amount of air will be flowing to indoor for all cases with fixed opening size. Similarly, surface temperatures were only slightly affected by this increase, Figure 9.18. For instance, the maximum change in temperature increase of the inner surface of the inner glass was equal to that for office's ventilation rate but opposite; i.e. surface temperature increase decreased by 6% for 1.0m when office's flow rate increased by 6%.

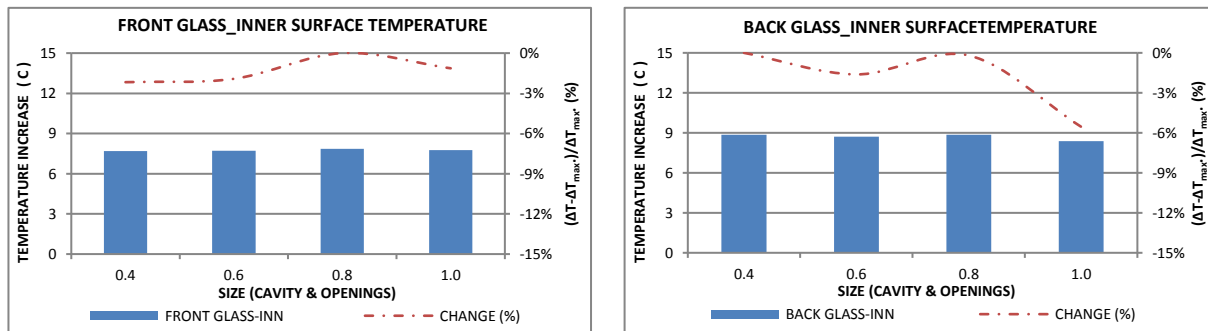


Figure 9.18: variation in surface temperature increase (surface temperature-outdoor temperature) averages for inner surface of outer glass (left) and inner glass (right) panes, with changed cavity width and fixed opening size.

Given correlations (9.23) and (9.24) could be used for further expansion of results of both front and back glass panes, respectively.

$$\Delta T = -7.7275 w^3 + 15.548 w^2 - 9.5767 w + 9.5234 \quad ; (R^2 = 1) \quad (9.23)$$

$$\Delta T = -18.096 w^3 + 35.931 w^2 - 22.895 w + 13.43 \quad ; (R^2 = 1) \quad (9.24)$$

9.4.2 Winter Conditions:

The work under this section primarily aimed at uniting the cavity width for both summer and winter conditions that have a different optimum width as discussed before. Optimum size and arrangement were used for outer and inner openings as 0.1m and 0.2m; respectively. Same structure was investigated again but with new widths as following: 0.6, 0.8 and 1.0m. Glass transmittance fixed to $t=0.8$.

- **Airflow rate:**

In winter, while effect of changing the cavity's width with fixed flow vents on office's ventilation would be relatively small; i.e. increased by 6% when width changed from 0.2m to 1.0m, corresponding change for cavity's flow would be more evident and around 58.5% for the same change range; Figure 9.19. This is expected as the change was in cavity structure leading to less flow resistance along its height rather than changing the vents to indoor.

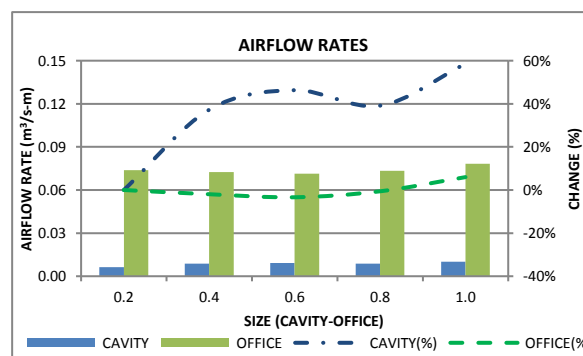


Figure 9.19: airflow rates and changes for both office and entire structure, with varied cavity width and fixed opening size to 0.1m and 0.2m for outer and inner, respectively.

Whereas maximum flow rates for office ($0.078\text{m}^3/\text{s-m}$) and cavity ($0.01\text{m}^3/\text{s-m}$) were with wider cavity (1.0m), lowest rate for cavity was found to be with the narrowest cavity (0.2m) and that for office was with size of 0.6m after which flowrate started to increase toward smaller cavities drawing different trend for changes compared to cavity. For instance, the case of 0.2m offered higher office's flow rate than case of 0.6m. Velocity contours showed that with the smallest cavity, having shortest distance, air would pass through the second vent with relatively higher angle compared to the size of 0.6 and continue upward along the inner glass's surface as being heated up before turning down again; Figure 9.20. Additional heat gained through flowing along the glass surface would give the flow an extra force so more air being dragged to inside compared to 0.6m-cavity. Furthermore, with smallest cavities, the short distance would prevent the flow from turning upward inside the cavity but continuing toward the indoor thus office ventilation shares a larger part of overall flow with smallest cavities (92% with 0.2m) compared to largest ones (88.6% with 1.0m).

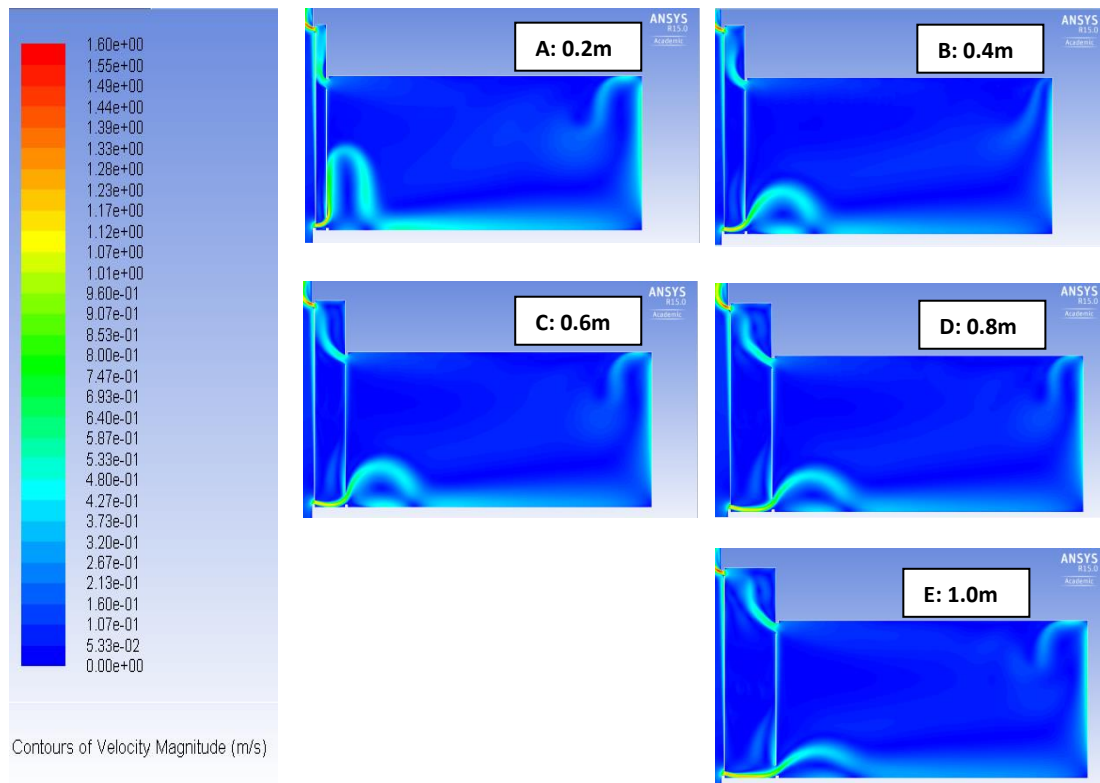


Figure 9.20: contours of velocity magnitude (m/s) for structure with different cavity sizes (0.2-1.0), where openings sizes fixed to its optimum.

Furthermore, in winter, adjusting the cavity width with fixed openings would have a slightly higher influence on office's ventilation compared to summer; e.g. when width changed from 0.4m to 1.0m, indoor flow increased by 8.1% for winter compared to 6% for summer. However, for same change range, cavity's flow rate would be less influenced under winter compared to summer, i.e. 15.5% and 27.1%, respectively. Indeed, when both winter and summer performances are being compared, one more thing should be taken into consideration that flow vents are not typical under both scenarios as summer vents' size (both out & inn: 0.4m) was four times the outer size for winter (out: 0.1m; inn: 0.2m). And, this is why the influence on cavity's flow for winter was much lower than summer as flow resistance accompanied with small winter's vents would be much higher than summer.

Following equations (9.25) and (9.26) could be used to express the correlation between the adjustable widths and calculated airflow rates for office and cavity, respectively.

$$Q_{\text{office}} = 0.0002 w^3 + 0.0007 w^2 - 0.001 w + 0.0754 \quad ; (R^2 = 0.9955) \quad (9.25)$$

$$Q_{\text{cavity}} = 0.0361 w^3 + 0.0709 w^2 - 0.045 w - 0.0001 \quad ; (R^2 = 0.9929) \quad (9.26)$$

- **Temperatures:**

For this work, indoor air temperatures were averaged for three different heights (0.5, 1.6 and 2.5m) along the office depth (6m depth); then the total average was calculated for the three averages for each size as shown in Figure 9.21. Results showed that temperature would decrease with increasing cavity size except for largest cavity (1.0m). From another perspective, both smallest and largest cavities (0.2m and 1.0m) would have highest total average temperatures although they would provide highest office's flow rate as discussed before.

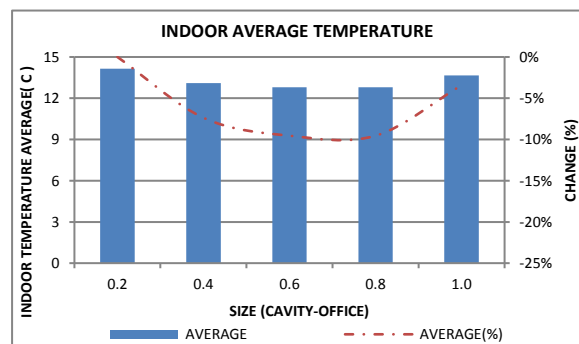


Figure 9.21: indoor temperature at height of 1.6m, with varied cavity width and fixed opening size to 0.4m.

Inner surface temperatures for both glass panes would be affected by changing cavity width while openings fixed to one size. This influence would be larger for middle-size cavities with a change up to 10% and 15%; respectively; Figure 9.22.

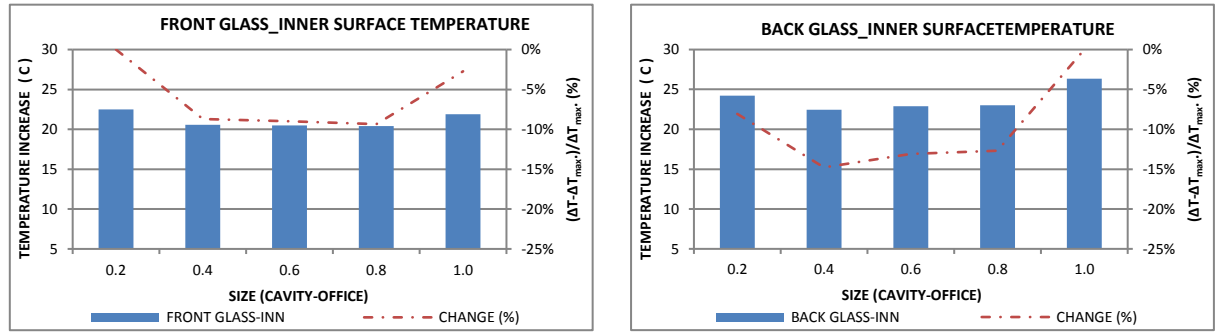


Figure 9.22: variation in surface temperature increase (surface temperature-outdoor temperature) averages for inner surface of outer glass (left) and inner glass (right) panes, with changed cavity width and fixed opening size.

Equations (9.27) and (9.28) represent the relationship between the adjustable widths and calculated surface temperatures for outer and inner glass panes, respectively.

$$\Delta T = 90.885 w^4 - 221.55 w^3 + 198.67 w^2 - 77.883 w + 31.766 \quad ; (R^2 = 1) \quad (9.27)$$

$$\Delta T = 159 w^4 - 370.97 w^3 + 313.79 w^2 - 112.31 w + 36.849 \quad ; (R^2 = 1) \quad (9.28)$$

To conclude, while widest cavity (1.0m) seems to be the best particularly for ventilation (0.078m³/s-m) and second for indoor air temperature (13.7°C), size of 0.6m was selected to merge with summer conclusion as well as it still provides sufficient ventilation and maintain indoor average temperature around 12.8°C in winter. In addition, wider cavity means less usable perimeter areas. The difference in temperature (0.9°C) between 0.6m and 1.0m could be compensated for by internal gains.

CHAPTER 10 DOUBLE SKIN FAÇADE (DSF)

INTEGRATED WITH SLATS

The work listed under this chapter aimed to further investigate and then optimize the installation of integrated shading slats inside the cavity of full mode (i.e. attached with office space). The configuration of the full model (office space and cavity) was based on the conclusion of the previous chapter. Variables for integrated slats were based on conclusions from precedent chapters in this work. Four main characteristics were again investigated in this chapter: size & angle, surface emissivity and position of slats. Simple flat shading devices (i.e. design#1) was chosen for this work. However, it is worth mentioning that the conclusion of this chapter and any following outcomes should mainly be limited to the simple flat design (of integrated slats) unless stated otherwise.

10.1 Size and Inclination Angle:

10.1.1 Summer Conditions

This part of the work aimed to investigate the influence attributed to integrated slats' characteristics on both airflow and thermal performance of cavity and indoor space. Here, the relative size of integrated slats was investigated with two different inclination angles: 45 and 60 degrees. Those angles were selected based on conclusions from the previous similar study, conducted within this work for the simplest cavity. Both cavity width and openings size were fixed to 0.4m. Other parameters like glass transmittance and slats emissivity were kept constant during this work and set to 0.8 and 0.2; respectively. Also, a slat set was placed at the middle axis of cavity dividing it into two sub-cavities with the possibility of air moving in-between.

- **Airflow rate:**

Results showed that relative size of integrated slats would have limited impact on overall airflow rates that would be decreased by 10% for actual size equals half of cavity width (50%) but with an inclination angle of 45 degrees; Figure 10.1. However, corresponding influence on indoor ventilation would be even smaller and less uniform. This is mainly caused by the non-uniform arrangement of integrated slats (different in size then offset) placed in front of both office inlets and outlets, which led to relatively different openness ratios and consequently non-uniform flow resistance; Figure 10.3. However, both the changes in openness ratio and office ventilation were relatively small as maximum was about 5%. Average ventilation rate for office would be around $0.053\text{m}^3/\text{s-m}$ which is 10 times more than minimum fresh air

requirement. However, such increase is still recommended for removing unwanted heat from indoor during hot summer times. On the other hand, the relative size of integrated slats would have an evident influence on cavity flow rate as flow would be decreased, as size increasing, with maximum drop of 20.8% for 50%-size. This relatively significant impact on cavity's flow was due to the flow resistance accompanied with the presence of slats inside.

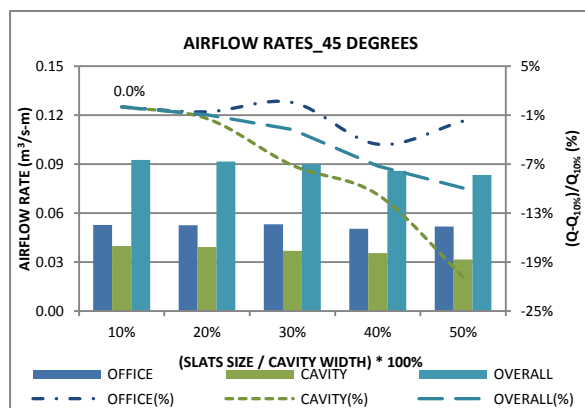


Figure 10.1: airflow rates and changes for both office and entire structure, with changes in size for 45 degrees slats.

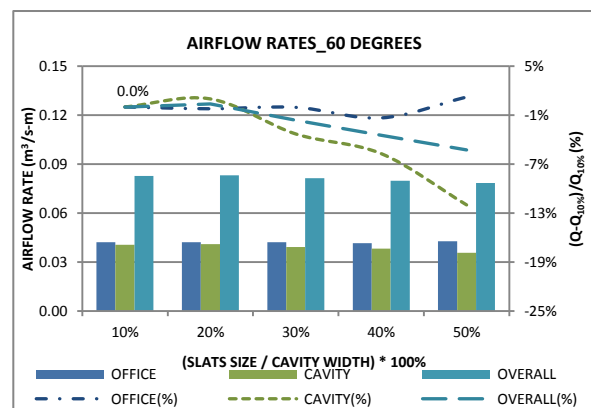


Figure 10.2: airflow rates and changes for both office and entire structure, with changes in size for 60 degrees slats.

Figure 10.2 shows findings of similar study but for slats with an inclination angle of 60 degrees. Generally, both overall and office's ventilation rates would have similar performance trends to those produced with 45 degrees. However, flow rate magnitudes (also, changes) were larger with 45° degrees as more heat would incident on inner glass (less shading factor) that heats it up while part of it penetrates toward indoors and enhance natural buoyancy. Also, the arrangement of slats with a higher angle (60° degrees) placed in front of office's inlet would have more flow resistance than in the case of 45° degrees for office's flow but less resistance for cavity flow. This is why cavity's flow rates with integrated slats of 60° degrees were larger than

those of 45° degrees while changes due to relative size increasing were smaller for the aforementioned.

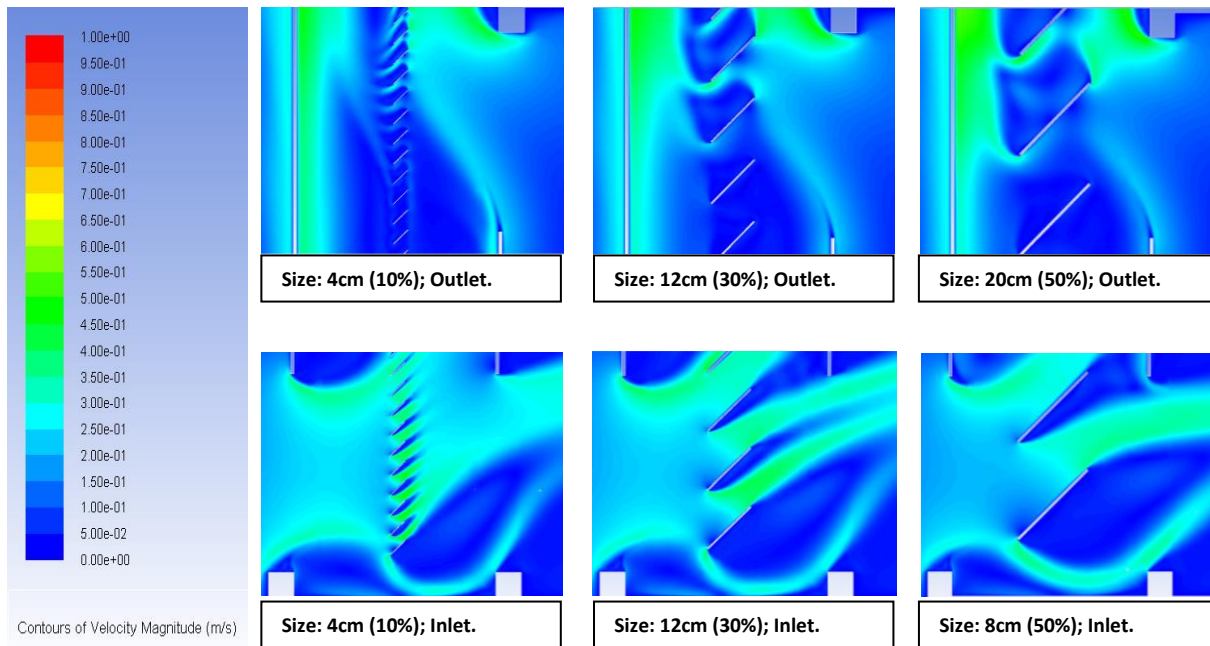


Figure 10.3: contours of velocity magnitude (m/s) at both inlets and outlets of each of 10% 30% and 50% cases; where size, offset and arrangements for 45 degrees integrated slats are shown.

Following correlations express (10.1), (10.2) and (10.3) revealed relationships between the relative size of slats (with 45° degrees) and calculated flow rate for office, cavity, and overall structure, respectively. Similarly, equations (10.4), (10.5) and (10.6) presents corresponding correlations but for slats with 60° degrees.

$$Q_{\text{office}} = 4.8796 r^4 - 5.583 r^3 + 2.1759 r^2 - 0.3383 r + 0.0699 \quad ; (R^2 = 1) \quad (10.1)$$

$$Q_{\text{cavity}} = -0.072 r^3 + 0.0217 r^2 - 0.0114 r + 0.0408 \quad ; (R^2 = 0.9885) \quad (10.2)$$

$$Q_{\text{overall}} = 0.2005 r^3 - 0.2213 r^2 + 0.0476 r + 0.0897 \quad ; (R^2 = 0.9924) \quad (10.3)$$

$$Q_{\text{office}} = 1.2619 r^4 - 1.3923 r^3 + 0.5281 r^2 - 0.0808 r + 0.0462 \quad ; (R^2 = 1) \quad (10.4)$$

$$Q_{\text{cavity}} = 0.0478 r^3 - 0.0797 r^2 - 0.0208 r + 0.0393 \quad ; (R^2 = 0.978) \quad (10.5)$$

$$Q_{\text{overall}} = 0.1698 r^3 - 0.1772 r^2 + 0.0428 r + 0.0801 \quad ; (R^2 = 0.9955) \quad (10.6)$$

- **Temperatures:**

Figure 10.4 presents indoor temperature profile at height of 1.6m along the office's depth, with integrated slats of 45° degrees. While magnitude difference was small ($<0.5^{\circ}\text{C}$), the relative change in reference to temperature increase with 10%-size was up to 13% as indoor temperature would generally increase with increasing slats' size; Figure 10.5. This was due to increasing total openness area in front of glass so more solar penetrates to inside.

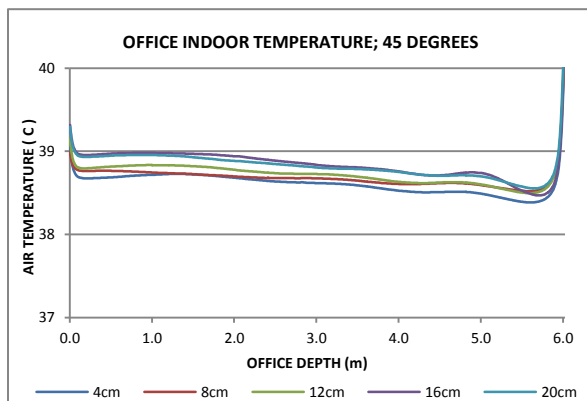


Figure 10.4: Indoor temperature at height of 1.6m for integrated slats with different sizes and angle of 45 degrees.

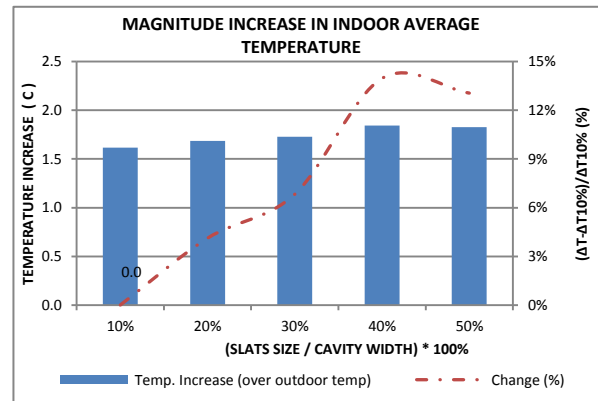


Figure 10.5: increase in indoor average temperature with relative changes at height of 1.6m for integrated slats with different sizes and angle of 45 degrees.

With slats of 60° degrees, indoor temperature would have an almost same profile as that of 45° degrees; Figure 10.6. Also, magnitude increase in averages would be around 1.5°C and relative changes from 10%-size less than 9%; Figure 10.7.

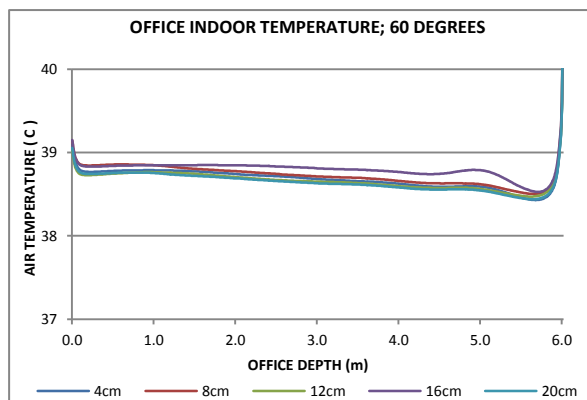


Figure 10.6: Indoor temperature at height of 1.6m for integrated slats with different sizes and angle of 60 degrees.

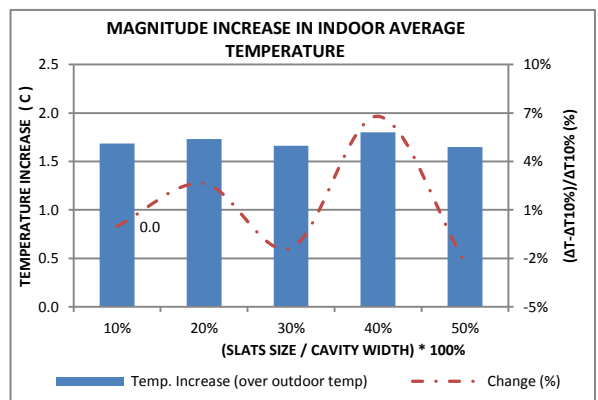


Figure 10.7: increase in indoor average temperature with relative changes at height of 1.6m for integrated slats with different sizes and angle of 60 degrees.

With inclination angle of 45° degrees, surface's temperature changes from those of 10%-size were always less than 2% except for the size of 20% (8cm) and in particular for inner glass as it dropped by 7%; Figure 9.3. Fluctuating patterns for changes in surface temperature do match, in some way, those for changes in office's ventilation rates.

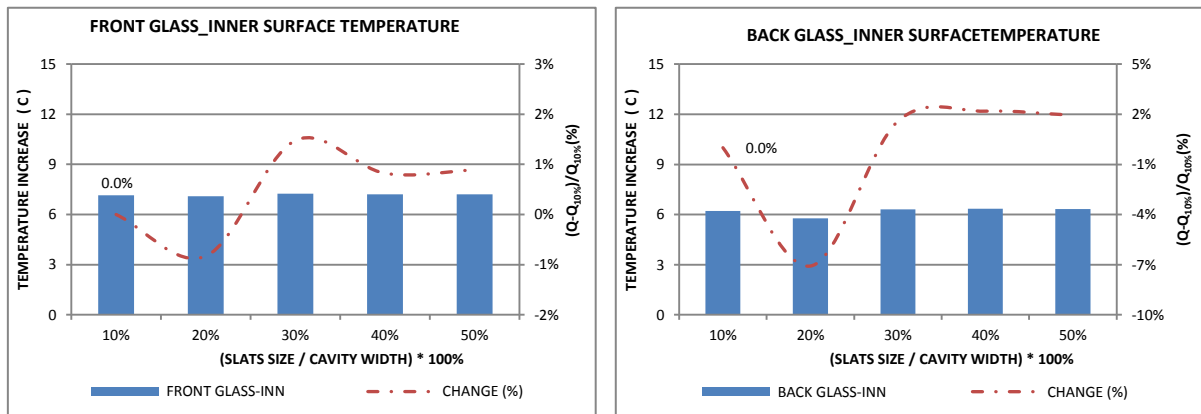


Figure 10.8: surface temperature averages for inner surfaces of outer glass (left) and inner glass (right) panes, with changes in cavity/openings size. Inclination angle 45 degrees.

Similarly, surface's temperature changes were limited and less than 2% for all sizes with an angle of 60 degrees; Figure 10.9. For outer glass, an increasing relationship was revealed compared to fluctuated one for inner glass.

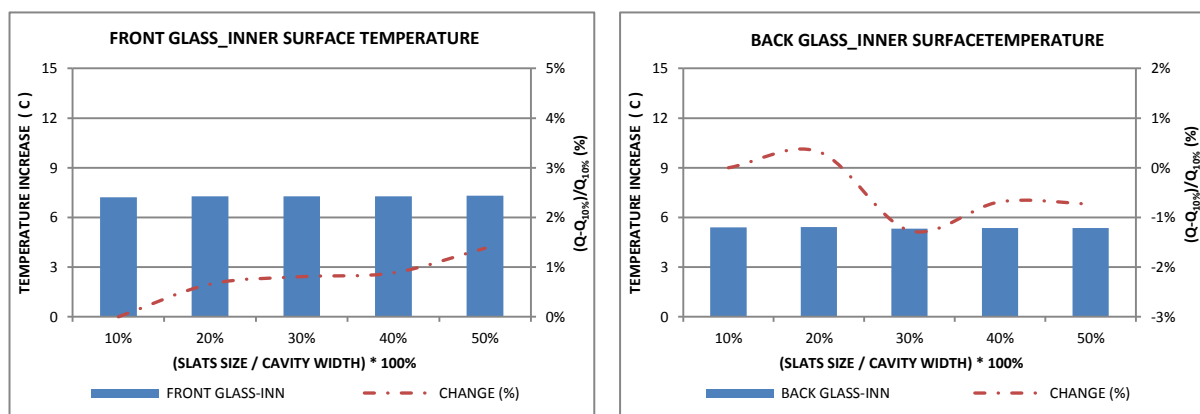


Figure 10.9: surface temperature averages for inner surfaces of outer glass (left) and inner glass (right) panes, with changes in cavity/openings size. Inclination angle 60 degrees.

Equations (10.7) and (10.8) could be used to find out relevant surface temperature increase for front and back glass panes, respectively, under the

effect of integrated slats with 45 degrees. Similarly, equations (10.9) and (10.10) would work the same but with an inclination angle of 60 degrees.

$$\Delta T_{\text{front_45}^\circ} = 291.41 r^4 - 364.12 r^3 + 156.84 r^2 - 26.53 r + 8.5644 \quad ; (R^2 = 1) \quad (10.7)$$

$$\Delta T_{\text{back_45}^\circ} = 803.94 r^4 - 1050.7 r^3 + 478.37 r^2 + 86.424 r + 4.6843 \quad ; (R^2 = 1) \quad (10.8)$$

$$\Delta T_{\text{front_60}^\circ} = 5.5517 r^3 - 5.2007 r^2 + 1.6485 r + 7.1004 \quad ; (R^2 = 1) \quad (10.9)$$

$$\Delta T_{\text{back_60}^\circ} = -154.26 r^4 + 190.87 r^3 - 81.097 r^2 + 13.454 r + 4.6843 \quad ; (R^2 = 1) \quad (10.10)$$

Based on these outcomes, and for the given cavity width of 0.4m, integrated slats with the size of 8cm (20%) and with an inclination angle of 45 degrees showed better overall performance in terms of ventilation rates and also temperatures. Also, slats with the angle of 45 degrees were preferred over 60 degrees as the aforementioned allows for better in-out visual continuity. So, the relative size of 20% of actual cavity width would be considered for further studies from now on.

10.1.2 Winter Conditions

Similar to summer, the work presented, here, aimed to show the impact of having shading slats inside the cavity on both ventilation and thermal performance of the structure in winter. In addition to inclination angles of 45 and 60 degrees, 30 degrees angle was also tested. This small angle was in response to winter sun's low angle. Slats size was fixed to agreed size after summer investigation; 12cm (20% of 0.6m cavity width). The set was placed at position P8 (clear distance from the outer glass is 8.16cm) and had an emissivity of 0.2. Cavity width was 0.6m with vents size of 0.1m and 0.2m for outer and inner skins, respectively. Other characteristics for various structure

elements were typical to those mentioned in corresponding work for summer conditions.

- **Airflow rate:**

Winter scenario results, Figure 10.10, revealed that installed slats would have more significant influence on system performance than summer scenario. This is mainly due to two reasons: low angle of sun and close position of slats (next to outer glass compared to middle position for summer). These two factors would increase the interaction between incoming solar radiation and integrated elements.

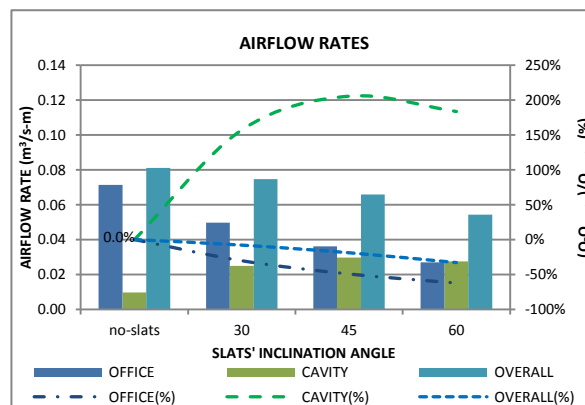


Figure 10.10: airflow rates and changes for both office and entire structure, with changes in size for 60 degrees slats.

Comparing to no-slats case, having slats with the angle of 30° degrees would lead to a drop in office ventilation by up to 30.3% while this reduction rose to 62.4% with a large angle as of 60° degrees. This is expected as less heat would be admitted to indoors with larger inclination angles. Such reduction in office ventilation should not be a problem as more heat could be used inside while sufficient fresh air being naturally supplied with a rate exceeding minimum requirements.

Alongside, cavity ventilation would be enhanced with the presence of slats. Generally, slats would absorb part of incident radiation leading to better buoyancy around. The minimum increase was 157% with 30° degrees and maximum was 206% for 45° degrees, Figure 10.10. Lowest inclination angle (30° degrees) would catch less radiation while having larger flow resistance to upward flow. On the other hand, an angle of 60° degrees would have lowest flow resistance (better than 30° degrees) but would block more radiation on the inner glass so less buoyancy in second sub-cavity resulting in lower total flow rate than 45° degrees. In total, the overall flow rate would be reduced due to the presence of slats. This reduction could reach up to 33% with 60° degree angle.

Following equations (10.11), (10.12) & (10.13) express mathematical relationships between slat's inclinations angle (θ) and calculated flow rate for different structures; i.e. cavity.

$$Q_{\text{office}} = 1\text{e-}05 \theta^2 - 0.0016 \theta + 0.0897 \quad ; (R^2 = 1) \quad (10.11)$$

$$Q_{\text{cavity}} = -2\text{e-}05 \theta^2 + 0.0015 \theta - 0.005 \quad ; (R^2 = 1) \quad (10.12)$$

$$Q_{\text{overall}} = -6\text{e-}06 \theta^2 - 0.002 \theta + 0.0848 \quad ; (R^2 = 1) \quad (10.13)$$

Figure 10.11 presents contour of velocity magnitude (m/s) for discussed cases. Both indoor airflow rate and distribution were affected by either installing the devices or adjusting its angle. With the presence of slats, flow toward indoor would be reduced as less heat would enter the space, which also reduced further with angle increasing. Also, the change in air distribution was more evident next to the back-wall and ceiling that became more obvious

with angle adjustment. For the cavity, airflow was significantly changed inside as it was divided into two sub-cavities. Airflow in back sub-cavity became turbulent, which increased with angle increasing as less heat penetrated to second glass then had a lower temperature and smaller buoyancy effect causing the air to turn down after a certain height. For the front sub-cavity, it had a relatively laminar flow that enhanced and became denser with increasing the inclination angle due to the more heat being absorbed by the slats surface.

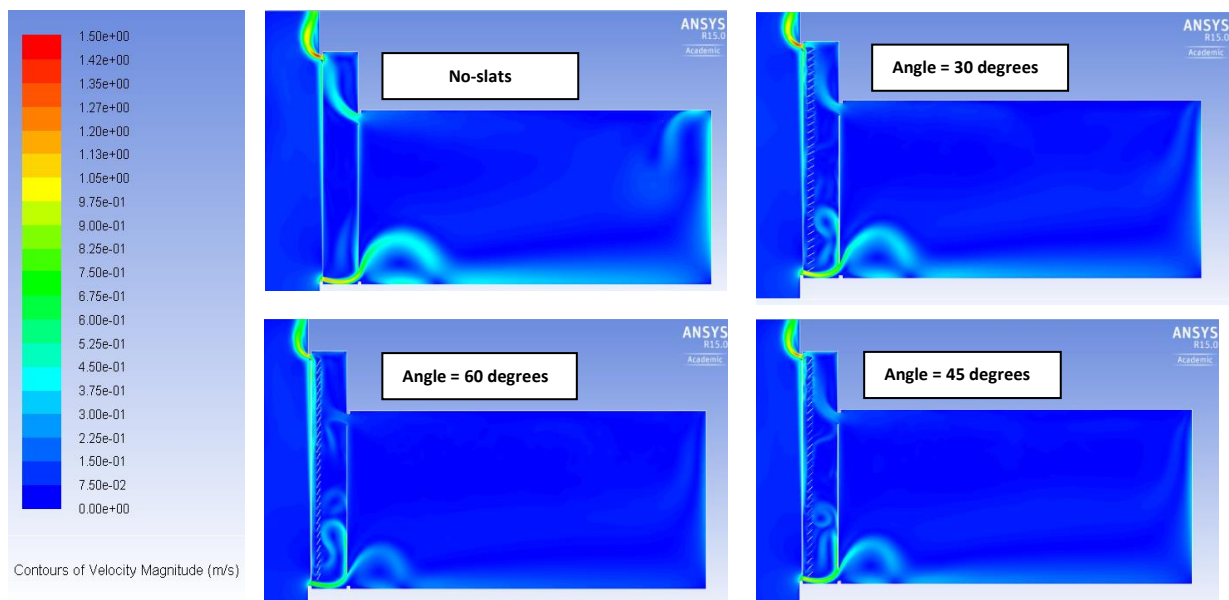


Figure 10.11: contours of velocity magnitude (m/s) showing variations in both flow rates and distribution inside cavity and attached office; under the effect of adjusting slats' inclination angles.

- **Temperatures:**

Average for indoor temperature increase (at $h=1.6\text{m}$), Figure 10.12, would diminish with the presence of slats except for inclination angle of 30 degrees as it increased by only 0.5c or 5.7%; Figure 10.13. Despite the fact that a bit less solar would be admitted to indoor with 30 degrees slats, the average temperature would slightly increase as the flow rate would significantly decrease (30.3%) due to additional flow resistance at offices'

vents leading to more accumulated heat inside. For a large angle of 60 degrees, indoor average temperature dropped by 50.4%, in reference to no-slats case, as less solar gains were admitted with the aforementioned. This finding agrees with the significant reduction in office flow rate with large inclination angles as discussed before.

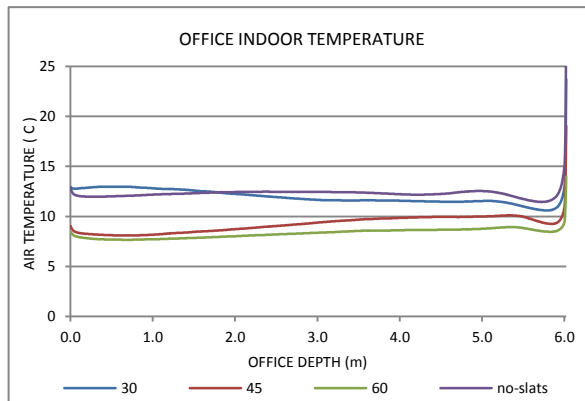


Figure 10.12: Indoor temperature at height of 1.6m with the effect of adjusting slats' inclination angles during winter.

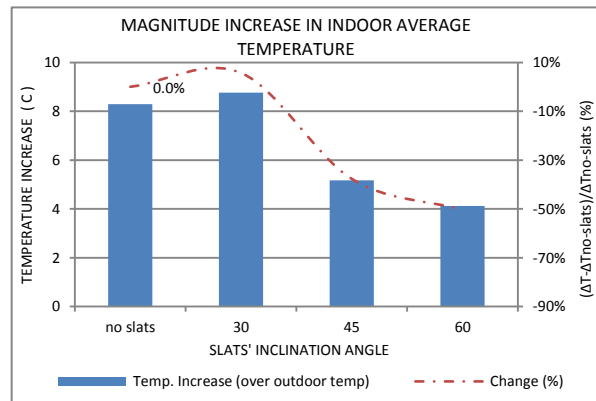


Figure 10.13: increase in indoor average temperature with relative changes at height of 1.6m with the effect of with adjusting slats' inclination angles during winter.

Outer glass's surface temperature would decrease up to 3.3% for all angles except for 45° degrees at which it would increase by <1%; Figure 10.14. Regarding inner glass, the change trend was more obvious as surface average temperature decreased as angle increased. This decrease would reach 56.7% with 60° degrees angle. Such decrease is expected as less solar gain incident on back glass pane with higher inclination angles.

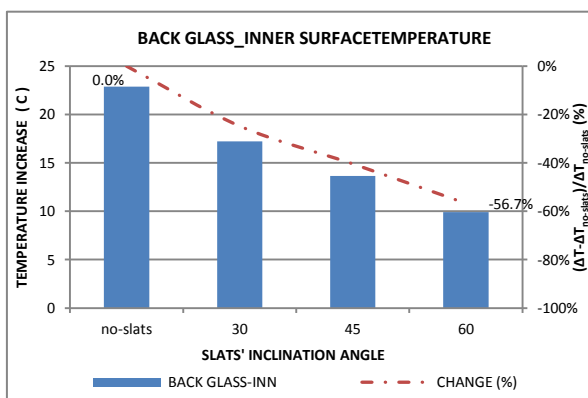
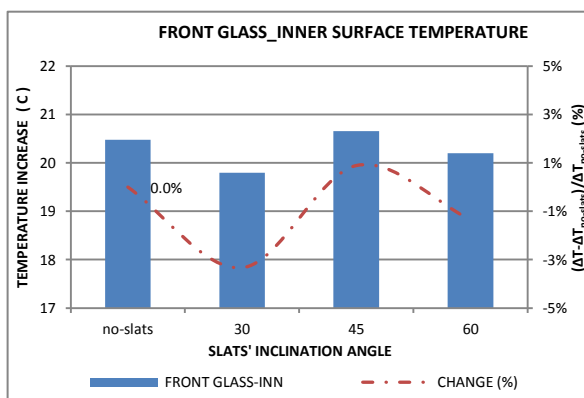


Figure 10.14: surface temperature averages for inner surfaces of outer glass (left) and inner glass (right) panes, with the effect of adjusting slats' inclination angles during winter.

For cases with integrated slats, the increase in surface's average temperature for front glass could be estimated using the revealed polynomial equation (10.14). Also, a linear relationship (10.15) was revealed for the back glass. In general, more cases (points) are needed to confirm such relationships.

$$\Delta T_{\text{front}} = -0.0029 \theta^2 + 0.2783 \theta + 14.092 \quad ; (R^2 = 1) \quad (10.14)$$

$$\Delta T_{\text{back}} = -0.2437 \theta + 24.549 \quad ; (R^2 = 0.9999) \quad (10.15)$$

Referring to these results, installing shading slats at angle of 30 degrees would produce best thermal conditions as well as maintain better ventilation rate. So, an angle of 30 degrees was selected for further investigation from now on for winter.

10.2 Slats' Surface Emissivity:

10.2.1 Summer Conditions

This work was conducted to explore the effect of integrated slats' surface emissivity on thermal and flow performance of cavity and the space behind. Cavity width was finally set to 0.6m instead of 0.4m as concluded from relative part of work regarding uniting its width for both summer and winter conditions. Glass transmittance was set to 0.8. Those slats had a size of 12cm and inclination angle of 45 degrees. Slats were placed at the middle of the cavity; this position is denoted hereafter as P5. Three different values for emissivity were investigated, which were 0.2, 0.5 and 0.8.

- **Airflow rate:**

Results revealed that ventilation would be reduced for office while increased for cavity itself. As a result, the overall rate would be changed very little. However, all these changes are related to the value of emissivity; Figure 10.15. Several reasons would contribute to such drop in office ventilation, including the reduction in solar gains penetrating to indoor and additional flow resistance at its inlet and outlet.

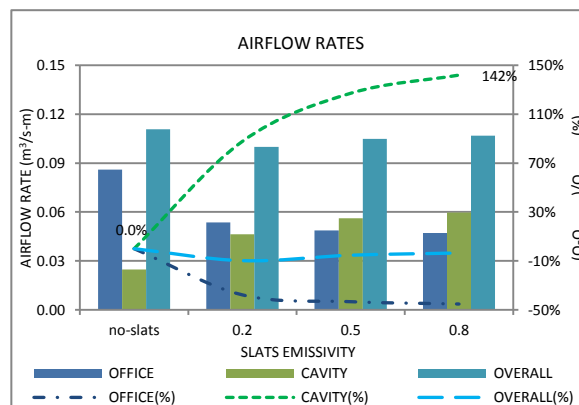


Figure 10.15: airflow rates and changes for both office and entire structure, with changes in integrated slats emissivity.

Moreover, office's flow rate would be reduced further by increasing surface emissivity; as more heat being absorbed by the integrated slats with higher emissivity resulting in less heat being transferred toward indoor thus less buoyancy force available. With emissivity of 0.8, office ventilation dropped by 45.3% compared to 37.8% with emissivity of 0.2; all in reference to no-slats case. At the same time, cavity flow rate increased as slats absorbing more solar gains then enhance natural buoyancy inside it; this increase could reach 142% with emissivity of 0.8; in reference to no-slats case.

Overall flow rate (office + cavity), would slightly be affected with emissivity of 0.8, just 3.5%. However, this change would reach about 10% with the lowest emissivity. Generally, the lowest emissivity (0.2) is recommended for daylighting purposes, thus was initially selected.

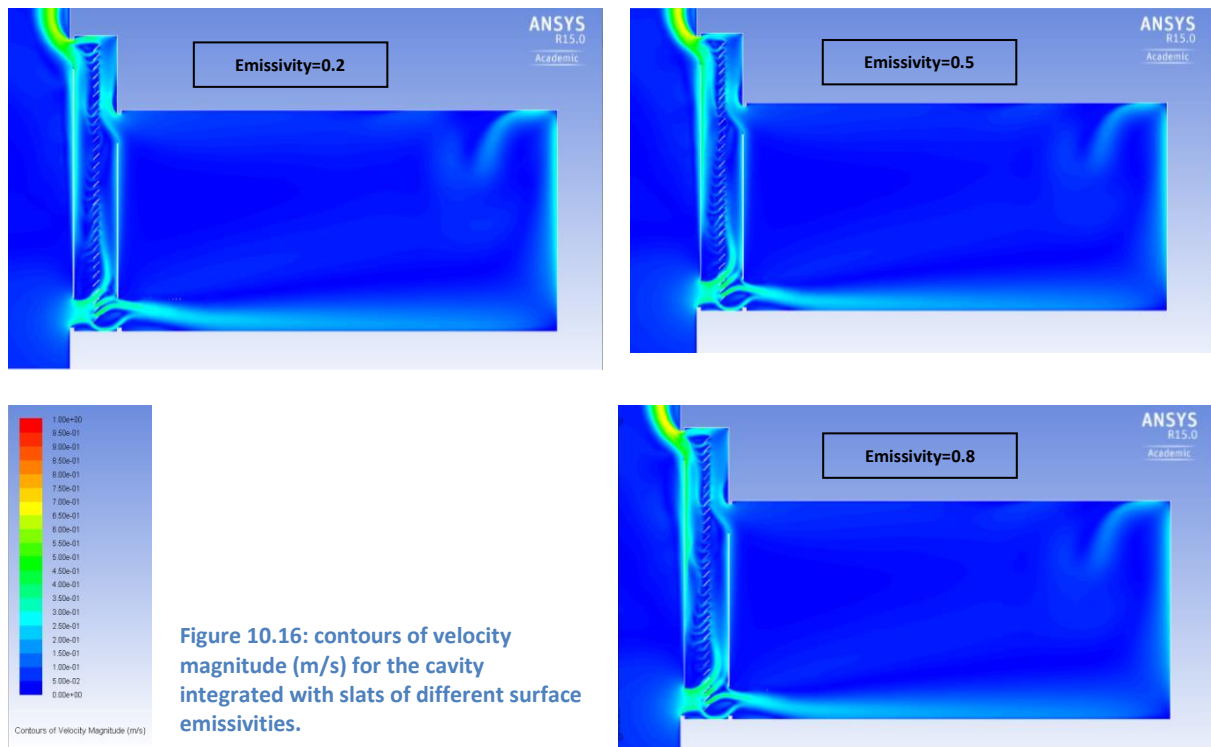
Revealed equations (10.16) to (10.18) express the mathematical relationship between surface emissivity (ϵ) of integrated slats and calculated airflow rate for the given part of the structure as denoted; e.g. Q_{office} : airflow rate for the office.

$$Q_{\text{office}} = 0.0175 \epsilon^2 - 0.0282 \epsilon + 0.0585 \quad ; (R^2 = 1) \quad (10.16)$$

$$Q_{\text{cavity}} = -0.0336 \epsilon^2 + 0.0559 \epsilon + 0.0365 \quad ; (R^2 = 1) \quad (10.17)$$

$$Q_{\text{overall}} = -0.0161 \epsilon^2 + 0.0277 \epsilon + 0.095 \quad ; (R^2 = 1) \quad (10.18)$$

As shown in Figure 10.16, indoor air distribution is nearly the same with slight variations that could be a result of turbulent flow. Cavity flow was more intense with emissivity of 0.8, particularly inside the cavity.



- **Temperatures:**

Indoor temperature average would slightly increase with the integrated slats; Figure 10.17. The increase depends on the surface emissivity of those slats. Although indoor gain heat is expected to be minimized with installed shading elements thus a drop in indoor temperature would be expected, the temperature increased instead mainly due to considerable reduction in the ventilation rate as discussed before. Then, as a result, a bit heat is being accumulated inside leading to a slight increase in temperature. To overcome this issue, office's vents should be kept free of any obstacles so have less flow resistance or opening size could be increased.

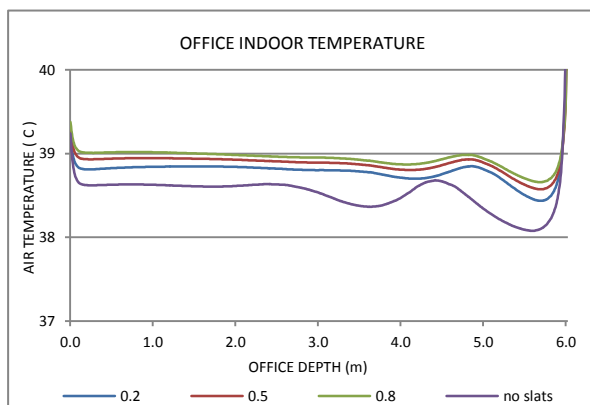


Figure 10.17: Indoor temperature at height of 1.6m for integrated slats with different surface emissivities for slats.

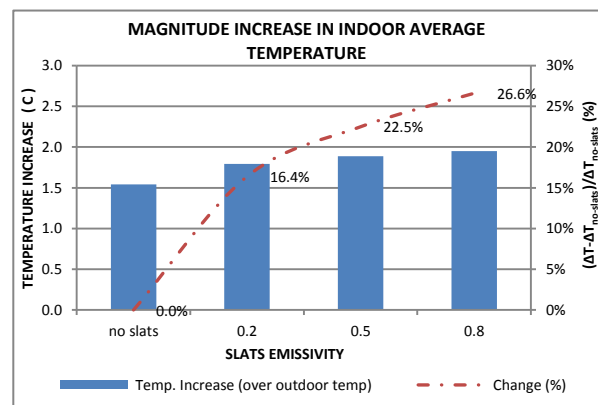


Figure 10.18: increase in indoor average temperature with relative changes at height of 1.6m for integrated slats with different surface emissivities.

For a better explanation, Figure 10.18 presents both magnitude and relative increase in indoor temperature with reference to no-slats case. Whereas having slats with low emissivity as of 0.2 would cause an increase of 16.4%, this increase would be more as of 26.6% with higher emissivity, 0.8. Furthermore, slight variations are seen for indoor temperature under the effect of different emissivities while it is clearer for cavity structure itself; Figure 10.20.

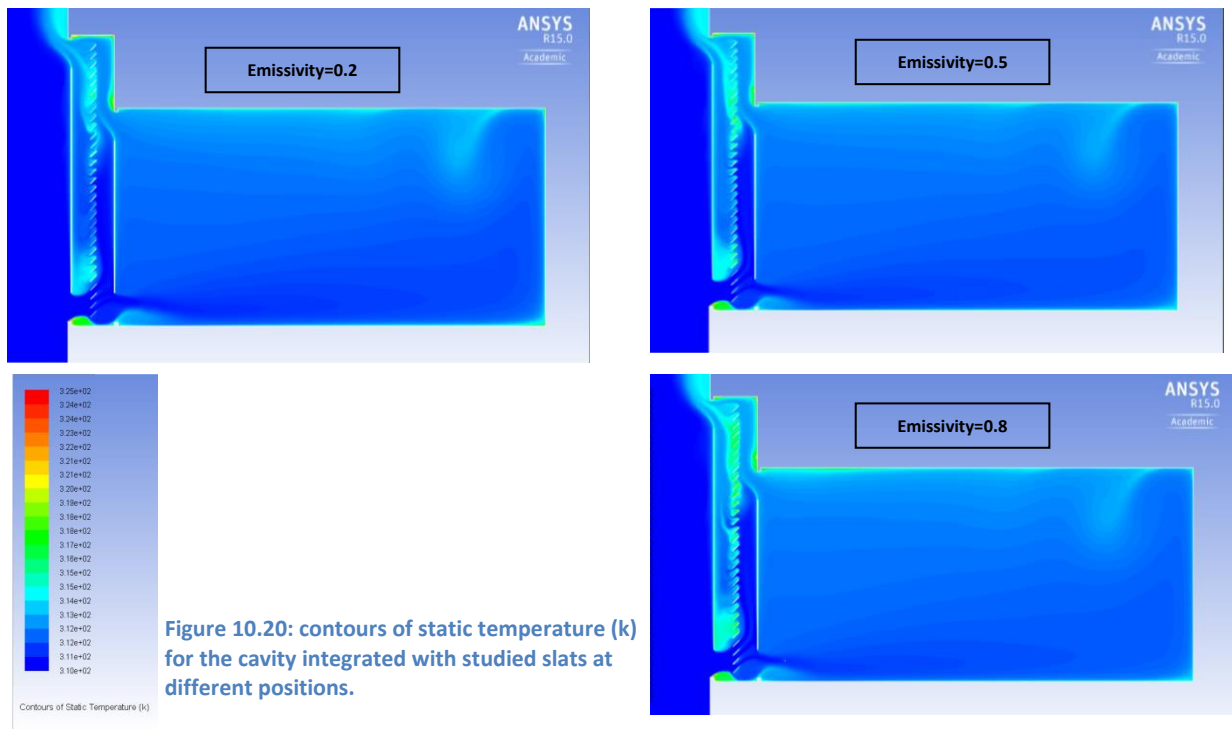


Figure 10.20: contours of static temperature (k) for the cavity integrated with studied slats at different positions.

Results showed that surface temperature would drop with installing shading slats inside the cavity, Figure 10.19; as part of solar gains either reflected to either side or absorbed by slats' surface before being removed through convection process. However, this change was found to be limited for outer glass pane, <7%, compared to inner one, maximum about 32%. The relatively small influence on outer glass was due to the fact that it would receive solar radiation first before being interfered by the slats so less influenced by the presence of these elements in contrast with the inner glass where it was partially blocked.

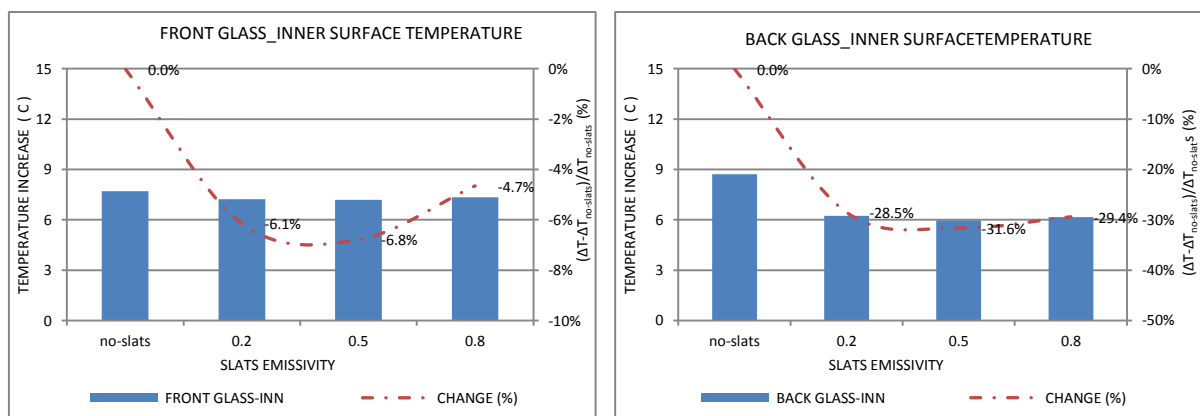


Figure 10.19: surface temperature averages for inner surfaces of outer glass (left) and inner glass (right) panes under the effect of varied slats surface emissivity; and relative changes in reference to no-slats case.

Shown expressions (10.19) to (10.21) could be used for predicting corresponding surface temperatures of different elements as denoted by each expression. Similarly, equation (10.22) would give the increase in indoor temperature average along the office depth at height of 1.6m.

$$\Delta T_{\text{front}} = 1.1887 \varepsilon^2 - 0.9965 \varepsilon + 7.3836 \quad ; (R^2 = 1) \quad (10.19)$$

$$\Delta T_{\text{back}} = 2.5783 \varepsilon^2 - 2.7056 \varepsilon + 6.6704 \quad ; (R^2 = 1) \quad (10.20)$$

$$\Delta T_{\text{slats}} = -5.6322 \varepsilon^2 + 11.52 \varepsilon + 3.2155 \quad ; (R^2 = 1) \quad (10.21)$$

$$\Delta T_{\text{indoor}_h=1.6\text{m}} = 0.2621 \varepsilon + 1.7447 \quad ; (R^2 = 0.9875) \quad (10.22)$$

This reduction for outer glass temperature could also be interpreted as cavity airflow would significantly be enhanced leading to the efficient removal of heat thus cooling down surfaces temperature. Another contributed reason could be the surface temperature of slats, depending on its emissivity, which determines the radiation exchange efficiency with outer glass based on the temperature difference. For instance, slats surface temperature found to be smaller than inner glass temperature for emissivity of 0.2.

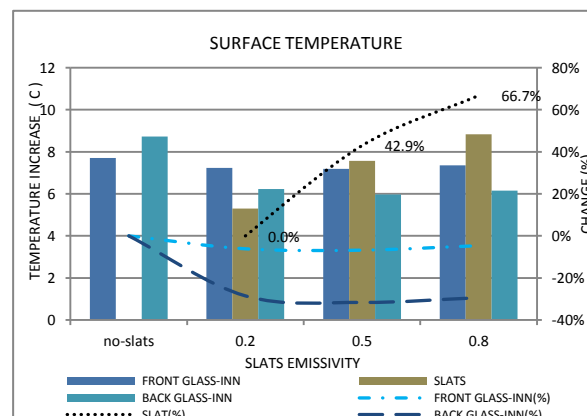


Figure 10.21: Temperature averages for outer glass's inner surface, inner glass's inner surface and slats' surface under the effect of varied slats surface emissivities. Relative changes are in reference to no-slats case for glass surfaces; and in reference to emissivity of 0.2 for slats surface; all for summer conditions.

Figure 10.21 shows surface temperature averages, and relative changes, for the three main structure's components: outer glass, inner glass, and integrated slats.

To conclude, having slats would cause a reduction in both office and overall ventilation but an increase for cavity itself. Indoor temperature average would experience a slight increase that might not be directly contributed to the presence of slats within the cavity, in general, rather than flow resistance at vents in particular. Inner glass's surface temperatures would drop significantly. In addition to thermal performance, the importance of installing those slats emerges from their role in controlling daylight and enhancing its quality, especially with more advanced elements. Finally, among tested values, the emissivity of 0.2 would provide higher office ventilation and then lowest indoor average temperatures even though it had a slightly higher inner glass surface temperature. Also, it would perform better in reflecting daylight toward the indoors.

10.2.2 Winter Conditions

The work, in this section, shows the effect of varied surface emissivities for integrated slats' surfaces on thermal and flow performance of the given system in winter. Cavity had a width of 0.6m and a glass transmittance of 0.8. Integrated slats had the size of 12cm and inclination angle of 30 degrees placed at position P8 (next to outer skin). Emissivities of 0.2, 0.5 and 0.8 were investigated.

- **Airflow rate:**

As for summer conditions, office's ventilation in winter would be reduced with higher slats emissivities as more heat being absorbed by those elements so less being reflected to inside. While ventilation dropped by 29.9% with emissivity of 0.2, this reduction went down to 57.5% with emissivity of 0.8; Figure 10.22. Consequently, cavity flow increased dramatically from 0.01m³/s-m with no integrated slats up to 0.038m³/s-m with emissivity of 0.8. As a result, the total flow rate would reduce by a maximum of 15.4% with the highest emissivity. The lowest emissivity of 0.2 would lead to a drop of 8.2% in overall ventilation, however, it is still recommended for better daylighting purposes.

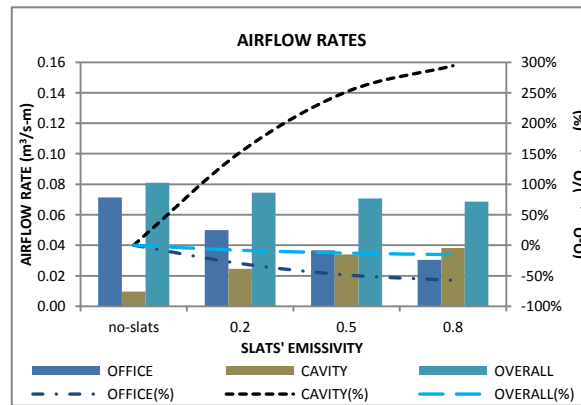


Figure 10.22: airflow rates and changes for both office and entire structure, with changes in integrated slats emissivity.

To predict discussed airflow rates for further emissivity values (ϵ), following expressions (10.23) to (10.25) could be used.

$$Q_{\text{office}} = 0.0399 \epsilon^2 - 0.0727 \epsilon + 0.063 \quad ; (R^2 = 1) \quad (10.23)$$

$$Q_{\text{cavity}} = -0.0304 \epsilon^2 + 0.0533 \epsilon + 0.015 \quad ; (R^2 = 1) \quad (10.24)$$

$$Q_{\text{overall}} = 0.0095 \epsilon^2 - 0.0193 \epsilon + 0.078 \quad ; (R^2 = 1) \quad (10.25)$$

Indoor air velocity would be influenced with the integrated slats. This influence would be larger with higher surface's emissivities. Clearly, flow inside the cavity would be changed dramatically and flow turbulence becomes more evident; Figure 10.23.

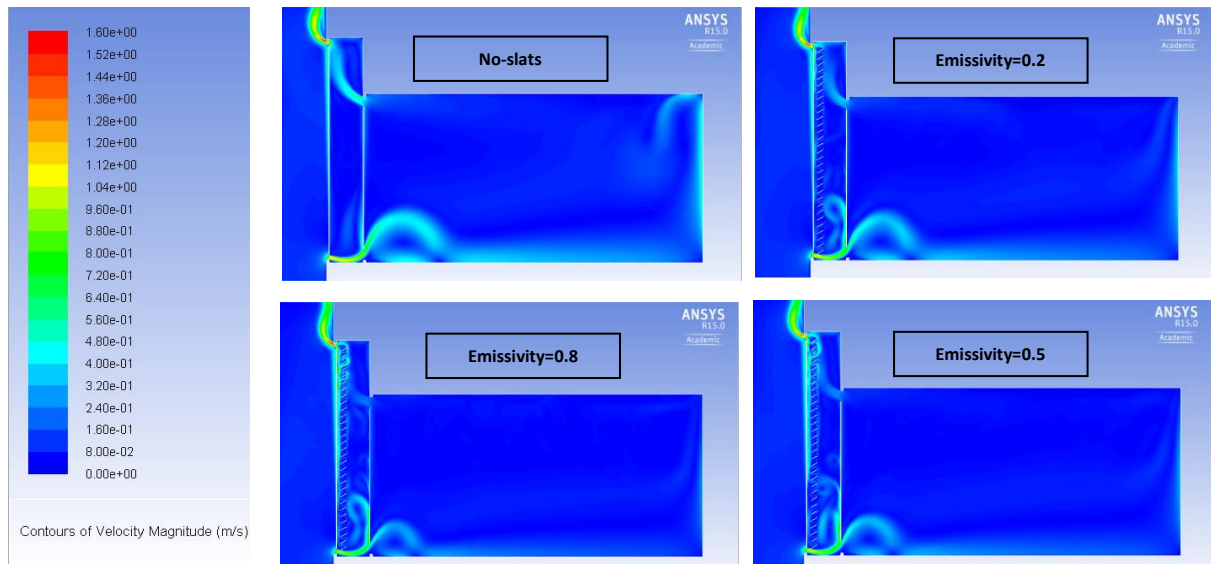


Figure 10.23: contours of velocity magnitude (m/s) for the office, under the effect of surface emissivity for cavity integrated slats.

- ### Temperatures:

Average for Indoor temperature would increase with the presence of slats, Figure 10.24, which depends on surface emissivity. Maximum increase was found to be with higher emissivity, 0.8, with a change of 28.6% and 21.7% from cases of no-slats and emissivity of 0.2, respectively; Figure 10.25. Indoor temperature would increase with slats' emissivity increase; due to expected decrease in office's ventilation.

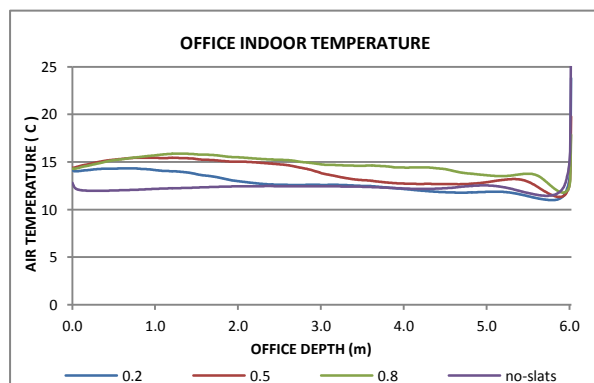


Figure 10.24: Indoor temperature at height of 1.6m for integrated slats with different surface emissivities during winter.

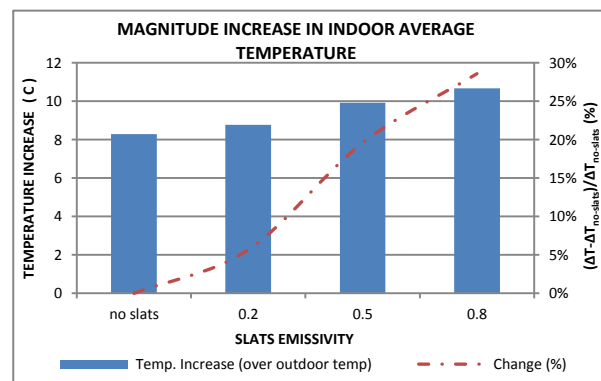


Figure 10.25: increase in indoor average temperature wit relative changes at height of 1.6m for integrated slats with different surface emissivities during winter.

Indoor Temperature contours, Figure 10.26, show the expected change inside both office and cavity with the presence of cavity slats and under the change of its emissivity. Generally, cavity temperature would increase particularly at the top as more heat was trapped inside. This would help in providing an additional thermal buffer zone between office and cold outdoor. Also, the temperature inside the office would experience more variation especially between bottom and top of the space. Such difference would increase with lower emissivities as more solar being directed to inside compared to high emissivity; i.e. more absorption by slats.

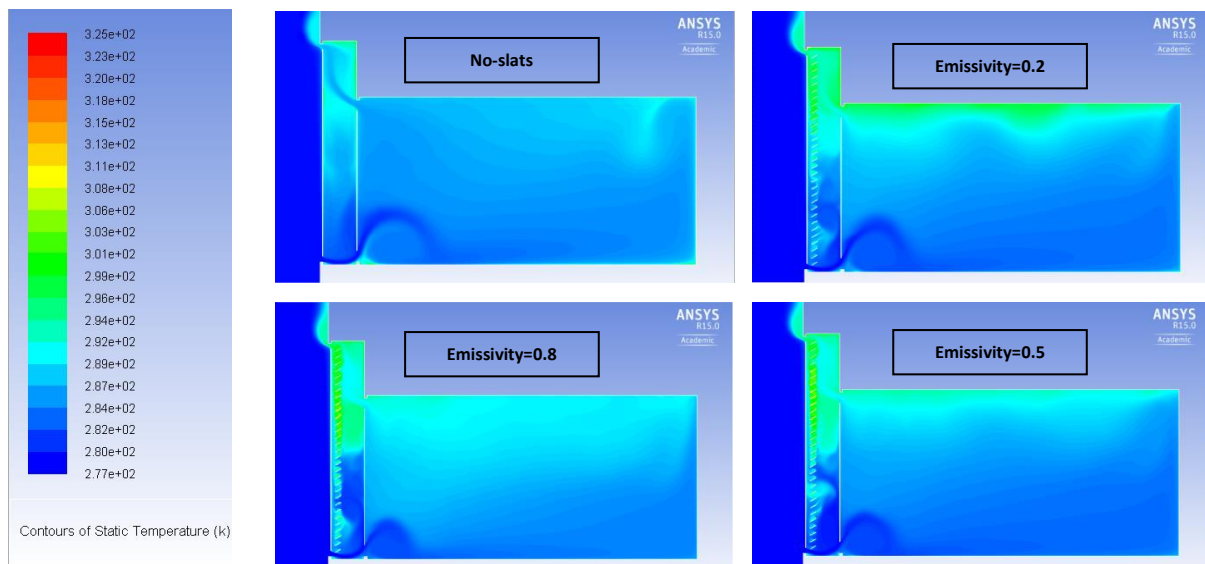


Figure 10.26: contours of static temperature (k) for the office, under the effect of surface emissivity for cavity integrated slats.

Limited variation, up to 5%, was revealed for the surface temperature of outer glass; Figure 10.27, but corresponding changes were more evident for inner glass and up to 31.5% for both 0.5 and 0.8 emissivities. Rates of change were found to be close to those for summer despite the differences in both solar magnitude and incident angles, as well as position if slats were inside the cavity. Figure 10.28 shows magnitude values and relative changes in surface temperature for glass panes and integrated slats. It is obvious that

integrated slats would experience a dramatic increase in its surfaces' temperature with a direct relationship to its emissivity while the inner glass temperature would decrease with increasing emissivity up to 0.5 and then remain constant.

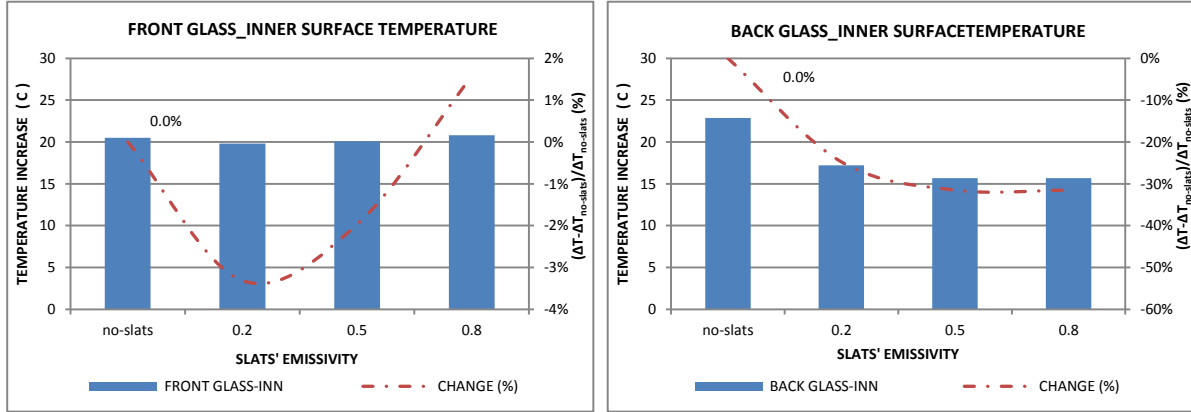


Figure 10.27: surface temperature averages for inner surfaces of outer glass (left) and inner glass (right) panes under the effect of varied slats surface emissivity; and relative changes in reference to no-slats case.

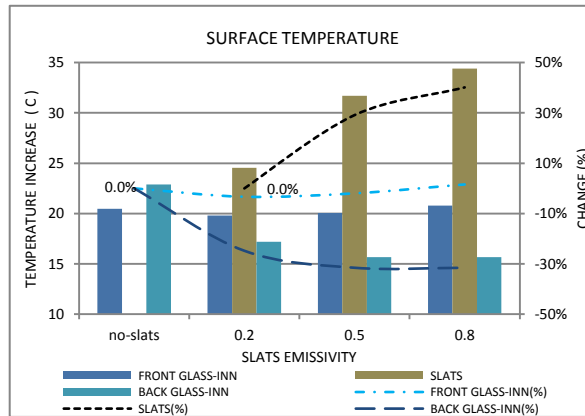


Figure 10.28: Temperature averages for outer glass's inner surface, inner glass's inner surface and slats' surface under the effect of varied slats surface emissivities. Relative changes are in reference to no-slats case for glass surfaces; and in reference to emissivity of 0.2 for slats surface; all for winter conditions.

Given equations (10.26) to (10.28) could also express the presented results for temperature increase for glass and slats surfaces in relation to their surface's emissivity (ϵ).

$$\Delta T_{\text{front}} = 2.4946 \epsilon^2 - 0.8279 \epsilon + 19.863 \quad ; (R^2 = 1) \quad (10.26)$$

$$\Delta T_{\text{back}} = 8.5563 \epsilon^2 - 11.134 \epsilon + 19.095 \quad ; (R^2 = 1) \quad (10.27)$$

$$\Delta T_{\text{slats}} = -24.686 \epsilon^2 + 41.09 \epsilon + 17.309 \quad ; (R^2 = 1) \quad (10.28)$$

Equation (10.29) expresses the increase in indoor temperature average along the office depth at height of 1.6m due to the change in slats surface emissivity (ϵ):

$$\Delta T_{\text{indoor}_h=1.6\text{m}} = -2.2669 \epsilon^2 + 5.4278 \epsilon + 7.7638 \quad ; (R^2 = 1) \quad (10.29)$$

To conclude, whereas both office and overall ventilation rates would decrease with installed slats, indoor temperature would experience an increase and surface temperature would generally drop. Compared to other investigated emissivities, the emissivity of 0.2 would produce highest office's flow rate and highest inner glass's surface temperature but lowest indoor temperature average at $h=1.6\text{m}$. However, it is still preferred for providing natural daylighting at deep parts of space (better reflecting).

10.3 Slats' Position:

10.3.1 Summer Conditions

After investigating the influence of relative size for integrated slats, its inclination angle and its surface emissivity, this part of work continued to explore the effect of its position inside the cavity. Cavity width was set to 0.6m. Inclination angle was 45° degrees and size of slats was 12cm (20% * 0.6m). Finally, glass transmittance and slats surface emissivity were fixed to 0.8 and 0.2; respectively. Three different positions were tested, which were P2, P5, and P8. For example, P2 indicates that the central axis of integrated slats' set to be placed far from the inner glass at a distance exactly equals to 20% of the cavity width; i.e. 12cm.

- **Airflow rate:**

Simulation showed that both office and overall flow rates would be reduced due to having the integrated slats within the cavity and in any position, Figure 10.29, this is due to the additionally occurred flow resistance. Obviously, this drop would be more evident for office ventilation as less heat would be transferred to indoor also its inlet and outlet would partially be blocked. However, this reduction is slightly getting smaller when the set was moved away from inner glass (38.4% for P2) toward outer glass (36.6% for P8).

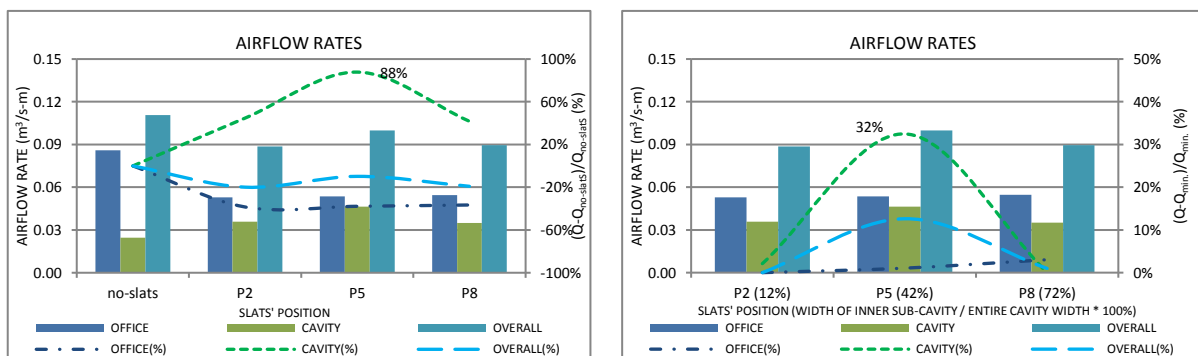


Figure 10.29: airflow rates and changes for both office and entire structure, with changes in position of integrated slats. Left: All changes in reference to no-slats case. Right: Results' changes in reference to their minimum values.

On the other hand, cavity flow would be largely enhanced by those slats as it is being heated up and causing an additional source for buoyancy driven flow. While cavity's flow could be increased by 88% with set placed at middle position (P5), this increase, however, would largely depend on such position. Moreover, as the slats' set moved to either side, flow rate decreased by about 32% in reference to P5. This is expected as new positions (P2 or P8) would cause an interfering to the boundary layers formed next to heated glass surfaces, which largely contributes to the total cavity flow rate. In total, overall flow rate would be reduced by having those elements. The smaller reduction was found to be for position P5, just less than 10%, whereas such reduction

was nearly doubled with either position P2 or P8. Based on given results, following expressions (10.30) to (10.32) were derived that could be used for further calculations on expanded range of positions (P) using the corresponding proportional width (δ) for back sub-cavity; i.e. $\delta=12\%$ or 0.12 for P2.

$$Q_{\text{office}} = 0.0027 \delta^2 + 0.0004 \delta + 0.0529 \quad ; (R^2 = 1) \quad (10.30)$$

$$Q_{\text{cavity}} = -0.1222 \delta^2 + 0.1012 \delta + 0.0254 \quad ; (R^2 = 1) \quad (10.31)$$

$$Q_{\text{overall}} = -0.1195 \delta^2 + 0.1016 \delta + 0.0783 \quad ; (R^2 = 1) \quad (10.32)$$

Figure 10.30 shows the velocity magnitude contours inside the same cavity served with same slats but with different positions. Obviously, having those elements would cause the flow to experience more turbulence. Also, additional flow resistance formed at inlets and outlets. Those slats with the current inclination angle (45° degrees) would help in turning the incoming flow upward inside the cavity.

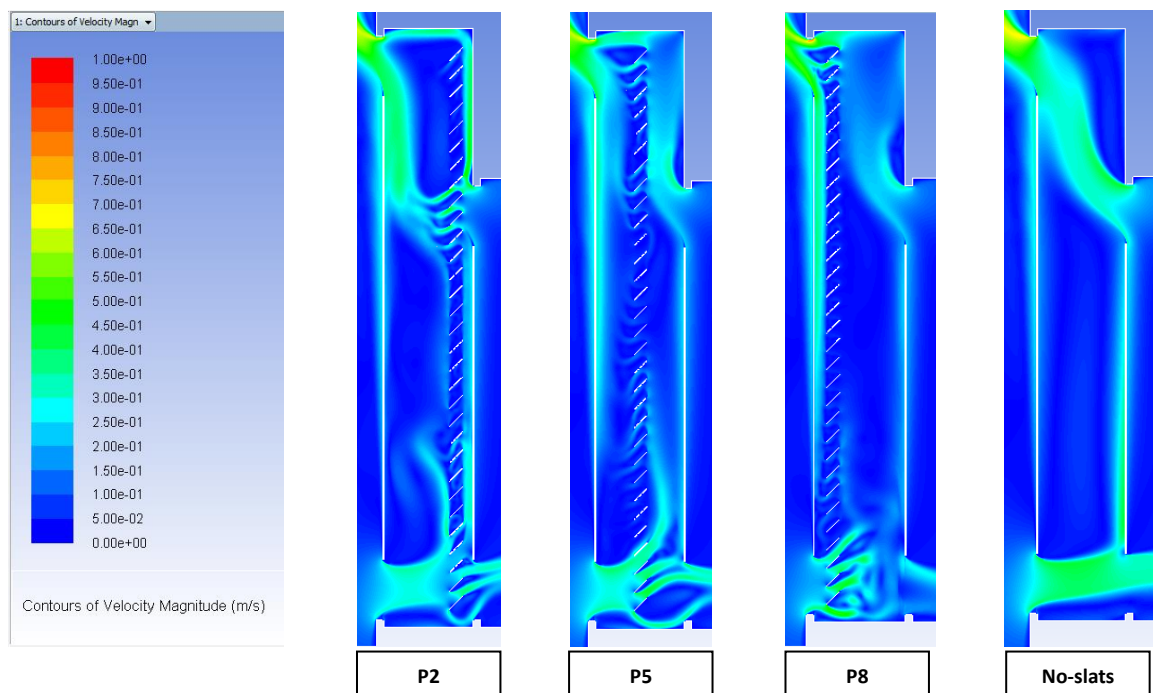


Figure 10.30: contours of velocity magnitude (m/s) for the cavity integrated with studied slats at different positions.

- **Temperatures:**

Indoor temperature at height of 1.6m is presented in Figure 10.31. In general, it would slightly increase ($<0.5^{\circ}\text{C}$) by having the integrated slats. However, this increase would relatively become larger with positions close to inner glass; i.e. P2, where it would reach 16.4%; Figure 10.32. This occurs as P2 would more heat up the inner glass as more heat trapped in-between. Furthermore, it would relatively reflect more heat toward indoor compared to far positions that would efficiently reflect incident radiation toward outdoor; e.g. slats with P8 would just increase indoor temperature by 3.6%. Despite the effect of shading and reduction for incoming solar gains, such little increase in temperature was due to the dominant reduction in office ventilation as discussed before. Removing a few slats in front of the office inlet and outlet would possibly help in recovering part of the reduced ventilation thus achieve the expectation from installing the shading elements in reducing indoor temperature in summer.

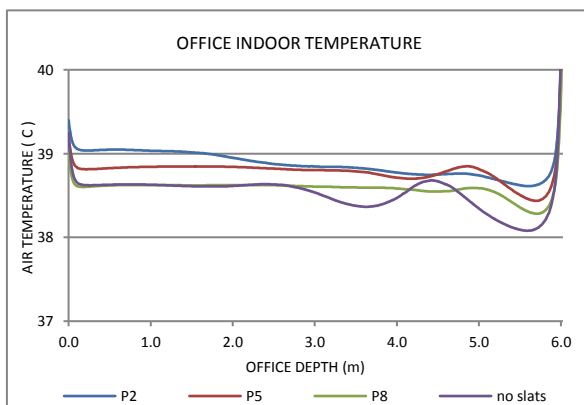


Figure 10.31: Indoor temperature at height of 1.6m for integrated slats with different sizes and angle of 45 degrees.

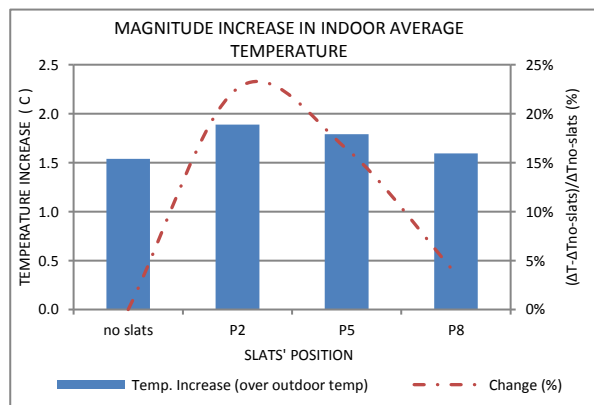


Figure 10.32: increase in indoor average temperature with relative changes at height of 1.6m for integrated slats with different sizes and angle of 45 degrees.

Following equations (10.34) to (10.36) express the relationship between calculated temperature increase (ΔT) and relative width of back sub-cavity (δ) that corresponds to position of slats' set.

$$\Delta T_{\text{front}} = 0.4753 \delta + 7.0286 \quad ; (R^2 = 0.9994) \quad (10.34)$$

$$\Delta T_{\text{back}} = 1.9231 \delta^2 - 1.9999 \delta + 6.7329 \quad ; (R^2 = 1) \quad (10.33)$$

$$\Delta T_{\text{slats}} = 7.6483 \delta^2 - 6.1043 \delta + 6.5091 \quad ; (R^2 = 1) \quad (10.35)$$

$$\Delta T_{\text{indoor}_h=1.6\text{m}} = -0.5608 \delta^2 - 0.0159 \delta + 1.8972 \quad ; (R^2 = 1) \quad (10.36)$$

Figure 10.33 presents variations in temperature contours of the cavity due to changing installation positions for its integrated slats. Also, it is clear how temperature distribution inside the cavity would be significantly changed after having the slats in particular at the bottom and top of the cavity where heat would be less trapped with the new installation.

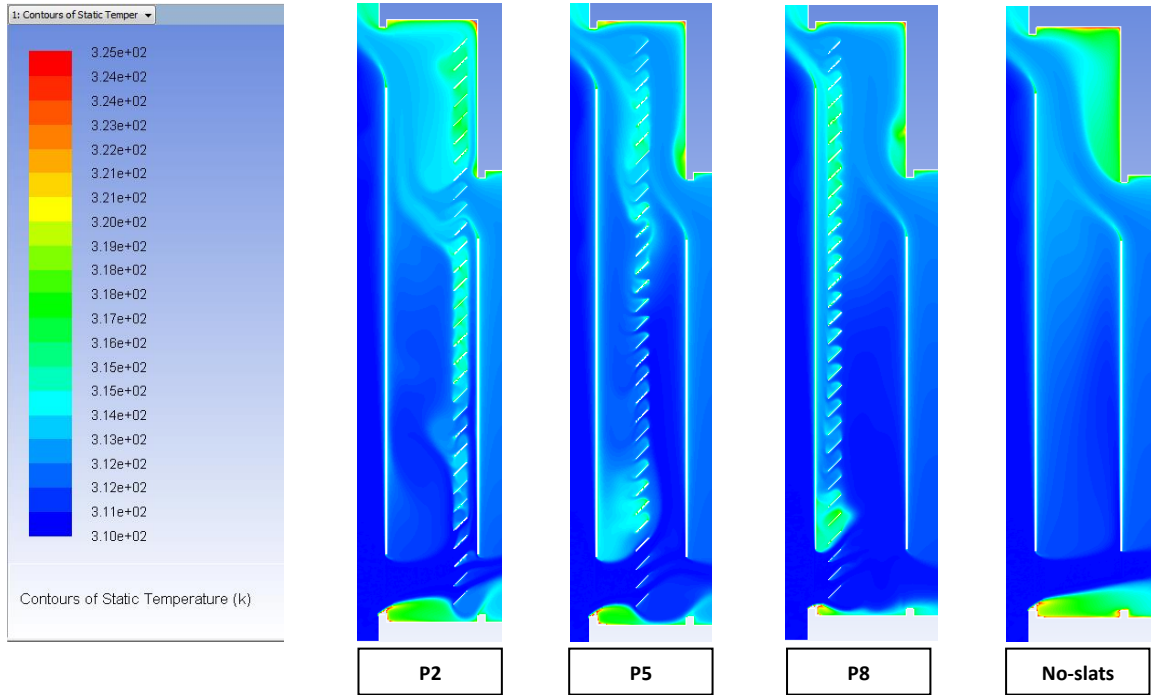


Figure 10.33: contours of static temperature (k) for the cavity integrated with studied slats at different positions.

Generally, surface temperature would drop with installing shading slats inside cavity; Figure 10.34. However, this change was found to be limited for outer glass pane (<10%) compared to inner one (up to 30%). Relatively small influence on outer glass was due to the fact that it would receive solar radiation first before being interfered by the slats. However, such reduction

could be interpreted as the slats (with emissivity=0.2) would have lower surface temperature than inner glass with no slats at all. This would produce a larger temperature difference between outer glass and slats surfaces as opposite surface. Consequently, outer glass surface would lose more heat under radiation exchange, as it has the higher temperature. For inner glass, surface temperature would be higher when slats placed at position P2 compared to P8, as the aforementioned would affect the airflow next to surface then lead to less efficient heat transfer. Slats' surface would have the lowest temperature with position P5 as the slats would be well ventilated from both sides; Figure 10.35.

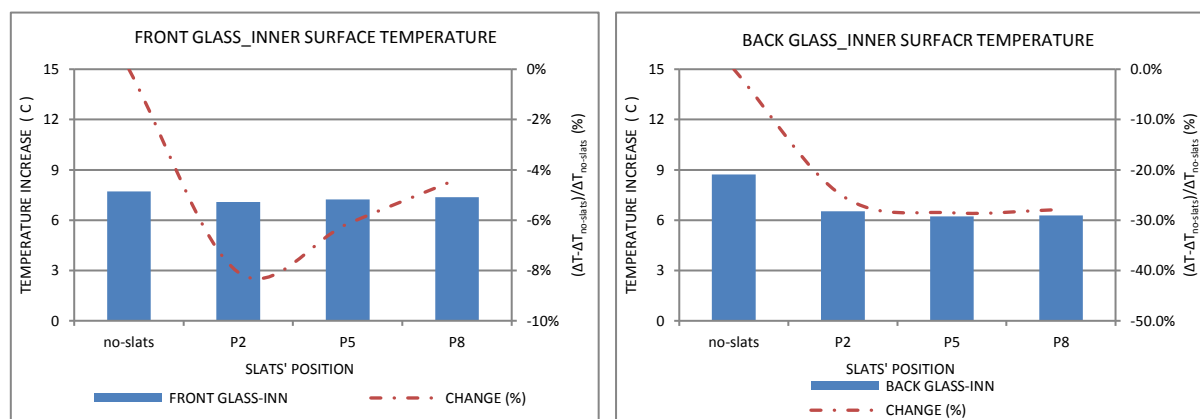


Figure 10.34: surface temperature averages for inner surfaces of outer glass (left) and inner glass (right) panes, with varied slats positions; and relative changes in reference to no-slats case.

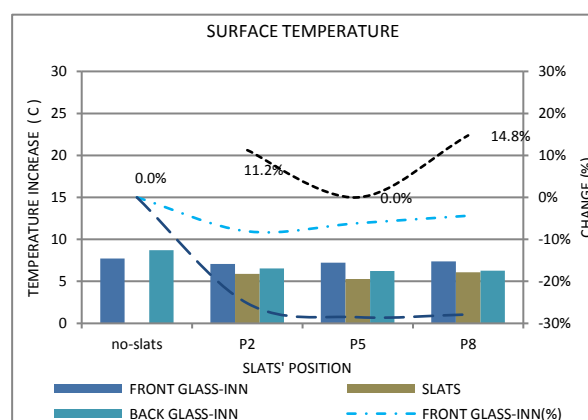


Figure 10.35: Temperature averages for outer glass's inner surface, inner glass's inner surface and slats' surface under the effect of changing integrated slats position. Relative changes are in reference to no-slats case for glass surfaces; and in reference to emissivity of 0.2 for slats surface; all for summer conditions.

To conclude, having slats would cause a reduction in both offices and overall ventilation but an increase for cavity itself. Whereas P5 would give the smallest increase to inner glass's surface temperature with a negligible change from P8, the later maintains lowest indoor temperature among shaded cavities with a slight increase of 3.6% compared to non-shaded cavity. Thus, P8 was selected to carry out the study from now on for summer conditions.

10.3.2 Winter Conditions

Three different positions were investigated for the integrated slats under winter conditions. Those are similar to summer positions: P2, P5, and P8. All other parameters, except emissivity, were kept as those used for emissivity study. However, emissivity was fixed to 0.2 as an outcome of that study.

- **Airflow rate:**

Similar to summer's findings, with the presence of cavity integrated slats, office's ventilation rate would reduce as well as overall flow; Figure 10.36. As mentioned earlier, this is due to the reduction of office's heat gain also the additional flow resistance at office vents.

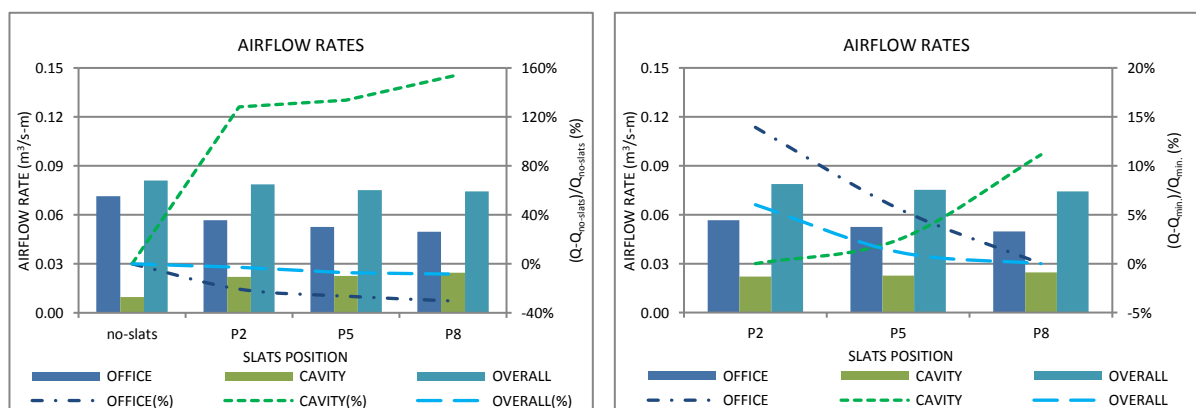


Figure 10.36: airflow rates and changes for both office and entire structure, with changes in position for integrated slats. Left: All changes in reference to no-slats case. Right: Results' changes in reference to their minimum values.

In reference to no-slats case, maximum reduction for office's ventilation, in winter, was 30.3% and associated with position P8 (close to outer glass) compared to 20.6% as minimum reduction for P2 (close to inner glass). As both had emissivity of 0.2; with the later, considerable part of reflected heat would be either directed to office or cavity unlike, for P8, being rejected to outdoor. Also, results revealed that installation position would have more significant influence on office ventilation during winter than summer as winter's sun would be much lower in position than summer one. Another reason was the change in inclination angle between summer and winter. Furthermore, cavity's airflow would generally be enhanced due to installing those elements however associated variations between different positions (about 11% from minimum) are much less than those for summer (up to 32% from minimum). As a result, the total flow rate would be reduced by 8.4% with position P8 as a maximum change from no-slats case, compared to 19.9% with position P2 for summer scenario. P2 showed better results among other positions as it would result in lowest office and overall reductions in ventilation.

Based on given results, following expressions (10.37) to (10.39) were derived that could be used for further calculations on expanded range of positions (P) using the corresponding proportional width (δ) for back sub-cavity; i.e. $\delta=72\%$ or 0.72 for P8.

$$Q_{\text{office}} = -0.0115 \delta + 0.0578 \quad ; (R^2 = 0.988) \quad (10.37)$$

$$Q_{\text{cavity}} = 0.0077 \delta^2 - 0.0024 \delta + 0.0223 \quad ; (R^2 = 1) \quad (10.38)$$

$$Q_{\text{overall}} = 0.015 \delta^2 - 0.0201 \delta + 0.0809 \quad ; (R^2 = 1) \quad (10.39)$$

Figure 10.37 shows the velocity magnitude contours inside the same cavity served with same slats but with different positions. Obviously, having those elements would cause the flow to experience turbulence. Turbulence was more obvious with position P8, in other words, when second sub-cavity had its largest width. The reason behind that is the relatively low temperature for inner glass surface (facing cavity) that would not be enough to support the air that was directed upward by the inner glass. Further details on temperature averages and changes for structure surfaces are discussed in the following section.

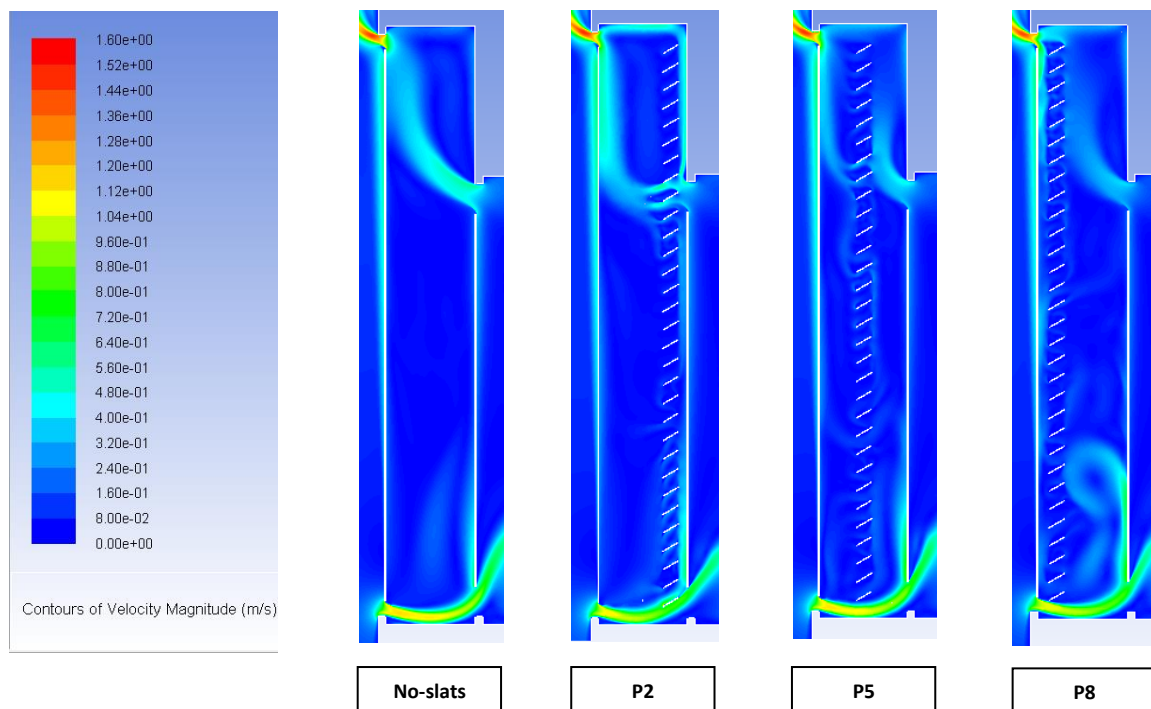


Figure 10.37: contours of velocity magnitude (m/s) for the cavity integrated with studied slats at different positions., during winter.

- **Temperatures:**

In winter, the average for indoor temperature would increase due to the presence of integrated slats and with all positions; Figure 10.38. The increase is mainly due to reduced office's ventilation rate. However, such increase

would vary depending on the position; Figure 10.39. Installing shading slats next to inner glass pane P2, would maintain indoor with relatively higher average temperature than placing those slats on the opposite side of the cavity, P8, and even middle of it, P5. For shaded cases (P2-P8), revealed temperature changes correlate with those for office's ventilation rates as both ventilation and indoor temperature would consequently decrease as width of back sub-cavity increases. This is largely contributed to the varied efficiency of slats with different positions. For instance, where those slats are installed next to outer glass, it would allow less heat penetrating to indoor then maintain lower indoor temperature and causing lower ventilation through. Figure 10.40 shows changes in temperature contours inside the cavity under the effect of various positions for slats.

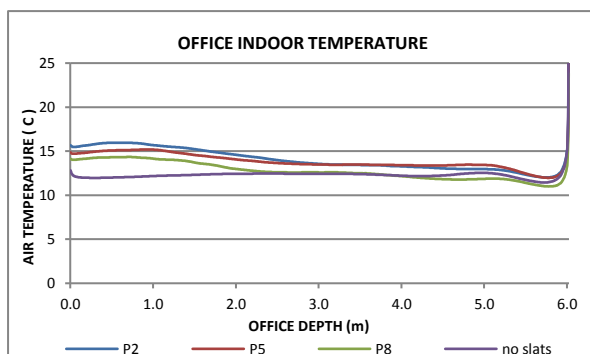


Figure 10.38: Indoor temperature at height of 1.6m with integrated slats having different positions.

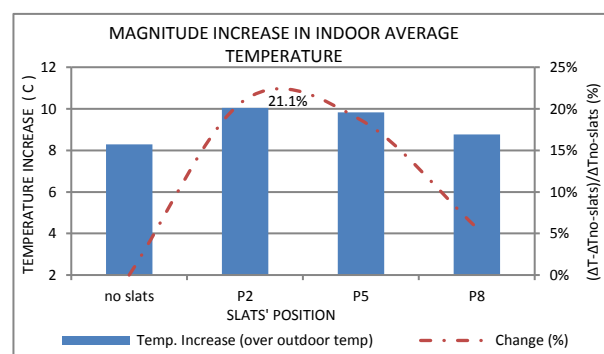


Figure 10.39: Increase in indoor average temperature at height of 1.6m and relative changes, with integrated slats having different positions.

Compared to no-slats case, surface temperature of the outer glass would slightly increase with P2 while decrease with P5 and P8, Figure 10.42. This increase could be attributed to the reflected solar radiation, but increase in air velocity due to narrowing front sub-cavity with case P8 and P5 compared to P2 leads to lower surface temperature (due to higher convective heat

transfer coefficient at the glass surface, even air velocity is not part of direct relationship: $h=q/\Delta T$). However, all changes were limited and less than 6% compared to summer (10%).

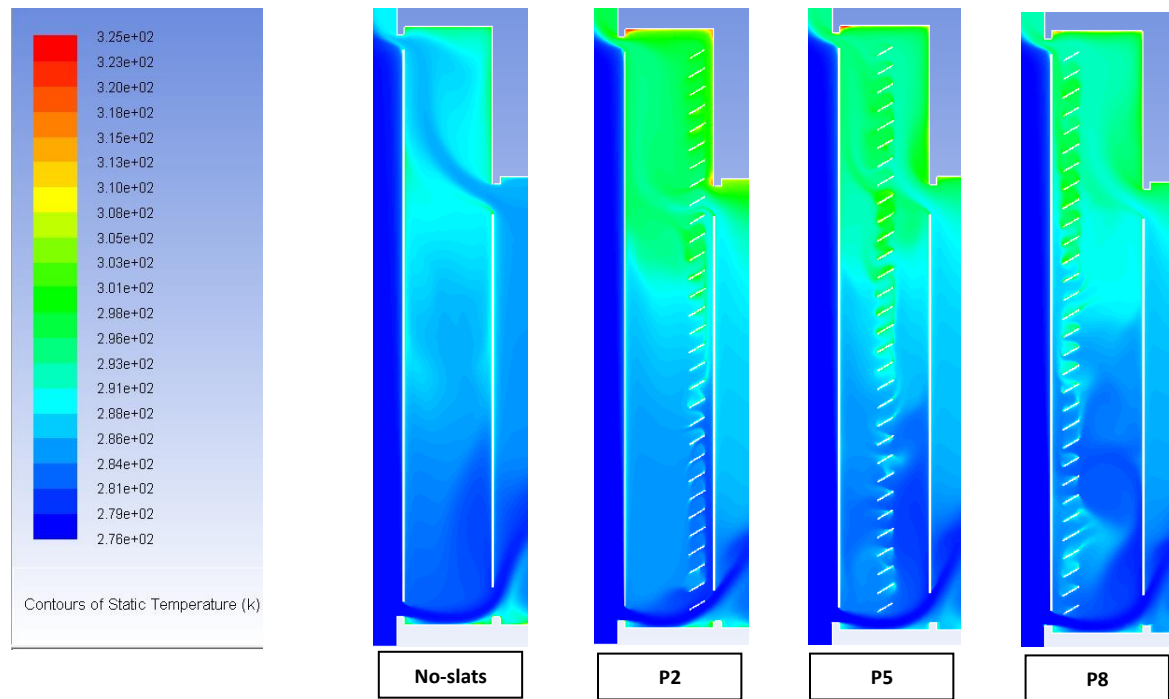


Figure 10.40: contours of static temperature (k) for the cavity integrated with studied slats at different positions in winter.

On the other hand, the inner glass would experience a significant drop in its surface temperature under the effect of installing such elements; which could reach 24.6% for position P8 compared to 27.9% in summer as discussed before. Obviously, reduction in surface temperature would increase with increasing width for second sub-cavity resulting in better ventilation and lower temperature; Figure 10.42. In addition, Figure 10.41 shows surface temperature averages for different elements: front glass, inner glass and cavity-integrated slats.

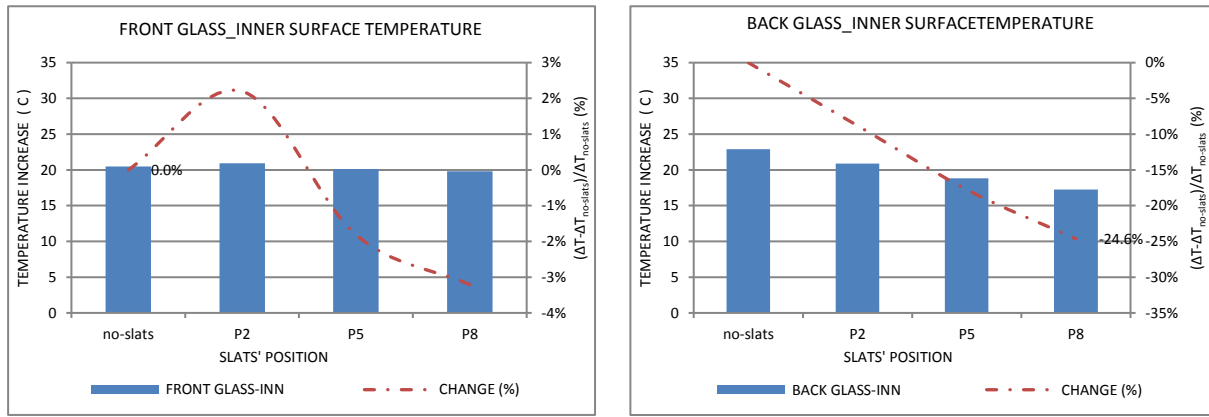


Figure 10.42: surface temperature averages for inner surfaces of outer glass (left) and inner glass (right) panes, with varied slats positions; and relative changes in reference to no-slats case.

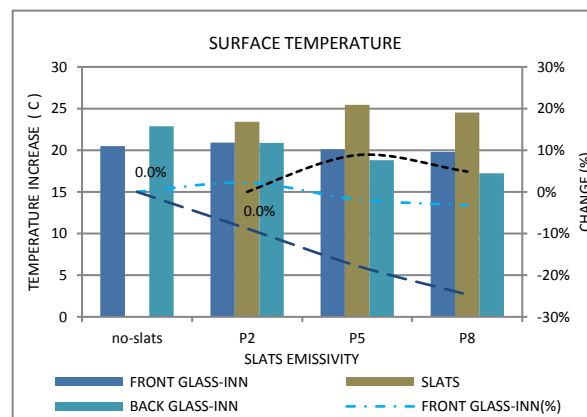


Figure 10.41: Temperature averages for outer glass's inner surface, inner glass's inner surface and slats' surface under the effect of changing integrated slats position. Relative changes are in reference to no-slats case for glass surfaces; and in reference to emissivity of 0.2 for slats surface; all for winter conditions.

Following equations (10.40) to (10.42) express the relationship between calculated temperature increase (ΔT) for structure surfaces and relative width of back sub-cavity (δ) that related to position of integrated slats. Based on this relative width, equation (10.43) could be used for calculating air average temperature at height of 1.6m along the space.

$$\Delta T_{\text{front}} = 2.9727 \delta^2 - 4.3378 \delta + 21.401 \quad ; (R^2 = 0.9994) \quad (10.40)$$

$$\Delta T_{\text{back}} = -6.0363 \delta + 21.506 \quad ; (R^2 = 0.9943) \quad (10.41)$$

$$\Delta T_{\text{slats}} = -16.621 \delta^2 + 15.842 \delta + 21.744 \quad ; (R^2 = 1) \quad (10.42)$$

$$\Delta T_{\text{indoor}_h=1.6\text{m}} = -4.8457 \delta^2 + 1.9357 \delta + 9.8736 \quad ; (R^2 = 1) \quad (10.43)$$

To conclude, having slats would cause a reduction in both offices and overall ventilation but an increase for cavity itself. Such reduction in office ventilation should not be a problem in winter as the minimum requirement (10L/s-person) for fresh air is still achieved. At the same time, temperature average for indoor would experience a noticeable increase with a maximum of 21.1% associated with position P2. For surface temperatures, P2 would perform the best among other positions as inner glass surface temperature would drop by just 8.8%. Therefore, installing such elements is recommended with position P2. Further works for winter conditions would be carried out considering this position, P2, then.

CHAPTER 11 EFFECT OF INTERNAL HEAT GAINS

This chapter shows the effect of including internal heat gains, in simulation, on the performance of the full model. Simulations were repeated for both summer and winter conditions.

11.1 Summer Conditions

Presented work, here, shows the effect of adding internal heat gains on thermal and ventilation performance of both office and attached cavity. The structure (office and cavity) and slats' parameters (size, emissivity, and position) were based on final results of previous tasks within this work. Internal heat gains include the three main components: occupants, equipments and artificial lighting. Assigned magnitudes were based on given values discussed in relevant benchmarks. Sensible heat gains for occupancy were found to be 6.25W/m^2 . Equipment heat gains were 15W/m^2 whereas gains due to artificial lighting were 12W/m^2 . For better distribution and representation, both occupant and equipment gains were assigned to floor structure while lightings were to the ceiling.

- **Airflow rate:**

As expected, including the internal heat gains would result in increasing office's ventilation due to having more heat inside and then larger buoyancy force to drive the incoming air through the office. This increase was found to be 28.8%. Also, cavity flow rate was enhanced by 5.3%; Figure 11.1. This is due to maintaining the integrated slats with relatively higher surface temperature, in conjunction with having the internal gains, as radiation exchange rate between those elements and either floor or ceiling would be

lower than before. Inner glass temperature, which bounds the cavity from the indoor side, would be higher as well. As a result, overall ventilation would be increased by 19.3%.

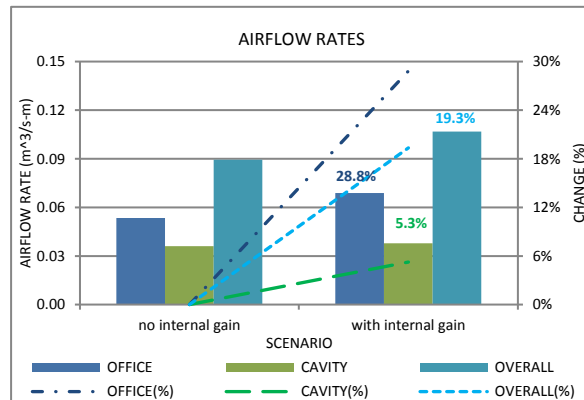


Figure 11.1: airflow rates and changes for office, cavity and entire structure for both scenarios: with and without internal heat gains.

Figure 11.2 shows contours of velocity magnitude for the entire structure with both scenarios. Generally, velocity magnitude increased after adding the internal heat gains however contour maps (relative variations) were the same except for the first half of cavity.

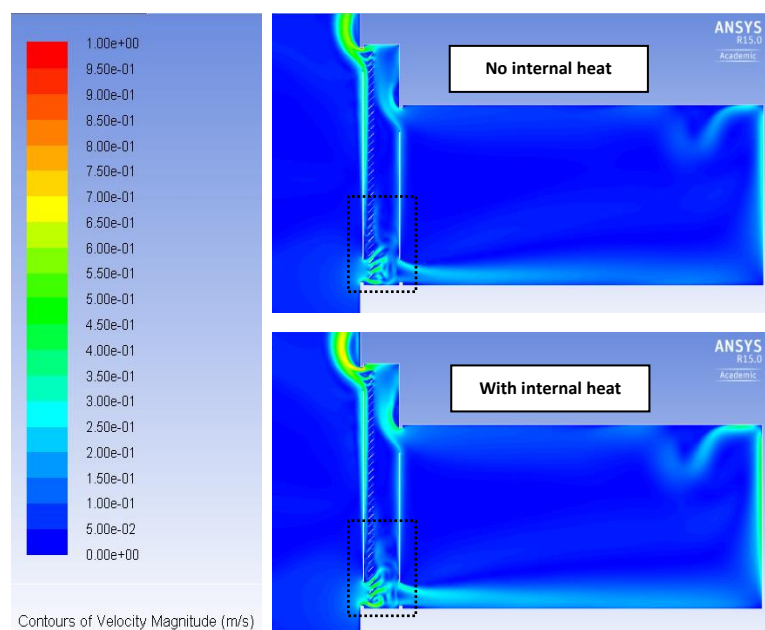


Figure 11.2: contours of velocity magnitude (m/s) for the office and attached cavity integrated with slats, for two scenarios: with and without internal heat gains.

- **Temperatures:**

Simulation showed that indoor temperature profile would experience an increase with the additional internal heat gains, Figure 11.3, even though office ventilation was enhanced as discussed before. This increase was small in magnitude, 0.6c, but still significant in its relative change, 38.7%, in reference to the increase above inlet air temperature, 37°C; Figure 11.4. Temperature contour maps, Figure 11.5, indicate that increase in magnitude and highlight the areas where the significant rise was dominant; i.e. floor, ceiling, and back-wall.

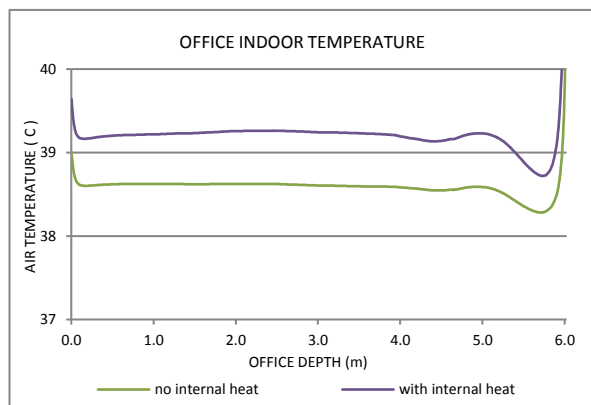


Figure 11.3: Indoor temperature at height of 1.6m for studied scenarios: with and without internal heat gains.

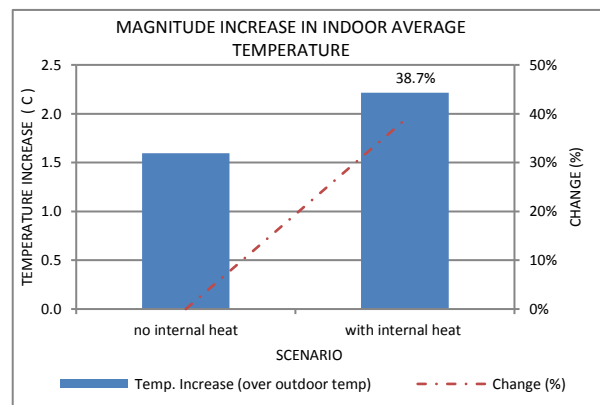


Figure 11.4: increase in indoor average temperature at height of 1.6m with relative changes for studied scenarios: with and without internal heat gains.

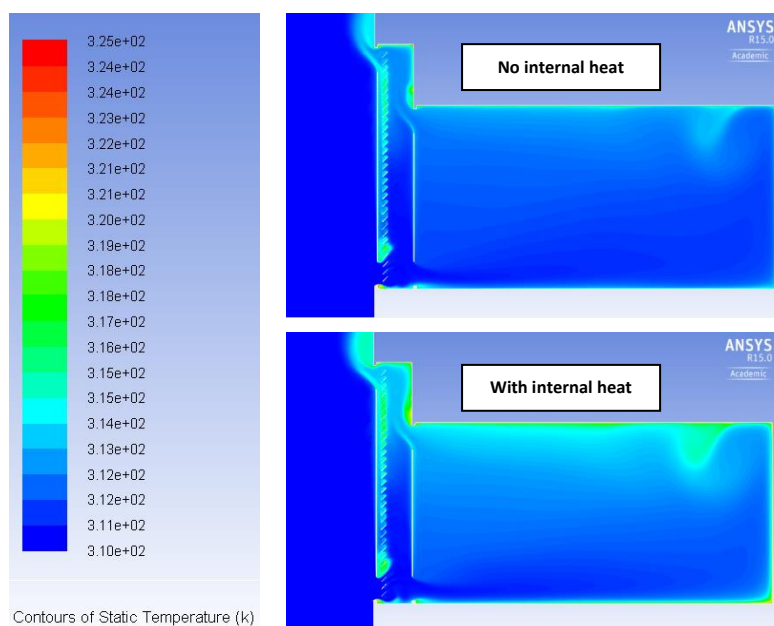


Figure 11.5: contours of static temperature (k) for the office and attached cavity integrated with slats, for two scenarios: with and without internal heat gains.

Averages for surface temperature for both glass panes would rise after including the internal heat gains; Figure 11.6. This increase was found to be 8.4% and 37.8% for outer glass and inner glass, respectively. At the same time, slats temperature would increase by about 10.9%. These increases for different structure elements were mainly attributed to the expected drop in radiation exchange rate with indoor surfaces, which are partially heated up by internal heat gains. This is why the temperature increased more for the surfaces close to indoor; e.g. 37.8% for inner glass compared to just 8.4% for outer glass.

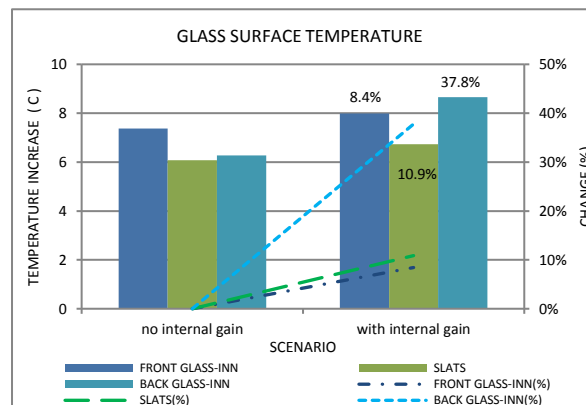


Figure 11.6: surface temperature averages for inner surfaces of outer glass (left) and inner glass (right) panes, with varied slats positions; and relative changes in reference to no-slats case.

To conclude, including internal heat gains would produce more realistic predictions for ventilation as well as temperature values. Office ventilation was found to be 0.069m³/s-m (69L/s-m) that is about 14 times of minimum required fresh air (5L/s-m). However, the extra flow rate is highly recommended during summer to remove accumulated heat from inside so to maintain indoor temperature at least close to incoming air temperature (37°C). Moreover, indoor temperature was 39.2°C (2.2°C above ambient temperature), which is still much higher than summer's comfort band (24°C -

28.5°C). Also, inner glass temperature was 43.74°C that would affect the radiation temperature. Therefore, results indicate the necessity for mechanical cooling aid to bring the indoor temperature to thermal comfort conditions and achieving occupant's satisfaction.

As part of this work, next chapter shows the influence of having mechanical cooling on the indoor thermal environment and investigates relevant design parameters including size and arrangement for assistant cooling vents as well as exhausts.

11.2 Winter Conditions

For winter, simulation was re-run with the additional internal heat gains, similar to summer case, to investigate changes in airflow and thermal conditions. Various characteristics and parameters for the tested structure match those agreed and concluded by relevant task within this work. Values and distribution for internal heat gains are typical to those for summer study.

- **Airflow rate:**

Initially, simulation was just re-run for the structure with concluded characteristics from previous work, which is named as "0.100" indicating that external opening height equals 0.1m. Results showed that office ventilation would increase by 14% compared to the scenario with no internal heat gains; Figure 11.7. However, the overall increase was just 7.6% as cavity flow rate would drop by 8.8% where less air would flow through the cavity while compensation amount would be dragged into the office due to having higher heat gains compared to no-internal-heat case.

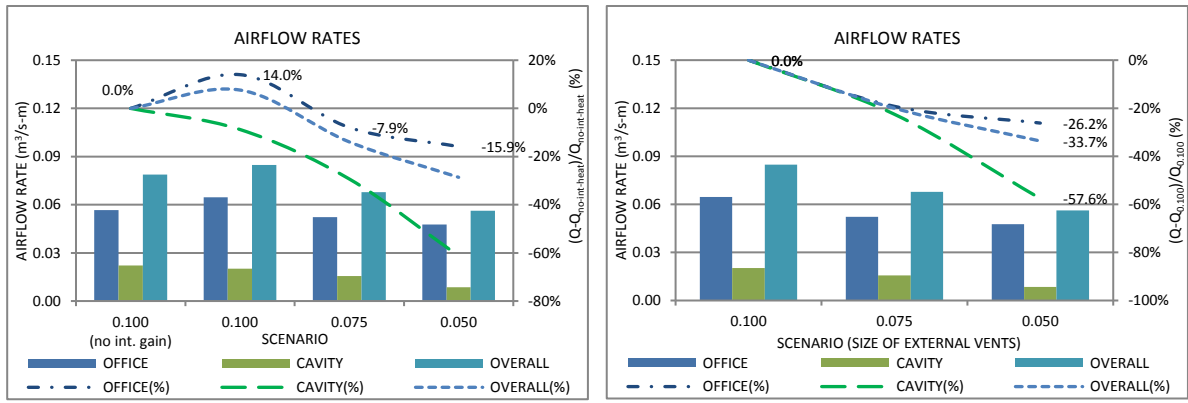


Figure 11.7: airflow rates and changes for office, cavity and entire structure for both scenarios: with and without internal heat gains. Left: All changes in reference to "no int. gain" case. Right: Results' changes in reference to their minimum values.

After that, two more cases were investigated, where outer openings' size was adjusted to control the ventilation so maintain the indoor temperature close to thermal comfort conditions while achieving minimum fresh air requirements. New sizes were 0.075m and 0.05m that applied to both external inlet and outlet of the cavity. However, inner openings (vents located at the inner skin of structure) were kept with primary size as of 0.2m. With the new adjustments, both office and overall ventilation rates would be reduced by a maximum of 26.2% and 33.7%, respectively, that was associated with the smallest size, 0.05m. However, office ventilation is still 0.048m³/s-m (48L/s-m).

Following equations (11.1) to (11.3) could be used to predict airflow rates (Q) for different parts of the structure as denoted, based on the height of external vents (h).

$$Q_{\text{office}} = 6.3369 h^2 - 0.612 h + 0.0625 \quad ; (R^2 = 1) \quad (11.1)$$

$$Q_{\text{cavity}} = -2.0235 h^2 + 0.5358 h - 0.0132 \quad ; (R^2 = 1) \quad (11.2)$$

$$Q_{\text{overall}} = 4.3135 h^2 - 0.0762 h + 0.0493 \quad ; (R^2 = 1) \quad (11.3)$$

Figure 11.8 shows contours of velocity magnitude for the entire structure before and after adding the internal heat gains. Also, cases with adjusted external vents are shown. While magnitudes were increased with additional gains and further with reducing external vents, air flow patterns seem to be similar for indoors but varied for the cavity.

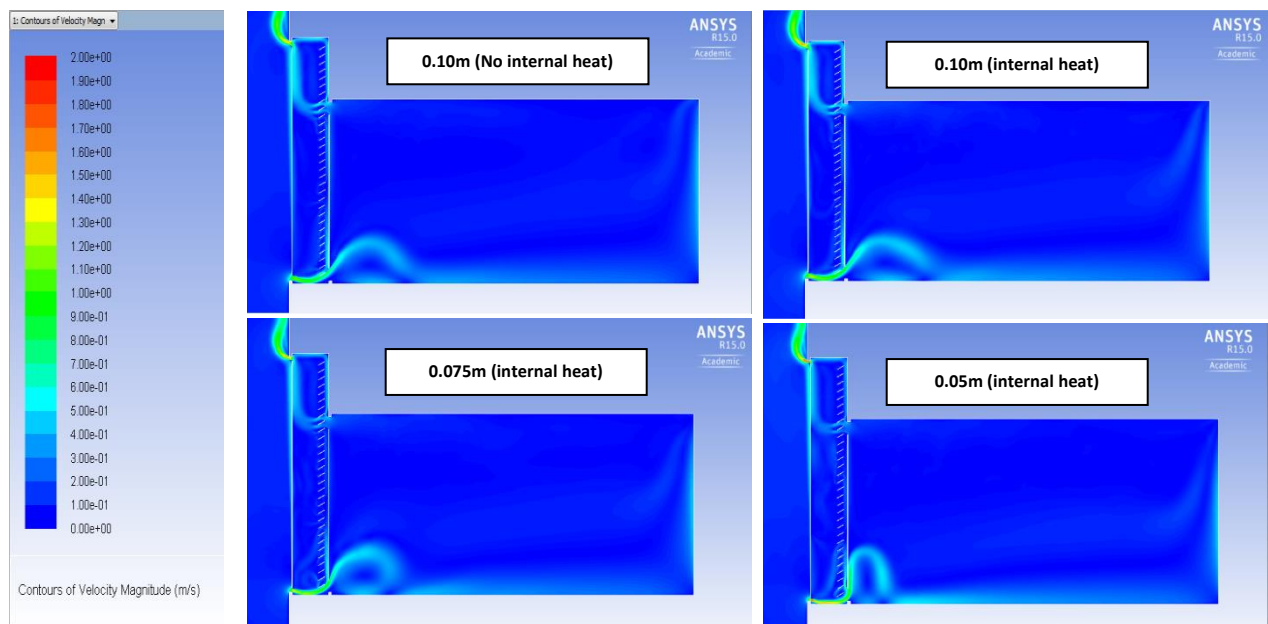


Figure 11.8: contours of velocity magnitude (m/s) for the office and attached cavity integrated with slats, for different scenarios.

- **Temperatures:**

With the additional gains, and having same vent size, average indoor temperature at height of 1.6m would increase from 13.07°C to 14.21°C, Figure 11.9, which is beneficial for the heating season. In addition, by adjusting external vents from 0.1m to 0.075m, the temperature would keep increasing. A significant increase was revealed with setting those vents to the size of 0.05m as more heat being trapped indoor. Generally, such increases were a direct result of reducing office flow rate.

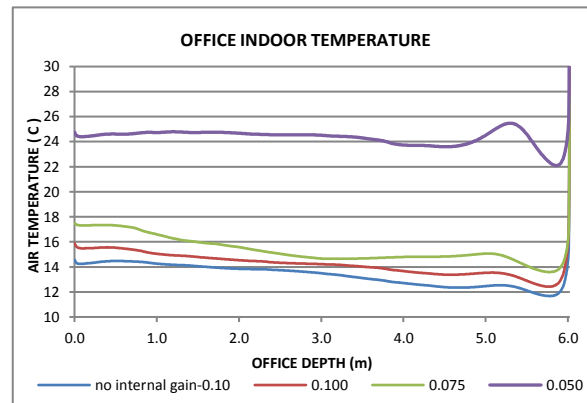


Figure 11.9: Indoor temperature at height of 1.6m for studied scenarios: with and without internal heat gains.

For the three studied cases, air temperature was measured at various levels (v) and depths (h), and then averages were calculated for these measurement lines; Figure 11.10. For each case, and despite the external vent size, results show that average temperature would largely vary with indoor height, (Graph B), as heat being accumulated at the top of space before being transferred to cavity then outdoor. The different levels share relatively close rates of change (8.2%-10.8%) with the size of 0.075m, but varied rates (66.4%-73.3%) with the smallest size, 0.05m. On the other hand, for assigned depths (Graph C), rates of change would experience similar trends to those given by levels but with lower maximums. Moreover, for individual cases, depths' averages were close except for deepest measurement line (h5.5) with the smallest size, 0.05m. Finally, Graph (D) shows two averages for different heights and different depths separately in addition to one overall average. The later was found to be 14.5°C, 15.7°C and 23.9°C for sizes of 0.1, 0.075 and 0.05m; respectively. Therefore, adjusting the external openings' size toward 0.05m would help in achieving indoor thermal comfort conditions (18.5-24°C) without the need to use artificial heating. Further

investigation is recommended for the range of sizes: 0.05-0.075m as the increase rate for temperature averages was significantly high.

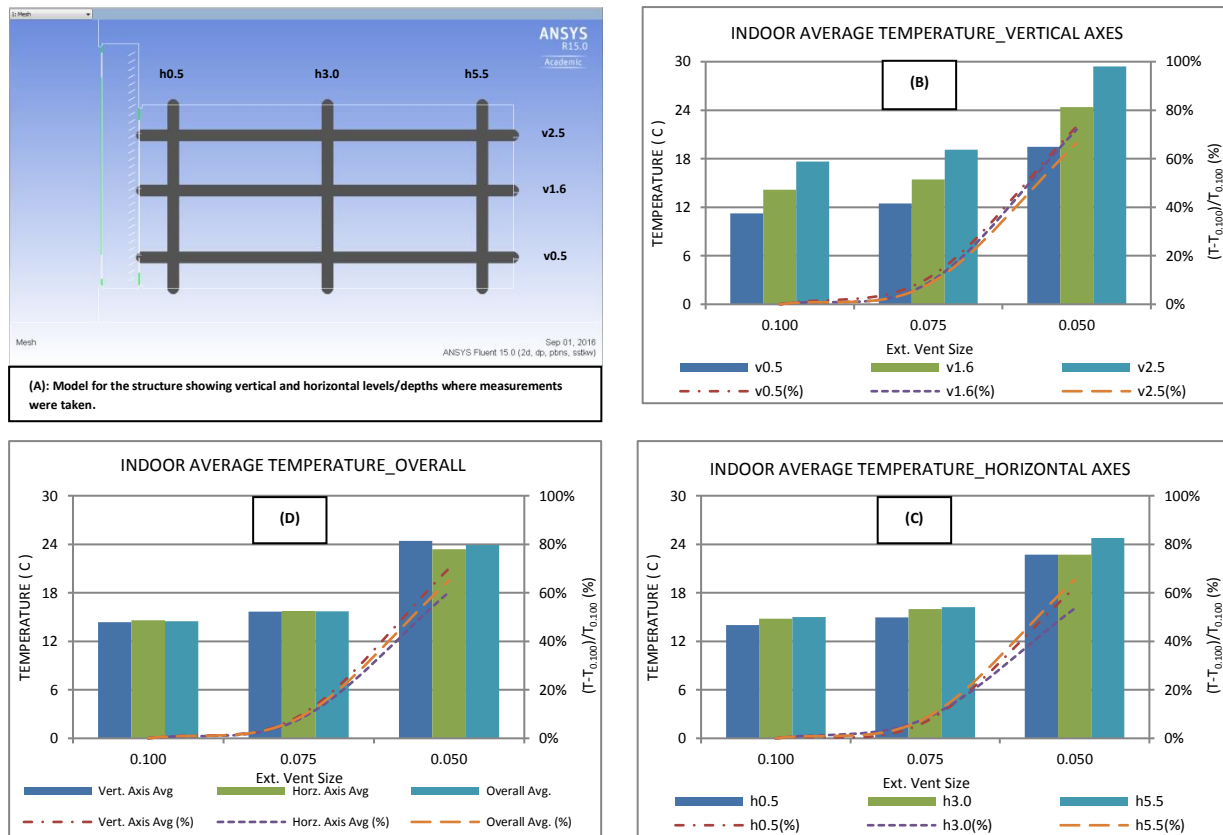


Figure 11.10: increase in indoor average temperature and relative changes at various levels and depths; for adjusted external vents.

Using the size (h) of external vents, revealed mathematical expressions (11.4) to (11.6) could be used to find out corresponding air temperature average (T) as denoted by each equation.

$$T_{\text{vertical}} = 5965 h^2 - 1096 h + 64.317 \quad ; (R^2 = 1) \quad (11.4)$$

$$T_{\text{horizontal}} = 5232.2 h^2 - 960.85 h + 58.363 \quad ; (R^2 = 1) \quad (11.5)$$

$$T_{\text{overall}} = 5598.6 h^2 - 1028.4 h + 61.34 \quad ; (R^2 = 1) \quad (11.6)$$

The average temperature for various indoor surfaces was calculated based on its calculated surface temperature and area; Figure 11.11. These surfaces were: inner glass (3*8m²), floor (6*8m²), ceiling (6*8m²) and back-

wall ($3 \times 8 \text{ m}^2$); in addition to the two side-walls (each $3 \times 6 \text{ m}^2$) that were not modelled with the 2D calculations but their temperature was assumed to be equal to back-wall one.

Generally, the surface temperature would increase after reducing vent's size due to reduced ventilation causing lower heat transfer from those surfaces to flowing air. The rate of the temperature-increase varied from a minimum of 17.6% for the ceiling to a maximum of 27.6% for back-glass (inner glass). However, the overall average temperature for all surfaces was increased by 22.2% from 32.77°C to 40.05°C that still indicates a too high radiant temperature for thermal comfort. However, occupied zone is usually smaller than the entire perimeter of the space; e.g. a perimeter up to 0.5m would not be used thus, in practice, such high surface temperature should not be a critical issue for occupant comfort. However, decreasing the surface temperature would require either allowing more incoming air but this should be balanced with indoor air temperature, or reducing glass transmittance to a point that less solar gains would get in although this would affect daylight performance. Finally, painting the walls with colours having lower emissivity values than used here (0.9) would also help.

For thermal comfort, operating temperature is the target rather than either air or surface temperatures; Figure 11.12. So, taking in consideration both values, operating temperature would be around 23.63°C and 31.98°C for vent's sizes of 0.1m and 0.05; respectively. Referring to winter's thermal comfort that is $18.5\text{-}24^\circ\text{C}$, the size of 0.10m would finally be selected when

the sun shines but could be adjusted to a smaller size when it is cloudy or raining.

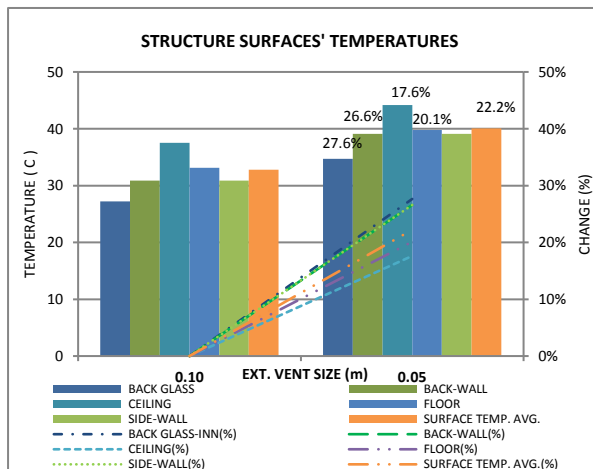


Figure 11.11: Temperature averages for different inner surfaces of space with relative changes as a result of adjusting external vent size.

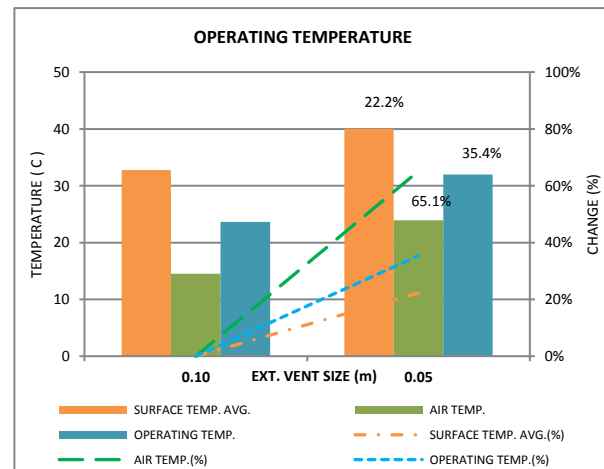


Figure 11.12: Averages for indoor surfaces temperature, air temperature and operating temperature with relative changes as a result of adjusting external vent size.

To conclude, the studied structure with given characteristics for integrated slats would be able to achieve both fresh air requirement and thermal comfort conditions during winter and by just relying on outdoor boundary conditions. Two vital factors were revealed: characteristics of integrated slats (size, position, and emissivity) and sizing of openings, in particular, outdoor ones. Most importantly, there would be no need for any artificial heating means.

CHAPTER 12 SUMMER ARTIFICIAL COOLING

This chapter presents requirements of summer artificial cooling for the designated office space (with DSF system). As part of this work, a set of parameters were further investigated. This included arrangement of supply air vents, arrangement of exhaust air vents, supply air temperature and the possibility of using ceiling air vents.

12.1 Arrangement of Supply Vents:

After passively optimizing the main parameters for the office and attached DSF with integrated shading devices, it was revealed that mechanical cooling is still required to achieve summer thermal comfort (24°C - 28.5°C). So, based on calculated solar gains and estimated internal gains, the total amount of indoor heat was determined. Then, initial inlet temperature (artificial cooling) was set to be 18°C. Consequently, difference between initial inlet temperature and indoor target temperature increase (average of thermal comfort band, 26.25°C) was computed to be 8.25°C; simply, this means that indoor temperature would be allowed to increase by a maximum of 8.25°C above cooling air temperature (18°C). Intuitively, this increase would be a result of both solar and internal heat gains after natural ventilation effect. The rest of accumulated heat should be extracted to outdoor with relatively cold supplied air. Finally, using initial temperature increase allowance (difference) and total heat gains, preliminary mass flow rate ($\text{kg}^3/\text{s-m}$) was calculated then volume flow rate ($\text{m}^3/\text{s-m}$). However, due to non-uniformity of solar heat distribution on various indoor surfaces and difficulty to match exact requirements of inlet temperature and corresponding flow rate, several runs

have to be conducted with adjustment of either inlet temperature, mass flow rate or even both. Table 12.1 presents both internal and solar heat gains used to calculate the mass flow rate. Mass flow rate was found to be 0.115kg/s-m that is equivalent to 0.095m³/s-m.

Table 12.1: Internal and solar heat gains used to calculate mass flow rate for initial setting of the artificial cooling loads.

	AVERAGE (w/m²)	AREA (m²-m)	TOTAL (w-m)
OCCUPANTS	6.25	6	37.5
LIGHTING	12	6	72
EQUIPMENTS	15	6	90
INTERNAL GAINS			199.5
SOLAR GAINS	126.08	6	756.48
SUM			955.98

Table 12.2 shows a group of potential sizes for artificial cooling vents and corresponding air velocity to achieve required air flow rate.

Table 12.2: Adjusted sizes and corresponding velocity to achieve required flow rate (0.095m³/s-m)

Adjusted sizes and corresponding velocity						
Vent's size (m²-m)	0.05	0.10	0.15	0.20	0.25	0.30
Velocity (m/s)	1.90	0.95	0.63	0.47	0.38	0.32

Initially, three different proposals were set for openings arrangement and size as following, Table 12.3 and Figure 12.1:

Table 12.3: Vent's sizes and arrangements for the three investigated proposals.

CASE	VENTS LOCATION	LEVEL (m)	SIZE (m)	VELOCITY (m/s)
A	Back-wall	2.6	1*0.2	0.47
B	Back-wall	0.2	1*0.2	0.47
C	Back-wall	0.2, 1.5, 2.7 (3 different positions)	3*0.1	0.32

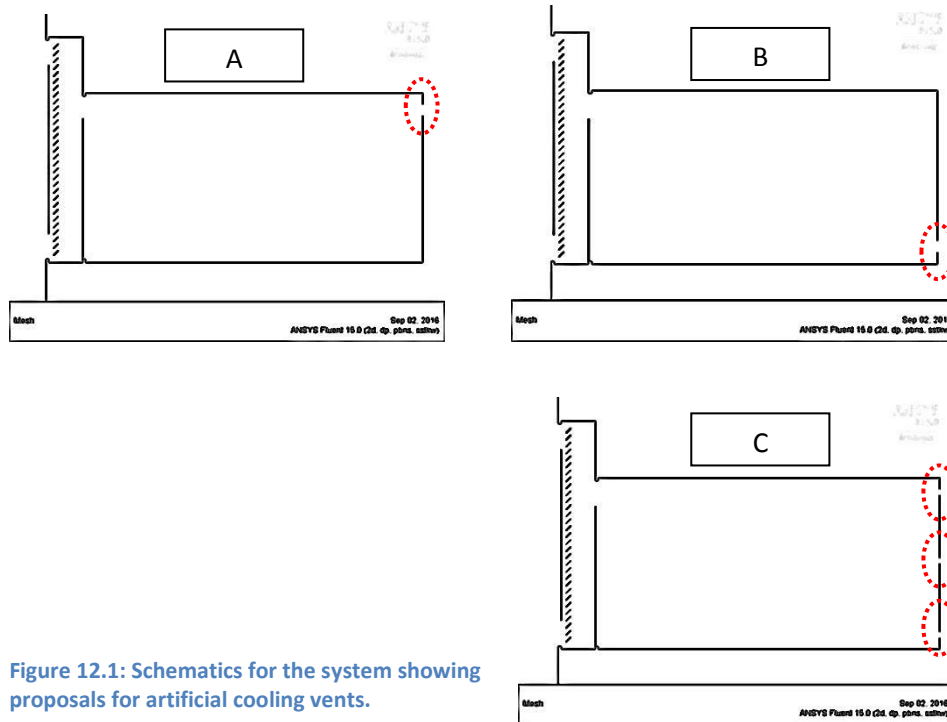


Figure 12.1: Schematics for the system showing proposals for artificial cooling vents.

- Airflow rate:**

For all cases (positions of office's supply vents), office supply ventilation rate was fixed to $0.095\text{m}^3/\text{s-m}$. However, cavity natural ventilation rate changed in response to office's outlet temperature, which was different based on indoor flow distribution. Maximum cavity ventilation was $0.058\text{m}^3/\text{s-m}$ (CASE-A) compared to $0.018\text{m}^3/\text{s-m}$ (CASE-B) as minimum with drop of 68.7%; Figure 12.2. The importance of having higher cavity ventilation emerged from its efficiency in cooling down glass structure thus reducing secondary radiation effect to indoor and maintain indoor surfaces'

temperatures relatively lower. In the end, CASE-A would provide highest flow rate.

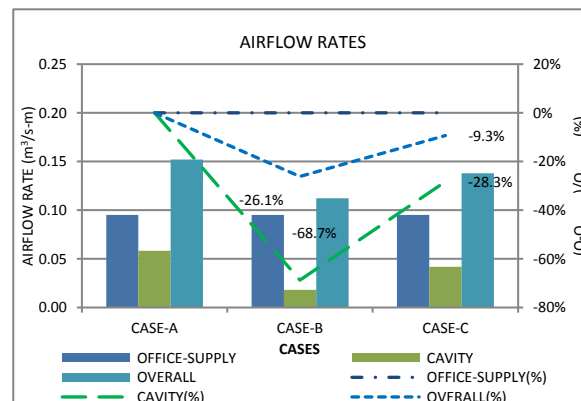


Figure 12.2: airflow rates and changes for office, cavity and entire structure various proposals for artificial cooling vents.

Simulation showed the difference in flow distribution between the three cases; Figure 12.3. Case-A would give better air distribution that would efficiently help in removing solar and internal heat gains so further reducing indoor temperature as will be discussed later. Also, variations in cavity airflow were clear. As office's outlet air temperature was always lower than ambient air temperature (37°C), air would drop down after getting out from office due to the higher density. This works also for cavity's outlet air temperature.

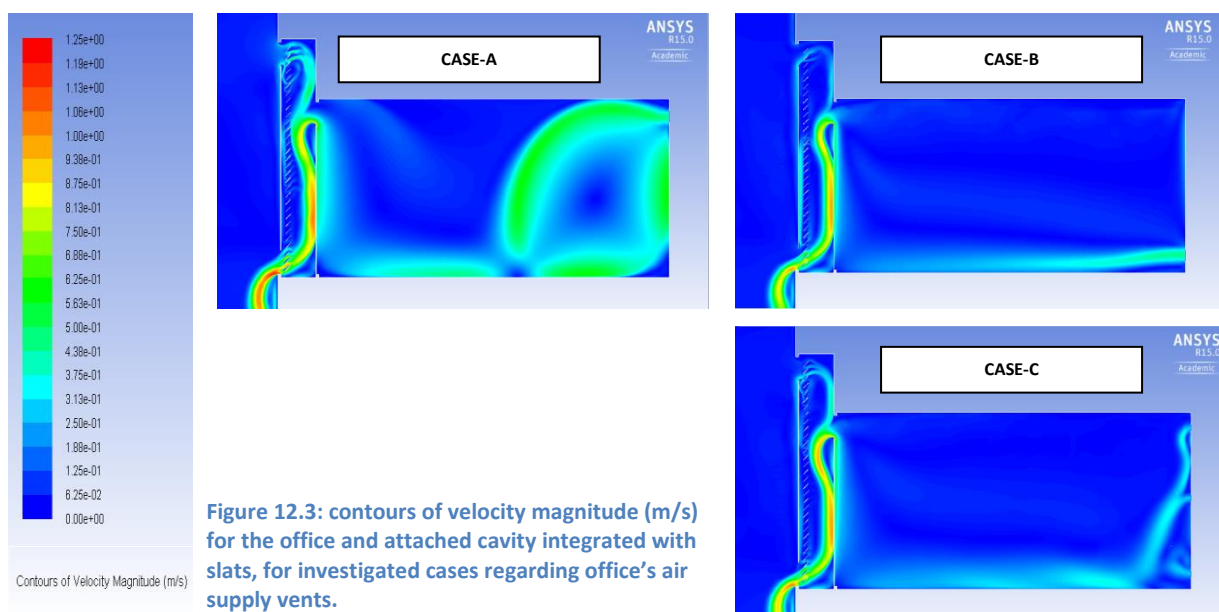


Figure 12.3: contours of velocity magnitude (m/s) for the office and attached cavity integrated with slats, for investigated cases regarding office's air supply vents.

- **Temperatures:**

Figure 12.4 presents the temperature profile at $h=1.6\text{m}$ along the office's depth. Referring to velocity contours Figure 12.3, temperature decreased at the areas where velocity was higher. Generally, CASE-A would maintain a more uniform profile for indoor temperature with the lowest average, 21.7°C , that means initial inlet temperature (18°C) for artificial cooling could be increased to higher values to save energy while meeting comfort requirements (24°C - 28.5°C). A separate study on this point is presented later on.

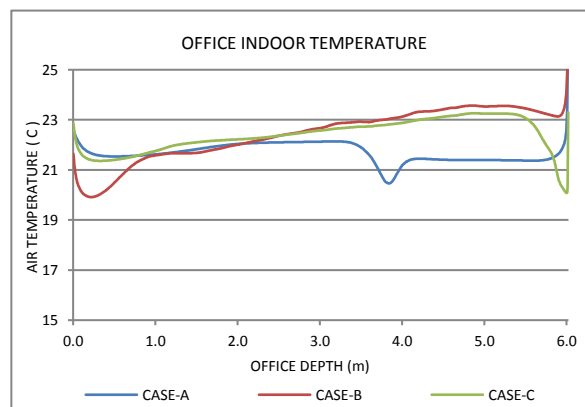


Figure 12.4: Indoor temperature at height of 1.6m for different proposals for indoor air supply vents.

Figure 12.5 shows contours for indoor temperature for different cases. As shown in Figure 12.6, average temperatures at measurement levels (v0.5-v2.5) were close for CASE-A while varied for both CASE-B and CASE-C. Moreover, CASE-B had a highest average temperature for both v1.6 and v2.5 but lowest for v0.5 as the later would directly be served with cooling air coming from the lower vent. As both inlet temperature and flow rate were fixed, these changes were a result of different flow distribution inside. Similarly, temperature averages for various depths (h0.5-h5.5) would be higher for CASE-B (Figure 12.6-C). However, those averages within the same

case would be close. Finally, CASE-A would provide lowest air temperature averages for the set of levels and set of depths as well as overall average (Figure 12.6-D). The later was 21.8°C for CASE-A compared to 23.8°C and 23.2°C for CASE-B and CASE-C; respectively.

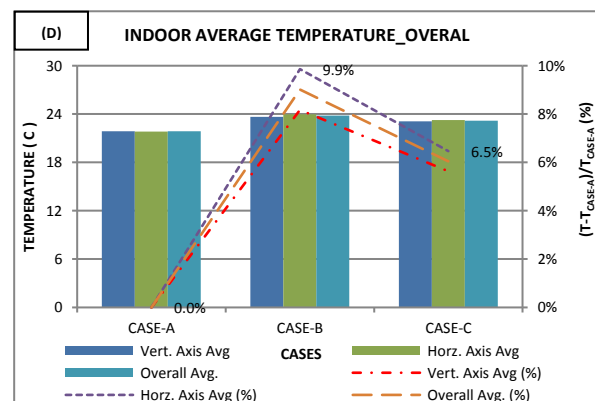
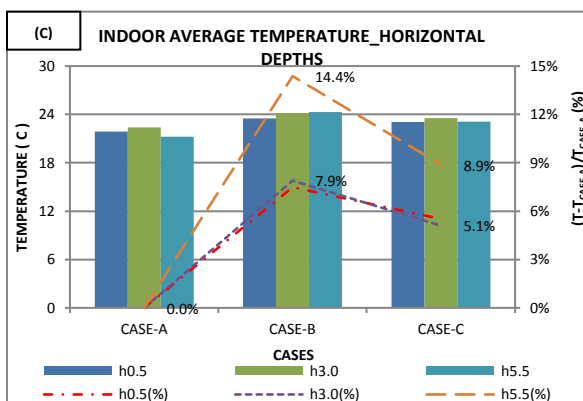
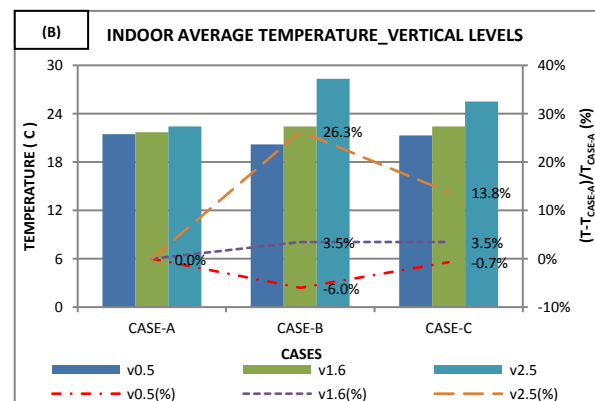
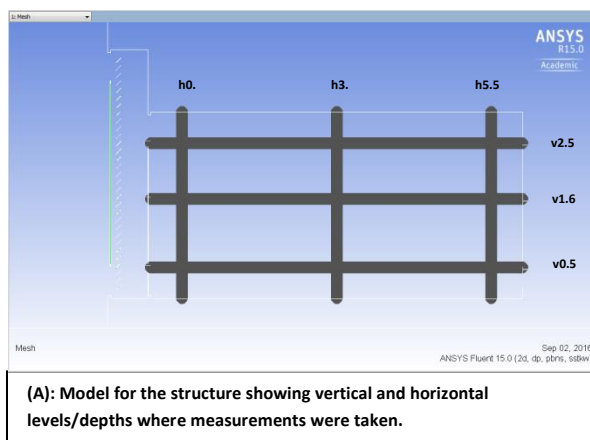
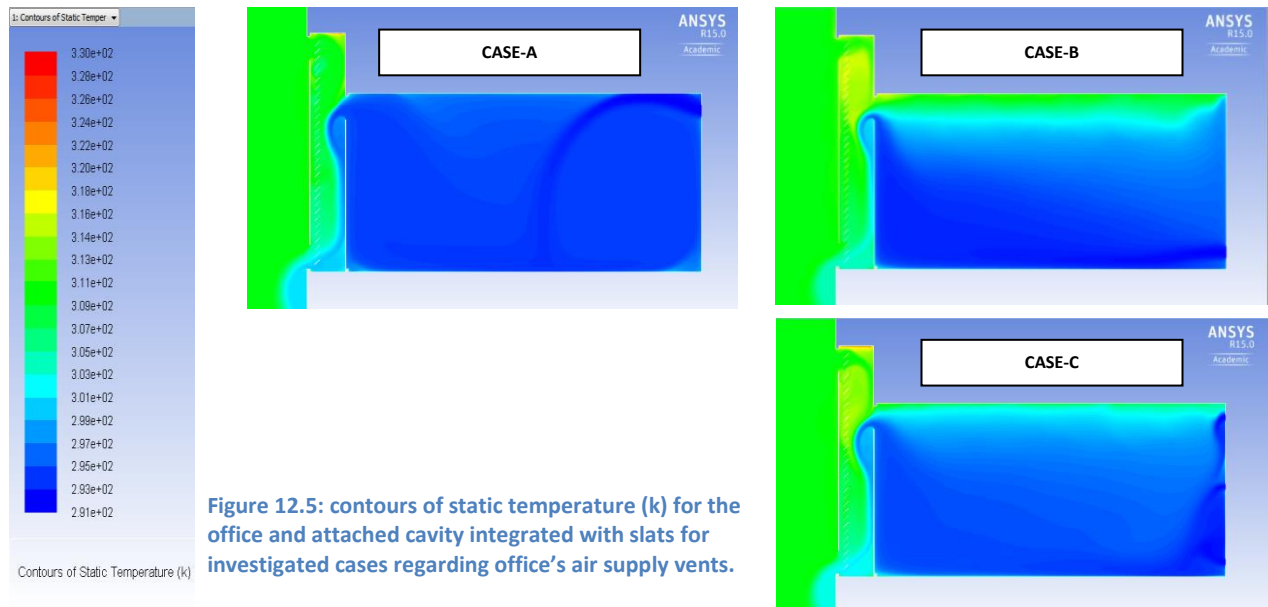


Figure 12.6: Indoor temperature averages and relative changes at various levels and depths; for investigated cases regarding office's air supply vents.

After discussing air temperature, averages for indoor surfaces' temperature were reported; Figure 12.8. For different surfaces, CASE-A showed lowest temperature values whereas CASE-B had the highest. For CASE-A, surfaces' overall temperature was 28.78°C while it was 34.66°C for CASE-B with an increase of 20.4%. Figure 12.7 shows overall temperature averages for air, surfaces and operating temperatures. CASE-A would always provide lowest values for the two components as well as operating one, which was 25.31°C for CASE-A so falls in summer's thermal comfort band (24-28.5°C).

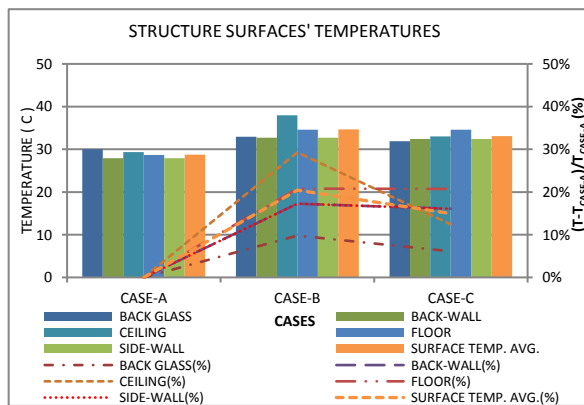


Figure 12.8: Temperature averages for different inner surfaces of space with relative changes for investigated cases regarding office's air supply vents.

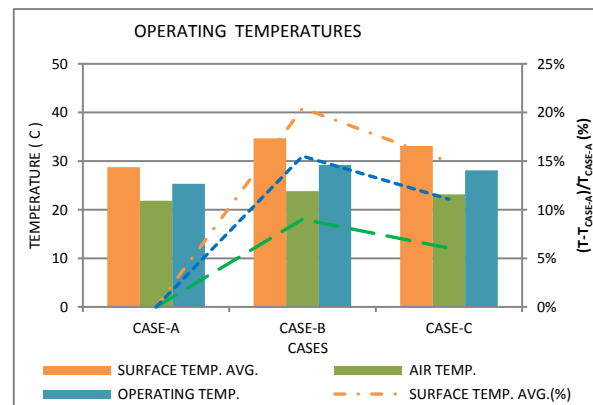


Figure 12.7: Averages for indoor surfaces temperature, air temperature and operating temperature with relative changes for investigated cases regarding office's air supply vents.

To conclude, whereas CASE-A was selected among other presented cases, following part of this work discusses results of related study on the arrangement of exhaust vents at both layers of front façade (DSF structure).

12.2 The arrangement of Exhaust Vents:

This section presents results of the study on arrangement of exhaust vents at both layers of front façade (DSF structure). Based on selected case, CASE-A, another two cases were generated with openings adjustments, as shown in Figure 12.9. While CASE-A intended to provide fresh air from outdoor to help cooling down the cavity structures, it was found that exhaust air from

office still had a lower temperature so new adjustments intend to rely on that air for such purpose. Hence, the external inlet for cavity was closed and new designs (A1&A2) would just have a single vent connected to ambient environment to work as an outlet.

In addition, CASE-A1 would have both the bottom and top vents at inner skin kept opened. However, CASE-A2 would work with just bottom vents at the inner skin. For the three cases, airflow rates and temperatures are presented here.

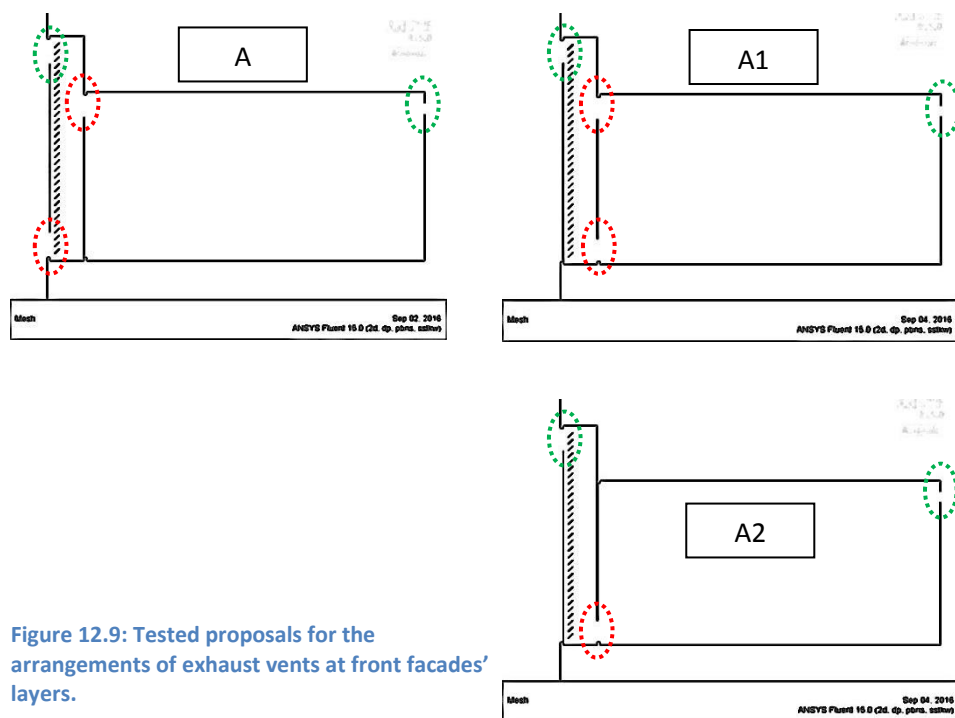


Figure 12.9: Tested proposals for the arrangements of exhaust vents at front facades' layers.

- **Airflow rate:**

Figure 12.10 shows airflow rates for both office ventilation and overall ventilation and for the three different designs. Clearly, office ventilation rate was constant, $0.095\text{m}^3/\text{s-m}$, for the three designs as it exclusively depended on mechanical supply from the back-wall single vent. However, indoor air distribution was largely varied in particular between CASE-A and the others,

which was due to the additional bottom vent at the external skin with CASE-A. And, that is why overall flow rate for new design (A1&A2) was about 38% less than original case (A).

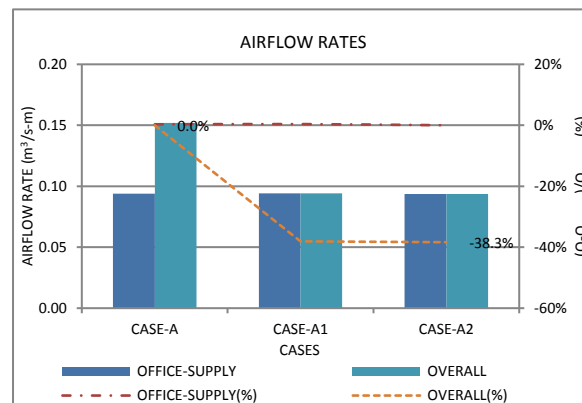
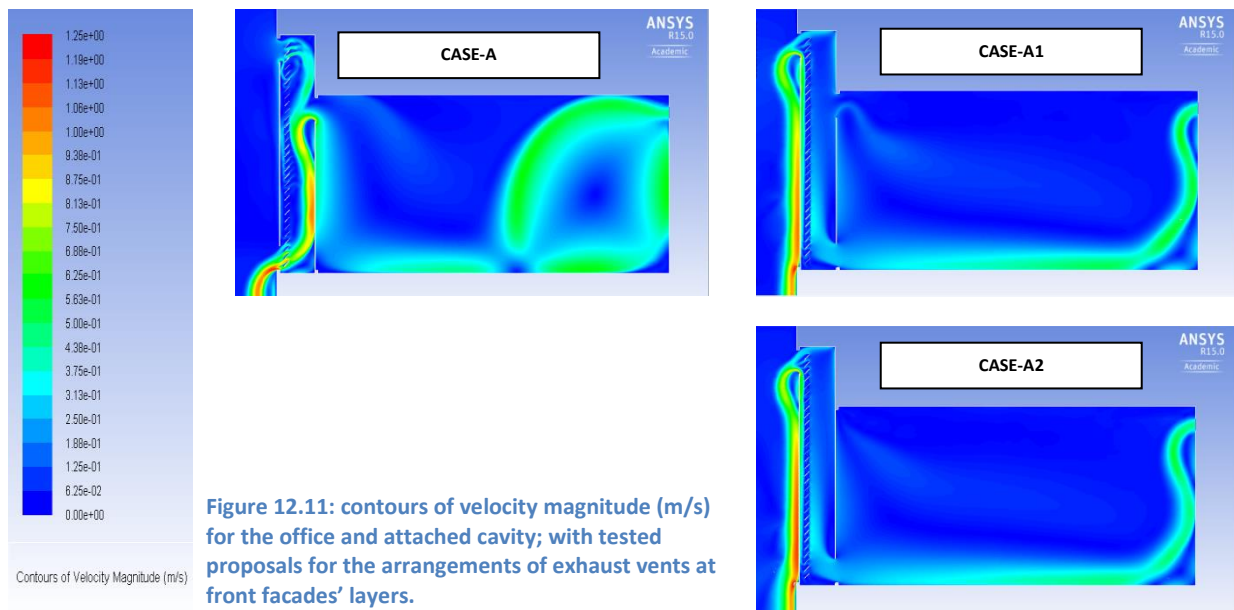


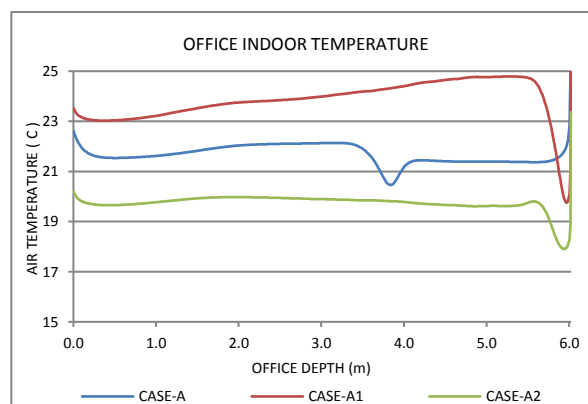
Figure 12.10: airflow rates and changes for office and entire structure with tested proposals for the arrangements of exhaust vents at front facades' layers.

Simulation results show how re-arranging exhaust vents would affect dramatically the flow patterns inside the space and cavity; Figure 12.11. With one external vent and two vents at the inner skin, CASE-A1, cooling air would drop down along the back-wall then continue along the floor before exhausting the space mainly from its bottom vent. However, there was a reverse flow from the cavity entering the space through the top vent, CASE-A1. To avoid that reverse flow, the top vent was closed, CASE-A2; so the indoor flow was slightly changed. Obviously, cavity flow with new designs (A1&A2) was smaller but more uniform than with CASE-A. Most importantly, the cavity would be fed with relatively low-temperature air than the later.



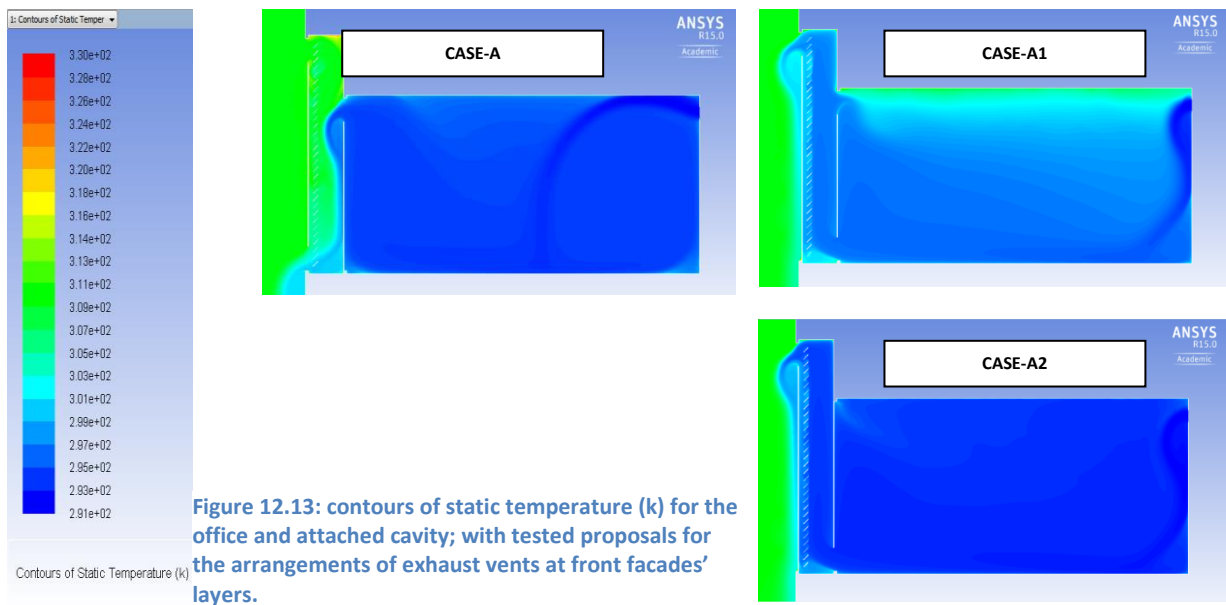
- **Temperatures:**

Temperature profile at $h=1.6$, Figure 12.12, would significantly be changed due to the adjustment of exhaust vents, which causes changes in airflow patterns inside then temperature contours; Figure 12.13.



Also, closing the upper vent at the inner skin (CASE-A2) would reduce the solar gains by 20% (additional effect of the second glass pane with a transmittance of 0.8) for that specific height (0.4m; mainly affects ceiling and the top part of volume). While keeping this vent opened for both CASE-A and CASE-A1, it would be the only exhaust vent for the aforementioned so main

airflow stream would help removing accumulated heat at the top of space. On the other hand, this vent would cause reverse flow from the cavity into the office with relatively higher temperature air.



As a result of changing airflow patterns and then its efficiency in extracting trapped heat from indoor, temperature averages for various levels (v0.5-v2.5) and depths (h0.5-h5.5) would be changed but with varied rates; Figure 12.14. Whereas they all increased for CASE-A1, all corresponding averages dropped for CASE-A2 with more efficient office exhaust vent. Compared to CASE-A with an overall indoor air temperature average of 21.8°C, such average was 24.7°C (+13.1%) for CASE-A1 and 19.8°C (-9.2%) for CASE-A2; Graph-D.

Simulation showed that surfaces' temperatures would differently increase with CASE-A1 while decrease with CASE-A2 by a maximum of +17.1% and -12.9%, respectively, Figure 12.15. However, surfaces' overall average temperature would have an increase of 7.7% and a decrease of 9.9% with CASE-A1 and CASE-A2, respectively. Including air temperature effect,

operating temperature was found for the three cases. Results show that operating temperature would respectively be changed as it recorded a rise of 2.54°C (10%) and drop of 2.43°C (-9.6%) for CASE-A1 and CASE-A2, respectively, Figure 12.16.

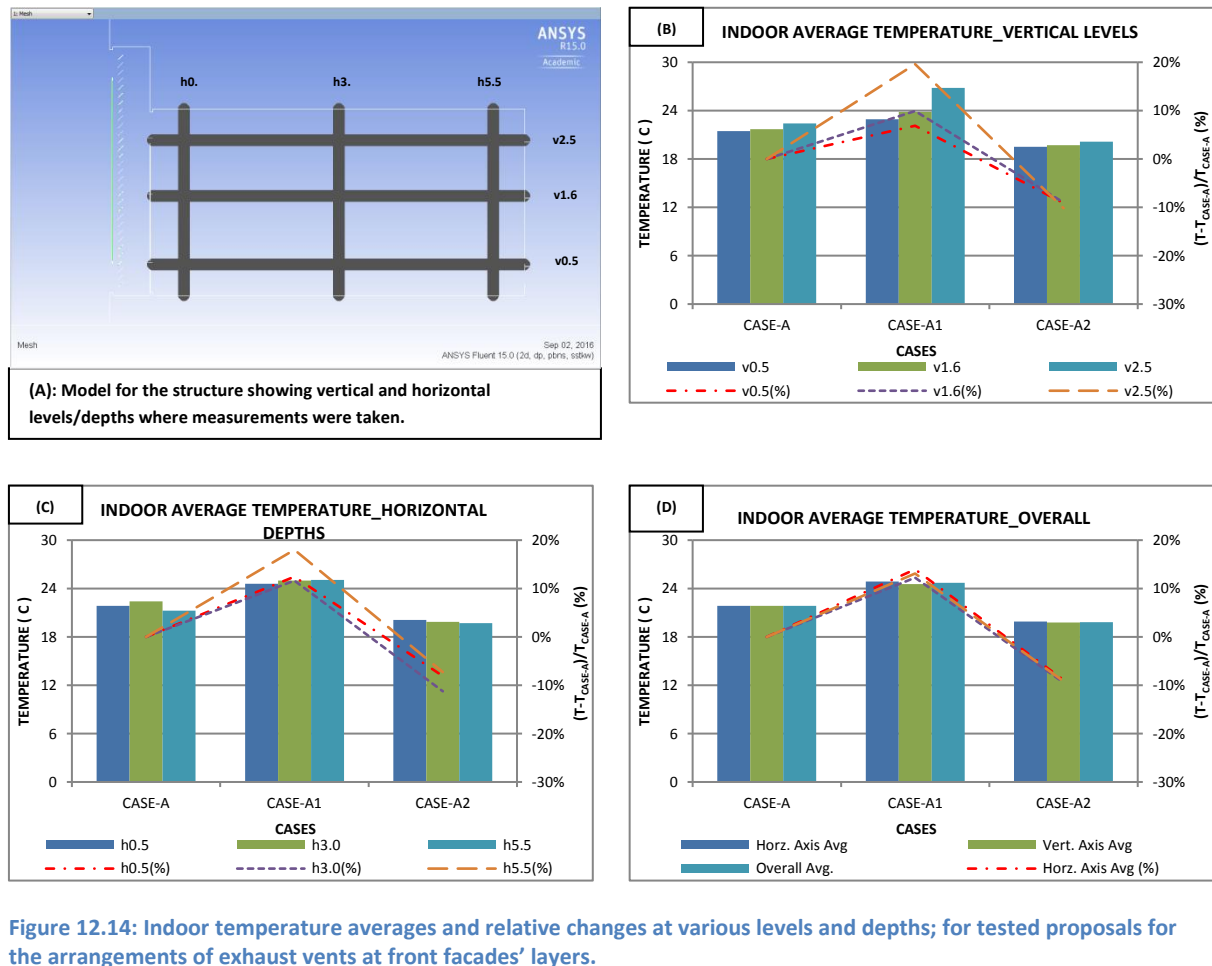


Figure 12.14: Indoor temperature averages and relative changes at various levels and depths; for tested proposals for the arrangements of exhaust vents at front facades' layers.

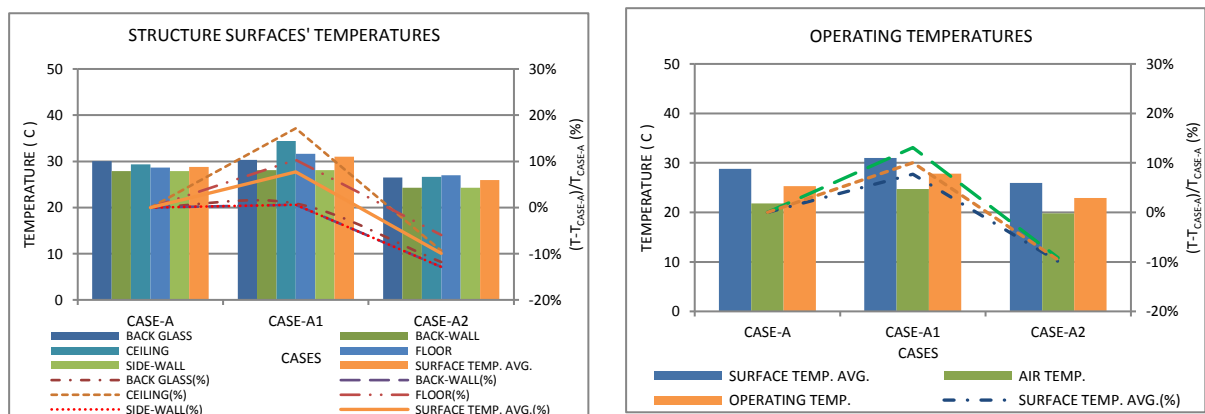


Figure 12.15: Temperature averages for different inner surfaces of space with relative changes for investigated cases regarding office's air supply vents.

Figure 12.16: Averages for indoor surfaces temperature, air temperature and operating temperature with relative changes for investigated cases regarding office's air supply vents.

To conclude, having single exhaust vent for each of inner and outer skins of the cavity, with shifted arrangement, would allow for better indoor airflow circulation and comfort operating temperature where cooling air supplied from a single vent located at the top of the back-wall, as well.

Next, inlet temperature would be adjusted for better energy saving. After that, one more case would be investigated with supply vents being located at the ceiling.

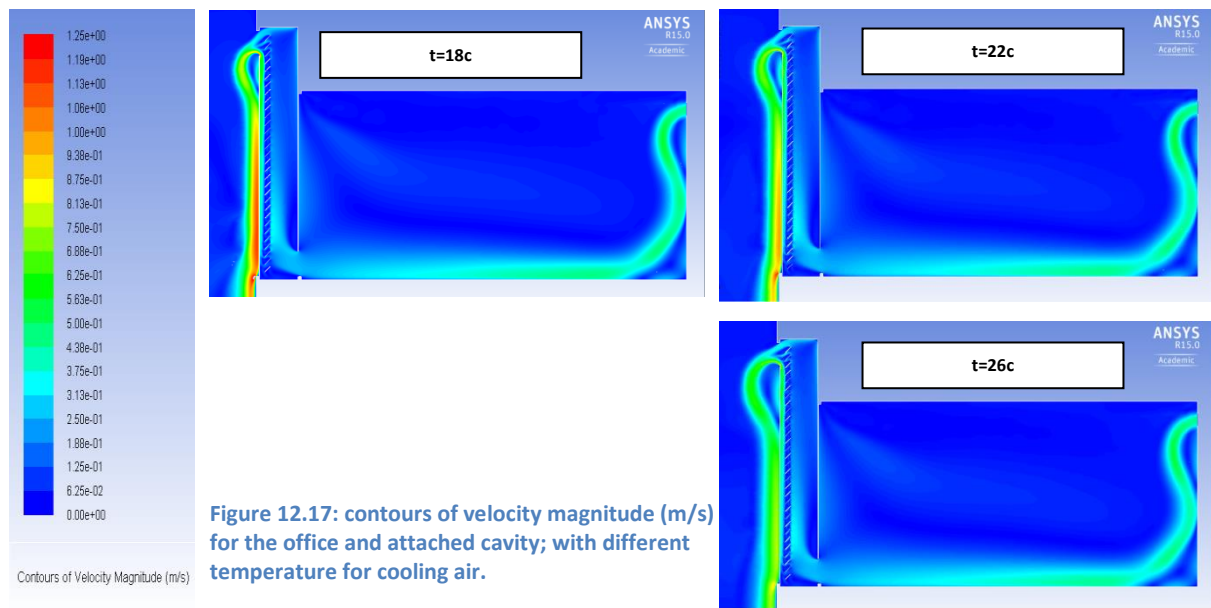
12.3 Supply Air Temperature:

Under this section, the effect of changing the temperature of office's inlet air (mechanical supply) on indoor thermal comfort was investigated. The aim was to achieve targeted summer thermal comfort (24-28.5°C) with highest available air temperature so saving cooling energy. In addition to the preliminary temperature of 18°C, four temperatures were tested: 20°, 22°, 24° and 26°C.

- **Airflow rate:**

Airflow rate was constant, $0.095\text{m}^3/\text{s-m}$, for all cases. Furthermore, simulation showed that indoor air distribution and velocity were nearly typical for different inlet temperatures; Figure 12.17. However, the angle of outgoing air at cavity's external vent would be changed. Also, velocity for outlet air along the external surface of outer skin would be significantly decreased as inlet air temperature increases. The reason is that temperature difference between external passing air and solar-heated surface would be smaller in

response to initially larger inlet temperature. This would attenuate convection process that is important to induce air moving away.



- **Temperatures:**

Effect of increasing inlet air temperature was direct on indoor air temperature average as shown in Figure 12.18. Temperature profiles, except their magnitudes, were nearly typical as there were no changes in airflow patterns as discussed before (Figure 12.17).

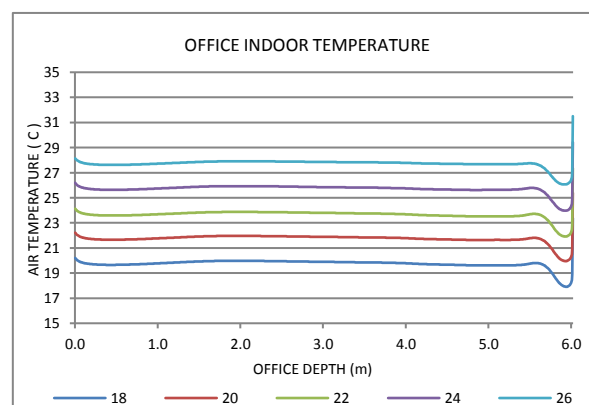


Figure 12.18: Indoor temperature at height of 1.6m for different temperatures of inlet air.

Figure 12.19 shows the temperature contours inside the space with almost minimum and maximum computed temperature range (scale: 18°C-57°C); such high temperatures were recorded for cavity frames surfaces

(aluminium with emissivity=0.9). Temperature maps would slightly be changed with varied weights for different temperature slots.

For better display and analysis, temperature scale was shortened to intended thermal comfort range: 24°C -28.5°C; Figure 12.20. It is clear that lowest inlet air temperature would produce a relatively lowest indoor temperature that would be even lower than the minimum threshold for summer thermal comfort (24°C). However, with a gradual increase in inlet air temperature, the designated empty area (indicates the area out of thermal comfort, mainly lower) was diminished. At the same time, areas out of comfort zone (with higher temperatures) were simultaneously enlarged, particularly at the corners. Whereas inlet temperature of 24°C would create a more convenient indoor environment, the temperature of 26°C would still act as good option as areas where air temperature would exceed upper band (28.5°C) were limited to corners and within the perimeter of 0.5m, which is usually outside the occupied zone. However, it is important to highlight that these maps and results express air temperature exclusively so are not final and need to be averaged with indoor surfaces' temperatures to produce total operating temperature. Also, it is important mentioning that the key behind working with highest possible inlet temperature is to save energy as basically inlet temperature has to mechanically be cooled down from ambient temperature, 37°C.

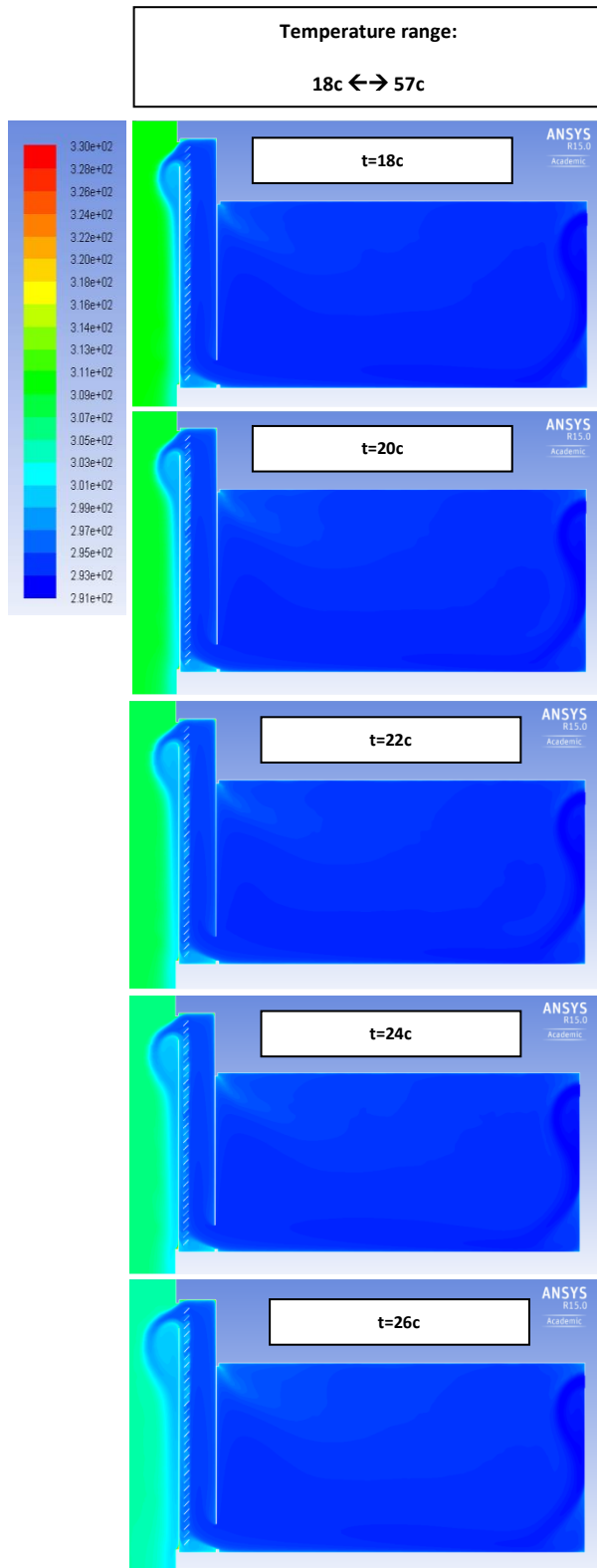


Figure 12.19: contours of static temperature (k) for the office and attached cavity; for different temperatures of inlet air. Scale range: 18-57°C.

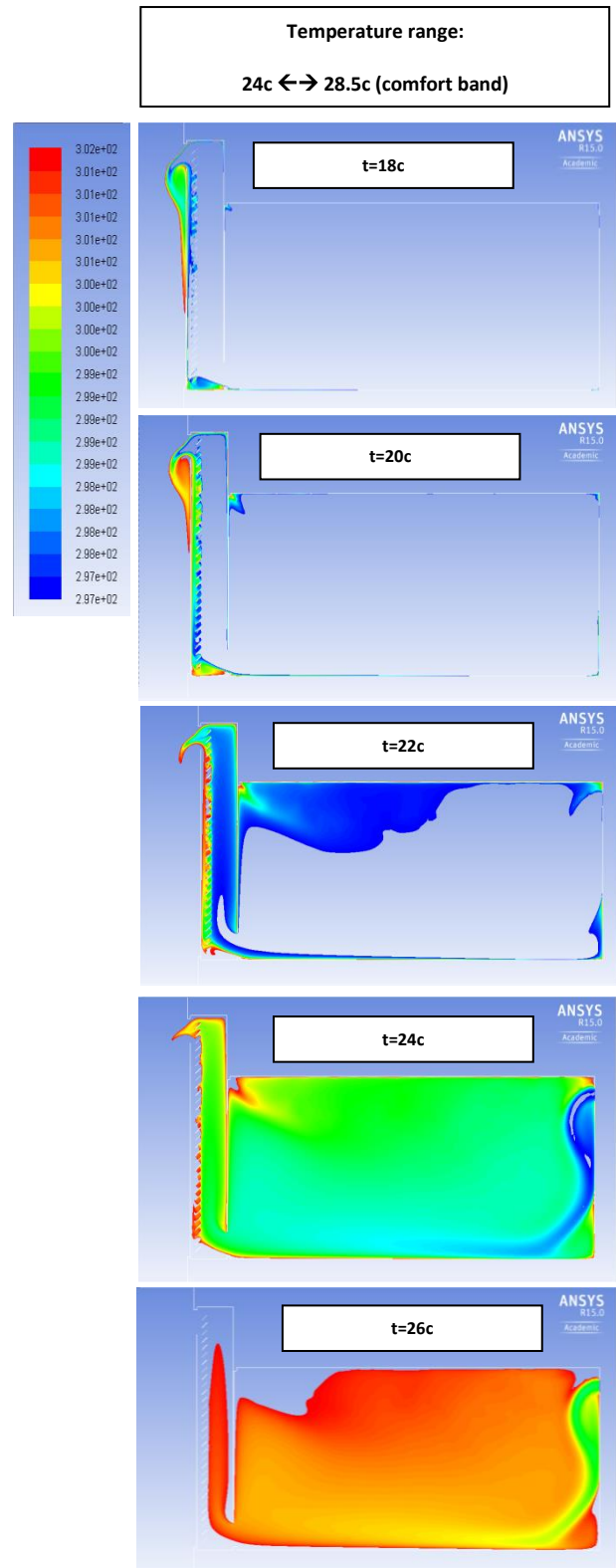


Figure 12.20: contours of static temperature (k) for the office and attached cavity; for different temperatures of inlet air. Scale Range: 24-28.5°C.

Temperature averages for imaginary rakes marked in Figure 12.21-A had a strong direct relationship with inlet air temperature for all vertical, horizontal and overall averages. This is expected as any increase in inlet temperature would be reflected to space air temperature before any increase being added due to solar or internal heat gains. Presented results (Figure 12.21-D) show that maximum overall average air temperature was 27.8°C for the inlet temperature of 26°C. However, corresponding value would be 23.7°C with an the initial temperature of 22°C. Both outcomes are still within the thermal comfort range (24°C -28.5°C).

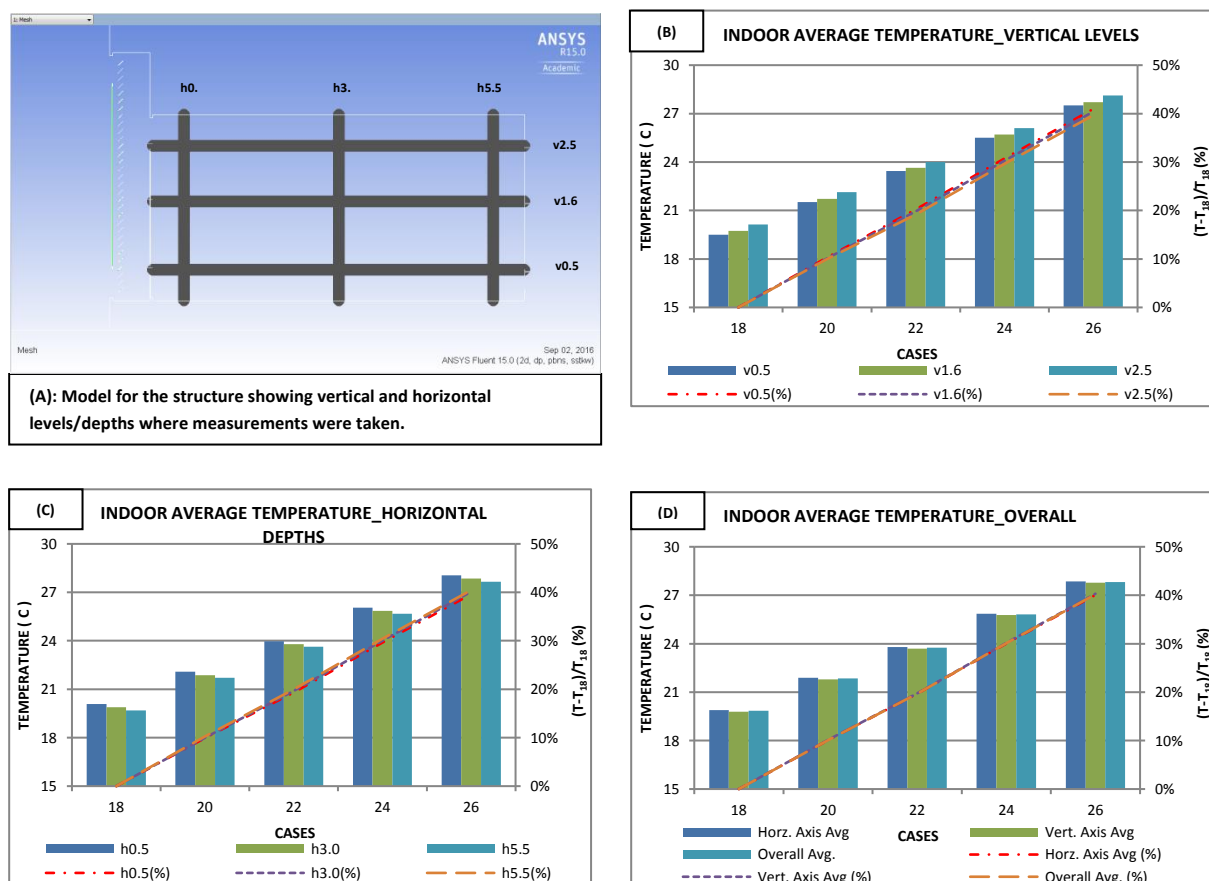


Figure 12.21: Indoor temperature averages and relative changes at various levels and depths for different temperatures of inlet air.

Following mathematical expressions (12.1) to (12.3) could be used for prediction of air temperature averages for different designated rakes as well as overall as denoted next to each equation.

$$T_{\text{air.vertical}} = 0.9966 T_{\text{inlet}} + 1.8412 \quad ; (R^2 = 0.9998) \quad (12.1)$$

$$T_{\text{air.horizontal}} = 0.995 T_{\text{inlet}} + 1.9674 \quad ; (R^2 = 0.9999) \quad (12.2)$$

$$T_{\text{air.all}} = 0.9958 T_{\text{inlet}} + 1.9043 \quad ; (R^2 = 0.9999) \quad (12.3)$$

In addition, due to the importance of surface temperature, it was reported for all indoor surfaces as averages; Figure 12.22. Surface temperature would be left higher in response to higher inlet temperature as temperature difference would decrease so convection rate would be reduced. Figure 12.23 presents the temperature averages for both indoor space's air and surfaces. Results show that surface temperature would always be higher than air temperature with an average of 6.3°C. Furthermore, the rate of increase for air temperature was larger than that for surfaces. For instance, maximum change was about 40% for air temperature compared to 32% for surfaces. Most importantly, operating temperature average would directly rise with both increases. Starting with 22.98°C for an inlet temperature of 18°C, operating temperature averages increased to 24.99°C, 26.81°C, 28.95°C and 31.11°C for inlet temperatures of 20°C, 22°C, 24°C and 26°C; respectively. Having said that thermal comfort band is 24°C -28.5°C, the inlet temperature of 22°C would be good enough to produce an operating temperature (26.81°C) that falls in that band.

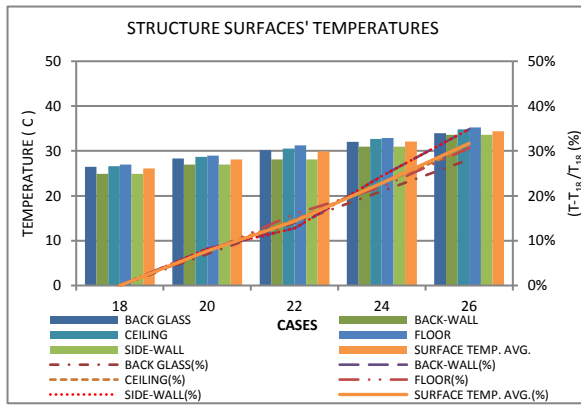


Figure 12.22: Temperature averages for different inner surfaces of space with relative changes for investigated cases regarding office's air supply vents.

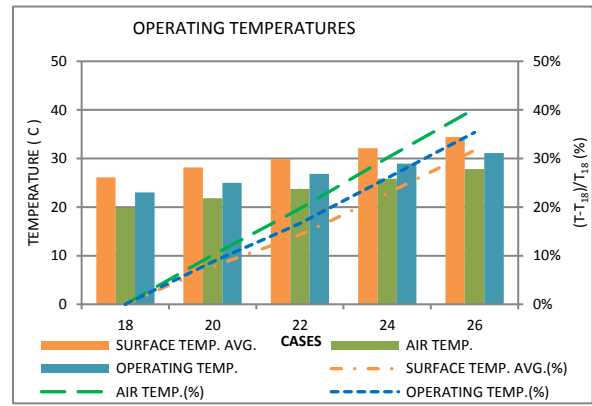


Figure 12.23: Averages for indoor surfaces temperature, air temperature and operating temperature with relative changes for investigated cases regarding office's air supply vents.

However, similar to air temperature average equation (12.3), equations (12.4) and (12.5) could be used to calculate both surfaces' temperature average and operating temperature; respectively.

$$T_{\text{surface.avg.}} = 1.0253 T_{\text{inlet}} + 7.5634 \quad ; (R^2 = 0.9972) \quad (12.4)$$

$$T_{\text{operating.temp.}} = 1.0105 T_{\text{inlet}} + 4.7339 \quad ; (R^2 = 0.999) \quad (12.5)$$

To conclude, inlet air temperature could be increased from its initial value (18°C) to up to 22°C while indoor thermal comfort is still achieved with an average of 26.81°C for operating temperature average. However, with an upper threshold of 28.5°C for summer thermal comfort, slightly higher inlet temperature can still be used; i.e. inlet temperature of 23.5°C is expected to produce an operating temperature of 28.48°C based on the revealed correlation for operating temperature, equation (12.5). With a suggested inlet temperature of 23.5°C, ambient fresh air (with a temperature of 37°C) has to be cooled down by 13.5°C.

12.4 Ceiling Cooling Vents:

Here, inlet vents for cooling air were placed on the ceiling instead of back-wall. This work aimed to investigate the effect of new positions of supply air vents on airflow and thermal distribution maps and compare that to back-wall cases. Three different temperatures were used for inlet air; those were: 18°C, 20°C, and 22°C. However, just one arrangement was used for the ceiling vents, Figure 12.24, as four split vents were created at the ceiling. Each was 0.25m²-m that results in 1.0m²-m as total area. However, to maintain same supply airflow rate (0.095m³/s-m), air velocity was set to 0.095m/s.

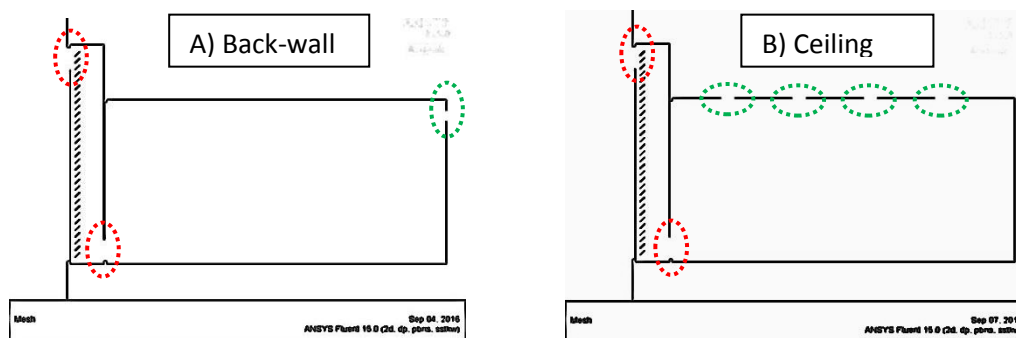
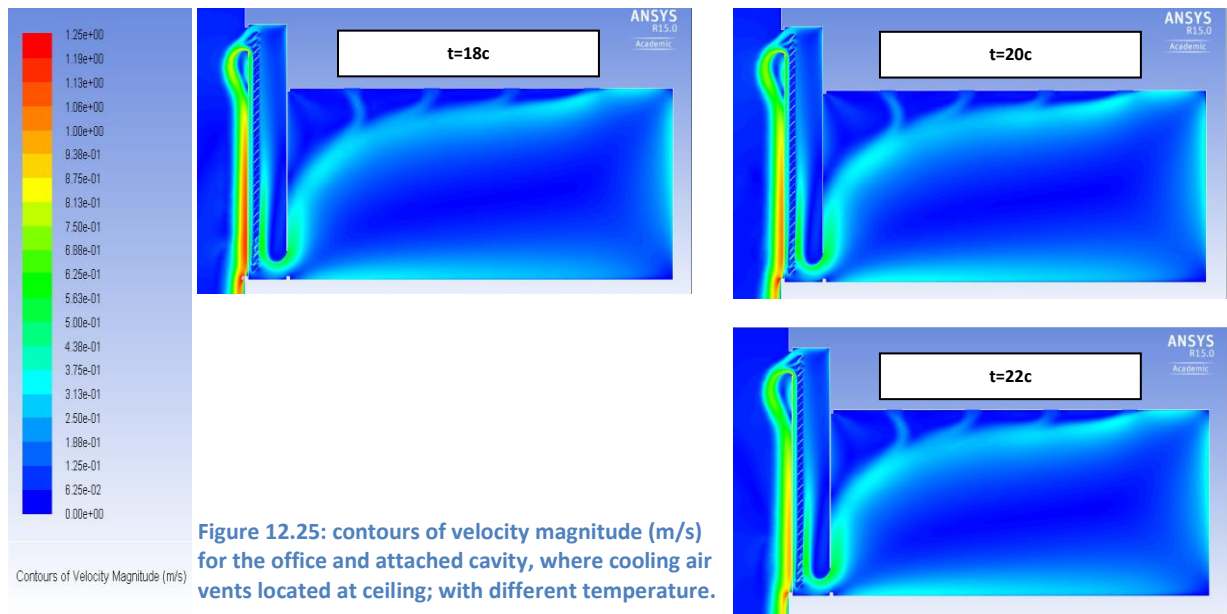


Figure 12.24: Tested proposal for placing cooling air vents at ceiling (B) instead of back-wall (A).

- **Airflow rate:**

As mentioned before, airflow rate was constant, 0.095m³/s-m. Similar to the previous study on back-wall vents, simulation showed that indoor air distribution and velocity were nearly typical for different inlet temperatures; Figure 12.25. However, maximum velocity would be increased with lower inlet temperature and that would be for external flow as discussed earlier.



- Temperatures:**

Similar to back-wall study, temperature profiles were nearly typical but varied in magnitudes, Figure 12.26, as there were no changes in airflow patterns as discussed before. For inlet temperature of 18°C, indoor temperature average at height of 1.6m was 21.8°C. In reference to that, increase in average was 3.3°C and 5.3°C for inlet temperatures of 20°C and 22°C; respectively.

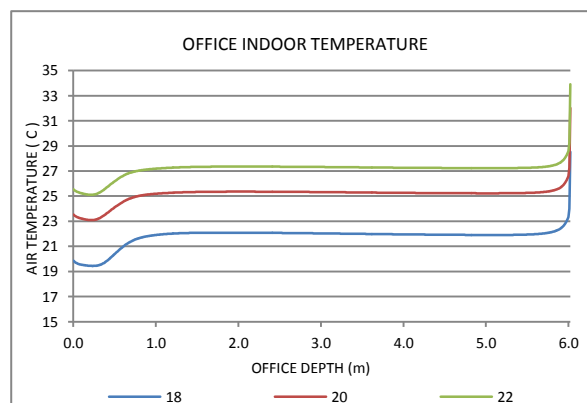


Figure 12.26: Indoor temperature at height of 1.6m for different temperatures of inlet air.

Figure 12.28 shows the temperature contours inside the space with almost minimum and maximum computed temperature range (scale: 18°C - 57°C). Changes in temperature contours were due to the change in inlet

temperature, which is clear in areas next to surfaces; e.g. ceiling. The cavity would also have higher air temperature with higher inlet temperature. The reason is that with higher inlet temperature, convection would be lower.

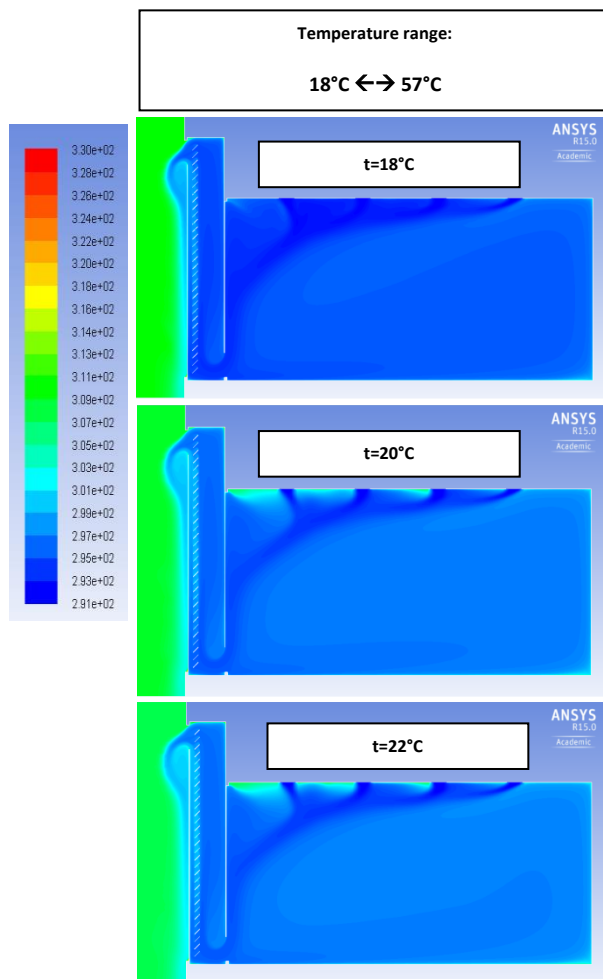


Figure 12.28: contours of static temperature (k) for the office and attached cavity; where cooling air vents located at ceiling; with different temperature. Scale Range: 18-57°C.

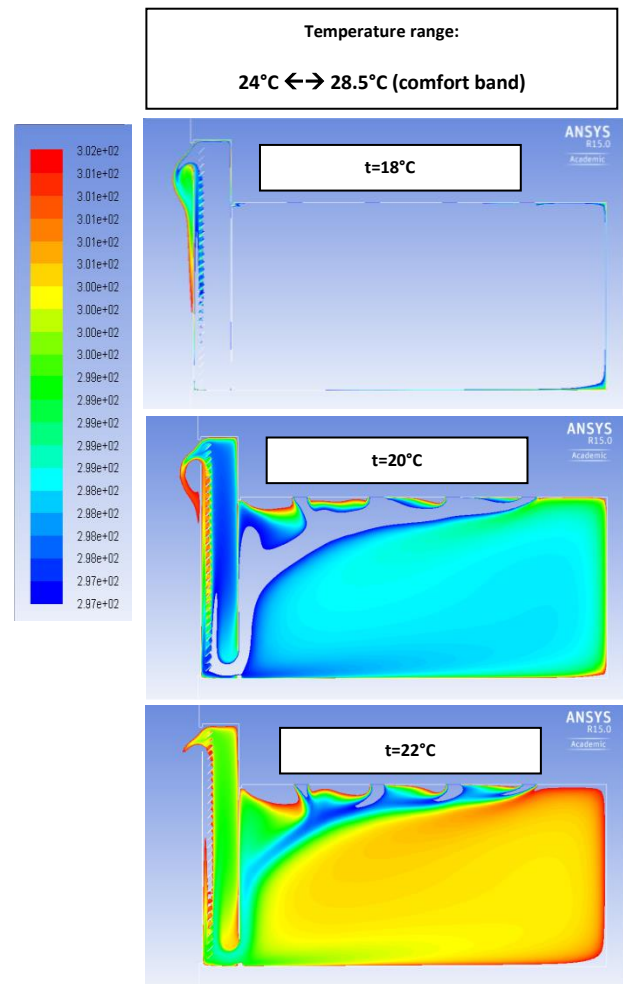


Figure 12.27: contours of static temperature (k) for the office and attached cavity; where cooling air vents located at ceiling; with different temperature. Scale range: 24-28.5°C.

Figure 12.27 shows same results but with a temperature scale equals thermal comfort (24°C - 28.5°C). It is clear that supplying the office with air at a temperature of 18°C would nearly produce an indoor environment that entirely has air temperature lower even than the bottom threshold of comfort (24°C). Next, the inlet temperature of 20°C would produce higher air temperature that almost falls in thermal comfort except for areas of main

stream of cooling air. Finally, the temperature of 22°C would visually make a reasonable output as almost all the indoor space is matching the thermal comfort; again except boundaries of cooling vents. However, extended areas for boundary layers next to surfaces would have a temperature that exceeds the upper threshold of thermal comfort but these are usually outside the occupied zone.

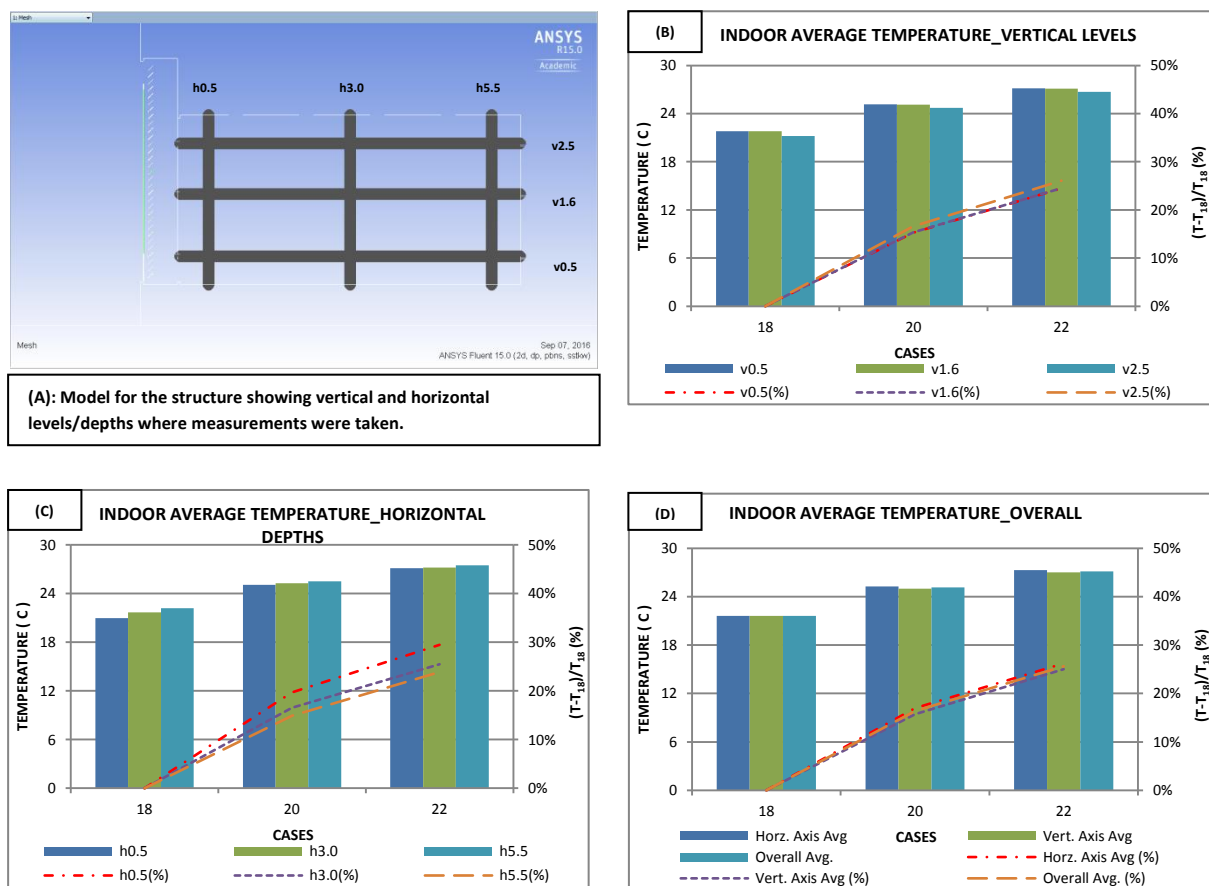


Figure 12.29: Indoor temperature averages and relative changes at various levels and depths for different temperatures of inlet air.

Similar to back-wall supply, indoor air temperature average would be increased with increasing inlet air temperature. However, with a same increase for inlet air temperature, rates of change for ceiling-vents design were higher than those for back-wall design, which applies for vertical, horizontal and overall averages; Figure 12.29. This was mainly due to

significant changes in airflow patterns inside so any increase in inlet air temperature would be treated differently. For example, with an inlet temperature of 22°C, overall change was 25.6% and 19.7% for ceiling-vents and back-wall; respectively.

Using inlet air temperature (T_{inlet}), indoor air temperature averages (e.g. $T_{air,vertical}$) could be predicted using the revealed polynomial equations of second degree (12.6) to (12.8).

$$T_{air,vertical} = -0.1735 T_{inlet}^2 + 8.2906 T_{inlet} - 71.417 \quad ; (R^2 = 1) \quad (12.6)$$

$$T_{air,horizontal} = -0.2096 T_{inlet}^2 + 9.8004 T_{inlet} - 86.883 \quad ; (R^2 = 1) \quad (12.7)$$

$$T_{air,all} = -0.1916 T_{inlet}^2 + 9.0455 T_{inlet} - 79.15 \quad ; (R^2 = 1) \quad (12.8)$$

Next, surfaces' temperatures had to be reported to find out operating temperature that matters the occupant thermal comfort. Surfaces' temperature averages would also be increased with a maximum change of 24.6% for ceiling element with inlet temperature of 22°C; Figure 12.30. As a result, operating temperature would be increased as well; Figure 12.31.

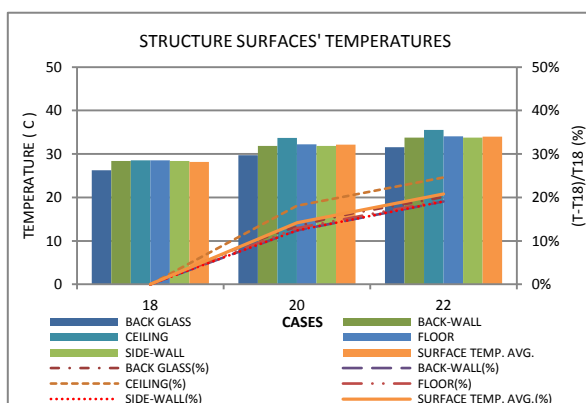


Figure 12.30: Temperature averages for different inner surfaces of space with relative changes for investigated cases regarding office's air supply vents.

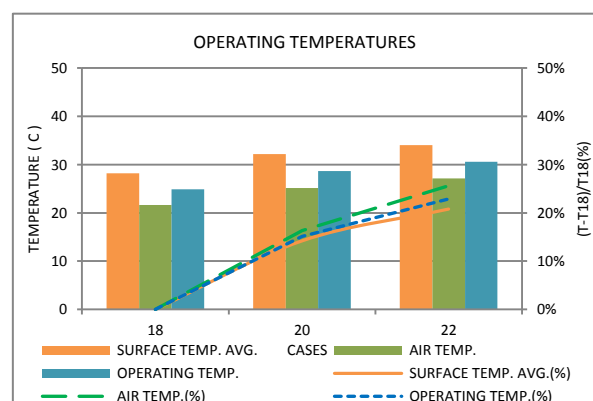
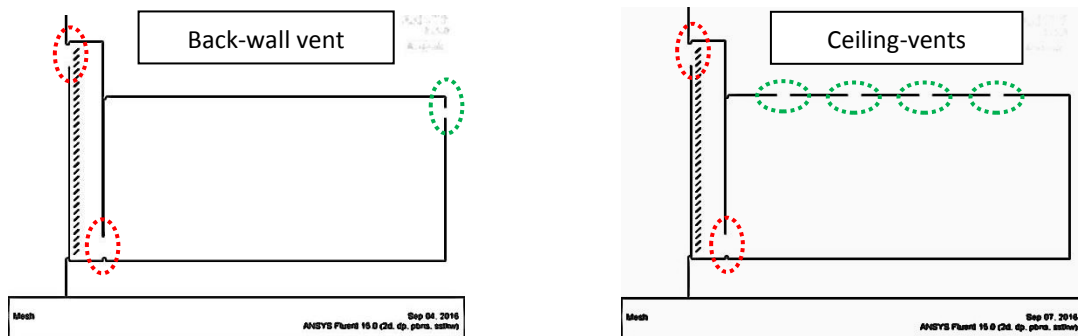
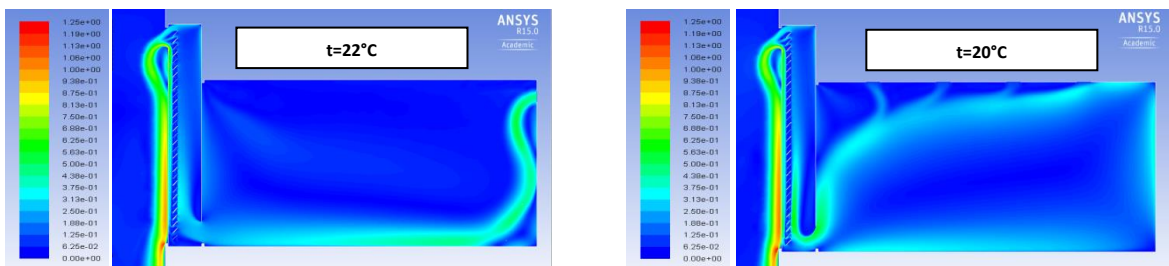


Figure 12.31: Averages for indoor surfaces temperature, air temperature and operating temperature with relative changes for investigated cases regarding office's air supply vents.

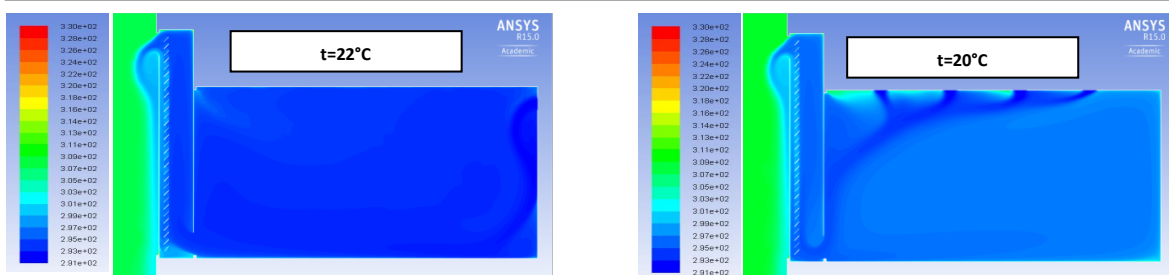
While inlet air temperature of 18°C would produce operating temperature of 24.9°C that falls in thermal comfort, setting inlet air temperature to either 20°C or 22°C would lead to a thermal discomfort as operating temperature was found to be 28.7°C and 30.6°C , respectively, which exceed upper threshold of thermal comfort (28.5°C).



(A): Structure schematic for both designs: Back-wall vent (Left) and Ceiling-vents (Right).



(B): contours of velocity magnitude (m/s) for the office and attached cavity. Left: Back-wall vents with inlet temperature= 22°C . Right: Ceiling-vents with inlet temperature= 20°C . Both could achieve thermal comfort.



(C): contours of static temperature (K) for the office and attached cavity. Left: Back-wall vents with inlet temperature= 22°C . Right: Ceiling-vents with inlet temperature= 20°C . Both could achieve thermal comfort.

Figure 12.32: Comparison between Back-wall vent and Ceiling-vents designs. Structures' schematic (A), Contours of Velocity magnitude (B) and Static temperature (C).

Referring to previous findings for back-wall design, indoor thermal comfort could easily be achieved with an inlet temperature of 22°C (even up to 23.5°C) however, it was revealed that the highest inlet temperature could

be used to maintain intended thermal comfort, should not exceed 20°C with ceiling-vents design. Figure 12.32 shows a comparison between both proposals.

Having known that ambient temperature is 37°C, it needs to be cooled down by 17°C with ceiling-vents compared to 13.5°C with back-wall vents. Therefore, sticking to back-wall design where cooling air enters the space from a single vent located at top of the wall seems to be the best option for better energy saving as well as achieving thermal comfort.

However, to save energy for cooling, a heat recovery device could be used to recover cooling from the exhaust air, which is at a much lower temperature than ambient air.

CHAPTER 13 OPTIMIZATION OF THE SYSTEM

(SUMMARY AND APPLICATION)

This chapter summarizes the main outcomes of previously discussed parametric studies on optimization of the office and DSF. This includes all part of the structure: office's indoor attached Double Skin Façade (DSF) and Cavity-Integrated Devices. The study was conducted for the two main climatic scenarios: summer and winter; where the day of peak conditions (air temperature °C and solar radiation) was considered for each. For these selected days, investigation and simulation were exclusively conducted for noontime, 12 pm. In general, main outcomes and recommendations could be applied to the rest hours of the day and extended to similar days. However, further detailed analysis with the hourly basis and for more design days is recommended to be continued in the future work.

The office has the dimensions of 6m (depth), 8m (width) and ceiling height of 3m. The cavity was designed with a width of 0.6m. Each skin of the structure consists of a glass with a transmittance of 0.8 for better daylighting. Also, there would be two separated vents located at bottom and top of each skin; these vents designed to be adjustable in size that depends on the operation conditions and mode. A set of shading devices (slats) would be installed inside the cavity. Those slats would be with a flat design and made of aluminum. Each slat would have a width of 120mm (20% of cavity's width) and a thickness of 3mm. Also, slats surface's emissivity is 0.2.

Also, the set's position would be adjustable between winter (P2: close to the inner skin) and summer (P8: close to the outer skin) as maximums. Another adjustable parameter for integrated slats is their inclination angle, which would be 30° and 45° for winter and summer; respectively.

13.1 Winter Scenario:

This section summarizes the final findings and design recommendations for winter conditions.

As discussed before, final agreed design for winter conditions would totally rely on natural ventilation and heating process. There would be two separated vents located at bottom and top of each skin. The recommended size for these vents would be 0.1m²-m and 0.2m²-m for outer and inner; respectively.

- **Airflow rate:**

Results show that the system would be able to provide sufficient fresh air requirements, about 0.065m³/s-m (65L/s-m), which even exceeds minimum requirements of 5L/s-m. Also, cavity flow rate was found to be about 0.02m³/s-m. However, cavity's flow would not be beneficial unless it is being used for preheating of incoming air into office, which is not the case here. Figure 13.1 presents the velocity fields inside the structure.

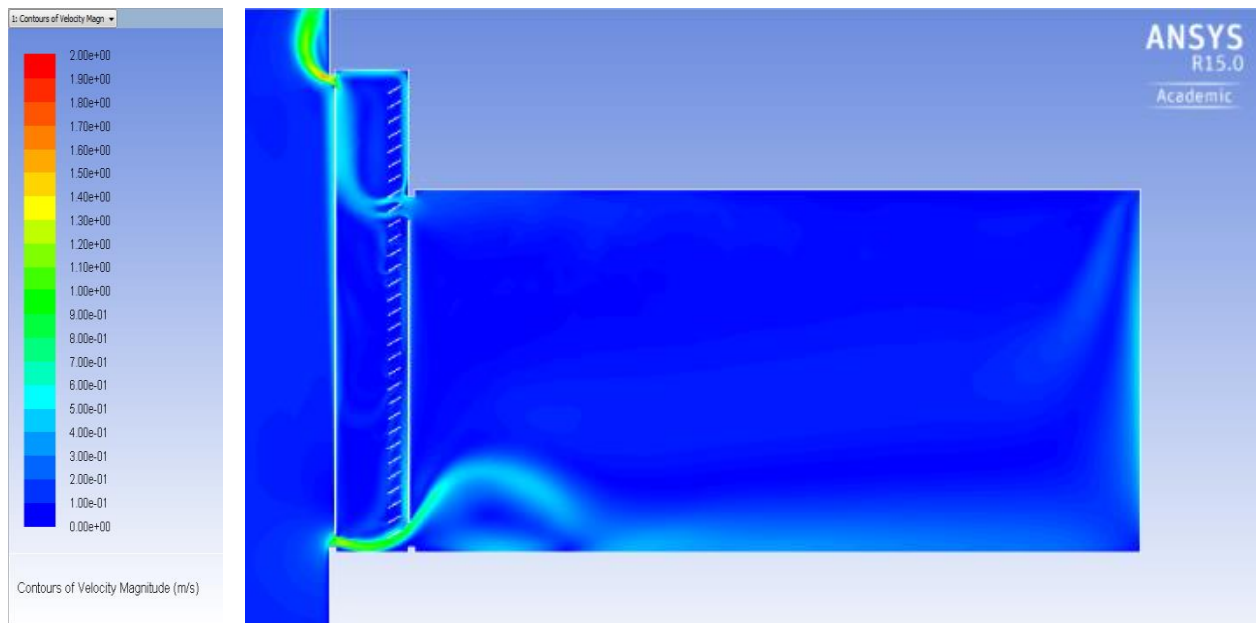


Figure 13.1: contours of velocity magnitude (m/s) for the office and attached cavity integrated with slats.

- Temperatures:**

Figure 13.2 shows the air temperature profile at height of 1.6m along the office depth. The average temperature was found to be about 14.21°C with maximums next to boundaries as 15.87°C and 19.63°C for inner glass's inner surface and back-wall; respectively.

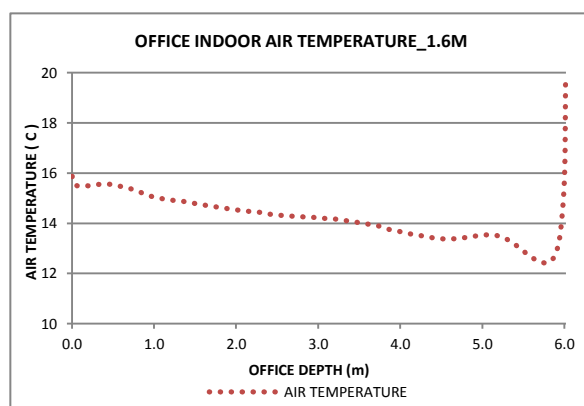


Figure 13.2: Indoor Air temperature at height of 1.6m with external vent size of 0.1m and internal size of 0.2m.

For the final selected design, Figure 13.3 presents the average temperate for different vertical and horizontal rakes assigned before. Results show that vertical measurements would have more significant variations than

horizontal ones, however, both would increase with distance increases: distance from the floor toward the ceiling for the aforementioned (e.g. v2.5) and distance from inner glass skin toward back-wall for the later (e.g. h5.5). Maximum magnitude difference for verticals was 6.4°C and changes from their average were -22% for v0.5m and 23% for v2.5. On the other hand, maximum variation for horizontals was less than 1°C and maximum change from average was about 4% for h0.5. Averages for vertical, horizontal and overall were 14.4°C, 14.6°C and 14.5°C; respectively.

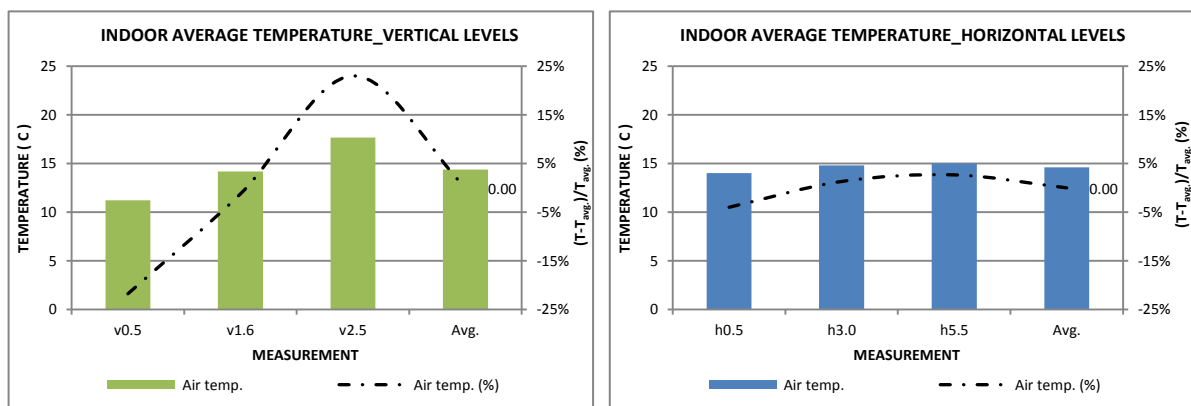


Figure 13.3: Indoor average temperature and relative changes at various levels (Left) and depths (Right) with external vents size of 0.1m.

Equation (13.1) could be used to calculate average temperature (T_{vertical}) along the office's depth at a given height (v). Similarly, equation (13.2) could be used to find out average temperature ($T_{\text{horizontal}}$) along any vertical axes placed certain distance (h) from inner glass skin.

$$T_{\text{vertical}} = 0.5949 v^2 - 1.4302 v + 10.374 \quad ; (R^2 = 1) \quad (13.1)$$

$$T_{\text{horizontal}} = -0.046 h^2 + 0.4703 h + 13.794 \quad ; (R^2 = 1) \quad (13.2)$$

Temperature averages for different indoor surfaces are presented in Figure 13.4. Total average was found to be about 32.77°C, which with air

temperature average resulted in an operating temperature of 23.63°C that falls in the required thermal comfort (18.5-24°C) for winter condition.

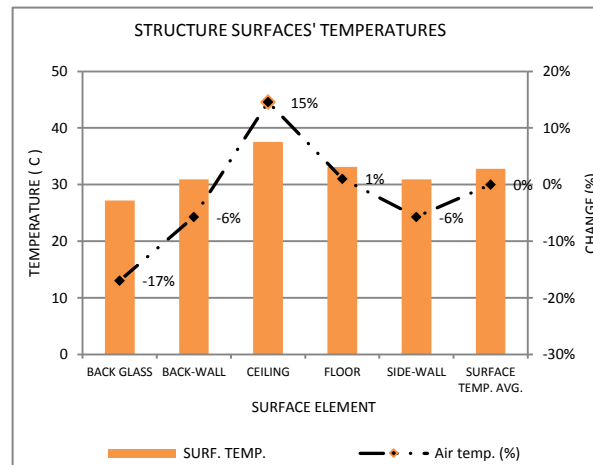


Figure 13.4: Temperature averages for different inner surfaces of space with relative changes during winter.

To conclude, the optimized design for investigated structure with integrated slats would be able to achieve both fresh air requirement and thermal comfort conditions during winter by just relying on outdoor boundary conditions, as there would be no need for any artificial heating means.

13.2 Summer Scenario:

This section summarizes the final findings and design recommendations for summer conditions.

For summer, a passive operation for the optimized system would not be capable to achieve thermal comfort where operating temperature would excessively exceed recommended thermal comfort (24°C-28.5°C). Therefore, it would be necessary to use mechanical air conditioning for cooling purposes.

Comparing to winter operation for the cavity's vents, just lower vents at the inner skin and upper vent at outer skin would be open to allow exhaust air getting out. Recommended size for each vent is 0.4m²-m. In addition, fresh

cooling air would be supplied from a vent ($0.2\text{m}^2\text{-m}$) located at the top of the back-wall.

- **Airflow rate:**

With an estimated solar gains of $755.2\text{W}/\text{m}^2\text{-m}$ and internal gains of $199.5\text{W}/\text{m}^2\text{-m}$, air flow rate was found to be about $0.095\text{m}^3/\text{s-m}$ with an inlet air temperature of 18°C , which was managed to be increased to about 23.5°C later on. This amount is required for two purposes: providing fresh air for occupants and helping continuously to remove accumulated contaminant from inside. Figure 13.5 presents the velocity fields inside the structure with artificial cooling with inlet air temperature of 24°C .

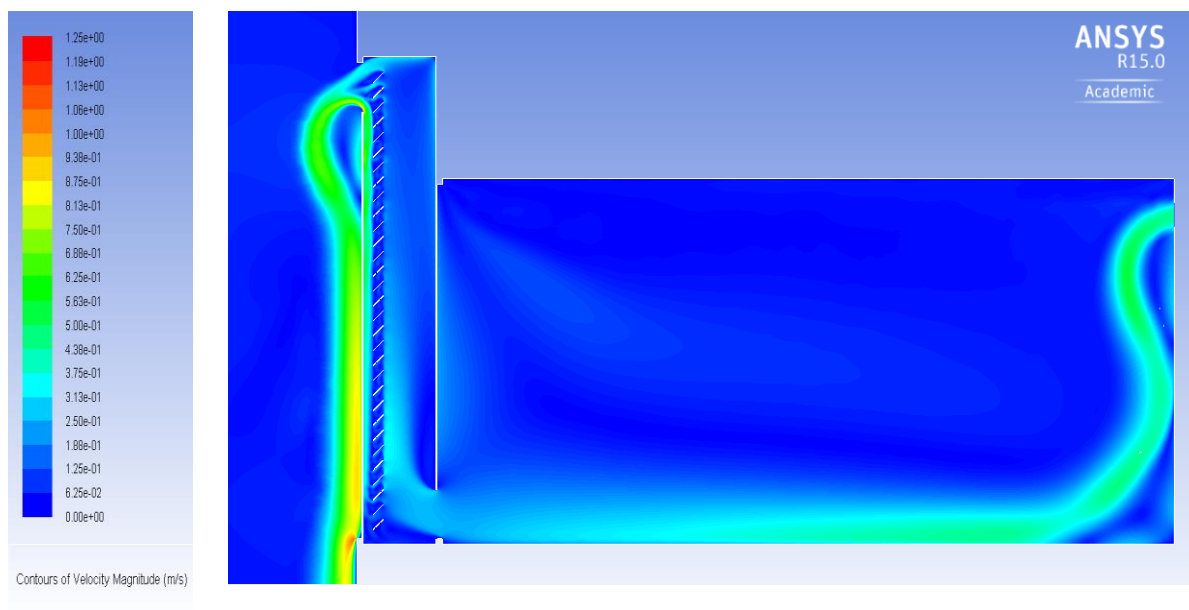


Figure 13.5: contours of velocity magnitude (m/s) for the office and attached cavity served with artificial cooling with 24°C during summer conditions.

- **Temperatures:**

Figure 13.6 shows the air temperature profile at height of 1.6m along the office depth with applying artificial cooling with inlet air temperature of 24°C (its 0.5°C higher than recommended value). The average air

temperature was found to be about 25.7°C with maximums next to boundaries as 26.19°C and 24.93°C for inner glass's inner surface and back-wall; respectively. Generally, the temperature profile is uniform except for the last half meter (next to back-wall).

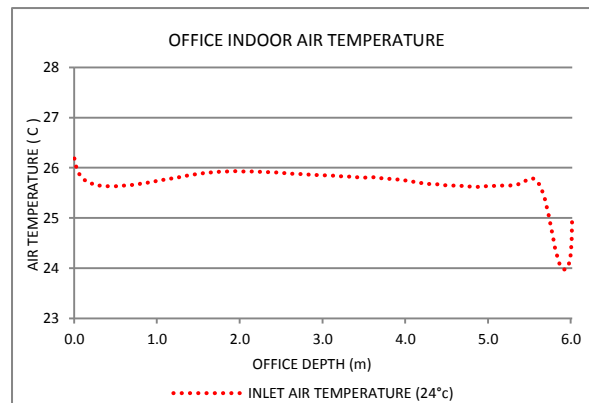


Figure 13.6: Indoor temperature at height of 1.6m for different temperatures of inlet air.

Furthermore, average temperature for different vertical and horizontal rakes assigned are presented in Figure 13.7. In general, and due to forced airflow, air temperature would be with high uniformity and nearly negligible variations ($<1\%$).

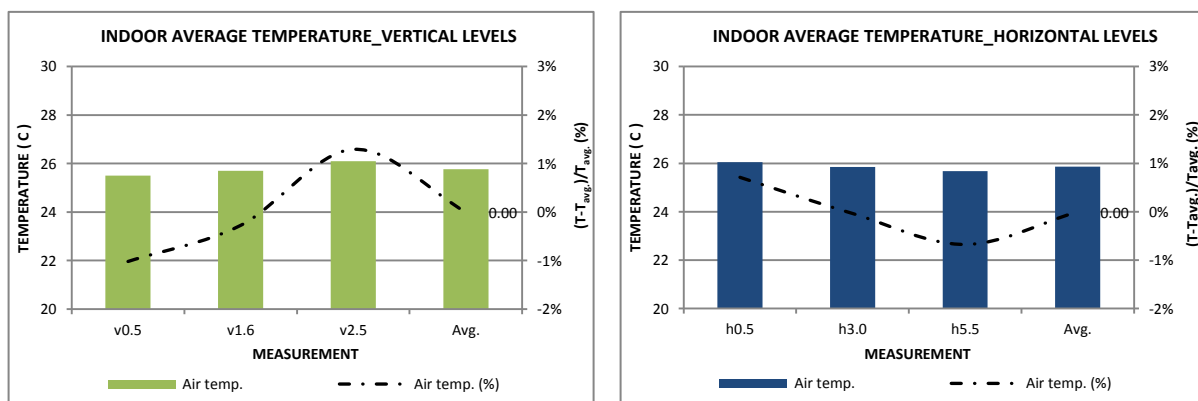


Figure 13.7: Indoor average temperature and relative changes at various levels (Left) and depths (Right) with external vents size of 0.1m.

Figure 13.8 shows the contours of temperature for the structure. It's clear how nearly the entire space would be within the comfort band (24°C-28.5°C), and its good uniformity.

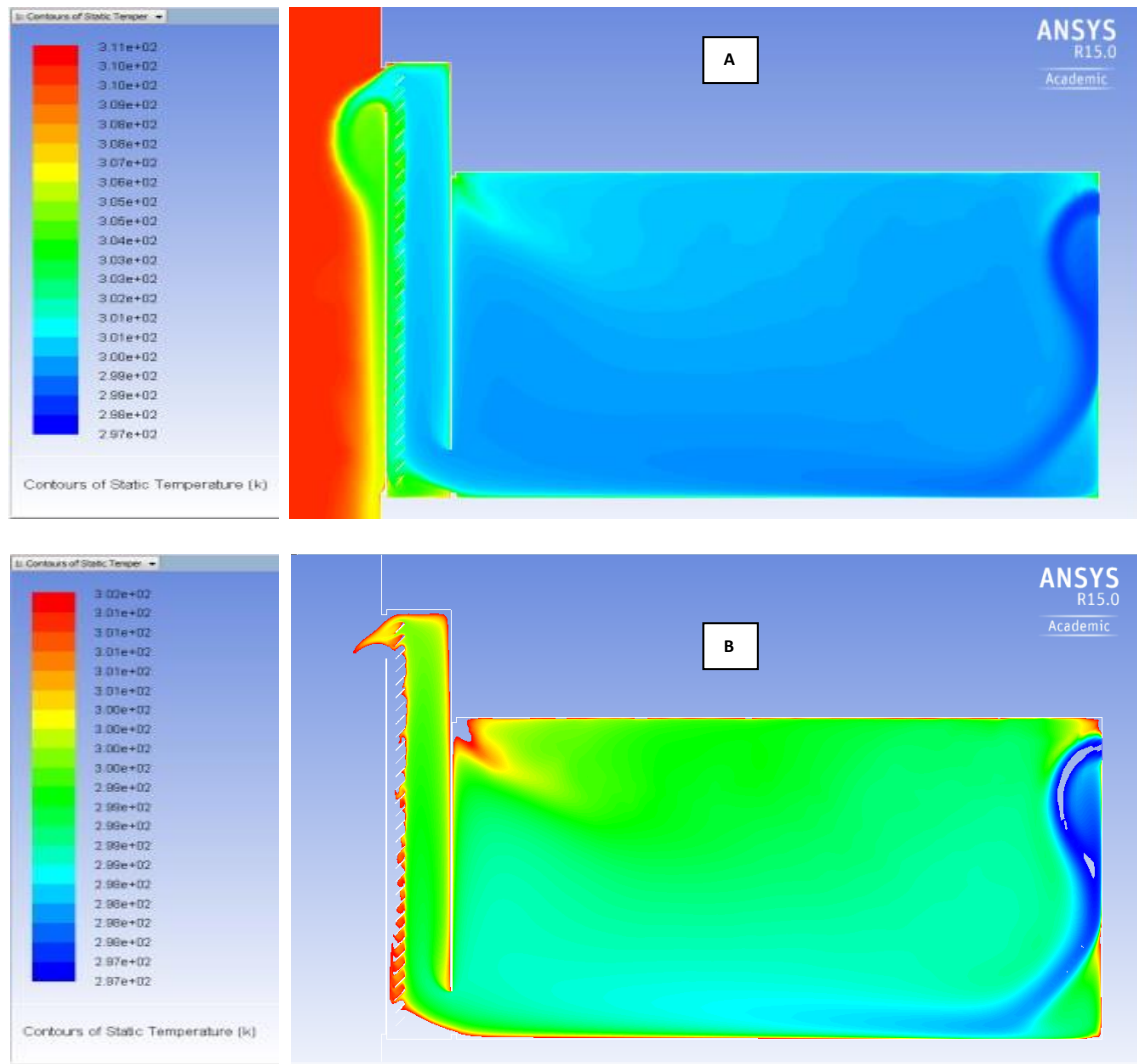


Figure 13.8: contours of static temperature (k) for the office and attached cavity integrated with slats. Temperature scale: A) 296°C - 311°C. B) 297.15°C - 301.65 “thermal comfort”.

Equations (13.3) and (13.4) could be used to find out average temperatures for vertical (T_{vertical}) and horizontal levels ($T_{\text{horizontal}}$); respectively.

$$T_{\text{vertical}} = 0.1369 v^2 - 0.113 v + 25.529 \quad ; (R^2 = 1) \quad (13.3)$$

$$T_{\text{horizontal}} = -0.0716 h + 26.072 \quad ; (R^2 = 0.9981) \quad (13.4)$$

Furthermore, temperature averages for different indoor surfaces were calculated as shown in Figure 13.9. The average temperature for all surfaces was 32.1°C. In contrast to winter, changes in surface temperature in reference

to average were limited to 3%. Having found that air temperature average was 25.8°C, operating temperature was found to be 28.95°C that is 0.45°C higher than recommended thermal comfort (24°C-28.5°C) for occupants in summer. This increase was expected as presented results for an inlet temperature of 24°C while recommended temperature is 23.5°C, calculated from revealed equation.

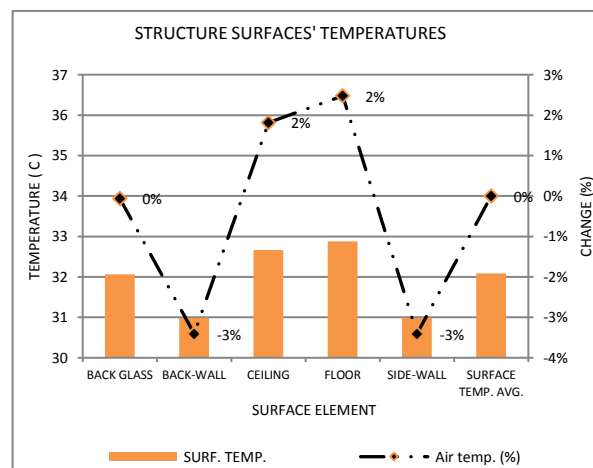


Figure 13.9: Temperature averages for different inner surfaces of space with relative changes during summer.

To conclude, while the requirement for fresh air was easily achieved with the passive optimization of the structure, it was necessary to have artificial cooling to achieve thermal comfort, as the ambient temperature is 37°C. With the optimization for artificial cooling, cooling air at a temperature of 23.5°C would enter the space from a single vent (0.2m²-m) located at the top of back-wall. After which, operating temperature average would be around 28.48°C.

CHAPTER 14 CONCLUSION, RECOMMENDATIONS AND FUTURE WORKS

14.1 Summary:

Double Skin Facade (DSF) system has many advantages that put it as a promising passive technology for building facades. Although many studies support the concept that DSF could work as a passive cooling strategy, there are still clear concerns regarding its thermal effectiveness during hot conditions. Whereas DSF's cavity and indoor space could experience summer overheating, enhancing DSF with cavity-integrated shading elements accompanied with proper ventilation mechanisms could help to overcome this issue. However, optimization of these elements is highly necessary.

This research aimed to further investigate the performance of DSF system for office space under both summer and winter scenarios. Moreover, special attention was given to the role of cavity-integrated shading slats and how they could affect the performance of DSF and indoors. Thus, an intensive parametric study was carried out concerning different design parameters of these slats. To achieve these objectives, a detailed computational model (CFD) for fluid and associated heat transfer was developed using ANSYS Fluent solver. Consequently, the developed model was intensively validated against experimental data and well-established general expressions (i.e. dimensionless number: Nu , Re). The model showed a good capability to simulate the proposed problem and predict airflow rate, air temperature, and surface temperature values.

The validation study showed that following parameters and factors should be carefully considered in computational modelling of similar problems. These include (1) detailed representation of the structure and its mediums (e.g. glass, air) with accurate solar and thermal characteristics, (2) accurate representation of the solar source in terms of magnitude, components (beam and diffuse) and angle of incidence, (3) quality and independence of mesh (4) proper selection for turbulence model, both RNG k- ϵ and SST k- ω were used as turbulence models, (5) external extension of the computational domain (six times the cavity width/openings).

A new method for more accurate representation "ACTUAL METHOD" of the solar source within Fluent model was introduced, and compared to conventional representation method "EQUIVALENT METHOD". The aforementioned method showed better representation for solar radiation, which would better serve designated objectives by this work. For example, with the simple cavity and vertical vents, the difference in airflow rate between the two methods changed from 4.2% for diffuse characteristics to -11.8% for specular characteristics. Moreover, this difference increased from 9% (for diffuse) to 28% (for specular) for the surface temperature of the inner glass.

First of all, a general parametric study was conducted on simple cavity with vertical vents and common parameters of design (e.g. cavity's width), to indicate vital parameters for controlling specific aspect of the system. Both cavity's width and opening size showed a significant role in controlling DSF's performance. Next, cavity-integrated shading elements were extensively investigated with several characteristics and design parameters such as size,

inclination angle, the shape of slat-unit and surface characteristics. The study showed that these parameters would differently affect DSF's performance. For cavity airflow, the size of slats would be the most influential parameter followed by surface's emissivity. For instance, cavity's airflow rate increased by 42% when slats' surface emissivity increased from 0 to 1. For inner glass surface temperature, the inclination angle of slats and their position inside the cavity would be the vital factors. For example, the increase in surface temperature of inner glass decreased by 29%, from 4.8°C to 3.4°C, as slats' inclination angle changed from 0° (fully opened) to 75°.

Moreover, results showed that cavity's aspect ratio (H/W) would dramatically affect its performance. For instance, with simple cavity of horizontal vents, this influence could reach 77% for airflow and up to 26% for back glass surface's temperature. At the same time, the influence of integrated slats was found to be dependent on the configuration of DSF (i.e. H/W). Furthermore, the detailed design of integrated slats could influence the system performance. However, this influence is still controlled by the cavity's aspect ratio (H/W), ambient boundary conditions (sun rays' angle of incidence), surface characteristics of these slats and properties of glass panes.

The proposed DSF was implemented into an office space and investigated under the climate of Amman. The study showed different optimum values for glass transmittance based on seasonal conditions. Optimum transmittance value was found to be 0.9 and 0.7 for summer and winter seasons, respectively. However, it was concluded that $t=0.8$ would be good enough to ensure indoor thermal comfort and ventilation rate for the

year. Similarly, optimum sizes for both cavity and openings were varied and dependent on seasonal conditions. However, size of the cavity was finally set to 0.6m for year-round. Yet, wider cavities are still recommended for summer but would lead to less usable perimeter areas while slightly affect DSF's performance. The size of openings was finally set to 0.4m for summer. For winter, inner and outer openings are recommended to be 0.2m and 0.1m, respectively. However, outer skin openings should further be controlled during winter conditions.

Finally, the proposed DSF integrated with flat shading slats was investigated with several parameters, and for office space in Amman. For better ventilation and thermal performance, optimum size for integrated slats was found to be 20% of cavity's size. Moreover, the inclination angle is recommended to be 45° for summer and 30° for winter. Furthermore, slat's surface emissivity of 0.2 would produce highest office's flow rate thus lowest indoor air temperature. However, it would slightly increase inner glass surface temperature. Yet, it is still preferred for enhancing natural daylighting at the deep part of space (better reflecting). For the position of slats, installing the integrated slats next to the outer glass pane (e.g. P9) would perform better for both indoor air temperature and the surface temperature of inner glass during summer. On the other hand, placing these devices next to inner glass (e.g. P2) is recommended in winter for same aspects. However, keeping an offset distance between the slats and adjacent surfaces is highly recommend to ensure sufficient ventilation for these surfaces and avoid overheating especially during summer. Whereas it is possible to achieve both seasonal

recommendations using a slider, these slats could be placed in the middle of the cavity (i.e. P5) instead. Moreover, it is still recommended to investigate the influence of slats' position on indoor natural daylight.

To conclude, the optimized design for the investigated system with integrated slats would be able to achieve both fresh air requirement (10L/s/person) and thermal comfort conditions (defined as 18.5°-24°C) passively in **winter** when there is sunshine. Thus, there would be no need for any artificial heating means. In **summer**, with an ambient temperature of 37°C, artificial cooling is still needed to achieve indoor thermal comfort (defined as 24°-28.5°C). Ventilating the office mechanically with cooling air at 23.5°C temperature would maintain the indoor operative temperature around 28.48°C thus ensure indoor thermal comfort assuming that other factors (e.g. air velocity) of indoor thermal comfort are within their normal ranges.

14.2 Conclusion, Key outcomes & Recommendations:

Based on conclusion and key outcomes of the conducted research, following recommendations are derived:

Modelling Perspective:

- The importance of detailed modelling of the problem and its parameters of interest, e.g. materials, configurations, aspect ratio, boundary conditions, etc.
- The necessity of accurate representation of the solar source in a way that serves objectives of the study. For example, including actual angle of incidence and both beam and diffuse magnitudes with different solar bands.

- The need to study the structure as a whole problem instead of investigating different parameters separately, as the performance of any parameter is highly influenced and controlled by other parameters and characteristics of the structure; such as aspect ratio and semi-transparent properties.

Design Perspective:

- Giving special attention to the configuration of the cavity; in particular, openings size & arrangement, cavity width & aspect ratio, solar and thermal characteristics of its elements.
- Using cavity-integrated slats to avoid summer overheating. In addition, giving special attention to their design parameters as following: size, inclination angle, surface emissivity (absorptivity) and position. However, this order in priority is varied and depends on the targeted perspective (e.g. ventilation rate, the temperatures of surfaces and/or air).
- The detailed design (e.g. effective height of slat-unit) of integrated slats should be considered carefully not only for natural daylighting but also for both thermal and ventilation. The difference between several designs could reach 20% for ventilation and 25% for surfaces' temperature increase, both depend on surfaces' characteristics and boundary conditions.
- In Amman city, using DSF system is generally recommended for office buildings, as it would work passively toward achieving indoor thermal comfort in heating seasons without the need for artificial means. In summer, the performance of DSF is still acceptable as it would reduce total solar gains; however, using integrated shading slats is highly recommended to further reduce direct solar gains (to mitigate indoor overheating). Yet, DSF should be well ventilated to avoid cavity overheating. However, simulation showed that artificial cooling is still needed to ensure thermal comfort in extreme hot times. On the hottest day, ambient air should be cooled down by around 13.5°C to be efficiently used for indoor cooling.

- Cavity width to be at least 0.6m (with 4m high structure). Wider cavities are possible however it would reduce usable perimeter areas.
- Single pane clear-glass (6mm) is recommended for both skins. The optimum value for glass transmittance was found to be 0.7-0.9 ($t=0.8$ is good to ensure thermal comfort for both summer and winter while allowing more natural daylighting).
- The need to control openings' size during heating times. Preferable to be controlled by occupant themselves or automatically programmed based on their preferences.
- The optimum size for integrated slats is 20% of cavity's size.
- In the case of flat slats, the inclination angle of 45° degrees is recommended in summer and angle of 30° degrees in winter; therefore, adjusting tilt angle is generally recommended.
- Slats to be made (or coated) with high-reflective surfaces (low absorptivity) to reflect solar radiation toward outdoor and enhance indoor daylighting.
- Slats to be placed next to outer glass during cooling times, and next to inner glass during winter times; therefore, adjusting their position is also recommended using a slider.

Application Perspective:

- The need to combine between good shading technique and proper ventilation strategy.
- The possibility to rely just on natural ventilation and solar gains for winter thermal comfort "operating temperature" as a passive design strategy.
- The need to use mechanical cooling to ensure summer thermal comfort.

14.3 Contribution to the Body of Knowledge:

The novelty of this of this research and its contribution to the body of knowledge are substantiated by following achievements:

- Development of a Fluent model that is more suitable for investigating glazed structures (e.g. DSF) with varied and complex designs of integrated slats (compared to 2D model); and at a reasonable cost in terms of time and computing resources (compared to 3D with solar load model).
- Demonstration of the importance of accurate representation (including the angle of incidence) of solar radiation in case of modelling of complex fenestration systems; and how inappropriately simplifying this factor could affect the validity of predictions.
- Establishment of a framework for schematic validation process of computational models concerning the finite volume method and more specifically deal with fluid and heat transfer problems. This covers independence of mesh, extension of the computational domain, selection of proper turbulence model.
- Expansion of the established literature on how DSF would perform under hot summer and cold winter conditions, including further exploration of the vital parameters that control its performance; e.g. H/W aspect ratio.
- Expansion of the established knowledge regarding the role of cavity-integrated shading elements (as complex fenestration system) on the performance of DSF system and indoors. This covers their design parameters (i.e. size, angle, position) and various surface's characteristics (i.e. emissivity and diffusivity).
- Exploration of the performance (airflow and thermal) of various designs of solar shading and daylighting products and providing an insight into how they would perform as integrated elements of DFS.
- Investigation into the role of the detailed design of integrated slats and to what extent this would influence their function. Most importantly, exploring the relation between their performance and characteristics of

the structure (i.e. H/W). This proves the necessity for more comprehensive investigation based on a realistic combination of various design parameters and operation conditions (e.g. boundary conditions).

- Generation of a set of empirical mathematical correlations for the performance of DSF system based on its configuration characteristics. These correlations could be used for further analysis of the system and as a design guidance.
- Filling the knowledge gap regarding the performance of DSF systems (with and without integrated shading elements) in the city of Amman, through providing a good insight into the potential operation of DSF systems over there. Moreover, some recommendations and guidelines for designers and engineers were developed. In addition, outcomes of this research form a good platform for further studies on such system in Amman or similar cities of Jordan.

14.4 Research Limitations:

As any research and project with time-frame, there were some restrictions and limitations that influenced the research outcomes; so it is highly recommended to be avoided in future works. Most of these limitations are related to time and facilities. Following points highlight these limitations:

- It was not possible to carry out a distinctive experimental work for this study due to facilities and time limitations.
- The work was carried out with two-dimensional (2D) model due to complexity of modelling thus highly time-dependent progress.
- All simulations were conducted with steady state assumptions.
- The work was limited to just summer and winter scenarios; and even, to just two design days (peak summer and winter) with one design hour (12 pm).
- The study was limited to the airflow and thermal performance of the system as the visual performance was not investigated.

- The study was carried out for one-storey office building. Yet, it is still recommended to investigate its performance with multi-storeys building and different functions and varied urban context.

14.5 Future Works:

Based on outcomes and understanding of this project, a set of suggestions and plans for future works are summarized as follows:

- As the existing experimental data for DSF are not of sufficient details or quality for comprehensive validation of a computational model, new experimental work should be carried out that allow for more technical details and precise measurements. Such experimental work would more effectively serve the objectives of similar research in future and provide more comprehensive data for the purpose of validation of computational models.
- Use unsteady (transient) simulations to provide insight into the dynamic performance of DSF system.
- Use three-dimensional (3D) modelling to examine all possible directions and angles of incidence of sunrays using the solar load model in FLUENT to avoid any unintended simplifications.
- Expand the work to cover more design days and weather conditions of Amman city.
- Apply the system to multi-storey buildings and with different functions in Amman city. Also, investigate other types of DSF (e.g. corridor type). Moreover, investigate the possibility of two-side ventilation.
- Use more comprehensive modelling techniques (i.e. building energy simulation (BES) tools with hourly-based climate data coupled with CFD), which allow for overall evaluations of the system and for year-round.
- Study the visual performance of DSF with cavity-integrated elements of various designs. This includes indoor daylight requirements and glare issues. This would allow for more comprehensive optimization for DFS and integrated elements towards multi-functional design (tripartite: solar shading, natural ventilation, and visual performance).

- Examine more materials for integrated slats such as phase change materials (PCMs) and investigate the possibility of night-time ventilation. Also, develop these elements as energy storage systems (e.g. solar water heating).
- Consider further issues related to glazed structures with wet and cold conditions such as condensation.

REFERENCES:

- ABDALI-BOULEVARD. 2013. BOULEVARD - The Walk of the Town [Online]. Available: <http://www.abdali-boulevard.jo/> [Accessed 1/11/2013].
- ABDALI. 2012a. ABOUT THE ABDALI PROJECT: BUSINESS, LIVING & LEISURE [Online]. Economic and Commerce Bureau, Embassy of Jordan. Available: <http://www.abdali.jo/index.php?r=site/page&id=4> [Accessed 19-10-2013].
- ABDALI. 2012b. SUSTAINABILITY: Green Initiative for Clean Environs [Online]. ABDALI. Available: <http://www.abdali.jo/index.php?r=site/page&id=24> [Accessed 19-10-2013].
- ABDALI. 2013a. CONSTRUCTION PROGRESS [Online]. Available: <http://www.abdali.jo/index.php?r=construction/index> [Accessed 1/11/2013].
- ABDALI. 2013b. Panoramic Image - Abdali, the new downtown of Amman [Online]. Available: <http://www.abdali.jo/index.php?r=site/page&id=10> [Accessed 1-11-2013].
- ABU-ZOUR, A., RIFFAT, S. & GILLOTT, M. 2006. New design of solar collector integrated into solar louvres for efficient heat transfer. *Applied thermal engineering*, 26, 1876-1882.
- AFONSO, C. & OLIVEIRA, A. 2000. Solar chimneys: simulation and experiment. *Energy and Buildings*, 32, 71-79.
- AHMED, M., ABEL-RAHMAN, A., ALI, A. & SUZUKI, M. 2016. Double Skin Façade: The State of Art on Building Energy Efficiency. *Journal of Clean Energy Technologies*, Vol. 4, 84-89.
- AL-ASAD, M. 2005. Ever-growing Amman-Urban Crossroads #42.
- AL-ASAD, M. 2013. The Newest Phase of Amman's Growth, Urban Crossroads #130. [Accessed 19-10-2013].
- AL-SALAYMEH, A., AL-HAMAMRE, Z., SHARAF, F. & ABDELKADER, M. R. 2010. Technical and economical assessment of the utilization of photovoltaic systems in residential buildings: The case of Jordan. *Energy Conversion and Management*, 51, 1719-1726.
- ALIBABA, H. Z. & OZDENIZ, M. B. 2011. Thermal comfort of multiple-skin facades in warm-climate offices. *Scientific Research and Essays*, 6, 4065-4078.
- ALZOUBI, H. H. & AL-ZOUBI, A. H. 2010. Assessment of building façade performance in terms of daylighting and the associated energy consumption in architectural spaces: Vertical and horizontal shading devices for southern exposure facades. *Energy Conversion and Management*, 51, 1592-1599.
- AMAIREH, I. 2012. Improving the Performance of PV Integrated Shading Devices (PVSD) for Glazed Facades of Commercial Buildings in JORDAN: Investigation and Design. MSc, The University of Nottingham.
- AMAIREH, I. 2016. CLIMATE DATA FOR AMMAN CITY OF JORDAN-EXCEL SHEET.
- AMARALA, A. R., RODRIGUESA, E., GASPARA, A. R. & GOMESB, Á. 2015. A PARAMETRIC STUDY ON WINDOW-TO-FLOOR RATIO OF DOUBLE WINDOW GLAZING AND ITS SHADOWING USING DYNAMIC SIMULATION. 3 EJIL - LAETA Young Researchers Meeting. ADAI, Coimbra.
- ANGELI, D. & DAMA, A. 2015. Modelling Natural Ventilation in Double Skin Facade. *Energy Procedia*, 78, 1537-1542.
- ARCHITECTS, F. F. 2011. High Judiciary House / CategoryFuture Projects - Competition entries / LocationAmman, Jordan [Online]. Available: <http://www.worldbuildingsdirectory.com/project.cfm?id=3475>.
- ARCHITECTS, R. P. 2012. Understanding overheating – where to start: An introduction for house builders and designers [Online]. Richards Partington Architects. Available: <http://www.nhbcfoundation.org/Researchpublications/NF44zmagstest/tabid/517/language/en-US/Default.aspx>.
- ARONS, D. M. 2000. Properties and applications of double-skin building facades. Massachusetts Institute of Technology.
- ASFOUR, O. S. & GADI, M. B. 2007. A comparison between CFD and Network models for predicting wind-driven ventilation in buildings. *Building and Environment*, 42, 4079-4085.

- ASHRAE 1992. *Standard 55 - Thermal environmental conditions for human occupancy*, Atlanta, USA, American Society of Heating, Refrigerating and Air-conditioning Engineers Inc.
- AWADALLAH, T. 2013a. *Climate data for University of Jordan's weather station in Amman*. Excel Sheet. Amman, Jordan.
- AWADALLAH, T. 2013b. *Psychometric Chart of Amman "University of Jordan's weather station"*. Excel Sheet. Amman, Jordan.
- AWADALLAH, T., ADAS, H., OBAIDAT, Y. & JARRAR, I. 2009. *Energy Efficient Building Code for Jordan*. GCREEDER 2009. Amman-Jordan.
- BALDINELLI, G. 2009. Double skin façades for warm climate regions: Analysis of a solution with an integrated movable shading system. *Building and Environment*, 44, 1107-1118.
- BALOCCO, C. 2002. A simple model to study ventilated facades energy performance. *Energy and Buildings*, 34, 469-475.
- BANFILL, P. P. The risk of buildings overheating in a low-carbon climate change future. ICEBO conference, 2012.
- BANI-DOMI, M. 2005. *Trend Analysis of Temperatures and Precipitation in Jordan*. Dept. of Geography Yarmouk University, Irbid-Jordan.
- BATAINEH, K. & FAYEZ, N. Thermal performance of building attached sunspace in Jordan climate. Nuclear & Renewable Energy Conference (INREC), 2010 1st International, 21-24 March 2010 2010. 1-6.
- BATAINEH, K. & FAYEZ, N. 2011. Analysis of thermal performance of building attached sunspace. *Energy and Buildings*, 43, 1863-1868.
- BBRI, B. B. R. I. 2002. *Source book for a better understanding of conceptual and operational aspects of active façades*, Department of Building Physics, Indoor Climate and Building Services, Belgian Building Research Institute.
- BIRD, R. E. & RIORDAN, C. 1984. *Simple Solar Spectral Model for Direct and Diffuse Irradiance on Horizontal and Tilted Planes at the Earth's Surface for Cloudless Atmospheres*, Technical Report No. SERI/TR-215-2436, Golden, CO: Solar Energy Research Institute.
- BOAKE, T., HARRISON, K., COLLINS, D., BALBAA, T., CHATHAM, A., LEE, R. & BOHREN, A. 2008. The tectonics of the double skin: green building or just more hi-tech hi-jink?—What are double skin façades and how do they work? University of Waterloo.
- BOHRA, D., SHAILY, G., VATS, S. & ZUMBRE, S. V. 2016. RETROFITTING VIKAS MINAR - FAÇADE TREATMENT - "WAYS TO REDUCE ENERGY CONSUMPTION OF A BUILDING THROUGH FAÇADE TREATMENT" [Online]. SlideShare. Available: <https://www.slideshare.net/RudraJaisal/retrofitting-of-vikas-minar-facade-design-final> [Accessed 9/1/2017].
- BRANDL, D., MACH, T., GROBBAUER, M. & HOCHENAUER, C. 2014. Analysis of ventilation effects and the thermal behaviour of multifunctional façade elements with 3D CFD models. *Energy and Buildings*, 85, 305-320.
- BRIEF, G. P. 2014. Horizon Group Opens USD \$423 Million "The Boulevard" in Amman [Online]. Available: <http://stonecreek-partners.com/qpb/horizon-group-opens-usd-423-million-boulevard-amman/> [Accessed 9/1/2017].
- BROWNARCH3230. 2011. *Personal Preferences and their role in Building Systems Design*. [Accessed 30/08/2013].
- BSI, B. S. I. 2005. *Ergonomics of the thermal environment. Analytical determination and interpretation of thermal comfort using calculation of the PMV and PPD indices and local thermal comfort criteria*, London, BSI.
- BSI, B. S. I. 2007. *Indoor Environmental Input Parameters for Design and Assessment of Energy Performance of Buildings Addressing Indoor Air Quality, Thermal Environment, Lighting and Acoustics*, London, BSI.
- CHAN, A., CHOW, T., FONG, K. & LIN, Z. 2009. Investigation on energy performance of double skin facade in Hong Kong. *Energy and Buildings*, 41, 1135-1142.
- CHOW, W. K. & HUNG, W. Y. 2006. Effect of cavity depth on smoke spreading of double-skin façade. *Building and Environment*, 41, 970-979.

- CIBSE 2006. *Environmental Design, Guide A*. The Chartered Institution of Building Services Engineers, London.
- COMMISSION, R. J. 2007. *Summary-Updated Master Strategy of Energy Sector in Jordan for the period (2007-2020). First Part* [Online]. Jordan. Available: <http://www.jordanecb.org/library/634448574517466250.pdf> [Accessed 1-11-2013].
- CRESPO, A. M. L. 1999. *3x2: Three Takes on Double Skins*. Harvard University.
- D.LITE. 2017. *Light Shelves - System Description* [Online]. Available: http://www.d-lite.org/page/light_shelves_p101.php [Accessed 9/1/2017].
- D'INGÉNIERIE, T. E. S. S. A. 2014. *Rotana Hotel - Construction of the Rotana hotel tower, Amman, Jordania* [Online]. Available: <http://www.tess.fr/en/projet/rotana-hotel#> [Accessed 9/1/2017].
- DATABASE, W. B. D.-O. 2011. *High Judiciary House* [Online]. Available: <https://www.worldbuildingsdirectory.com/content/high-judiciary-house?co=203&t=&page=1> [Accessed 9/1/2017].
- DENGEL, A. 2012. *Overheating in new homes-A review of the evidence*. NHBC Foundation.
- DENGEL, A., SWAINSON, M., ORMANDY, D. & EZRATTY, V. 2016. *Guidance Document: Overheating in dwellings*. Building Research Establishment (BRE).
- DENTON, G. S. 2009. *CFD simulation of highly transient flows*. UCL (University College London).
- DIGERT, N. E., CARLSBAD, CA (US) & HOLTZ, M. J., BOULDER, CO (US). 2002. *MINI-OPTICAL LIGHT SHELF DAYLIGHTING SYSTEM*. USA patent application 09/776,319.
- DING, W., HASEMI, Y. & YAMADA, T. 2005. *Natural ventilation performance of a double-skin façade with a solar chimney*. *Energy and Buildings*, 37, 411-418.
- E-ARCHITECT. 2013. *Queen Alia International Airport Building, Gateway to Amman, Design: Foster + Partners* [Online]. Available: http://www.e-architect.co.uk/jordan/queen_alia_international_airport.htm [Accessed 9/1/2017].
- EICKER, U., FUX, V., BAUER, U., MEI, L. & INFELD, D. 2008. *Façades and summer performance of buildings*. *Energy and Buildings*, 40, 600-611.
- ELSAGHEER, M. 2013. *Energy Situation in Jordan*. Jordan: Ministry of Planning and International Cooperation.
- FANGER, P. O. 1970. *Thermal comfort: Analysis and applications in environmental engineering*, Danish Technical Press.
- FLUENT 2005. *Fluent User's Guide - Version 6.2*. Fluent Inc., Centerra Resource Park, Lebanon, NH: ANSYS, Inc.
- FLUENT 2012a. *14.5 Theory Guide*. Canonsburg, PA, USA: ANSYS Inc.
- FLUENT 2012b. *14.5 User's Guide*. Fluent Inc., Lebanon, NH.
- FOSTER+PARTNERS. 2007. *Work starts on new mixed-use development in Amman* [Online]. Available: <http://www.fosterandpartners.com/news/archive/2007/06/work-starts-on-new-mixed-use-development-in-amman/> [Accessed 9/1/2017].
- FREEWAN, A. A. *Improving thermal performance of offices in JUST using fixed shading devices*. World Renewable Energy Congress in Sweden, May, 2011. 8-13.
- GADI, M. B. 2010. *27 - Application of design and passive technologies for thermal comfort in buildings in hot and tropical climates A2 - Hall, Matthew R. Materials for Energy Efficiency and Thermal Comfort in Buildings*. Woodhead Publishing.
- GAN, G. 2011a. *General expressions for the calculation of air flow and heat transfer rates in tall ventilation cavities*. *Building and Environment*, 46, 2069-2080.
- GAN, G. 2011b. *Prediction of heat transfer and air flow in solar heated ventilation cavities*. In: MURPHY, A. D. (ed.) *Computational fluid dynamics: theory, analysis and applications*. New York: Nova Science Publishers.
- GAVAN, V., WOLOSZYN, M., KUZNIK, F. & ROUX, J. 2010. *Experimental study of a mechanically ventilated double-skin façade with venetian sun-shading device: A full-scale investigation in controlled environment*. *Solar Energy*, 84, 183-195.
- GAVAN, V., WOLOSZYN, M., ROUX, J., MURESAN, C. & SAFER, N. *An investigation into the effect of ventilated double-skin Facade with venetian blinds: Global simulation and assessment of energy performance*. *Proceedings*, 2007. 127-133.

- GOVERNMENT, D. F. C. A. L. 2012. *Investigation into Overheating in Homes - Literature Review*. UK: Department for Communities and Local Government.
- GRATIA, E. 2006. *Thermique des immeubles de bureaux*, Presses univ. de Louvain.
- GRATIA, E. & DE HERDE, A. 2004a. Is day natural ventilation still possible in office buildings with a double-skin façade? *Building and Environment*, 39, 399-409.
- GRATIA, E. & DE HERDE, A. 2004b. Natural cooling strategies efficiency in an office building with a double-skin facade. *Energy and Buildings*, 36, 1139-1152.
- GRATIA, E. & DE HERDE, A. 2004c. Natural ventilation in a double-skin facade. *Energy and Buildings*, 36, 137-146.
- GRATIA, E. & DE HERDE, A. 2004d. Optimal operation of a south double-skin facade. *Energy and Buildings*, 36, 41-60.
- GRATIA, E. & DE HERDE, A. 2007a. Are energy consumptions decreased with the addition of a double-skin? *Energy and Buildings*, 39, 605-619.
- GRATIA, E. & DE HERDE, A. 2007b. Greenhouse effect in double-skin facade. *Energy and buildings*, 39, 199-211.
- GRATIA, E. & DE HERDE, A. 2007c. The most efficient position of shading devices in a double-skin facade. *Energy and Buildings*, 39, 364-373.
- HAASE, M. & AMATO, A. 2006. Design considerations for double-skin facades in hot and humid climates. *Envelope Technologies for Building Energy Efficiency*.
- HAASE, M., MARQUES DA SILVA, F. & AMATO, A. 2009. Simulation of ventilated facades in hot and humid climates. *Energy and Buildings*, 41, 361-373.
- HADLOCK, C. Modelling and Optimization of an Airflow Window with Between-the-Panes Shading Device. *Masters Abstracts International*, 2006.
- HAMZA, COOK & CROPPER 2011. COMPARATIVE ANALYSIS OF NATURAL VENTILATION PERFORMANCE IN NON-UNIFORM DOUBLE SKIN FACADES IN TEMPERATE CLIMATES.
- HAMZA, N. 2004. The performance of double skin facades in office building refurbishment in hot arid areas; PhD Thesis. PhD, University of Newcastle upon Tyne.
- HAMZA, N. 2008. Double versus single skin facades in hot arid areas. *Energy and Buildings*, 40, 240-248.
- HAMZA, N., DUDEK, S. & ELKADI, H. S. Impacts of changing facade configurations on office building energy consumption in hot arid climates. *CLIMA 2000*, September 15–18 2001 Napoli, Italy.
- HAMZA, N., GOMAA, A. & UNDERWOOD, C. Daylighting and thermal analysis of an obstructed double skin façade in hot arid areas. *Proceedings of Clima*, 2007.
- HASHEMI, N., FAYAZ, R. & SARSHAR, M. 2010. Thermal behaviour of a ventilated double skin facade in hot arid climate. *Energy and Buildings*, 42, 1823-1832.
- HAZEM, A., AMEGHCHOUCHE, M. & BOUGRIOU, C. 2015. A numerical analysis of the air ventilation management and assessment of the behavior of double skin facades. *Energy and buildings*, 102, 225-236.
- HEIM, D., JANICKI, M. & SZCZEPANSKA, E. Thermal and visual comfort in a office building with double skin façade. *Indoor Air 2011*, 2011 Austin, Texas, USA.
- HENDRIKSEN, O. J., SORENSEN, H., SVENSON, A. & AAQVIST, P. 2000. Double skin façades—fashion or a step towards sustainable buildings. *Proceedings of ISES, Eurosun*, 2000.
- HENSEN, J., BARTAK, M. & DRKAL, F. 2002. Modeling and simulation of a double-skin façade system. *ASHRAE Transactions*, 108, 1251-1259.
- HIEN, LIPING, CHANDRA, PANDEY & XIAOLIN 2005. Effects of double glazed facade on energy consumption, thermal comfort and condensation for a typical office building in Singapore. *Energy and Buildings*, 37, 563-572.
- HRAYSHAT, E. S. 2007. Analysis of renewable energy situation in Jordan. *Renewable and Sustainable Energy Reviews*, 11, 1873-1887.
- HUB, Z. C. 2015. IMPACTS OF OVERHEATING_EVIDENCE REVIEW. London.
- HUMPHREYS, M. 1975. Field studies of thermal comfort compared and applied, *Building Research Establishment*.
- HUMPHREYS, M. 1976. Comfortable indoor temperatures related to the outdoor air temperature. *Building Service Engineer*, 44, 5-27.

- HUMPHREYS, M. A. 1974. *Classroom Temperature, Clothing and Thermal Comfort--A Study of Secondary School Children in Summertime*. Building Research Establishment Current Paper 22/74. Reprinted from *The Building Services Engineer (JHVE)*, 41, 191-202.
- INSTRUMENTS., T. A. 2015. *AIRFLOW MEASUREMENT INSTRUMENTS: TSI-AIRFLOW 2014 CATALOG*.
- IYI, D., HASAN, R., PENLINGTON, R. & UNDERWOOD, C. 2014. Double skin façade: Modelling technique and influence of venetian blinds on the airflow and heat transfer. *Applied Thermal Engineering*, 71, 219-229.
- Ji, Y., COOK, M. J., HANBY, V. I., INFELD, D. G., LOVEDAY, D. L. & MEI, L. CFD MODELLING OF DOUBLE-SKIN FAÇADES WITH VENETIAN BLINDS. *Building Simulation*, 2007. 1491-1498.
- JIRU, T. E. & HAGHIGHAT, F. 2008. Modeling ventilated double skin façade—A zonal approach. *Energy and Buildings*, 40, 1567-1576.
- JORDAN, M. O. E. A. M. R.-. 2012. Ministry of Energy and Mineral Resources-Annual Report 2012 [Online]. Available: <http://eis.memr.gov.jo/publication/2016-04-03-07-59-21/annual-report/81-annual-report-2012> [Accessed 1-11-2013].
- JORDAN, M. O. E. A. M. R.-. 2014. ENERGY 2014 - Facts & Figures [Online]. Available: <http://www.memr.gov.jo/EchoBusV3.0/SystemAssets/PDFs/EN/Brchure%202014.pdf> [Accessed 08-05-2017].
- KISCHKOWEIT-LOPIN, M. 2002. An overview of daylighting systems. *Solar Energy*, 73, 77-82.
- KOTTEK, M., GRIESER, J., BECK, C., RUDOLF, B. & RUBEL, F. 2006. World map of the Koppen-Geiger climate classification updated. *Meteorologische Zeitschrift*, 15, 259-264.
- KRAGH, M. 2000. *Building Envelopes and Environmental Systems*. Paper presented at Modern Façades of Office Buildings Delft Technical University. The Netherlands.
- KUHN, T. E. 2006. Solar control: A general evaluation method for facades with venetian blinds or other solar control systems. *Energy and buildings*, 38, 648-660.
- LA PICA, A., RODONÒ, G. & VOLTERRA, R. 1993. An experimental investigation on natural convection of air in a vertical channel. *International Journal of Heat and Mass Transfer*, 36, 611-616.
- LANG, W. & HERZOG, T. 2000. Using multiple glass skins to clad buildings. *Architectural Record*, 7, 171-182.
- LARSON, G. W., SHAKESPEARE, R., EHRLICH, C., MARDALJEVIC, J., PHILLIPS, E. & APIAN-BENNEWITZ, P. 1998. *Rendering with radiance: the art and science of lighting visualization*, Morgan Kaufmann San Francisco, CA.
- LEE, E., SELKOWITZ, S., BAZIANAC, V., INKAROJIT, V. & KOHLER, C. 2002. High-performance commercial building facades.
- LESLIE 2003. Capturing the daylight dividend in buildings: why and how? *Building and Environment*, 38, 381-385.
- LEVIN, H. 1995. Physical factors in the indoor environment. *Occup Med*, 10, 59-94.
- LITTLEFAIR, AIZLEWOOD & BIRTLES 1994. The performance of innovative daylighting systems. *Renewable Energy*, 5, 920-934.
- LOONEN, R., SINGARAVEL, S., TRČKA, M., CÓSTOLA, D. & HENSEN, J. 2014. Simulation-based support for product development of innovative building envelope components. *Automation in Construction*, 45, 86-95.
- MANZ, SCHAEELIN & SIMMLER 2004. Airflow patterns and thermal behavior of mechanically ventilated glass double façades. *Building and Environment*, 39, 1023-1033.
- MANZ, H. 2003. Numerical simulation of heat transfer by natural convection in cavities of facade elements. *Energy and Buildings*, 35, 305-311.
- MANZ, H. 2004. Total solar energy transmittance of glass double façades with free convection. *Energy and Buildings*, 36, 127-136.
- MANZ, H. & FRANK, T. 2005. Thermal simulation of buildings with double-skin façades. *Energy and Buildings*, 37, 1114-1121.
- MASAR. 2013. The Abdali Boulevard [Online]. Available: <http://www.masarunited.com/category/projects/jordan/jordan-buildings/page/2/> [Accessed 9/1/2017].

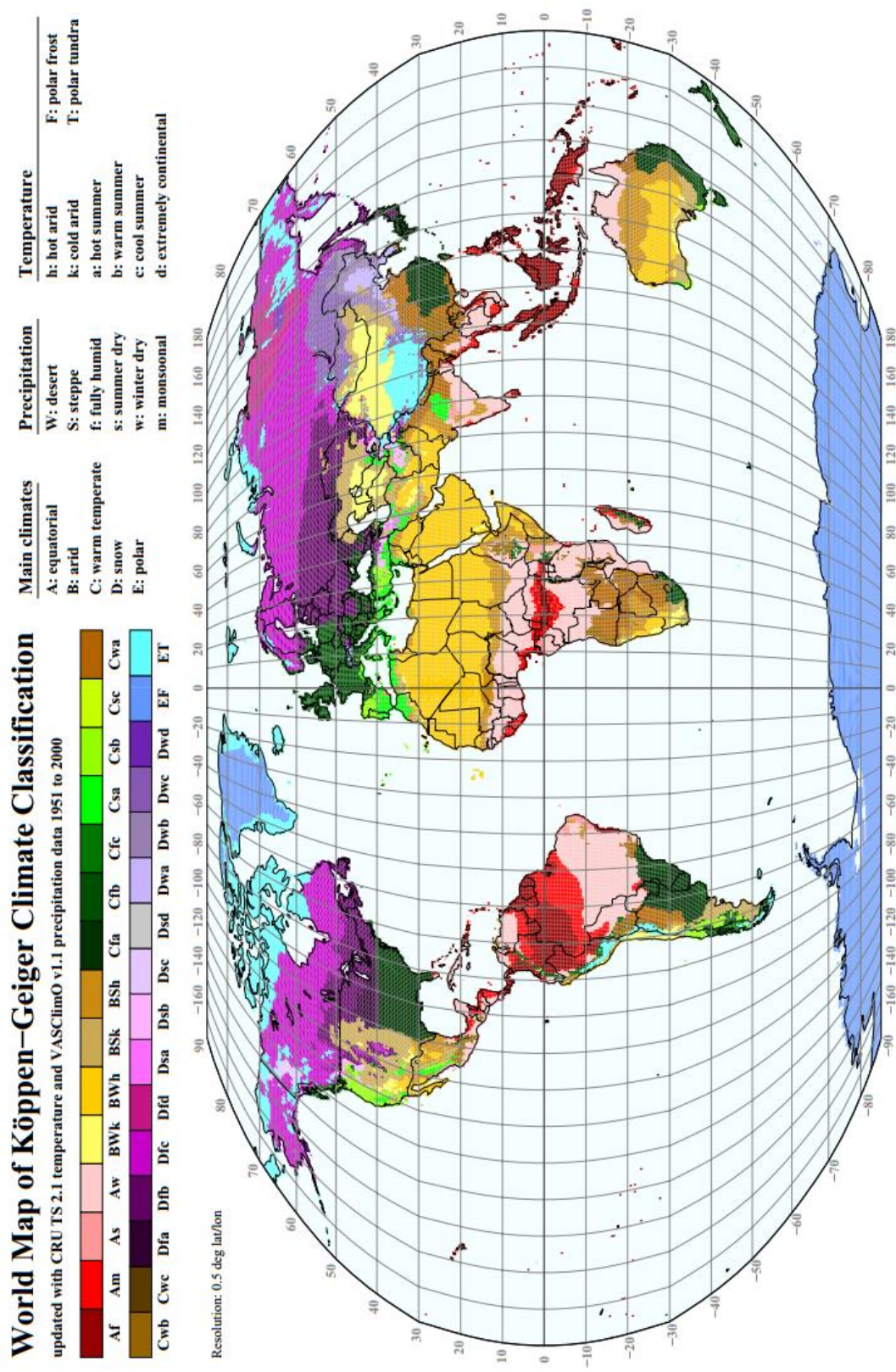
- MATOUQ, M., EL-HASAN, T., AL-BILBISI, H., ABDELHADI, M., HINDIYEH, M., ESLAMIAN, S. & DUHEISAT, S. 2013. The climate change implication on Jordan: A case study using GIS and Artificial Neural Networks for weather forecasting. *Journal of Taibah University for Science*, 7, 44-55.
- MCNAMARA, W. 2013. *Down The Boulevard*. Jordan Business.
- MEI, L., LOVEDAY, D., INFELD, D., HANBY, V., COOK, M., LI, Y., HOMLES, M. & BATES, J. The influence of blinds on temperatures and air flows within ventilated double-skin Façades. *Clima 2007 WellBeing Indoors*, 2007.
- METZ, H. C. Jordan: A country study. 1989. Library of Congress, Federal Research Division.
- MGAE, M. G. A. E.-. 2017. Managing Energy Costs in Congregational Buildings [Online]. Available: https://www.mge.com/saving-energy/business/bea/article_detail.htm?nid=1734 [Accessed 9/1/2017].
- MINGOTTI, CHENVIDYAKARN & WOODS 2011. The fluid mechanics of the natural ventilation of a narrow-cavity double-skin facade. *Building and Environment*, 46, 807-823.
- MITCHELL, R., KOHLER, C., CURCIJA, D., ZHU, L., VIDANOVIC, S., CZARNECKI, S., ARASTEH, D., CARMODY, J. & HUIZENG, C. 2013. THERM 6.3 / WINDOW 6.3 NFRC Simulation Manual. Lawrence Berkeley National Laboratory.
- MUBĀRAK, A. 1969. *Al-Khiṭaṭ al-Tawfīqīyah al-jadīdah li-Miṣr al-Qāhīrah wa-mudunihā wa-bilādihā al-qadīmah wa-shahīrah* (الخطط التوفيقية الجديدة لمصر القاهرة ومدنها وبلادها القديمة والشهيرة), مطبعة دار الكتب،
- MUSA, M. 2014. Constructing global Amman: petrodollars, identity, and the built environment in the early twenty-first century. University of Illinois at Urbana-Champaign.
- NES, N. E. S. 2008. ROTANA AMMAN HOTEL; Amman, Jordan.
- NICOL, J. F. & HUMPHREYS, M. A. 2002. Adaptive thermal comfort and sustainable thermal standards for buildings. *Energy and Buildings*, 34, 563-572.
- OCHOA, C. E. & CAPELUTO, I. G. 2006. Evaluating visual comfort and performance of three natural lighting systems for deep office buildings in highly luminous climates. *Building and Environment*, 41, 1128-1135.
- OESTERLE, E., LIEB, R.-D., LUTZ, M. & HEUSLER, W. 2001. Double Skin Facades – Integrated Planning.
- OKALUX. [n.d.]-a. OKASOLAR - Leistungsfähige Systeme zur Tageslichtnutzung - Glazing with Integral Daylight Control [Online]. Available: https://www.okalux.de/fileadmin/user_upload/aktuell/Downloads/Prospekte/Prospekt_OKASOLAR.pdf [Accessed 18-5-2017].
- OKALUX. [n.d.]-b. OKASOLAR RETRO O/U - Glazing with Integral Sun Control Louvres [Online]. Available: http://03ccde5.netsolhost.com/wordpress1/wp-content/uploads/2015/07/i_okasolar_retro_e.pdf [Accessed 9/5/2017].
- OMRAN, D. A. 2013a. Architecture, Office - ALABDALI OFFICE BUILDING COMPETITION - AMMAN, JORDAN - 2006 [Online]. Available: <http://www.daralomran.com/?portfolio=alabdali-office-building-competition> [Accessed 31/10/2013].
- OMRAN, D. A. 2013b. Architecture, Office - ARAB INSURANCE COMPANY OFFICE BUILDING - AMMAN, JORDAN - 2008 [Online]. Available: <http://www.daralomran.com/?portfolio=arab-insurance-company-office-building> [Accessed 31/10/2013].
- PARK, AUGENBROE, MESSADI, THITISAWAT & SADEGH 2004. Calibration of a lumped simulation model for double-skin façade systems. *Energy and Buildings*, 36, 1117-1130.
- PARRA, J., GUARDO, A., EGUSQUIZA, E. & ALAVEDRA, P. 2015. Thermal Performance of Ventilated Double Skin Façades with Venetian Blinds. *Energies*, 8, 4882-4898.
- PARSONS, K. 2014. Human thermal environments: the effects of hot, moderate, and cold environments on human health, comfort, and performance. Crc Press.
- PASQUAY, T. 2004. Natural ventilation in high-rise buildings with double facades, saving or waste of energy. *Energy and Buildings*, 36, 381-389.
- PASUT, W. & DE CARLI, M. 2012. Evaluation of various CFD modelling strategies in predicting airflow and temperature in a naturally ventilated double skin façade. *Applied Thermal Engineering*, 37, 267-274.

- PÉREZ-GRANDE, I., MESEGUER, J. & ALONSO, G. 2005. Influence of glass properties on the performance of double-glazed facades. *Applied Thermal Engineering*, 25, 3163-3175.
- POIRAZIS, H. 2004. *Double Skin Façades for Office Buildings*. Sweden: Lund University, Lund Institute of Technology, Lund.
- POIRAZIS, H. Double skin façade glazed office buildings; A parametric study for optimized energy and thermal comfort performance. 2nd PALENC Conference and 28th AIVC Conference on Building Low Energy Cooling and Advanced Ventilation Technologies in the 21st Century., 2007. Citeseer.
- RADHI, H., SHARPLES, S. & FIKIRY, F. 2013. Will multi-facade systems reduce cooling energy in fully glazed buildings? A scoping study of UAE buildings. *Energy and Buildings*, 56, 179-188.
- RESEARCH, A. O. 2015. GLAD Theory Manual: Ver. 5.9.
- ROGERS, Z. L., LAYFAYETTE, CO (US), HOLTZ, M. J., BOULDER, CO (US) & CLEVINGER, C. M., BOULDER, CO (US). 2003. MINI-OPTICAL LIGHT SHELF DAYLIGHTING SYSTEM. USA patent application 10/293,689.
- ROGERS, Z. L., LAYFAYETTE, CO, HOLTZ, M. J. B., CO, CLEVINGER, C. M., BOULDER, CO & DIGERT, N. E., WESTMINSTER, CO. 2004. Mini-optical light shelf daylighting system. 10/293,689.
- SAELEN, D. 2002. *Energy Performance Assessments of Single Storey Multiple-Skin Facades*. PhD, Catholic University of Leuven, Belgium.
- SAELEN, D., BLOCKEN, B., ROELS, S. & HENS, H. Optimization of the energy performance of multiple-skin facades. *Proceedings of IBPSA International Conference on Building Simulation*, 2005. 1-8.
- SAELEN, D., CARMELIET, J. & HENS, H. 2003. Energy performance assessment of multiple-skin facades. *HVAC&R Research*, 9, 167-185.
- SAELEN, D., ROELS, S. & HENS, H. 2008. Strategies to improve the energy performance of multiple-skin facades. *Building and Environment*, 43, 638-650.
- SAFER, N., GAVAN, V., WOLOSZYN, M. & ROUX, J. Double-skin façade with Venetian blind: global modelling and assessment of energy performance. *EPIC Conference*, 2006.
- SAFER, N., WOLOSZYN, M. & ROUX, J. Influence of solar radiation on heat and air flow transfers in double skin façades with Venetian blinds. 9th International Conference on Air Distribution in Rooms (ROOMVENT 2004), Coimbra Portugal, 2004a.
- SAFER, N., WOLOSZYN, M. & ROUX, J. Global modelling of double skin facades equipped with venetian blind model based on CFD approach. *CONFERENCE INTERNATIONALE ENERGIE SOLAIRE ET BATIMENT*, 2005a. EPFL, Lausanne, 179-184.
- SAFER, N., WOLOSZYN, M. & ROUX, J. 2005b. Three-dimensional simulation with a CFD tool of the airflow phenomena in single floor double-skin facade equipped with a venetian blind. *Solar Energy*, 79, 193-203.
- SAFER, N., WOLOSZYN, M., ROUX, J., RUSAOUËN, G. & KUZNIK, F. Modeling of the double-skin facades for building energy simulations: radiative and convective heat transfer. 9th International IBPSA Conference Building Simulation, 2005c. 1067-1074.
- SAFER, N., WOLOSZYN, M., RUSAOUËN, G. & ROUX, J. Numerical studies with CFD approach of the heat and air flow transfers combined with solar radiation in double-skin facades. *The 21th Conference on Passive and Low Energy Architecture (PLEA 2004)*, Eindhoven The Netherlands, 2004b.
- SECRETARIAT, E. C. 2010. *THE HASHEMITE KINGDOM OF JORDAN; Regular Review of Energy Efficiency Policies. Part I: Trends in energy and energy efficiency policies, instruments and actors* [Online]. Available: http://www.energycharter.org/fileadmin/DocumentsMedia/EERR/EERR-Jordan_2010_en.pdf [Accessed 1-11-2013].
- SHARIAH, A., TASHTOUSH, B. & ROUSAN, A. 1997. Cooling and heating loads in residential buildings in Jordan. *Energy and Buildings*, 26, 137-143.
- SIMMLER, H. & BINDER, B. 2008. Experimental and numerical determination of the total solar energy transmittance of glazing with venetian blind shading. *Building and environment*, 43, 197-204.
- SINGH, M. C., GARG, S. N. & JHA, R. 2008. Different glazing systems and their impact on human thermal comfort—Indian scenario. *Building and Environment*, 43, 1596-1602.
- STRAUBE, J. F. & VAN STRAATEN, R. 2001. *The technical merit of double facades for office buildings in cool humid climates*. White Paper. University of Waterloo. Canada.

- TECHNOLOGIES, W. B. 2008. WEATHER DATA FOR ENERGY CALCULATIONS [Online]. Available: <http://weather.whiteboxtechnologies.com/>.
- TSI UNDERSTANDING, A. 2012. AIR VELOCITY TRANSDUCERS MODELS 8455, 8465, AND 8475. U.S.A.
- UUTTU, S. 2001. Study of Current Structures in Double-Skin Facades. MSc thesis in Structural Engineering and Building Physics.
- WANG, F., DAVIES, M., CUNLIFFE, B. & HEATH, P. The design of double skin façade: Modelling study on some design parameters affecting indoor thermal conditions. *Proceedings CIBSE National Conference*, 1999. 540-567.
- WANG, Y., CHEN, Y. & ZHOU, J. 2016. Dynamic modeling of the ventilated double skin façade in hot summer and cold winter zone in China. *Building and Environment*, 106, 365-377.
- WARD, G. J. 1992. RADIANCE Visual Comfort Calculation. LESO-EPFL, April, 6, 1992.
- WAREMA 2009. WAREMA Competence Center, Marktheidenfeld / Germany. Germany.
- WEBB, A. R. 2006. Considerations for lighting in the built environment: Non-visual effects of light. *Energy and Buildings*, 38, 721-727.
- WEBSTER, N. 2014. *Comfort, health and indoor air quality*.
- WELTY, J. R., WICKS, C. E., RORRER, G. & WILSON, R. E. 2009. *Fundamentals of momentum, heat, and mass transfer*, John Wiley & Sons.
- WIENOLD, J. & CHRISTOFFERSEN, J. 2006. Evaluation methods and development of a new glare prediction model for daylight environments with the use of CCD cameras. *Energy and buildings*, 38, 743-757.
- WIGGINTON, M. 1996. *Glass in architecture*, Phaidon London.
- WIGGINTON, M. & HARRIS, J. 2002. *Intelligent Skins*, Butterworth-Heinemann.
- WONG, P. C., PRASAD, D. & BEHNIA, M. 2008. A new type of double-skin façade configuration for the hot and humid climate. *Energy and Buildings*, 40, 1941-1945.
- XU, L. & OJIMA, T. 2007. Field experiments on natural energy utilization in a residential house with a double skin façade system. *Building and environment*, 42, 2014-2023.
- XU, X.-L. & YANG, Z. 2008. Natural ventilation in the double skin facade with venetian blind. *Energy and Buildings*, 40, 1498-1504.
- YAKHOT, V. & ORSZAG, S. A. 1986. Renormalization group analysis of turbulence I. Basic theory. *J. Sci. Comput.*, 1, 3-51.
- ZENG, Z., LI, X., LI, C. & ZHU, Y. 2012. Modeling ventilation in naturally ventilated double-skin façade with a venetian blind. *Building and Environment*, 57, 1-6.
- ZHANG, Y. 2013. Multi-Slat Combination Blind of Up-Down-Movement Type. US Patent 20,130,037,224.
- ZHOU, J. & CHEN, Y. 2010. A review on applying ventilated double-skin facade to buildings in hot-summer and cold-winter zone in China. *Renewable and Sustainable Energy Reviews*, 14, 1321-1328.
- ZÖLLNER, A., WINTER, E. & VISKANTA, R. 2002. Experimental studies of combined heat transfer in turbulent mixed convection fluid flows in double-skin-facades. *International Journal of Heat and Mass Transfer*, 45, 4401-4408.

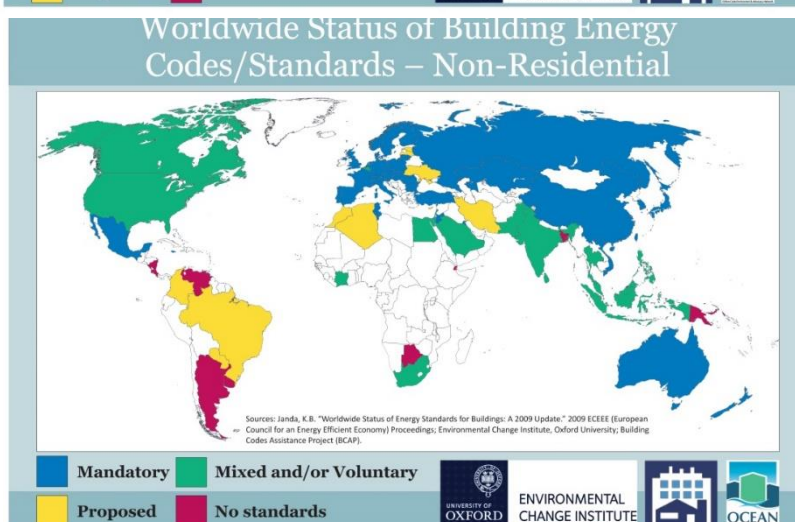
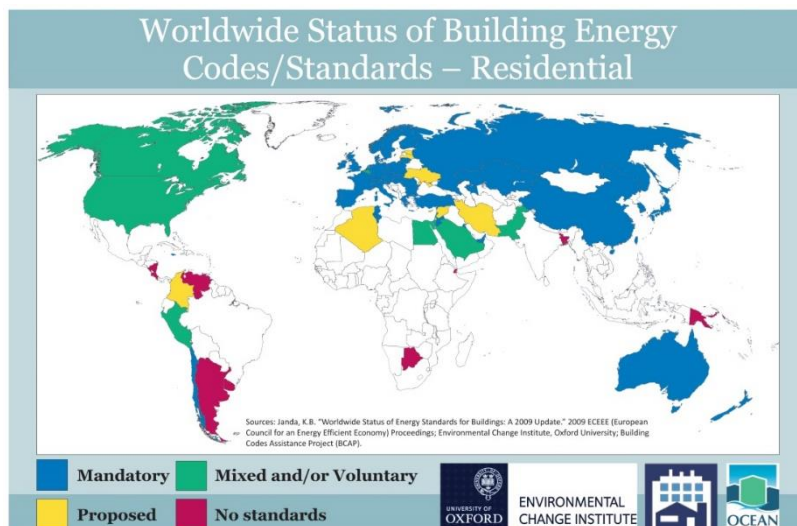
APPENDICES:

APPENDIX A: World Map of Koppen-Geiger Climate Classification.



KOTTEK, M., GRIESER, J., BECK, C., RUDOLF, B. & RUBEL, F. 2006. World map of the Köppen-Geiger climate classification updated. *Meteorologische Zeitschrift*, 15, 259-264.

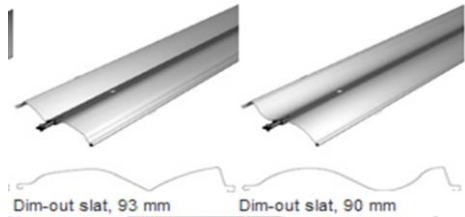


APPENDIX B: Jordan status in terms of applying Building Energy Code for residential and non-residential sectors. Worldwide Status of Building Energy Code/Standards.




JANDA, K. B. 2009. "Worldwide Status of Energy Standards for Buildings: A 2009 Update." 2009 ECEEE (European Council for an Energy Efficient Economy) Proceedings; Environmental Change Institute, Oxford University; Building Codes Assistance Project (BCAP). [Online]. Available: <http://bcapcodes.org/code-status/country/worldwide-status-residential/> [Accessed 17-5-2017].

APPENDIX C: Design and Specifications for Various Available Daylighting Products.

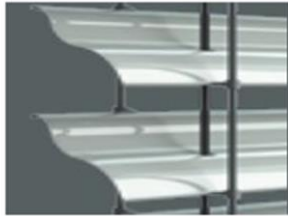
APPENDIX C-1: Design and specifications for different daylighting products – Surface-Slat “A” (Cont'd).

CATEGORY	(A) Surface-slat				
CODE	POSITION	PRODUCT NAME	FEATURE S	DESCRIPTION/GRAPHS	COMMENTS
A1	Exterior Louver Systems.	WAREMA Dim Out External Venetian Blinds ^{1,2,3}	WAREMA Dim Out External Venetian Blinds		<ul style="list-style-type: none">- Reduce solar heat gain- Eliminating glare- Redirecting daylighting
	<div><div></div><div></div><div></div></div>				
<div>¹ WAREMA. [n.d.]-a. <i>Dim-out external venetian blinds</i> [Online]. Available: http://www.warema.com/en/PRIVATE_CUSTOMERS/PRODUCTS/External_venetian_blinds/Dim-out_external_venetian_blinds.php [Accessed 17-5-2017].</div> <div>² SHADEFACOR. [n.d.]-a. <i>external venetian blinds :: dim-out</i> [Online]. Available: http://www.shadefactor.com.au/external-venetian-blinds/external-venetian-blinds/item/64-dim-out-external-venetian-blinds [Accessed 15-1-2014].</div> <div>³ SHADEFACOR. [n.d.]-b. <i>external venetian blinds :: dim-out</i> [Online]. Available: http://www.shadefactor.com.au/external-sunshading/external-venetian-blinds/external-venetian-blinds-dim-out [Accessed 17-5-2017].</div>					

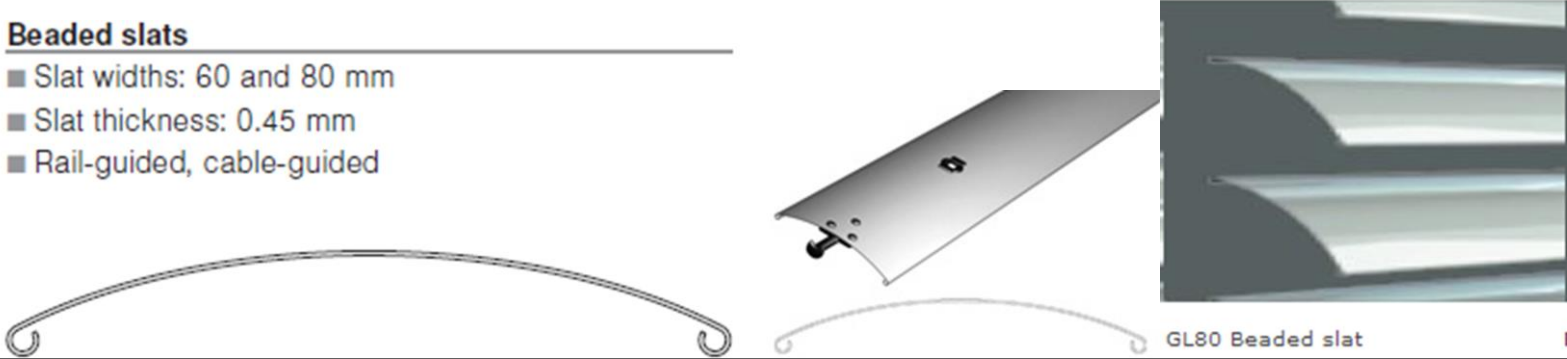
APPENDIX C-2: Design and specifications for different daylighting products – Surface-Slat “A” (Cont'd).

CATEGORY		(A) Surface-slat			
CODE	POSITION	PRODUCT NAME	FEATURES	DESCRIPTION/GRAPHS	COMMENTS
A2	Exterior Louver Systems ^{1,2}	Wind Stable External Venetian Blinds	<ul style="list-style-type: none"> -Rolled edge slat. -S shape: braced plane against wind pressure. -Multi-fold geometry → better rigidity. 		<ul style="list-style-type: none"> - Similar to above. - Rigid against wind up to 90 km/h - Daylight features available! - Needs more considerations/investigations regarding airflow.
<p>¹ WAREMA. [n.d.]-c. <i>Wind-stable external venetian blinds</i> [Online]. Available: http://www.warema.com/en/PRIVATE_CUSTOMERS/PRODUCTS/External_venetian_blinds/Wind-stable_external_venetian_blinds.php [Accessed 17-5-2017].</p> <p>² SHADEFACOR. [n.d.]-a. <i>external venetian blinds :: dim-out</i> [Online]. Available: http://www.shadefactor.com.au/external-sunshading/external-venetian-blinds/external-venetian-blinds-dim-out [Accessed 17-5-2017].</p>					

APPENDIX C-3: Design and specifications for different daylighting products – Surface-Slat “A” (Cont'd).

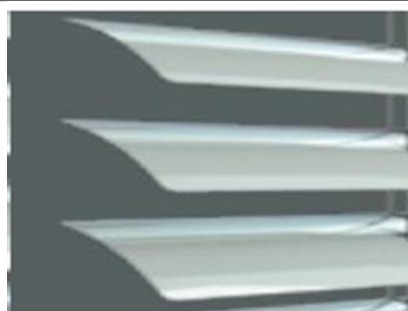
CATEGORY (A) Surface-slat					
CODE	POSITION	PRODUCT NAME	FEATURES	DESCRIPTION/GRAPHS	COMMENTS
A3	Exterior Louver Systems ^{1,2}	Exterior blinds: DBL70 Three-fold slat		 <p>DBL70 Three-fold slat</p>	<ul style="list-style-type: none"> - Similar to above. - Daylight features available! - Needs more considerations/investigations regarding airflow.
<p>¹ LUXUSHAUS, I. L. [n.d.]-a. <i>Exterior blinds: DBL70 Three-fold slat</i> [Online]. Available: https://www.luxushaus.com/shading/roma/triple-curve-slat.php [Accessed 15-1-2014].</p> <p>² DUNDM. 2010. <i>Front mounting systems with roller shutters or exterior blinds</i> [Online]. Available: http://www.dundm.com/d_und_m/en/Downloads/Downloads/Front%20mounting/Brochure.pdf [Accessed 18-5-2017].</p>					

APPENDIX C-4: Design and specifications for different daylighting products – Surface-Slat “A” (Cont'd).

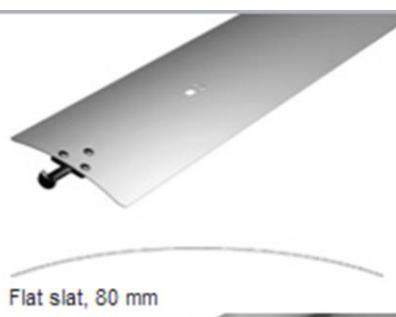
CATEGORY (A) Surface-slat					
CODE	POSITION	PRODUCT NAME	FEATURES	DESCRIPTION/GRAPHS	COMMENTS
A4	Exterior Louver Systems ^{1,2,3}	Exterior blinds: GL80 Beaded slat			<ul style="list-style-type: none"> - Similar to above. - Daylight features available! Needs more considerations/investigations regarding airflow.
<p>Beaded slats</p> <ul style="list-style-type: none"> ■ Slat widths: 60 and 80 mm ■ Slat thickness: 0.45 mm ■ Rail-guided, cable-guided  <p>GL80 Beaded slat</p>					
<p>¹ LUXUSHAUS, I. L. [n.d.]-c. <i>Exterior blinds: GL80 Beaded slat</i> [Online]. Available: http://www.luxushaus.com/shading/roma/triple-curve-slat.php [Accessed 15-1-2014].</p> <p>² SHADEFACOR. [n.d.]-d. <i>WAREMA External Venetian Blind Range - External venetian blinds - Modern Sun Shading</i> [Online]. Available: http://www.shadefactor.com.au/external-sunshading/external-venetian-blinds/external-venetian-blinds-standard#cedar-slat [Accessed 18-5-2017].</p> <p>³ DUNDM. 2010. <i>Front mounting systems with roller shutters or exterior blinds</i> [Online]. Available: http://www.dundm.com/d_und_m/en/Downloads/Downloads/Front%20mounting/Brochure.pdf [Accessed 18-5-2017].</p>					

APPENDIX C-5: Design and specifications for different daylighting products – Surface-Slat “A” (Cont'd).

CATEGORY	(A) Surface-slat				
CODE	POSITION	PRODUCT NAME	FEATURES	DESCRIPTION/GRAPHS	COMMENTS
A5	Exterior Louver Systems ^{1,2,3}	Exterior blinds: FL80 Flat slat			<ul style="list-style-type: none"> - Similar to above. - Rigid against wind up to 90 km/h - Daylight features available! - Needs more considerations/investigations regarding airflow.



FL80 Flat slat



Flat slats

- Slat widths: 50, 60, 80, 100 and 150 mm
- Slat thickness: 0.45 mm
- Rail-guided, cable-guided

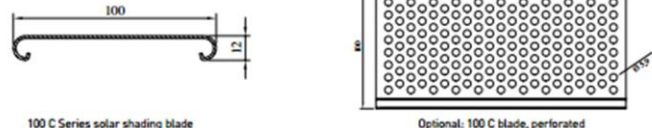
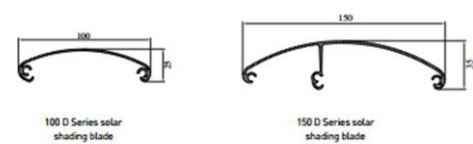




¹ LUXUSHAUS, I. L. [n.d.]-b. *Exterior blinds: FL80 Flat slat* [Online]. Available: <http://www.luxushaus.com/shading/roma/triple-curve-slat.php> [Accessed 15-1-2014].

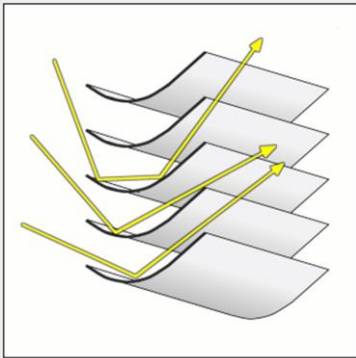
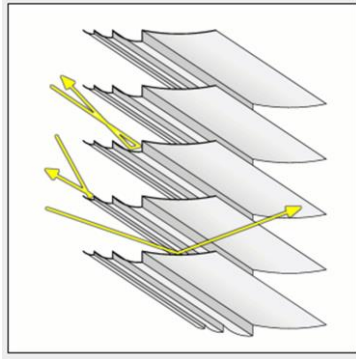
² SHADEFACOR. [n.d.]-d. *WAREMA External Venetian Blind Range - External venetian blinds - Modern Sun Shading* [Online]. Available: <http://www.shadefactor.com.au/external-sunshading/external-venetian-blinds/external-venetian-blinds-standard#cedar-slat> [Accessed 18-5-2017].

³ DUNDM. 2010. *Front mounting systems with roller shutters or exterior blinds* [Online]. Available: http://www.dundm.com/d_und_m/en/Downloads/Downloads/Front%20mounting/Brochure.pdf [Accessed 18-5-2017].

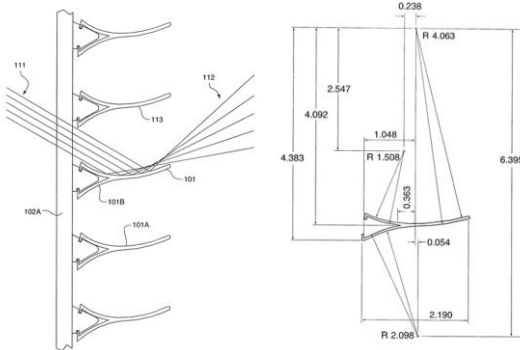
APPENDIX C-6: Design and specifications for different daylighting products – Surface-Slat “A” (Cont'd).

CATEGORY	(A) Surface-slat				
CODE	POSITION	PRODUCT NAME	FEATURES	DESCRIPTION/GRAPHS	COMMENTS
A6	Exterior Louver Systems ^{1,2}	Exterior: DucoSun 100 C vertical	<ul style="list-style-type: none"> - C-shape - Perforated → airflow! 	<p>→ Solar shading blades</p>  <p>100 C Series solar shading blade</p> <p>Optional: 100 C blade, perforated</p>	<ul style="list-style-type: none"> - Solar shading - Airflow (Perforated) - Daylight (perforated)
<p>¹ SIMON, R. [n.d.]-a. <i>DucoSun 100 C vertical</i> [Online]. Available: http://www.simonairmanagement.co.uk/content_images/products_pdf/folder_sun_UK.pdf [Accessed 15-1-2014].</p> <p>² DUCO, V. S. C. 2009. <i>NATURAL COMFORT INSIDE</i> [Online]. Available: https://www.barbourproductsearch.info/folder%20sun%20UK-file033137.pdf [Accessed 18-5-2017].</p>					
A7	Exterior Louver Systems ^{3,4}	Exterior: DucoSun 100 D/150 D vertical Appealing with <i>bullnose design</i>	<ul style="list-style-type: none"> - D-shape. - Bullnose design. 	<p>→ Solar shading blades</p>  <p>100 D Series solar shading blade</p> <p>150 D Series solar shading blade</p> <p>→ DucoSun 100 D vertical</p>  <p>100 D</p> <p>→ DucoSun 150 D vertical</p>  <p>150 D</p> <p>Solar shading</p>	
<p>³ SIMON, R. [n.d.]-b. <i>DucoSun 100 D/150 D vertical</i> [Online]. Available: http://www.rwsimon.co.uk/content_images/products_pdf/folder_sun_UK.pdf [Accessed 15-1-2014].</p> <p>⁴ DUCO, V. S. C. 2009. <i>NATURAL COMFORT INSIDE</i> [Online]. Available: https://www.barbourproductsearch.info/folder%20sun%20UK-file033137.pdf [Accessed 18-5-2017].</p>					

APPENDIX C-7: Design and specifications for different daylighting products – Surface-Slat “A” (Cont'd).

CATEGORY (A) Surface-slat					
CODE	POSITION	PRODUCT NAME	FEATURES	DESCRIPTION/GRAPHS	COMMENTS
A8	Interior Louver Systems ¹	Curved Metallic Louvers	<ul style="list-style-type: none"> - Curve concave surface. - High gloss surface. 		<ul style="list-style-type: none"> - Simple daylighting redirecting system.
¹ KNOWLEDGEBASE, L. D. A. S. 2013b. <i>Daylight Redirection Systems - Interior Louver Systems</i> [Online]. Available: http://www.schorsch.com/en/kbase/redir/louvers.html [Accessed 18-5-2017].					
A9	Interior Louver Systems ²	Folded Metallic Louvers	<ul style="list-style-type: none"> - Simple curvature top surface. - The external half is folded. 		<ul style="list-style-type: none"> - Reject the high-angle light. - Redirect/reflect the low-angle light.
² KNOWLEDGEBASE, L. D. A. S. 2013b. <i>Daylight Redirection Systems - Interior Louver Systems</i> [Online]. Available: http://www.schorsch.com/en/kbase/redir/louvers.html [Accessed 18-5-2017].					



APPENDIX C-8: Design and specifications for different daylighting products – Surface-Slat “A” (Cont'd).

CATEGORY	(A) Surface-slat			
CODE	POSITION	PRODUCT NAME	FEATURES	DESCRIPTION/GRAPHS
A10	Interior Louver Systems ¹	Patent US 6480336 B2: Mini optical light shelf daylighting system with slats	<ul style="list-style-type: none">- Optically shaped top surface.- Two adjoining arcs + radii- Leading edge deals with high angles; has:<ol style="list-style-type: none">1. Small-surface portion2. a tighter radius3. steeper reflecting angle- Trailing edge deals with low-angles, has:<ol style="list-style-type: none">1. Large-surface portion2. Flatter surface3. Large radius curve.	
	<ul style="list-style-type: none">- Light will not strike the bottom of the adjacent slat thus no glare causing at this bottom- Design of surface will ensure receiving different-angle incident light by different portion of the surface.- Receive daylight from different angles (input) and redirect through specific range of angles (output).			
¹ NEALL EDWARD DIGERT, C., CA (US) & MICHAEL JOSEPH HOLTZ, B., CO (US). 2002. <i>MINI-OPTICAL LIGHT SHELF DAYLIGHTING SYSTEM</i> . USA patent application 09/776,319.				

APPENDIX C-9: Design and specifications for different daylighting products – Surface-Slat “A” (Cont'd).

CATEGORY	(A) Surface-slat				
CODE	POSITION	PRODUCT NAME	FEATURES		DESCRIPTION/GRAPHS
A11	Interior Louver Systems ¹	Patent US 6239910 B1: Mini optical light shelf daylighting system with slats	<ul style="list-style-type: none">- Optically shaped top surface.- Two main different shapes regarding the vertical element		<ul style="list-style-type: none">- Collect & redirect light- Shading (block direct light)- Optical geometry & characteristics of the reflective curved top surface determine the efficiency of the lighting louver.- Providing uniform & glare-free daylighting.- Receive daylight from different angles (input) and redirect through specific range of angles (output).
¹ NEALL EDWARD DIGERT, W., CO (US). 2001. MINI-OPTICAL LIGHT SHELF DAYLIGHTING SYSTEM. USA patent application 09/249,664.					

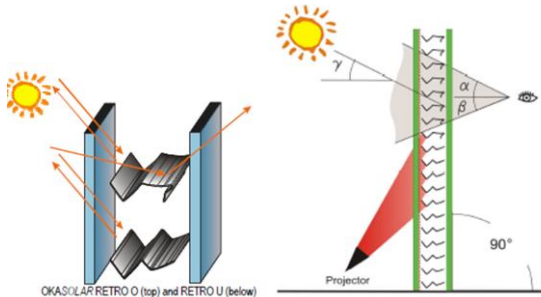
APPENDIX C-10: Design and specifications for different daylighting products – Surface-Slat “A” (Cont'd).

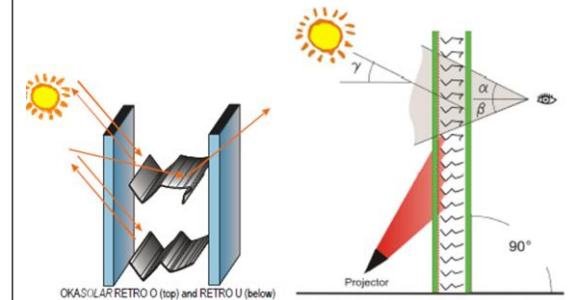
CATEGORY	(A) Surface-slat				
CODE	POSITION	PRODUCT NAME	FEATURES		DESCRIPTION/GRAPHS
A12	DSF cavity (also; Exterior and internal)	Genius slats (WAREMA) ^{1,2}	<ul style="list-style-type: none">- Symmetry shape.- Folded slat- with low reflectivity finish- Exterior face is with high reflectivity finish	<ul style="list-style-type: none">- Used in DSF- Not sure if it's ventilated!	
	<div><div></div><div><p>Genius slats</p><ul style="list-style-type: none">■ Slat widths: 50 and 80 mm■ Slat thickness: 0.27 mm / 0.45 mm■ Cable-guided, rail-guided, freely suspended</div></div>				

¹ SHADEFACOR. [n.d.]-c. Warema - Light control venetian blinds with Genius special slats C 50/80 Genius, E 50/80 Genius [Online]. Available: <http://www.shadefactor.com.au/internal-sunshading/day-light-guidance-venetian-blinds> [Accessed 18-5-2017].

² WAREMA. [n.d.]-b. Genius light guidance venetian blind [Online]. Available: http://www.warema.com/en/BUSINESS_PARTNERS/PRODUCTS/Light_guidance_systems/Light_guidance_venetian_blind/Light_guidance_venetian_blind_Genius.php# [Accessed 18-5-2017].

APPENDIX C-12: Design and specifications for different daylighting products – Surface-Slat “A” (Cont'd).

CATEGORY	(A) Surface-slat																										
CODE	POSITION	PRODUCT NAME	FEATURES			DESCRIPTION/GRAPHS																					
A14	Integrated Vertical Double Glazing	OKASOLAR RETRO O/U ¹ Design 1	<div>Table 1: Geometry of the different OKASOLAR RETRO types</div> <table><tr><th>Type OKASOLAR</th><th>Angle of louvre [°]</th><th>Distance of louvre [mm]</th><th>Horizontal trough-vision %</th><th>Trough-vision to above α [°]</th><th>lower β [°]</th><th>Look out angle γ [°]</th></tr><tr><td>RETRO U</td><td>90</td><td>12.5</td><td>57</td><td>26</td><td>30</td><td>26</td></tr><tr><td>RETRO O</td><td>90</td><td>12.5</td><td>55</td><td>28</td><td>22</td><td>28</td></tr></table>			Type OKASOLAR	Angle of louvre [°]	Distance of louvre [mm]	Horizontal trough-vision %	Trough-vision to above α [°]	lower β [°]	Look out angle γ [°]	RETRO U	90	12.5	57	26	30	26	RETRO O	90	12.5	55	28	22	28	<ul style="list-style-type: none">- Façade-integrated- Enable daylight (directionally selective light transmission)- Effective solar shading (directionally selective solar control)- Partially through-vision
Type OKASOLAR	Angle of louvre [°]	Distance of louvre [mm]	Horizontal trough-vision %	Trough-vision to above α [°]	lower β [°]	Look out angle γ [°]																					
RETRO U	90	12.5	57	26	30	26																					
RETRO O	90	12.5	55	28	22	28																					
	<ul style="list-style-type: none">- Through-vision: approx. 56% of total glazed area- Three-dimensional shape- Highly reflective profile- Two different types of louvers: U & O- Type U: work to reflect daylight outwards (retro-reflection) + glare protection- Type O: redirect daylighting into the room.- Both types can be used in one vertical elements: type O should be not used within height of 1.8 m- Function:<ol style="list-style-type: none">1. Direct light with High or medium angles: total solar energy transmittance as low as 8% + glare protection + <u>daylighting by type O</u>2. Direct light with low angles: partial transmittance of direct light + <u>daylighting by type O</u>3. Diffuse light: daylighting penetration			<div></div>																							
¹ OKALUX. [n.d.]-d. OKASOLAR RETRO O/U - Glazing with Integral Sun Control Louvres [Online]. Available: http://03ccde5.netsolhost.com/wordpress1/wp-content/uploads/2015/07/i_okasolar_retro_e.pdf [Accessed 9/5/2017.																											



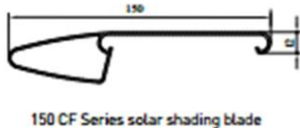
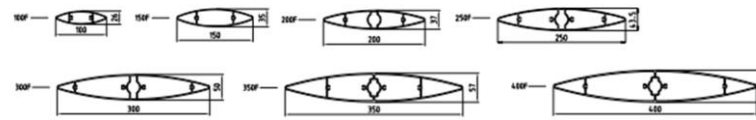
¹ OKALUX. [n.d.]-d. OKASOLAR RETRO O/U - Glazing with Integral Sun Control Louvres [Online]. Available: http://03ccde5.netsolhost.com/wordpress1/wp-content/uploads/2015/07/i_okasolar_retro_e.pdf [Accessed 9/5/2017].

APPENDIX C-13: Design and specifications for different daylighting products – Surface-Slat “A”.

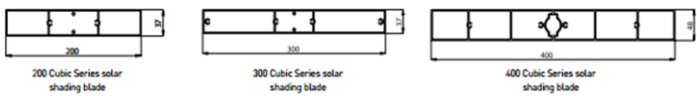
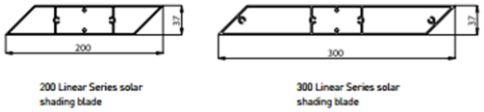
CATEGORY	(A) Surface-slat			
CODE	POSITION	PRODUCT NAME	FEATURES	DESCRIPTION/GRAPHS
A15	Integrated Vertical Double Glazing	OKASOLAR RETRO O/U ¹ Design 2	<ul style="list-style-type: none">- Type U: work to reflects daylight at sharp angles toward the ceiling ... this make free-glare daylighting ... good view to outside- Type O: redirects daylight at flat angle toward the ceiling ... this flat angle (horizontally) allows daylighting to penetrate deeply in the room.	

¹ OKALUX. [n.d.]-b. OKASOLAR + OKAFLEX - Optisch geregelter Sonnenschutz, flexible Lichtsteuerung - Glazing with integral sun control louvres, flexible light control [Online]. Available: <http://www.vena-ltd.co.uk/images/brochures/OKASOLAR-Brochure.pdf> [Accessed 18-5-2017].

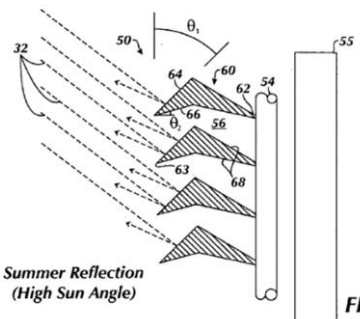
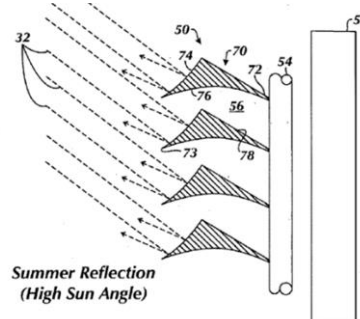
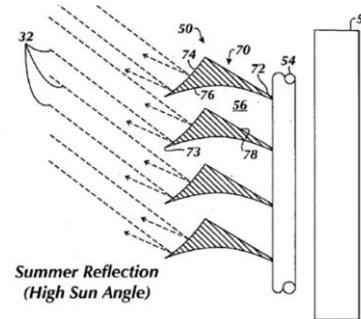
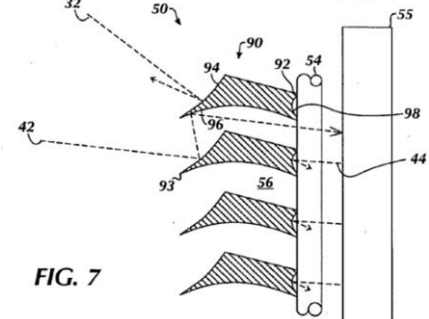
APPENDIX C-14: Design and specifications for different daylighting products – Simple Body-slat “B”.

CATEGORY		(B) Simple Body-slat			Comments
Code	Position	Product Name	Features	Description/Graphs	
Category-B		Simple Body-slat			
B1	Exterior Louver Systems	Exterior: DucoSun 150 CF vertical Appealing with <i>ellipsoid</i> <i>design</i> ^{1,2}	<ul style="list-style-type: none"> - CF-shape - Ellipsoid design 	 <p>150 CF Series solar shading blade</p>	<ul style="list-style-type: none"> - Solar shading - Strong → more in-between spans
<p>¹ SIMON, R. [n.d.]-c. <i>DucoSun 150 CF vertical</i> [Online]. Available: http://www.simonairmanagement.co.uk/content_images/products_pdf/folder_sun_UK.pdf [Accessed 15-1-2014].</p> <p>² DUCO, V. S. C. 2009. <i>NATURAL COMFORT INSIDE</i> [Online]. Available: https://www.barbourproductsearch.info/folder%20sun%20UK-file033137.pdf [Accessed 18-5-2017].</p>					
B2		Exterior: DucoSun Ellips ^{3,4}	<ul style="list-style-type: none"> - Ellips-shape (ellipsoid shape) - Different sizes (7 proportional sizes) 	<p>Basic components</p> <p>→ Solar shading blades</p> 	<ul style="list-style-type: none"> - Admit high diffused daylight - Optimal shading performance
<p>³ SIMON, R. [n.d.]-e. <i>DucoSun Ellips</i> [Online]. Available: http://www.rwsimon.co.uk/content_images/products_pdf/folder_sun_UK.pdf [Accessed 15-1-2014].</p> <p>⁴ DUCO, V. S. C. 2009. <i>NATURAL COMFORT INSIDE</i> [Online]. Available: https://www.barbourproductsearch.info/folder%20sun%20UK-file033137.pdf [Accessed 18-5-2017].</p>					

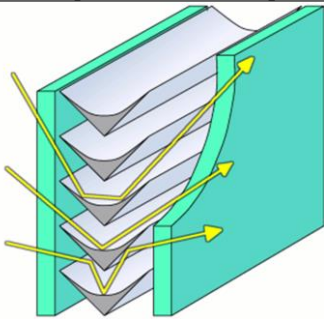
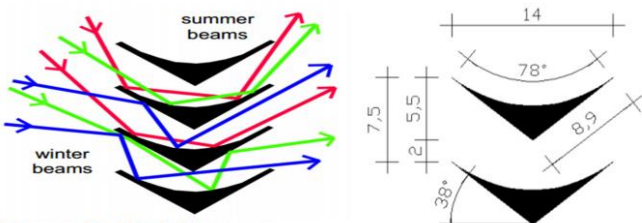
APPENDIX C-15: Design and specifications for different daylighting products – Simple Body-slat “B”.

CATEGORY		(B) Simple Body-slat			Comments
Code	Position	Product Name	Features	Description/Graphs	
Category-B		Simple Body-slat			
B3		Exterior: DucoSun Cubic ^{1,2}	- Cubic-shape	<p>Basic components</p> <p>→ Solar shading blades</p> 	- Not optimal for Airflow !
<p>¹ SIMON, R. [n.d.]-d. <i>DucoSun Cubic</i> [Online]. Available: http://www.rwsimon.co.uk/content_images/products_pdf/folder_sun_UK.pdf [Accessed 15-1-2014].</p> <p>² DUCO, V. S. C. 2009. <i>NATURAL COMFORT INSIDE</i> [Online]. Available: https://www.barbourproductsearch.info/folder%20sun%20UK-file033137.pdf [Accessed 18-5-2017].</p>					
B4		Exterior: DucoSun Linear ^{3,4}	- parallelogram shaped solar shading blade	<p>Basic components</p> <p>→ Solar shading blades</p> 	<p>- atheistic appearance</p> <p>- Not optimal for Airflow!</p>
<p>³ SIMON, R. [n.d.]-f. <i>DucoSun Linear</i> [Online]. Available: http://www.simonairmanagement.co.uk/content_images/products_pdf/folder_sun_UK.pdf [Accessed 15-1-2014].</p> <p>⁴ DUCO, V. S. C. 2009. <i>NATURAL COMFORT INSIDE</i> [Online]. Available: https://www.barbourproductsearch.info/folder%20sun%20UK-file033137.pdf [Accessed 18-5-2017].</p>					

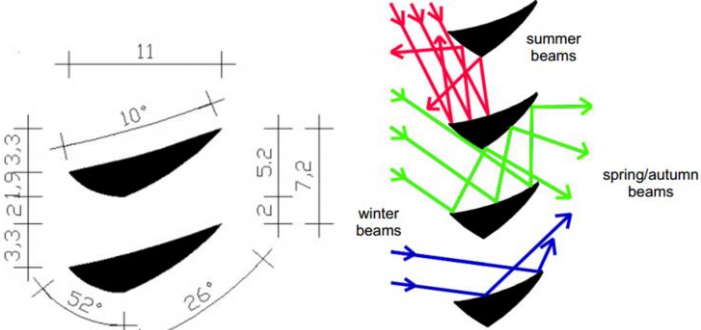
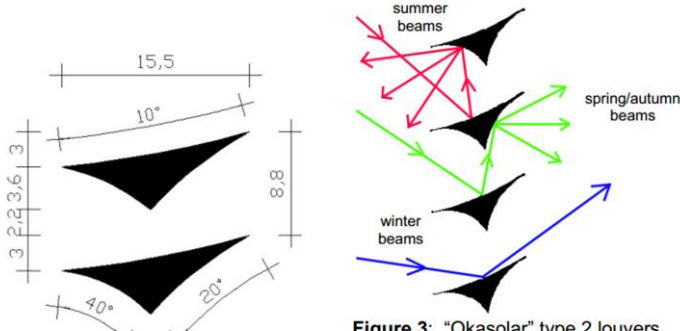
APPENDIX C-16: Design and specifications for different daylighting products – Compound Body-slat “C” (Continue).

Category-C		Compound Body-slat		
C1	Integrated Vertical Double Glazing	Patent US 2010/010156 5 A1: Passive solar wire screens for building ¹	<ul style="list-style-type: none">- Enclosure shape (cross-section)- External shading- Four different shaped.	<ul style="list-style-type: none">- Mainly for passive solar shading.- Block and reject high solar light- Redirect and reflect the low solar light onto indoor- With increasing the offset distance, some low solar light will penetrate directly to indoor.
<div><div><p>FIG. 4A</p></div><div><p>FIG. 5A</p></div><div><p>FIG. 5A</p></div><div><p>FIG. 7</p></div></div>				
¹ RLCHARD C. MAXSON, M. G., MN (US) & MICHAEL EKHOLM, M., MN (US). 2010. PASSIVE SOLAR WIRE SCREENS FOR BUILDINGS USA patent application 12/258,796.				

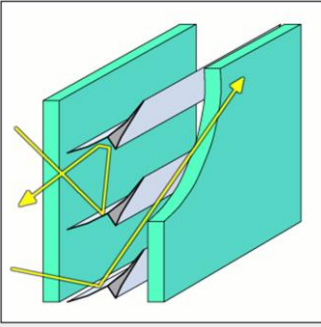
APPENDIX C-17: Design and specifications for different daylighting products – Compound Body-slat “C” (Continue).

Category-C		Compound Body-slat		
C2	Integrated Vertical Double Glazing	Symmetric Metallic Profiles ¹	<ul style="list-style-type: none"> - Redirect (allow) most of the incident light and over the year. - Micro-scale. - No airflow consideration. 	-Needs more considerations & investigations regarding airflow.
¹ KNOWLEDGEBASE, L. D. A. S. 2013a. <i>Daylight Redirection Systems - Integrated in Vertical Double Glazing</i> [Online]. Available: http://www.schorsch.com/en/kbase/redir/vertglas.html [Accessed 18-5-2017].				
C3	Interior Louver Systems	Fish Louvers ²	<ul style="list-style-type: none"> - Similar concept to integrated into glazed surfaces.  <p>Figure 1: “Fish” louvers</p>	<ul style="list-style-type: none"> - Allow light from different angles. - Can block direct ones (depends on the offset)
² HEIM, D. & KIESZKOWSKI, K. Shading Devices Designed to Achieve the Desired Quality of Internal Daylight Environment. PLEA2006 - The 23rd Conference on Passive and Low Energy Architecture, 6-8 September. 2006 Geneva, Switzerland.				

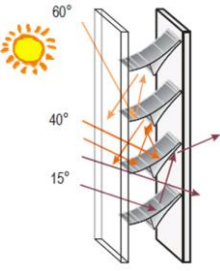
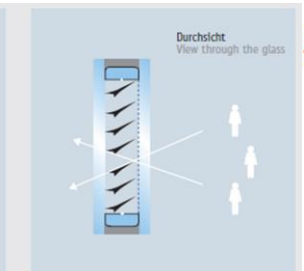
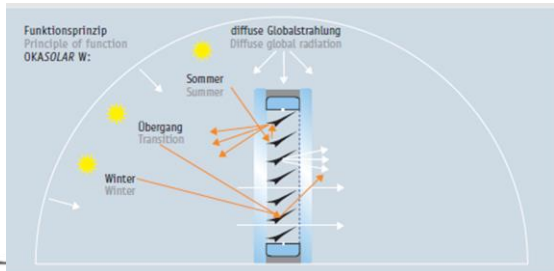
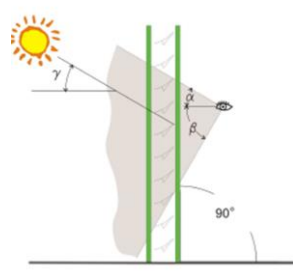
APPENDIX C-18: Design and specifications for different daylighting products – Compound Body-slat “C” (Continue).

Category-C		Compound Body-slat			
C4	Interior Louver Systems	Okasolar-1 Louvers ¹		 <p>Figure 2: “Okasolar” type 1 louvers</p>	<ul style="list-style-type: none"> - Block high-angle light - Redirect the others - Allow for good in-out view offset, while still deal with horizontal light properly (not allow as direct but reflected). - Possibility of downward reflections; which may cause glare.
		¹ HEIM, D. & KIESZKOWSKI, K. Shading Devices Designed to Achieve the Desired Quality of Internal Daylight Environment. PLEA2006 - The 23rd Conference on Passive and Low Energy Architecture, 6-8 September. 2006 Geneva, Switzerland.			
C5	Interior Louver Systems	Okasolar-2 Louvers ²		 <p>Figure 3: “Okasolar” type 2 louvers</p>	<ul style="list-style-type: none"> - Block high-angle light - Redirect the others - Allow for good in-out view offset, while still deal with horizontal light properly (not allow as direct but reflected). - Possibility of downward reflections; which may cause glare.
		² HEIM, D. & KIESZKOWSKI, K. Shading Devices Designed to Achieve the Desired Quality of Internal Daylight Environment. PLEA2006 - The 23rd Conference on Passive and Low Energy Architecture, 6-8 September. 2006 Geneva, Switzerland.			

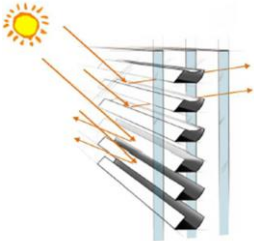
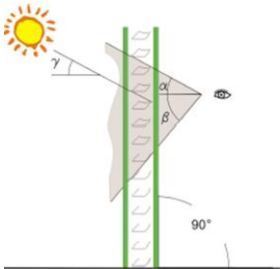
APPENDIX C-19: Design and specifications for different daylighting products – Compound Body-slat “C” (Continue).

Category-C		Compound Body-slat		
C6	Integrated Vertical Double Glazing	Asymmetric Metallic Profiles ¹	<ul style="list-style-type: none"> - Reflect part of the incident light (high angles of summer) - Redirect (allow) most of low-angle incident light (winter) - Provide summer shading - Micro-scale. - No airflow consideration- 	 <ul style="list-style-type: none"> - Block high-angle light - Redirect the others - Allow for good in-out view offset, while still deal with horizontal light properly (not allow as direct but reflected). - Possibility of downward reflections; which may cause glare.
¹ KNOWLEDGEBASE, L. D. A. S. 2013a. <i>Daylight Redirection Systems - Integrated in Vertical Double Glazing</i> [Online]. Available: http://www.schorsch.com/en/kbase/redir/vertglas.html [Accessed 18-5-2017].				

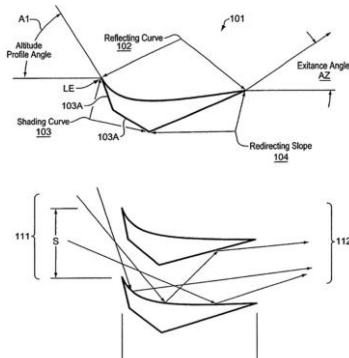
APPENDIX C-20: Design and specifications for different daylighting products – Compound Body-slat “C” (Continue).

C7	Integrated Vertical Double Glazing	OKASOLAR W ^{1,2}	<table><tr><th colspan="6">Table 1: Geometry of the different OKASOLAR W types</th></tr><tr><th>Type OKASOLAR</th><th>Angle of louvre [°]</th><th>Distance of louvre [mm]</th><th>Horizontal through-vision %</th><th>Through-vision to above α [°]</th><th>lower β [°]</th><th>Look out angle γ [°]</th></tr><tr><td>W 50/17</td><td>50</td><td>17</td><td>38</td><td>25</td><td>64</td><td>25</td></tr><tr><td>W 55/17</td><td>55</td><td>17</td><td>41</td><td>28</td><td>62</td><td>28</td></tr><tr><td>W 60/17</td><td>60</td><td>17</td><td>45</td><td>30</td><td>60</td><td>30</td></tr></table>	Table 1: Geometry of the different OKASOLAR W types						Type OKASOLAR	Angle of louvre [°]	Distance of louvre [mm]	Horizontal through-vision %	Through-vision to above α [°]	lower β [°]	Look out angle γ [°]	W 50/17	50	17	38	25	64	25	W 55/17	55	17	41	28	62	28	W 60/17	60	17	45	30	60	30	<ul style="list-style-type: none">- Highly reflective profile- Function:<ol style="list-style-type: none">1. For Direct light with High or medium angles: total solar energy transmittance as low as 11% + glare protection2. For Direct light with low angles: partial transmittance of direct light + partial light reflection upwards to ceiling.3. For Diffuse light: daylighting penetration	<ul style="list-style-type: none">- Façade-integrated- Enable daylight (directionally selective light transmission)- Effective solar shading (directionally selective solar control)- Partially through-vision
			Table 1: Geometry of the different OKASOLAR W types																																				
Type OKASOLAR	Angle of louvre [°]	Distance of louvre [mm]	Horizontal through-vision %	Through-vision to above α [°]	lower β [°]	Look out angle γ [°]																																	
W 50/17	50	17	38	25	64	25																																	
W 55/17	55	17	41	28	62	28																																	
W 60/17	60	17	45	30	60	30																																	
<div></div>																																							
<p>¹ OKALUX. [n.d.]-a. <i>OKASOLAR - Leistungsfähige Systeme zur Tageslichtnutzung - Glazing with Integral Daylight Control</i> [Online]. Available: https://www.okalux.de/fileadmin/user_upload/aktuell/Downloads/Prospekte/Prospekt_OKASOLAR.pdf [Accessed 18-5-2017].</p> <p>² OKALUX. [n.d.]-e. <i>OKASOLAR W - Isolierglas mit optisch geregeltem Sonnenschutz</i> [Online]. Available: https://www.okalux.de/fileadmin/user_upload/aktuell/Downloads/Infotexte/Infotext_OKASOLAR_W.pdf [Accessed 18-5-2017].</p>																																							

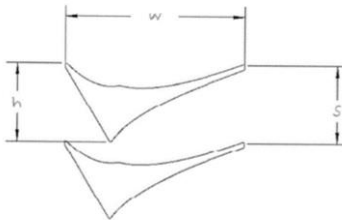
APPENDIX C-21: Design and specifications for different daylighting products – Compound Body-slat “C”.

C8	Integrated Vertical Double Glazing	OKASOLAR F ¹	<ul style="list-style-type: none">- Similar to <u>OKASOLAR RETRO O/U but:</u><ol style="list-style-type: none">1. With different profiles for U & O profiles.2. And, Through-vision: approx. 57% of total glazed area instead of 56%.3. Total solar energy transmittance <u>as low as 9% instead of 8%</u> with medium angles.- Façade-integrated- Enable daylight (directionally selective light transmission)- Effective solar shading (directionally selective solar control)- Partially through-vision																											
	<div>Table 1: Geometry of the different OKASOLAR F types</div> <table><tr><th>Type OKASOLAR</th><th>Angle of louvre [°]</th><th>Distance of louvre [mm]</th><th>Horizontal trough-vision %</th><th colspan="2">Trough-vision to</th><th>Lock out angle</th></tr><tr><td></td><td></td><td></td><td></td><th>above α [°]</th><th>lower β [°]</th><th>γ [°]</th></tr><tr><td>FO</td><td>0</td><td>9.5</td><td>57</td><td>28</td><td>50</td><td>28</td></tr><tr><td>FU</td><td>0</td><td>9.5</td><td>57</td><td>28</td><td>50</td><td>28</td></tr></table> <div></div>			Type OKASOLAR	Angle of louvre [°]	Distance of louvre [mm]	Horizontal trough-vision %	Trough-vision to		Lock out angle					above α [°]	lower β [°]	γ [°]	FO	0	9.5	57	28	50	28	FU	0	9.5	57	28	50
Type OKASOLAR	Angle of louvre [°]	Distance of louvre [mm]	Horizontal trough-vision %	Trough-vision to		Lock out angle																								
				above α [°]	lower β [°]	γ [°]																								
FO	0	9.5	57	28	50	28																								
FU	0	9.5	57	28	50	28																								
¹ OKALUX. [n.d.]-c. <i>OKASOLAR F - Isolierglas mit optisch geregeltem Sonnenschutz</i> [Online]. Available: https://www.okalux.de/fileadmin/user_upload/aktuell/Downloads/Infotexte/Infotext_OKASOLAR_F.pdf [Accessed 18-5-2017].																														

APPENDIX C-22: Design and specifications for different daylighting products – Compound Body-slat “C”.

C9	Interior Louver Systems	Patent US 6714352: Mini optical light shelf daylighting system with slats. 1,2	<p>→ No CPC profile. → Reflective louver. → Width-height ratio is 2.75 (large!). → Slat geometry:</p> <ol style="list-style-type: none">1. Optically shaped-curvature reflected top surface: it is optically shaped with curve. It is work to collect the incident light on its surface and immediately redirect it onto the ceiling ...2. light redirecting segment (part of bottom surface): this segment works to redirect the incoming (reflected) light from the opposite reflecting segment of the adjacent louver, onto the ceiling.3. light shading segment (part of bottom surface): it works to block low angle “but not less than 5-degrees” daylighting rays from passing toward the space through the adjacent slats.
		<ul style="list-style-type: none">- Con: The diffused inclined external surface of the louver will reject large portion of the incoming light! (<u>Lose more daylighting!</u>)- Con: Allow some low-angle light to pass directly to indoor → <u>glare!</u>- Act as shading louver (large than 5 degrees)- Pro: Collimates output light horizontally deeper. Pro: Redirect the incoming daylight onto the ceiling as diffuse light → source of light Design: Optical geometry & characteristics of the reflective curved top surface determine the efficiency of the lightinglouver. Design: Vertical window height used for the system is determining the effective depth of the system (lit ceiling). Pro: It works for all altitude angles. And, providing uniform & glare-free daylighting.	
<p>¹ ROGERS, Z. L., LAYFAYETTE, CO (US), HOLTZ, M. J., BOULDER, CO (US) & CLEVENGER, C. M., BOULDER, CO (US). 2003. MINI-OPTICAL LIGHT SHELF DAYLIGHTING SYSTEM. USA patent application 10/293,689.</p> <p>² ROGERS, Z. L., LAYFAYETTE, CO, HOLTZ, M. J. B., CO, CLEVENGER, C. M., BOULDER, CO & DIGERT, N. E., WESTMINSTER, CO. 2004. Mini-optical light shelf daylighting system. 10/293,689.</p>			

APPENDIX C-23: Design and specifications for different daylighting products – Compound Body-slat 2 (CPS) “D”.

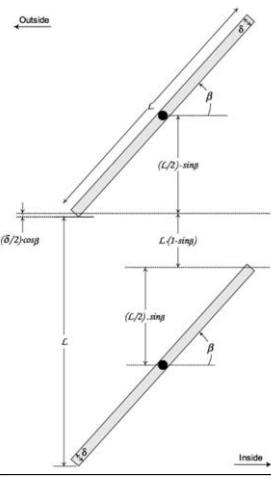
Category-D		Compound Body-slat 2 (CPC)	
Code	Position	Product Name	Features
D1	Integrated Vertical Double Glazing	Patent US 8462437 B2 ^{1,2} 2013	<ul style="list-style-type: none">- Tilting toward ceiling- No direct light (diffuse all light)- Anidolic curve concept.- Surfaces:<ul style="list-style-type: none">1. CPC: redirect the light to ceiling or at least horizontal2. Single parabolic reflector: collect and redirect high-angle light to the CPC3. Inclined flat surface: reflect/redirect low-angle light (horizontal) to single parabolic surface.- Concept of cut-off angle: no horizontal light till 26 degrees will enter → loss! <p>Predetermined output angle. -20 to +20 from the centreline of CPC. With tilting the CPC itself, the output range angle becomes +40 over horizontal.</p>
	 <p>Figure 16</p>	<ul style="list-style-type: none">- Con: The diffused inclined external surface of the louver will reject large portion of the incoming light! (<u>Lose more daylighting!</u>)- Con: Allow some low-angle light to pass directly to indoor → <u>glare!</u>- Act as shading louver (large than 5 degrees)- Pro: Collimates output light horizontally deeper.- Pro: Redirect the incoming daylight onto the ceiling as diffuse light → source of light- Design: Optical geometry & characteristics of the reflective curved top surface determine the efficiency of the lightinglouver.- Design: Vertical window height used for the system is determining the effective depth of the system (lit ceiling)- Pro: It works for all altitude angles. And, providing uniform & glare-free daylighting.	

¹ THUOT, K. W. 2011. *The Soralux Daylighting System: Passive Solar Illumination for Deep-Plan Building Spaces* [Online]. Master Thesis. Department of Mechanical Engineering. The Massachusetts Institute of Technology. MIT, USA. Available: <https://dspace.mit.edu/handle/1721.1/67824> [Accessed 18-5-2017].

² KEVIN W. THUOT, A., TX (U S) & MARLLYNE ANDERSEN, P. C. 2013. *PASSIVE LOUVER-BASED DAYLIGHTING SYSTEM*. USA patent application 13/222,533.

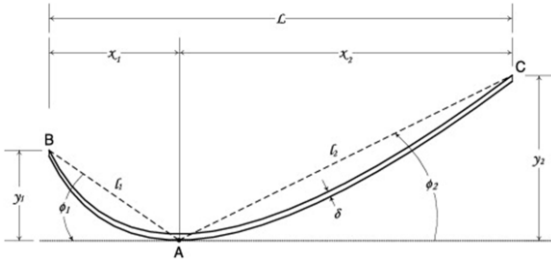
APPENDIX D: Design and Specifications for Common Shading Products.

APPENDIX D-1: Design and specifications for different Shading Designs –Surface Slat “E” (Cont'd).

CATEGORY		(E) Surface-slat			Comments
Code	Position	Product Name	Features	Description/Graphs	
E1	Exterior + Interior	Flat Slats ¹			<ul style="list-style-type: none"> The analysis showed that there is no extra shading (for any tilt angle) due to slat thickness when $D \leq 5\%$ – in reality, most available commercial products have a dimensional ratio less than 5%. ($D = \delta/L$).

¹ TZEMPELIKOS, A. 2008. The impact of venetian blind geometry and tilt angle on view, direct light transmission and interior illuminance. *Solar energy*, 82, 1172-1191.

APPENDIX D-2: Design and specifications for different Shading Designs –Surface Slat “E”.

E2	Exterior + Interior	Curved blind: Arc-of-circle slat ¹		<ul style="list-style-type: none">- For small central angles, the blind could perform similarly to flat-shaped (theoretically for $\theta = 0$). Most of the common products have central angles close to 90°.- Two basic characteristics parameters for the arc-of-circle slat are:<ul style="list-style-type: none">• Circle radius• Central angle- Other parameters are being calculated based on these parameters:<ul style="list-style-type: none">• The chord length or distance between the two blind ends (L): $L = 2R \sin (\theta/2)$.• The height of the arced portion, sagitta (h): $h = R(1 - \cos (\theta/2))$.• The chord length of the arc AC (l): $l = 2R \sin (\theta/4)$.• The apothem (k): $k = R \cos (\theta/4)$.• The sagitta (z): $z = R(1 - \cos (\theta/4))$. <p>The characteristic angle (ϕ): $\phi = \frac{\theta}{4}$ (perpendicular sides).</p>
E3	Exterior + Interior	Curved blind: Arbitrary curved slat ² (two connected curves)		
^{1,2} TZEMPELIKOS, A. 2008. The impact of venetian blind geometry and tilt angle on view, direct light transmission and interior illuminance. <i>Solar energy</i> , 82, 1172-1191.				